Ricardo H. Bardales *Editor*

The Invasive Cytopathologist

Ultrasound Guided Fine-Needle Aspiration of Superficial Masses

Essentials in Cytopathology
Series Editor
Dorothy L. Rosenthal

Springer

The Invasive Cytopathologist

Essentials in Cytopathology

Dorothy L. Rosenthal, MD, FIAC, Series Editor

For further volumes:
http://www.springer.com/series/6996

Ricardo H. Bardales
Editor

The Invasive Cytopathologist

Ultrasound Guided Fine-Needle Aspiration of Superficial Masses

Springer

Editor
Ricardo H. Bardales, MD, MIAC, ECNU
Department of Pathology
and Cytopathology
Outpatient Pathology Associates
Sacramento, CA
USA

ISBN 978-1-4939-0729-8 ISBN 978-1-4939-0730-4 (eBook)
DOI 10.1007/978-1-4939-0730-4
Springer New York Heidelberg Dordrecht London

Library of Congress Control Number: 2014942864

Printed on acid-free paper

Springer is part of Springer Science+Business Media (www.springer.com)

Dedicated To

Waldetrudis, Ricardo, Angela, Ricky, and Angie for their encouragement, support, and for being my role models.

My mentors Abel Mejia, Benjamin Koziner, Leopold G. Koss, Klaus Schriber, Michael W. Stanley, and Norwin Becker.

My Pathology residents and Cytology fellows.

Foreword

Dr. Bardales has reviewed the history of fine needle aspiration, placing this volume at the forefront of this discipline. Before it was applied to current methods, it began as a tool in the hands of our clinical colleagues who sent us specimens for microscopic interpretation. These punctures were directed mostly at palpable lesions. Those active in this field today can imagine the interpretive difficulties that must have arisen in an era when virtually every specimen seemed new. Such difficulties continue to arise and are the subject of our enlarging collective published experience.

In many settings, fine needle aspiration of palpable masses moved into the hands of pathologists. This provided the possibility of immediate interpretation, repeat of inadequate samples and close correlation of clinical with cytologic findings. Many pathologists made the required pilgrimage to study with the method's masters in Sweden during the 1970s and 1980s. As our diagnostic prowess increased, our enthusiasm and confidence grew as well. Many clinicians welcomed the expanding role of pathologists in specimen acquisition, as improved specimen preparation and concentration of clinical and cytologic assessment were merged into a single pair of hands. Many of us have found that pathologist-performed fine needle aspiration simply works better than asking busy clinicians to be responsible for aspiration, preparation and triage to special studies without adequate training. In other words, what happens at the microscope is limited by what happened at the bedside. What happens at the bedside is predicated on what is expected to happen at the microscope.

Dr. Bardales has for some years been associated with Outpatient Pathology Associates (OPA) in Sacramento, California, USA. These academically productive inhabitants of private practice cytology have long been leaders in our field. Many will recall his previous book *Practical Urologic Cytopathology* as the definitive source in the field. We cannot review this history here, but many of us will recall having met and learned from other members of this school, including Dr. John Abele and Dr. Ted Miller. It seems only natural that this group should move decisively into practicing the newest methods that patients will perceive as efficient, high quality one-stop cytologic diagnosis. Dr. Bardales' new book, *The Interventional Cytopathologist: US Guided FNA of Superficial Masses*, reports on OPA's capabilities and expands Dr. Bardales' experience with many thousands of palpable-lesion biopsies to pathologist-performed ultrasound-guided sampling of more deeply situated or more palpably subtle masses.

Many of us have been intimidated by learning to perform and interpret ultrasound, or by the method's seeming complexity or by the instrumentation's cost. As emphasized by Dr. Bardales, the latter two have been ameliorated considerably of late. The former is dealt with early in this book. Issues as basic, but as essential, as concepts of echogenicity are described and illustrated. More traditional issues such as the basics of aspiration technique and specimen preparation remain keys to ultimate diagnostic success and are also considered here.

It is reasonable that the thyroid is addressed extensively. For many of us, this is the most frequent site of needle aspiration biopsies. The thyroid is also one of the sites in which ultrasound imaging is most helpful. Many thyroid lesions are difficult to palpate with confidence. Others are confused by their presence in the setting of multinodular goiter. Called to do a thyroid aspirate in this setting, one is sometimes unsure that his selected target is the same as that for which the aspiration referral was originally made. Diagnostic considerations in thyroid cytology are placed firmly within Bethesda

System terminology, criteria and follow-up recommendations. The parathyroid glands can be clinical, cytomorphologic and anatomic cousins to the larger organ. Most such aspirations require ultrasound guidance. One may also perform parathormone chemistry on samples obtained during aspiration to great effect.

Other head and neck sites, as well as lymph nodes in many areas, also benefit from ultrasound-guided aspiration. A portion of the book is dedicated to breast cytology with a much needed update of diagnostic criteria. While OPA and other practices remain very active in breast aspiration, many of us have long since conceded this area to those wielding much larger core biopsy instruments and using guidance by either stereotactic or ultrasound methods. It is tempting to speculate that pathologists' use of ultrasound might regain some of this territory, allowing patients to enjoy more rapid interpretations.

I predict that this book will not only allow but will encourage pathologists to enter the realm of ultrasound-guided fine needle aspiration. The tools are here.

Michael W. Stanley, MD
Department of Pathology
United Hospital
St. Paul, MN, USA

Series Editor Foreword

The days of the reclusive pathologist are receding. Many cytopathologists have embraced the opportunity to meet patients in the clinics and aspirate palpable lesions. Others involved in cytopathology have experienced direct patient contact as rapid-on site evaluation (ROSE) has become the standard to make sure that fine needle aspirate (FNA) specimens are adequate and triaged appropriately. We are still often invisible, behind a curtain or in an adjacent room while the invasive radiologist obtains the sample.

With the advent of inexpensive ultra-sound machines and the explosive demand for FNA of superficial lesions, especially of the thyroid, pathologists have responded with an unexpected enthusiasm. Professional societies have augmented the response with courses providing instruction toward ultrasonographer certification. Dr. Bardales and his colleagues share their experience learning the interpretation of ultrasound (US) images, and obtaining optimal samples from superficial tumors.

Although other volumes in the *Essentials in Cytopathology* Series cover some of the same material, the presentation in this volume emphasizes the role of the invasive cytopathologist as first clinician in the line of patient managers. Finally, the pathologist will no longer be invisible. We will know that we have "arrived" when the evening news interviews the pathologist, rather than the surgeon, to learn the diagnosis of a noteworthy personality. After all, we are now first in line, as we always have been!

Baltimore, MD, USA Dorothy L. Rosenthal, MD, FIAC

Preface

The use of ultrasonography (US) has become essential in the evaluation of superficial palpable and nonpalpable lesions. In addition to its diagnostic benefit, US can be used as a tool for needle guidance in diagnostic US-guided fine-needle aspiration (USG-FNA), therapy, e.g., cyst drainage, and administration of agents, e.g., alcohol ablation. These procedures can be done in an outpatient office or hospital setting.

This book provides a comprehensive review of the cytology of palpable and/or US-visible superficial neoplastic and non-neoplastic disease processes, as obtained by percutaneous USG-FNA, particularly of the head and neck, breast, lymph nodes, as well as skin and soft tissue. The most salient US features for the most common entities are also provided. Emphasis will be placed on thyroid US, cytology, and molecular tests because they provide fundamental information for personalized therapy.

Sacramento, CA, USA

Ricardo H. Bardales,
MD, MIAC, ECNU

Acknowledgements

Special thanks to the personnel of Outpatient Pathology Associates who contributed in retrieving archival material, making endless phone calls to inquire about patient follow-up, and consenting to obtain ultrasound images of their normal superficial organs. I thank Pathology Residents and Fellows, who throughout the years have contributed with cases that always occupy special places in the library of my brain and heart. Also, I thank Ms. Connie Walsh, Developmental Editor for Springer, and Richard Hruska, Senior Editor for Springer, for their constant support and patience. Last but not least, my special gratitude to Mrs. Elisabeth Lanzl, Senior Editor at the University of Chicago, for her undaunted effort to improve the English grammar and syntax of my manuscripts to transform them into readable documents. I learned so much, and there are still lots of room for improvement.

Sacramento, CA, USA

Ricardo H. Bardales,
MD, MIAC, ECNU

Contents

Contributors

Ricardo H. Bardales, MD, MIAC, ECNU Department of Pathology and Cytopathology, Outpatient Pathology Associates, Sacramento, CA, USA

Eugenio Leonardo, MD, PhD Pathology Department, University Hospital of Trieste, Trieste, Italy

Chapter 1
Ultrasound: General Considerations

Ricardo H. Bardales

The Ultrasound System

The US equipment should have a linear-array transducer probe having a 3.5–5.0-cm footprint and multiple frequency settings ranging from 7.5 to 14 MHz. The system should also have the capacity to do power and color-flow Doppler imaging. We, at Outpatient Pathology Associates (OPA), use a Siemens Acuson ×300 ultrasound system featuring a VF 11.5 MHz linear-array Acuson ×300 transducer probe, a panel of adjustable controls, and a 15' flat screen display for routine evaluation of palpable and non-palpable superficial lesions. We also use MyLab50 ultrasound system (Esaote North America, Inc., Indianapolis, IN) (Figs. 1.1, 1.2, 1.3, and 1.4).

R.H. Bardales, MD, MIAC, ECNU
Department of Pathology and Cytopathology,
Outpatient Pathology Associates,
7750 College Town Drive, Sacramento, CA 95826, USA
e-mail: rhbardales@aol.com

R.H. Bardales (ed.), *The Invasive Cytopathologist*, Essentials in Cytopathology 16, DOI 10.1007/978-1-4939-0730-4_1,

FIGURE 1.1 Siemens Acuson ×300 ultrasound system

Basic Concepts in Ultrasound

The following are a few basic important concepts with which any professional using US should be familiar:

1. Sound is a form of mechanical energy that needs a transmitting material (air, fluid, soft tissue, etc.) to travel. The

FIGURE 1.2 MyLab50. Panel of adjustable controls. (1) System on/off switch; (2) preset key allows the user to select from various menu items; (3) gain alters the amplification of the received signals in the image and by changing it the image brightness can be increased or decreased; (4) time gain compensation and depth gain compensation manual controls are useful to control the amount of amplification at different depths particularly when there is low attenuation of the image; (5) depth alters the image, and better view of the surrounding anatomy and less artifacts can be viewed in a large depth image; (6) the zoom function is used to magnify a region of the image on the screen; (7) the freeze function captures the image on the screen and allows to apply focus, measure, and save the image; (8) the calipers used to mark the area to be measured; (9) the image function saves the image in the system; (10) the clip function allows to take a video clip of various durations; (11) Doppler gain; (12) the start/end key saves the patient data and makes the system to be ready for the next study; (13) the archive review key permits the review of a specific exam and to save the entire session to an external drive, i.e., DVD and USB

speed of sound depends on and is constant for a specific material and does not change with sound frequency or wavelength.

2. Sound travels longitudinally and is represented by a sine wave which is the result of compression (the peaks) and rarefaction (the troughs or valleys) of molecules in space.

FIGURE 1.3 MyLab50. Flat screen display monitor

FIGURE 1.4 Linear-array transducer probe

3. Frequency is the number of cycles per time of the vibration of the sound waves and it is measured in hertz. A hertz (Hz) is defined as one cycle per second.
4. The frequency of sound waves in the audible spectrum ranges from 30 to 20,000 Hz. The frequency of sound waves used in diagnostic US ranges from 5 to 15 million cycles per second (5–15 MHz).

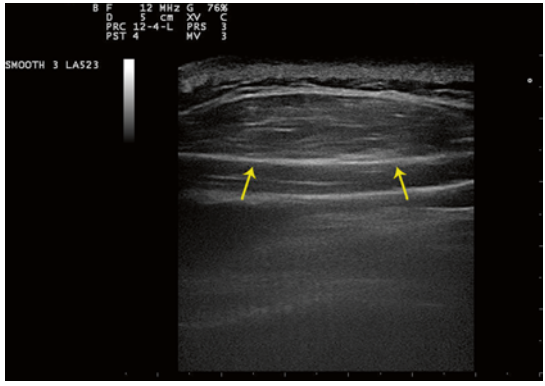

FIGURE 1.5 Superficial US showing the skin in the upper edge of the frame. Lipoma is seen as oval-shaped image horizontally below the skin (*arrows*)

5. The US machine produces and transmits short pulses of high-frequency sound through the transducer into the tissues and waits for part of the US to be reflected back from the tissues and to be captured by the transducer to be converted into electric signals. This process repeats many times per second. The result is the creation of a two-dimensional gray-scale image in the screen monitor. The upper edge of the image corresponds to the surface of the skin (Fig. 1.5).
6. Higher frequencies of sound waves are associated with higher resolution and also with greater attenuation (reduction in amplitude and intensity with increasing distance traveled). As a result, the depth of imaging, or the tissue penetration, is inversely proportional to the US frequency. Superficial organs such as the breast and thyroid can be scanned at high frequencies (10–15 MHz); the abdomen and pelvis are typically scanned at 2.5 MHz.
7. The transducer has an array of piezoelectric crystals that detect US waves and produce electricity (piezoelectric effect). Conversely, when electricity is applied to the crystals, they vibrate and produce sound (reverse piezoelectric effect). Thus, a transducer converts electric to mechanical energy and vice versa.

8. Linear-array transducers are normally used for evaluation of superficial organs. Curved-array transducers with lower frequencies are commonly used for evaluation of abdominal and pelvic organs.
9. The speed of sound in the soft tissues of the body is all (excluding fat) within 5 % of the average value of 1,540 m/s. The US equipment uses this average speed of the sound. The coupling gel transmits the US waves at similar value of 1,540 m/s and removes the air pockets between the transduced footprint and the patient's skin.
10. When US enters soft tissue, it can be transmitted, reflected, or both.
11. Acoustic impedance is the inverse of the capacity of a material to transmit sound (resistance to the passage of the US waves) and depends on the density (concentration of matter) and stiffness (capacity to change shape) of the material and the speed of sound.
12. The soft tissues of a given anatomic region have different (heterogeneous) acoustic impedance with different amounts of reflection of the sound waves, leading to the generation of a characteristic US pattern. The mass of a given organ may have a characteristic pattern as well.
13. A cyst has uniformly low impedance with high sound transmission and no reflected sound and will appear anechoic. The echogenicity of a nodule or mass is compared with the brightness of the adjacent tissue (adipose or muscle). When masses have uniform echoes, they can be hypoechoic (slightly darker than fat or muscle), isoechoic (light gray like fat or muscle), or hyperechoic (slightly brighter than fat or muscle) (Figs. 1.6, 1.7, and 1.8).
14. Benign lesions usually have smooth, lobulated, and well-defined pushing rather than infiltrating margins (Fig. 1.9). A malignant tumor is usually hypoechoic and heterogeneous, with ill-defined, irregular, and angulated borders due to infiltration of the malignant growth into the surrounding tissue (Fig. 1.10).
15. *Acoustic shadowing* is an artifact that refers to a dark shadow seen behind a calcified nodule due to near or total lack of sound transmission, e.g., an eggshell calcification in a thyroid nodule (Fig. 1.11).

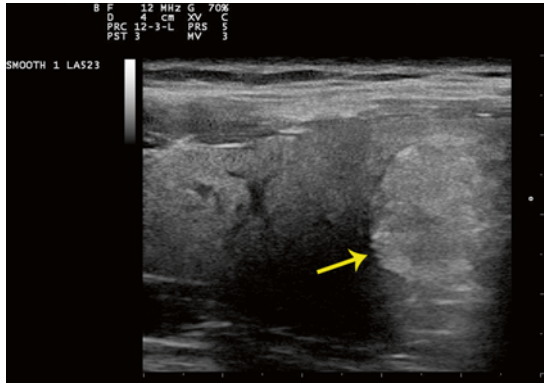

FIGURE 1.6 Hyperechoic mass (*arrow*). The echogenicity is brighter than that of surrounding thyroid tissue

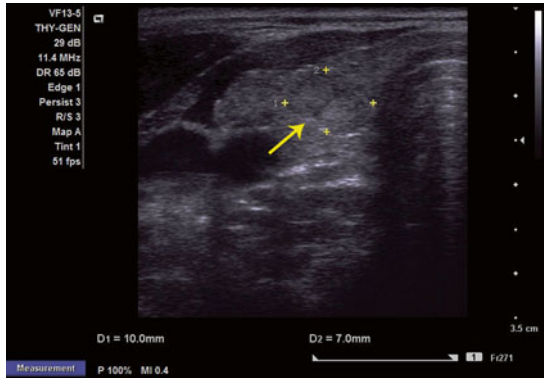

FIGURE 1.7 Isoechoic nodule (*arrow*). The echogenicity is similar to that of surrounding thyroid tissue

16. *Acoustic enhancement* is an artifact that refers to a bright shadow seen behind a nodule with little attenuation due to great intensity of sound waves behind the nodule, e.g., cystic lesions, colloid-rich thyroid nodules, or even homogeneous solid nodules, e.g., lipid-rich nodules. Both acoustic shadowing and enhancement are artifacts due to attenuation and occur when sound travels between two extreme interfaces (Fig. 1.12).

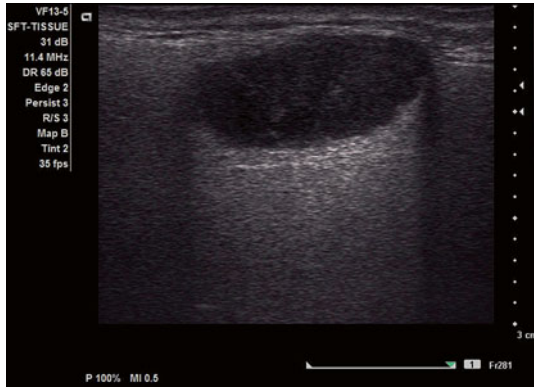

FIGURE 1.8 Hypoechoic nodule. The echogenicity is darker than that of the surrounding tissue

FIGURE. 1.9 Hypoechoic nodule with lobulated edges and pushing borders (benign mixed tumor)

17. Doppler US is used for evaluation of the vascularity of tissues and plays an important role in thyroid imaging. *Color-flow Doppler* provides information regarding the direction and speed of blood flow within the tissue and is particularly useful in vascular studies. *Power Doppler* provides information on the total amount of blood flow

FIGURE 1.10 Hypoechoic mass with ill-defined borders and irregular, angulated, and infiltrating margins (mammary carcinoma)

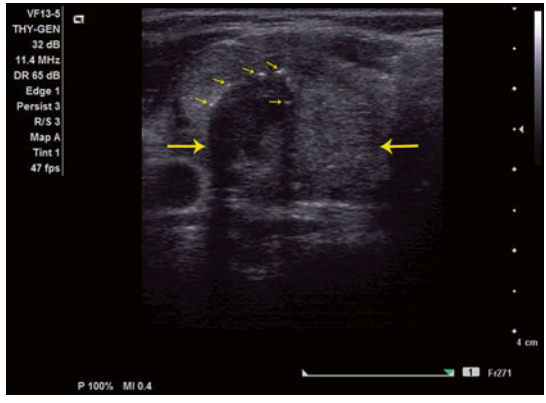

FIGURE 1.11 Posterior acoustic shadowing. The thyroid nodule is demarcated by the *big arrows*. The *small arrows* point the calcified fragmented rim that projects dark irregular shadows of various lengths due to lack of sound transmission

present, independent of the direction or speed, and is generally the preferred modality for evaluating tissue vascularity (Figs. 1.13 and 1.14).

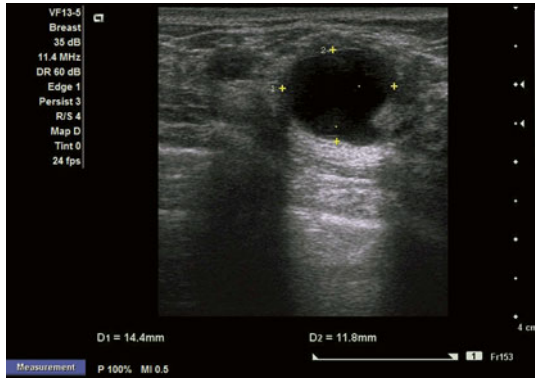

FIGURE 1.12 Posterior acoustic enhancement. A uniform bright shadow is projected posterior to this cystic lesion

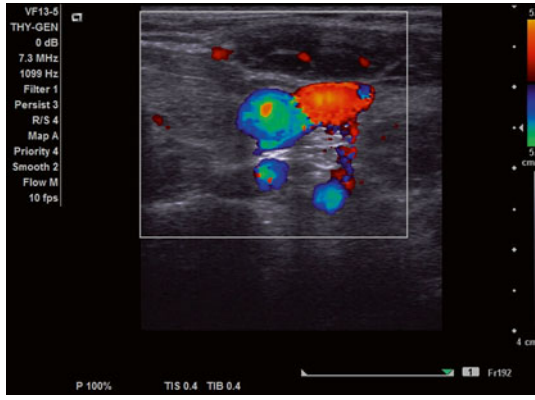

FIGURE 1.13 Color-flow Doppler provides information regarding the direction and speed of blood flow within the tissue

The Ultrasound (US) Exam

The US examination of a patient starts with the selection of a particular default setting the US system may have, i.e., breast or small body parts, selection of the appropriate transducer, and enter patient's demographics.

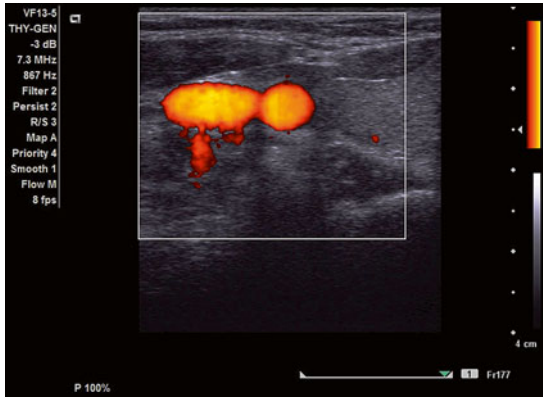

FIGURE 1.14 Power Doppler provides information on the total amount of blood flow present and is generally the preferred modality for evaluating tissue vascularity

1. The operator holds the transducer in contact with the skin surface of the patient.
2. The transducer produces short pulses of US, which travel through the patient's skin and underlying tissue planes/organs. The depth of US penetration depends on the US frequency.
3. The pulses of US are reflected and/or transmitted from the tissue planes back to the transducer in a repetitive manner.
4. The transducer converts the different amounts of reflected US echoes into electric signals.
5. The electric signals lead to the generation of a characteristic US pattern that corresponds to the echoes reflected from the underlying tissue planes.
6. The system processor forms an image of the anatomic structure based on the information received, i.e., direction of the US pulses and speed of reflection. The result is the creation of a two-dimensional gray-scale B-mode image (B for brightness) in the screen monitor, which can be stored as static image or video clip.

Suggested Reading

Baskin HJ, Duick DS, et al. Thyroid ultrasound and ultrasound-guided FNA. New York: Springer; 2013.

Lieu D. Ultrasound physics and instrumentation for pathologists. Arch Pathol Lab Med. 2010;134(10):1541–56.

Lieu D. Breast imaging for interventional pathologists. Arch Pathol Lab Med. 2013;137(1):100–19.

Martin K. Basic equipment, components, and image production. In: Allan PL, Baxter GM, Weston MJ, editors. Clinical ultrasound, vol. 1. London: Churchill Livingstone Elsevier; 2011. p. 16–30.

McDicken WN, Anderson T. Basic physics of medical ultrasound. In: Allan PL, Baxter GM, Weston MJ, editors. Clinical ultrasound, vol. 1. London: Churchill Livingstone Elsevier; 2011. p. 3–15.

Chapter 2
The Interventional Cytopathologist

Ricardo H. Bardales

The role of the interventional cytopathologist evolves parallel to the evolution of the cytopathology and the fine-needle aspiration (FNA) technique. One of the first manuscripts on the subject was published in 1904 by Grieg and Gray, who described the aspiration of lymph nodes with a needle of unstated caliber for identification of trypanosomes in patients with sleeping sickness in Uganda. Years later, Martin and Ellis in 1930 and Fred Stewart in 1933 wrote seminal articles describing the use of 18-gauge needles to sample palpable tumors predominantly from the head and neck. The latter article details the needle aspiration technique and the use of local anesthesia. Whereas cytopathology remained dormant in the United States for the next four decades, it became a strong diagnostic modality in Europe, pioneered by the Karolinska Institutet in Stockholm, Sweden.

Ultrasound (US) imaging is a technology that allows the transmission of sound waves to a computer screen as images. In the 1940s, US was used in medicine mainly for research and therapeutic purposes. In the 1950s, US technology made it possible to visualize and measure breast nodules with 90 % accuracy. US evaluation of thyroid nodules started in

R.H. Bardales, MD, MIAC, ECNU
Department of Pathology and Cytopathology,
Outpatient Pathology Associates,
7750 College Town Drive, Sacramento, CA 95826, USA
e-mail: rhbardales@aol.com

R.H. Bardales (ed.), *The Invasive Cytopathologist*, Essentials in Cytopathology 16, DOI 10.1007/978-1-4939-0730-4_2,

the late 1960s in the hope that, with this technology, one could distinguish benign from malignant processes. Currently, US is accurate in demonstrating the characteristics of a nodule or mass, but is less accurate for the diagnosis of malignancy. The combination of FNA and US to improve the accuracy of the cytologic diagnosis of thyroid nodules was first described in the 1970s. Doppler US was developed in the 1980s, allowing for the detection of blood flow within a lesion, which is important for assessment of the likelihood of malignancy and for minimizing blood contamination during FNA sampling.

The use of bedside US for better visualization and guidance (USG) of the needle and improvement in the diagnostic accuracy of USG-FNA has become indispensable. Currently, USG-FNA is universally accepted as a simple, inexpensive, accurate, safe, and rapid technique that, when properly used, yields valuable information for adequate clinical management.

The USG-FNA technique, simplistically outlined as "insert the needle in the target," "obtain the sample," "prepare and stain smears," and "read them in the microscope," must be practiced by well-trained professionals with full understanding of the pitfalls behind every step of the procedure. All steps are strongly linked to one another, and a successful microscopic evaluation depends on and is directly related to the other steps. It is accepted that the FNA accuracy is highest when the same professional examines the patient, performs the procedure, prepares the smears, and performs the microscopic examination. Also, the cytopathologist who performs several FNAs a day is probably the person with more experience in assessing superficial palpable masses and performing USG-FNAs than persons who seldom do them. Following along these lines, we will describe our experience in performing USG-FNA. Table 2.1 shows the numbers and types of FNAs evaluated at Outpatient Pathology Associates (OPA), including "clinic cases" and "sent-in cases." The outpatient FNA biopsy clinic was founded in 1982 by Drs. John A. Abele and Anthony J. Mathios.

Table 2.1 Outpatient Pathology Statistics for cases 1984–2013

Site/cases	2013 (%)	1984–2013 (%)
Thyroid	4,875 (82)	75,440 (52)
Breast	143 (2)	32,370 (22)
Soft tissue and lymph node	749 (13)	28,306 (19)
Salivary gland	187 (3)	5,478 (4)
Prostate	0	2,980 (2)
Miscellaneous	8 (0)	1,169 (1)
	5,962 (100)	145,743 (100)

We introduced USG-FNA in 2003 and currently we perform an average of 10 biopsies a day. All patients referred to our clinic have palpable or non-palpable but US-visible lesions, and the US evaluation of the lesion is a routine component of the brief but thorough focused physical examination. In our FNA clinic, we see approximately 2,500 patients a year, and 60 % of them are thyroid USG-FNAs, often performed in more than one nodule. In 2013, we accessioned close to 6,000 clinic and referral FNA cases from more than 200 physicians in more than 20 states within the United States. Details for setting up an outpatient clinic have been reviewed by Abele and Miller.

Clinical Evaluation

The clinical evaluation is of paramount importance for an accurate FNA diagnosis. In our practice, the referring clinical team submits the pertinent clinical information and imaging study reports prior to a patient appointment. This information is reviewed by the cytopathologist before he/she sees the patient.

An information brochure mailed to the patient in advance and also available at our clinic reception desk is helpful

FIGURE 2.1 Outpatient Pathology Associates FNA clinic, reception room

for having the patient informed about the visit and what to expect (Fig. 2.1). The following are sequential steps prior to performing the USG-FNA:

1. *Anamnesis*

- The interview helps the cytopathologist to take a concise, complete history of the lesion and other significant medical problems, explain the procedure step by step, and provide reassurance to the patient.
- The anamnesis is often more accurate and pertinent to the mass diagnosis when the cytopathologist directly obtains it from the patient than when it is read from the data provided by the clinical team.
- The patient should be given the option to ask questions, particularly at the end of the anamnesis.

FIGURE 2.2 Outpatient Pathology Associates FNA clinic, exam room

2. *Clinical examination*
    - Findings of a careful and focused clinical examination provide valuable information about the mass and narrow the differential diagnosis.
3. *Ultrasound evaluation*
    - The US is part of the clinical examination and complements the tactile physical examination, helping the cytopathologist to plan the FNA procedure (Fig. 2.2).
4. *Sample triage*
    - The prior considerations supported by a rapid on-site cytology interpretation will prompt the cytopathologist to allocate material for special studies, e.g., bacterial or fungal cultures, flow cytometry, cytogenetics, cell block for

FIGURE 2.3 Immediate FNA evaluation and specimen triage section

immunohistochemistry, and molecular tests, or to perform a USG-core biopsy (CBx) for tissue confirmation in soft tissue or breast tumors to assess invasion and perform hormonal studies and HER2 in breast cancer (Fig. 2.3).

The Aspiration Procedure

The operator must be familiar with the materials needed and the step-by-step procedures to perform FNA of palpable lesions described in various cytology treatises, including the textbook *Fine Needle Aspiration of Palpable Masses*, skillfully written by Michael W. Stanley, M.D., and Torsten Löwhagen, M.D. In the next paragraphs, we describe our experience performing USG-FNA. As a general rule, patient positioning should provide patient comfort, a good US evaluation, and good aspiration.

We perform the USG-FNA by using the Zajdela technique without aspiration or by capillarity. In our experience, this

technique offers sensitivity, specificity, and diagnostic accuracy, which are very similar to if not better than the conventional FNA (with aspiration) for evaluating superficial masses, especially of the head and neck, and in particular thyroid nodules. For thyroid nodule and lymph node sampling, we use 27- and 25-gauge needles respectively. Our sample adequacy rate is >99 %.

Contraindications for USG-FNA

There are few, if any, instances that may preclude doing the procedure. The only absolute contraindication may be a severe bleeding disorder or coagulopathy. In some cases, stopping anticoagulant or antiplatelet therapy for 24 h may be necessary. Relative contraindications include the use of warfarin products or heparin; however, local bleeding can be controlled with manual pressure at the site of puncture. Mild sedation may be given to the anxious patient.

Approaches Used in USG-FNA Sampling

1. *Perpendicular approach*. The needle placed in the center of the upper lateral border of the US probe intersects the US beam perpendicularly and travels through the tissue in a noncontinuous fashion, resulting in visualization of the needle tip only in the screen display (Fig. 2.4).
2. *Parallel approach*. The needle placed in the center of one of the tips of the US probe travels parallel to the US beam in a continuous fashion, allowing the visualization of the entire needle length, emerging from the right upper corner in the screen display if the procedure is done with the right hand. The needle plane must coincide with the US beam for the needle length to be visualized (Fig. 2.5).

We often use the perpendicular approach for USG-FNA sampling and the parallel approach for USG-CBx and occasionally for USG-FNA. Of note, because any needle is visualized with modern high-resolution US equipment, there is no need to use echogenic needles for routine USG-FNA. Likewise, use of heparinized needles is not necessary.

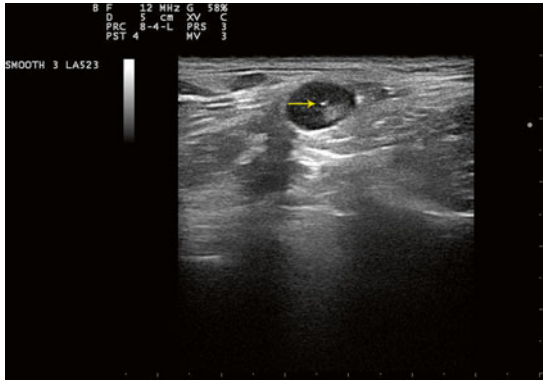

FIGURE 2.4 Perpendicular approach. The needle tip seen as a bright spot (*arrow*)

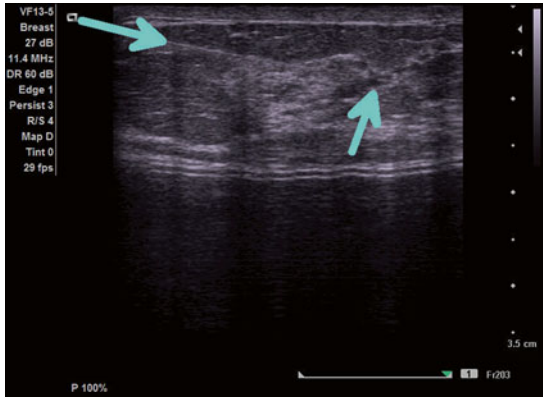

FIGURE 2.5 Parallel approach. Then entire needle length is visualized (*arrows*). USG-FNA performed with the left hand

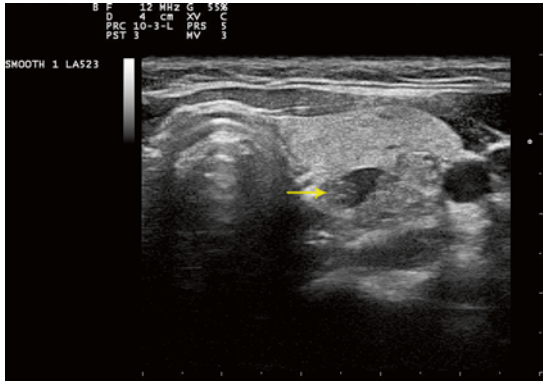

FIGURE 2.6 The target is positioned in the center of the screen (*arrow*)

Steps Prior to USG-FNA (Perpendicular Approach)

The following steps should be followed sequentially:

1. Patient in supine position. For thyroid nodules, apply a soft pillow beneath the neck and shoulders. A semi-sitting position may be recommended for patients having limitations to adopting a supine position.
2. Apply sterile coupling gel to the transducer face.
3. Find the target lesion with the US probe. The transducer should be held at a 90° angle to the target lesion.
4. Document US characteristics of the lesion, including power Doppler evaluation.
5. Center the intended biopsy site of the lesion in the screen display (Fig. 2.6).

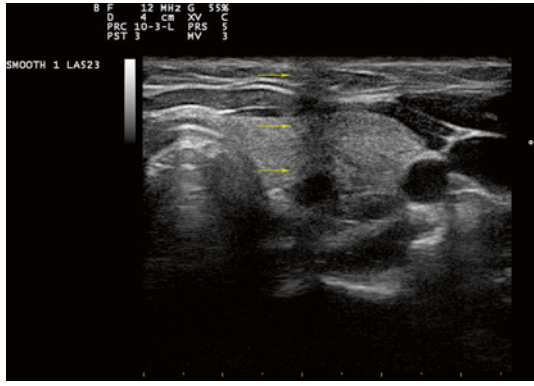

FIGURE 2.7 Shadow of the tip of pen coinciding with the target to be sampled (*arrows*)

6. Use a pen or pencil and make its tip shadow coincide with the intended biopsy site of the lesion (Fig. 2.7).
7. Withdraw the US probe and keep the pen or pencil tip on the skin surface.
8. Dot the skin surface under the tip of the pen or pencil with an erasable cutaneous marker (Fig. 2.8).
9. Reposition the US probe over the marked skin to make sure that the biopsy site is centered in the screen display.
10. Clean *all* US gel from the skin.
11. Thoroughly disinfect the skin with alcohol.
12. Apply local 2 % lidocaine hydrochloride with epinephrine or epinephrine-free 3 % Carbocaine, using equipment available from dental supply stores. The syringe uses a 30-gauge disposable needle, a tubular 2-ml disposable cartridge of lidocaine or Carbocaine, and a reusable metallic injection handle. This step may be considered optional; however, it is always welcomed by our patients. Make sure that the strap muscles of the neck anterior to the target are properly anesthetized. Carbocaine *must* be used for sampling of lesions of the breast areola or nipple, tips of fingers or toes, and penis (Fig. 2.9).
13. Wait 1 or 2 min.

FIGURE 2.8 The *center blue dot* corresponds to the underlying target lesion. The lateral *short blue lines* coincide with the lateral edges of the linear US transducer

USG-FNA (Perpendicular Approach)

1. Disinfect the skin with alcohol.
2. Insert the 25- or 27-gauge needle through the marked skin. We use a 1 1/2″ (3.8 cm) long needle for most USG-FNAs. Needles thicker than 23-gauge often cause more bleeding rather than better specimens (Fig. 2.10).

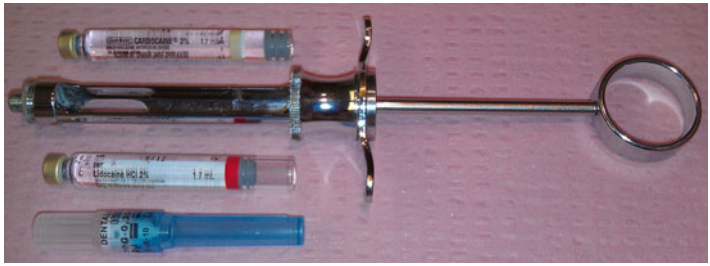

FIGURE 2.9 Local anesthesia supplies

3. Apply the US probe with a *small* amount of coupling gel on the skin.
4. Identify the bright image of the needle tip on the screen.
5. Advance and/or reposition the needle tip into the biopsy site as shown in Fig. 2.4.
6. Perform the FNA using the Zajdela technique, moving the needle repeatedly back and forth within the mass.

   (a) We perform 3–4 passes or punctures.
   (b) Solid vascular thyroid nodules can best be sampled with 27-gauge (0.4-mm-diameter) needles. Each pass lasts no more than 3 s, with a cadence of 3 movements or thrusts per second. Doppler findings must be kept in mind to minimize blood contamination.
   (c) Cyst drainage can be done with a 25- or 23-gauge needle attached to an IV 4-ml extension 34" long male Luer (Baxter) and to a 10-cc or 20-cc size syringe in an FNA pistol. A second person is needed who maneuvers the pistol and aspirates the fluid (Fig. 2.11).
   (d) Sampling of stroma-rich nodules can be performed by the use of a 25-gauge (0.5-mm-diameter) needle and the same IV extension to apply negative pressure while the operator gently moves the needle within the target as indicated before. A 23-gauge (0.6-mm-diameter) needle can be used particularly for soft tissue stromal nodules.

FIGURE 2.10 Perpendicular approach. Insert the needle in the marked skin overlying the target lesion and then position the US transducer to avoid gel contamination

7. Remove the needle from the patient.
8. Apply pressure to the puncture site with sterile gauze after each pass.
9. Apply a Band-Aid when the procedure has been finished.

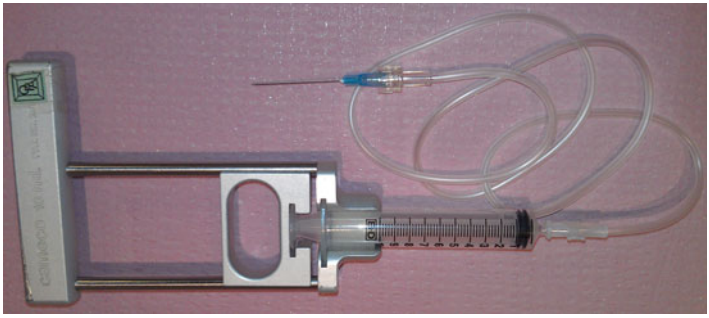

FIGURE 2.11 Cyst drainage supplies

FIGURE 2.12 Parallel approach. The dot placed in the skin at the edge of the US transducer lateral to the target lesion is the entry site (*arrow*)

Steps Prior to USG-FNA (Parallel Approach)

Follow steps 1–13 for the perpendicular approach.

For step 5, position the mass/intended biopsy site in the lateral 1/3 of the screen close to the needle entry site on the skin.

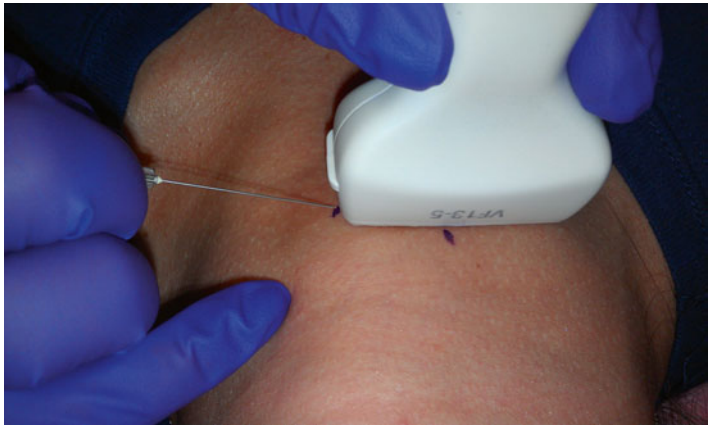

FIGURE 2.13 Parallel approach. Insert the needle first and then place the US probe to avoid gel contamination

For step 8, dot the skin surface under the tip of the pen or pencil *as well as* the midportion of each of the two lateral tips of the US probe with an erasable cutaneous marker. This step is helpful for orientation and repositioning of the US probe.

The skin entry site is the dotted lateral one closest to the target mass (Fig. 2.12).

USG-FNA and USG-CBx (Parallel Approach)

Disinfect skin with alcohol.

For USG-FNA

1. Insert the 25- or 27-gauge needle through the dotted skin in the midportion of the lateral tip of the US probe closer to the mass (Fig. 2.13).
2. Apply the US probe to the skin. The transducer should be held at a 90° angle to the mass.

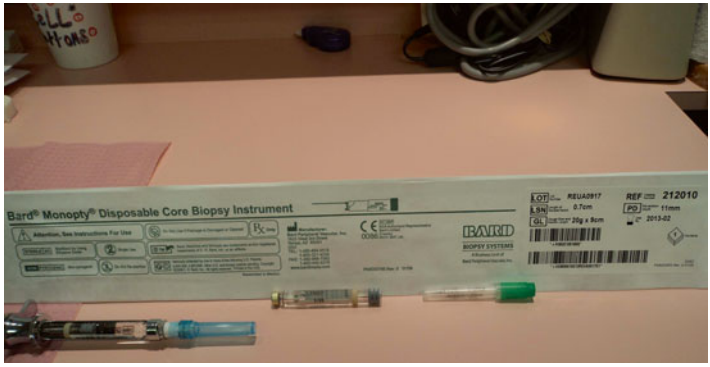

FIGURE 2.14 Core needle biopsy supplies

3. Make sure the target is closer to the needle insertion site.
4. Advance and guide the needle into the biopsy site. The needle will travel parallel to the midplane (azimuthal) of the transducer probe length and will be visualized in its entirety as shown in Fig. 2.5.
5. Perform the USG-FNA as described in step 6 of the perpendicular approach.

For USG-CBx

The steps are similar to those described for USG-FNA by the parallel approach.

1. Using an 18-gauge needle tip edge, gently open a 1.5-mm entry site in the dotted skin corresponding to the lateral tip of the US probe closest to the mass.
2. The core needle is carefully guided to the periphery of the mass.
3. We use a BARD®MONOPTY® Disposable Core Biopsy Instrument (20 gauge × 9 cm) with a penetration depth of 11 mm (Fig. 2.14). Three core biopsies are usually obtained.
4. The biopsy site is carefully evaluated, and local pressure with sterile gauze is applied after each core biopsy.

5. Follow the instructions of the manufacturer to retrieve the cores of tissue.
6. Place the tissue in formalin or other tissue fixative.

USG-FNA Specimen Handling

The selection of the smearing technique depends on the type of FNA material obtained and on the operator's skill and preference. In general, we use the one-step method for small volume specimens as it allows better control of the pressure applied to the specimen and yields excellent smears and the two-slide-pull method for larger volume specimens, the two-step method for liquid specimens, or the modified two-step method for larger volumes of blood or fluid.

We encourage the reader to consult textbooks and Internet sources such as the Papanicolaou Society of Cytopathology (www.papsociety.org) for details on how to handle FNA specimens. All steps are crucial and should be mastered by the operator to obtain a smear with well-preserved cells, thinly spread to allow for adequate staining and light microscopy interpretation. In the following lines, we summarize how we handle the material obtained by USG-FNA.

(The material is in the needle cylinder and hub)

1. Fill a 10-cc slip-tip syringe with air.
2. Replace the needle with the material onto the syringe.
3. Keep the needle tip in contact with the slide's surface with the bevel facing down at a 45° angle. This maneuver will prevent specimen dispersion and desiccation.
4. Gently express the specimen onto the surface of a non-frosted glass slide.
5. Place the spreader slide onto the droplet, applying gentle pressure without crushing the droplet.
6. Draw the spreader slide along the length of the lower slide in a constant and steady manner. It is important to remember that the long axes of both glass slides must be perpendicular, but the flat surfaces parallel. When smearing is properly done, no residual material is left in the spreader glass slide.

7. Gently wave the smear in the air for a few seconds or place the smear in front of a small battery-powered electric fan for quick drying and then staining with May–Grünwald–Giemsa (MGG) stain. Alternatively, immerse the smear in 96 % ethyl alcohol for subsequent Papanicolaou or H&E stain. In general, both types of smears should be prepared; however, we prefer air-dried smears in most thyroid USG-FNAs.
8. Immediate interpretation of the smear can be done with toluidine blue stain after 1 min of 96 % ethyl alcohol smear fixation. The stain also works on air-dried smears. The smear can be placed back into and left in 96 % ethyl alcohol, if previously fixed for conventional Papanicolaou or H&E stain, or removed from the alcohol and rapidly dried if previously air-dried for subsequent MGG stain. It is our experience that the cytopathologist performing both the US evaluation and USG-FNA, and doing 3–4 passes, reduces the numbers of unsatisfactory/nondiagnostic specimens. We can count as <10 unsatisfactory specimens after performing over 5,000 USG-FNAs of nodules in superficial organs, predominantly the thyroid.
9. Clotted blood or fluid with minute fragments of tissue is placed in 10 % formalin for cell block embedding as histologic specimen.
10. Cyst fluid may be processed by centrifugation or liquid-based techniques following the manufacturer's specifications. We avoid the use of the latter to evaluate FNAs from solid lesions and prefer the use of conventional smearing techniques instead.

Suggested Reading

Abele JS. The case for pathologist ultrasound-guided fine-needle aspiration biopsy. Cancer. 2008;114(6):463–8.

Abele JS. Putting aspiration back into thyroid fine-needle biopsy-the re-emerging role of vacuum assistance. Cancer Cytopathol. 2012;120(6):366–72.

Abele JS, Miller TR. Implementation of an outpatient needle aspiration biopsy service and clinic: a personal perspective. In: Schmidt WA, editor. Cytopathology annual. Baltimore: Williams & Wilkins; 1993. p. 43–71.

Ammanagi AS, Dombale VD, et al. On-site toluidine blue staining and screening improves efficiency of fine-needle aspiration cytology reporting. Acta Cytol. 2012;56(4):347–51.

Baskin HJ, Duick DS, et al. Thyroid ultrasound and ultrasound-guided FNA. New York: Springer; 2013.

Cibas ES, Alexander EK, et al. Indications for thyroid FNA and pre-FNA requirements: a synopsis of the National Cancer Institute Thyroid Fine-Needle Aspiration State of the Science Conference. Diagn Cytopathol. 2008;36(6):390–9.

de Carvalho GA, Paz-Filho G, et al. Adequacy and diagnostic accuracy of aspiration vs. capillary fine needle thyroid biopsies. Endocr Pathol. 2009;20(4):204–8.

Lieu D. Cytopathologist-performed ultrasound-guided fine-needle aspiration and core-needle biopsy: a prospective study of 500 consecutive cases. Diagn Cytopathol. 2008;36(5):317–24.

Lieu D. Value of cytopathologist-performed ultrasound-guided fine-needle aspiration as a screening test for ultrasound-guided core-needle biopsy in nonpalpable breast masses. Diagn Cytopathol. 2009;37(4):262–9.

Lieu D. Ultrasound physics and instrumentation for pathologists. Arch Pathol Lab Med. 2010;134(10):1541–56.

Lieu D. Breast imaging for interventional pathologists. Arch Pathol Lab Med. 2013;137(1):100–19.

Ljung BM, Langer J, et al. Training, credentialing and re-credentialing for the performance of a thyroid FNA: a synopsis of the National Cancer Institute Thyroid Fine-Needle Aspiration State of the Science Conference. Diagn Cytopathol. 2008;36(6):400–6.

Martin K. Basic equipment, components, and image production. In: Allan PL, Baxter GM, Weston MJ, editors. Clinical ultrasound. London: Elsevier; 2011. p. 16–30.

McDicken WN, Anderson T. Basic physics of medical ultrasound. In: Allan PL, Baxter GM, Weston MJ, editors. Clinical ultrasound. London: Elsevier; 2011. p. 3–15.

Oertel YC. Emerging role of the interventional pathologist. Diagn Cytopathol. 2004;30(5):295–6.

Pitman MB, Abele J, et al. Techniques for thyroid FNA: a synopsis of the National Cancer Institute Thyroid Fine-Needle

Aspiration State of the Science Conference. Diagn Cytopathol. 2008;36(6):407–24.
Stanley MW, Löwhagen T. Equipment, basic techniques, and staining procedures. In: Fine needle aspiration of palpable masses. Boston: Butterworth-Heinemann; 1993a. p. 1–58.
Stanley MW, Löwhagen T. The patient: clinical techniques and results reporting. In: Fine needle aspiration of palpable masses. Boston: Butterworth-Heinemann; 1993b. p. 58–118.
Wu M. A comparative study of 200 head and neck FNAs performed by a cytopathologist with versus without ultrasound guidance: evidence for improved diagnostic value with ultrasound guidance. Diagn Cytopathol. 2011;39(10):743–51.
Zajdela A, de Maublanc MA, et al. Cytologic diagnosis of orbital and periorbital palpable tumors using fine-needle sampling without aspiration. Diagn Cytopathol. 1986;2(1):17–20.

Chapter 3
The Thyroid Gland

Ricardo H. Bardales

The Normal Thyroid Gland Seen by US (Fig. 3.1)

The thyroid lobes have a pear shape and a bright homogeneous echotexture. The thyroid gland lobes measure 4.5–5.5 cm in length (longitudinal), 2–3 cm in width (transverse), and ≤2 cm in depth (anteroposterior), and the isthmus measures ≤0.5 cm in thickness. The right lobe is slightly larger than the left lobe. The gland has the following boundaries:

- Anterior: platysma and strap muscles of the neck (sternohyoid, sternothyroid, and omohyoid).
- Lateral: sternocleidomastoid muscle, carotid artery, and the internal jugular vein.
- Posterior: *longus colli* muscle.
- Medial: trachea.
- The esophagus may be seen in the left lateral border. The parathyroid glands are not visible unless they are enlarged.

R.H. Bardales, MD, MIAC, ECNU
Department of Pathology and Cytopathology,
Outpatient Pathology Associates,
7750 College Town Drive, Sacramento, CA 95826, USA
e-mail: rhbardales@aol.com

R.H. Bardales (ed.), *The Invasive Cytopathologist*, Essentials in Cytopathology 16, DOI 10.1007/978-1-4939-0730-4_3,

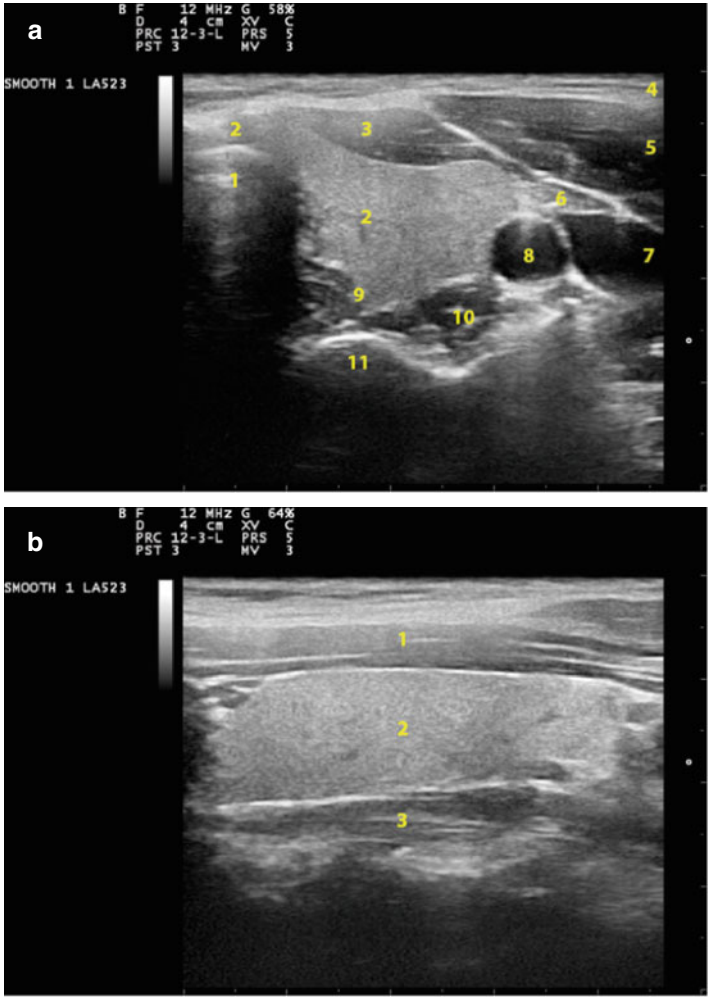

FIGURE 3.1 (**a**). Normal thyroid gland. Axial or transverse ultrasound of the left lobe. (1) Trachea, (2) thyroid, (3) strap muscles (sternohyoid and sternothyroid), (4) platysma muscle, (5) sternocleidomastoid muscle, (6) omohyoid muscle, (7) internal jugular vein, (8) common carotid artery, (9) esophagus, (10) *longus colli*, and (11) C6 vertebral body. (**b**) Normal right thyroid, longitudinal ultrasound. (1) Strap muscles, (2) thyroid, (3) *longus colli* muscle

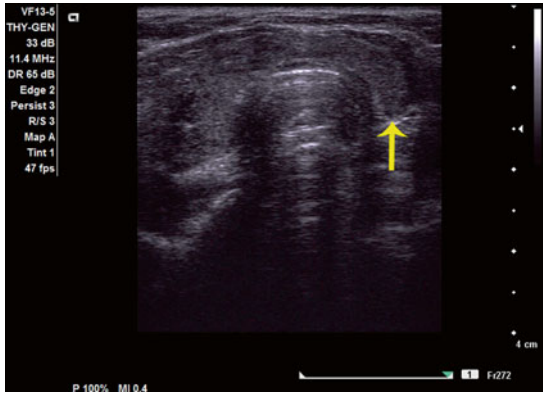

FIGURE 3.2 Agenesis of the left thyroid lobe (*arrow*). Background of chronic thyroiditis. The right thyroid lobe shows a nodule

Thyroid and Nonthyroidal Anomalies Seen by US

Hemiagenesis of the thyroid gland has an incidence of 1 in 2,500 and affects predominantly the left lobe (Fig. 3.2).

Aberrant thyroid can be seen anywhere in the neck from the base of the tongue to above the larynx and is undivided and of small/normal size. Occasionally, it can be located in the lateral neck.

Esophageal diverticulum is visualized as an outpouching, usually adjacent to the left posterior thyroid lobe (Fig. 3.3). The wall shows concentric hyperechoic and hypoechoic layers, and moving contents are visualized in the center of the diverticulum when the patient swallows. The importance of recognizing this anomaly is to avoid mistaking it for a thyroid nodule.

Undescended thymus is seen inferior to the thyroid gland, and a thyrothymic ligament is visualized, allowing for the movement of the thymus along with the thyroid gland while the patient swallows.

Ectopic intra- or perithyroidal thymic and parathyroid tissues are congenital anomalies that, on imaging studies, may

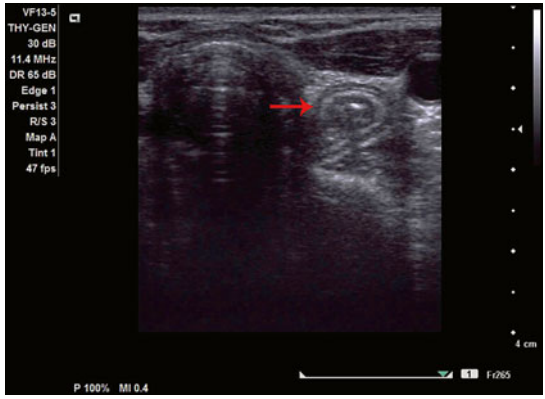

FIGURE 3.3 Esophagus. Concentric bright and dark layers (*arrow*) with bright luminal esophageal contents

be mistaken for a thyroid nodule. The smears of ectopic thymic tissue show single and aggregated benign predominantly small lymphocytes and bland-appearing thymic epithelium showing large cells with abundant clear cytoplasm and round nuclei; the epithelial elements are obscured by lymphocytes (Fig. 3.4a, b). Ultrasound features recapitulate the gross anatomy including a well-circumscribed hypoechoic fusiform lesion with well-defined margins and multiple punctate and or linear microreflectors that mimic microcalcifications; however, they show no posterior acoustic shadowing (Fig. 3.4c).

The Patient with Thyroid Nodules

Patients with thyroid nodules are candidates for USG-FNA. However, palpable "nodules" are not always true nodules by US in up to 30 % of patients, and a palpable "not nodular" thyroid gland may have a small and/or posterior nodule that may not be palpable, but may be amenable to USG-FNA. Because US alters the clinical management, patients with

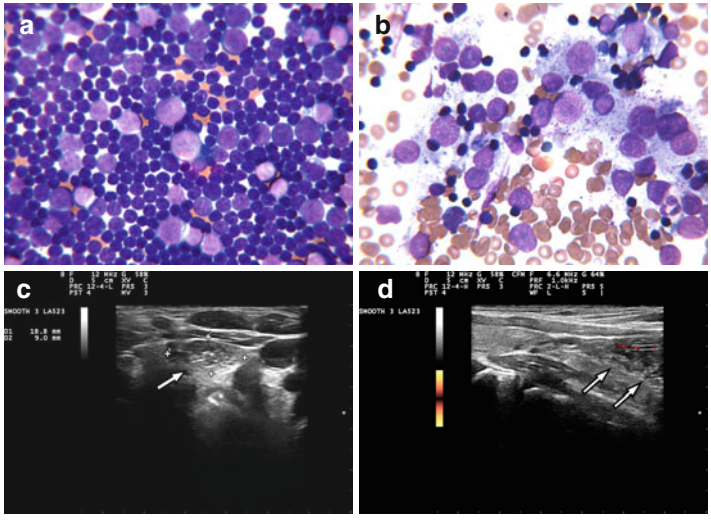

FIGURE 3.4 Ectopic thymic tissue. (**a**) Population of predominantly small lymphocytes along with scattered larger lymphocytes. (**b**) Sheet of thymic epithelial cells showing ample clear cytoplasm, red cytoplasmic granules, and round nuclei; the cells are obscured by overlapping lymphoid elements. (**c**) Ultrasound exam shows a fusiform lesion with well-defined margins, marked hypoechogenicity, and numerous internal punctate and linear echogenic foci (*arrow*). (**d**) Doppler examination shows no increased internal vascularity (*arrows*). (**a**, **b**, MGG stain, high magnification)

suspected thyroid nodules, goiter, and palpable thyroid nodule(s) or have risk factors for malignancy should undergo US examination of the thyroid gland and soft tissue of the neck, in addition to a complete clinical history, physical examination mainly of the head and neck, and serum levels of thyroid-stimulating hormone (TSH).

Patients with normal or high TSH levels and US-visible nodule(s) may be candidates for USG-FNA. Patients with low TSH levels and US-visible nodule(s) should have a radionuclide thyroid scan. A functioning nodule often does not need to undergo FNA, because the possibilities of malignancy

are extremely low. When abnormal lymph nodes are present, USG-FNA of the lymph node for cytology and thyroglobulin (TG) levels in needle rinses should be performed at the time of USG-FNA of the thyroid nodule.

Clinical Evaluation

The clinical evaluation identifies pertinent risk factors predicting malignancy in a thyroid nodule, such as:

- Male gender.
- Patient's age <20 years or >60 years.
- History of head and neck irradiation for thymic and tonsillar hypertrophy, acne, etc. or radiotherapy of any kind.
- Family history of thyroid cancer. Papillary thyroid carcinoma (PTC) can be familial in up to 10 % of cases. There is an eightfold increased risk of developing thyroid cancer when there is such a history in a first-degree relative.
- Personal history of syndromes or malignancy associated with thyroid cancer in a first-degree relative, i.e., Cowden or Wermer syndrome, familial polyposis, Carney complex, and multiple endocrine neoplasia (MEN) types 1 and 2. PTC can occur in association with acromegaly, papillary renal cell carcinoma, parathyroid tumors, paragangliomas, and ataxia–telangiectasia.
- Rapid nodule growth, firm, and fixed to adjacent tissues.
- Hoarseness, vocal cord paralysis, dysphonia, dysphagia, and dyspnea.
- Enlarged ipsilateral neck lymph nodes.

Epidemiologic and Clinical Aspects of Thyroid Nodules and Thyroid Cancer

Thyroid nodules in adults are found by palpation in 4–8 %, by US in 10–40 %, and in postmortem exam in 50 %. The prevalence is higher in women and increases with age and in

individuals with iodine deficiency and a history of radiation exposure.

The overall incidence of malignancy in thyroid nodules undergoing FNA is the same (10–13 %) regardless of the number of nodules identified by US or if the nodules were incidentally identified or nonpalpable.

In patients with multiple thyroid nodules, cancer is found in two-thirds of cases in the dominant nodule and in one-third of cases in a nondominant nodule.

Thyroid nodules occur less frequently in children than in adults, and the diagnostic approach and management should be the same as that of adults. The frequency of thyroid cancer in children varies and has been reported as being higher than or similar to that of adults.

There is an increase in the incidence of thyroid cancer, predominantly PTC (with *RET/PTC* rearrangement), in patients exposed to low-dose (therapy for acne and thymic or tonsillar hypertrophy) and high-dose (therapy for Hodgkin lymphoma) radiation. A well-known example is the Chernobyl nuclear accident, where the population is at increased risk for thyroid cancer.

Ultrasound Characteristics of Thyroid Nodules

The Society of Radiologists in Ultrasound issued a consensus statement in 2004 to determine which thyroid nodules should or should not undergo USG-FNA based on US characteristics. It was concluded that (1) the various US features studied are not specific in separating benign from malignant thyroid nodules due to overlapping characteristics and (2) FNA diagnosis is required before the patient undergoes thyroid surgery for a possible thyroid malignancy.

The US evaluation of a thyroid nodule includes size, echogenicity (isoechoic, hypoechoic, or hyperechoic), composition (cystic, solid, mixed), calcifications (fine, coarse), halo,

Table 3.1 US predictive features of thyroid cancer

US feature	Sensitivity (%)	Specificity (%)	PPV (%)	NPV (%)
Microcalcifications	26–59	86–95	24–71	42–94
Marked hypoechogenicity	27–87	43–94	11–68	74–94
Irregular margins, no halo	17–78	40–85	9–60	40–98
Solid echotexture	69–75	53–60	16–27	88–92
Intranodular vascularity	54–74	79–81	24–42	86–97
Taller than wide in the transverse dimension	33–84	82–93	67	75

Modified from Frates et al. (2005), Kim et al. (2002), Alexander et al. (2004)
Abbreviations: *PPV* positive predictive value, *NPV* negative predictive value

margins (regular, irregular), and vascularity determined by Doppler. The value of these features to predict malignancy is highly variable (Table 3.1). A single abnormal US finding is seen approximately in 70 % of benign thyroid nodules. Thus, a combination of features such as marked hypoechogenicity, solid echotexture, irregular borders, microcalcifications, and central intranodular blood flow increases the likelihood of thyroid cancer.

Thus, the indications for a USG-FNA of a given thyroid nodule are determined mainly by the US characteristics of the nodule and less by the number of nodules or the nodule size.

1. *Echotexture*. A purely cystic nodule (Fig. 3.5), a spongiform-appearing nodule (multiple microcystic components in >50 % (Fig. 3.6), or a complex nodule more than 50 %

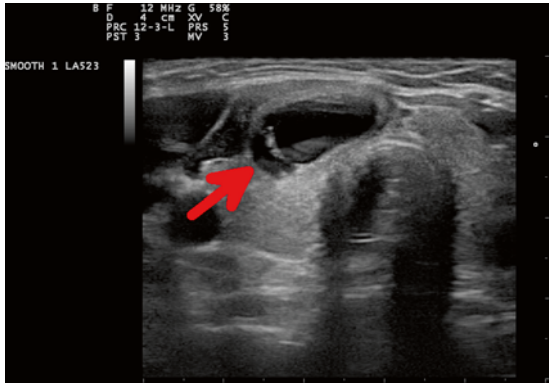

FIGURE 3.5 Cystic thyroid nodule (*arrow*) with a thick uniform wall, best seen opposite to the *arrow*. USG-FNA diagnosis was benign thyroid nodule

FIGURE 3.6 Spongiform nodule. USG-FNA diagnosis was benign thyroid nodule

cystic (Fig. 3.7) is highly predictive for being benign. However, malignancy should be considered in cysts with an irregular/thick wall and microcalcifications or when a mural nodule has an increased vascularity (Fig. 3.8). Of

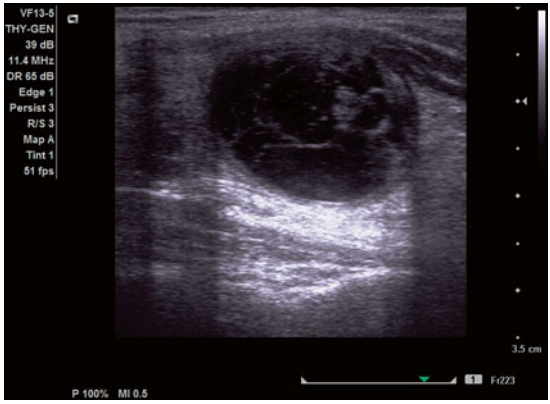

FIGURE 3.7 Complex nodule, more than 50 % cystic. USG-FNA diagnosis was benign thyroid nodule

note, a macrofollicular variant of PTC may show a spongiform pattern. A solid echotexture (Fig. 3.9) has high sensitivity but low specificity and a low positive predictive value for malignancy.

2. *Echogenicity*. Marked hypoechogenicity is very suggestive of malignancy, and iso- and hyperechogenicities are more commonly seen in benign thyroid nodules (Fig. 3.10). Follicular neoplasms, particularly follicular carcinoma, and rarely PTC may be hyperechogenic.
3. *Calcifications*. Any calcification increases the likelihood of malignancy. Calcifications are classified as micro, coarse, and eggshell calcifications.

   - Microcalcifications or microreflectors are less than 1 mm in size and do not produce acoustic shadowing, are associated with a threefold increase in cancer risk in a solid nodule, and may represent aggregated psammoma bodies (Fig. 3.11a).
   - Macrocalcifications are larger than 2 mm and produce posterior acoustic shadowing, are associated with a

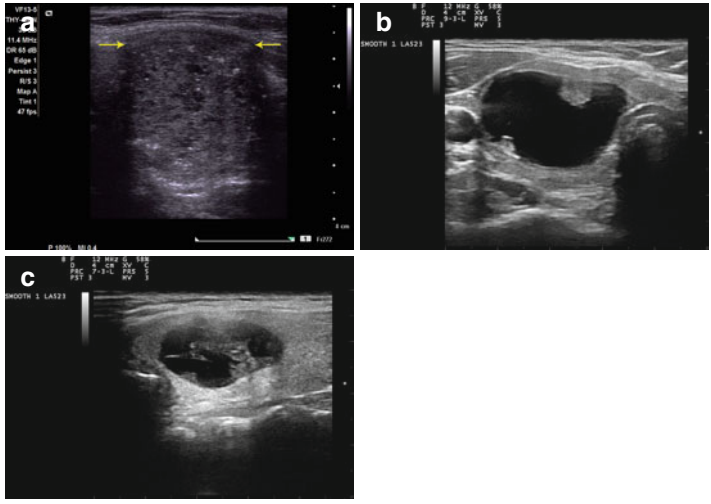

FIGURE 3.8 (**a**) Predominantly solid nodule with irregular thick wall (*arrows*), microcalcifications, and ill-defined edges. USG-FNA diagnosis was papillary thyroid carcinoma. (**b**) Predominantly cystic nodule with mural solid component, vascular by Doppler examination. USG-FNA diagnosis was benign thyroid nodule. (**c**) Predominantly cystic complex nodule with solid central component, vascular by Doppler examination. USG-FNA diagnosis was cystic papillary thyroid carcinoma

twofold increase in cancer risk in solid nodules, and represent dystrophic calcification in areas of fibrosis and degeneration; however, a central location within the nodule and association with microcalcifications raise the suspicion for malignancy (Fig. 3.11b).

- Eggshell calcification with smooth contours can be associated with benign or malignant thyroid nodules; however, eggshell with interrupted rim is suggestive of thyroid cancer permeating through the defect to invade the surrounding tissue (Fig. 3.11c–e).

4. *Margins*. The margins of a benign thyroid nodule are usually regular and well defined, with a smooth, thin surface

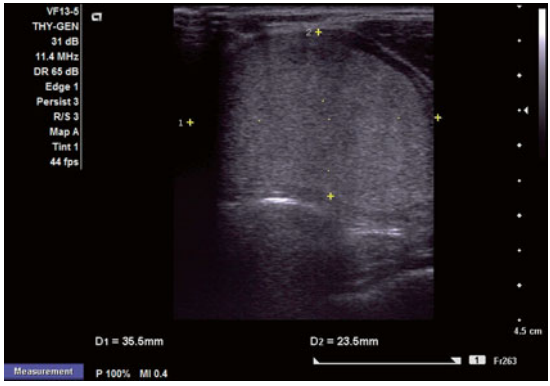

FIGURE 3.9 Solid homogeneous thyroid nodule. USG-FNA diagnosis was benign thyroid nodule

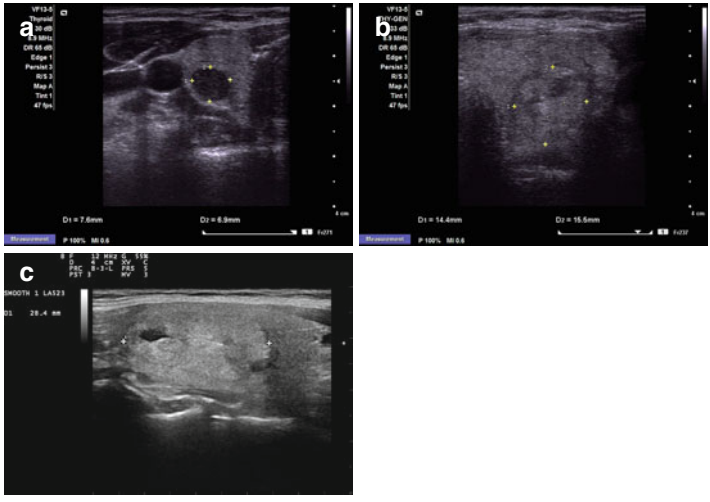

FIGURE 3.10 (**a**) Hypoechoic subcentimeter thyroid nodule. USG-FNA diagnosis was suspicious for papillary thyroid carcinoma. (**b**) Isoechoic nodule. USG-FNA diagnosis was benign thyroid nodule. (**c**) Hyperechogenic thyroid nodule. USG-FNA diagnosis was benign thyroid nodule

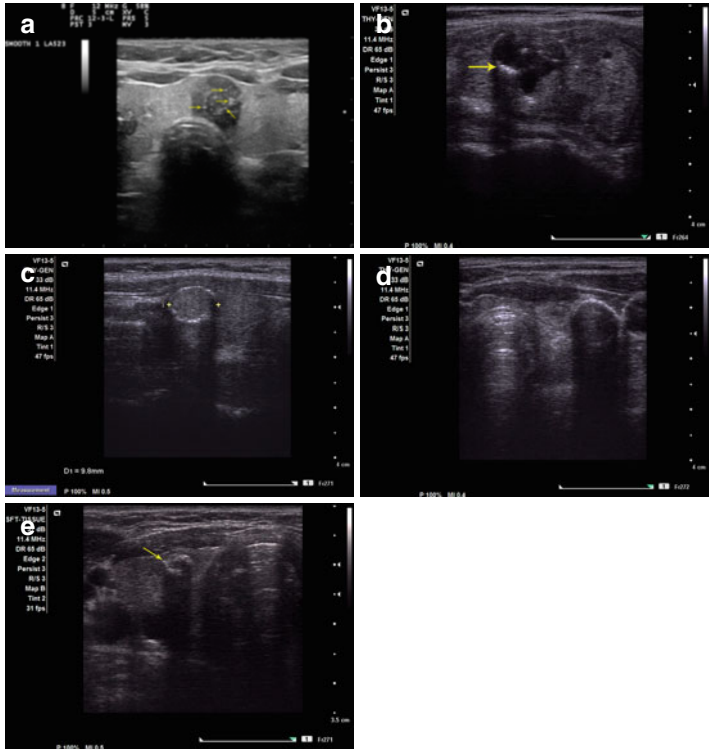

FIGURE 3.11 (**a**) Microcalcifications or microreflectors (*arrows*) in a hypoechoic nodule. USG-FNA diagnosis was papillary thyroid carcinoma. (**b**) Macrocalcifications with posterior acoustic shadow (*arrows*). USG-FNA diagnosis was chronic thyroiditis. (**c**) Eggshell calcification. USG-FNA diagnosis was benign thyroid nodule. (**d**) Eggshell calcification. USG-FNA was nondiagnostic, unable to penetrate needle through the wall of the calcified nodule. (**e**) Small nodule with interrupted (*arrow*) eggshell calcification. USG-FNA diagnosis was papillary thyroid carcinoma

(Fig. 3.12a). However, irregular, fuzzy, ill-defined, and microlobulated borders with a thick capsule or halo may be associated with a neoplastic nodule or malignancy (Fig. 3.12b).

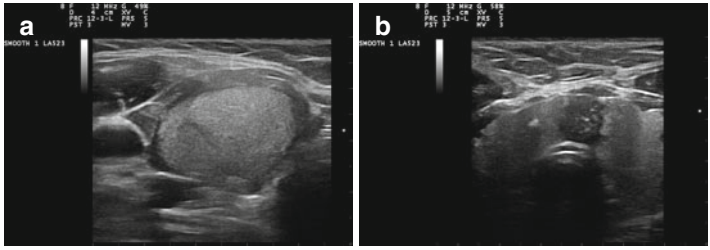

FIGURE 3.12 (**a**) Smooth, and well-defined margins. USG-FNA diagnosis was benign thyroid nodule. (**b**) Irregular margins. USG-FNA diagnosis was papillary thyroid carcinoma

5. *Halo.* The halo is a hypoechoic ring that surrounds an iso- or hyperechoic nodule and probably represents compressed peripheral thyroid tissue and vessels, usually associated with benignity (Fig. 3.13a). A thick halo produces an "edge" artifact (Fig. 3.13b). Both margins and halo may not be as helpful as originally thought for the differentiation of benign from malignant thyroid nodules, except when there is loss of halo or capsule due to invasion into surrounding tissue. The combination of a peripheral halo and interrupted eggshell-type calcification may be a high predictor for malignancy (Fig. 3.13c).
6. *Color and power Doppler*. Most benign nodules lack intranodular flow on power Doppler analysis, and most malignancies have central blood flow. Also, nodular peripheral blood flow suggests a benign nodule. However, lack of extensive vascularity cannot be used to exclude malignancy. Vascularity in a thyroid nodule can be categorized as follows:

    - Grade 1. Absent. No flow detectable (Fig. 3.14a)
    - Grade 2. Perinodular. Peripheral flow only (Fig. 3.14b)
    - Grade 3. Perinodular and intranodular. Peripheral blood flow and scant central flow (Fig. 3.14c)
    - Grade 4. Intranodular. High-intensity central flow (Fig. 3.14d)

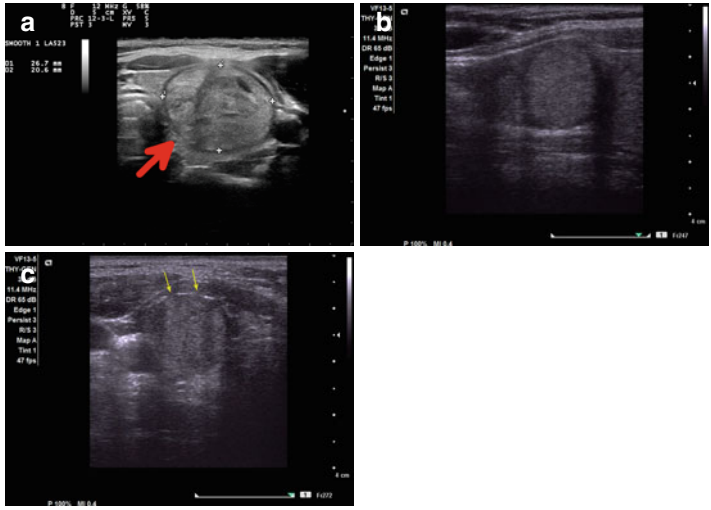

FIGURE 3.13 (**a**) Isoechoic nodule (*arrow*) with a smooth uniform halo. USG-FNA diagnosis was benign thyroid nodule. (**b**) Edge shadows from a thick halo. USG-FNA diagnosis was benign thyroid nodule. (**c**) Thin, irregular, inconspicuous halo and interrupted (*arrows*) eggshell calcification. USG-FNA diagnosis was papillary thyroid carcinoma

7. *Shape*. The nodule shape may help to predict malignancy and prompt one to perform a USG-FNA. Spherical shape and nodules that are taller (anteroposterior diameter) than wide (transverse diameter) in the transverse view statistically may be associated with a malignant diagnosis (Fig. 3.15).
8. *Comet-tail sign*. Comet tails are reverberation ("echo") artifacts that result from the reflection of sound waves off of the crystals present in the desiccated thick colloid, resulting in a bright signal; the crystals vibrate under the sound energy, producing the comet tail. This sign is reported to be almost pathognomonic for a benign thyroid nodule, particularly if present at the periphery of cystic nodules

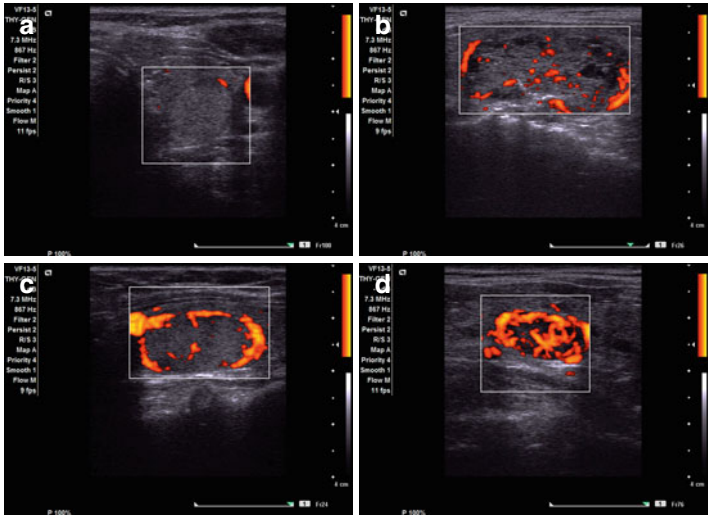

FIGURE 3.14 (**a**) Nodule vascularity. Grade 1. There is no blood flow. USG-FNA diagnosis was benign thyroid nodule. (**b**) Grade 2. There is peripheral blood flow and incipient central blood flow. USG-FNA diagnosis was benign thyroid nodule with cystic change. (**c**) Grade 3. There is marked peripheral and less prominent central blood flow. USG-FNA diagnosis was mixed pattern of benign thyroid nodule and chronic thyroiditis. (**d**) Grade 4. There is prominent peripheral and central blood flow. USG-FNA diagnosis was microfollicular tumor

(Fig. 3.16a). However, often it is difficult to state conclusively its presence in a given thyroid nodule. Comet tails have also been described in PTC, particularly in the cystic variant. Condensed colloid in a hypoechoic nodule ("cat's eye") correlates with a benign thyroid nodule (Fig. 3.16b).

Documentation of the following US features must be included in the USG-FNA report:

1. Nodule margins, i.e., well or poorly circumscribed, irregular, interrupted, spiculated, scalloped, and halo (thick, thin, irregular)
2. Nodule echotexture, i.e., heterogeneous and homogeneous

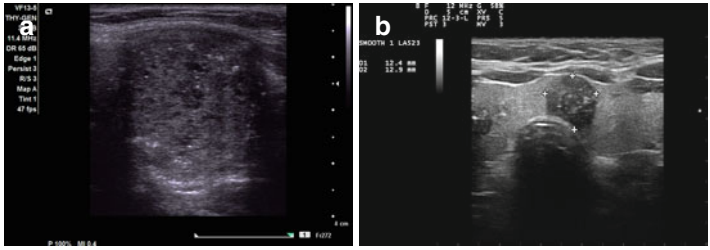

FIGURE 3.15 (**a**) Taller than wide with microcalcifications. USG-FNA diagnosis was papillary thyroid carcinoma. (**b**) Taller than wide with microcalcifications. USG-FNA diagnosis was papillary thyroid carcinoma

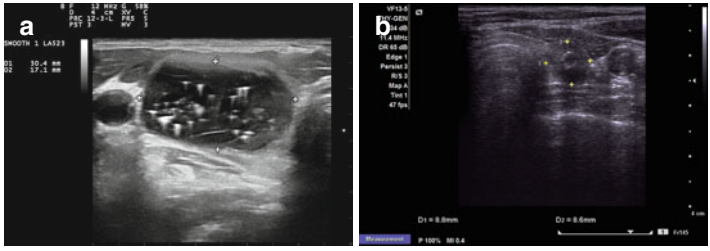

FIGURE 3.16 (**a**) Comet-tail artifact. USG-FNA diagnosis was colloid-rich benign thyroid nodule. (**b**) Cat's eye artifact. USG-FNA diagnosis was benign thyroid nodule

3. Nodule echogenicity with respect of the background thyroid, i.e., hyper-, hypo-, and isoechoic
4. Calcifications, i.e., micro, coarse, and eggshell (interrupted, continuous, displaced)
5. Intranodular blood flow pattern on Doppler exam (peripheral and/or central, mild or marked, uniform or chaotic)
6. Other intranodular features, i.e., cystic change and comet tails
7. Echotexture of the surrounding thyroid

Metastasis to cervical lymph nodes, usually pre- and paratracheal and anterior cervical (neck compartment VI) is the first manifestation of the disease in an average of 20 % of adults with thyroid carcinoma, often PTC. This presentation is much

higher in patients younger than 20 years. Other aggressive malignancies including lymphoma have lymph node involvement at initial diagnosis.

We should emphasize that (1) according to the American Thyroid Association guidelines, US is the imaging modality of choice in the evaluation of thyroid nodules, surveillance of multinodular goiter, and preoperative evaluation of patients with known differentiated thyroid cancer (DTC), (2) the US features of a thyroid nodule are helpful in predicting malignancy or benignity, but they do not replace the need to perform USG-FNA, and (3) US examination is particularly useful in the selection of the nodule for USG-FNA in multinodular goiter.

Indications for USG-FNA of Thyroid Nodules

The indications are summarized in Table 3.2. USG-core needle biopsies are not recommended for thyroid nodules due to lack of appropriate sampling, particularly in follicular neoplasms or lesions, and serious complications such as bleeding and pain, nerve injury, tracheal perforation, and architectural distortion that preclude accurate histologic interpretation in subsequently excised specimens. USG-core needle biopsies may be complementary to FNA in selected cases such as diffuse Hashimoto's thyroiditis and perhaps an advanced malignant neoplasm.

Thyroid USG-FNA Approach

The superficial location of the thyroid gland facilitates tactile examination, US evaluation, and FNA. Adequate patient positioning is crucial for achieving success. With the patient in the supine position, a pillow should be placed under the shoulders to produce slight overextension of the neck. Then, US evaluation of both lobes in the transverse and

Table 3.2 Recommendations for USG-FNA: various societies

A. Thyroid nodules that are ≥1.0 cm

1. All societies except the SRUS recommend USG-FNA of all nodules ≥1.0 cm
2. Solitary nodule with microcalcifications if ≥1 cm (SRUS)
3. Solitary nodule with coarse calcifications or solid nodule if ≥1.5 cm (SRUS)
4. Solitary predominantly cystic with a solid mural component or mixed solid and cystic nodule if ≥2 cm (SRUS). Other societies recommend USG-FNA of all nodules if ≥2 cm
5. Solitary nodule having a substantial growth since prior US examination. The ATA considers 20 % increase in 2 of the 3 diameters (≥2 mm each) as reasonable nodule growth
6. If multiple nodules are present, select the one(s) for USG-FNA, applying the previous 2–5 criteria for solitary nodules (in that order)
7. If abnormal cervical lymph node(s) is present, USG-FNA of the lymph node and or any ipsilateral thyroid nodule should be done regardless of the US characteristics
   (a) The US features associated with cancer in a lymph node include loss of fatty hilum, round shape, well-defined edges, taller than wide, calcifications, cystic areas, and increased peripheral vascularity regardless of size (Fig. 3.17)
   (b) Thyroid cancer most commonly metastasizes to neck levels III, IV, and VI. Malignancy is confirmed by cytologic evaluation and/or measurement of thyroglobulin levels in needle rinses
8. If the nodule is entirely cystic, or stable in size, or none of the above listed features is seen, then probably USG-FNA is unnecessary
9. For a diffusely enlarged thyroid gland with no US-visible nodules, USG-FNA is probably unnecessary

Table 3.2 (continued)

B. Special considerations for USG-FNA of nodules <1 cm
1. Ultrasound features suggestive of malignancy (calcifications, solid, increased intranodular blood flow on power Doppler, or taller than wide in the transverse view on US). Nodules can be accurately aspirated by USG-FNA with >90 % diagnostic rate (Fig. 3.18)
2. Abnormal neck lymphadenopathy. US criteria as described in the prior section
3. History of head and neck irradiation in childhood or adolescence
4. History of thyroid cancer in one or more first-degree relatives
5. History of prior hemithyroidectomy with incidentally found thyroid cancer
6. Nodule incidentally found by 2-deoxy-2[^{18}F]fluoro-D-glucose positron emission tomography (^{18}FDG-PET) imaging for other reasons. The risk of malignancy in these nodules is 15–50 %, and cancers may be more aggressive. Most are PTC and others are follicular or Hurthle cell neoplasms
7. Nodule incidentally found by sestamibi scan, a nuclear medicine scan for parathyroid gland disorders and confirmed by thyroid US, has a high incidence of malignancy (22–66 %) and should be sampled

ACT Academy of Clinical Thyroidologists, *ATA* American Thyroid Association, *AACE* American Academy of Clinical Endocrinologists, *SRUS* Society of Radiologists in Ultrasound

longitudinal planes is performed (Fig. 3.19). Of note, the US evaluation should include the entire neck, looking for abnormal lymph nodes, enlarged parathyroid glands, and other masses. Once a nodule is identified, USG-FNA is performed as described previously.

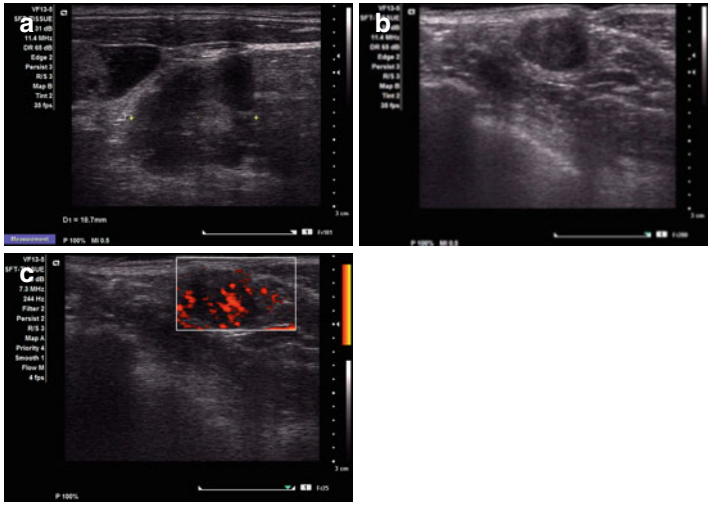

FIGURE 3.17 (**a**) Large cervical lymph node with irregular lobulated borders, complex echotexture, and loss of fatty hilum. USG-FNA diagnosis was metastatic papillary thyroid carcinoma. (**b**) Left cervical lymph node with abnormal US features (lack of hilum, marked hypoechogenicity, and round shape with irregular borders). USG-FNA diagnosis was metastatic papillary thyroid carcinoma. (**c**) Left cervical lymph node (b) with diffuse chaotic vascularity by Doppler examination

USG-FNA is the gold-standard technique for screening and diagnosis of thyroid nodules. USG-FNA is recommended particularly for nonpalpable, predominantly cystic, or posteriorly located nodules; however, USG-FNA should be used for sampling of *all* types of thyroid nodules. It is highly accurate in experienced hands and is quick, safe, and cost-effective and can be performed in an outpatient clinic. Contraindications to thyroid USG-FNA are perhaps limited to uncooperative patients and those with a severe bleeding diathesis. Complications are extremely rare and include local hematoma, and nodule infarction particularly, in Hurthle cell neoplasms. Needle track seeding of a thyroid malignancy has been reported anecdotally. Of note, the operator should try to

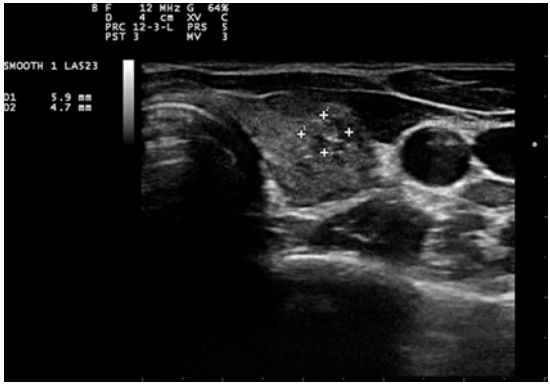

FIGURE 3.18 Subcentimeter thyroid nodule with microcalcifications and ill-defined fuzzy margins. USG-FNA diagnosis was papillary thyroid carcinoma

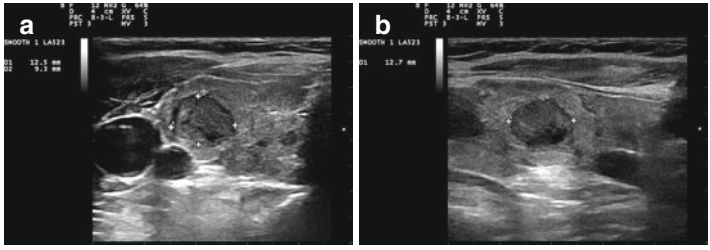

FIGURE 3.19 Transverse (**a**) and longitudinal (**b**) views of a right thyroid nodule. The USG-FNA diagnosis was benign thyroid nodule

avoid possible injury of neck organs, particularly in patients with nonpalpable or distorted anatomic landmarks.

Advantages of US and USG-FNA

1. The US test is cost-effective and relatively available and does not involve ionizing radiation.
2. The US test provides the characteristics of the thyroid gland and is of particular use in thyroiditis and hyperthyroidism.

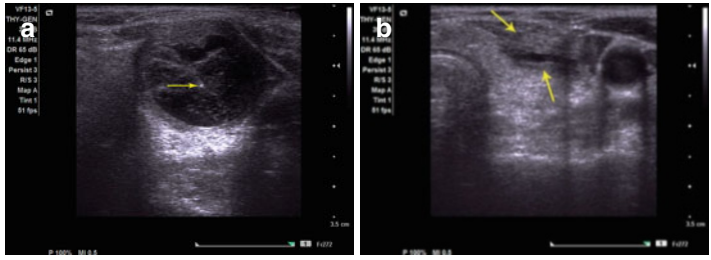

FIGURE 3.20 (**a**) Cystic nodule with posterior acoustic enhancement. Tip of needle (*arrow*) is visualized in the transverse plane. (**b**) Collapsed cystic nodule after fluid drainage (*arrows*). USG-FNA diagnosis of the solid component was benign

3. The US test identifies and characterizes US features for selecting of the most dominant or the most suspicious nodule to be sampled by USG-FNA.
4. US provides precise needle placement for nodule sampling in obese or muscular patients.
5. It provides visualization and sampling of nonpalpable or small nodules with high accuracy, making sure the needle tip is within the nodule.
6. *Drainage of fluid in cystic lesions*. Careful needle guidance to the cystic component for drainage of the fluid will allow better visualization and sampling of the residual solid-phase component after drainage (Fig. 3.20). Initial avoidance of the solid component is important to avoid intralesional bleeding in highly vascular lesions (Fig. 3.21). The cyst fluid should be processed by centrifugation or by liquid-based techniques aimed mainly at ruling out a cystic variant of PTC.
7. *Sampling of highly vascular lesions*. Nodules with central vascularity by Doppler US usually yield bloody aspirates. The amount of blood present in the smears is directly proportional to the needle caliber, syringe suction, and dwelling time. Excellent samples can be obtained by performing the Zajdela technique (no syringe suction) with 27-gauge (0.4 mm diameter) needles and monitoring of intranodular

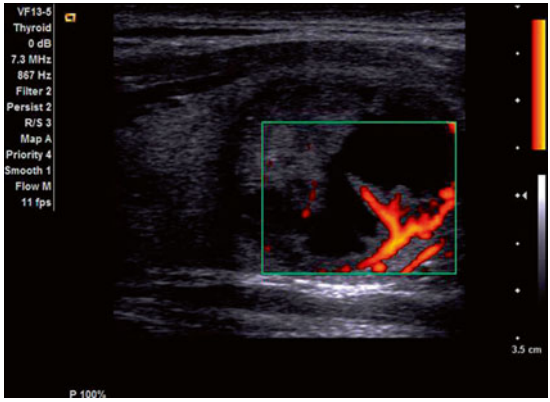

FIGURE 3.21 Cyst drainage is needed to accurately sample the posterior vascular solid component and avoid smear dilution with blood and cyst contents. USG-FNA diagnosis was papillary thyroid carcinoma

needle motion as mentioned before. These steps minimize blood contamination and increase the likelihood of a diagnostic aspirate.

8. Sampling of hypoechoic areas or suspicious features in heterogeneous nodules, i.e., microcalcifications, high vascular flow, etc. (Fig. 3.22).
9. Increases the diagnostic accuracy, sensitivity, and specificity of palpation-guided FNA in the diagnosis of thyroid nodules. For thyroid nodules with a benign FNA diagnosis, the false-negative rate is higher with palpation FNA (2–5 %) than with USG-FNA (0.6 %).

The use of the Zajdela technique is most useful particularly for evaluating small thyroid nodules. The needle grip provides an excellent control for sampling of the lesion and adds an exquisite degree of sensitivity to perceiving the tissue texture changes along the path the needle travels, to the point that the operator is able to "feel" when the periphery of the target is penetrated.

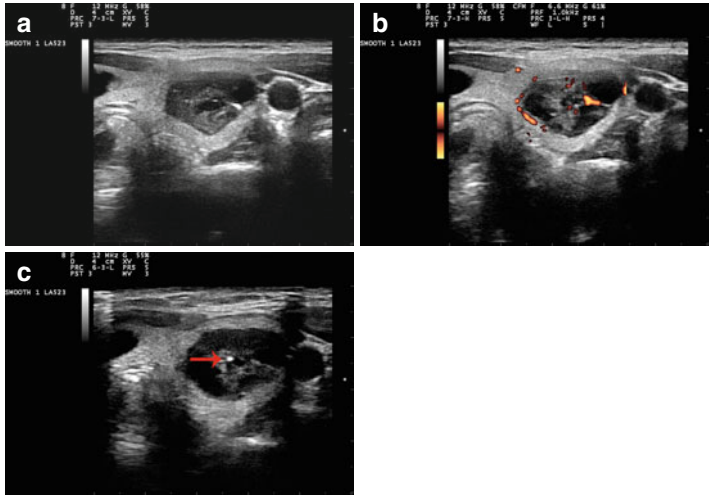

FIGURE 3.22 (**a**) Complex solid and cystic left thyroid nodule. (**b**) The central solid component has increased vascular blood flow by Doppler examination. (**c**) Needle tip (*arrow*) samples the solid component. USG-FNA diagnosis was papillary thyroid carcinoma with prominent cystic change

Important Concepts in Thyroid FNA

- All FNAs must have well-preserved and well-prepared material for interpretation.
- The size of normal follicular epithelial cell nuclei is about the size of a red blood cell or lymphocyte (8–10 μm in diameter). The diameter of a normal three-dimensional follicle averages 200 μm (Fig. 3.23). Thus, the inner diameter of a 27-gauge needle allows for the passage of such structures or even small stromal–epithelial fragments.
- The adequacy of an FNA specimen is dictated by the presence of a minimum of six groups of at least 10 follicular epithelial cells each, preferably on a single slide.
- Cyst fluid with less than six groups of 10 follicular cells may be considered nondiagnostic.

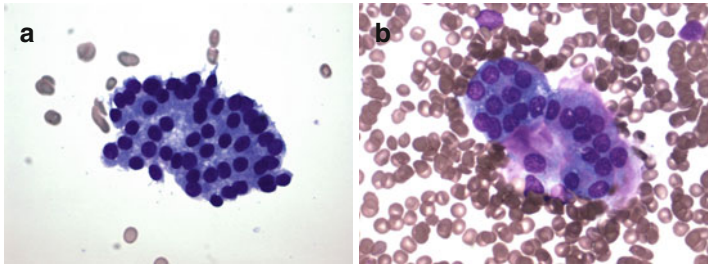

FIGURE 3.23 Benign follicular cell sheet, atrophic (**a**) and partially ruptured benign thyroid follicle (**b**). The nuclear sizes of the follicular cells are similar or slightly larger than those of red blood cells. (MGG stain, high power)

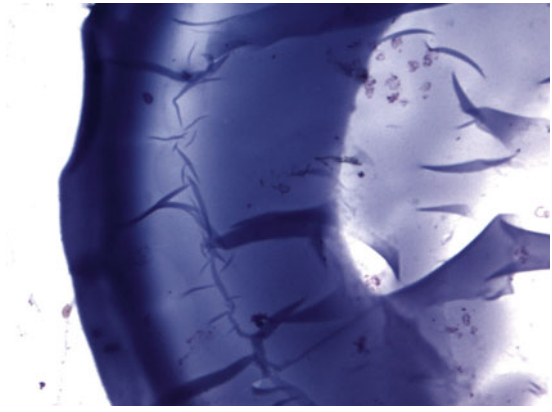

FIGURE 3.24 Thick colloid. (MGG stain, low power)

- The presence of thick colloid reliably identifies most benign processes and overrules the absence or paucity of follicular epithelial cells, and the specimen is considered adequate (Fig. 3.24).
- Inflammatory entities such as thyroiditis or thyroid abscess do not require the presence of follicular elements for specimen adequacy.
- If cytologic atypia is seen, it must be reported regardless of specimen adequacy, including cell count.
- Poorly prepared, poorly stained, or obscured follicular cells are considered nondiagnostic specimens (Fig. 3.25).

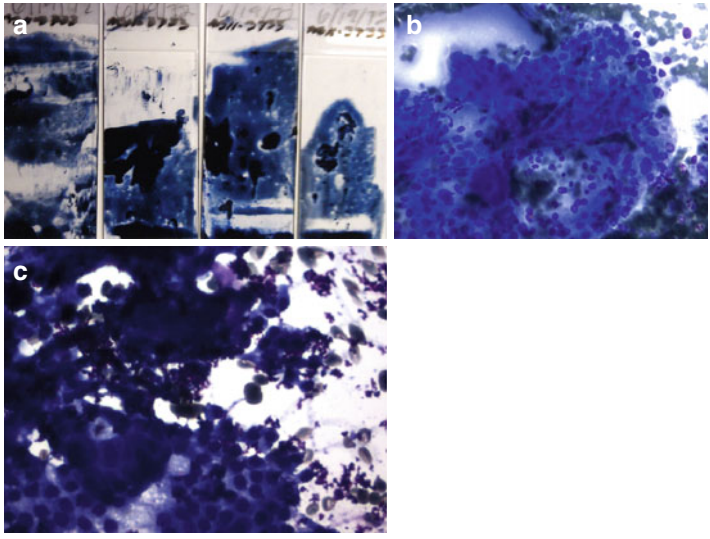

FIGURE 3.25 (**a**) Nondiagnostic smears with extensive clotting. (**b**) Obscuring blood clot and fibrin strands. (**c**) Obscuring ultrasound gel. (**b**, **c**, MGG stain medium power)

- The numbers of follicular cell groups may not be important for specimen adequacy in liquid-based smears. A total individual count of 180–320 cells has been proposed as sufficient. Further validation of these findings is needed. We discourage the use of liquid-base cytology in thyroid nodules, except for evaluating cyst fluid.

USG-FNA and the Bethesda System (TBS) for Reporting Thyroid Cytopathology

The National Cancer Institute (NCI) sponsored the NCI Thyroid Fine Needle Aspiration (FNA) State of the Science Conference on October of 2007 in Bethesda, MD. Six committees were formed to review (1) indications/pre-FNA requirements, (2) training and credentialing, (3) technique, (4) terminology and morphologic criteria, (5) ancillary

studies, and (6) post-FNA options for testing and treatment. The summary reports have been published.

The Bethesda system diagnostic categories (Table 3.3) are (1) nondiagnostic, (2) benign, (3) atypia of undetermined significance (AUS) or follicular lesion of undetermined significance (FLUS), (4) follicular neoplasm or suspicious for follicular neoplasm (specify if oncocytic type), (5) suspicious for malignancy, and (6) malignant.

Table 3.3 TBS diagnostic categories: significance, common underlying disease processes, and helpful tips for diagnosis

1. Nondiagnostic
(a) *Underlying causes*. Few or no follicular epithelial cells as seen in a pure cyst, thick or calcified capsule, hypervascular or necrotic lesion, and benign or malignant sclerotic lesions
(b) *Preventable cause*. Poor technique includes a missed target, obscuring blood, clot artifact, mechanical distortion, and slow air-drying
(c) *Helpful tips*. Look for stripped atrophic nuclei in the smear edges; look for inconspicuous sheets of atrophic cells in bloody smears with thin colloid; correlate with US features, because simple colloid cysts may yield only colloid and macrophages with no or limited follicular elements
2. Benign thyroid nodule
(a) *Underlying causes*. Hyperplastic nodule, thyroiditis, thyroid nodule with cystic change, and colloid-rich benign thyroid nodule
(b) *Helpful tips*. Make the diagnosis only if there is good cell representation and preservation. PTC may have a prominent cystic change. Chronic thyroiditis may coexist with PTC
3. AUS or FLUS
(a) *Underlying causes*. Follicular neoplasm, hyperplastic thyroid nodule, lymphocytic thyroiditis, thyroid cancer

Table 3.3 (continued)

(b) *Cytologic findings*. Cytologic and/or architectural atypia. Microfollicular pattern and/or oncocytic cell pattern in variable proportions. Oncocytic cells forming microfollicles are seen in lymphocytic thyroiditis. Metaplastic cells with squamoid features may be the cyst-lining cells

(c) *Helpful tips*. Look for cell sheets comprising >50–75 % of smear cellularity that may indicate a mixed macro- and microfollicular-pattern nodule. Look for intact or entangled lymphocytes to exclude lymphocytic thyroiditis. Repeat or perform USG-FNA in not less than 3 months is strongly recommended. Consider doing molecular testing for thyroid cancer; a split sample for cytology and molecular testing should be obtained

4. Follicular neoplasm or suspicious for follicular neoplasm (specify if oncocytic)

(a) *Underlying causes*. Follicular and oncocytic (Hurthle) cell neoplasms. Histologic diagnoses include adenoma, carcinoma, and follicular variant of PTC

(b) *Cytologic findings*. Hypercellular smears, cell monotony, microfollicular arrangements, and minimal or absent colloid and absent lymphoid cells

(c) *Helpful tips*. Look for lymphoid cells to exclude chronic thyroiditis. Atrophy mimics microfollicles. Presence of colloid, follicular cell sheets, and Hurthle cells is more in favor of a hyperplastic nodule. Make the diagnosis only if there is good cell representation and preservation; otherwise, repeat USG-FNA in not less than 3 months

5. Suspicious for malignancy

(a) *Underlying cause*. Usually thyroid cancer

(b) *Cytologic findings*. Cytologic criteria are short for making a malignant diagnosis

(c) *Helpful tips*. Make the diagnosis only if there is good cell representation and preservation; otherwise, repeat USG-FNA in not less than 3 months

(continued)

Table 3.3 (continued)

6. Malignant
(a) *Underlying causes*. PTC, medullary carcinoma, anaplastic (undifferentiated) carcinoma, squamous cell carcinoma, lymphoma, miscellaneous thyroid malignancies, and metastasis
(b) *Cytologic findings*. Cytologic criteria fulfill the diagnosis of malignancy
(c) *Helpful tips*. PTC has overlapping features mainly with hyalinizing trabecular tumor. Degenerative changes, inadequate specimen, and lack of cytopathologist's experience are main causes for a false-positive diagnosis

Reported statistics for the various diagnostic categories are as follows: nondiagnostic (10–15 %), benign (60–80 %), FLUS and neoplasms (10–20 %), suspicious (3–10 %), and malignant (4–10 %)
Abbreviations: *TBS* the Bethesda System, *US* ultrasound, *PTC* papillary thyroid carcinoma, *AUS* atypical cells of undetermined significance, *FLUS* follicular lesion of undetermined significance, *USG-FNA* ultrasound-guided fine-needle aspiration

Impact of FNA Diagnosis on Clinical Management

The FNA diagnosis dictates the management modality for patients, including the selection for surgery, with a positive impact on the cancer diagnoses and a negative impact on the number of unnecessary surgeries for benign conditions (Table 3.4).

FNA Diagnosis of Benign Thyroid Nodule

A benign thyroid nodule is the most common (80 %) condition of the thyroid gland in adults and children. This diagnosis conveys the presence of a hyperplastic disorder, either nodular (nodular hyperplasia and dyshormonogenetic

Table 3.4 Clinical management of thyroid nodules based on the FNA diagnosis

Diagnosis	Risk of malignancy and management
Nondiagnostic	The risk of malignancy is probably 5–10 %. Repeat FNA under US guidance in not less than 3 months and perform rapid cytology evaluation if available. If again nondiagnostic, surgery may be considered, particularly in the case of solid nodules
Benign	Carries up to 3 % risk of malignancy. Clinical follow-up including US in 6–18 months and repeat FNA if nodule volume grows >50 %. Carries a false-negative rate of <5 % (<1 % by USG-FNA)
Indeterminate (AUS, FLUS)	Carries 5–15 % risk of malignancy. Repeat USG-FNA in 6 months. Molecular markers may be considered to help guide management
Follicular neoplasm	Carries 65–85 % risk of neoplasm and 15–30 % risk of malignancy. Lobectomy or total thyroidectomy if the nodule is autonomous by ^{123}I scan
Hurthle cell neoplasm	Carries 20–30 % risk of malignancy. Lobectomy or total thyroidectomy
Suspicious for PTC	Carries 60–75 % risk of malignancy. Lobectomy or total thyroidectomy
Malignant	Carries <1 % false-positive diagnosis. Near-total or total thyroidectomy. Further diagnostic workup is recommended for anaplastic carcinoma, lymphoma, and metastasis before surgery

Abbreviations: US ultrasound, *FNA* fine-needle aspiration, *USG* ultrasound guided, *FLUS* follicular lesion of undetermined significance, *PTC* papillary thyroid carcinoma

goiter) or diffuse (Graves' disease). The diagnosis of the specific entity cannot be made on FNA cytology only, but needs clinical correlation, and the patient is followed up

conservatively. Of note, the macrofollicular type of follicular adenoma cannot be distinguished from the other entities on FNA cytology.

Nodular Hyperplasia

Nodular hyperplasia, also known as nodular or multinodular goiter, adenomatoid goiter, and adenomatous hyperplasia, is the most common thyroid disorder. It can be endemic (related to iodine deficiency in the diet) or sporadic (unknown cause). Incidental carcinoma is seen in 5–10 % and is usually microcarcinoma of the papillary type.

Clinical findings. Patients usually are euthyroid and have a visible goiter.

Histopathology. The nodules may have macrofollicles, microfollicles, and areas of follicles with Hurthle cell changes and even a papillary architecture. Rupture of the follicles may produce a foreign body-type granulomatous reaction to the colloid. Calcification and fresh and old hemorrhage can be seen. Chronic inflammation is variably seen and is usually related to the development of hypothyroidism.

Molecular profile. Monoclonality, cytogenetic abnormalities, aneuploidy, and oncogenic mutations have been seen in some hyperplastic nodules. Thus, there is debate whether hyperplastic nodules are in fact neoplastic. *BRAF* mutation and *PAX8/PPARγ* rearrangement have not been identified in hyperplastic nodules; however, occasional *RAS* mutations have been reported.

FNA findings. Common findings include colloid of variable quantity and/or quality and variable numbers of benign follicular epithelial cells, Hurthle cells, macrophages, and lymphocytes. Follicular cells may be arranged in monolayer sheets, spheres, and intact follicles or singly. The amount of cytoplasm is variable and may range from hyperplastic to atrophic, commonly seen as stripped small nuclei. The nucleolus is small or inconspicuous. Cytoplasmic lipofuscin and/or hemosiderin pigment granules may be seen. Occasional

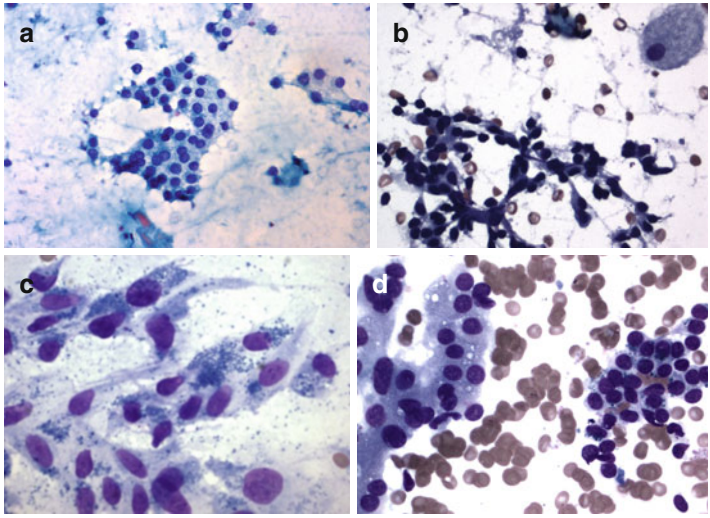

FIGURE 3.26 Benign thyroid nodule. (**a**) Sheets of follicular epithelial cells and colloid. (**b**) Atrophic follicular cells, colloid, and macrophages indicating cystic change. (**c**) Cohesive cyst-lining cells with elongated and "reparative" appearance and cytoplasmic lipochrome granules. (**d**) Sheets of cells with oxyphilic (*left*) and atrophic (*right*) changes. (**a**, Papanicolaou stain, high power; **b–d**, MGG stain, high power)

microfollicles may be seen, usually comprising less than 10 % of the cell representation. Cyst-lining cells with reparative features may be present in cystic nodules; the recognition is important to avoid a misdiagnosis of cystic PTC (Fig. 3.26).

US features (Fig. 3.27)

- Hyperplastic and adenomatoid nodules cannot be distinguished by US.
- Solid, usually isoechoic nodules with well-defined margins.
- Presence of comet tails, the result of crystals of desiccated colloid.
- Cystic degeneration is common.
- Heterogeneous echogenicity.

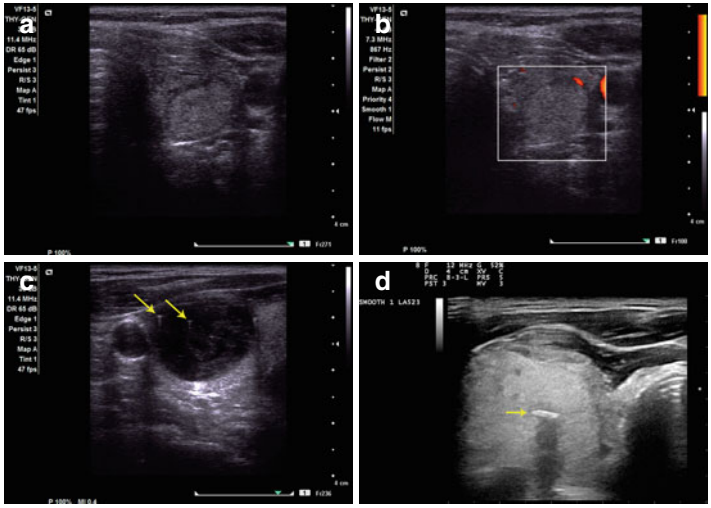

FIGURE 3.27 Ultrasound features of benign thyroid nodules. (**a**, **b**) Isoechoic nodule with well-defined margins, thick halo, and minimal focal peripheral vascular blood flow by Doppler examination. (**c**) Hypoechoic predominantly cystic nodule with comet tails (*arrows*). (**d**) Coarse curve-shaped calcification (*arrow*) with posterior shadow in a hyperechoic nodule

- Calcifications are coarse or curved, peripheral, or dysmorphic.
- Rare microcalcifications can occur in 5 % of adenomatoid nodules.
- Variable vascularity, often Grades 1 and 2 pattern.

Dyshormonogenetic Goiter

This type of goiter is caused by genetically determined errors in thyroid hormone synthesis and metabolism, in part due to loss-of-function mutation genes.

Histopathology. The thyroid gland is large and nodular and histologically shows a solid and microfollicular pattern with

cytologic atypia, mitoses, and a scant amount of colloid. Rare cases of follicular adenoma and carcinoma and even rarer cases of PTC have been reported.

Graves' Disease

Graves' disease is an autoimmune process that targets the thyroid follicles. Thyroid-stimulating immunoglobulin (TSI) and thyrotropin-binding inhibitor immunoglobulin (TBII) are involved in the pathogenesis of this disease. Patients develop autoantibodies to thyroid peroxidase, thyroglobulin, and TSH receptor; this stimulates the TSH receptor and increases the production of thyroid hormone. Thymic hyperplasia may be seen.

Clinical findings. Diffuse toxic goiter occurs more frequently in young females and is accompanied by exophthalmos in 25–50 % of cases. It can also occur in children. The gland shows mild to moderate symmetric, diffuse enlargement; however, large and/or cold thyroid nodules may be present and may be targeted by USG-FNA. Other causes of hyperthyroidism include "toxic" follicular adenoma, "toxic" sporadic nodular goiter, various thyroiditides, and iatrogenic causes such as amiodarone.

Histopathology. There is follicular hyperplasia with small follicles with scant thin colloid and occasional papillary fronds. The lining epithelium is columnar with nuclear hyperchromasia and usually clear cytoplasm. Lymphoid follicles are present in the stroma, which has prominent vascularity. In late stages, the gland is nodular with oncocytic changes, fibrosis, and follicular atrophy. Incidental microcarcinomas of papillary type have been found in Graves' disease with an incidence equal to that found in normal glands.

FNA findings. Smears are usually cellular, showing sheets of cohesive cuboidal or columnar cells with abundant slightly clear cytoplasm, a round nucleus, and conspicuous nucleoli. A few microfollicular aggregates, lymphocytes, and oncocytes may be seen. Romanowsky-stained smears may show follicular cells with microlobulated cytoplasmic borders/microvacuoles

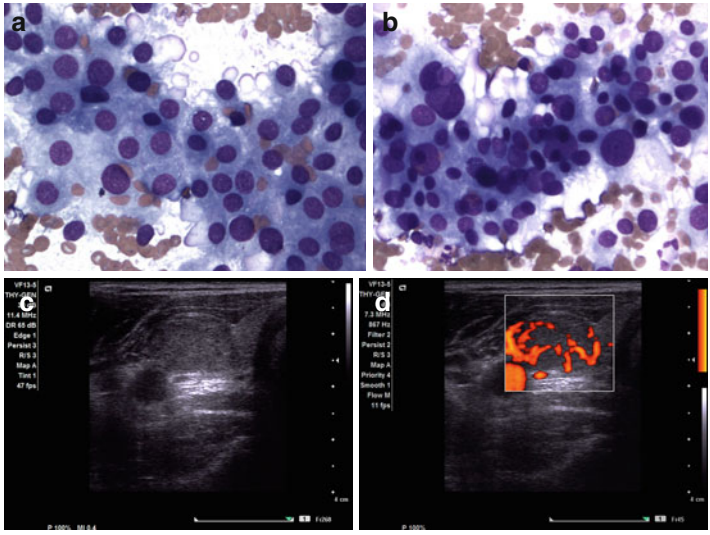

FIGURE 3.28 Treated Graves' disease. (**a**, **b**) Slightly complex sheets of large cells with slightly granular cytoplasm, prominent anisocytosis and anisonucleosis, and microlobulated cytoplasmic borders/microvacuoles exhibiting accentuated red-pink edges. (MGG stain, high power). (**c**, **d**) There is an ill-defined slightly hypoechogenic nodule in the right thyroid lobe with increased vascular blood flow by Doppler examination

exhibiting accentuated red-pink edges; however, they are not specific for Graves' disease and may be seen in other benign and malignant thyroid conditions. Smears from treated patients may have significant architectural and cytologic atypia (Fig. 3.28a, b).

US features (Fig. 3.28c, d)

- The gland is enlarged and may show normal echotexture, but it is usually hypoechogenic, corresponding to the lymphoid infiltrates and decreased amounts of colloid seen histologically. Occasionally, the parenchyma shows small 2–3-mm hypoechoic foci.
- Blood flow is increased (thyroid "inferno") on Doppler examination.

- The incidence of thyroid nodules and thyroid cancer in Graves' disease equals that seen in the general population.

FNA Diagnosis of Thyroiditis

All forms of thyroiditis are more common in women than in men. They can be classified as autoimmune (chronic lymphocytic or Hashimoto's), subacute granulomatous (De Quervain's), subacute lymphocytic, acute suppurative, and chronic fibrous (Riedel's) thyroiditides. Rare causes of granulomatous thyroiditides include tuberculosis, localized or systemic sarcoidosis, Wegener's granulomatosis, Langerhans cell histiocytosis, foreign body reactions, and "palpation" thyroiditis.

Ultrasonography is helpful in evaluation of the echotexture of the gland and the presence of nodules. The US characteristics of thyroiditis are variable along the course of the disease and may show focal or diffuse hypoechogenicity. If diffuse, the parenchyma also looks heterogeneous, with hyperechoic streaks representing fibrosis. Likewise, once the inflammatory process improves or resolves, the US appearance is also variable, ranging from normal to hypoechoic nodular or atrophic.

Thyroiditides have distinct cytologic findings allowing for a specific FNA diagnosis in most cases.

Autoimmune (Chronic Lymphocytic and Hashimoto's) Thyroiditis

Clinical findings. Autoimmune thyroiditis is a clinicopathologic and serologic entity that shows varying degrees of thyroid dysfunction, thyroid tissue diffuse lymphocytic infiltration, and positive serum thyroid autoantibodies to thyroid peroxidase (TPO), thyroglobulin, and TSH receptors. However, serology may be negative in rare cases.

Hashimoto's thyroiditis commonly affects women over the age of 40 years as well as children and adolescents who present with diffuse symmetric, slightly asymmetric, or multinodular goiter. Mild hyperthyroidism usually occurs in the initial

phases of the disease process and hypothyroidism in late stage. Hashimoto's thyroiditis is the leading cause of hypothyroidism in areas with no iodine-deficient diet. It is commonly associated with autoimmune processes in other organs, and it predisposes to the development of lymphoma. The rate of epithelial malignancy in thyroid nodules in a background of Hashimoto's thyroiditis is at least as high as or possibly higher than that in normal thyroid glands.

Histopathology. The presence of diffuse lymphoid infiltration with germinal center formation is characteristic of autoimmune thyroiditis. Small colloid-depleted thyroid follicles lined with "normal" epithelium are seen in lymphocytic thyroiditis, and those with "oncocytic" epithelium, in Hashimoto's thyroiditis. Hashimoto's thyroiditis also shows plasma cells, histiocytes, and multinucleated giant cells as well as squamous metaplasia and extensive fibrosis. Large cysts lined with metaplastic squamous epithelium and surrounded by hyperplastic lymphoid follicles may be seen. Hyperplastic nodules may be present, particularly in multinodular Hashimoto's thyroiditis; also, a follicular or Hurthle cell adenoma can occur in the same setting. While diffuse reactive cellular changes are commonly seen in autoimmune thyroiditis, microscopic foci of cells showing pronounced architectural and cytologic atypia (lack papillary architecture or intranuclear cytoplasmic invaginations) are not uncommonly seen and are called "follicular epithelial dysplasias" and may be the precursors of papillary thyroid carcinoma.

Immunoprofile. The immunophenotype of oncocytic cells in Hashimoto's thyroiditis and PTC is similar. Thus, these findings may provide an indication that patients with Hashimoto's thyroiditis have a small but real risk of developing PTC. Medullary carcinoma is exceedingly rare to occur in a background of autoimmune thyroiditis. In contrast to reactive cellular changes that are negative or weak and focal for HMBE-1, CK 19, and galectin-3, "follicular epithelial dysplasias" are positive in 86, 96, and 40 %, respectively, and support the concept that these lesions are precursors of papillary thyroid carcinoma that shows similar immunoreactivity.

Molecular profile. It is suggested that multiple genes with variable penetrance are involved in the development of autoimmune thyroiditis. *RET/PTC* may provide a link between PTC and Hashimoto's thyroiditis. Patients who developed PTC in the Chernobyl accident developed associated chronic autoimmune thyroiditis.

FNA findings. Smears are usually cellular, although the presence of follicular or Hurthle cells is not required for specimen adequacy. The background shows a polymorphous population of benign reactive lymphocytes and plasma cells. Lymphoid elements may be entangled with the epithelial cells. Of note, Hurthle cells may have prominent anisonucleosis, which may be a source for an erroneous diagnosis of atypia, Hurthle cell neoplasm, or even PTC. Lymphoma should be considered in the presence of monomorphic lymphoid cells (Fig. 3.29).

US features

- The US appearance is highly variable and correlates with the progression of histopathologic changes along the course of the disease. The lymphoid and oncocytic cell components appear homogeneous on US, and fibrous tissue elements as hyperechoic septa.
- Early in the course of the disease, the gland appears diffusely enlarged and profoundly hypoechoic, which correlates with lymphocytic infiltration and colloid depletion without fibrosis. Subclinical thyroid dysfunction is common at this stage.
- As the disease progresses, there is mild hyperechogenicity, heterogeneity, and pseudo-micronodularity ("moth-eaten" or cotton weave) that is the result of destruction of thyroid tissue.
- Poorly outlined hypoechoic pseudonodules may be variably present, often transient, and may represent coalescent aggregates of lymphoid cell-rich tissue, which may be surrounded by echogenic septa. A "Swiss-cheese" appearance on US, the result of small cystic lesions, may be seen in the course of the disease.

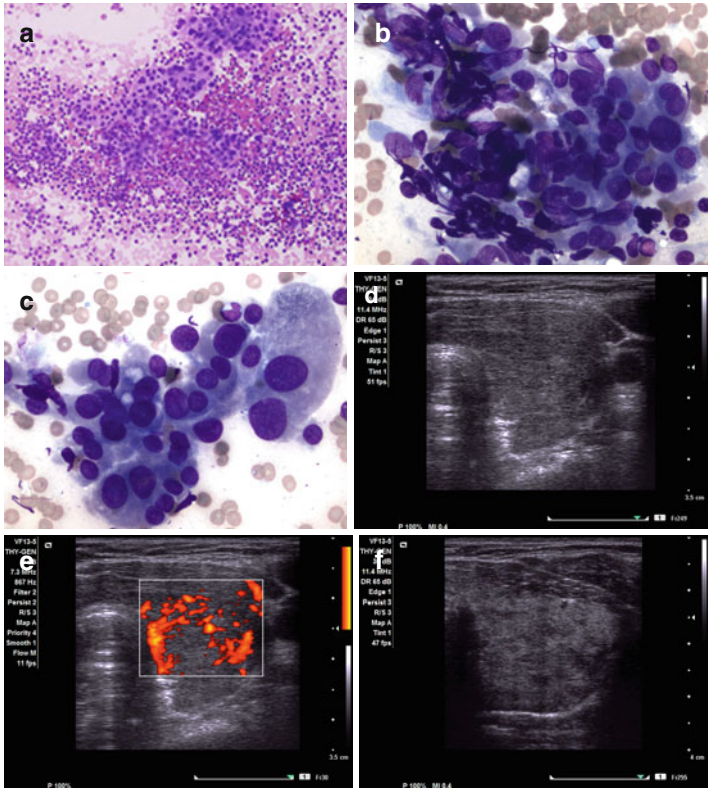

FIGURE 3.29 Autoimmune thyroiditis. The smear shows sheets of Hurthle cells and lymphocytes (**a**). The Hurthle cells are both single and clustered, the lymphocytes are both single and entangled with Hurthle cells, and there is lack of colloid (**b**, **c**). Ultrasound features show a diffusely enlarged slightly hypoechoic thyroid gland (**d**) and increased blood flow by Doppler examination (**e**). Progressively the gland develops a "moth-eaten" pseudo-micronodularity (**f**), echogenic septa surrounding hypoechogenic pseudonodules (**g**), hyperechoic regenerative pseudonodules ("white knight", *arrow*) (**h**), cobblestone appearance ("giraffe skin," **i**), and detached pseudonodules (**j**, calipers) (**a**, Diff-Quik stain low power. Courtesy of Dr. Javier Saenz de Santamaria, Badajoz, Spain; **b**, **c**, MGG stain, high power)

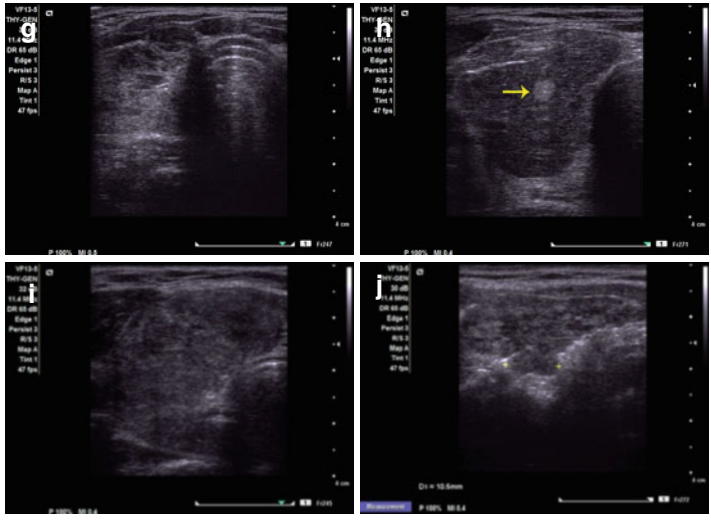

FIGURE 3.29 (continued)

- Hyperechogenic pseudonodules may be seen in "regenerative" nodules or as a result of aggregated fibrous tissue ("white knight").
- "Detached" tissue nodules may be seen in chronic stages.
- Blood flow is variable; it ranges from absent to normal to increased on Doppler examination.
- The gland is small, atrophic, hypoechoic, and heterogeneous in end-stage disease.
- True distinct hypoechogenic thyroid nodules with or without calcifications may be seen and need USG-FNA sampling to rule out PTC or lymphoma. Cytologic material for confirmatory flow-cytometry studies can be easily obtained by this means.
- A "speckled" pattern is occasionally seen and probably needs a USG-FNA, because the numerous "colloid bodies" may be difficult to distinguish from the numerous psammoma bodies present in the sclerosing variant of PTC.
- Prominent lymph nodes in the central and lateral neck are almost always present.

Subacute Granulomatous (De Quervain's) Thyroiditis

Subacute thyroiditis is a transient self-limited inflammatory process. The etiology is unknown but is generally believed to be of viral origin (mumps, measles, influenza, Coxsackie, Epstein–Barr, and adenovirus). It may also be drug induced.

Clinical findings. Middle-aged women are usually affected and develop a sore throat and anterior lower neck tenderness of rapid onset, accompanied by fever and malaise. The process commonly follows a viral illness, usually in patients with HLA-Bw35 antigen. The acute phase lasts approximately 1 month with a hyperthyroid stage, followed by several months of hypothyroidism before the patient returns to a euthyroid stage. Thyroid autoantibodies are negative. The glandular involvement is usually asymmetric, and the affected areas are firm.

Histopathology. There is a granulomatous inflammatory reaction with multinucleated cells of the giant cell type. Colloid is often seen within the giant cells.

FNA findings. The FNA procedure may be painful, which limits adequate sampling of the nodule. Smears show variable cellularity, multinucleated giant cells, isolated histiocytes, granulomas, chronic inflammation, and neutrophils, particularly in the early phase of the disease process. Fibrosis and scant cellularity are seen in late phases of the process (Fig. 3.30a–c).

US features

- The US shows diffuse or localized hypoechogenicity in the affected painful or tender areas. When localized, the US features mimic those of carcinoma or lymphoma (Fig. 3.30d, e).
- No increased vascularity is seen in the affected areas; however, vascularity may be increased in the recovery phase.
- The US appearance usually returns to normal in the recovery phase.

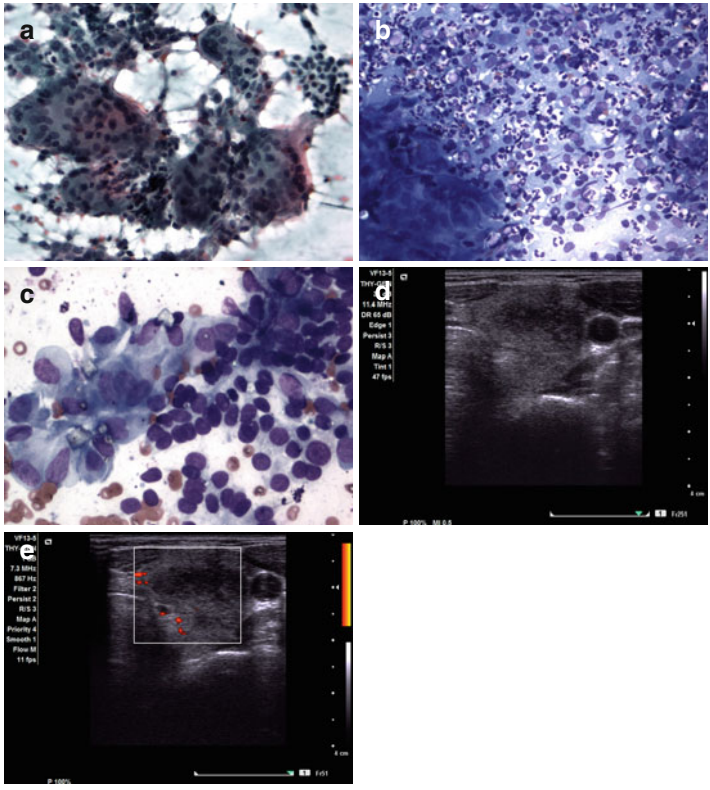

FIGURE 3.30 Subacute thyroiditis. Multinucleated giant cells with numerous nuclei (**a**), granulomas (**b**, **c** left lower side), acute inflammatory cells (**b**), and benign follicular cells (**c**) are present. Ultrasound shows poorly defined heterogeneous and irregular areas of hypoechogenicity (**d**) with lack of vascular blood flow by Doppler examination (**e**). (**a**, Papanicolaou stain low power; **b**, **c** MGG stain, high power)

Subacute Lymphocytic (Sporadic or Postpartum) Thyroiditis

This type of thyroiditis is an autoimmune process with positive thyroid antibodies that develops in the first year after the delivery. Patients initially have transient hyperthyroidism and a nontender thyroid gland, followed by lymphocytic thyroiditis.

Acute Suppurative Thyroiditis

Acute suppurative thyroiditis is uncommon. The etiology is bacterial, usually due to staphylococci and streptococci, or fungal secondary to hematogenous or lymphatic dissemination (sepsis in an immunocompromised individual or malnourished infant), contiguous spread from adjacent sites (infections of the upper aerodigestive tract), or superinfection of congenital anomalies such as thyroglossal duct cyst or pyriform sinus fistula. Most patients have an underlying thyroid disorder. In the presence of acute suppurative unilateral thyroiditis or abscess in the thyroid or surrounding tissue, a persistent pyriform sinus-thyroid fistula resulting from a fourth branchial cleft anomaly or a persistent embryonal thymopharyngeal duct from the third pouch, usually left-sided should be excluded and surgically treated to avoid recurrent infections.

Clinical findings. Patients complain of anterior lower neck swelling and pain developing over a period of days to weeks, accompanied by fever, dysphagia, dysphonia, hoarseness, and palpable cervical lymphadenopathy. Thyroid function tests are normal, although there may be transient hyper- or hypothyroidism; autoantibodies are negative.

Histopathology. There is acute inflammation and tissue necrosis with eventual abscess formation.

FNA findings. Smears show a purulent smear pattern with necrosis and blood. Organisms may be seen particularly in immunosuppressed patients. Occasional reactive follicular cells may be seen; however they are not a requirement for specimen adequacy. Samples for bacterial cultures should be obtained. Treatment includes antibiotics and abscess drainage.

US features

- The thyroid gland is diffusely hypoechoic and edematous with intermixed hyperechoic trabeculae and mildly increased vascularity.
- A thyroid abscess may develop in the course of the disease and shows a complex echotexture, irregular borders, and posterior acoustic enhancement in the cystic areas.

Chronic Fibrous (Riedel's) or Ligneous Thyroiditis

This rare entity has an unknown etiology and probably represents a primary inflammatory dense fibrotic process replacing the thyroid tissue. Rarely, it may be part of a multisystemic fibrosclerotic syndrome.

Clinical findings. This process affects predominantly adult or elderly female patients. The fibrosis extends to the tissues surrounding the thyroid, compressing adjacent structures and causing hoarseness and stridor. Shortness of breath and dysphagia develop if the fibrosis extends into the mediastinum. The thyroid gland is enlarged and has a stony consistency. Tenderness or cervical lymphadenopathy is absent. Most patients are euthyroid, but 30 % have hypothyroidism. Cases of hypoparathyroidism have been described due to fibrosis. Similar signs and symptoms are seen in anaplastic thyroid carcinoma.

Histopathology. There are areas of complete obliteration of the thyroid parenchyma next to areas with preserved architecture. Microscopically, there is extensive fibrosis that extends to the surrounding perithyroidal tissue planes. Chronic inflammation is patchy, and multinucleated cells are lacking.

FNA findings. Smears are pauci- or acellular, showing rare strands of fibrocollagenous tissue. Rare lymphocytes and bland-appearing spindle cells may be seen. Colloid and follicular cells are usually absent (Fig. 3.31). Open surgical biopsy is often needed for definitive diagnosis and exclusion of malignancy.

US features

- The gland may be enlarged or poorly defined and has a diffuse, homogeneous hypoechogenicity.

FNA Diagnosis of Follicular Neoplasm

The FNA diagnosis of "follicular neoplasm" reflects the lack of ability of cytology to distinguish accurately among a hyperplastic nodule in nodular goiter, follicular adenoma, and follicular carcinoma due to overlapping cytologic features. The follicular variant of PTC may be considered in this group when nuclear features of papillary carcinoma are

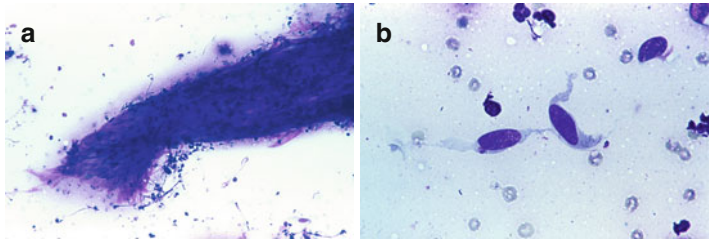

FIGURE 3.31 Reidel's thyroiditis (From the American Society of Cytology slide seminar 2005). Paucicellular smears showing a fibrocollagenous tissue fragment with damaged inflammatory cells (**a**) and rare bland stromal cells (**b**). (Diff-Quik stain, low and high power)

inconspicuous. Parathyroid adenoma shows cytologic features similar to those of a follicular neoplasm and is often misinterpreted as such; this issue will be discussed under parathyroid adenoma/carcinoma.

Follicular Adenoma and Carcinoma

Follicular adenoma is the most common thyroid neoplasm. Follicular carcinomas are rare, although they are more common in iodine-deficient geographic areas.

Lobectomy is necessary for differentiation between adenoma and carcinoma. Thus, the diagnosis is made histopathologically only.

Clinical findings. Most patients are euthyroid and have a solitary "cold" nodule on thyroid scan. Few adenomas are "hot" and may cause hyperthyroidism ("Plummer adenoma"). Follicular carcinomas often measure >5 cm, and they occur predominantly in women of the fifth decade or older; however, it may occur in children and adolescents as well. Metastases are hematogenous rather than lymphatic. Thus, regional lymph node metastases are unusual. Distant visceral metastases include the lung, bone, kidney, etc. The prognosis is slightly worse than that of PTC, with a 75–95 % 10-year survival.

Histopathology. Adenoma is surrounded by a thin capsule that is grossly and histologically complete, lacking

capsular, vascular, or thyroid invasion. The pattern may be microfollicular, normofollicular, macrofollicular, trabecular, solid, and/or papillary. Cells are usually monomorphic, but occasionally there is cellular pleomorphism with large bizarre hyperchromatic nuclei; however, other features of malignancy are absent. Nuclear features of PTC are absent. Mitoses are rare or absent. Cystic degeneration, spindle cells, and adipose and cartilaginous metaplasia may be seen particularly in large-sized adenomas. Clear cell changes (cytoplasmic glycogen, lipid, mucin) are more common in carcinomas than in adenomas. In contrast, signet ring cells (cytoplasmic thyroglobulin) are more common in adenomas. Adenomas can also show black pigment (minocycline related).

Follicular carcinoma can be subclassified as minimally invasive or widely invasive. Follicular carcinomas measuring less than 2 cm have not been associated with metastatic disease. Widely invasive carcinomas with necrosis and/or mitoses have a worse prognosis.

Immunoprofile. Normal follicular tissue, follicular adenoma, and follicular carcinoma have similar profiles including positivity for thyroglobulin, TTF-1, low-molecular-weight keratin, EMA, laminin, and type IV collagen.

Molecular profile. No molecular test is able to differentiate between follicular adenoma and follicular carcinoma. Mutually exclusive *RAS* point mutations and *PAX8/PPARγ* rearrangements are seen in both follicular adenomas and carcinomas (70–75 %) (Figs. 3.32, 3.33, and 3.34).

- *RAS* mutation is related to follicular architecture in thyroid tumors and is typically detected in 20–40 % of conventional-type follicular adenomas, 40–50 % of conventional-type follicular carcinomas, and 10–20 % of the follicular variant of PTC and not in conventional PTC. A lower incidence has been seen in oncocytic tumors.
- Many studies on thyroid follicular tumors have reported the presence of somatic mutations to three forms of *RAS*: *HRAS*, *KRAS*, and *NRAS*. The rate of gene mutations is significantly higher in the carcinomas than in the adenomas. *RAS* mutations in follicular carcinoma have

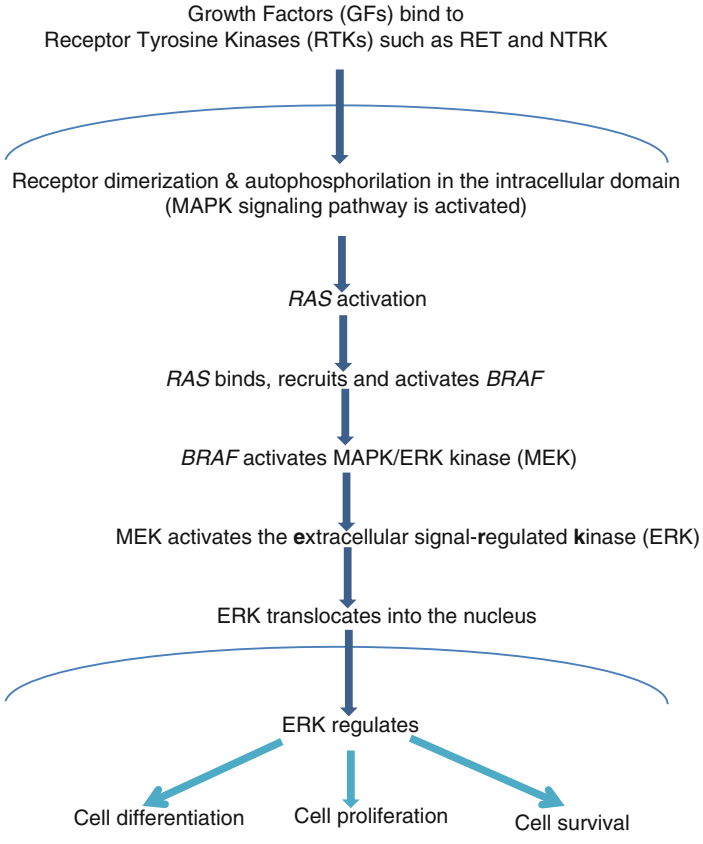

FIGURE 3.32 MAPK signaling pathway

been correlated with an unfavorable prognosis and poor overall patient survival and may be correlated with tumor dedifferentiation as they are prevalent in anaplastic carcinoma. The *NRAS* codon 61 mutation in follicular carcinomas is positively associated with distant metastases.

- *PAX8/PPARγ* rearrangements occur in 12–40 % of conventional follicular carcinomas, with lower prevalence in oncocytic (Hurthle) carcinomas. They have also been found in the follicular variant of PTC (38 %, particularly the encapsulated ones), follicular adenomas (2–13 %),

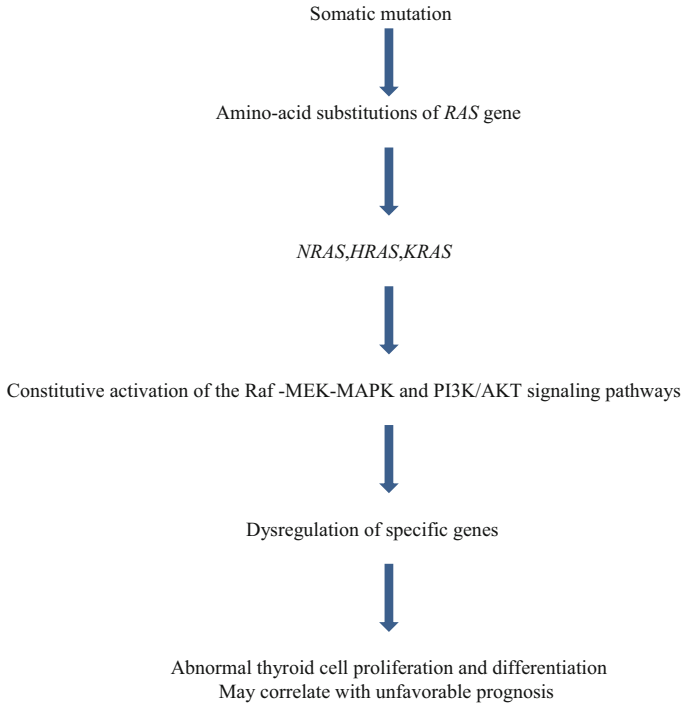

FIGURE 3.33 *RAS* in follicular carcinoma (40–50 %)

hyperplastic thyroid nodules, and anaplastic and poorly differentiated carcinomas (7 %). Tumors tend to occur at a young age, be of small size, and have vascular invasion.

- "Hot" adenomas typically have *TSHR* and *GNAS1* activating mutations. The PI3K/PTEN/AKT pathway is rarely activated in follicular adenomas; however, this pathway is activated in follicular carcinoma associated with Cowden, Carney complex type I, and Wermer syndromes.
- Loss of heterozygosity on 7q and 3p loci is frequently encountered in follicular carcinomas.

FNA findings. (Microfollicular adenoma, Fig. 3.35a–d. Follicular carcinoma, Fig. 3.35e–g). Smears are cellular and show microfollicular and trabecular patterns, as well

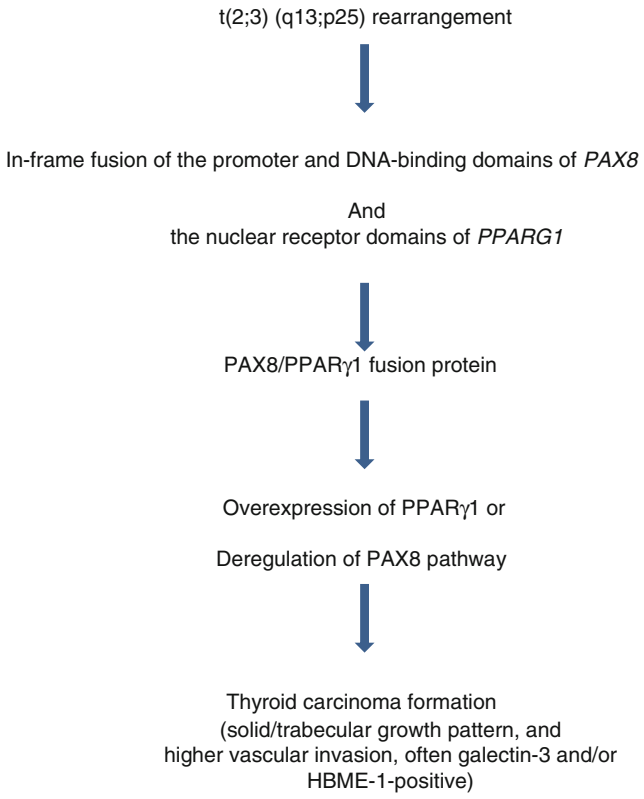

FIGURE 3.34 *PAX8/PPARγ* in follicular carcinoma (30–40 %)

FIGURE 3.35 Follicular adenoma (**a–d**). High cellularity and a trabecular arrangement (**a**, **b**). Microfollicles showing cells with high nuclear to cytoplasmic ratio, large nuclei, and molding (**c**). Signet ring cells (cytoplasmic thyroglobulin) are seen in a different case (**d**). Follicular carcinoma (**e–g**). Cells with oxyphilic change are seen in a microfollicular pattern (**e**, **f**). Vascular invasion is seen in the resection specimen (**g**). Follicular adenoma, ultrasound features (**h–k**). These two cases show single hypoechoic nodules [1.6 and 5.5cm (composite image between *arrows*) in maximum diameter], slightly heterogeneous echotexture, well-defined margins, no halo, and Grade 4 vascular blood flow on Doppler examination. (**a–c**, **e** and **f**, MGG stain, high power; **d**, Papanicolaou stain, high power; **g**, hematoxylin and eosin stain, low power)

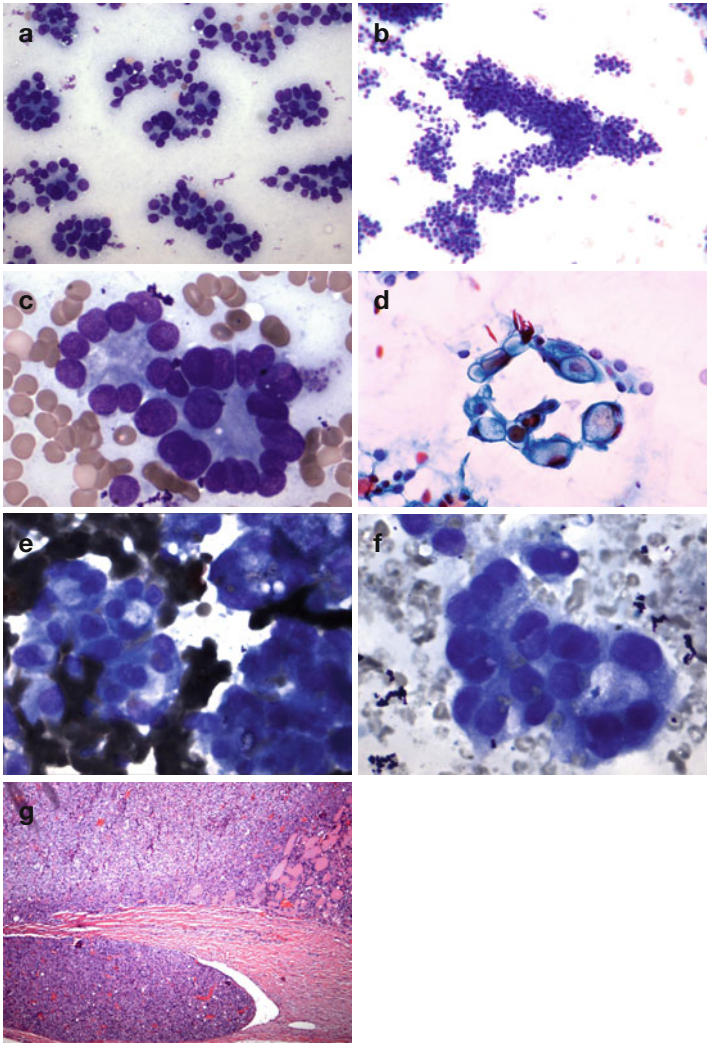
a
b
c
d
e
f
g

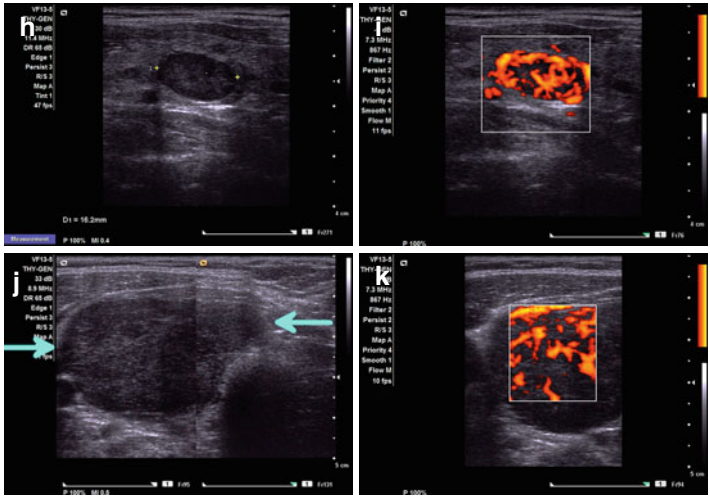

FIGURE 3.35 (continued)

as single cells. A microfollicle is characterized by less than 15 crowded and overlapped cells. Cells may be slightly or markedly enlarged with scant cytoplasm, a round nucleus, slightly coarse chromatin, and an inconspicuous nucleolus. Rare atypical cells may be seen. There is nuclear overlapping and molding, but nuclear features for PTC are absent. Colloid is scant or absent; however, dense colloid may be seen in the lumen of the microfollicle. Occasional sheets of cells with no overlapping and small cell and nuclear size may be seen indicating a macrofollicular component, usually comprising less than 25 % of smear cellularity. Macrophages indicating cystic change may be present in large tumors. Psammoma bodies are absent and squamous metaplasia is rare.

US features (Fig. 3.35h–k)

- US features cannot separate follicular adenoma from follicular carcinoma.

- Nodules are commonly solitary or dominant, hypoechoic, homogeneous or slightly heterogeneous, and solid.
- Oval or round shape, regular and well-defined margins, hypoechoic halo 1–3-mm thick, and an intact capsule are US features strongly suggestive of adenoma.
- An inhomogeneous internal texture, an irregular ill-defined margin, and an absent or discontinuous thick and irregular halo suggest follicular carcinoma. However, these findings are not sensitive or specific, because follicular carcinomas may be hyper- or isoechoic and may have a halo.
- Cystic change is absent or minimal and calcifications are rare in adenomas, except in large tumors.
- Vascularity is usually present and peripheral in adenomas; however, no vascularity is seen in a few follicular adenomas. Intranodular vascularity is more common in carcinomas than in adenomas. A lack of blood flow by Doppler examination in follicular neoplasms makes malignancy very unlikely.
- Widely invasive tumors often show a heterogeneous mulberry-like echotexture and ring calcifications.

Oncocytic (Hurthle Cell) Neoplasm

Approximately 20 % of follicular neoplasms are oncocytic; they may be benign or malignant. Hurthle cell adenomas are cured by excision. Carcinomas are highly aggressive.

Clinical findings. Most patients have single or multiple nodules. Hurthle cell carcinomas are larger than adenomas, tend to occur in an older age group, and do not show much female preponderance. Lesions >4 cm are often (80 %) malignant. The prognosis seems to be worse than conventional follicular carcinoma, with a greater risk of distant metastasis (30 %), 20–40 % mortality at 5 years, and a 40 % 10-year survival rate. Lungs and bone are common sites for metastasis.

Histopathology. Similar to follicular neoplasms, the distinction between a benign and a malignant oncocytic neoplasm is histologic, following the same histologic criteria. The architectural pattern may be follicular, trabecular, solid, or papillary. The follicular pattern is commonly seen in adenomas and the solid/trabecular pattern in carcinomas. Cellular pleomorphism and prominent nucleoli are common in both. Massive infarction may be present particularly after FNA.

Immunoprofile. No ancillary technique distinguishes between Hurthle cell adenoma and carcinoma. Oncocytes show reactivity with thyroglobulin, mitochondrial antigens, glucose transport 4 (GLUT-4), keratin, and in particular CK14, CEA, S-100 protein, and HMB-45.

Molecular profile. No specific chromosomal abnormality has been described. *RAS* mutations also occur in these tumors, although less frequently than in follicular tumors. *PAX8/PPARγ* rearrangements are virtually never seen in Hurthle cell carcinoma; in contrast, this abnormality is seen in 25–50 % of follicular carcinomas. Mutations of the mitochondrial DNA may be the responsible for the mitochondrial dysfunction and for the increased numbers of mitochondria characteristic of these cells. In contrast to PTC with oncocytic features that is diploid, both Hurthle cell adenomas and carcinomas are aneuploid.

FNA findings (Fig. 3.36). The smears are cellular and composed almost exclusively of loosely cohesive Hurthle cells of variable cell, nuclear, and nucleolar size. Syncytial aggregates and crowded groups with or without capillaries may be seen. Large and small "dysplastic" Hurthle cells have been described. Cells from carcinoma are smaller, more monomorphic, and have a high nuclear to cytoplasmic ratio. Nuclear atypia is unreliable for the diagnosis of a Hurthle cell neoplasm, because marked nuclear atypia can be seen in metaplastic nonneoplastic oncocytes of nodular goiter and Hashimoto's thyroiditis. The background lacks colloid and lymphocytes. PTC, medullary

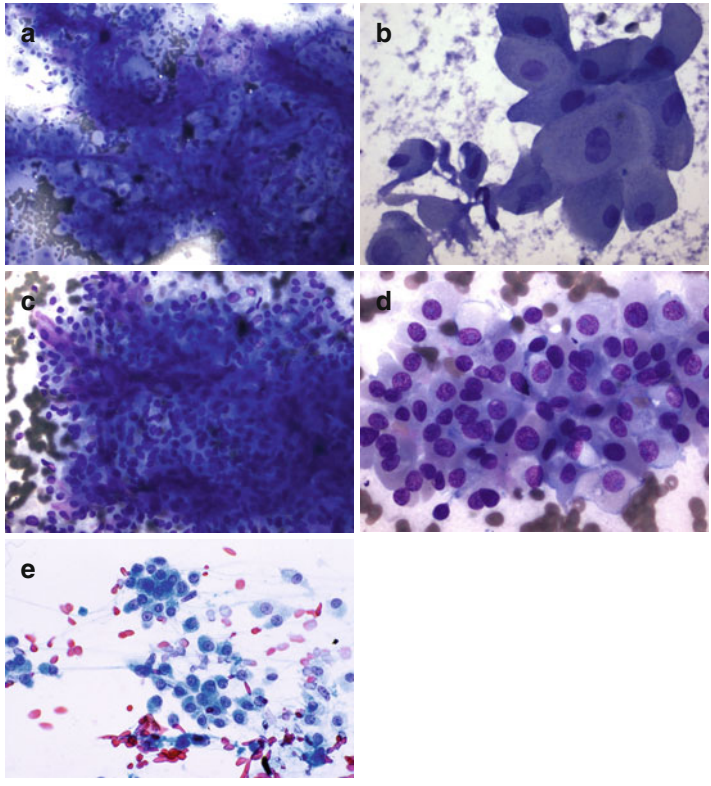

FIGURE 3.36 Hurthle cell adenoma (**a**, **b**). Smear shows high cellularity with crowded fragments of large cells and fine capillaries (**a**); cells show anisocytosis, round nuclei with prominent nucleoli and granular eosinophilic cytoplasm (**b**). Hurthle cell carcinoma (**c–e**). Complex aggregate of monomorphic cells supported by a fine capillary network (**c**); bland-appearing Hurthle cells are smaller than those of the prior case, monomorphic, and lack cytologic features of malignancy (**d**, **e**). (**a**, **c** and **d**, MGG stain, high power; **b** and **e**, Papanicolaou stain, high power)

carcinoma, and parathyroid tumors should also be considered in the differential diagnosis. Medullary carcinoma cells often lack nucleolus, and parathyroid tumors show a "salt-and-pepper" chromatin. Immunochemical stains are also helpful.

US features

- The US criteria are unreliable for differentiation among follicular neoplasm, Hurthle cell adenoma, and Hurthle cell carcinoma.
- Nodules have mixed hyper- and hypoechoic echogenicity, are often solid and ill-defined with incomplete halo, and lack calcifications.
- Nonspecific type intranodular vascularity as seen in follicular neoplasms may be present.

Hyalinizing Trabecular Tumor

It has been suggested that this tumor is the morphologic variant of PTC that behaves in a benign fashion. Until this is clarified, it is preferable to call it a tumor instead of adenoma.

Histopathology. This tumor has a characteristic trabecular arrangement of follicular cells surrounded by a prominent hyalinized collagenized stroma (type IV collagen). Cells show a cytoplasmic paranuclear yellow inclusion body (intermediate filaments) with a refractile appearance. The tumor shares morphologic features (psammoma bodies, nuclear inclusions, and groves) with PTC.

Immunoprofile. The tumor is consistently positive for thyroglobulin and TTF-1 and in 50 % for CK19 and galectin-3. Immunoreactivity for S-100 protein and neuroendocrine markers may be rarely seen. Calcitonin and CEA are negative.

Molecular profile. Rare cases of hyalinizing trabecular tumor share *RET/PTC* translocations as seen in PTC, but no *RAS* or *BRAF* mutations have been found. Of note, *RET/PTC* has also been seen in Hashimoto's thyroiditis, Hurthle cell adenoma, and hyperplastic nodules.

FNA findings. The smears are variably cellular and show single dispersed cells and complex cell aggregates embedded in a dense "amyloid-like" and fibrillary metachromatic

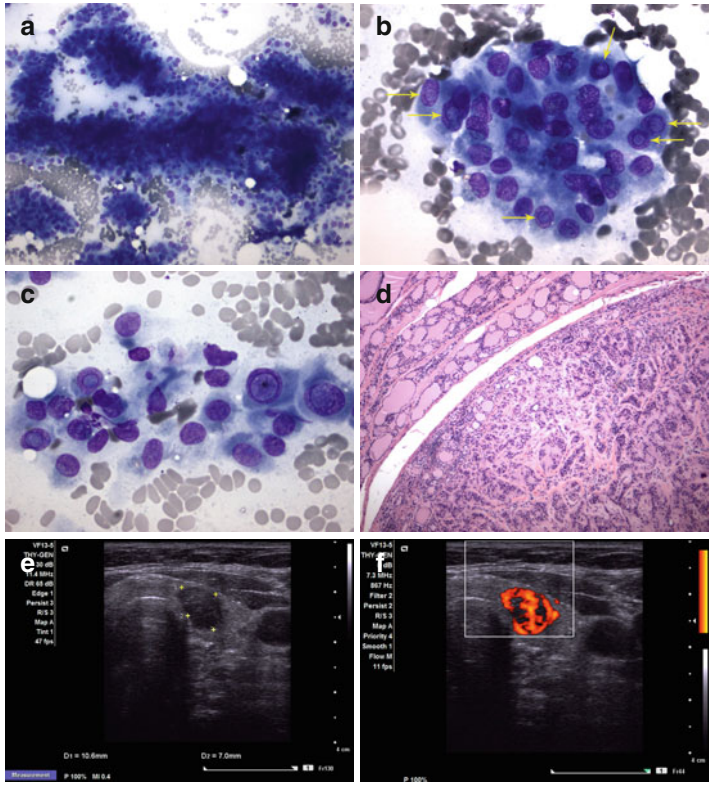

FIGURE 3.37 Hyalinizing trabecular tumor. Smear is cellular (**a**) showing complex aggregates of large cells surrounded by an "amyloid-like" stroma (**b**). Cells have ill-defined wispy cytoplasmic borders, nuclear grooves, and numerous intranuclear cytoplasmic invaginations (**b** (*arrows*), **c**). Tissue section shows a circumscribed tumor with a trabecular architecture supported by a dense hyalinized stroma (**d**). Ultrasound features include an oval well-circumscribed homogeneous hypoechoic nodule with Grade 4 vascular pattern by Doppler examination (**e**, **f**). (**a**–**c**, MGG stain, high power; **d**, hematoxylin and eosin, low power)

material. The cells are large with usually ill-defined cytoplasmic whispy/filamentous borders, dense cytoplasm, and numerous intranuclear cytoplasmic invaginations and nuclear grooves (Fig. 3.37a–d). Psammoma bodies and cytoplasmic

paranuclear yellow inclusions (light green on Papanicolaou stain) may be present. Often, this tumor is interpreted as PTC or less often as medullary carcinoma.

US features (Fig. 3.37e, f)

- These tumors share US features with follicular neoplasms, including the follicular variant of PTC, but rarely with those of PTC.
- Tumors often show a hypoechoic solid echotexture, oval to round shape, well-defined margins, a hypoechoic halo, and no calcifications. A heterogeneous echotexture is seen in some cases.

FNA Diagnosis of Thyroid Malignancies

The American Cancer Society statistics for 2014 estimates that 62,980 ($M = 15{,}190$ and $F = 47{,}790$) new cases of thyroid cancer will be diagnosed and 1,980 ($M = 830$ and $F = 1{,}060$) will die of thyroid malignancy in the United States.

In adults and children, most thyroid malignancies are PTCs (75–80 %) followed by follicular (10–20 %), medullary (3–5 %), and anaplastic (1–2 %) carcinomas. Thyroid lymphoma, sarcoma, and metastases are rare.

PTC, follicular carcinoma, and Hurthle cell carcinoma are grouped as differentiated thyroid cancer (DTC). Poorly differentiated thyroid carcinoma (PDTC) includes those tumors with no glandular component and instead insular, trabecular, and solid histologic tumor architecture and at least one of the following: convoluted nuclei, mitoses (>3/10 HPF), or necrosis. Based on its biologic behavior, DTC is treated with total or near-total thyroidectomy with lymph node dissection, depending on the extent of intra- and extrathyroidal and metastatic disease, followed by ^{131}I. In contrast, PDTC is treated with a more aggressive surgical approach, often postoperative ^{131}I, and in some cases external-beam radiotherapy. Of note, PDTC and anaplastic thyroid carcinoma are 2 distinct clinicopathologic entities whose therapeutic management is different. PDTC may represent an intermediate entity in the progression from DTC to anaplastic thyroid

carcinoma. Medullary carcinoma is a distinct tumor treated with thyroidectomy and lymph node dissection. Somatostatin inhibitors, repeat surgery, and external-beam radiation are used in recurrent and metastatic medullary carcinoma.

Papillary Thyroid Carcinoma

Papillary thyroid carcinoma is the most common type of thyroid malignancy in children and adults, affecting more women than men and predominating in the fifth decade of life. There has been almost a threefold increment in the incidence of PTC in the last three decades, mostly due to an increase in detection and not in the true occurrence. Tumors less than 5 mm are considered micropapillary carcinomas, the occurrence of which ranges between 5 and 36 %, and the natural history is not well understood.

The long-term prognosis is very good, particularly in children and adolescents. The survival rate is 99 and 95 % at 20 years and 30 years after surgery, respectively. Adverse prognostic factors include male sex; older patients; large tumor size; extracapsular extension or vascular invasion; distant metastases; tall-cell, columnar cell, and sclerosing variants at histology; and high postoperative thyroglobulin levels. Cervical lymph node metastasis does not seem to affect the prognosis.

DNA ploidy, circulating tumor cells detected by RT-PCR assay for thyroglobulin RNA, and detection of *BRAF* V600E mutation are also considered adverse prognostic factors.

Clinical findings. Patients are usually asymptomatic and euthyroid. Lymph node involvement is common particularly in young patients and may be the first manifestation of the disease. Hematogenous metastases are less common. *BRAF* mutations have been associated with lymph node and lung metastases. Extrathyroidal extension is seen in 25 % of patients at the time of surgery.

Histopathology. The tumor shows a papillary architecture with fibrovascular cores lined with columnar, cuboidal, and at times hobnail epithelium. A follicular component is

commonly seen. The cytologic findings include ground-glass nuclei (absent in frozen sections and FNA material), intranuclear cytoplasmic invaginations (present in frozen sections and FNA material), nuclear groves, and nuclear microfilaments seen in rare cases as intranuclear clearing. Psammoma bodies are seen in 50 % of cases and, when present, are almost always indicative of PTC; however, they can be seen in medullary carcinoma. A clear cell change may occur as a result of glycogen accumulation. Chronic inflammation is seen in 25 % of cases.

Immunoprofile. PTC shows positivity for CK/CK19/TTF-1, thyroglobulin (TG), HBME-1, PAX8, S-100 protein, vimentin, and EMA, among others. CK20 is negative. These markers are rarely used because the diagnosis is made by morphology in most cases. However, the most specific and useful markers for determination of the cell lineage are TG and TTF-1. Because the oncocytic cells of Hashimoto's thyroiditis share their immunoprofile with PTC, HBME-1 and CK19 are most useful for differentiating between the two.

Molecular profile. The mitogen-activated protein kinase (MAPK) pathway, physiologically activated by growth factors binding to receptor tyrosine kinases in the cytoplasmic membrane, propagates signals to the nucleus and regulates cell proliferation, differentiation, and survival (see Fig. 3.32).

- In PTC, activation of this pathway is secondary to point mutations of *RAS* and *BRAF* genes or results from RET/PTC and TRK rearrangements involving the *RET* and *NTRK1* genes, respectively (Figs. 3.38 and 3.39). RET/PTC is the major molecular marker for PTC, and at least15 types of *RET/PTC* chimeric oncogene have been identified in PTC. All of these mutations and rearrangements are present in 70 % of PTCs and were initially thought to be mutually exclusive; however, a simultaneous occurrence of these genetic abnormalities has been shown in some PTCs, although it is not clear whether in the same or different cells within the tumor.
- Activating mutations of the *BRAF* oncogene are highly specific for PTC and related tumor types, are seen in 40–70 % of PTCs with the presence of valine in residue

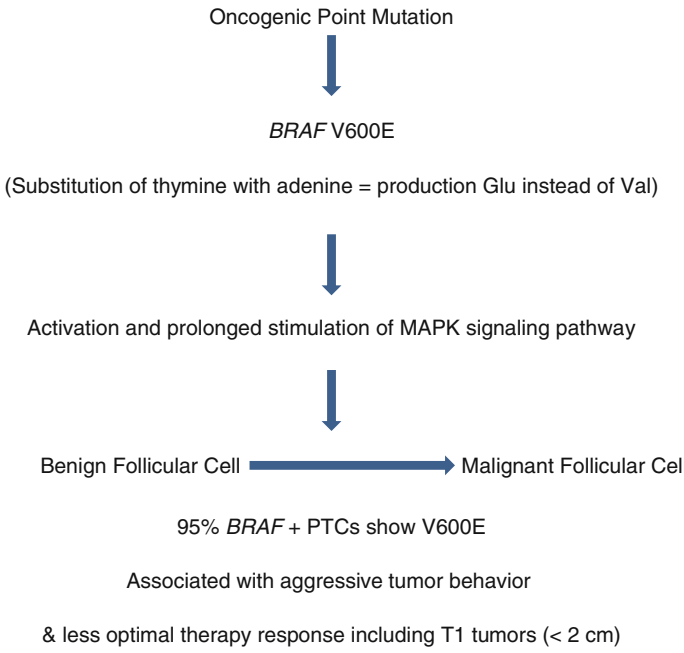

FIGURE 3.38 *BRAF* in papillary carcinoma (50 %)

600 of protein (V600E) in most cases, and correlate directly with the tumor papillary architecture. Most PTCs carrying the *BRAF* V600E mutation are classic, tall-cell, oncocytic/Warthin-like variants, and subcapsular sclerosing microcarcinomas. The mutation is present in about 20 % of the follicular variant of PTC and absent from the cribriform–morular variant. Of note, *BRAF* and *NRAS* gene mutations have been identified in 24 and 8 % of diffuse large B-cell thyroid lymphomas, respectively.

- *BRAF* V600E mutation is an early event in thyroid carcinogenesis and has been associated with male gender, older age at diagnosis, classic nuclear features of PTC, infiltrative growth, stromal fibrosis, psammoma bodies, extrathyroidal extension, lymph node metastasis, a higher

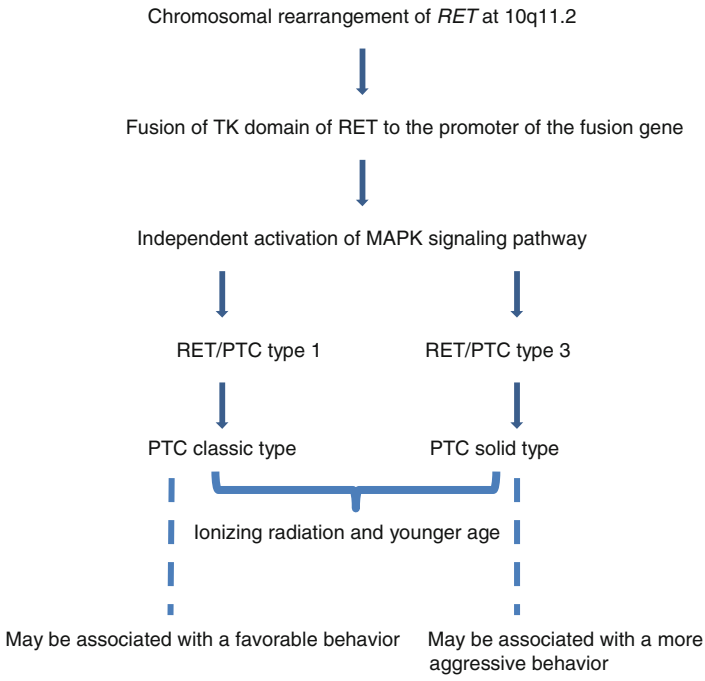

FIGURE 3.39 *RET* in papillary carcinoma (20–30 %)

risk of persistent disease, and more aggressive tumors that are refractory to radioiodine therapy. These prognostic implications are of particular importance in PTCs ≤2 cm, including microcarcinomas. Thus, detection of *BRAF* V600E mutation preoperatively may play a role in a more aggressive surgical approach, postsurgical therapy, and closer follow-up.

- *BRAF* V600E mutations are uncommon in PTC occurring in children and in relation to radiation exposure and have not been found in benign thyroid nodules or follicular carcinoma. They can be reliably detected by molecular techniques in paraffin-embedded tissue and FNA samples.

- Gene rearrangements occur in 20–40 % of PTCs, mostly involving *RET*, a transmembrane tyrosine kinase receptor. Clonal *RET/PTC* rearrangement is a strong indicator of PTC and has a variable incidence, being detected in 10–20 % of adult sporadic PTC, 50–80 % of tumors from patients with a history of therapeutic or environmental radiation exposure (detected in 87 % of post-Chernobyl PTC), and 40–70 % of PTC in children and young adults. The identification is made by use of RT-PCR or FISH. Of note, activating *point* mutations of the same *RET* oncogene are detected in medullary carcinoma.
- *RAS* mutation occurs in about 10 % of PTCs and almost always correlates with a follicular architecture, less prominent nuclear features, more frequent encapsulation, and a low rate of lymph node metastasis.
- *NTRK1* is a gene that encodes a transmembrane tyrosine kinase receptor that binds the nerve growth factor. Rearrangement of this gene is identified in 5 % of PTCs, and the clinicopathologic features are similar to those of PTCs associated with *RET/PTC* rearrangement. However, it is uncommon in PTC related to radiation exposure.
- VEGF, binding to two receptor tyrosine kinases (VEGFR1 and VEGFR2), also triggers MAPK signaling, and the intensity of expression correlates with a poor prognosis and *BRAF* mutation status.

FNA findings (Fig. 3.40a–e). PTCs of all conventional and variant types share the same cytomorphologic criteria. Smears are usually cellular and show monolayered sheets, complex tridimensional aggregates (without fibrovascular cores), and single cells. Corrugated or "onion-skin" cell sheets and papillary clusters with fibrovascular cores may occasionally be seen. Cellular overlapping, crowding, and molding are important diagnostic features. Cells are enlarged and show dense cytoplasm with well-defined cytoplasmic borders. Squamous metaplasia and focal oncocytic change may also be seen.

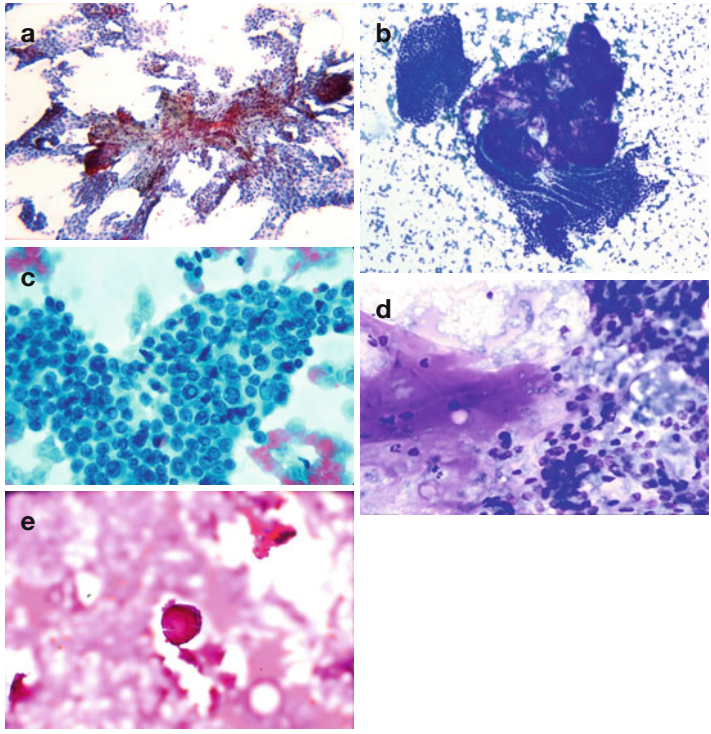

FIGURE 3.40 Papillary thyroid carcinoma. FNA cytology showing papillary fronds (**a**), corrugated sheets of neoplastic cells (**b**), cohesive cell sheets with nuclear grooves and intranuclear cytoplasmic invaginations (**c**), stringy "bubble-gum"-like colloid (**d**), and psammoma bodies (**e**). Ultrasound features of papillary carcinoma (**f–o**) include nodule(s) of variable size, usually solid echotexture with incomplete halo, hypoechogenicity, irregular lobulated (**f**, **h**) and spiculated (**g**, *arrow*) margins, micro-, macro-, or interrupted eggshell calcifications (**i**, **j**, and **k** *arrow*), and variable blood flow on Doppler examination (**l**, **m**, **o**). Hyperechogenicity may be seen in rare cases accompanied with chaotic internal vascularity on Doppler examination (**n–o**) (**a**, Papanicolaou stain, low power; **b**, DiffQuik stain, low power; **c** and **e**, Papanicolaou stain, medium power; **d**, DiffQuik stain, medium power)

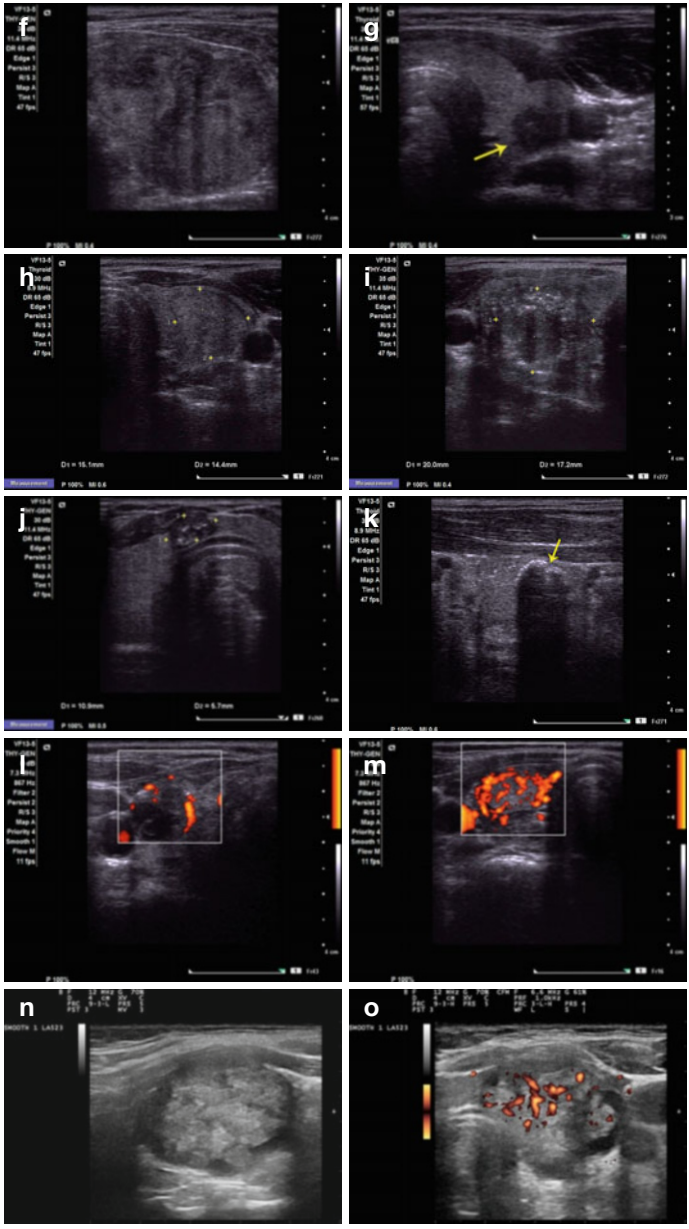

FIGURE 3.40 (continued)

Enlarged oval or irregularly shaped nuclei with longitudinal linear groves, intranuclear cytoplasmic invaginations, powdery clear chromatin, and small, eccentrically placed nucleoli are characteristic diagnostic nuclear findings. The background may show stringy, ropy, "bubble-gum"-like colloid and variable numbers of macrophages and lymphocytes. Psammoma bodies and multinucleated giant cell may also been seen.

None of the mentioned features is specific of PTC, and the FNA diagnosis is based on a conjunction of cytologic, architectural, and background features. Intranuclear cytoplasmic invaginations, although crucial for the diagnosis of PTC, are not specific; they are also seen in medullary carcinoma, anaplastic carcinoma, and poorly differentiated carcinoma and rarely in benign thyroid nodules and chronic thyroiditis. Similarly, psammoma bodies can be seen in medullary carcinoma, goiter, and chronic thyroiditis.

In general, the cytoplasmic features including intranuclear cytoplasmic invaginations are best seen in Romanowsky-stained smears; in contrast, nuclear features are best appreciated with Papanicolaou and hematoxylin and eosin stains.

Specific architectural, cytoplasmic, nuclear, and background features characterize specific variants and will be addressed under the specific variant.

US features (Fig. 3.40f–o)

- A halo is seen in 15–30 % of cases, frequently incomplete, and represents encapsulation.
- Irregular margins and hypoechogenicity occur in 75–90 %. Hyperechogenicity is rare.
- Most have a solid composition (70 %); however 20–30 % are variably cystic and even purely cystic in rare instances.
- Microcalcifications or microreflectors are seen in 25–45 %. Coarse and eggshell calcifications are less common.
- Multifocality occurs in 10–20 % of cases. Associated microcarcinomas are more common.
- Increased vascularity is almost always seen, but is not specific. Probably low vascularity has a good negative predictive value for a given nodule.
- In summary, papillary thyroid carcinomas may be solid and hypoechoic, with microcalcifications; blurred, irregular,

and lobulated margins; lack of a complete halo; and high intranodular blood flow on power Doppler.
- Invasion of adjacent tissue may be present.
- Lymph node metastasis may be seen with calcifications or cystic degeneration.

Variants of PTC

All share similar nuclear features, and the prognosis may be different when compared with the conventional type. However, the initial surgical approach is usually similar.

Follicular Variant

The follicular variant represents approximately 30 % of PTCs in some series. The prognosis is similar to that of the classical variant.

Histopathology. This variant shows an entirely or almost entirely microfollicular pattern with nuclear features diagnostic of papillary thyroid carcinoma. An abortive papilla, psammoma bodies, and dense eosinophilic colloid support the diagnosis. Associated minor histologic patterns of this variant include solid and macrofollicular ones, both with nuclear features of classical PTC and with well-differentiated features. Follicular variant of PTC is further sub-categorized in encapsulated and invasive.

Molecular profile. RAS mutation and *PAX8/PPARγ* rearrangement have been identified in the encapsulated follicular variant of PTC. *BRAF* and *RAS* mutations and *PAX8/PPARγ* rearrangement have been found in the nonencapsulated/invasive follicular variant of PTC. The *PAX8/PPARγ* rearrangement may be associated with angio-invasiveness.

FNA findings (Fig. 3.41a–c). The smear pattern is that of a microfollicular neoplasm with variable numbers of cells showing nuclear features of PTC. However, nuclear findings are usually inconspicuous, including intranuclear cytoplasmic invaginations and nuclear grooves. Occasional sheets of cells of normal size are also seen. Dense colloid may be seen in the

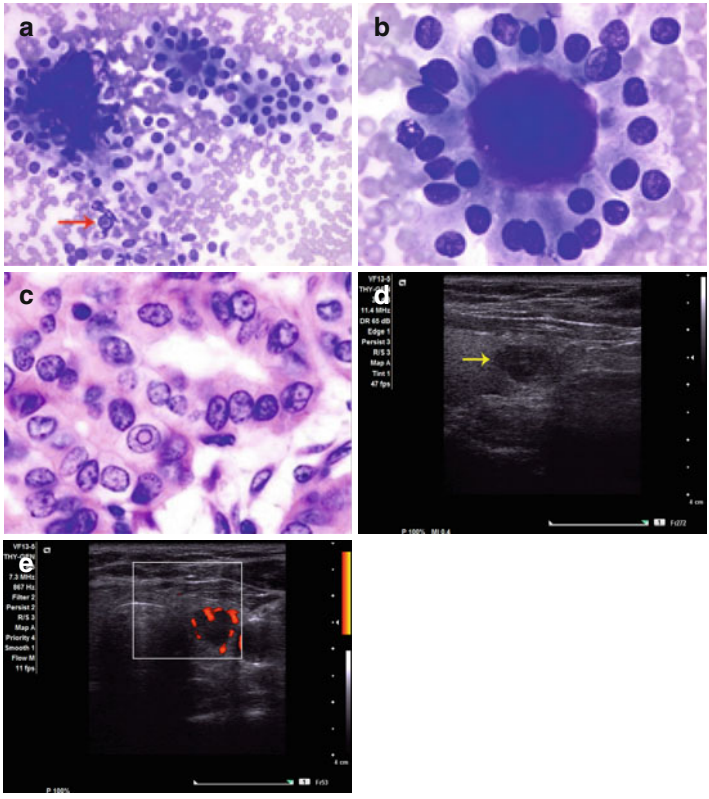

FIGURE 3.41 Papillary thyroid carcinoma, follicular variant. FNA smear shows high cellularity (**a**) with microfollicles containing central dense colloid (**b**) and rare intranuclear cytoplasmic invaginations (**a**, *arrow*) recapitulating tissue section findings (**c**). Ultrasound features are not specific and include a hypoechoic solid nodule with irregular infiltrating margins (**d**, *arrow*), focal fuzzy edges, and Grade 2 blood flow by Doppler examination (**e**) (**a**, **b** Diff-Quik stain, high power; **c**, hematoxylin and eosin stain, high power. Courtesy of Dr. Javier Saenz de Santamaria, Badajoz, Spain)

background and in the follicular lumens. Unless diagnostic nuclear features are seen, the USG-FNA diagnosis is usually "follicular neoplasm," with a note addressing the various entities included in the differential diagnosis.

US features (Fig. 3.41d, e)

- The follicular variant of PTC often has a benign US appearance, i.e., ovoid to round and iso- to hyperechoic, with a halo.
- Hypoechoic in 50 % of cases.
- Solid and regular or irregular, well-defined margins.
- A minority of tumors (5 %) are taller than wide.
- Microcalcifications are rare.

Macrofollicular Variant

Histologically, more than 50 % of the follicles are arranged as macrofollicles.

FNA findings (Fig. 3.42). The smears are cellular and show sheets of cells of variable size and thin colloid, which, at low power, resemble the findings of a benign thyroid nodule. The nuclear diagnostic features of PTC must be evaluated at high microscopic power. However, similarly to the follicular variant, the nuclear features are often inconspicuous.

Diffuse Sclerosing Variant

This variant occurs commonly in young women, and cervical lymph node and lung metastases are more common than in the classic variant of PTC, conferring a less favorable prognosis.

Histopathology. There are diffuse involvement of one or both thyroid lobes, extensive solid foci, squamous metaplasia, fibrosis, a marked lymphocytic infiltrate, numerous psammoma bodies, and vascular permeation.

Molecular profile. RET/PTC rearrangement has been identified, but *BRAF* mutations are rare.

FNA findings (Fig. 3.43a, b). Smears may be modestly cellular and show numerous psammoma bodies along with cytologic features of PTC, including sheets of follicular cells with pleomorphic nuclear enlargement, irregular nuclear membranes, grooves, and intranuclear cytoplasmic invaginations

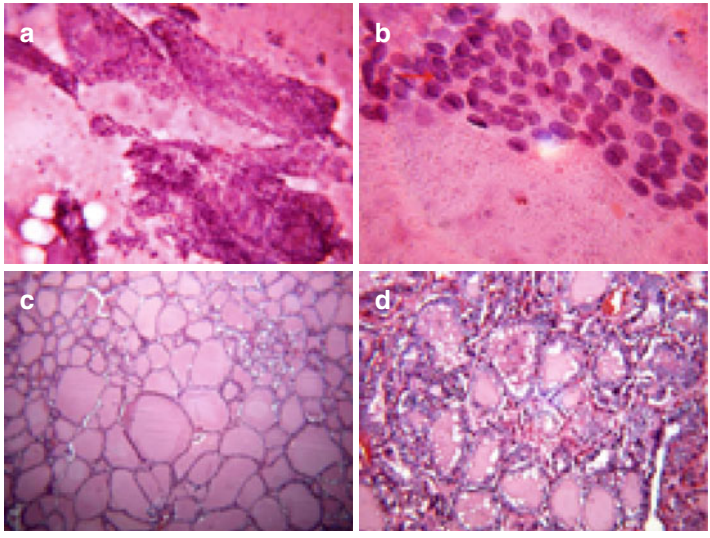

FIGURE 3.42 Papillary thyroid carcinoma, macrofollicular variant. FNA smear shows large cell sheets and colloid, findings that at low magnification resemble those of benign thyroid nodule (**a**). Nuclear hypochromasia, grooves, and rare intranuclear cytoplasmic invaginations (**b**, *red arrow*) are seen at high magnification. Similarly, the histologic examination requires careful search for nuclear features of papillary carcinoma (**c**, **d**). (**a**–**d**, hematoxylin and eosin stain)

commonly present in a background of chronic thyroiditis. Squamous metaplastic cells may be seen.

US features (Fig. 3.43c, d)

- Large, heterogeneous solid tumors with irregular margins often involving one entire thyroid lobe diffusely; the involvement may be bilateral.
- There is hyper- or hypoechogenicity.
- Scattered microcalcifications are present ("snowstorm" pattern), most commonly diffuse and rarely focal.
- Metastatic cervical lymph nodes are almost always present.

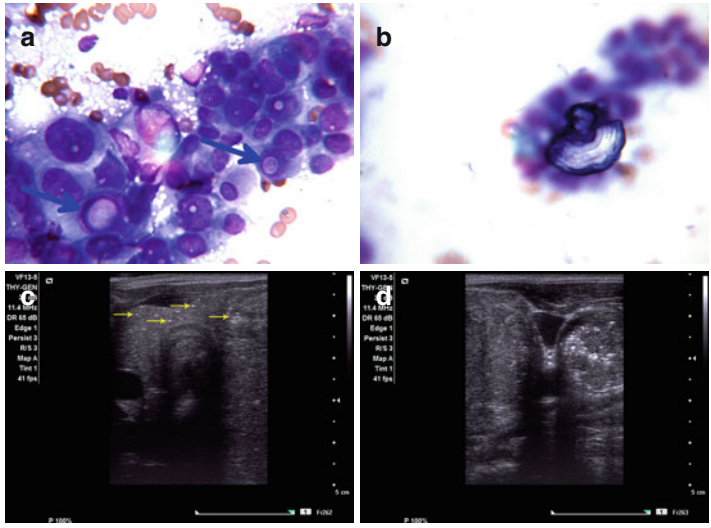

FIGURE 3.43 Papillary thyroid carcinoma, sclerosing variant. FNA smears show cytologic features of papillary carcinoma including complex cellular aggregates and intranuclear cytoplasmic invaginations (**a**, *blue arrows*), and numerous psammoma bodies (**b**). Ultrasound shows numerous diffuse microcalcifications scattered in the thyroid parenchyma (**c**, *arrows*), a large left thyroid lobe iso- to hyperechoic mass (**d**, *left side of frame*), and lymph node metastasis (**d**, *right side of frame*) both with numerous diffuse microcalcifications ("snowstorm" pattern). (**a**, **b** MGG stain, high power view)

Cystic Variant

This variant occurs in 5 % of PTCs, and the associated lymph node metastases are often cystic.

Histopathology. The amount of cystic change varies, and most retain a papillary architecture.

FNA findings (Fig. 3.44a, b). Smears show a background of abundant thin, watery fluid, numerous macrophages with variable cytoplasmic hemosiderin, and tumor cells often with vacuolated cytoplasm ("histiocytoid" cells).

The epithelial component may be inconspicuous but usually shows sufficient diagnostic criteria for diagnosis. Cells may be arranged in small aggregates, papillae, and small

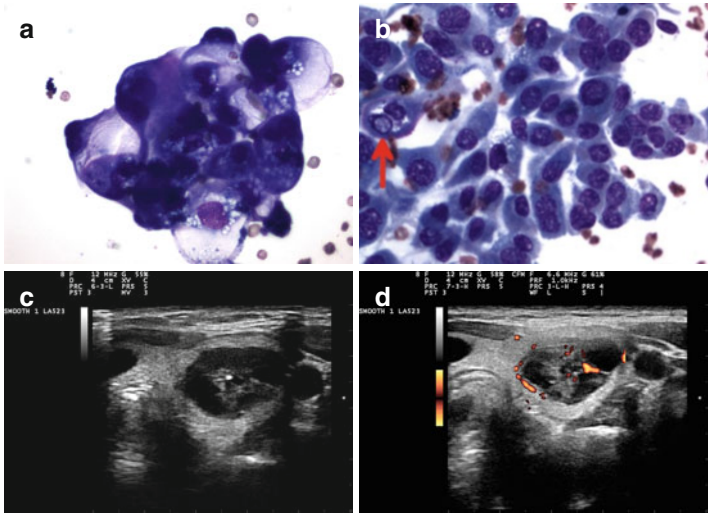

FIGURE 3.44 Papillary thyroid carcinoma, cystic variant. FNA smear shows aggregates of large cells with ballooned cytoplasm containing large vacuoles ("histiocytoid cells") in a background of watery fluid (**a**). Occasional intranuclear cytoplasmic invaginations are seen in the metaplastic cells (**b**, *red arrow*). Ultrasound shows a predominantly cystic complex nodule with a bright dot corresponding to the 27-gauge needle tip in the solid component (**c**); blood flow by Doppler examination is evident in the solid portion (**d**). (**a**, **b** MGG stain, high power)

follicles. Cyst-lining epithelium and metaplastic cells may be present. This variant should be kept in mind in cases showing a dominant or entirely cystic and/or hemorrhagic smear pattern.

US features (Fig. 3.44c, d)

- Cystic tumors are often taller than wide and have spiculated margins.
- A solid hypervascular nodule is almost always seen in the cyst wall.
- A "comet-tail" sign can be observed, particularly in cystic metastases to lymph nodes.
- Microcalcifications may be seen in the solid component.

Oncocytic Variant

The growth pattern may be papillary or follicular. In this variant, the cells are polygonal and have abundant granular eosinophilic cytoplasm and nuclear features of PTC. The subvariant showing heavy lymphocytic infiltrate in the papilla is named the Warthin-like variant of PTC and has *BRAF* mutations and *RET/PTC* rearrangements. The prognosis is similar to that of the classic PTC.

FNA findings. Smears are variably cellular and show a predominance of oncocytic cells arranged in papillae, in sheets, or as isolated cells with nuclear changes of PTC. The background shows rare or no lymphocytes (Fig. 3.45a).

When a papillary architecture is prominent and lymphoid cells are numerous, a Warthin-like variant must be considered (Fig. 3.45b–e). When lymphocytes are absent, the differential diagnosis includes Hurthle cell neoplasms. Thus, this variant should be searched for when the smear pattern shows a predominance of Hurthle cells. However, if lymphocytes are present, the Warthin-like variant may be overlooked and the tumor diagnosed as Hashimoto's thyroiditis. Of note, nucleoli are more prominent in Hashimoto's thyroiditis than in any of the Hurthle-cell-rich variants.

Tall-Cell Variant

This tumor tends to occur in elderly people, particularly men. The course is aggressive and often presents as a bulky tumor with extrathyroidal extension and often lymph node metastasis.

Histopathology. The growth pattern is papillary and the cells are "tall" (three times taller than wide), the cytoplasm is eosinophilic, and the nuclear features are those of PTC.

Molecular profile. The tumor expresses a *BRAF* V600E mutation in 80 % of cases and has been associated with *RET/PTC3* translocation.

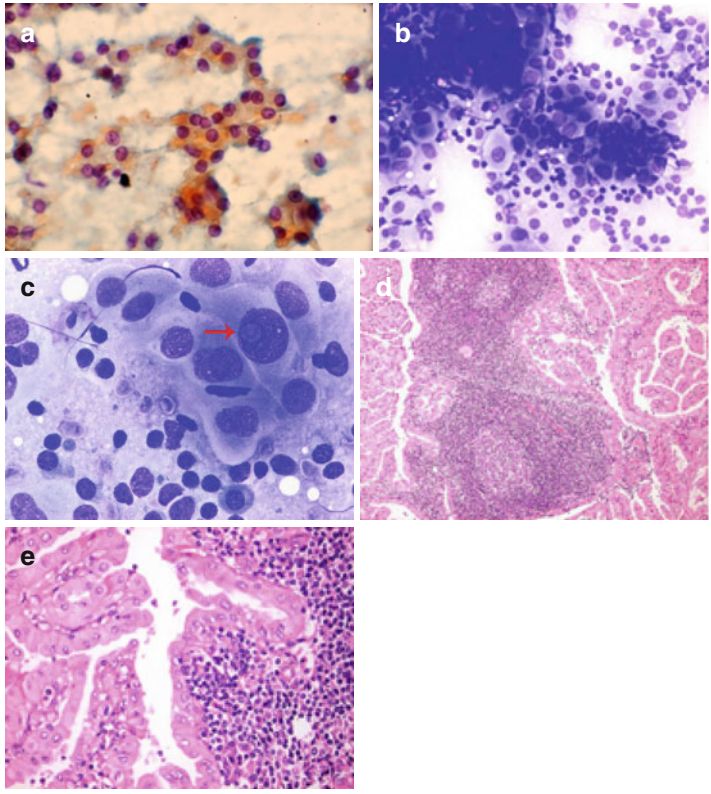

FIGURE 3.45 The smears of the papillary thyroid carcinoma, oncocytic variant, show small sheets and circumferential aggregates of cells with eosinophilic cytoplasm, nuclear features of papillary carcinoma, and lack of lymphoid cells (**a**). The smears of the papillary thyroid carcinoma, Warthin's subtype, show aggregates of large cells exhibiting eosinophilic granular cytoplasm and nuclear features of papillary carcinoma including intranuclear cytoplasmic invaginations (**c**, *arrow*) in a background of numerous lymphocytes and plasma cells (**b**, **c**). Histologic sections confirm the diagnosis (**d**, **e**). (**a**, Papanicolaou stain, medium power; **b**, Diff-Quik stain, medium power; **c**, Diff-Quik stain, high power; **d**, **e**, hematoxylin and eosin stain, low and medium power. Courtesy of Dr. Javier Saenz de Santamaria, Badajoz, Spain)

FNA findings. Smears show papillary fragments with no nuclear pseudostratification and tall tumor cells (three times taller than wide) showing cytoplasmic eosinophilia and nuclear features of PTC, including multivacuolated/septated ("soap bubble like") intranuclear cytoplasmic invaginations.

US features

- Microlobulated markedly hypoechoic nodules with microcalcifications
- Extrathyroidal extension

Columnar Cell Variant

The columnar cell variant of PTC is an aggressive and rare neoplasm.

Histopathology. The architecture is papillary and shows prominent nuclear pseudostratification, which is reminiscent of that of the endometrium. The nuclei are oval and hyperchromatic with supra- or subnuclear cytoplasmic vacuoles.

FNA findings (Fig. 3.46). Cells are arranged in aggregates, sheets, and papillae and show clear cytoplasm and nuclear pseudostratification. The nuclear features of PTC, such as nuclear grooves and intranuclear cytoplasmic invaginations, are focal and less prominent, the nuclei show hyperchromasia, and colloid and cystic changes are typically absent. Mitoses can be found. These features may be a factor in not making an accurate diagnosis.

Cribriform–Morular Variant

The architecture of this tumor shows cribriform and morular formations, as the name implies. There is nuclear clearing, but distinct nuclear features for PTC are absent. Nuclei stain positively for β-catenin. The diagnosis may lead to early detection of associated polyposis coli.

FNA findings. Smears are cellular with elongated cells arranged in papillary aggregates, a cribriform pattern, and morules. Cells exhibit nuclear clearing. The background shows macrophages, but colloid is absent.

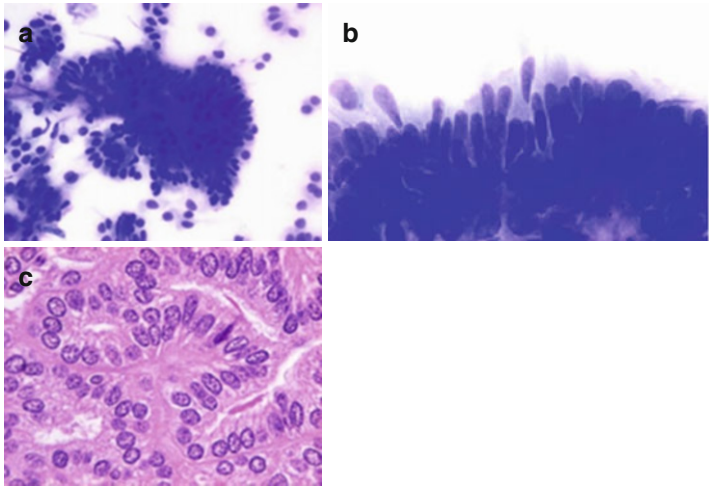

FIGURE 3.46 Papillary thyroid carcinoma, columnar cell variant. Smears show complex cellular aggregates and pseudopapillary structures composed of elongated cells with slight clear cytoplasm and pseudostratification reminiscent of that of the endometrium (**a**, **b**). This cell pattern correlates with the tumor tissue sections (**c**) (**a**, **b** Diff-Quik stain medium and high power. **c**, hematoxylin and eosin stain, medium power. Courtesy of Dr. Javier Saenz de Santamaria, Badajoz, Spain)

Thyroid Cancer Recurrences

These usually occur in the thyroid bed. Lymph node metastasis can also occur, often in neck compartments III, IV, and VI. USG-FNA is required for exclusion of a nonneoplastic process such as a fibrous nodule, a suture-related foreign body-type granulomatous reaction, etc. (Fig. 3.47).

US features

- Nodules of recurrent thyroid cancer in the thyroid bed are often hypoechoic, irregular, and vascular. Hyperechogenicity may correlate with fibrosis.

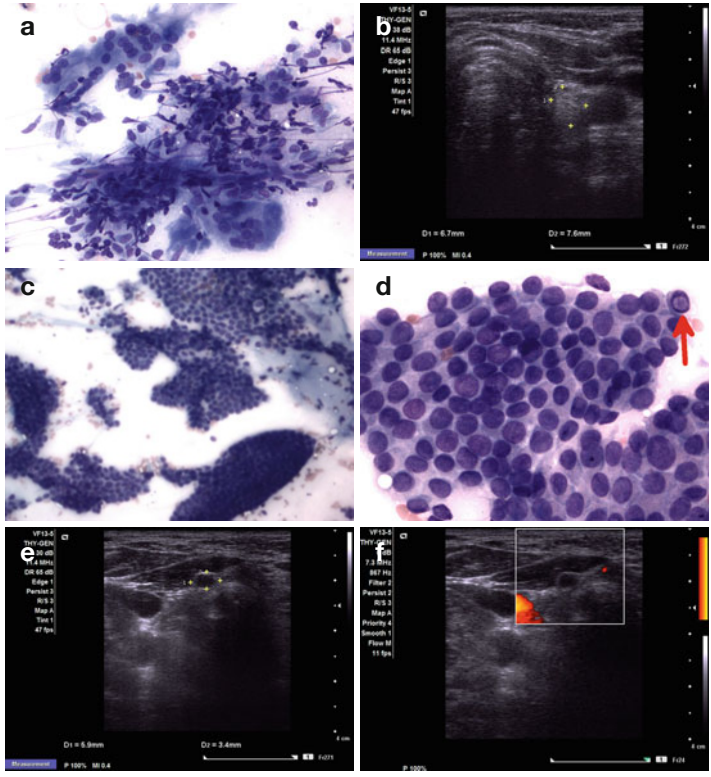

FIGURE 3.47 Thyroid bed nodules. Granulation tissue and foreign body-type giant cell reaction is noted in this benign nodule (**a**). The patient had thyroidectomy for PTC 15 years before and the US evaluation shows a slightly hyperechoic nodule (**b**). Recurrent PTC was the diagnosis in the smears obtained from this 0.6-cm hypoechoic, round, well-circumscribed, and bulging nodule (**c–e**). An intranuclear cytoplasmic invagination is seen in figure **d** (*red arrow*). Doppler examination showed no vascular blood flow (**f**). (**a**, **c**, **d** MGG stain, medium and high power)

Lymph Node Metastasis in PTC

Lymph node metastases of PTC are present in 50 % of cases at diagnosis and may be the first manifestation of the carcinoma in up to 20 %. Ninety percent are micrometastases to

neck lymph nodes and do not influence disease-free survival. Close to 90 % of lymph node metastases involve the level VI compartment, regardless of involvement of other compartments. Pure solitary lymph node cystic metastases are seen particularly in patients under the age of 35 years.

Surgical management is altered in the presence of neck US-visible metastases, and patients undergo central or lateral neck dissection and total or near-total thyroidectomy for improved survival. Lymph node detection by other imaging modalities (CT, MRI, PET) is not recommended by ATA guidelines. US has limited resolution in evaluation of the level VI compartment, particularly posterior tracheal and tracheoesophageal groove lymph nodes.

USG-FNA of lymph nodes should include cytology and needle rinses for thyroglobulin level measurements in all cases of differentiated thyroid cancer. Suspicious lymph nodes less than 5–8 mm in the greatest diameter may be followed by US; if the node grows or threatens vital structures, USG-FNA should be performed.

FNA findings (Fig. 3.48a, d, f, g). Because lymph node metastases may show variable degrees of cystic degeneration, the FNA shows characteristic features of PTC and variable numbers of macrophages. Pure solitary lymph node cystic metastases show macrophages only, and they must be considered in the differential diagnosis of congenital neck cysts such as branchial cleft cyst, particularly when there is no US-visible primary thyroid malignancy. High thyroglobulin levels in the aspirated fluid help in the diagnosis. Cystic metastatic squamous cell carcinoma, although uncommon in young patients, should also be included in the differential diagnosis.

The differential diagnosis of an enlarged lymph node includes primary hematolymphoid processes, metastasis other than from the thyroid, and lymphoid hyperplasia secondary to an inflammatory or infectious process, including sarcoidosis and other granulomatous processes.

US features (Fig. 3.48b, c, e, h, i). While not limited to PTC, US features that suggest metastatic malignancy to a lymph node include loss of fatty hilum, rounded rather than oval shape, marked hypoechogenicity, cystic change,

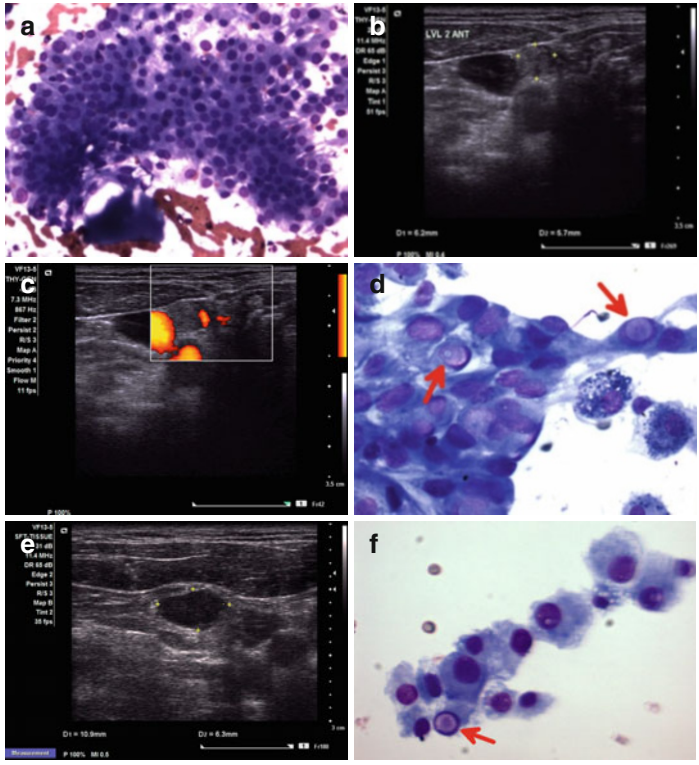

FIGURE 3.48 Differentiated thyroid cancer metastatic to neck lymph nodes. A complex aggregate of bland-appearing epithelial cells with oxyphilic change (**a**) were seen in the smears obtained from a 0.6-cm right level II heterogeneous and slightly hyperechoic lymph node with focal peripheral vascularity (**b**, **c**) 22 years after having total thyroidectomy for thyroid carcinoma. An aggregate of metaplastic-appearing cells with intranuclear cytoplasmic invaginations (*arrows*) and macrophages (**d**) were obtained from a 1.1-cm hypoechoic cystic cervical lymph node with irregular and fuzzy margins (**e**, radio 3–6) in a patient with history of PTC. Large cells with vacuolated cytoplasm, intranuclear cytoplasmic invaginations (**f**, *arrow*), and psammoma bodies (**g**) were obtained from a patient with history of PTC. The US of the neck showed a level IV 1.8-cm heterogeneous mass with lobulated and fuzzy margins and slight central blood flow by Doppler examination (**h**, **i**). (**a**, **d**, **f** MGG stain, high power; **g**, Papanicolaou stain, medium power)

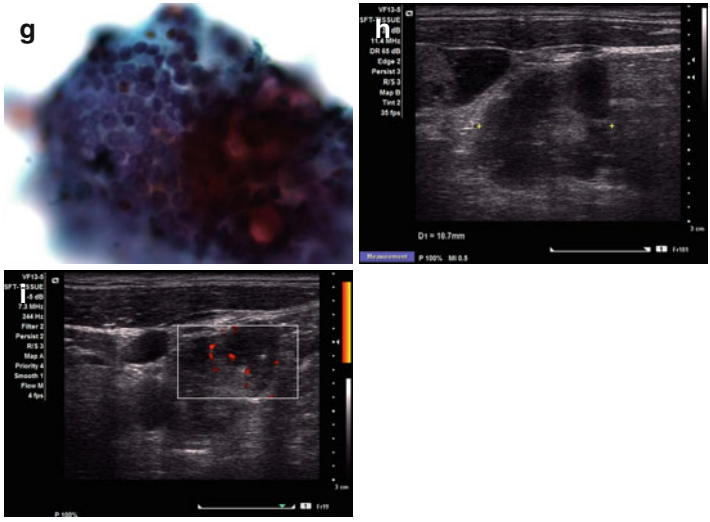

FIGURE 3.48 (continued)

microcalcifications, and increased vascularity. Nodal metastasis may show the following US characteristics:

- They are located in the middle and lower jugular chains (compartments III and IV) and ipsilateral in 70–85 %. Pre- and paratracheal nodes (compartment VI) are also common but less often found at US.
- They have absent echogenic hilum. A hilum may be seen in reactive lymph nodes; however, it is not seen by US in reactive nodes less than 5 mm in diameter.
- They have a round (anteroposterior/transverse ratio >0.5 in the transverse view) appearance instead of flattened or oval shape <0.5.
- They have well-defined margins.
- They have a chaotic (central and peripheral) vascularity.
- They have a marked hypoechogenicity.
- They have microcalcifications in 50 % and mainly seen in solid metastases. Dense macrocalcifications or entirely calcified lymph nodes may be seen post ^{131}I therapy.

- Variable cystic degeneration is seen in 20–50 %. Pure solitary cystic metastasis, although rare, is seen particularly in young patients.
- Features such as size and well-defined borders are less important than morphology.

Medullary Thyroid Carcinoma

Medullary carcinoma arises from the neuroendocrine calcitonin-secreting parafollicular or "C" cells found in the middle to upper third of the lateral thyroid lobes, accounts for approximately 3–7 % of thyroid carcinomas, and can be sporadic (75 %) or heritable (25 %). The heritable form may be a part of multiple endocrine neoplasia [MEN 2A (pheochromocytoma and hyperparathyroidism), MEN 2B (pheochromocytoma, mucosal neuromas, gastrointestinal ganglioneuromatosis, and marfanoid habitus)] or be isolated, with no other tumors (familial medullary carcinoma syndrome). Medullary carcinoma is likely to be present when the serum calcitonin level is >10 pg/mL. Ultrastructurally, "C" cells contain neurosecretory dense-core granules.

Clinical findings. Patients with sporadic medullary carcinoma are in the fifth decade of life or older, and they almost always have a solitary tumor. The heritable form is autosomal dominant with virtually complete penetrance and is more aggressive than the sporadic form, affects young patients usually in the first three decades of life, and is often multiple and bilateral.

Medullary carcinoma is an aggressive tumor that spreads through hematogenous and lymphatic channels. Most patients have regional cervical and mediastinal lymph node and/or distant organ metastases (bone, liver, and lung) at diagnosis. The only effective treatment is total thyroidectomy and radical neck dissection and only before metastatic dissemination. The tumor does not respond to chemotherapy, radioactive iodine, or radiotherapy. Poor prognostic factors include old age and an advanced tumor stage at diagnosis. The 5-year survival rate is 75 %.

Thyroid US screening should be performed only in patients with *RET* proto-oncogene mutations and no clinical evidence of thyroid disease.

Histopathology. Medullary carcinoma is usually, but not always, invasive and may present as firm encapsulated masses. The heritable forms may be multifocal. The classic tumor shows a solid proliferation of round to polygonal cells with granular cytoplasm, vascular stroma, hyalinized collagen, and amyloid. The architectural pattern may be trabecular, carcinoid-like, paraganglioma-like, neuroblastoma-like, angiosarcoma-like, papillary, pseudopapillary, or glandular. The cytomorphology is also highly variable. Calcifications may be present, and true psammoma bodies may be identified.

Immunoprofile. Tumor cells are positive for keratin, CEA, TTF-1, chromogranin, synaptophysin, and calcitonin and negative for thyroglobulin. Cells also express BCL2 and MYC. Hurthle cells that may resemble medullary carcinoma cells stain positively for thyroglobulin and negatively for calcitonin and chromogranin.

Molecular profile. Activation of the *RET* proto-oncogene by point mutations located on chromosome segment 10p11.2 is seen in 95 % of heritable and 50 % of sporadic forms of medullary carcinoma (Fig. 3.49). It is known that clinical behavior varies according to the germline and somatic *RET* mutations. The three forms of MEN2 (A, B, and familial) have specific activating point mutations in the *RET* proto-oncogene. MEN2A often carry *RET* mutations in codon 634 encoding cysteine and have high risk of lymph node metastasis and often affect patients by age 20 years. Most MEN2B patients have *RET* mutation in exon 16 that is found as a germline mutation and correlates with an aggressive disease. Familial forms carry mainly *RET* mutations in codons 609, 611, and 618 as well as in the intracellular exons 13 and 15. Of note, screening of at-risk family members for medullary carcinoma should be done by testing for germline mutations in the *RET* proto-oncogene. This screening may also detect MEN2 in 5 % of sporadic medullary carcinoma cases, and these patients may benefit from prophylactic total thyroidectomy.

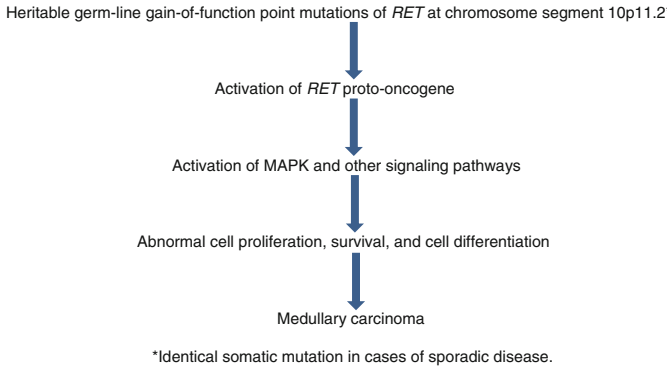

FIGURE 3.49 *RET* in medullary carcinoma (95 %)

Recently, *PROM1* gene has been found to be significantly overexpressed in aggressive medullary carcinoma associated with *RET* M918T mutation that confers resistance to therapy; thus, decrease in *PROM1* expression opens a venue for targeted therapy at this level.

FNA findings (Fig. 3.50a–g). Smears are moderately to highly cellular, showing cell aggregates and numerous single cells with ill-defined cytoplasmic borders and mild to moderate pleomorphism. Cells may be spindle, cuboidal, plasmacytoid, oncocytic, squamoid, clear, small, giant multinucleated, pleomorphic, pigmented, or melanin producing. Again, the architecture and cytomorphology are highly variable.

Neuroendocrine features are present and include plasmacytoid cells, red cytoplasmic granules seen with Romanowsky stains, "salt-and-pepper" chromatin, inconspicuous nucleoli, binucleation, and ill-defined cytoplasmic borders. Nuclei are round and eccentric. Amyloid is present in most cases as dense amorphous "puffy cloud"-appearing matter in the background. Intranuclear cytoplasmic invaginations are present in 50 % of cases. Cytoplasmic vacuoles and psammoma bodies may be present, although rarely.

Calcitonin levels in needle rinses can be used in selected cases; a very high level, usually >80 pg/ml, is diagnostic of medullary carcinoma.

The differential diagnosis includes PTC, hyalinizing trabecular tumor, Hurthle cell neoplasms, anaplastic carcinoma, and metastases including melanoma, among others. Cytomorphology including nuclear and nucleolar features, calcitonin levels in needle rinses and serum, and judicious uses of immunohistochemistry are helpful. Calcitonin immunostain and Congo-red stain for amyloid can be made in cytology smears and cell block.

US features (Fig. 3.50h–j). A solid hypoechoic mass with dense and coarse echogenic calcific foci is present in 80–90 % of cases, representing amyloid with associated calcifications, and these may have a posterior acoustic shadowing.

- Involvement is localized in the mid- to upper third of the thyroid lobe in the early sporadic form and diffuse and/or bilateral in the familial type.
- Disorganized and chaotic hypervascularity, predominantly Grade 3 pattern, is present.
- Cervical and mediastinal lymph node metastases are hypoechoic, with echogenic foci similar to those of the primary tumor. Cystic change is rare.

FIGURE 3.50 Medullary thyroid carcinoma. The smears show characteristic features including high cellularity (**a**, **b**), cellular pleomorphism with aggregated and dissociated cuboidal, multinucleated, spindle, and plasmacytoid cells exhibiting hyperchromasia; lack of nucleoli; and granular ("salt-and-pepper") chromatin (**c**–**e**). Variable numbers of intranuclear cytoplasmic invaginations (**f**) may be present resembling PTC. The finding of fine cytoplasmic metachromatic granules supports the diagnosis (**d**). The smear background shows amyloid in variable amounts and textures (**a**, **g**), which may be identified by Congo-red stain in cytology preparations and evaluated under polarized light (**g**). Binucleation with a distinct nuclear disposition (**c**, *circle*) is often seen. The US often shows a large hypoechoic mass with irregular borders, ill-defined margins, variable calcific foci, and high vascularity. One case shows a large ill-defined slightly hyperechogenic mass (**h**, *arrow*); a different case shows a 2.2-cm oval mass invading the surrounding thyroid parencyma (**i**, *left upper* and *right lower borders*), microcalcifications (*arrows*), and a peripheral and intranodular vascular pattern by Doppler examination (**j**). (**a**, **e** Papanicolaou stain, low and high power; **b**–**d**, **f**, **g** Diff-Quik stain, high power; **g**, Congo-red stain, high power) (**b**–**d**, **g** Courtesy of Dr. Javier Saenz de Santamaria, Badajoz, Spain)

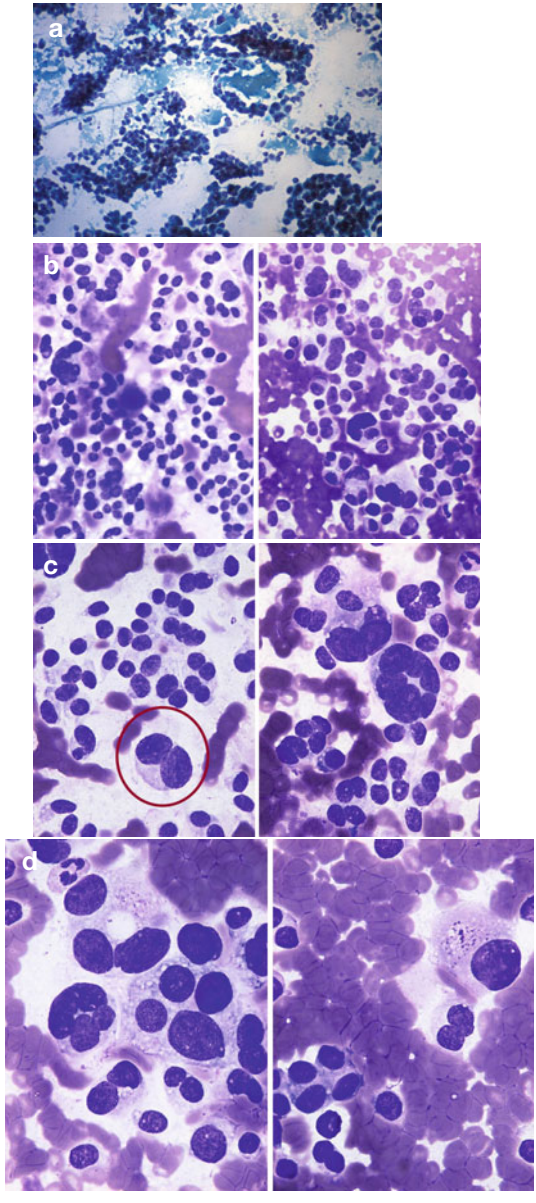
a
b
c
d

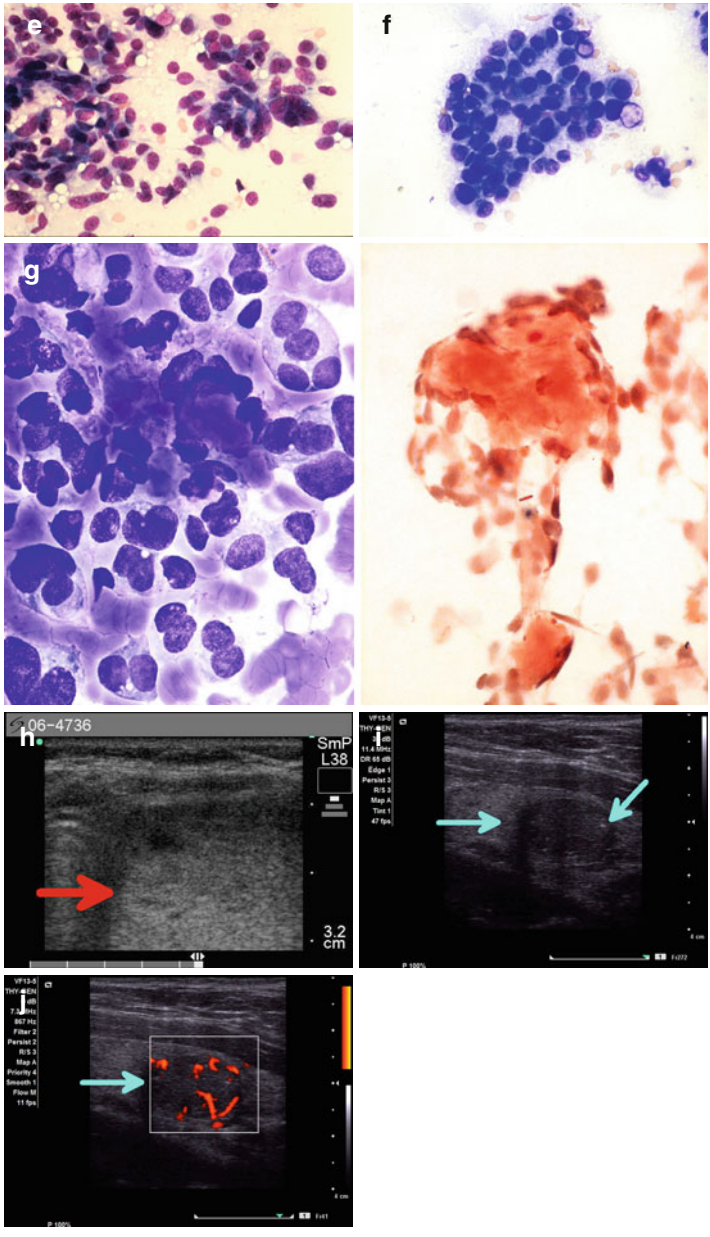

FIGURE 3.50 (continued)

Poorly Differentiated Carcinoma

Poorly differentiated carcinoma is a rare thyroid malignancy (5 %) that falls between DTCs (papillary, follicular, and Hurthle) and undifferentiated (anaplastic) carcinoma. The clinical behavior is aggressive and also falls between DTC and anaplastic carcinoma. The mean 5-year survival rate is 50 %. The definitive diagnosis is made histologically.

Clinical findings. Poorly differentiated carcinoma occurs in patients older than those with the DTCs and often presents at an advanced stage, recurs locally, and metastasizes to the cervical lymph nodes and distant organs, particularly the lung and bones.

Histopathology. Tumor cells are small and uniform and form a characteristic nesting growth pattern surrounded by a delicate rim of stroma (insular type). Solid and trabecular patterns are also present (noninsular type). Variable mitoses and necrosis are present. Occasionally, DTCs may show focal poorly differentiated features.

Immunoprofile. The tumor shows positivity for thyroglobulin and TTF-1. Calcitonin and CEA are negative. Often there is focal weak positivity with neuroendocrine markers.

Molecular profile. Molecular alterations include those seen in differentiated thyroid carcinomas *(BRAF* and *RAS* mutations) and those of poorly differentiated carcinomas (*TP53* mutation in 40 % and *CTNNB1* mutation in 30 %, with expression of p53 and β-catenin by immunohistochemistry, respectively). *RAS* mutation is seen in 20–50 % of cases and *PAX8/PPARγ* translocation in 7 %.

FNA findings (Fig. 3.51a–g). The smears show high cellularity, a nesting (insular) and trabecular pattern, and often necrosis. The smear pattern is usually homogeneous; however, some cases show cell pleomorphism. In the pure form, cells lack features of PTC and have scant cytoplasm, a high nuclear to cytoplasmic ratio, small round or convoluted nuclei, and hyperchromasia. The nuclei may show a "salt-and-pepper" chromatin, inconspicuous nucleolus, and mild atypia in some cases. The architecture, marked crowding, dissociated cells, and a high nuclear to cytoplasmic ratio are helpful for the diagnosis. However, the FNA diagnosis in most cases is either carcinoma including PTC (25 %) or follicular neo-

plasm (45 %), and the specific diagnosis is made in 30 %. A microfollicular, papillary, or Hurthle cell pattern may be seen when there is a DTC component.

The differential diagnosis includes medullary carcinoma and metastases, particularly melanoma and hematolymphoid malignancies. Judicious use of immunohistochemistry and serum calcitonin levels is helpful. Of importance, TTF1 is positive in both poorly differentiated and medullary carcinoma. Anaplastic thyroid carcinoma shows marked cellular pleomorphism.

US features (Fig. 3.51h–j)

- Tumors are usually large and show US features of extrathyroidal extension.
- The shape is irregular and lobulated and has irregular indistinct borders.
- Heterogeneous echotexture and hypoechogenicity with areas of cystic necrosis are noted.
- A peripheral halo is absent.
- There is variable and chaotic vascularity; the viable areas are vascular.
- Cervical lymphadenopathy is common.

Undifferentiated (Anaplastic) Carcinoma

Clinical findings. Anaplastic carcinoma is a rare and highly aggressive malignancy with a poor prognosis that affects

FIGURE 3.51 Poorly differentiated carcinoma. Insular (**a**, **e**) and trabecular/microfollicular (**b–d**, **f**) patterns are seen in these tumors. Occasional cellular pleomorphism (**f**) is present. Immunostains for thyroglobulin and TTF1 are positive (**g**). Cytology and histology findings of this case of insular carcinoma show unequivocal correlation (**d**, **e**). Ultrasound exam shows a large odd-shaped, heterogeneous, and hypoechoic mass with irregular, angulated, and microlobulated margins invading the surrounding thyroid parenchyma and skeletal muscles (**h–j**). (**a**, **f**, Diff-Quik stain, low and high power; **b**, **c** MGG stain, medium and high power; **d**, **e** Diff-Quik and hematoxylin and eosin, high power; **g**, immunoperoxidase stain) (**a**, **d–g** Courtesy of Dr. Javier Saenz de Santamaria, Badajoz, Spain)

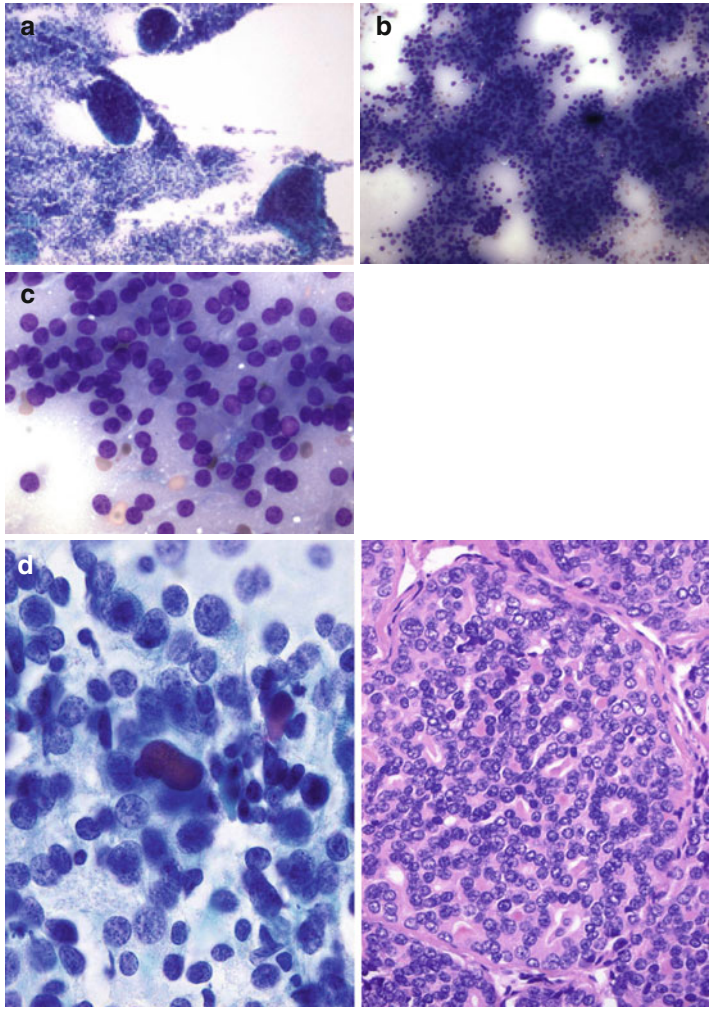
a
b
c
d

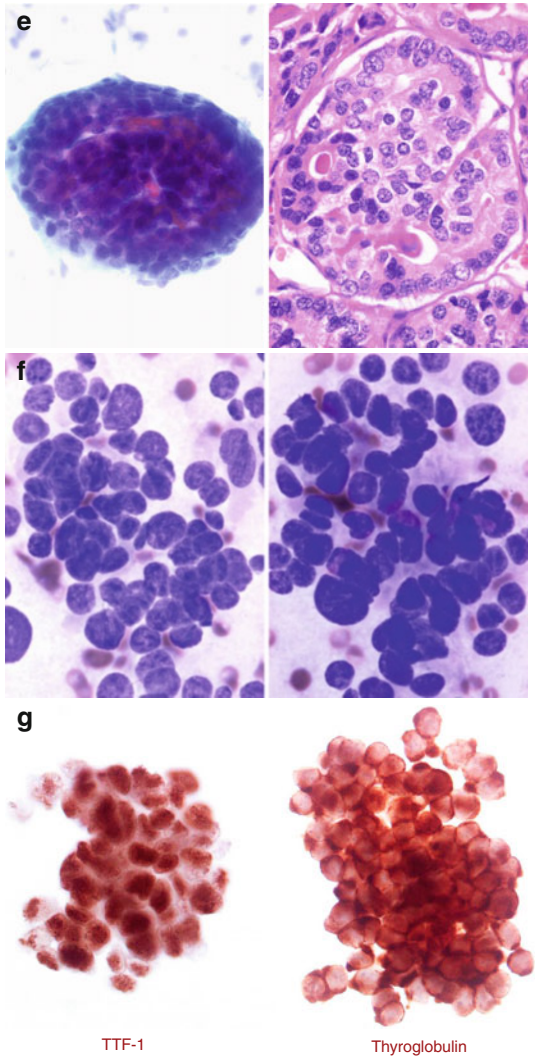

FIGURE 3.51 (continued)

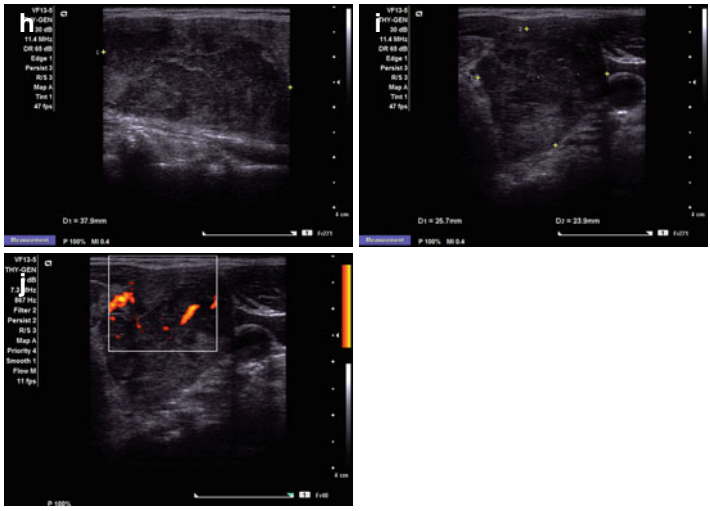

FIGURE 3.51 (continued)

middle-aged to elderly patients. Patients usually are euthyroid and have compressive and obstructive symptoms in the upper airways and esophagus. They may have recurrent laryngeal nerve palsy and neck pain resulting from local tumor invasion. The clinical and imaging differential diagnosis for this rapidly enlarging thyroid mass is non-Hodgkin lymphoma. The average survival rate is 9 months; patients usually die of compression of the aerodigestive tract.

Histopathology. Microscopically, there is a variety of features including squamoid cells; spindle cells; giant cells; osteoclast-like multinucleated giant cells; foci of neutrophilic infiltrate; foci of keratinization; bone, cartilage, and skeletal muscle differentiation; variable fibrosis and hyalinization; hemorrhage; and necrosis. A clear cell change may be seen as a result of glycogen accumulation.

Immunoprofile. Positivity for keratin is seen. Vimentin is also positive, particularly in the spindle cells; stromal positivity for laminin and focal positivity for CEA and EMA are seen in the squamoid type. Thyroglobulin and TTF-1 are usually negative.

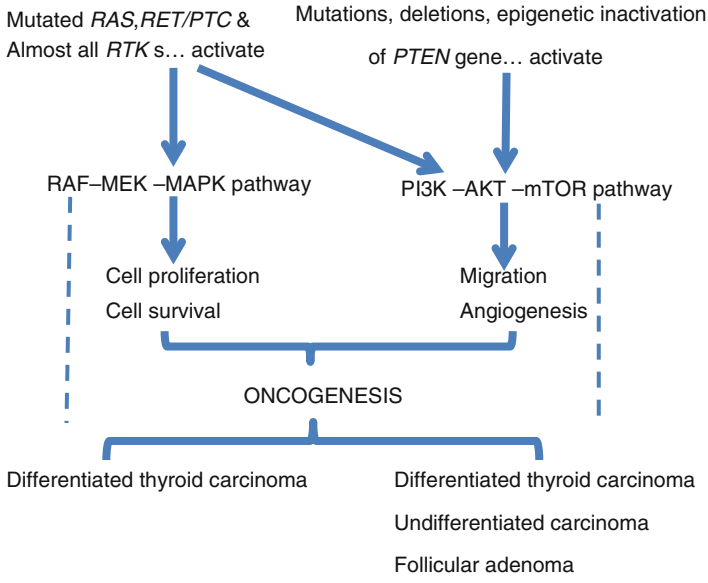

FIGURE 3.52 Synergistic signaling pathways

Molecular profile. The PI3K/PTEN/AKT pathway is altered (Fig. 3.52). The molecular alterations are similar to those seen in poorly differentiated carcinoma but occur with greater frequency. *TP53* mutations coding for p53 are seen in 50–80 % of cases. Mutation in the gene *CTNNB1* coding for β-catenin is found in 66 % of cases. *PIK3CA* and *PTEN* mutations are also observed in a minority of cases and frequently coexist with *RAS* and *BRAF* V600E mutations, suggesting an origin from and/or coexistence with DTC. *RET/PTC* and *PAX8/PPARγ* rearrangements are usually absent. Epithelial–mesenchymal transition [loss of E-cadherin (CDH1) expression due to activation of E-cadherin repressors] is accepted as a key mechanism in the development and progression of anaplastic thyroid carcinoma.

FNA findings (Fig. 3.53a–e). The FNA should avoid necrotic areas. Smears show high cellularity and highly pleomorphic malignant cells with nuclear enlargement, irregular nuclear membranes, clumped chromatin, macronucleoli, and

atypical mitoses. Cells may have squamoid features, be multinucleated (osteoclast type and bizarre), and have a spindle appearance. The background shows variable necrosis and scattered neutrophils.

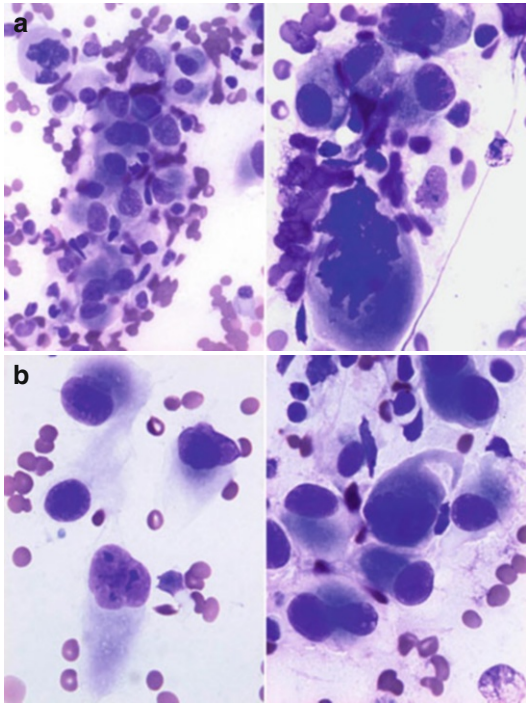

FIGURE 3.53 Undifferentiated (anaplastic) carcinoma. Smears show large single and multinucleated pleomorphic cells with atypical mitoses, variable amounts of cytoplasm, and a necrotic background with neutrophils both extra- and intracellular (**a**, **b**, **d**, **e**). A rhabdoid phenotype with dense cytoplasmic aggregates of intermediate filaments may be evident and show immunostain positivity for vimentin (**c**). Ultrasound in this particular case shows a large hypoechogenic mass with slight heterogeneous echotexture, slightly irregular, lobulated, and fuzzy borders with moderate vascularity by Doppler examination (**f**, **g**) (**a–c** Courtesy of Dr. Javier Saenz de Santamaria, Badajoz, Spain)

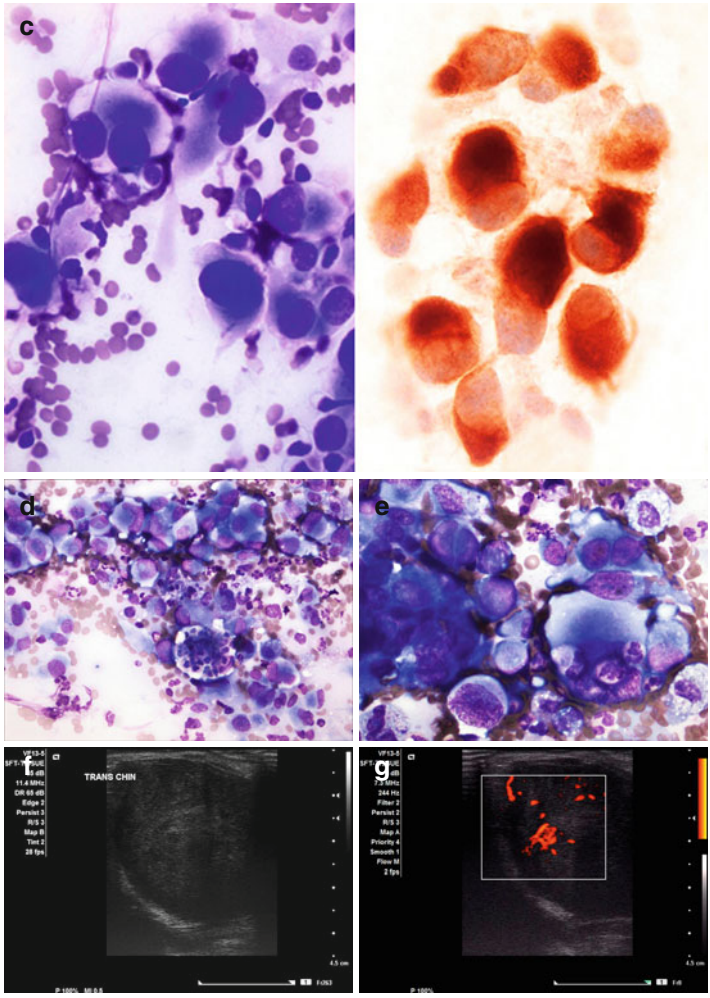

FIGURE 3.53 (continued)

The differential diagnosis includes metastases to the thyroid, particularly from lung, melanoma, and sarcomatoid renal cell carcinoma. Medullary carcinoma may be considered in cases with absent necrosis or multinucleated cells,

because they are almost always absent in medullary carcinoma. Again, judicious use of immunostains is helpful. We should emphasize that a diligent search of malignant cells should be conducted in hypocellular specimens so that a misdiagnosis of Riedel thyroiditis is avoided.

US features (Fig. 3.53f–g)

- Diffuse and usually large mass with heterogeneous and hypoechoic echotexture, frequently seen in a background of multinodular goiter.
- Dense coarse amorphous calcification is present in 60 %.
- Necrosis is common (80 %) and may be extensive.
- Cervical lymphadenopathy is common (80 %) and usually heterogeneous and shows necrosis.
- US evidence of local invasion of adjacent neck structures including blood vessels is seen.
- Viable areas are vascular, and areas of necrosis are hypovascular.

Thyroid Lymphoma

Thyroid lymphoma, either primary or secondary, is rare. Secondary involvement is more common, because 20 % of disseminated lymphomas involve the thyroid. Plasmacytoma, Hodgkin lymphoma, Langerhans cell histiocytosis, Rosai–Dorfman disease, and extramedullary hematopoiesis (Fig. 3.54a, b) can involve the thyroid gland, often presenting as thyroid nodules.

Clinical findings. Patients with primary lymphoma usually have Hashimoto's thyroiditis; however, only a minority of patients with Hashimoto's develops lymphoma. Patients are usually women with a median age of 60 years. The clinical presentation is similar to that of anaplastic carcinoma, including a rapidly enlarging thyroid mass, dysphagia, and hoarseness. The response to chemotherapy and radiotherapy is favorable, and the prognosis is better than that for patients with anaplastic carcinoma. The prognosis is better

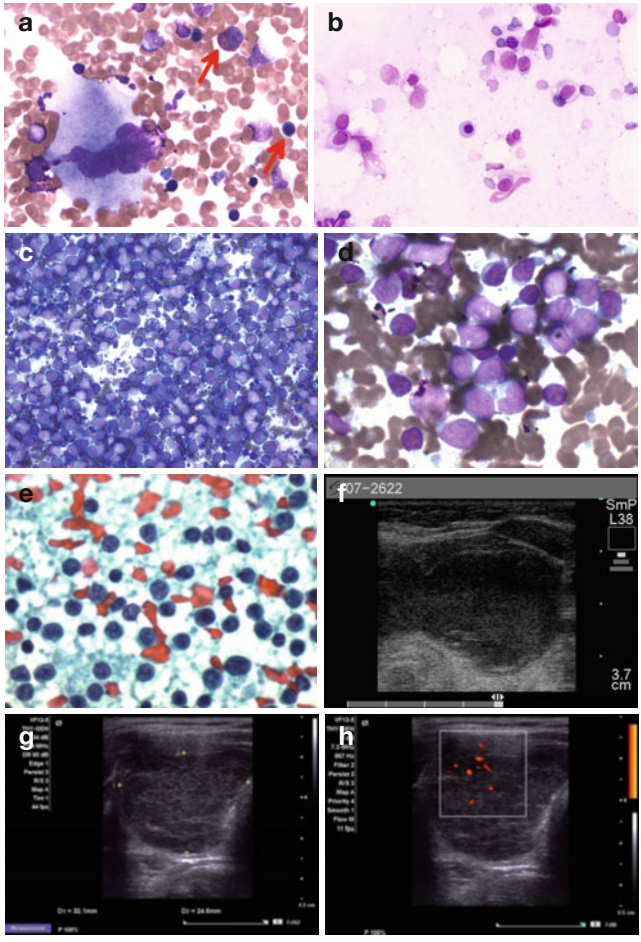

FIGURE 3.54 Smears of extramedullary hematopoiesis showing a single megakaryocyte, nucleated red blood cell (**a**, *right arrow*; **b**, *center*), myeloblasts (**b**), and one immature eosinophil (**a**, *upper arrow*). Smear from non-Hodgkin lymphoma shows a monotonous population of small cells (**c**) with nuclear clefts (**d**), coarse chromatin, and conspicuous nucleoli (**e**). These two cases of lymphoma show similar US features including a large homogeneous hypoechoic solid mass with posterior acoustic enhancement ("pseudocystic" appearance) and minimal vascularity by Doppler examination (**f**–**h**). (**a**–**d**, MGG stain high power; **e**, Papanicolaou stain, high power)

for marginal zone B-cell lymphoma than for diffuse large B-cell lymphoma.

Histopathology. Almost all thyroid lymphomas are B-cell non-Hodgkin lymphoma, mainly of the diffuse large cell type (70 %) and less commonly of the MALT type (marginal zone B-cell lymphomas) (15 %), and only rarely are true follicular lymphomas. Primary thyroid T-cell lymphomas are exceedingly rare.

Immunoprofile. A consideration in the evaluation of B-cell lymphomas in a background of chronic thyroiditis is the detection of clonal B-cell populations that have not yet evolved into lymphoma. Thus, careful interpretation of results is advised.

Molecular profile. *BRAF* and *NRAS* gene mutations have been identified in 24 and 8 % of diffuse large B-cell thyroid lymphomas, respectively. *HRAS* and *KRAS* mutations or *PAX8/PPARγ* have not been detected.

FNA findings (Fig. 3.54c–e). Smears are cellular and show a monomorphic noncohesive lymphoid cell population in a background of red blood cells and numerous lymphoglandular bodies. Cells of marginal zone lymphoma are of medium size and have a plasmacytoid appearance. Cells of large cell lymphoma may have a fragile cytoplasm, and numerous stripped nuclei may be present along with intact cells showing a basophilic cytoplasm and prominent nucleoli. Occasionally, there is a mixed lymphoid cell population.

US features (Fig. 3.54f–h)

- A diffuse or focal hypoechoic homogeneous mass is often seen. Occasionally, the thyroid is nodular, mimicking multinodular goiter, or enlarged with no obvious abnormality.
- The focal lymphomatous nodule may be profoundly hypoechoic with posterior enhancement resembling a thyroid cyst (“pseudocystic” appearance).
- In contrast to anaplastic carcinoma, calcifications, cystic degeneration, and necrosis are rare.

- Vascularity is variable, from almost absent, to marked, and to chaotic.
- The background thyroid parenchyma often has US features of Hashimoto's thyroiditis.
- Associated lymph nodes may be large, round, homogeneous, and very hypoechoic with posterior acoustic enhancement, and they often lack calcifications or necrosis.

Rare Primary Thyroid Tumors

Squamous cell and mucoepidermoid carcinoma have been described only rarely in the thyroid. The diagnosis is histologic and should be made after exclusion of PTC with a squamous or mucoepidermoid component or a metastatic deposit. A distinct subtype of mucoepidermoid carcinoma is the sclerosing type with eosinophilia, which often arises in a background of Hashimoto's thyroiditis with fibrosis. The eosinophils tend to cluster around the moderately pleomorphic squamous cells. Keratin is positive, and TTF-1 and thyroglobulin are usually negative. The clinical course is usually indolent.

Other rare tumors of the thyroid gland include teratomas, which usually occur in the first decade of life, neuroblastomas, thymic and parathyroid tumors, and amyloidosis causing the so-called amyloid goiter (Fig. 3.55). Mixed medullary–follicular, mixed medullary–papillary, thyroid paraganglioma, and small cell carcinoma are other neuroendocrine tumors described in the thyroid.

Benign mesenchymal tumors such as lipoma, hemangioma, leiomyoma, schwannoma, granular cell tumor have been described in the thyroid. Sarcomas including spindle, epithelioid, and pleomorphic cell types are exceedingly rare and should be considered after exclusion of anaplastic carcinoma. Angiosarcoma has also been described in the thyroid, particularly in patients from European Alpine countries (Fig. 3.56).

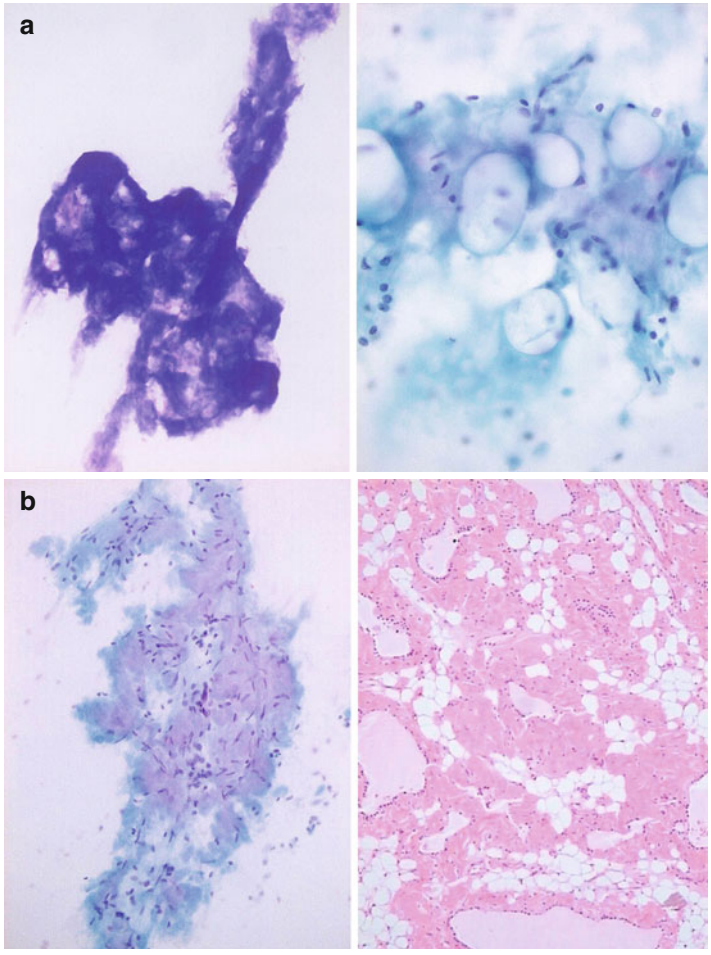

FIGURE 3.55 Amyloid goiter. Smear shows ill-defined fragments of amorphous cottony material ("puffy clouds") admixed with benign stromal elements (**a**, **b**), which correlate with the tissue findings (**b**) (**a**, **b** Diff-Quik and Papanicolaou stains, high power; **b**, hematoxylin and eosin, medium power. Courtesy of Dr. Javier Saenz de Santamaria, Badajoz, Spain)

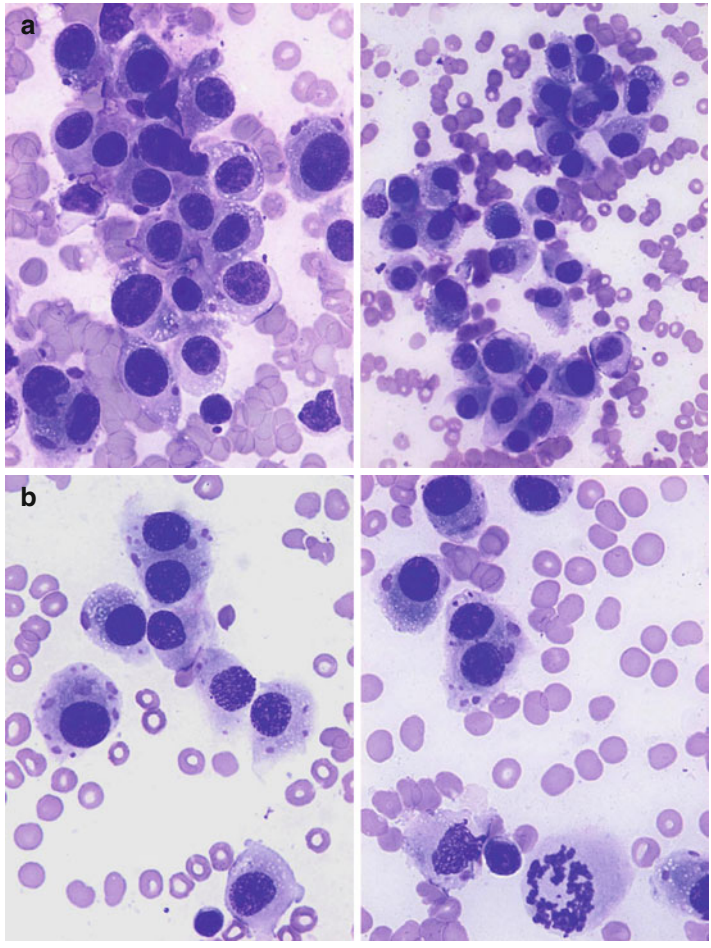

FIGURE 3.56 Primary thyroid angiosarcoma. Epithelioid angiosarcoma resembles either primary or metastatic poorly differentiated malignancy. Cells have mild to moderate pleomorphism and may show small cytoplasmic vacuoles (**a**, **b**). Immunocytochemical stains for factor VIII and CD10 are confirmatory (**c**) (**a**, **b** Diff-Quik stain, high power; **c**, immunocytochemistry, high power. Courtesy of Dr. Javier Saenz de Santamaria, Badajoz, Spain)

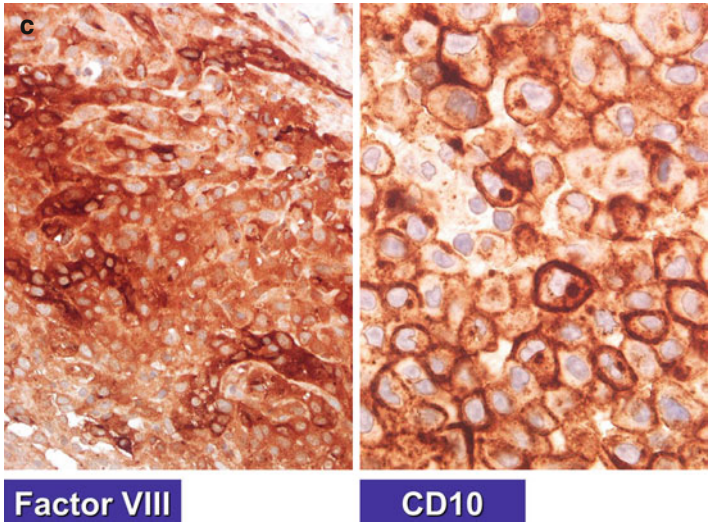

FIGURE 3.56 (continued)

Metastases

Clinically significant metastases to the thyroid gland are not unusual and are seen in approximately 2 % of patients who have surgery for suspected thyroid cancer and 10 % of patients who die of malignancy other than thyroid. The most common primary sites for thyroid metastases include the kidney (48 %), colorectum (10 %), lung (8 %), breast (8 %), and sarcomas (4 %). Aggressiveness of the tumor and host susceptibility account for the incidence and time of detection of the metastasis after the primary tumor. Local invasion from primary malignancies of adjacent organs is less common and is seen only in advanced disease.

Clinical findings. Thyroid metastases are commonly (40 %) solitary; however, they may be multiple or diffuse and are commonly the result of an advanced and disseminated malignancy. Regional lymphadenopathy is common in thyroid metastasis. Forty-four percent of metastases to the thyroid occur in glands with underlying benign thyroid conditions and primary thyroid neoplasms. In general, the

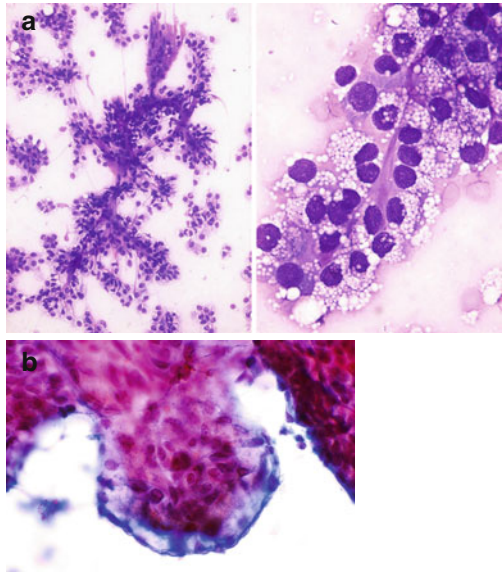

FIGURE 3.57 Metastases to the thyroid. Examples of metastatic clear cell renal cell carcinoma (**a**) and metastatic squamous cell carcinoma of the esophagus (**b**). (**a**, Diff-Quik stain, low and high power; **b**, Papanicolaou stain, medium power)

clinical suspicion for a metastatic malignancy is high except for renal cell carcinoma. Renal cell carcinoma can present as a thyroid nodule years or decades after the diagnosis of the primary tumor.

FNA findings. Cytologic features are those described in the primary tumors. Briefly, renal cell carcinoma shows aggregates of cells with finely granular, clear, or microvacuolated cytoplasm, large round to oval nuclei, and often large nucleoli. In melanoma, the smear is cellular with cellular pleomorphism including anaplastic, spindle, and plasmacytoid cells, eccentric nuclei, prominent nucleoli, occasional intranuclear cytoplasmic invaginations, and fine granular cytoplasmic pigment. A uniform population of polygonal cells may be seen in metastatic adenocarcinoma. The smear background often shows necrosis and acute inflammation (Fig. 3.57).

The clinical history, cytomorphology, comparison with the primary tumor tissue, and wise use of immunohistochemical markers are of paramount importance for the diagnosis. In metastatic carcinoma, it is important to remember that a lung primary shows a TTF-1 inmunoreactivity. The presence of cytoplasmic mucin in the malignancy strongly favors a metastatic deposit.

US features

- Solid, large, and well-defined hypoechoic and homogeneous mass affecting predominantly the lower poles of the thyroid.
- Diffuse involvement is unusual; a heterogeneous echo pattern may be seen.
- Calcifications and necrosis are uncommon.
- A nonspecific vascular pattern is seen on Doppler examination.
- Cervical lymph node and systemic involvement is often present.

FLUS and AUS: FNA Diagnosis and Ancillary Tests

USG-FNA cytology is highly accurate and has a sensitivity and specificity of more than 95 % in the diagnosis of benign and malignant thyroid nodules (in our experience at Outpatient Pathology Associates (OPA) evaluating over 70,000 samples). Follicular and Hurthle cell neoplasms remain the most challenging in FNA cytology and constitute the majority of the Bethesda System for Reporting Thyroid Cytopathology indeterminate category. In contrast to published statistics that report 20 % rate for indeterminate diagnoses, the rate in OPA is well below 4 %.

Cytologic Considerations for Reducing the Indeterminate FNA Diagnosis Rate

We should keep in mind the following considerations:

1. The presence of lymphoid cells, both single and entangled, along with microfollicles, which may be oncocytic, strongly

suggests chronic thyroiditis. Correlation with clinical findings including serology and US features is needed (Fig. 3.58a).
2. A two-cell pattern including microfollicles and sheets of follicular cells indicates a mixed micro- and macrofollicular pattern nodule. If macrofollicles comprise more than 25 %, repeat USG-FNA in 6 months (Fig. 3.58b).
3. Modest cellularity with few microfollicles is not sufficient for a diagnosis of a microfollicular-pattern nodule. Render a descriptive diagnosis and repeat USG-FNA in not less than 3 months (Fig. 3.58c).
4. Nuclear features short of malignancy are not sufficient for the diagnosis of malignancy. Render a descriptive diagnosis and repeat USG-FNA in not less than 3 months (Fig. 3.58d).
5. A cystic background and scattered metaplastic cells may be seen in papillary carcinoma. Render a descriptive diagnosis and repeat USG-FNA in not less than 3 months, with sampling of the solid-phase component (Fig. 3.58e).
6. "Pseudo-microfollicles," seen in benign thyroid nodules with atrophy, show cell and nuclear sizes similar or slightly bigger than those of red blood cells, lack intact cytoplasm, and lack molding and overlapping in contrast with true microfollicles (Fig. 3.58f).

Currently, no ancillary test or molecular marker replaces the USG-FNA diagnoses of follicular lesion or suspicion of malignancy. However, their use may be considered in selected cases. Many potential thyroid cancer biomarkers have been studied, including *BRAF*, *RAS*, *RET/PTC*, *PAX8/PPARγ*, galectin-3, HBME-1, MRC2, HMGA2, SFN, and miRNAs. The value of these tests in the diagnosis of specific thyroid malignancies and indeterminate FNA results varies from institution to institution and depends heavily on the molecular or immunohistochemistry laboratory and the expertise of the cytopathologist, who should use these tests judiciously. Likewise, galectin-3, cytokeratin-19, HBME-1, thyroid peroxidase, and DAP IV are proteins detected by immunoperoxidase stains that vary from laboratory to laboratory. Galectin-3 is overexpressed in thyroid malignancies, and HBME-1 is overexpressed in PTC.

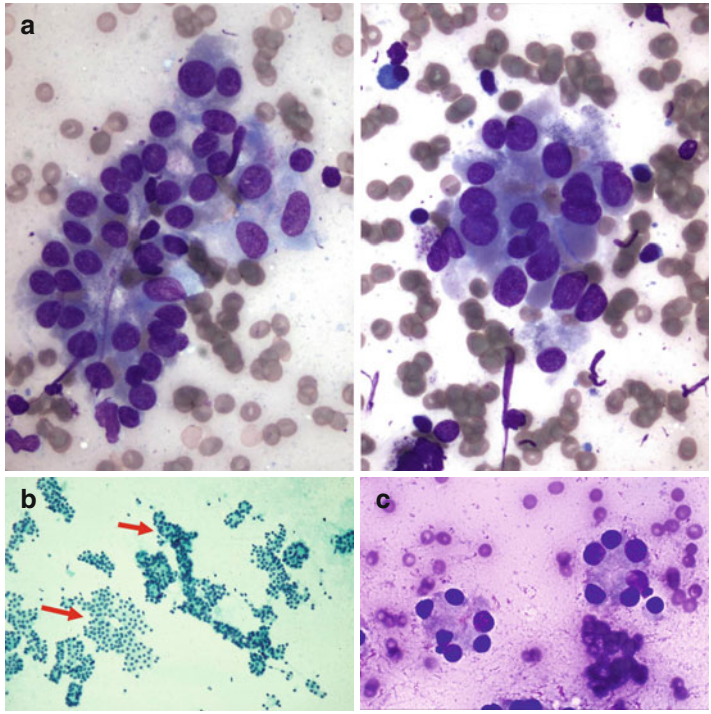

FIGURE 3.58 Cytologic clues to avoid erroneous diagnoses. Oxyphilic cells forming microfollicles are often seen in chronic thyroiditis, and a microfollicular tumor diagnosis should be avoided (**a**). The predominance of a macrofollicular architecture in a mixed macrofollicular (**b**, *left arrow*) microfollicular (**b**, *top arrow*) pattern nodule merits repeat FNA under US guidance in not less than 3 months (**b**). The diagnosis of microfollicular tumor should be avoided in the presence of rare microfollicles; thus, repeat FNA under US guidance in not less than 3 months (**c**). When cellular findings suspicious for malignancy are seen (medullary carcinoma in this case), correlate the cytology with clinical findings (serum calcitonin levels in this case) (**d**, *arrow* indicates a distinct type of binucleation). Metaplastic cells and macrophages are findings that may be seen in PTC (**e**), and further sampling under US guidance is required, particularly when there is a solid component. Pseudo-microfollicles may be seen in benign thyroid nodules with atrophic pattern; small nuclear and cell size, fragile cytoplasm, and lack of molding are seen in atrophy and not in true microfollicles (**f**)

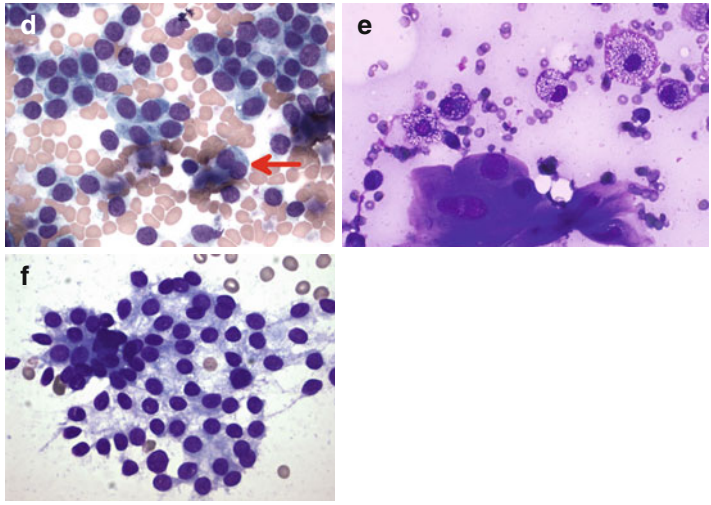

FIGURE 3.58 (continued)

Table 3.5 provides general guidelines to perform additional tests based on cytomorphologic findings to help clarify the diagnosis under consideration.

Molecular Markers

In follicular cells, the mitogen-activated protein kinase (MAPK) signaling pathway regulates cell proliferation, differentiation, and survival and is physiologically activated by growth factors binding to receptor tyrosine kinases. The signal is transmitted to the nucleus through proteins and cytoplasmic kinases including RAS, RAF, MEK, and ERK. Thyroid tumors frequently have genetic alterations leading to the nonregulated spontaneous activation of the MAPK signaling pathway (see Fig. 3.32 and Table 3.6).

Molecular markers are currently not recommended for routine use in diagnosis of thyroid tumors. The American Thyroid Association guidelines recommendation is that

Table 3.5 Reflex ancillary tests based on the cytopathology interpretation

USG-FNA diagnosis	Ancillary tests	Remarks
AUS/FLUS	None	Repeat FNA under US guidance in 3–6 months. See molecular markers
Papillary carcinoma	None	Surgery
Anaplastic carcinoma	IHC for keratin	Preferably done in cell block. Rule out melanoma, lung, pancreas, as distant primaries
Lymphoma	Immunophenotype by flow cytometry	Submit one or two dedicated passes in RPMI medium
Medullary carcinoma	Serum calcitonin, IHC for calcitonin, CEA, thyroglobulin, synaptophysin, chromogranin	Preferably done in cell block
Metastasis from the thyroid	IHC for TTF-1	Preferably done in cell block
	Needle rinses for thyroglobulin and thyroglobulin antibody levels	Obtain needle rinses in 1 ml. of normal saline
Metastasis to the thyroid	IHC for TTF-1. If negative, clinical correlation and proceed with additional IHC tests. If positive, still consider lung primary	Preferably done in cell block
Parathyroid	IHC for PTH, TTF-1, and chromogranin	Preferably done in cell block
	Needle rinses for PTH levels	Obtain needle rinses in normal saline and freeze them

Abbreviations: *AUS/FLUS* atypia of undetermined significance/follicular lesion of undetermined significance, *FNA* fine-needle aspiration, *IHC* immunohistochemistry, *RPMI* Roswell Park Memorial Institute, *CEA* carcinoembryonic antigen, *TTF-1* thyroid transcription factor, *PTH* parathyroid hormone

Table 3.6 Common genetic alteration in thyroid tumors

Tumor	Genetic alteration (in various proportions)
Papillary thyroid carcinoma	*BRAF* and *RAS* point mutations
	RET/PTC rearrangement
	TRK rearrangement
Follicular carcinoma	*RAS* mutations
	PAX8/PPARγ rearrangement
Medullary carcinoma	*RET* point mutations
Poorly differentiated carcinoma	*RAS* mutations
	CTNNB1 (β-catenin) mutations
	TP53 mutations
Anaplastic carcinoma	*TP53* mutations
	CTNNB1 (β-catenin) mutations
	RAS mutations
	BRAF mutations

BRAF, *RAS*, *RET/PTC*, and *PAX8/PPARγ* gene alterations may be considered for patients with indeterminate FNA cytology to help guide management.

Cytology Correlation

The following are useful considerations regarding the various genetic alterations in thyroid tumors and should be taken into account in the cyto-molecular correlation:

1. *BRAF*, a growth promoter thought to be specific for PTC, is only seen in about 50 % of these tumors. Thus, a negative BRAF result in a patient with an indeterminate FNA diagnosis will create more uncertainty, and the clinical management has to be based on the cytology diagnosis. If there is a false-positive BRAF result, although unlikely in a patient with an indeterminate FNA diagnosis, the result will be an

unnecessary surgery for a neoplasia that in most cases is not life-threatening.
2. Finding both *BRAF and RET* is a strong indication of malignancy, *RAS* strongly suggests malignancy, and *PAX8/PPARγ* correlates with a follicular pattern, but is not diagnostic of malignancy.
3. The specificity of *RET/PTC* has been questioned because of the identification of *RET/PTC* in nonneoplastic follicular cells in Hashimoto's thyroiditis, oncocytic tumors, and other benign lesions.
4. *PAX8/PPARγ*, a growth inhibitor thought to be specific for follicular carcinoma, not only detects 50 % of them but also is expressed in follicular adenomas and the encapsulated follicular variant of PTC.
5. It is suggested that thyroid tumors showing *RAS* mutations need surgical excision. Such tumors exhibit a follicular pattern that includes follicular adenoma, follicular carcinoma, and the follicular variant of papillary carcinoma as well as Hurthle cell neoplasms. When these are correctly diagnosed by FNA cytology, the patient will benefit from surgery.
6. Thus, it is only in selected cases that the analysis of some types of *RAS* mutations and *PAX8/PPARγ* rearrangement are helpful for deciding a surgical approach. *PAX8/PPARγ* rearrangement should be used as an indication for an exhaustive search for hallmarks of malignancy in a surgically excised follicular-pattern tumor.

Cytology material is particularly suitable for molecular analysis of thyroid nodules. The rate of PTC in *BRAF*-positive nodules tested by FNA is 99.8 %, showing that this test is highly accurate in the diagnosis. However, in our experience at Outpatient Pathology Associates, PTC is also confidently diagnosed by FNA cytology in more than 99 % of cases; thus, in an experienced cytology laboratory, *BRAF* mutation or *RET/PTC* rearrangement analysis may be unnecessary for the diagnosis of PTC. Similarly, the clinical history, FNA cytology, and serum calcitonin levels will allow one to diagnose almost all medullary carcinomas, and *RET* proto-oncogene analysis may not be necessary.

Besides the established thyroid cancer biomarkers, *BRAF*, *RET/PTC*, *RAS*, and *PAX8/PPARγ*, that represent well-understood mutations with regard to activating pathways of growth, recently, upregulated genes (*MRC2*, *HMGA2*, *SFN*) with a potential effect on neoplastic growth have been described as useful discriminators for thyroid cancer in indeterminate FNA diagnosis. Also, it has been suggested that miRNA analysis could be a useful adjunct in the management algorithm of patients with thyroid nodules, based on 100 % sensitivity and 86 % specificity (96 % specificity when Hurthle cell lesions were excluded) at differentiating malignant from benign indeterminate FNA thyroid lesions. Recently, a gene expression classifier using a cocktail of 167 genes has shown promise in improving preoperative risk assessment; however, close follow-up and repeat cytology is most appropriate in cases with a negative molecular test.

It is important to stress that (1) thyroid molecular tests are expensive, performed only in few molecular laboratories, not easily accessible, and not standardized yet; (2) a molecular panel that includes *BRAF* V600E and *RAS* point mutations and *RET/PTC* and *PAX8/PPARγ* rearrangements will be able to identify a group of patients (70 %) with almost 100 % probability of malignancy; however, 30 % of thyroid cancers have no detectable molecular markers, a fact that is difficult to ignore clinically; and (3) thyroid molecular markers have high specificity for malignant lesions, but do not have a good negative predictive value for cytology-indeterminate lesions. It has been shown that 7.6–16.2 % of patients with indeterminate cytology diagnosis (well above the 3.9 % in our laboratory) and negative molecular testing had thyroid carcinoma on surgical excision. Thus, it is still necessary to find out what is the appropriate clinical management when a patient with an undetermined FNA diagnosis has molecular-panel-negative results.

The efficacy of these studies must be assessed carefully, considering the laboratory standards and clinical scenario, including imaging studies. The so-called "reflex" BRAF testing is clinically beneficial for the patient and for the health-care system when the cytology diagnosis is indeterminate or suspi-

cious for PTC in less than the acceptable 5 % rate; otherwise health care becomes molecular test dependent and unnecessarily expensive. We must emphasize that the operator needs training to obtain a diagnostic specimen and/or the cytopathologist needs to reassess the diagnostic criteria to lower the rate of undetermined FNA diagnoses.

Therapeutic Implications of Molecular Markers

1. *Surgical therapy*. Conventional therapy for most patients with DTC includes surgery, radioactive iodine, and TSH-suppressive thyroid hormone therapy. When metastatic disease occurs, radioactive iodine can be curative. However, for those patients with DTC whose disease progresses despite conventional therapy, no effective therapy exists. The advent of molecular markers opens the horizons for a possibly different initial surgical approach and targeted therapy. The suggested surgical management scenarios for patients with positive molecular markers are:
   - BRAF+= total thyroidectomy and more aggressive and extended surgical exploration.
   - RET/PTC+= total thyroidectomy and more aggressive and extended surgical exploration if RET/PTC3+. The test should be done by RT-PCR, because highly sensitive assays such as Southern blotting have 13 % false-positive diagnoses.
   - RAS+= hemithyroidectomy.
2. *Targeted therapy*. A minority of patients with DTC develop a more aggressive, metastatic, recurrent, and life-threatening disease. Targeted therapies for thyroid cancer with kinase inhibitors based on molecular and cellular pathogenetic pathways are being evaluated clinically for potential use in patients who are not surgical candidates, patients with metastatic thyroid carcinoma unresponsive to traditional therapy, or preoperatively. Patients with progressive metastatic medullary carcinoma also benefit from biologically targeted therapy. The hypothesis is that the targeting of these kinases could block tumor growth and ultimately induce cell death.

Because agents that target RET and RET/PTC also inhibits VEGF receptors and other kinases, only some BRAF inhibitors used as therapy for PTC have entered clinical trials.

Therapies by categories include:

1. Tyrosine kinase inhibitors. These agents can target a single kinase (such as BRAF) or multiple kinases in the MAPK signaling pathway, which is activated in most PTCs. Inhibitors of RET, RAS, RAF, and MEK kinases target different points in the same pathway.

   (a) RAF inhibitors: induce growth arrest and apoptosis.
   (b) PLX 4032 inhibits specifically mutant *BRAF* V600E, with no effect on wild-type *BRAF* or other RAF kinases. XL281 inhibits both wild-type and mutant BRAF kinases. Both appear to control stable disease in advanced PTC with *BRAF* mutation.
   (c) Selumetinib also seems to target *BRAF* V600E.

2. *Modulators of apoptosis*. Apoptosis is targeted by PPARγ activators, including COX2 inhibitors, rexinoids, bortezomib, and derivatives of geldanomycin.
3. *Inhibitors of angiogenesis*. Physiologically, proangiogenic factors such as VEGF bind tyrosine kinase receptors that trigger angiogenesis as well as MAPK signaling. Neoangiogenesis is an event that is needed for tumor growth. Tyrosine kinase inhibitors (motesanib, sorafenib, sunitinib, vandetanib, and pazopanib) and humanized antibodies against VEGFs (bevacizumab) target VEGF receptors responsible of neoangiogenesis, particularly in papillary and medullary oncogenesis. These agents have a strong antiangiogenic effect in thyroid carcinoma.

   (a) Sorafenib also targets RET and BRAF kinases. The anti-RET activity makes this agent of potential use for medullary thyroid carcinoma.
   (b) Sunitinib also targets RET and RET/PTC1 and 3 kinases with potential use for papillary, follicular, and medullary carcinoma.

(c) Vandetanib also targets RET kinase, with potential use for medullary carcinoma as well as PTC.
(d) Axitinib has a strong antiangiogenic effect and does not block RET or other mutated kinases. It is effective in the treatment of advanced medullary, papillary, and follicular carcinomas including Hurthle cell carcinoma. Thus, the effect is primarily antiangiogenic.
(e) Pazopanib has a strong antiangiogenic effect and does not block RET, RET/PTC, or BRAF kinases. Its efficacy in treating advanced DTC and medullary carcinoma is under investigation, and the results appear promising. The effect is primarily antiangiogenic.

4. Immunomodulators
5. Gene therapy

Earlier studies claimed that *BRAF* and *RAS* mutations and *RET/PTC* rearrangements were mutually exclusive in PTC, but recent studies have shown the coexistence of *RET/PTC*, *BRAF* V600E, and phosphatase and tensin homolog (*PTEN*) rearrangements in some PTCs. Thus, it may be more effective to provide therapeutic agents with a broader inhibitory profile (kinases and growth factor receptors) than using single targeted therapy agents.

The success of the mentioned biologic targeted therapies has not been dramatic and varies according to the agent and dosage; side effects such as hypertension, heart conduction system abnormalities, photosensitivity, mucositis, nausea, vomiting, diarrhea, fatigue, a high incidence of cutaneous squamous cell carcinoma have been reported. We emphasize that targeting angiogenesis by blocking of VEGF tyrosine kinase receptors is very promising for the management of DTC and medullary carcinoma because of the synergistic effect on angiogenesis and on MAPK signaling pathways (see Fig. 3.52). However, we are still waiting for the development of a selective agent to a specific target within the neoplastic cell that prevents the development and maintenance of the malignant phenotype with high therapeutic efficacy and without side effects.

Handling of Cytologic Specimens for Molecular Marker Studies

The following summarizes the steps involved in the procurement, handling, and submission of material for molecular testing from thyroid nodules obtained by USG-FNA.

Because paired samples for cytology and molecular tests are obtained during the same procedure, this should be performed not sooner than 3 months after prior FNA to avoid finding reactive cytologic changes that may interfere with the cytology interpretation.

1. Perform the USG-FNA of the thyroid nodule with 25- or 27-gauge needles, as described before.
2. Prepare the smears for cytologic interpretation in the conventional manner, as described before.
3. Rinse the FNA needles with the solution provided by the molecular test manufacturer.
4. Perform two passes exclusively for the molecular test. Rinse the needle in the solution as in step 3.
5. If the molecular test is performed by an outside laboratory, submit the vial for molecular tests following the instructions of the manufacturer. Include 1 or 2 smears for molecular cytology correlation.
6. Stain the rest of the cytology smears by using standard staining techniques, preferably Romanowsky and Papanicolaou stains.
7. The cytopathologist should perform the cytologic interpretation without knowing the molecular test results to avoid bias.

Minimally Invasive Procedures Guided by US

Percutaneous ethanol injection may be curative for thyroid cysts, particularly if it is unilocular and simple. Recurrences are common in large, multilocular, and predominantly cystic complex nodules, and surgery is often the final therapy.

Percutaneous laser ablation has been proposed for decreasing the volume and improving local symptoms in patients who decline surgery or are at surgical risk. The ablation is done with local anesthesia, and the results are promising; however, long-term follow-up results are not yet available.

Suggested Reading

Abele JS. The case for pathologist ultrasound-guided fine-needle aspiration biopsy. Cancer. 2008;114(6):463–8.

Abele JS. Putting aspiration back into thyroid fine-needle biopsy-the re-emerging role of vacuum assistance. Cancer Cytopathol. 2012;120(6):366–72.

Abele JS, Levine RA. Diagnostic criteria and risk-adapted approach to indeterminate thyroid cytodiagnosis. Cancer Cytopathol. 2010; 118(6):415–22.

Ahuja AT. The thyroid and parathyroids. In: Ahuja A, Evans R, editors. Practical head and neck ultrasound. London: Greenwich Medical Media Limited; 2000. p. 35–64.

Aiken AH. Imaging of thyroid cancer. Semin Ultrasound CT MR. 2012;33(2):138–49.

Alexander EK, Kennedy GC, et al. Preoperative diagnosis of benign thyroid nodules with indeterminate cytology. N Engl J Med. 2012;367(8):705–15.

Alexander EK, Marqusee E, et al. Thyroid nodule shape and prediction of malignancy. Thyroid. 2004;14(11):953–8.

Ali SZ, Cibas ES. The Bethesda system for reporting thyroid cytopathology. New York: Springer; 2010.

American Thyroid Association Guidelines Taskforce on Thyroid Nodules and Differentiated Thyroid Cancer, et al. Revised American Thyroid Association management guidelines for patients with thyroid nodules and differentiated thyroid cancer. Thyroid. 2009;19(11):1167–214.

Bardales RH, Suhrland MJ, et al. Cytologic findings in thyroglossal duct carcinoma. Am J Clin Pathol. 1996;106(5):615–9.

Baskin HJ, Duick DS, et al. Thyroid ultrasound and ultrasound-guided FNA. New York: Springer; 2013.

Bishop JA, Owens CL, et al. Thyroid bed fine-needle aspiration: experience at a large tertiary care center. Am J Clin Pathol. 2010; 134(2):335–9.

Boos LA, Dettmer M, et al. Diagnostic and prognostic implications of the PAX8-PPARgamma translocation in thyroid carcinomas-a TMA-based study of 226 cases. Histopathology. 2013;63: 234–41.

Brose MS. In search of a real "targeted" therapy for thyroid cancer. Clin Cancer Res. 2012;18(7):1827–9.

Buehler D, Hardin H, et al. Expression of epithelial-mesenchymal transition regulators SNAI2 and TWIST1 in thyroid carcinomas. Mod Pathol. 2013;26(1):54–61.

Chan JKC. Tumors of the thyroid and parathyroid glands. In: Fletcher CDM, editor. Diagnostic histopathology of tumors, vol. 2. Philadelphia: Churchill Livingstone Elsevier; 2007. p. 997–1079.

Chui MH, Cassol CA, et al. Follicular epithelial dysplasia of the thyroid: morphological and immunohistochemical characterization of a putative preneoplastic lesion to papillary thyroid carcinoma in chronic lymphocytic thyroiditis. Virchows Arch. 2013; 462(5):557–63.

Chung AY, Tran TB, et al. Metastases to the thyroid: a review of the literature from the last decade. Thyroid. 2012;22(3):258–68.

Cibas ES, Ali SZ. The Bethesda system for reporting thyroid cytopathology. Thyroid. 2009;19(11):1159–65.

Clark DP, Faquin WC. Thyroid cytopathology. New York: Springer; 2010.

Cozens N. Thyroid and parathyroid. In: Allan PL, Baxter GM, Weston MJ, editors. Clinical ultrasound, vol. 2. London: Elsevier; 2011. p. 867–89.

Dellis RA, Lloyd RV, et al. Tumors of the thyroid and parathyroid. In: Pathology and genetics tumours of endocrine organs. Lyon: IARC Press; 2004. p. 49–133.

Filie AC, Asa SL, et al. Utilization of ancillary studies in thyroid fine needle aspirates: a synopsis of the National Cancer Institute Thyroid Fine Needle Aspiration State of the Science Conference. Diagn Cytopathol. 2008;36(6):438–41.

Finkelstein A, Levy GH, et al. Papillary thyroid carcinomas with and without BRAF V600E mutations are morphologically distinct. Histopathology. 2012;60(7):1052–9.

Frates MC, Benson CB, et al. Management of thyroid nodules detected at US: Society of Radiologists in Ultrasound consensus conference statement. Radiology. 2005;237(3):794–800.

Geisinger KR, Stanley MW, et al. Thyroid gland fine needle aspiration. In: Modern cytopathology. Philadelphia: Churchill Livingstone; 2004. p. 731–80.

Gharib H, Papini E, et al. American Association of Clinical Endocrinologists, Associazione Medici Endocrinologi, and EuropeanThyroid Association Medical guidelines for clinical practice for the diagnosis and management of thyroid nodules. Endocr Pract. 2010;16 Suppl 1:1–43.

Hassell LA, Gillies EM, et al. Cytologic and molecular diagnosis of thyroid cancers: is it time for routine reflex testing? Cancer Cytopathol. 2012;120(1):7–17.

Juliano AF, Cunnane MB. Benign conditions of the thyroid gland. Semin Ultrasound CT MR. 2012;33(2):130–7.

Kim EK, Park CS, et al. New sonographic criteria for recommending fine-needle aspiration biopsy of nonpalpable solid nodules of the thyroid. AJR Am J Roentgenol. 2002;178(3):687–91.

Kim TY, Kim WB, et al. Metastasis to the thyroid diagnosed by fine-needle aspiration biopsy. Clin Endocrinol (Oxf). 2005;62(2): 236–41.

Lee YYP, Wong KT, et al. Ultrasound investigations in head and neck cancer patients. In: Bernier J, editor. Head and neck cancer: multimodality management. New York: Springer; 2011. p. 221–33.

Ljung BM. Thyroid fine-needle aspiration: smears versus liquid-based preparations. Cancer. 2008;114(3):144–8.

Maliszewska A, Leandro-Garcia LJ, et al. Differential gene expression of medullary thyroid carcinoma reveals specific markers associated with genetic conditions. Am J Pathol. 2013;182(2):350–62.

Moysich KB, McCarthy P, et al. 25 years after Chernobyl: lessons for Japan? Lancet Oncol. 2011;12(5):416–8.

Nikiforov YE. Thyroid carcinoma: molecular pathways and therapeutic targets. Mod Pathol. 2008;21 Suppl 2:S37–43.

Nikiforov YE. Molecular diagnostics of thyroid tumors. Arch Pathol Lab Med. 2011;135(5):569–77.

Nikiforov YE, Ohori NP, et al. Impact of mutational testing on the diagnosis and management of patients with cytologically indeterminate thyroid nodules: a prospective analysis of 1056 FNA samples. J Clin Endocrinol Metab. 2011;96(11):3390–7.

Roh MH, Jo VY, et al. The predictive value of the fine-needle aspiration diagnosis "suspicious for a follicular neoplasm, hurthle cell type" in patients with hashimoto thyroiditis. Am J Clin Pathol. 2011;135(1):139–45.

Rosai J, Tallini G. Thyroid gland. In: Rosai and Ackerman's surgical pathology, vol. 1. Edinburgh: Elsevier Mosby; 2011. p. 487–564.

Ruggeri RM, Campenni A, et al. What is new on thyroid cancer biomarkers. Biomark Insights. 2008;3:237–52.

Sharma A, Gabriel H, et al. Subcentimeter thyroid nodules: utility of sonographic characterization and ultrasound-guided needle biopsy. AJR Am J Roentgenol. 2011;197(6):W1123–8.

Sherman SI. Targeted therapies for thyroid tumors. Mod Pathol. 2011;24 Suppl 2:S44–52.

Snozek CL, Chambers EP, et al. Serum thyroglobulin, high-resolution ultrasound, and lymph node thyroglobulin in diagnosis of differentiated thyroid carcinoma nodal metastases. J Clin Endocrinol Metab. 2007;92(11):4278–81.

Stelow EB, Woon C, et al. Interobserver variability with the interpretation of thyroid FNA specimens showing predominantly Hurthle cells. Am J Clin Pathol. 2006;126(4):580–3.

Virk RK, Van Dyke AL, et al. BRAF(V600E) mutation in papillary thyroid microcarcinoma: a genotype-phenotype correlation. Mod Pathol. 2013;26(1):62–70.

Wunderbaldinger P, Harisinghani MG, et al. Cystic lymph node metastases in papillary thyroid carcinoma. AJR Am J Roentgenol. 2002;178(3):693–7.

Zajdela A, de Maublanc MA, et al. Cytologic diagnosis of orbital and periorbital palpable tumors using fine-needle sampling without aspiration. Diagn Cytopathol. 1986;2(1):17–20.

Chapter 4
The Parathyroid Gland

Ricardo H. Bardales

The parathyroid glands usually have the size of a grain of rice and measure $5 \times 3 \times 1$ mm. The location of the lower parathyroid glands is more variable than that of the upper glands, and they may even have ectopic locations such as the mediastinum or a location around the carotid sheath and in the aortopulmonary window. Supernumerary glands may be seen in 5–15 % of individuals. Rarely, the parathyroid glands may be intrathyroidal, usually within the upper pole.

Embryologically, the lower and upper parathyroid glands develop from the third and fourth branchial cleft, respectively. The lower parathyroid glands share the embryologic origin with the thymus, all migrating caudally, leaving the parathyroid glands in the dorsal extracapsular aspect of the lower thyroid poles. The upper parathyroid glands descend with the thyroid gland and locate in the dorsomedial extracapsular aspect of the upper thyroid poles, usually at the level of the thyroid isthmus.

Histologically, the parathyroid glands are composed of one basic cell type, the chief cell which may have morphologic variations (oxyphilic, clear, transitional) reflecting different physiologic states of activity. *Chief cells* have a central nucleus

R.H. Bardales, MD, MIAC, ECNU
Department of Pathology and Cytopathology,
Outpatient Pathology Associates,
7750 College Town Drive, Sacramento, CA 95826, USA
e-mail: rhbardales@aol.com

R.H. Bardales (ed.), *The Invasive Cytopathologist*, Essentials in Cytopathology 16, DOI 10.1007/978-1-4939-0730-4_4,

and pale granular cytoplasm, which has secretory (parathormone or PTH) granules and variable amounts of glycogen. Increased secretory granules, prominent Golgi apparatus, and less glycogen are seen in response to hypocalcemia, reflecting increased PTH production. *Oxyphilic cells* have a deep eosinophilic cytoplasm that is rich in mitochondria, but has fewer secretory granules. *Water-clear cells* have clear cytoplasm and are more commonly seen in hyperplastic glands than in normal glands. *Transitional cells* may also be present. In addition, the parathyroid glands contain variable amounts of stromal fat that increases with the age of the individual; however, functional parenchymal elements remain constant. Cytoplasmic immunoreactivity with antibodies to PTH, keratin, chromogranin, and neuron-specific enolase is seen in all cell types.

Hyperparathyroidism

Hyperparathyroidism is the most common cause of hypercalcemia, occurring in 1/500–1/1,000 of the population. Most patients are asymptomatic, and a single parathyroid adenoma is the cause in 85–90 % of cases; multiple adenomas (4 %) and hyperplasia account for the rest. Parathyroid carcinoma is a rare cause (less than 1 %) of hyperparathyroidism. Secondary hyperparathyroidism due to parathyroid hyperplasia is commonly the result of chronic renal failure. All patients with hyperparathyroidism should undergo US so that the adenomatous/hyperplastic gland(s) is located and coexisting thyroid nodules are identified because the incidence of coexisting thyroid cancer is 2–6 %.

Parathyroid Adenoma

Parathyroid adenomas are more frequent in women than in men and occur at any age, including childhood, but are particularly common in the fourth decade of life. Most are single, and 75 % involve one of the lower glands. Adenomas have a thin capsule and may have cystic change, hemorrhage, and calcification.

Histologically, adenomas are cellular and are usually composed of chief cells; but it is common to find a combination of the other cell types. Cellular elements may be arranged in diffuse, trabecular, nested, follicular, or pseudopapillary patterns and may show cellular pleomorphism and hyperchromasia, but mitoses are usually absent (Fig. 4.1). Lymphoid cells and sometimes plasma cells may be present. Colloid-like material simulating thyroid tissue may be present. Oxyphilic adenoma is composed almost entirely of oxyphilic cells and is commonly nonfunctioning. Lipoadenomas are unusual and are composed of glandular and abundant adipose tissue.

Molecular genetic abnormalities of parathyroid adenomas are diverse and variable and are not conclusively distinct from parathyroid hyperplasia. Furthermore, clonality studies suggest that this feature is related to the "nodular architecture" seen in adenomas and hyperplasia, rather than being a feature of neoplasia, i.e., adenoma. Alterations in overexpression of

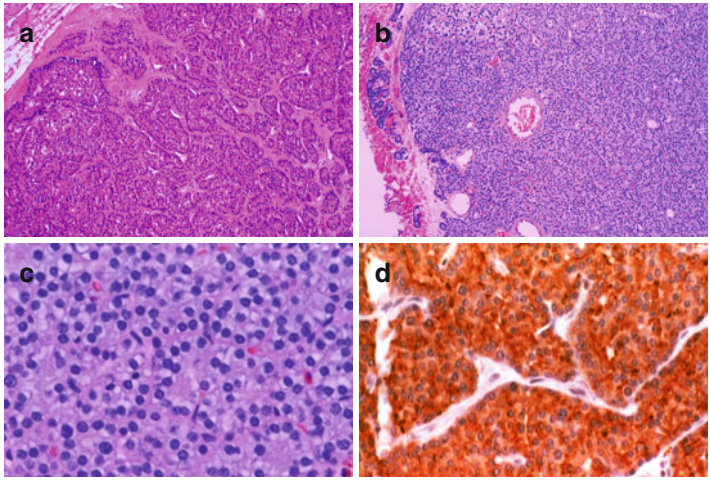

FIGURE 4.1 Parathyroid adenoma. Histologically, these two adenomas show thin capsules and trabecular (**a**) and follicular (**b**) architecture composed of small- to medium-sized cells without cellular atypia (**c**). Immunostain for parathormone is positive (**d**). (**a–c**, hematoxylin and eosin, low and medium power; **d**, immunoperoxidase stain for PTH, medium power)

cyclin D and chromosome 11q13 regions are characteristically seen in parathyroid nodular hyperplasia and adenoma.

Parathyroid Carcinoma

Parathyroid carcinoma is rare and may be seen as a component of MEN1. Hereditary predisposition for parathyroid carcinoma is seen in patients with the hyperparathyroidism–jaw tumor syndrome (parathyroid cysts, parathyroid carcinomas, fibro-osseous lesions of the jaw). Parathyroid carcinoma can be suspected when there is local invasion or nodal metastasis. Patients may have a firm, palpable neck mass, symptoms related to invasion of adjacent neck structures, and very high calcium and PTH serum levels. The relative survival at 5 years is 85 % and at 10 years ranges from 49 to 77 %.

Histologically, tumors show conspicuous dense, fibrous tissue bands, as well as spindle cells arranged in a trabecular pattern, and they commonly exhibit a high mitotic count and capsular invasion; vascular invasion is seen in some cases. Carcinomas composed of chief cells are more common than oxyphilic cell carcinomas.

Genetic analysis suggests that most parathyroid carcinomas do not arise from adenomas. Loss of parafibromin (the result of inactivating mutations of the tumor suppressor gene *HRPT2* which is responsible for the hyperparathyroidism–jaw tumor syndrome), loss of *Rb* gene expression, and overexpression of galectin-3 detected by antibodies may help in the diagnosis of parathyroid carcinoma. The cyclin D and *Rb* gene have frequently been found in parathyroid carcinoma.

Chief Cell Hyperplasia

Chief cell hyperplasia can be primary (related to MEN types 1 and 2a) or secondary to renal failure or malabsorption. The parathyroid glands are all enlarged in the classic primary condition; however, at times one gland may be grossly enlarged, with all being histologically hyperplastic. Parathyroid calcification is more common in hyperplasia

than in adenoma or carcinoma. Distinction between primary and secondary chief cell hyperplasia cannot be made histologically without the aid of clinical and laboratory information. Although it is difficult to evaluate, the compressed rim of normal parathyroid tissue seen in adenoma helps in the distinction from hyperplasia.

Water-Clear Cell Hyperplasia

Water-clear cell hyperplasia is rarely associated with hyperparathyroidism and is not associated with MEN syndrome. It affects predominantly the superior parathyroid glands, which may be large, weighing 100 g and more. Cells arranged in a solid or pseudoglandular pattern have well-defined cytoplasmic membranes, peripheral nuclei of variable sizes, and membrane-bound cytoplasmic vacuoles probably related to the Golgi apparatus.

Ultrasound (US) Examination of the Parathyroid Glands

The normal parathyroid glands are usually not seen by US. The use of US in the evaluation of the parathyroid glands is to look for parathyroid hyperplasia or adenoma in patients with borderline or elevated calcium levels with or without symptoms of hyperparathyroidism. The positive predictive value of US (anatomic study) in parathyroid adenomas is 97.5 % and that of 99Tc MIBI or sestamibi scan (functional study) is 83.7 %. Thus, the US evaluation has greater sensitivity than the sestamibi scan, is less expensive, and includes no ionizing radiation. In addition, the examination is rapid and allows for simultaneous thyroid evaluation. However, US is unable to detect small lesions, particularly if they are located in the mediastinum, and has limitations regarding distinction of parathyroid adenoma from lymph node or follicular thyroid neoplasms without cytology and PTH levels in needle rinses (PTH has more sensitivity than does cytology). CT and MRI are useful for detecting mediastinal and retrotracheal parathyroid glands.

US Features of Parathyroid Solid Lesions (Fig. 4.2)

- Parathyroid adenomas and carcinomas share similar US features.
- The capsule of the parathyroid lesion, which separates the lesion from the thyroid tissue, appears as an echogenic plane between the two.
- The lesion is homogeneous, hypoechoic, and solid, of variable size and shape, molding to the surrounding structures.
- Lesions posterior to the thyroid tissue are oval or flat and have a well-defined echogenic line that separates them from the thyroid gland. The surface is flattened due to lying against the fascial planes. The lesions are oval/round if they are located lower to the thyroid pole.
- In parathyroid carcinoma, the lesion often is more spherical than in adenoma.
- Calcifications are uncommon in adenomas, but more common in carcinoma and hyperplasia.
- Intrathyroidal adenomas are rare (1–2 %) and are hypoechoic with a sharp edge/border and prominent vascularity, similar to a "hot" thyroid nodule.
- Intranodular hypervascularity is common, with a predominant arterial pattern. Visualization of the feeding polar inferior thyroid artery in the vascular pedicle is a helpful feature. The vascular pedicle is caudal in the inferior glands and cranial in the superior glands.
- Avascular lesions (10 %) are usually less than 1 cm in diameter, cystic, and deep seated.
- Large lesions may be cystic; multiple cysts are more common than a single one. They may be entirely cystic.
- Invasion of adjacent structures and immobility on swallowing may be present in parathyroid carcinoma.
- Lymph node metastasis is seen in 25 % of cases of parathyroid carcinoma.
- The parathyroid lesion must be distinguished from the *longus colli* muscle, esophagus, blood vessels, lymph nodes, and thyroid nodules.

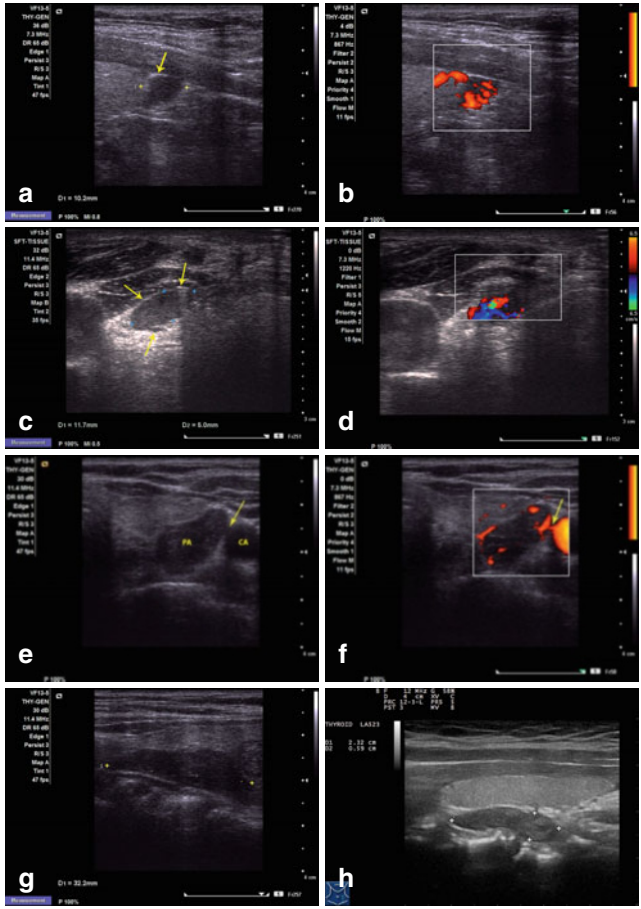

FIGURE 4.2 Ultrasound features of parathyroid adenoma. (**a**, **b**) Longitudinal view of an adenoma with intranodular hypervascularity, homogeneous hypoechogenicity, and focal echogenic rim (**a**, *arrow*) adjacent to the superior vascular pole (**b**). (**c**, **d**) Transverse view of an inferior adenoma showing an echogenic rim (**c**, *upper arrows*) and the inferior polar vessels (**c**, *lower arrow*; **d**). (**e**, **f**) Left inferior intrathyroidal adenoma (*PA*) adjacent to the left carotid artery (*CA*). Note the hypoechoic area that connects the adenoma and the artery (**e**, *arrow*) that corresponds to the feeding vessel (**f**, *arrow*); the surface of the adenoma is flattened lying against the surrounding structures (**g**, **h**)

US-Guided FNA of Parathyroid Solid Lesions

Not all parathyroid lesions need US-guided (USG)-FNA; however, USG-FNA is helpful when there are multiple lesions or when it is in an intrathyroidal or atypical neck location, particularly after failed surgery or prior to ethanol ablation. It is also useful to distinguish the parathyroid lesion from a lymph node. USG-FNA can also play a role in localizing the lesion in recurrent disease and can obtain material for cytology and to measure PTH levels in needle rinses.

Relative contraindications for USG-FNA include morbid obesity, respiratory movement problems, partial or complete obscuration by vessels, and anticoagulation.

The patient must lie supine with the neck hyperextended. Low-frequency transducers in the range of 7.5–10 MZ are recommended for evaluation of the deep neck structures and inferior parathyroid glands particularly in patients with a voluminous neck.

Sampling should be done by capillarity (Zajdela technique) with the use of a 27-gauge needle. Two or three quick thrusts are sufficient for obtaining diagnostic material. Samples are bloody, and when the operator sees that blood appears in the hub of the needle, he or she should withdraw the needle immediately. Thus, the material must be immediately and quickly smeared onto a glass slide to avoid clotting.

FNA Findings of Parathyroid Solid Lesions (Fig. 4.3)

Parathyroid lesions including cysts may be mistaken clinically as thyroid nodules. Furthermore, cytologic findings are similar to those of thyroid follicular tumors, and without clinical and US correlation, differentiating between the two is difficult. Smears are cellular and show dispersed single cells, complex aggregates, microfollicles, and pseudopapillary structures in a background of variable amounts of proteinaceous fluid and lymphoid cells. Epithelial cells are cuboidal with eccentric round or oval nuclei, inconspicuous nucleoli, granular coarse chromatin, and either non-oncocytic scant cytoplasm

(chief cells) or oncocytic ample cytoplasm and may show intranuclear cytoplasmic inclusions. Cytopathology cannot distinguish between parathyroid adenoma and carcinoma. Macrophages indicating cystic change are unusual. When

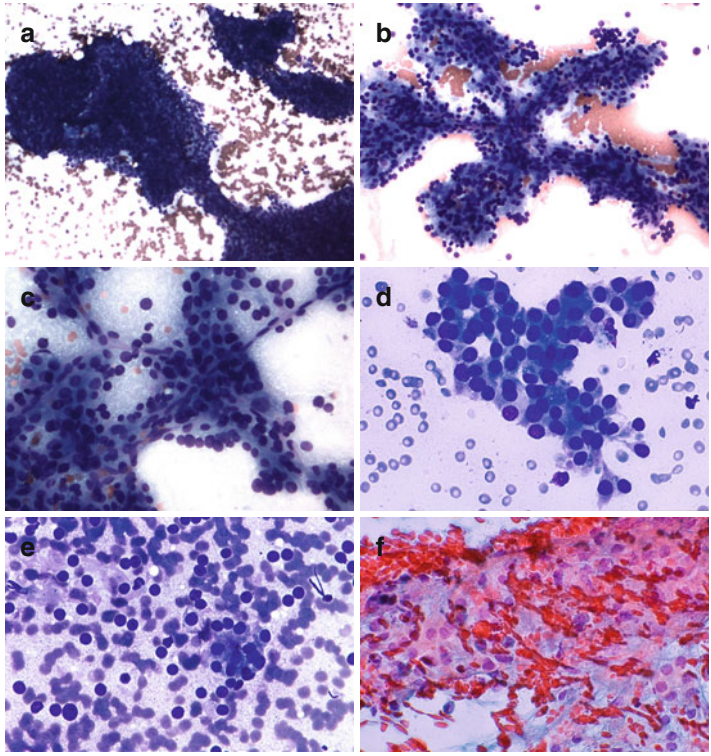

FIGURE 4.3 Smears from parathyroid adenoma (**a–f**) show complex cell aggregates (**a**) with papillary architecture (**b**), and a fine capillary network (**c**). The cells are monomorphous and cuboidal and show round nuclei, slight anisonucleosis, and granular chromatin and lack nucleoli. Microfollicles may be seen along with stripped nuclei, and the cytoplasm may be granular and eosinophilic (**d–f**). Smears from a melanocytic pigmented parathyroid carcinoma (**g–j**) show features similar to those found in the adenoma. In addition, cytoplasmic granular pigment and melanin-laden macrophages are also seen in this particular case. (**d**, **e** Diff-Quik stain, high power; **f**, Papanicolaou stain, high power; **a–c**, **g–j** MGG stain, high power)

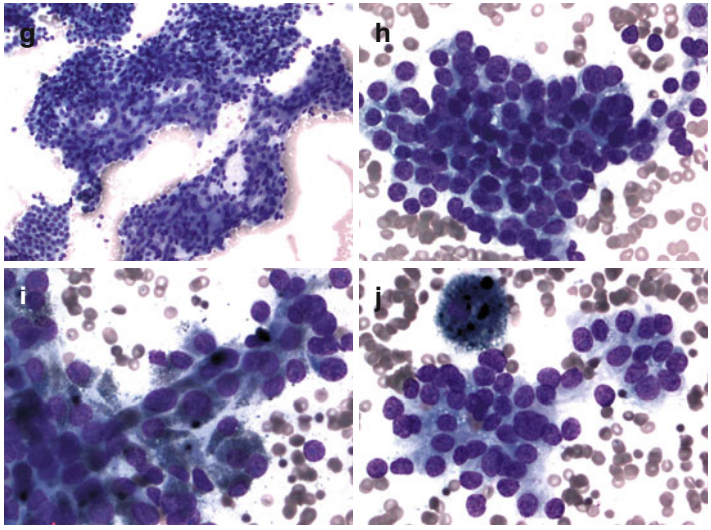

FIGURE 4.3 (continued)

clear cells predominate, the differential diagnosis includes metastasis from renal cell clear cell carcinoma. When oxyphilic cells predominate, the differential diagnosis includes oncocytic thyroid neoplasms or even metastatic malignancies to the thyroid or parathyroid gland. Parathyroid hormone measurements in needle rinses and immunostain for TTF1 are helpful in the differential diagnosis. Metastases to the parathyroid gland are exceedingly rare; one case of metastatic breast carcinoma was reported by Fulciniti F. et al.

Parathyroid Cysts

Parathyroid cysts are rare and more frequent in women than in men. Patients do not have hypercalcemia or hyperparathyroidism and are asymptomatic except for local pressure. The mean diameter is 4 cm, and the drained volume is variable, but may be 100 ml or more. The cyst wall has parathyroid tissue and is lined with cuboidal epithelium. The cyst contents are rich in PTH. Differential diagnosis includes thymic and thyroid cysts.

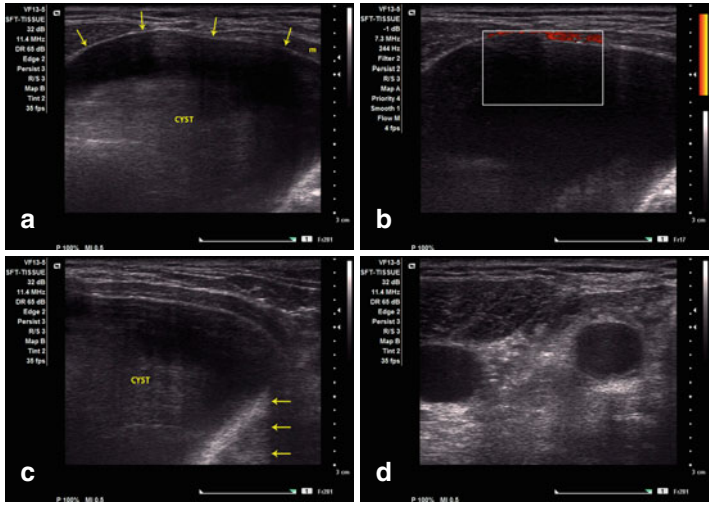

FIGURE 4.4 Ultrasound features of a parathyroid cyst. This large anechoic mass is compressing the muscle (*m*) and shows a thin uniform wall (**a**, *arrows*), no vascular blood flow (**b**), and posterior acoustic enhancement best seen in the lateral aspect (**c**, *arrows*). The cyst completely collapsed after fluid drainage (**d**)

US Features of Parathyroid Cysts (Fig. 4.4)

- Cysts are well defined and thin walled. They may be large and found within the lower neck region or in the upper mediastinum and may "dissect" the tissue planes and compress the adjacent structures, i.e., the trachea, esophagus, or recurrent laryngeal nerve.
- 2/3 of the cysts originate in the inferior parathyroid glands, and 95 % are located below the inferior thyroid border.

FNA Findings of Parathyroid Cysts (Fig. 4.5)

The fluid has a characteristic and almost pathognomonic clear, transparent, and water-like appearance, but can be yellow and cloudy, similar to thyroid cyst contents. Variable numbers of macrophages may be present.

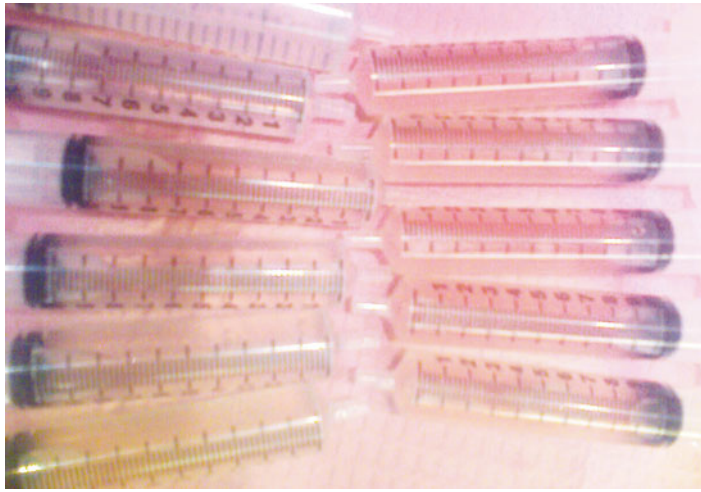

FIGURE 4.5 Parathyroid cyst contents. Approximately 100 cc of clear fluid was drained from the case shown in Fig. 4.4. PTH levels in the fluid were high and supported the diagnosis

Suggested Reading

Agarwal AM, Bentz JS, et al. Parathyroid fine-needle aspiration cytology in the evaluation of parathyroid adenoma: cytologic findings from 53 patients. Diagn Cytopathol. 2009;37(6):407–10.

Ahuja AT. The thyroid and parathyroids. In: Ahuja A, Evans R, editors. Practical head and neck ultrasound. London: Greenwich Medical Media Limited; 2000. p. 35–64.

Baskin HJ, Duick DS, et al. Thyroid ultrasound and ultrasound-guided FNA. New York: Springer; 2008.

Cozens N. Thyroid and parathyroid. In: Allan PL, Baxter GM, Weston MJ, editors. Clinical ultrasound, vol. 2. London: Elsevier; 2011. p. 867–89.

Dellis RA, Lloyd RV, et al. Tumors of the thyroid and parathyroid. In: Pathology and genetics tumours of endocrine organs. Lyon: IARC Press; 2004. p. 49–133.

Dimashkieh H, Krishnamurthy S. Ultrasound guided fine needle aspiration biopsy of parathyroid gland and lesions. Cytojournal. 2006;3:6.

El-Naggar AK. Cellular and molecular pathology of head and neck tumors. In: Bernier J, editor. Head and neck cancer: multimodality management. New York: Springer; 2011. p. 57–79.

Fulciniti F, Pezzullo L, et al. Metastatic breast carcinoma to parathyroid adenoma on fine needle cytology sample: report of a case. Diagn Cytopathol. 2011;39(9):681–5.

Ippolito G, Palazzo FF, et al. A single-institution 25-year review of true parathyroid cysts. Langenbecks Arch Surg. 2006;391(1):13–8.

Khati N, Adamson T, et al. Ultrasound of the thyroid and parathyroid glands. Ultrasound Q. 2003;19(4):162–76.

Lieu D. Cytopathologist-performed ultrasound-guided fine-needle aspiration of parathyroid lesions. Diagn Cytopathol. 2010; 38(5):327–32.

Owens CL, Rekhtman N, et al. Parathyroid hormone assay in fine-needle aspirate is useful in differentiating inadvertently sampled parathyroid tissue from thyroid lesions. Diagn Cytopathol. 2008; 36(4):227–31.

Paker I, Yilmazer D, et al. Intrathyroidal oncocytic parathyroid adenoma: a diagnostic pitfall on fine-needle aspiration. Diagn Cytopathol. 2010;38(11):833–6.

Papanicolau-Sengos A, Brumund K, et al. Cytologic findings of a clear cell parathyroid lesion. Diagn Cytopathol. 2013;41:725–8.

Phillips CD, Shatzkes DR. Imaging of the parathyroid glands. Semin Ultrasound CT MR. 2012;33(2):123–9.

Rosai J. Parathyroid glands. In: Rosai J, editor. Rosai and Ackerman's surgical pathology, vol. 1. Edinburgh: Elsevier Mosby; 2011. p. 565–84.

Tseng FY, Hsiao YL, et al. Ultrasound-guided fine needle aspiration cytology of parathyroid lesions. A review of 72 cases. Acta Cytol. 2002;46(6):1029–36.

Wei CH, Harari A. Parathyroid carcinoma: update and guidelines for management. Curr Treat Options Oncol. 2012;13(1):11–23.

Chapter 5
The Salivary Glands

Ricardo H. Bardales

Normal Salivary Glands

The three pairs of major salivary glands include the parotid, submandibular, and sublingual. The minor salivary glands are numerous and are located in the mouth and oropharynx.

All salivary glands are exocrine and have serous or mucous acini and excretory ducts. Serous acini have basally located nuclei, granular basophilic cytoplasm, and cytoplasmic zymogen PAS+ diastase-resistant granules, and they secrete amylase (Fig. 5.1). Mucous acini have basally located nuclei, clear vacuolated cytoplasm, and cytoplasmic sialomucin vacuoles, and they secrete mucin. The ductal system begins distally in the intercalated ducts, which are lined with cuboidal epithelium. The cells have central nuclei in communication with the larger striated ducts which are lined by mitochondria-rich columnar eosinophilic cells. The more proximal interlobular ducts are lined by pseudostratified columnar epithelium with scattered mucinous cells. Myoepithelial cells surround the secretory acini and the intercalated ducts.

R.H. Bardales, MD, MIAC, ECNU
Department of Pathology and Cytopathology,
Outpatient Pathology Associates,
7750 College Town Drive, Sacramento, CA 95826, USA
e-mail: rhbardales@aol.com

R.H. Bardales (ed.), *The Invasive Cytopathologist*, Essentials in Cytopathology 16, DOI 10.1007/978-1-4939-0730-4_5,

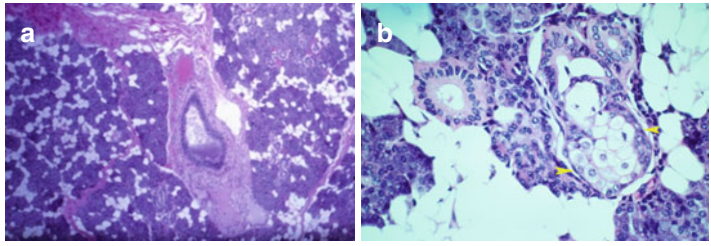

FIGURE 5.1 Normal histology of the parotid gland at low (**a**) and high magnification (**b**). Note the presence of adipose tissue and sebaceous glands (**b**, *arrowheads*) (Hematoxylin and eosin stain)

The parotid gland is a serous gland and contains lymphoid aggregates; lymph nodes may be present and contain ducts or occasionally acini. The submandibular gland is mixed serous and mucous; caps of serous cells may be seen in the mucous acini. The sublingual gland is also mixed but is predominantly mucous. The minor glands may be predominantly serous or mucous.

Ultrasound of the Salivary Glands

The parotid space extends from the external auditory canal superiorly to the angle of the mandible inferiorly, neighbors the nasopharyngeal area in the medial aspect, and is separated from the carotid space by the posterior belly of the digastric muscle. The space contains the parotid gland, facial nerve, retromandibular vein, external carotid area, and lymph nodes. The normal parotid gland has a homogeneous echotexture and is hyperechoic, more than the submandibular gland (Fig. 5.2). The facial nerve cannot be visualized; however, the retromandibular vein, seen as a well-defined hypoechoic tubular structure, is the landmark for the facial nerve. Intraparotid lymph nodes may be visualized, measure <5 mm, and are usually located in the superficial lobe. An accessory parotid gland may be seen in 20 % of patients and is located overlying the masseter muscle.

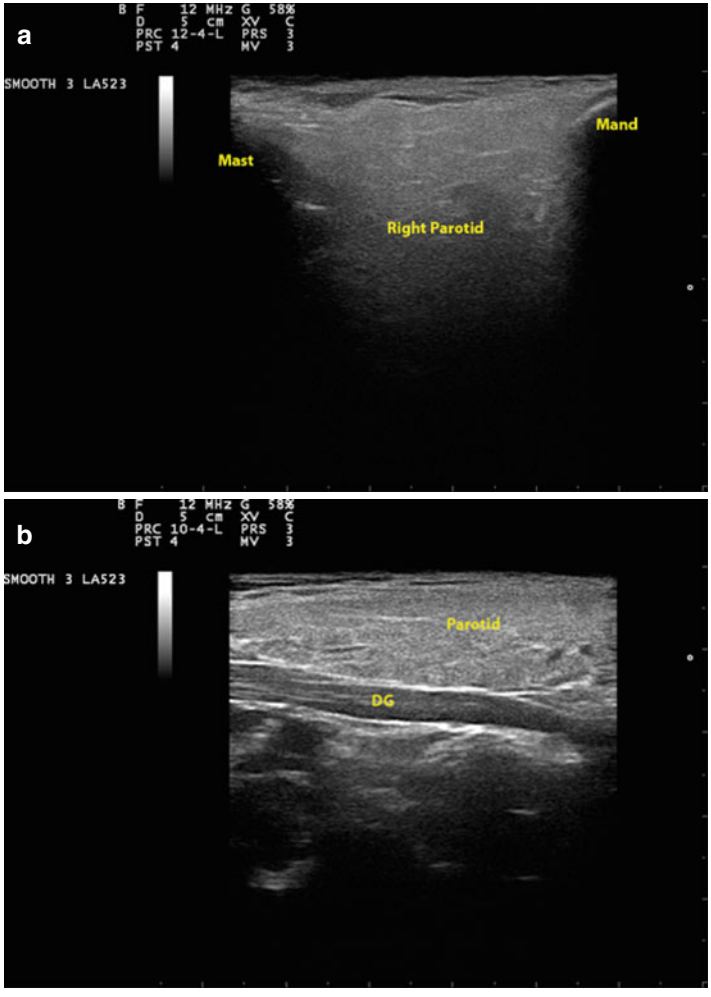

FIGURE 5.2 Normal US of the parotid space and parotid gland (**a**, right parotid; **b**, left parotid). *Mand* mandible, *Mast* mastoid process, *DG* posterior belly digastric muscle

The submandibular and sublingual spaces lay inferolateral and superomedial, respectively, and are divided by the mylohyoid muscle. The submandibular space contains

the anterior belly of the digastric muscle, the superficial lobe of the submandibular gland, lymph nodes, the facial artery and vein, the inferior part of the XII nerve, and fat. Different from the parotid gland, the lymph nodes are around and not within the submandibular gland. The sublingual space contains the anterior hyoglossus muscle, the deep lobe of the submandibular gland, sublingual gland and ducts, submandibular duct, lingual artery and vein, lingual nerve, and cranial nerves IX and XII. The submandibular and sublingual glands are homogeneous and slightly hyperechoic. The Wharton's duct is not normally seen, only when dilated (Fig. 5.3).

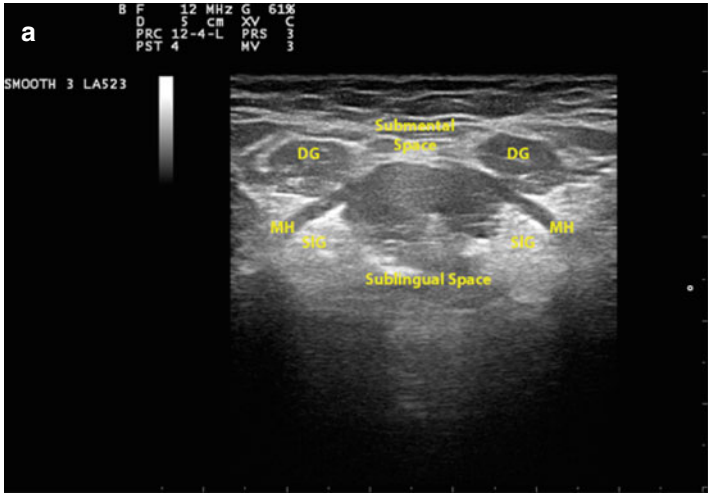

FIGURE 5.3 Normal US of the submental and sublingual (**a**, transverse view; **b**, longitudinal view), and submandibular (**c**) gland spaces and the submandibular gland. *DG* digastric muscle, *MH* mylohyoid muscle, *SlG* sublingual gland, *LN* lymph node, *SmG* submandibular gland, *DGa* anterior belly digastric muscle, *DGp* posterior belly digastric muscle, *HG* hyoglossus muscle, *T* tonsil

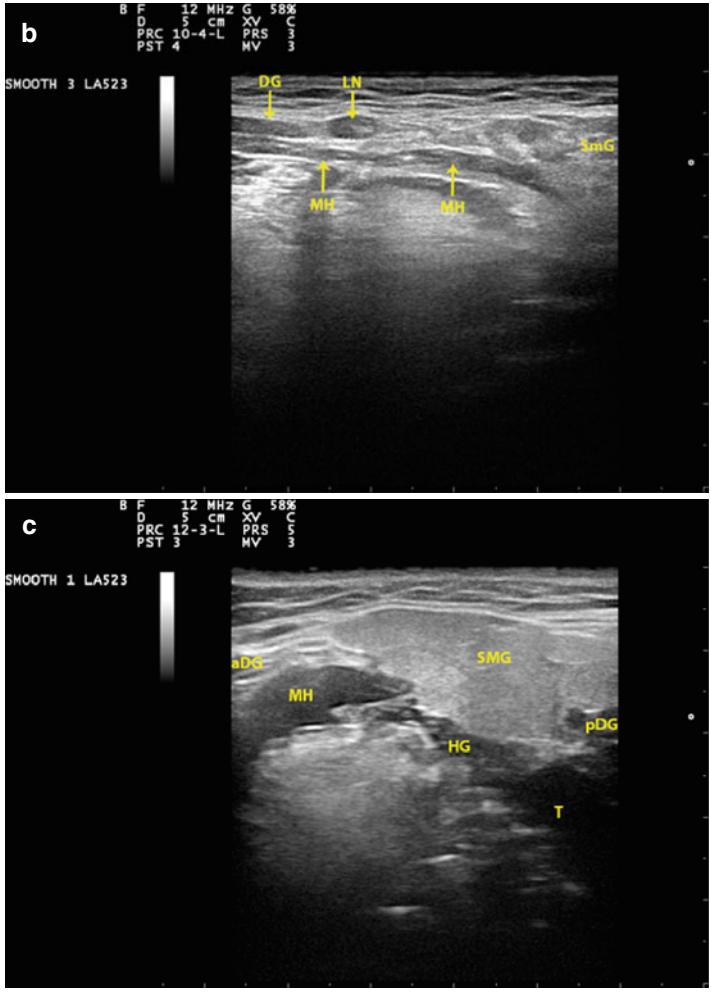

FIGURE 5.3 (continued)

US and Salivary Gland Masses

US imaging alone is usually sufficient for evaluation of most salivary gland masses. However, US has limitations: it cannot visualize the deep lobe of the parotid gland and the minor

salivary glands. Thus, masses arising deep in the parotid gland, oral cavity, tracheobronchial tree, or pharynx cannot be evaluated by US. In cases of salivary gland malignancies, US cannot evaluate bone, perineural, or deep-soft-tissue involvement or the retropharyngeal lymph nodes. Despite these limitations, US should be part of the initial evaluation of any accessible asymptomatic salivary gland mass, particularly when it develops in the parotid, submandibular, or sublingual areas. Of note, 20 % of masses clinically considered as being in the parotid gland are extra-glandular and reinforce the use of US. US characterizes a salivary gland mass, evaluates associated lymphadenopathy, and permits needle guidance and accurate sampling by fine-needle aspiration (USG-FNA). USG-FNA is the preferred diagnostic modality for any symptomatic or asymptomatic salivary gland mass.

US Features of Benign and Malignant Salivary Gland Masses

1. *Tumor edge*. Benign tumors have well-defined, regular, and smooth margins. Malignant tumors have irregular and ill-defined contours (Fig. 5.4).
2. *Internal architecture*. Benign tumors have a homogeneous echotexture and may have posterior acoustic enhancement as often seen in pleomorphic adenomas. Malignant tumors have heterogeneous internal architecture and may have areas of necrosis and cystic change/hemorrhage. However, benign tumors may have cystic change and complex internal architecture, i.e., Warthin's tumors or large pleomorphic adenomas. Calcification usually indicates a long-standing process, as seen in pleomorphic adenoma (Fig. 5.5).
3. *Tumor extent*. Extracapsular invasion into the surrounding tissue, including the skeletal muscle, subcutaneous tissue, and skin, may be seen, particularly in high-grade or long-standing malignant tumors (Fig. 5.6).

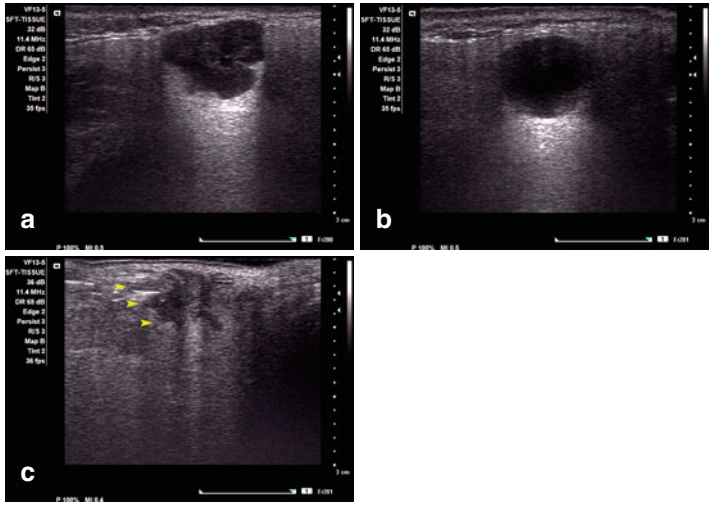

FIGURE 5.4 Tumor edge. Smooth, well-defined, and lobulated borders are often seen in benign mixed tumors or pleomorphic adenomas (**a**). Round and well-defined edges are seen in cystic lesions (**b**). Spiculated infiltrative borders (*arrow heads*) are seen in malignant tumors (**c** adenoid cystic carcinoma)

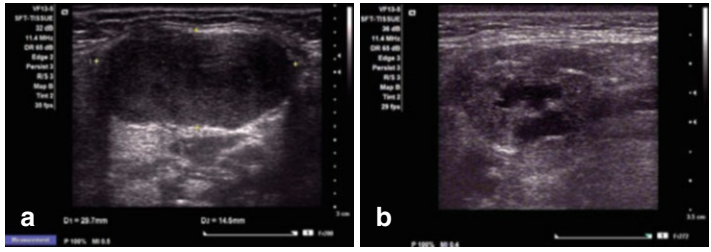

FIGURE 5.5 Internal architecture. Homogeneous echotexture is commonly seen in monomorphic and pleomorphic adenomas (**a** monomorphic adenoma). Heterogeneous echotexture may be seen in malignant tumors (**b** mucoepidermoid carcinoma), chronic sialadenitis (**c**), and benign tumors (**d** Warthin's tumor)

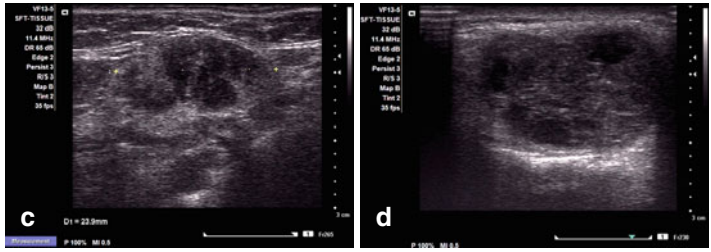

FIGURE 5.5 (continued)

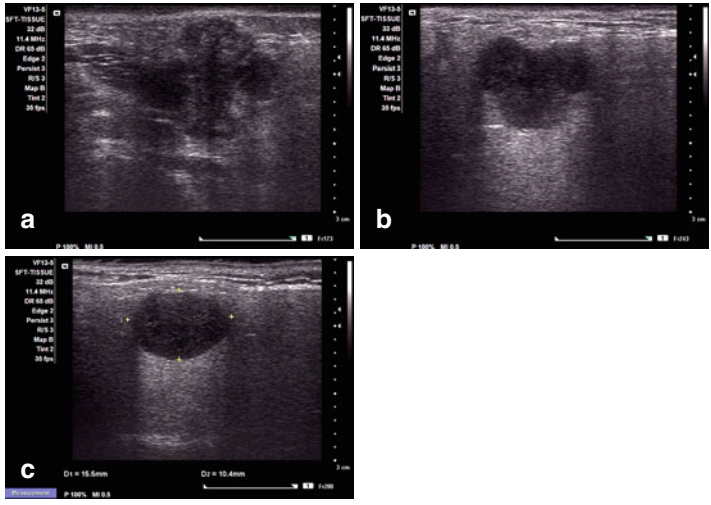

FIGURE 5.6 Tumor extent. Malignant tumors show spiculated and fuzzy borders with infiltration into surrounding tissue (**a** basal cell carcinoma). Smooth and distinct borders are seen in benign conditions (**b** monomorphic adenoma; **c** Warthin's tumor)

4. *Tumor vascularity*. Malignant tumors may show increased internal vascularity. Pleomorphic adenomas may have peripheral vascularity (Fig. 5.7).
5. *Lymphadenopathy*. An indirect sign of malignancy is the presence of cervical lymph nodes with abnormal US features in the region of lymphatic drainage.

The US distinction between benign and malignant salivary gland masses is not clear, and features overlap. Although US imaging is unable to differentiate among specific types of malignant salivary gland tumors, it helps to separate benign from malignant tumors. However, low-grade malignancies often share similar US features with benign tumors.

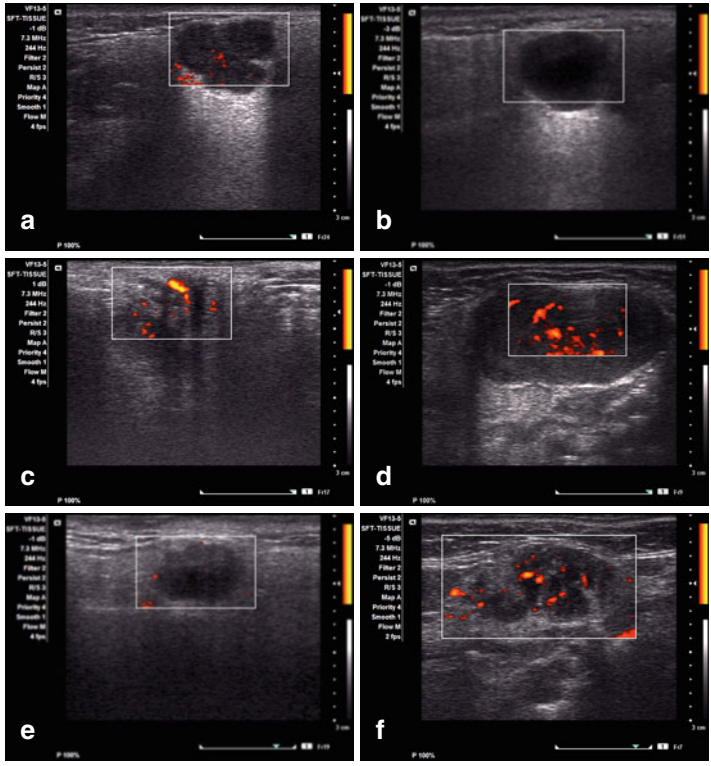

FIGURE 5.7 Tumor vascularity. Vascularity is variable and usually high in high-grade tumors. However, Warthin's tumors usually have high internal vascularity. The tumors shown correspond to those benign and malignant tumors and lesions listed in 4A–C (**a**, pleomorphic adenoma; **b**, cyst; **c**, adenoid cystic carcinoma), 5A–D (**d**, monomorphic adenoma; **e**, mucoepidermoid carcinoma; **f**, chronic sialadenitis; **g**, Warthin's tumor), and 6A–C (**h**, basal cell carcinoma; **i**, monomorphic adenoma; **j**, Warthin's tumor)

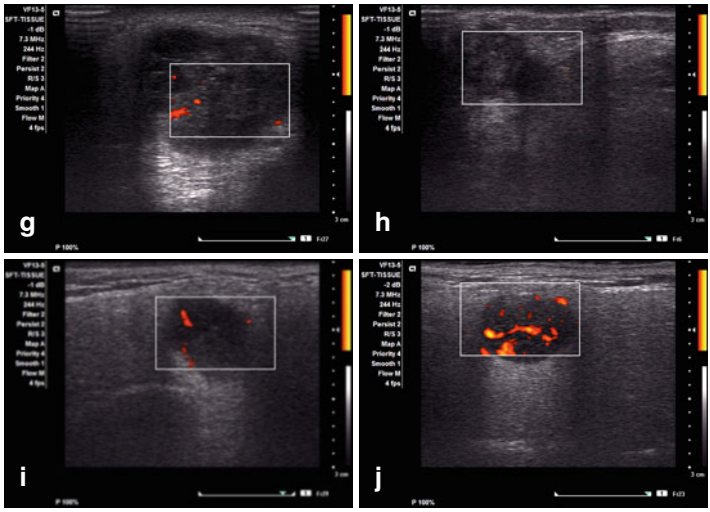

FIGURE 5.7 (continued)

Ultrasound-Guided FNA of Salivary Gland Masses

From the clinical perspective, it is relevant to remember that masses often develop in the parotid, submandibular, sublingual, and minor salivary glands in decreasing order. They may be present in heterotopic salivary gland tissue in various sites of the head and neck, including along Stensen's duct, and most are malignant, with mucoepidermoid carcinoma being the most common. Patient age is relevant because benign mixed tumor and Warthin's tumor occur in adulthood, and mucoepidermoid carcinoma is the most common salivary gland tumor in children. Local pain, facial nerve damage, and signs of local tumor invasion often indicate malignancy, but their absence does not exclude such a diagnosis.

Masses affecting the salivary glands may be broadly classified as infectious/inflammatory, nonneoplastic, and neoplastic with a vast resulting number of mass lesions. Superimposed alterations such as degeneration, chronic inflammation, cystic

change, or metaplasia of various types add challenges to the already at times difficult pathologic diagnosis.

We agree with Stanley, M. W. et al. that a practical approach to interpreting FNA material based on a pattern diagnosis recognition based on first impression key findings will result in a narrow differential diagnosis for that particular pattern. We will adopt this approach to discuss common salivary gland masses. Briefly, the salivary gland patterns include (1) normal, (2) inflammatory/infectious, (3) pleomorphic adenoma, (4) Warthin's tumor, (5) cystic, (6) small epithelial cells, (7) large epithelial cells, and (8) spindle cells. Benign mixed tumor and Warthin's tumor are included not only because they are common but also for their occasional diagnostic difficulties in differentiating them from other tumors. The most common salivary gland masses will be covered in this fashion, and the rare entities will be mentioned briefly.

The USG-FNA is performed with a 25-gauge needle without suction (Zajdela technique), as mentioned in the aspiration procedure section, early in this book. If the material obtained is limited, the use of an aspiration device may be indicated for applying moderate suction (3–4 ml of negative pressure). USG-FNA with a 22-gauge needle may be used for obtaining a bloody specimen, which is useful for preparation of a cell block for histologic evaluation and for ancillary tests including molecular studies; salivary gland tumors have significant and highly prevalent translocations. USG-FNA has 85, 96, and 94 % sensitivity, specificity, and accuracy, respectively, in the evaluation of salivary gland masses. USG-core biopsy may be considered in rare selected cases, solely when USG-FNA is nondiagnostic and the patient's risk for surgery is high.

Pattern I: Normal Salivary Gland Pattern

This pattern may be present in up to 20 % of salivary gland FNAs in some series. Cytologic smears are cellular and show predominantly acinar and less common ductal elements as well as variable amounts of adipose tissue. Acinar elements are arranged in small, round aggregates of cells with large

granulovacuolar cytoplasm, eccentric round nuclei, and small inconspicuous nucleoli. Acinar cells have a fragile cytoplasm; as a result, the smear background is granular and exhibits variable numbers of stripped nuclei that need to be distinguished from lymphocytes, which have a scant rim of basophilic cytoplasm. The ductal elements may be branching and show tubular structures and cell sheets with honeycomb architecture (Fig. 5.8a, b).

Sialosis

Sialosis is a nonneoplastic, asymptomatic salivary gland enlargement that affects principally the parotid gland and less commonly the submandibular gland. It is the result of

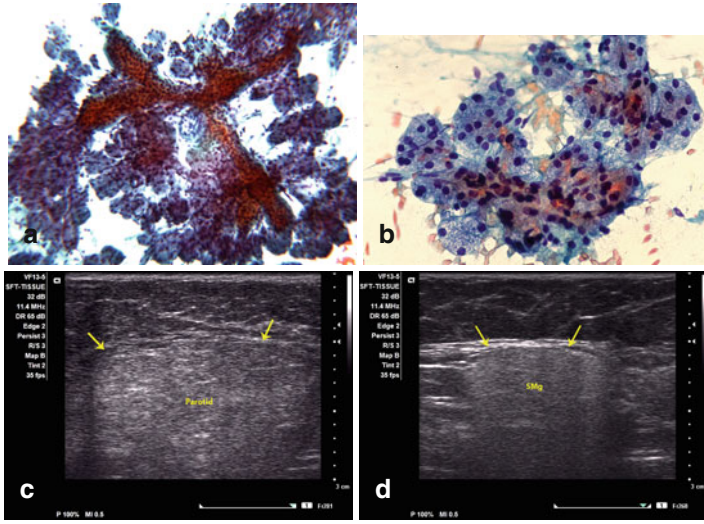

FIGURE 5.8 Normal salivary gland cytology showing cohesive branching ducts and acini (**a**, **b**). US imaging of the left parotid (**c**, *arrows*) and left submandibular (**d**, *arrows*) gland enlargement (sialosis) in a patient with type II diabetes mellitus shows both glands with diffuse homogeneous echotexture and no hyper- or hypoechoic masses. There is a slight hyperechogenicity in the parotid gland compared with the submandibular gland (**c**, **d**) (**a**, **b** Papanicolaou stain, low and high magnification) *SMg* submandibular gland

acinar hypertrophy and is usually bilateral. A related underlying cause is usually identified, i.e., diabetes mellitus, malnutrition, alcoholism, cirrhosis, obesity, hypothyroidism, HIV, drugs, etc.; however, it may be idiopathic. FNA smears show a normal salivary gland pattern, as mentioned before (Fig. 5.8a, b). It has been suggested that the cellular yield is greater than that of normal gland, and acinar cells are 20 % larger than normal cells, features that are difficult to evaluate in a high-quality FNA smear. The aspirates may contain variable amounts of adipose tissue, but they are devoid of inflammatory cells. The differential diagnosis includes failure to sample the target, and depending on the amount of adipose tissue present, a lipoma or a lipomatous salivary gland should be considered, all of which require clinical correlation, including imaging studies. The diagnostic accuracy is improved when the cytopathologist performs USG-FNA to reduce the sampling error.

US features. There is bilateral gland enlargement with normal echogenicity and no focal lesions or increased blood flow; however, the glands may be hyperechoic due to fat infiltration. The features are nonspecific (Fig. 5.8c, d).

Pattern II: Inflammatory/Infectious Pattern and Similar Processes

Acute Inflammation

Acute inflammatory processes most commonly affect the parotid gland but are rarely subject to FNA. Suspicion of an associated neoplastic process, abscess formation that needs drainage, a poor response to antibiotic therapy, or a clinically suspected infectious process in a setting of immunosuppression may prompt an FNA, best if done under US guidance. The FNA smear pattern is purulent and shows neutrophils, fibrin strands, and variable numbers of acinar and ductal cells, which may have marked reactive changes (Fig. 5.9a, b). The most common agents are bacterial organisms, e.g., *Staphylococcus*, and FNA material must be submitted for cultures. High-grade malignant neoplasms, either primary or secondary, may show a background of neutrophils and necrosis. Caution should be

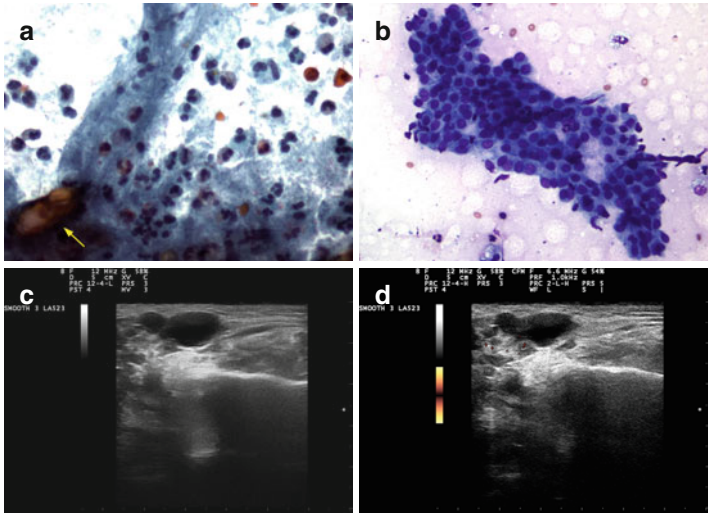

FIGURE 5.9 Parotid abscess. This patient had an episode of acute sialadenitis and developed an abscess after antibiotic therapy. A purulent pattern (**a**), stone fragments (**a**, *arrow*), and rare sheets of ductal cells with squamous metaplasia (**b**) are seen. US imaging shows a slightly irregular anechoic lesion with posterior acoustic enhancement and no vascularity by Doppler examination (**c**, **d**) (**a**, **b** MGG stain, high magnification)

exercised in diagnosing malignancy, particularly of low grade, in the presence of acute inflammation.

US features. A hypoechoic, ill-defined mass may be seen in early abscess formation; when liquefaction occurs, the mass becomes anechoic and well defined with posterior acoustic enhancement (Fig. 5.9c, d). The gland is hypervascular, and regional lymphadenopathy is often present. The enlarged gland is hypoechogenic with a heterogeneous pattern due to duct and cyst dilatation and microabscess formation.

Chronic Inflammatory Processes

The presence of chronic inflammatory cells needs clinical correlation because the majority of masses with this pattern represent salivary gland tumors with scant representation of

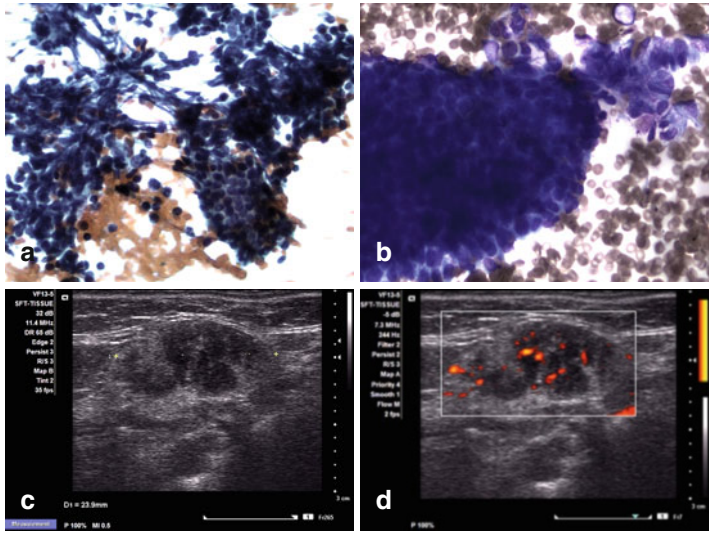

FIGURE 5.10 Chronic sialadenitis. Chronic inflammatory cells, predominantly entangled with benign salivary gland elements (**a**) and reactive aggregates of ductal cells with squamous metaplasia (**b**). Ultrasound shows a complex heterogeneous mass with anechoic foci, septae of slightly hyperechoic bands, and mild internal blood flow by Doppler examination (**c**, **d**)

epithelial cells and various degrees of nonspecific chronic inflammation, i.e., Warthin's tumor or, in some cases, intra- or peri-salivary gland lymph nodes. On US, the gland is of normal size or small, heterogeneous, and hypoechoic with multiple round hypoechoic foci. The vascularity is not increased (Fig. 5.10).

Postradiation sialadenitis produces a firm nodular and often tender salivary gland with fibrosis, acinar atrophy, and preservation of the ductal epithelial system. Smears are sparsely cellular and show fibrosis, chronic inflammatory cells, and epithelial and stromal elements with variable cytologic atypia that may pose difficulty in distinguishing this from a malignant process. The clinical history helps in the distinction. The gland is enlarged and hypoechoic in the acute phase and small, atrophic, and hypoechoic in the chronic fibrous stage.

Benign lymphoepithelial lesions present as bilateral salivary gland enlargement in patients with Mikulicz's disease or Sjögren's syndrome. Smears show a polymorphous population of lymphoid cells and epimyoepithelial islands or groups of myoepithelial cells, which may be inconspicuous. Clinical correlation is needed for consideration or support of the diagnosis. In contrast to the AIDS-related lymphoepithelial cyst, the cystic component seen in the autoimmune-related lesion is not prominent, and the normal salivary elements are almost absent. The gland is enlarged and shows normal echogenicity in the early stages. A gland with heterogeneous echotexture and multiple round hypoechoic areas or even cysts is seen in late stages. The incidence of lymphoma is greatly increased in patients with Sjögren's syndrome.

Lymphomas

The lymphomas rarely affect the salivary glands (Fig. 5.11a, b); more often is the involvement of the parotid or submandibular space lymph nodes (Fig. 5.11c). The immunophenotype as determined by flow cytometry is helpful for the diagnosis in these cases. Hodgkin lymphoma rarely involves the salivary glands, and if diagnostic Reed–Sternberg cells are not identified, these cases may be diagnosed as inflammatory process or reactive lymphoid hyperplasia. Non-Hodgkin lymphomas of low grade may be confused with reactive processes and vice versa. Occasionally, non-Hodgkin lymphoma of high grade, although often recognized as malignant, may be confused with poorly differentiated carcinoma or even small cell carcinoma.

US features. Lymphomatous deposits are markedly hypoechoic and may show through acoustic transmission with posterior acoustic enhancement the so-called "pseudocystic" appearance. The vascular pattern is increased and abnormal (Fig. 5.11d, e).

Granulomatous Processes

This pattern may be seen as a part of infectious, non-neoplastic, and neoplastic processes. Sarcoidosis, a commonly

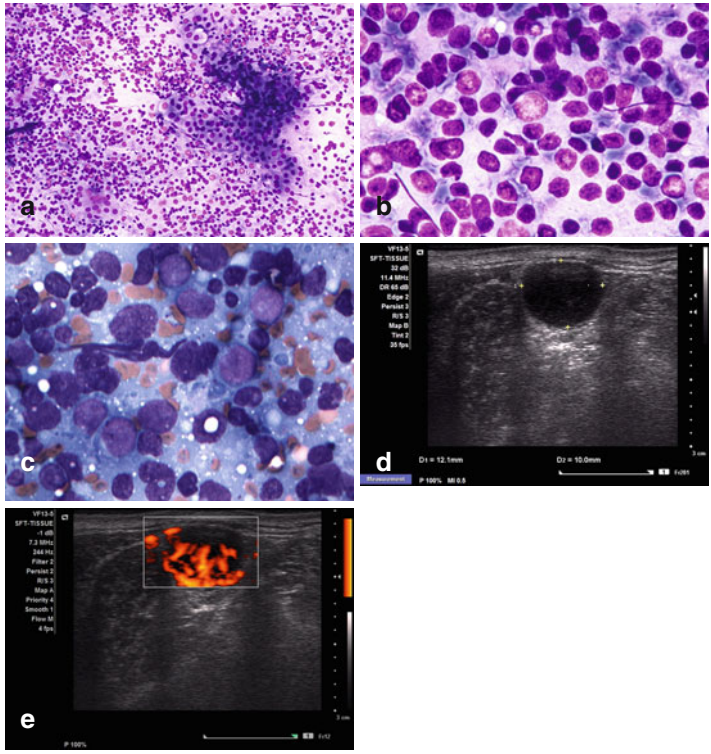

FIGURE 5.11 Mixed cell follicular lymphoma and Warthin's tumor of the parotid gland (**a**, **b**). Large B-cell lymphoma involving submandibular space lymph node (**c**). Ultrasound shows a round markedly hypoechoic lymph node with well-circumscribed margins, posterior acoustic enhancement, and chaotic internal blood flow by Doppler examination (**d**, **e**) (**a**, **b** Diff-Quik stain, medium and high magnification; **c** MGG stain high magnification)

non-necrotizing granulomatous process, may involve salivary glands or intragland lymph nodes (Fig. 5.12a, b). Necrotizing granulomatous inflammation, as in other body sites, is commonly associated with mycobacterial and fungal infections. Clinical correlation including cultures for organisms is always important. Of note, FNA material is perfectly suitable for ancillary studies, including cultures.

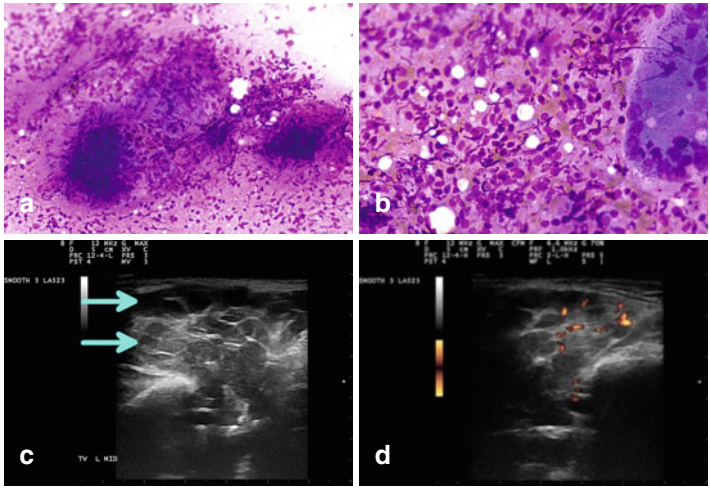

FIGURE 5.12 Sarcoidosis. Non-necrotizing granulomatous inflammation. Granulomas, chronic inflammation and tissue damage (**a**) and multinucleated giant cells are present (**b**). Ultrasound shows heterogeneous salivary gland echotexture with multiple hypechoic foci (**c**, *arrows*) vascularized septae on Doppler evaluation (**d**) (DiffQuik stain, medium and high magnification)

US features. The findings are non-specific and may show a normal or enlarged gland with diffuse hypoechogenicity or heterogeneous echotexture and lobulated gland borders (Fig. 5.12c, d).

Pattern III: Pleomorphic Adenoma (Benign Mixed Tumor), Variants, and Similar Processes

Pleomorphic Adenoma

Pleomorphic adenoma or benign mixed tumor is composed of epithelial and stromal elements. Some tumors are cellular, and others exhibit various architectural patterns that may challenge the diagnosis. Complete surgical excision with preservation of

the facial nerve is the treatment of choice. Local recurrence is rare and is often the result of incomplete resection or "spillage" of myxochondroid matrix. Complications include malignant transformation, particularly in large and long-standing tumors and in the so-called metastasizing pleomorphic adenoma.

Clinical findings. Pleomorphic adenoma is the most common tumor of the salivary glands and occurs predominantly in the tail of the parotid gland. It is rare in the sublingual glands. It is the most frequent tumor of the parapharyngeal space, followed by peripheral nerve sheath tumors. It has a slight female predominance, with variable age presentation, usually occurring in adults and the elderly. Familial occurrence is rare. Bilateral or multiple tumors are uncommon. Tumors are slowly growing over years, and except for compressive mechanical symptoms, patients are almost always asymptomatic. Tumors are firm, well circumscribed, with regular and lobulated borders, and of variable size.

Histopathology. All tumors have a capsule of variable thickness and may be non-visible, particularly in cases with abundant myxoid matrix.

Typical pleomorphic adenomas have a mixture of ductal epithelial, myoepithelial, and stromal elements. The epithelial component may show variable architectural patterns including trabecular, papillary, tubular, solid, or cystic, even within the same tumor. The islands and tubules have an inner layer of cuboidal/columnar/flattened epithelial cells and outer myoepithelial cell layer(s). The stromal component is myxoid, chondroid, or fibro-osseous alone or mixed. Crystalloids may also be present in the background. Squamous elements in the form of pearls or squamous cells as well as mucous cells, clear cells, spindle cells, plasmacytoid cells, sebaceous cells, oncocytic cells, calcification, and adipose tissue may be seen. Degenerative changes may be seen spontaneously or after FNA and include squamous metaplasia, reactive cellular changes, necrosis, and infarction.

Cellular pleomorphic adenomas may be rich in epithelial or myoepithelial cells, but every case shows the typical component described above, although it may be limited. There may be large atypical cells and rare non-atypical mitoses; as long as these features are focally present, they do not signify malignancy.

Most tumors are diagnosed without difficulty; however, those with a predominant cellular epithelial or myoepithelial component or those with variable architectural patterns must be recognized and distinguished from other tumors such as polymorphous low-grade adenocarcinoma when involving minor salivary glands or adenoid cystic carcinoma in the major salivary glands. Pleomorphic adenomas with predominant rich myxoid stroma must be distinguished from mesenchymal tumors, including but not limited to myxoid lipoma, myxoid neurofibroma, and myxoma.

Immunoprofile. Epithelial cells show keratin, CEA, and EMA positivity. Myoepithelial cells are positive for calponin, p63, actin, vimentin, S-100 protein, CD10, glial fibrillary acid protein, and keratin but are CEA and EMA negative. Podoplanin, a myoepithelial cell marker has been shown to be positive on the cell border and in the external periphery of the cells in pleomorphic adenoma and other salivary gland tumors with myoepithelial differentiation.

Molecular profile. Most pleomorphic adenomas have karyotypic abnormalities including 8q12 rearrangements, 12q14–15 rearrangements, or sporadic clonal changes. The 8q12 and the 12q14–15 abnormalities activate the target genes *PLAG1* and *HMGA2*, respectively, producing fusions that are specific and diagnostic for these tumors.

FNA findings. Ductal cells are small, cuboidal, and bland appearing and can be single or form sheets, acini, tubules, or branching aggregates (Fig. 5.13a). Cells show round, regular nuclei with fine chromatin and inconspicuous nucleoli and may have mild to moderate pleomorphism (arrows Fig. 5.13b); occasional intranuclear inclusions may be present. The epithelial component may have cystic change and squamous, clear cell, mucinous, oncocytic, and sebaceous metaplasia (Fig. 5.13c). Myoepithelial cells are usually dissociated or in small aggregates and show plasmacytoid or spindle shapes and may have moderate pleomorphism; they may be mistaken for hematopoietic cells (Fig. 5.13d). Myoepithelial cells appear faint with poorly defined cell borders when admixed with the stroma (Fig. 5.13e). The chondromyxoid matrix, in air-dried Romanowsky-stained slides, is characteristic and

appears metachromatic, dense, and fibrillary; the last feature is particularly visible in the frayed edges (Fig. 5.13e, f). The matrix is less conspicuous with Papanicolaou stain and appears pale and gray; and myoepithelial cells may appear stellate or spindle. Thus, Romanowsky-stained slides are advantageous for detection of small amounts of stromal elements, and they lower the possibility of an incorrect diagnosis. Necrosis and cellular atypia secondary to infarction may rarely be associated with prior FNA.

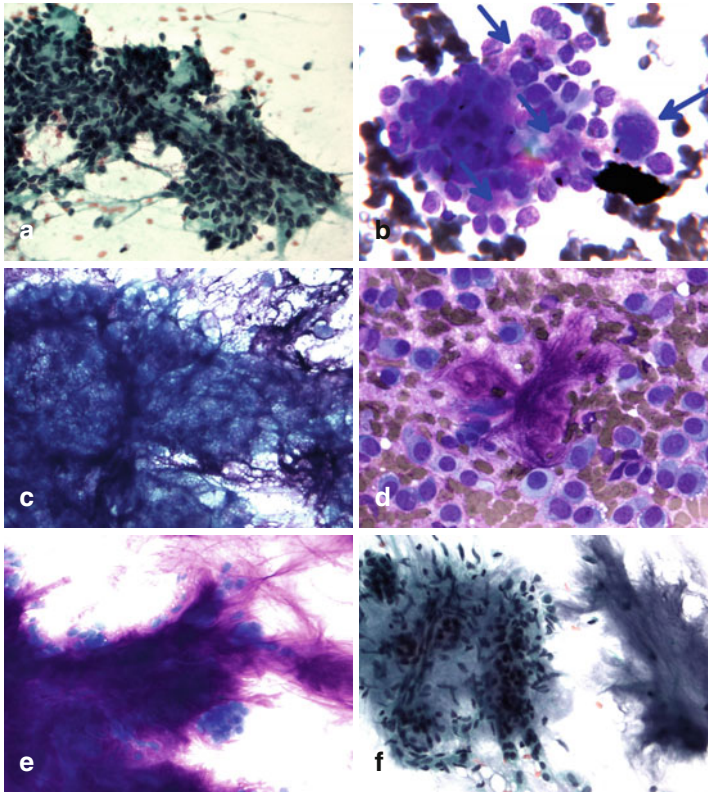

FIGURE 5.13 Benign mixed tumor. Cytologic features (**a–f**). Ultrasound characteristics (**g–l**) (**a–f** Papanicolaou and MGG stains, medium and high magnification)

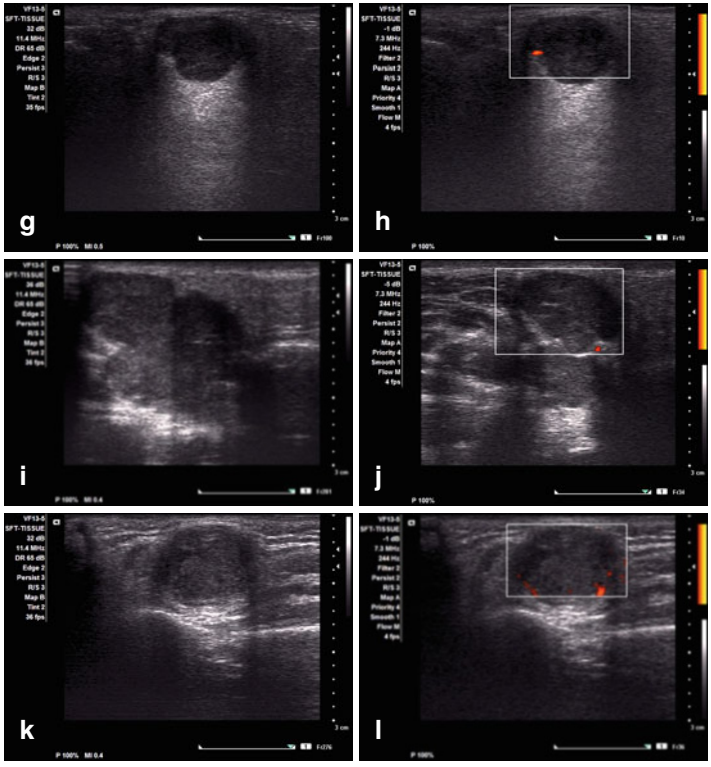

FIGURE 5.13 (continued)

It should be emphasized that finding fibrillary stroma overrides any ductal or myoepithelial cell atypia that may suggest malignancy including carcinoma ex-pleomorphic adenoma, which should be carefully considered due to its rarity particularly in the absence of facial nerve-related clinical findings.

Myoepithelioma should be considered when myoepithelial cells predominate. However, because the stroma is the most conspicuous element in the pleomorphic adenoma pattern, the differential FNA diagnosis includes mucoepidermoid carcinoma, polymorphous low-grade adenocarcinoma, and adenoid cystic carcinoma. Pleomorphic adenoma may resemble

mucoepidermoid carcinoma based on the presence of marked mucinous metaplasia, foam cells secondary to cystic change, and metaplastic squamous cells. Finding less dense stroma that, on careful examination appears fibrillary, is helpful for reaching the correct diagnosis.

Cellular pleomorphic adenoma with a cylindromatous pattern and limited stromal elements should be distinguished from adenoid cystic carcinoma and will be discussed in the section "small epithelial cell pattern." Except for the proclivity to affect minor salivary glands instead of the parotid gland and the perineural invasion seen in polymorphous low-grade adenocarcinoma, both polymorphous low-grade adenocarcinoma and pleomorphic adenoma have stromal and epithelial cell similarities that make FNA distinction difficult.

US features. A round or oval well-defined hypoechoic solid mass with a lobulated or bosselated surface is usually located in the superficial portion of the parotid gland. The mass is homogeneous and often displays a "through" transmission with posterior acoustic enhancement ("pseudocystic" appearance). Power Doppler often demonstrates peripheral blood flow. Irregular ill-defined margins and heterogeneity raise the possibility of malignancy. Cystic and hemorrhagic degeneration is usually not seen; however, it may be observed in tumors larger than 3 cm. Calcifications may occur in long-standing tumors (Fig. 5.13g–l).

Recurrent pleomorphic adenoma almost always occurs in or around the surgical excision site. Single or multiple nodules with smooth and well-defined borders, homogeneous echotexture, posterior acoustic enhancement, and peripheral vascularity may be present in these recurrent tumors.

Atypical Pleomorphic Adenoma

The atypical features of this tumor include high cellularity, cellular pleomorphism, increased mitoses, and/or necrosis. These features may suggest malignancy and should prompt extensive tissue sampling; however, they should not be mistaken for malignancy (Fig. 5.14).

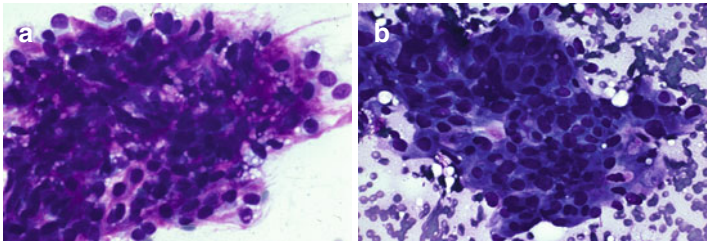

FIGURE 5.14 Benign mixed tumor with atypia and sebaceous (**a**) and squamous (**b**) metaplasia (Diff-Quik stain, high magnification)

Metastasizing Pleomorphic Adenoma

Deposits of otherwise typical pleomorphic adenoma may be seen occasionally in the lungs, mimicking pulmonary hamartoma, or in the bone, mimicking chondrosarcoma or myxoid malignant fibrous histiocytoma. Clinical and radiographic findings are required for adequate interpretation of the FNA findings.

Polymorphous Low-Grade Adenocarcinoma

Characteristically, this tumor shows bland cyto- and histomorphology, shows variable histologic patterns, and has low metastatic potential.

Clinical findings. This tumor originates almost exclusively in the minor salivary glands of the oral cavity, particularly the palate. It is more common in women and frequently occurs in the sixth to eighth decade of life. The patient has a non-tender mass that can last for months to years.

Histopathology. This well-circumscribed unencapsulated tumor shows various growth patterns, including a solid, cribriform, glandular, tubular, cystic, papillary, trabecular, or single cell linear pattern. Tumor cells are bland-appearing cuboidal and of medium size with round to elongated nuclei, granular fine chromatin, and inconspicuous nucleoli. Nuclear pleomorphism, necrosis, and mitoses are rare. The stroma is hyaline or mucoid and may have areas of hemorrhage.

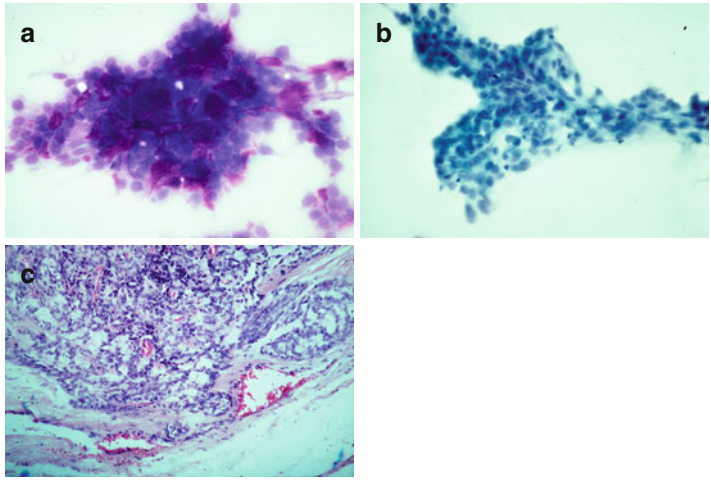

FIGURE 5.15 Polymorphous low-grade adenocarcinoma. Pseudopapillary aggregates with myxoid matrix are present (**a**). There are fine capillaries surrounded by bland-appearing epithelial cells (**b**). Histologic findings show glandular, cribriform, and trabecular patterns (**c**) (**a** MGG stain, high magnification; **b** Papanicolaou stain, medium magnification; **c** hematoxylin and eosin stain, medium magnification)

Squamous, oncocytic, or mucinous metaplasia may be seen as well as intratubular calcifications. Pseudoepitheliomatous hyperplasia of the overlying epithelium may be present.

Immunoprofile. Neoplastic cells show positive immunoreactivity for CEA, keratin, S-100 protein, vimentin, EMA, actin, CD117, Bcl-2, and galectin-3.

Molecular profile. Alterations of the 8q12 chromosome band, 12q rearrangements, and clonal t(6:9)(p21;p22) have been observed.

FNA findings. Smears are often of high cellularity and show epithelial cells, myoepithelial cells, and myxoid matrix. The epithelial cells are seen in aggregates or sheets and occasionally as branching pseudopapillary aggregates. Cells are cuboidal to spindle shaped with round to oval uniform nuclei, fine chromatin, inconspicuous nucleoli, and dense cytoplasm (Fig. 5.15). The cell features are important for distinguishing

this tumor from pleomorphic adenoma that has plasmacytoid myoepithelial cells or adenoid cystic carcinoma that shows more basaloid hyperchromatic cells and lacks cell pleomorphism or necrosis.

Pattern IV: Warthin's Tumor and Similar Processes

Warthin's Tumor

Warthin's tumor is the second most common salivary gland tumor, has cigarette smoking as the main risk factor, is more prevalent after the fourth decade of life, involves almost exclusively the parotid gland, is bilateral in 10 % of cases, and is slightly more common in men. Complete surgical excision is the treatment of choice.

Clinical findings. Tumors are softer than pleomorphic adenomas and may even be fluctuant when predominantly cystic. Patients are usually asymptomatic. Transformation to epithelial or lymphoid malignancy is exceedingly rare.

Histopathology. The epithelial component is oncocytic, arranged as a double layer with inner columnar and outer smaller cuboidal cells that decorate cystic, glandular, or papillary projections. The lymphoid elements are predominantly mature and may exhibit germinal centers. Mucous and goblet cells as well as sebaceous glands may be seen.

Immunoprofile. Epithelial cells show positivity for keratin and EMA and are negative for S-100 protein, p63, calponin, actin, and GFAP. Lymphoid cells lack light-chain restriction and are positive for mature B- and T-cell markers.

Molecular profile. The majority of these tumors show a normal karyotype. Approximately 10 % of tumors have cytogenetic abnormalities; 6p rearrangement and 11q;19p translocations are the most common and consistent abnormalities in this tumor.

FNA findings. Smears may show three components in various proportions: oncocytic cells, lymphocytes, and cyst fluid.

Oncocytic cells often occur in cohesive flat sheets showing abundant cytoplasm, well-defined cytoplasmic borders, round nuclei, and conspicuous nucleoli. The cytoplasm is granular and eosinophilic when stained with Papanicolaou stain or dense in air-dried Romanowsky-stained preparations (Fig. 5.16a, b). Sebaceous, mucinous, or squamous metaplasia may be seen (Fig. 5.16c). The lymphoid cells are usually small and may be scattered in the smear background or tangled among themselves or with the epithelial elements (Fig. 5.16d). The cystic component shows debris admixed with variable numbers of macrophages and lymphocytes (Fig. 5.16e). Cholesterol crystals may be seen.

In the presence of a lymphoid-rich FNA, chronic inflammation, reactive lymphoid hyperplasia, or even small cell-type non-Hodgkin lymphoma may be differential diagnostic considerations. Flow cytometry is helpful in questionable cases. Cyst content characteristics are highly suggestive of Warthin's tumor; however, the diagnosis cannot be made without the presence of oncocytic cells; then repeat FNA under US guidance should be performed for sampling of the solid component. Mucoepidermoid carcinoma may be considered when the oncocytic epithelium is not prominent, and squamous metaplasia is identified in a background of cyst fluid that may be mistaken for mucin (Fig. 5.16f). Cystic squamous cell carcinoma may be considered when atypical squamous metaplasia is apparent in a background of cystic elements. When oncocytic cells predominate and the cyst fluid is not prominent, the differential diagnosis includes oncocytic neoplasms, i.e., oncocytoma or oncocytic papillary cystadenoma, among others. Cells of acinic cell carcinoma may be difficult to differentiate from those of oncocytic neoplasms, particularly Warthin's tumor, because both lymphocytes and cystic fluid may be present in these tumors. In contrast to the fine granularity of Warthin's tumor, the coarse cytoplasmic zymogen granules of acinic cell carcinoma are more prominent in cell block slides. Necrosis, infarction, reactive changes, and hemorrhagic and granulation tissue may be encountered as a result of FNA sampling.

US features. This tumor is usually a well-circumscribed round or ovoid hypoechoic mass which is heterogeneous with solid and cystic areas or multiseptated with spongiform cystic architecture. This US pattern is highly suspicious for Warthin's tumor, but is not common. Power Doppler may show variable vascularity, particularly in the septa of the tumor (Fig. 5.16g–l).

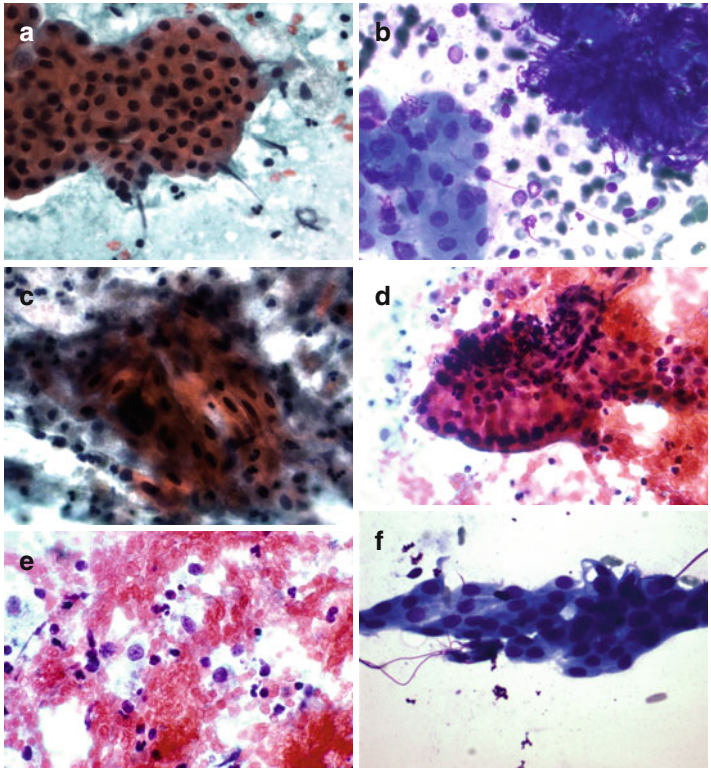

FIGURE 5.16 Warthin's tumor. Cytologic features (**a–f**). Ultrasound characteristics (**g–l**) (**a–f** Papanicolaou and MGG stains, medium and high magnification)

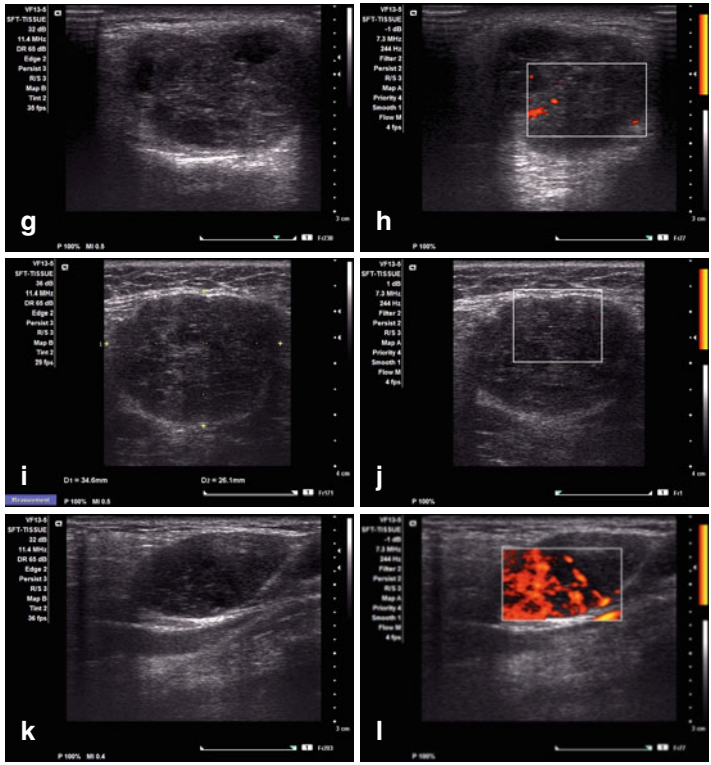

FIGURE 5.16 (continued)

Pattern V: Cystic Pattern and Similar Processes

The cyst contents obtained by FNA may be broadly classified as non-mucinous and mucinous. Each of these categories has a broad differential diagnosis that includes primary nonneoplastic and neoplastic benign or malignant lesions. It should be remembered that cystic change may also be the result of degeneration in solid tumors. The differential diagnosis is narrowed when other cellular or noncellular elements are visualized.

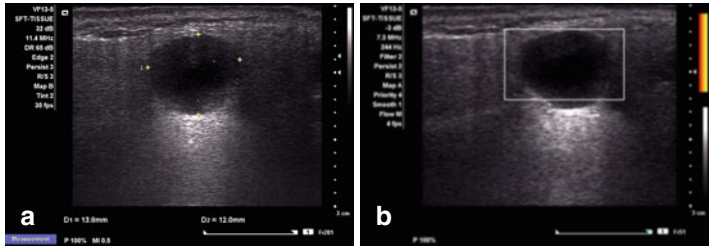

Figure 5.17 Parotid gland cyst. US shows a round nodule with well-defined margins, anechoic pattern, posterior acoustic enhancement, and no vascularity by Doppler exam

US features. Regardless of the etiology, cysts have similar characteristics, including well-defined edges, thin walls, anechoic pattern, posterior acoustic enhancement, and no vascularity (Fig. 5.17). If the cyst becomes infected, the wall becomes thick and there is internal debris.

Non-mucinous Cystic Lesions

Crystals in Cystic Lesions

Cysts may contain crystals, i.e., α-amylase and tyrosine.

Alpha-amylase crystals are not associated with malignant processes. Smears show polyhedral and multifaceted structures of variable size and thickness commonly associated with scant epithelial elements, predominantly oncocytic cells (Fig. 5.18). These crystals have been observed predominantly in cystic spaces lined with metaplastic oncocytic cells in Warthin's tumor, oncocytic papillary cystadenoma, pleomorphic adenoma, sialadenitis, and sialolithiasis. The crystals may be a product of oncocytic cell secretion.

Tyrosine crystals, on the contrary, have been found in malignant and nonmalignant neoplastic processes, more frequently in black patients.

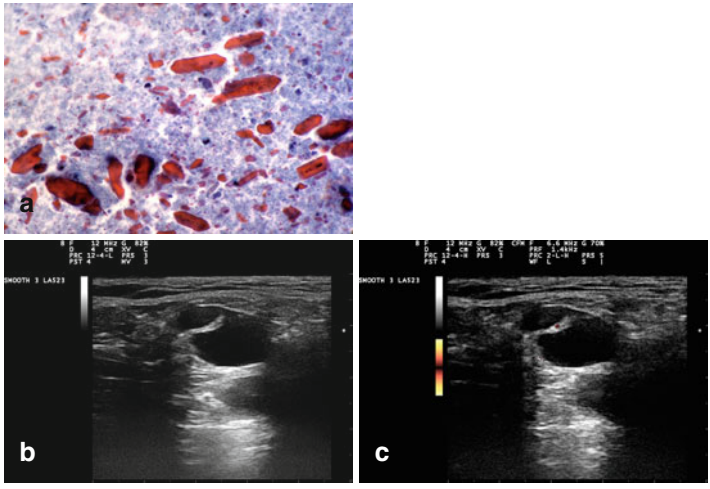

FIGURE 5.18 Parotid gland cyst with alpha-amylase crystals. Smear shows characteristic polyhedral and multifaceted crystals (**a**). US shows a septated cyst with posterior acoustic enhancement (**b**) and minimal vascularity in the septum by Doppler exam (**c**) (**a** SurePath preparation, high magnification)

Lymphoepithelial Cysts

This AIDS-related process affects principally the parotid gland, unilaterally or bilaterally, and shows hyperplastic lymphoid tissue lining cystic structures, which may show squamous, columnar ciliated or non-ciliated, or mucinous epithelium or even sebaceous glands (Fig. 5.19a). Cytologic findings include epithelial cells of the types described, polymorphous lymphoid cells, and a cystic background (Fig. 5.19b, c). The differential diagnosis depends on the predominant elements identified; however, clinical correlation is important, considering that reactive lymphoid hyperplasia and lymphoepithelial cysts are more common than malignant lymphoma, and Kaposi's sarcoma, the most common

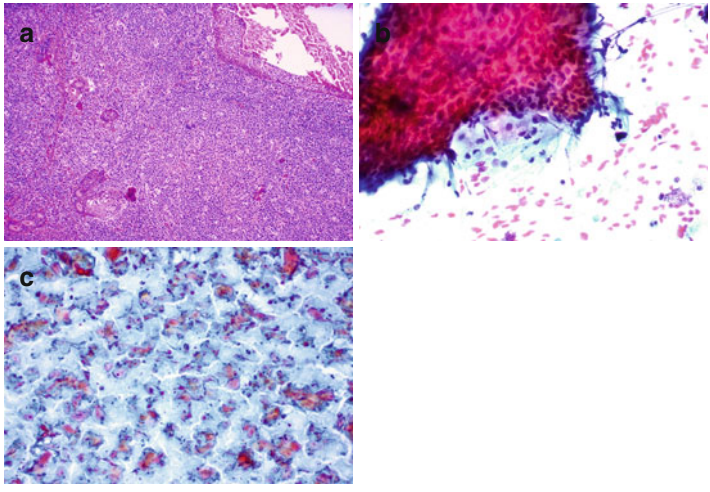

FIGURE 5.19 Lymphoepithelial cyst. Histologic section showing reactive follicular hyperplasia and a cyst lined with benign squamous epithelium (**a**). Squamous cells in complex aggregates and single are seen along with lymphocytes (**b**, **c**) (**a** hematoxylin and eosin stain, low magnification; **b**, **c** Papanicolaou stain, low and medium magnification)

malignancies in patients with AIDS. Some lymphoepithelial cysts may have a complex echotexture with solid and cystic areas resembling tumors.

Mucinous Cystic Lesions

Obstructive Sialopathy

These processes may be the result of fibrosis, adjacent masses, or sialolithiasis obstructing the ductal system, causing retrograde dilatation and mucin accumulation. As a result, acinar atrophy, chronic inflammation, and occasionally acute inflammation may occur. The lining epithelium of the dilated ducts is usually flattened or may show squamous, mucinous, or ciliated metaplasia. Foreign body reaction and stromal reactive

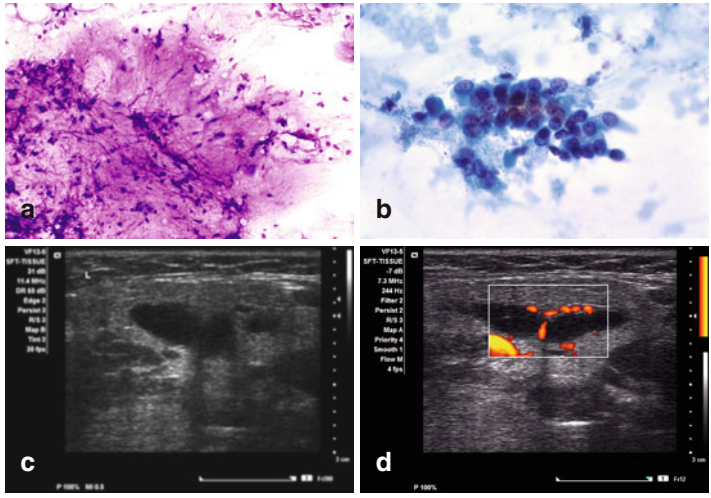

FIGURE 5.20 Obstructive sialopathy. Squamous metaplasia, chronic inflammation, and cyst contents were the findings in this submandibular gland lesion (**a**, **b**). US shows cystic cavity surrounded by a thick wall, vascular by Doppler examination (**c**, **d**) (**a**, **b** Papanicolaou stain, high magnification)

changes may occur if there is rupture of the dilated duct. Cytology preparations are similar, if not identical to those of a low-grade mucoepidermoid carcinoma (Fig. 5.20).

Sialolithiasis

This process is more common in women than in men and affects predominantly the submandibular gland, mainly as a unilateral lesion. Most calculi are single; 90 % of submandibular gland and 10 % of parotid gland stones are radiopaque. Clinically, patients classically present with pain at mealtime; however, they may be asymptomatic and have a firm mass suggestive of malignancy.

The FNA diagnosis can be made in the presence of stone fragments that may be associated with cell metaplasia,

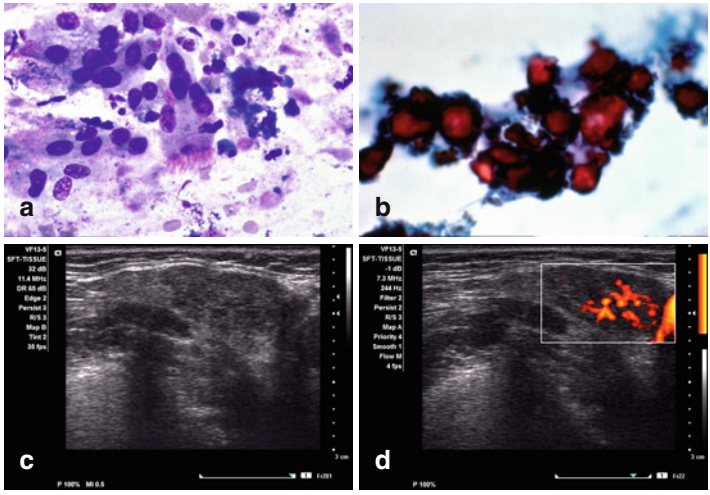

FIGURE 5.21 Sialolithiasis. Ciliated metaplasia and crystals are present in a mucoid background (**a**, **b**). US shows a hypoechoic area with lobulated edges and high vascular blood flow by Doppler exam (**c**, **d**) (**a**, **b** Papanicolaou stain, high magnification)

including ciliated columnar cells, which may be interpreted as a congenital cyst when stone fragments are not evident. The background is mucinous, with debris, and may be sparsely cellular (Fig. 5.21a, b).

The main differential diagnosis is low-grade mucoepidermoid carcinoma in the absence of stone fragments and ciliated metaplasia and in the presence of squamous metaplasia, foam cells, and reactive, bland ductal cells. In cases where mucus is only present, the FNA diagnosis of "mucinous smear pattern" is suggested, followed by a comment addressing the differential diagnosis.

US features. The gland appears enlarged and hypoechoic due to ectasia and has variably dilated ducts. Duct dilatation may be usually seen, with the duct stone showing a hyperechoic rim and posterior acoustic shadowing. Parenchymal stones can also be identified. Cyst and abscess formation may also be seen (Fig. 5.21c, d).

Low-Grade Mucoepidermoid Carcinoma

Mucoepidermoid carcinoma (MEC) is a malignant tumor composed of mucin-producing epithelium, squamous cells, intermediate cells, and mucus. Wide local surgical excision with preservation of the facial nerve is the treatment of choice.

Clinical findings. This is the most common salivary gland malignant neoplasm in both adults and children. It is more common in women than in men and occurs principally in the fifth decade of life, although it may occur in children in the second decade of life. It affects predominantly the parotid gland, the palate being the most frequent minor salivary site. The low-grade tumors are slowly growing and usually are asymptomatic, in contrast to the high-grade type, which are fast growing and cause pain. Low-grade tumors have an excellent prognosis, whereas high-grade ones have a poor prognosis.

Histopathology. The tumors are often cystic. Mucus cells usually compose <10 % of the tumor and are round and large and show well-defined cytoplasmic borders, clear or foamy cytoplasm, and small, dark eccentric nuclei. Epidermoid cells have a polygonal shape, dense eosinophilic cytoplasm, well-defined cytoplasmic borders, and vesicular nuclei. Keratinization is rare except in inflamed tumors. Intermediate cells may be small basal or large polygonal cells. Basal cells have round/oval nuclei and scant eosinophilic cytoplasm. Large polygonal cells are round to oval with more abundant cytoplasm. Clear cells may be present and are occasionally prominent, as in the rare clear cell variant of MEC. Oncocytic cells are seen in the oncocytic variant of MEC. Hyalinized or sclerosed stroma is seen in sclerosing MEC. Psammomatous MEC is another variant.

The histologic grading is fundamentally based on the predominance of the cystic component (low-grade MEC) or the solid component (high-grade MEC). Cellular pleomorphism, necrosis, mitosis, and hemorrhage are usually absent in low-grade tumors. The differential diagnosis depends on the tumor grade and includes obstructive sialopathy, necrotizing sialometaplasia, cystadenoma, and carcinomas including metastasis.

Immunoprofile. Epidermoid, intermediate, and columnar cells are cytokeratin and EMA positive. Mucous cells are cytokeratin and EMA negative. CK5/CK6 and p63 highlight squamous derivation, and PAS demonstrates mucus. Oncocytic variant is strongly positive for p63.

Molecular profile. Mutations are found mainly in high-grade tumors. The t(11;19)(q12;p13) in MEC is highly specific and results in fusion of the MEC translocated gene-1 or *MECT1* gene and the mastermind-like gene family or *MAML2* gene. The MECT1–MAML2 fusion transcript, which is present in more than half of all MECs, is associated with lower histologic grades and improved survival, suggesting both diagnostic and prognostic roles in clinical management. The translocation has not been seen in other salivary gland malignancies and can potentially be of diagnostic value using a FISH-based approach in FNA material, when MEC particularly of low grade is suspected.

FNA findings. The smear pattern is similar to that seen in obstructive sialopathy (Fig. 5.20a, b). Smears are acellular or hypocellular, and the background shows abundant mucin that, in contrast to pleomorphic adenoma, does not appear fibrillary and does not stain as intensely. Cellular elements appear singly or in aggregates (Fig. 5.22a, b). The epidermoid cells are bland appearing, and the mucous cells are plump with vacuolated cytoplasm indistinguishable from macrophages, well-defined cytoplasmic borders, and eccentric nuclei displaced by the cytoplasmic mucin (Fig. 5.22c). The mucous cells are fewer than the epidermoid cells. Intermediate cells are bland appearing and have moderate amounts of cytoplasm.

US features. Low-grade MEC is usually hypoechoic and well defined, and it shares US features with benign salivary gland tumors (Fig. 5.22d, e). In contrast, high-grade malignancies may be frankly infiltrative. Large tumors have a complex heterogeneous echotexture reflecting intratumoral necrosis or hemorrhage. Malignant tumors are more likely to have a disorganized vascular flow and have regional neck lymph node metastases.

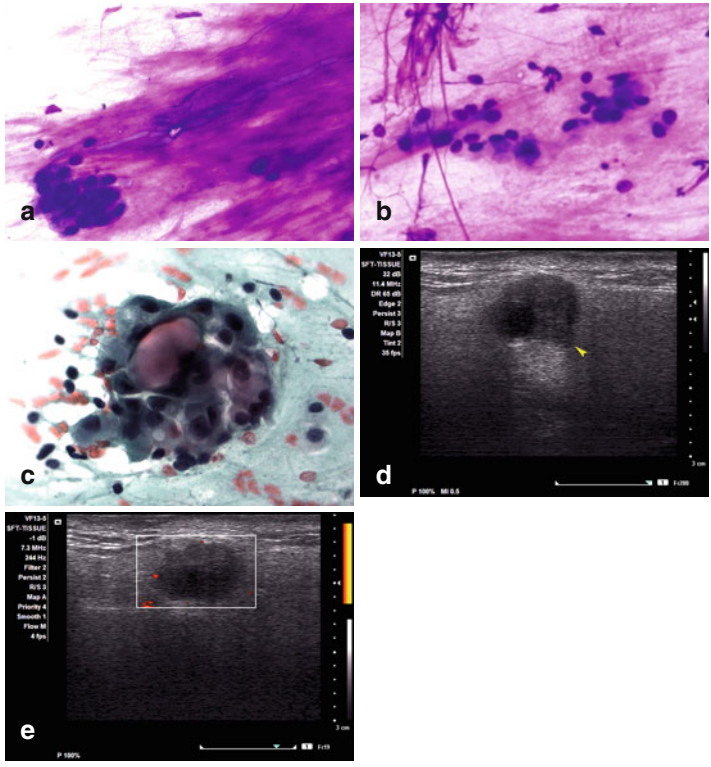

FIGURE 5.22 Low-grade mucoepidermoid carcinoma. Abundant mucus, scattered small cell groups, intermediate-type squamous cells, and few mucin-producing cells are characteristic, although not diagnostic findings, of this tumor (**a**–**c**). US features are not specific and overlap with those of benign cysts and tumors including marked hypoechogenicity and well-defined borders (**d**, **e**). The *arrowhead* points to an area of extracapsular invasion (**a**, **b** Diff-Quik stain, high magnification; **c** Papanicolaou stain, high magnification)

Pattern VI: Small Epithelial Cell Pattern

Various primary salivary neoplasms as well as dermal, adnexal, and even metastatic deposits should be considered in the differential diagnosis of this cytologic pattern. Primary

salivary gland neoplasms include monomorphic adenoma, pleomorphic adenoma with scanty stroma, adenoid cystic carcinoma, and rarely, primary small cell carcinoma and lymphoepithelioma-like carcinoma. Dermal eccrine cylindroma and pilomatrixoma, infiltrative or metastatic basal cell carcinoma, metastatic neuroendocrine carcinoma of the skin or lung, and lymphomas must be considered in light of the clinical findings. Differentiating monomorphic adenoma from adenoid cystic carcinoma may be one of the most difficult diagnostic problems in salivary gland cytology.

Monomorphic Adenoma (Basal Cell Adenoma)

This tumor is composed of small, uniform basaloid cells and absence of the myxochondroid stroma seen in pleomorphic adenoma. Cytologically, this tumor is often indistinguishable from pleomorphic adenoma, with scant stroma and adenoid cystic carcinoma. Complete surgical excision is the treatment of choice. Local recurrences are unusual.

Clinical findings. This rare tumor affects predominantly the parotid gland of adults, with no sex predilection. Patients often have an asymptomatic mass present for a variable period ranging from months to years. Superficial lobe tumors are detected earlier; thus, the size usually is <3 cm. Larger tumors are located in the deep lobe and tend to have cystic degeneration.

Histopathology. Tumors of major glands are encapsulated, whereas those of minor glands are often uncapsulated, although well circumscribed. Cells are columnar or cuboidal and are arranged in tubular, solid, trabecular, or membranous patterns of growth. All patterns, but in particular the solid pattern, may show squamous horns or eddies, and the membranous pattern shows thick eosinophilic hyaline membranes, which are reduplicated basement lamina similar to those of dermal cylindroma.

Immunoprofile. In the tubular component, epithelial cells are cytokeratin, EMA, and CEA positive. The myoepithelial cells are CD10, calponin, p63, actin, and S-100 protein positive.

Molecular profile. Loss of heterozygosity 16q12–13, a region related to the cylindromatosis gene *CYLD*, has been found. Trisomy of chromosome 8 and t(7;13) have also been reported.

FNA findings. Smears are cellular and show numerous blue cells and variable amounts of collagenous stroma that appears metachromatic on Romanowsky stains (Fig. 5.23a). Cellular dissociation and single cells may be numerous. The membranous basal cell adenoma shows features identical to those of adenoid cystic carcinoma, and the distinction between the two is almost impossible. When cellular complex aggregates with little or no stroma are the predominant pattern, the distinction from the solid (anaplastic) type of adenoid cystic carcinoma may be extremely difficult. The identification of spindle cells and capillaries within the arborizing collagenous stroma is useful for the correct identification of the tumor (Fig. 5.23b). Also, the stroma cell interface is fuzzy and fibrillary, with a subtle interconnection between the two instead of the sharp interface often seen in adenoid cystic carcinoma (Fig. 5.23c). However, adenoid cystic carcinoma may show a fibrillary desmoplastic stroma produced in the areas of invasion that is indistinguishable from the stroma of basal cell adenoma. The difficulty of the distinction is even more difficult in the solid type of adenoid cystic carcinoma that shows limited amounts of the characteristic globular cylindromatous metachromatic extracellular matrix. The well-demarcated cylinder cell interface may not be prominent in this type.

US features. Superficial tumors are solid and often round or oval, well circumscribed, and hypoechoic, with a homogeneous echotexture (Fig. 5.23d, e). Deep tumors are larger, often round and well circumscribed, and hypoechoic, with a variably heterogeneous echotexture due to cystic change, particularly in tumors measuring >3 cm (Fig. 5.23f, g). Almost all tumors show posterior acoustic enhancement.

Adenoid Cystic Carcinoma

This basaloid malignant tumor is composed of epithelial and modified myoepithelial cells and varying amounts of globular cylindromatous matrix. Surgery is the treatment of choice,

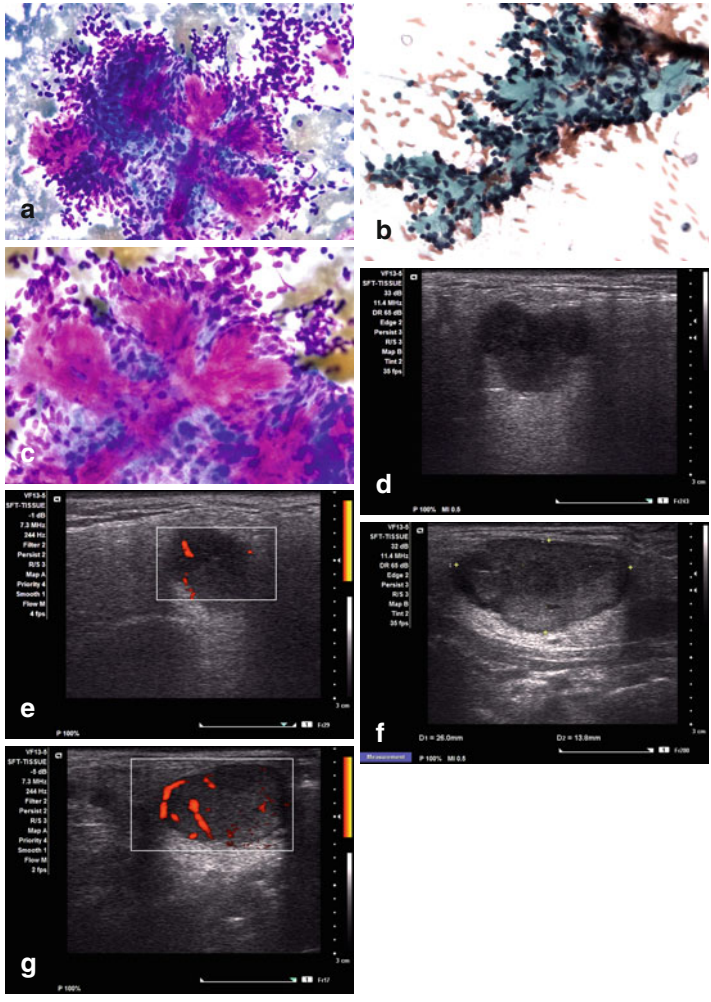

FIGURE 5.23 Monomorphic (basal cell) adenoma. Cytologic findings (**a**–**c**). Ultrasound features are not specific and overlap with those seen in benign mixed tumors including lobulated margins, hypoechogenicity with posterior acoustic enhancement (**d**, **e**), and slightly heterogeneous echotexture in larger tumors (**f**, **g**) (**a**, **c** Diff-Quik stain, high magnification; **b** Papanicolaou stain, medium magnification)

and radiation therapy may be considered in unresectable and/or deeply invasive tumors.

Clinical findings. This tumor comprises 10 % of salivary gland neoplasms and affects major and minor salivary glands. It occurs predominantly in adult and old individuals who present with a slow-growing mass with associated local pain, paresthesia, or even facial nerve paralysis. The prognosis is poor, and the outcome is usually fatal.

Histopathology. This infiltrative unencapsulated tumor has cells arranged in tubular, cribriform, and solid architectural patterns that are present in various proportions in the tumor. The lumens are filled with hyaline mucoid material. Perineural invasion is commonly seen.

Immunoprofile. No markers are specific for this tumor. Epithelial cells are keratin, CEA, and EMA positive. The myoepithelial cells are CD10, calponin, p63, actin, and S-100 protein positive. The tumor is reported to be positive for CD117 and bcl-2. Ki-67 immunostain may be helpful for distinguishing this tumor from polymorphous low-grade adenocarcinoma. The extracellular material is PAS and mucicarmine positive. Other biomarkers expressed in adenoid cystic carcinoma include p53, EGFR, and MYB.

Molecular profile. The t(6;9)(q22-23;p23-24) translocation in adenoid cystic carcinoma results in fusion and activation of the *MYB* gene at 6q22-23 and the *NFIB* gene at 9p23-24. The *MYB–NFIB* fusion transcript, present in at least one third of salivary gland adenoid cystic carcinomas, can be detected by new reverse transcription polymerase chain reaction screening methods and FISH, and has emerged as a potential therapeutic target. Frequently, there is overexpression of the c-kit protein; however, no *c-kit* gene mutations have been shown and no response to imatinib mesylate therapy has been reported.

FNA findings. Smears are cellular, and, depending on the histologic pattern, the cellular elements may be complex tridimensional, glandular, trabecular, and solid, composed of small blue cells (Fig. 5.24a). Cell dissociation is usually prominent,

and numerous stripped nuclei are present in the background. The cells are uniform, and nuclear features are usually bland-appearing with small nucleoli and do not show features of malignancy (Fig. 5.24b).

The stroma seen in adenoid cystic carcinoma is of two types: (1) the classic cylindromatous globular stroma resulting from basal membrane reduplication is acellular and avascular and has a sharp separating edge from the surrounding blue cells (Fig. 5.24c, d) and (2) the desmoplastic tumor stroma seen in the areas of invasion is fibrillary with fuzzy borders and interdigitates with the surrounding blue epithelial cells in a fashion similar to that seen in basal cell adenoma (Fig. 5.24e).

Two important features that may be seen in smears are necrosis and atypical mitoses that would favor the diagnosis of adenoid cystic carcinoma over basal cell adenoma; however, these features are found infrequently. Thus, considering the overlapping FNA cytology between these two tumors, the Swedish school of cytology recommends, based on its vast experience, that even in the presence of classical cytologic features of adenoid cystic carcinoma, such a conclusive diagnosis should be made only in the presence of symptoms and signs of facial nerve damage.

Neoplasms that have a cylindromatous pattern and mimic adenoid cystic carcinoma include pleomorphic adenoma, basal cell adenoma, epithelial–myoepithelial carcinoma, and polymorphous low-grade adenocarcinoma. Pilomatrixoma with prominent basaloid cell representation and scanty squamous ghost cells and calcific matter is another tumor that resembles solid adenoid cystic and basal cell adenoma. Clinical features and careful search for additional cytologic features are helpful for reaching the diagnosis. Likewise, basal cell adenocarcinoma primarily to the salivary gland and basal cell carcinoma of dermal origin show cytologic features very similar to those of solid adenoid cystic carcinoma and basal cell adenoma. Mitoses and necrosis, when present, help in the distinction of a malignant process from basal cell adenoma. Cytologic diagnosis of the specific type of malignancy is often less than impossible.

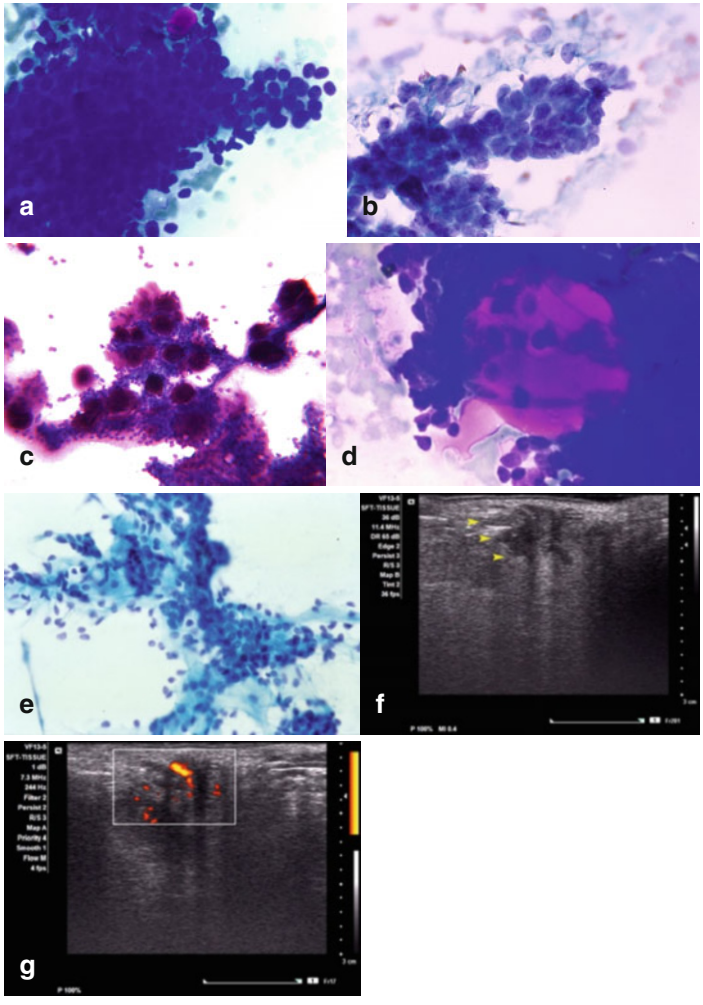

FIGURE 5.24 Adenoid cystic carcinoma. Cytologic findings (**a**–**e**). Ultrasound images show a mass with ill-defined margins, heterogeneous echotexture, and infiltrating borders (*arrowheads*); the needle length is seen emerging from the left upper corner (**f**, **g**) (**a** Diff-Quik, high magnification; **b**, **e** Papanicolaou stain, medium magnification; **c** MGG stain, medium magnification; **d** Diff-Quik stain, high magnification)

Metastasis from Merkel cell and small cell carcinoma should also be considered in the diagnosis.

US features. Small tumors are encapsulated, well defined, and hypoechoic. Large tumors are often infiltrative, hypoechoic, and heterogeneous with a complex echotexture reflecting areas of necrosis and hemorrhage (Fig. 5.24f, g).

Pattern VII: Large Epithelial Cell Pattern

These neoplasms can be arbitrarily divided into low-grade and high-grade types. The large cell low-grade tumors include acinic cell carcinoma, mammary analogue secretory carcinoma, oncocytic neoplasms, epithelial–myoepithelial carcinoma, clear cell adenocarcinoma, and metastasis. Those with a high-grade pattern include high-grade mucoepidermoid carcinoma, high-grade carcinoma NOS, squamous carcinoma, salivary duct carcinoma, and metastasis including, but not limited to, melanoma.

Acinic Cell Carcinoma

This is a malignant salivary gland neoplasm showing differentiation from intercalated duct/serous acinar cells. It contains cytoplasmic zymogen granules and forms various histologic patterns. Complete surgical excision is the treatment of choice; however, there is 35 % recurrence rate and 15 % metastatic rate.

Clinical findings. Acinic cell carcinoma represents approximately 20 % of salivary gland malignancies, often arises in the parotid gland, and is slightly more common in women, with a peak incidence in the seventh decade of life, but may occur at all ages, including in children, in whom it is the second frequent malignancy after mucoepidermoid carcinoma. Patients have a slow-growing mass that may be present for months or even years and are commonly asymptomatic, although some may cause vague and intermittent pain.

Histopathology. The tumor cells grow forming solid, microcystic, papillary–cystic, and follicular patterns, the first two being the most common. Papillary projections supported by

thin fibrovascular cores are present in the papillary–cystic pattern. The tumor is similar to thyroid parenchyma in the follicular-patterned tumor and has eosinophilic proteinaceous material lined by columnar or cuboidal cells.

The cellular elements may have variable proportions of *acinar cells* with polyhedral shape, eccentric round nuclei, and granular cytoplasm with zymogen granules that are characteristic of this tumor and are predominant in well-differentiated tumors. The granules are identified by electron microscopy as round electron-dense cytoplasmic secretory granules. Variable numbers of *intercalated ductal cells* with columnar or cuboidal shape, eosinophilic cytoplasm, and central nuclei, *clear cells*, and *vacuolated cells* may also be present. In summary, this tumor show different architectural patterns and cytologic findings within the same tumor. Chronic inflammation and hemorrhage may be seen. Cell pleomorphism and mitoses are usually absent.

Immunoprofile. Immunostains are not specific and show keratin positivity. Calponin, actin, and p63 are negative, with high expression for p53 and bcl-2. Acinar and intercalated cells are PAS + diastase resistant and mucicarmine negative. All other cells are PAS (-).

Molecular profile. Alterations of chromosome arms 4p, 5q, 6p, and 17p have been described.

FNA findings. Aspirates are usually cellular with cells both single and grouped, including formation of acinar arrangements (Fig. 5.25a). Thin vascular structures decorated with cellular elements of variable size and complexities are often present (Fig. 5.25b). The cytoplasmic membrane is friable, and the cells are easily damaged during the smear process, resulting in the presence of numerous naked nuclei and a granular background. Detached small fragments of vascular elements may also be found in the background. Macrophages are identified when cystic change is present.

In contrast to benign salivary gland tissue, well-differentiated acinic cell carcinoma often lacks ductal cells and adipose tissue, unless surrounding benign salivary gland tissue is inadvertently sampled. Lack of the narrow cytoplasmic rim permits the distinction of naked nuclei from small lymphocytes

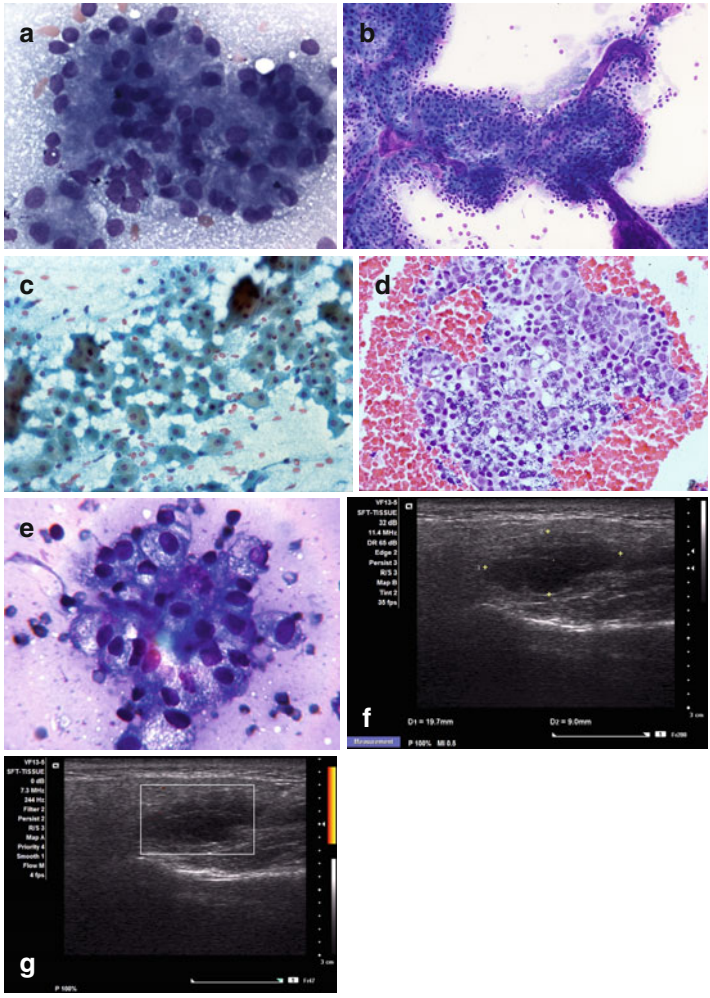

FIGURE 5.25 Acinic cell carcinoma. Cytologic features are shown in (**a**–**e**). The US images show an irregularly shaped hypoechoic mass with slight heterogeneous echotexture and no vascularity by Doppler examination (**f**, **g**) (**a**, **b**, **e** MGG stain, medium and high magnification; **c** Papanicolaou stain, medium magnification; **d** hematoxylin and eosin stain, medium magnification)

and avoids an erroneous diagnosis of Warthin's tumor, particularly in the presence of cystic change. Distinguishing oncocytoma from acinic cell carcinoma may be more challenging because the smear pattern, cellular features including nuclear characteristics, and smear background are almost identical (Fig. 5.25c). When cell block slides stained with H&E are available, the basophilic, coarse cytoplasmic granules are more conspicuous than the uniform eosinophilic granules of oncocytoma (Fig. 5.25d). Of note, clear cell change may be seen in both acinic cell carcinoma and oncocytoma, and even the possibility of epithelial–myoepithelial carcinoma, clear cell adenocarcinoma, and metastatic renal cell carcinoma may be entertained (Fig. 5.25e). Cystic acinic cell carcinoma may show vacuolated cells resembling low-grade mucoepidermoid carcinoma. Differential diagnosis includes other low-grade salivary gland neoplasms such as mucoepidermoid carcinoma and the recently described mammary analogue secretory carcinoma.

US features. The features are not specific, and the tumor is hypoechoic and heterogeneous, with areas of cystic degeneration (Fig. 5.25f, g).

Mammary Analogue Secretory Carcinoma

This tumor was described in 2010 and is strikingly similar to the secretory breast carcinoma not only morphologically but also at the molecular level with identical translocation.

Clinical findings. The tumor appears to be more common in men than in women with an average age of presentation of 45 years and predominantly affects major salivary glands. The tumor is considered of low grade, has a disease-free survival of 90 months, and may involve regional neck lymph nodes.

Histopathology. The architectural pattern is often microcystic; however, macrocystic and solid patterns have been described. Cytologically, the tumor often shows monomorphic large cells with finely vacuolated cytoplasm with bland-appearing round nuclei and small nucleoli. Few mitoses may

be present. Hobnailing, eosinophilic vacuolated cytoplasm, and variable mucin production have been described. This tumor must be distinguished from oncocytic tumors, acinic cell carcinoma, low-grade mucoepidermoid carcinoma, and salivary gland duct adenocarcinoma. The histo- and cytomorphology may be similar, and the final diagnosis rests upon the molecular detection of the specific and unique translocation.

Immunoprofile. The tumor is strongly positive for S-100 protein and mammaglobin. High-molecular-weight keratin, vimentin, and cytokeratin 19 are also positive.

Molecular profile. The translocation between the *ETV6* gene and the *NTRK3* gene located on chromosomes 12p13 and 15q25 is seen in almost 100 % of tumors and can be detected by FISH analysis in paraffin-embedded tissue or FNA cytology material.

FNA findings. Smears are cellular showing cell aggregates and single cells. Cell aggregates may have acinar, tight, small, tubular, or arborizing papillary patterns with transgressing capillaries. Cells have abundant finely granular and variably vacuolated cytoplasm, eccentrically placed round nuclei, and nucleoli of variable size. Ample eosinophilic cytoplasm, binucleation, signet ring cell-like cells, and mild to moderate nuclear atypia may be seen. Amorphous aggregates of mucin and stripped tumor cell nuclei may be seen in the background (Fig. 5.26).

Oncocytoma

This rare benign tumor that comprises <1 % of salivary gland neoplasms is composed of large cells with granular mitochondria-rich eosinophilic cytoplasm. Complete surgical excision is the treatment of choice.

Clinical findings. The tumor often occurs in the parotid gland, has no gender preference, and occurs in the sixth to eighth decade of life. Patients have a painless mass and are asymptomatic.

Histopathology. The tumor is encapsulated with a solid, organoid, and trabecular pattern composed of enlarged, polyhedral oncocytic cells with central round nuclei and conspicuous nucleoli. Cellular pleomorphism, necrosis, or mitoses

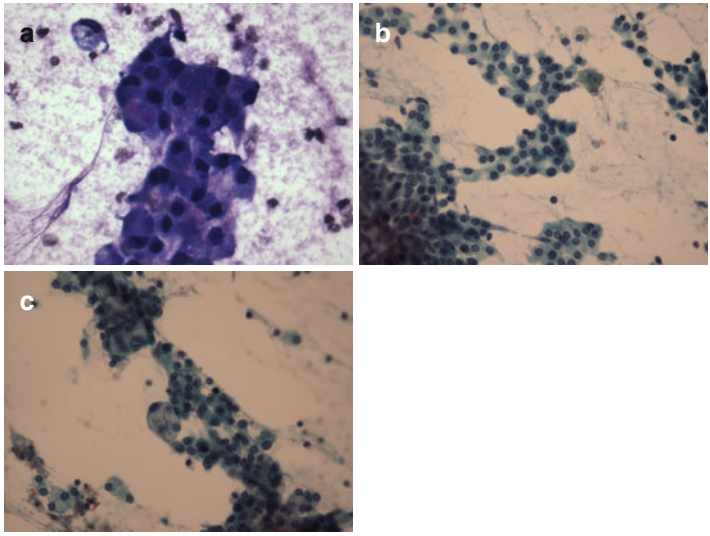

FIGURE 5.26 Mammary analogue secretory carcinoma. Smears are cellular and show cells with ample eosinophilic dense cytoplasm, granular background, and scattered stripped nuclei; large cytoplasmic vacuoles displacing the nucleus to the periphery ("signet ring-like" cells) are also noted (**a**). Papanicolaou-stained smears show sheets of large cells with eosinophilic cytoplasm, round central and eccentrically placed nuclei, and small inconspicuous nucleoli (**b**). Occasional cells with variable cytoplasmic vacuolization are also seen (**c**). Note the striking similarity with oncocytic neoplasms and acinic cell carcinoma (**a** Diff-Quik stain, high magnification; **b**, **c** Papanicolaou stain, high magnification. Courtesy, Dr. Edward B. Stelow, University of Virginia, Charlottesville, VA)

are absent. A clear cell variant, in part due to accumulation of cytoplasmic glycogen, with variable transitional cell areas may occur.

Immunoprofile. The epithelial elements show an immunoprofile similar to that of Warthin's tumor.

Molecular profile. Alterations in mitochondrial DNA mutations have not been consistently found.

FNA findings. The oncocytic cells are arranged in flat sheets, papillary clusters, and as individual cells (Fig. 5.27a–c). Cytologic atypia is focal or absent, and scattered lymphoid

cells may be present (Fig. 5.27d). Cystic changes may occur. The differential diagnosis includes oncocytosis or adenomatous hyperplasia, Warthin's tumor, pleomorphic adenoma, and salivary gland carcinoma with oncocytic cells such as mucoepidermoid carcinoma, acinic cell carcinoma, adenoid cystic carcinoma, or oncocytic carcinoma. When clear cells predominate, one should consider clear variants of epithelial–myoepithelial carcinoma, primary salivary gland adenocarcinoma, myoepithelioma, mucoepidermoid carcinoma, and metastatic renal cell carcinoma.

US features. There is no typical US pattern; this is similar to other benign lesions. The tumor is a round or oval, well-defined hypoechoic homogeneous mass. Power Doppler demonstrates peripheral and intratumor blood flow (Fig. 5.27e–h). Cystic and hemorrhagic degeneration may be seen in tumors >3 cm.

Epithelial–Myoepithelial Carcinoma

This rare, low-grade malignant neoplasm is composed of epithelial and myoepithelial cells. Complete surgical excision is the treatment of choice; however, there is a 30–50% recurrence rate and 20 % metastatic rate.

Clinical findings. The tumor often develops in the parotid gland, is slightly more common in women, and occurs in the sixth and seventh decade of life. Patients have a slow-growing, often painless mass. Facial nerve paralysis is infrequent.

Histopathology. Tumor cells often show tubular, cystic, solid, papillary, and trabecular growth patterns that are present in various proportions within the tumor. The neoplastic cells are of two types: epithelial cuboidal with scant eosinophilic cytoplasm and myoepithelial polyhedral, large cells with vacuolated clear cytoplasm. Epithelial cells are inconspicuous in solid tumors, where the myoepithelial cells predominate. Of note, the epithelial cell layer is single, but the myoepithelial cells may form several layers. A dual layer of inner epithelial and outer myoepithelial lining cells is visualized in tumors that have cystic and tubular components. The separating stroma may be fibrovascular, myxoid, hyaline, or

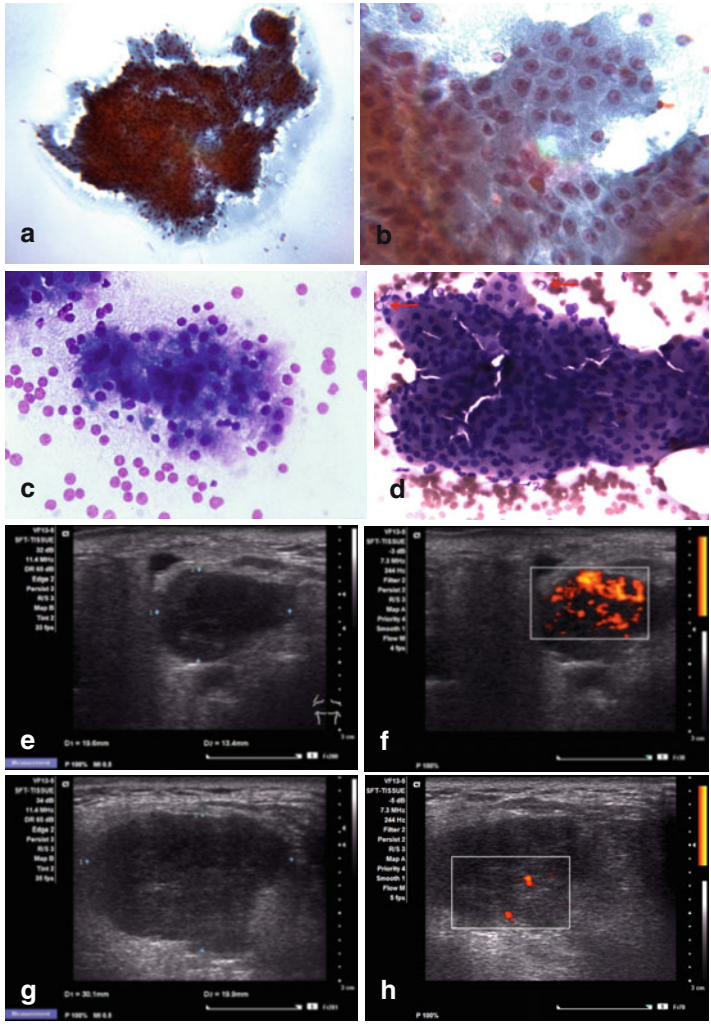

FIGURE 5.27 Oncocytoma. Cytologic features are shown in (**a**–**d**). The *red arrows* (**d**) point to rare lymphoid cells that may be found in oncocytoma. The ultrasonographic findings are not specific and are shown in (**e**–**h**) (**a**, **b** Papanicolaou stain, low and medium magnifications; **c** Diff-Quik stain, high magnification; **d** MGG stain, high magnification)

dense and is PAS positive. Mitoses, necrosis, or marked cellular anaplasia are not typically present. Oncocytic and sebaceous differentiation may occur.

Immunoprofile. The epithelial cells are positive for cytokeratin and EMA. Myoepithelial cells are p63, calponin, actin, and S-100 protein positive. Bcl-2 and c-kit are frequently positive.

Molecular profile. These tumors are reported to be aneuploid. The most frequent recurrent aberrations reported are gains of 8q (26 %) and gains of 1q (21 %) and chromosome 5 (21 %). Several oncogene candidates, including cyclin-dependent kinase 4 (*CDK4*), sarcoma-amplified sequence (*SAS*, aka tetraspanin 31 – *TSPAN31*), and glioma-associated oncogene homolog (*GLI1*), have been suggested.

FNA findings. Smears are usually cellular and show two patterns, small dark epithelial cells with scant dense cytoplasm and large myoepithelial cells with distinct borders and ample and clear cytoplasm. However, myoepithelial cells have a fragile cytoplasm and may be present as naked nuclei or cells without much cytoplasm. This may be the predominant pattern. Fragments of acellular hyaline material, which may be globular, may be present, suggesting adenoid cystic carcinoma. When clear cells predominate, alternate diagnoses to consider include clear cell adenocarcinoma, clear cell acinic cell carcinoma, or sebaceous carcinoma; however, these tumors do not exhibit a dual cell population. Thus, a thorough sampling is required for a correct diagnosis.

US features. Features of epithelial–myoepithelial carcinoma mimic those of a benign salivary gland tumor.

Clear Cell Adenocarcinoma

This is a rare malignant epithelial neoplasm composed of monotonous clear cells. The tumor has ductal but not myoepithelial cell differentiation. Complete surgical resection is the

treatment of choice for this low-grade neoplasm and the prognosis is excellent.

Clinical findings. The tumor often develops in the intraoral minor salivary glands and occurs mostly in females. There is no age preference. Patients present with swelling and may have pain and mucosal ulceration. Prognosis is good; however, local recurrence and lymph node metastases may be seen.

Histopathology. Polygonal to round cells with clear glycogen-rich cytoplasm, eccentric round nuclei, and small nucleoli are arranged in sheets, nests, and cords. Ductal structures are absent. There is mild to moderate nuclear pleomorphism, and mitoses are rare. The stroma is usually thin and fibrous, but may be broad and thick and hyalinized or loose. The differential diagnosis includes clear cell mucoepidermoid carcinoma, myoepithelial neoplasms, and metastatic renal cell carcinoma.

Immunoprofile. Tumors are strongly positive for p63, CEA, and EMA. Cytokeratin is positive. There is variable positivity with vimentin and GFAP. However, myoepithelial markers such as S-100 protein, calponin, and smooth muscle actin are usually negative.

Molecular profile. Tumors show a consistent translocation t(12;22) involving the *EWSR1* (Ewing sarcoma breakpoint region *1*) gene and the *ATF1* gene. This marker may be used to differentiate this tumor from other salivary gland tumors that do not harbor this translocation such as myoepithelioma, acinic cell carcinoma, pleomorphic adenoma, mucoepidermoid carcinoma, oncocytic neoplasms, salivary duct carcinoma, adenoid cystic carcinoma, and pleomorphic low-grade adenocarcinoma.

FNA findings. Smears are cellular and show groups and sheets of cells with well-defined cytoplasmic borders, uniform round nuclei, small nucleoli, and abundant clear cytoplasm. Hyaline globules are absent, although fragments of hyalinized stroma may be present.

Salivary Duct Carcinoma

This high-grade malignancy arises from the excretory ducts and resembles breast carcinoma on histology. Treatment of choice includes complete excision with radical neck dissection and postoperative radiotherapy. There is a 30–40 % recurrence rate, 50–60 % metastatic rate, and 60–80 % mortality rate.

Clinical findings. This rare tumor is more common in men, often occurs after the age of 50 years, and commonly affects the parotid gland. When the parotid gland is affected, patients have a rapidly growing mass, with or without local pain and/or facial nerve paralysis.

Histopathology. The tumor resembles the pathologic findings of intraductal and infiltrating ductal breast carcinoma, including comedo necrosis and cribriform, solid, cystic, and papillary patterns. Neoplastic cells are large with large hyperchromatic nuclei, prominent nucleoli, and slightly eosinophilic cytoplasm. Necrosis and mitosis are often present. Squamous metaplasia, oncocytic changes, chronic inflammation, and psammoma-like bodies may be present. Histologic variants including sarcomatoid, micropapillary, mucin-rich, and osteoclast-like giant cell may occur, as in breast carcinoma

Immunoprofile. Salivary duct carcinoma expresses some markers also found in breast carcinoma. Gross cystic disease fluid protein-15 (GCDFP-15) is found in 80 % of cases. HER2/neu is positive in 90 % of cases; however, it depends on the antibody clone used and scoring system. Cytokeratin, EMA, and CEA are also positive. ER and PR expression is exceptional; in contrast, androgen receptor (AR) positivity is seen in 67–83 % of cases. Myoepithelial differentiation markers including p63, calponin, smooth muscle actin, and vimentin are negative. Following the breast cancer molecular classification, attempt to classify 42 pure salivary duct carcinomas into molecular subtypes showed that 16.7, 69, 4.8, 9.5, and 0 % were of HER2, luminal AR-positive, basal-like,

indeterminate, and luminal phenotype, respectively. The prognostic implications of this classification and possible targeted therapy for these tumors need to be evaluated.

Molecular profile. There is loss of heterozygosity of polymorphic markers of chromosome locus 9p21 containing the tumor suppressor gene *p16*(INK4a/CDKN2/MTS1). The apoptosis-related genes *CASP10* and *MMP11* are overexpressed.

FNA findings. Smears are cellular and show complex tridimensional aggregates. Flat sheets are present arranged in cribriform, solid, and papillary patterns. Occasional psammoma bodies, squamous metaplastic cells, and comedo-like necrosis may be seen. Cells are large and polyhedral with granular or vacuolated cytoplasm, large hyperchromatic nuclei, prominent nucleoli, and increased mitotic activity (Fig. 5.28).

US features. In one reported case of salivary duct carcinoma of the extra-glandular segment of Stensen's duct, the scan showed an ill-defined hypoechoic tumor and a dilated and thickened wall of the duct connected with the tumor.

Malignant neoplasms showing large cells and a high nuclear grade, including metastases, are rare, and a specific FNA diagnosis cannot be made in most cases. It is sufficient to state the diagnosis of a high-grade malignancy and exclude direct extension of a head and neck tumor or metastasis to the salivary gland or intraparotid lymph node to avoid unnecessary surgery. A clinical history of previous malignancy is of extreme importance. In general, a metastatic deposit must be suggested when the smear pattern is different from that of known salivary gland malignancies (Fig. 5.29).

Pattern VIII: Spindle Cell Pattern

Processes showing this pattern can be divided into low grade and high grade. Myoepithelioma is the typical example of low-nuclear-grade lesions, and primary or secondary sarcomas, malignant myoepithelioma, and malignancies with

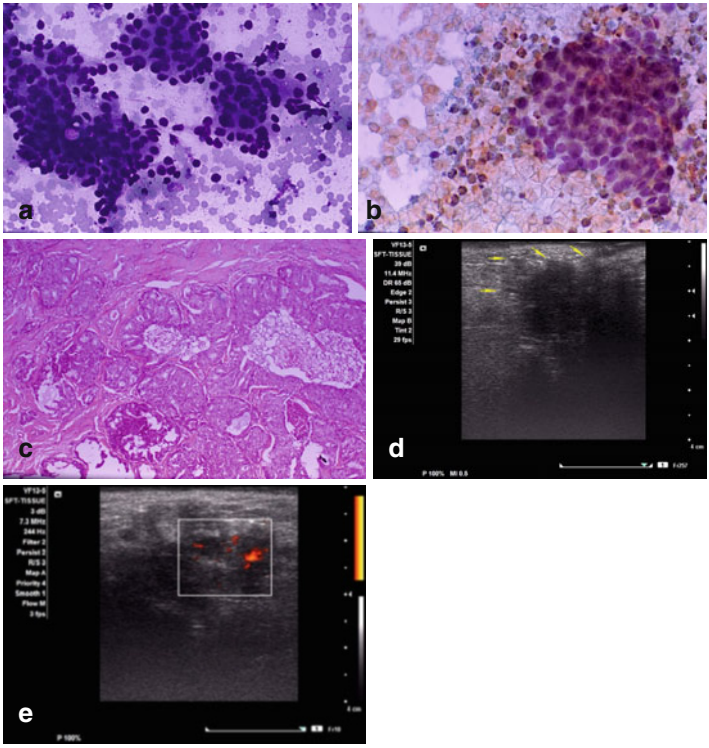

FIGURE 5.28 Salivary duct carcinoma. Cytologically and histologically, this tumor is almost indistinguishable from ductal breast carcinoma. Ultrasound imaging from a different case shows a heterogeneous mass with spiculated fuzzy borders (**d**, *arrows*) and irregular vascular flow by Doppler examination (**e**) (**a** Diff-Quik stain, medium power; **b** Papanicolaou stain, medium power; **c** hematoxylin and eosin stain, medial magnification)

spindle cell morphology including metastatic melanoma should be considered in the high-grade group. These tumors are rarely described in either the histopathology or cytology literature.

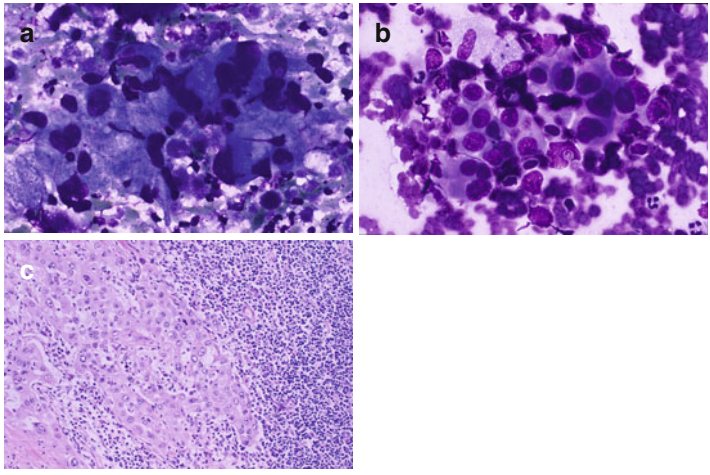

FIGURE 5.29 Metastatic adenocarcinoma from pulmonary origin (**a**). Metastatic squamous cell carcinoma to an intraparotid lymph node (**b**) with histologic correlation (**c**) (**a**, **b** Diff-Quik stain, high magnification; **c** hematoxylin and eosin stain, medial magnification)

Myoepithelioma

This tumor is a benign neoplasm composed of spindle, epithelioid, plasmacytoid, or clear cells. Complete surgical excision is the treatment of choice. Recurrence is related to incomplete excision.

Clinical findings. This slow-growing tumor is rare, has no gender predilection, often occurs in adults with an average age of 44 years, and develops preferentially in the parotid gland.

Histopathology. Spindle cells are arranged in interlacing fascicles resembling stroma. Plasmacytoid cells are often seen in myoepitheliomas arising in the minor salivary glands. The stroma is collagenous or mucoid.

Immunoprofile. Cells are positive for cytokeratins. Spindle cells show variable reactivity with actin, calponin, S-100 protein, GFAP, and smooth muscle myosin heavy chain.

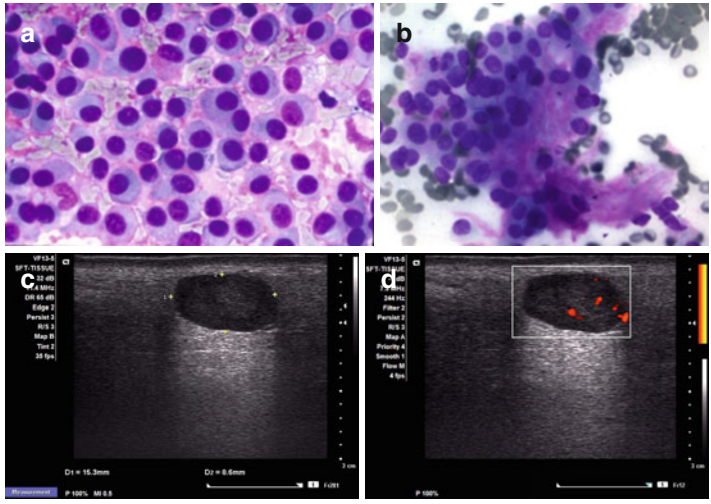

Figure 5.30 Myoepithelioma. Numerous myoepithelial cells are present both single and supported by a collagenous stroma with lack of fibrillary magenta features (**a**, **b**). The US findings are non-specific including oval, slightly lobulated well-defined tumor edges, marked hypoechogenicity, and minimal internal vascularity by Doppler examination (**c**, **d**) (**a** Diff-Quik stain; **b** MGG stain, high magnification)

Molecular profile. Alterations of chromosomes 1, 9, 12, and 13 have been detected.

FNA findings. Smears are cellular and show bland-appearing, uniform spindle, epithelioid/plasmacytoid, and stellate cells. Nuclear grooves and intranuclear inclusions may be present. Scant myxoid and fibrillary matrix may be seen and in some cases may have a globular appearance resembling adenoid cystic carcinoma (Fig. 5.30a, b).

US features. The sonographic characteristics of benign and malignant neoplasms have no significant differences. Thus, US cannot differentiate with certainty between benign and malignant cases, particularly in low-grade neoplasms

(Fig. 5.30c, d). US findings reported in a 7.8-cm tumor included a well-circumscribed mass with solid and cystic components and posterior acoustic enhancement.

Myoepithelial Carcinoma

This tumor is the malignant counterpart of myoepithelioma.

Clinical findings. This tumor is rare, has no gender predilection, occurs in adults, and commonly affects the parotid gland. Patients often have a slow-growing, asymptomatic mass.

Histopathology. Various proportions of spindle, plasmacytoid, epithelioid, and clear cells with variable nuclear pleomorphism are seen. Variable amounts of myxoid or mucoid stroma may be seen and, in some areas, may appear globular and eosinophilic. Cystic changes may be present. In the absence of malignant cytomorphology, invasion into surrounding tissue is the only indication of malignancy.

Immunoprofile. Cytokeratin is positive, as are myoepithelial markers such as calponin, p63, actin, S-100 protein, and vimentin.

Molecular profile. Infrequent cytogenetic alterations have been seen.

FNA findings. The findings are similar to those of myoepithelioma; however, marked nuclear pleomorphism, atypical mitosis, and necrosis may be present (Fig. 5.31a–c).

US features. One reported case describes a hypoechogenic and heterogeneous 2-cm tumor with irregular borders, invading the surrounding soft tissue including the masseter muscle and subcutaneous tissue; Doppler examination showed a hilar vascular pattern (Fig. 5.31d, e).

In summary, USG-FNA should be considered in the diagnostic evaluation of a patient with a salivary gland mass, allowing for optimal surgical planning and preoperative patient counseling. It has >90 % sensitivity and specificity, modifies or avoids surgery in 30 % of cases, and procures material for ancillary tests, including molecular studies potentially useful for targeted therapy.

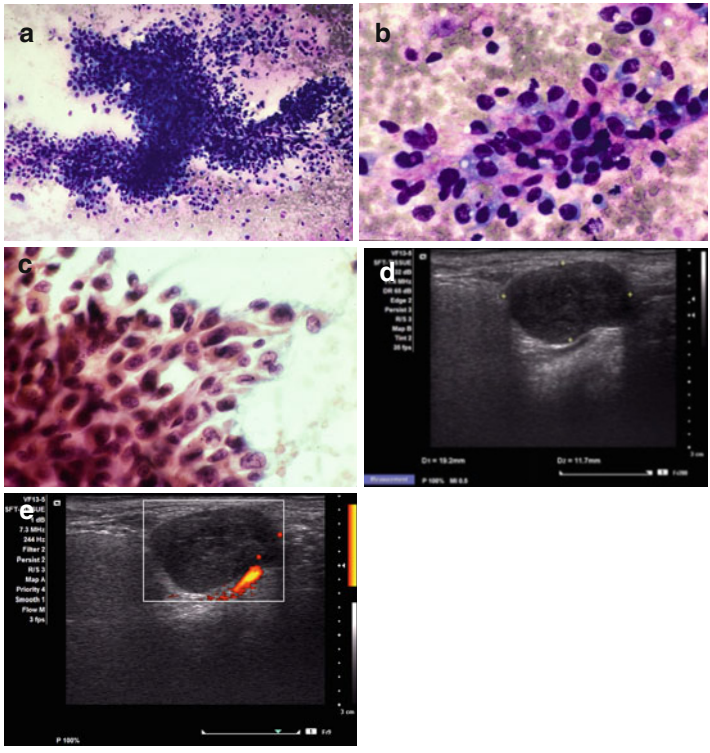

FIGURE 5.31 Malignant myoepithelioma. Smears show high cellularity, branching complex pseudopapillary aggregates, plasmacytoid and spindle cell features, and nuclear atypia (**a**–**c**). Ultrasound imaging shows a well-circumscribed homogeneous hypoechoic mass with posterior acoustic enhancement and minimal vascularity by Doppler examination (**d**–**e**) (**a**, **b** MGG stain, medium and high magnification; **c** Papanicolaou stain, high magnification)

Suggested Reading

Barnes L, Eveson JW, et al. Salivary glands. In: Barnes L, Eveson JW, Reichart P, Sidransky D, editors. Pathology and genetics of head and neck tumors. Lyon: IARC; 2005. p. 209–81.

Brill 2nd LB, Kanner WA, et al. Analysis of MYB expression and MYB-NFIB gene fusions in adenoid cystic carcinoma and other salivary neoplasms. Mod Pathol. 2011;24(9):1169–76.

Di Palma S, Simpson RH, et al. Salivary duct carcinomas can be classified into luminal androgen receptor-positive, HER2 and basal-like phenotypes*. Histopathology. 2012;61(4):629–43.

El-Naggar AK. Celular and molecular pathology of head and neck tumors. In: Bernier J, editor. Head and neck cancer: multimodality management. New York: Springer; 2011. p. 57–79.

Geisinger KR, Stanley MW, et al. Salivary gland masses. In: Modern cytopathology. Philadelphia: Churchill Livingstone; 2004. p. 781–811.

Griffith CC, Stelow EB, et al. The cytological features of mammary analogue secretory carcinoma: a series of 6 molecularly confirmed cases. Cancer Cytopathol. 2013;121(5):234–41.

Gupta S, Sodhani P, et al. Oncocytic papillary cystadenoma of parotid gland: a diagnostic challenge on fine-needle aspiration cytology. Diagn Cytopathol. 2011;39(8):627–30.

Henry-Stanley MJ, Beneke J, et al. Fine-needle aspiration of normal tissue from enlarged salivary glands: sialosis or missed target? Diagn Cytopathol. 1995;13(4):300–3.

Johnson FB, Oertel YC, et al. Sialadenitis with crystalloid formation: a report of six cases diagnosed by fine-needle aspiration. Diagn Cytopathol. 1995;12(1):76–80.

Kim J, Kim EK, et al. Characteristic sonographic findings of Warthin's tumor in the parotid gland. J Clin Ultrasound. 2004;32(2):78–81.

Klijanienko J, el-Naggar AK, et al. Comparative cytologic and histologic study of fifteen salivary basal-cell tumors: differential diagnostic considerations. Diagn Cytopathol. 1999a;21(1):30–4.

Klijanienko J, El-Naggar AK, et al. Fine-needle sampling findings in 26 carcinoma ex pleomorphic adenomas: diagnostic pitfalls and clinical considerations. Diagn Cytopathol. 1999b;21(3):163–6.

Klijanienko J, Lagace R, et al. Fine-needle sampling of primary neuroendocrine carcinomas of salivary glands: cytohistological correlations and clinical analysis. Diagn Cytopathol. 2001;24(3):163–6.

Klijanienko J, Vielh P. Fine-needle sampling of salivary gland lesions. I. Cytology and histology correlation of 412 cases of pleomorphic adenoma. Diagn Cytopathol. 1996;14(3):195–200.

Klijanienko J, Vielh P. Fine-needle sample of salivary gland lesions. V: Cytology of 22 cases of acinic cell carcinoma with histologic correlation. Diagn Cytopathol. 1997a;17(5):347–52.

Klijanienko J, Vielh P. Fine-needle sampling of salivary gland lesions. II. Cytology and histology correlation of 71 cases of Warthin's tumor (adenolymphoma). Diagn Cytopathol. 1997b;16(3):221–5.

Klijanienko J, Vielh P. Fine-needle sampling of salivary gland lesions. III. Cytologic and histologic correlation of 75 cases of adenoid

cystic carcinoma: review and experience at the Institut Curie with emphasis on cytologic pitfalls. Diagn Cytopathol. 1997c;17(1):36–41.
Klijanienko J, Vielh P. Fine-needle sampling of salivary gland lesions. IV. Review of 50 cases of mucoepidermoid carcinoma with histologic correlation. Diagn Cytopathol. 1997d;17(2):92–8.
Klijanienko J, Vielh P. Cytologic characteristics and histomorphologic correlations of 21 salivary duct carcinomas. Diagn Cytopathol. 1998a;19(5):333–7.
Klijanienko J, Vielh P. Fine-needle sampling of salivary gland lesions. VI. Cytological review of 44 cases of primary salivary squamous-cell carcinoma with histological correlation. Diagn Cytopathol. 1998b;18(3):174–8.
Klijanienko J, Vielh P. Fine-needle sampling of salivary gland lesions. VII. Cytology and histology correlation of five cases of epithelial-myoepithelial carcinoma. Diagn Cytopathol. 1998c;19(6):405–9.
Klijanienko J, Vielh P. Salivary carcinomas with papillae: cytology and histology analysis of polymorphous low-grade adenocarcinoma and papillary cystadenocarcinoma. Diagn Cytopathol. 1998d;19(4):244–9.
Lee YYP, Wong KT, et al. Ultrasound investigations in head and neck cancer patients. In: Bernier J, editor. Head and neck cancer: multimodality management. New York: Springer; 2011. p. 221–33.
Mukunyadzi P. Review of fine-needle aspiration cytology of salivary gland neoplasms, with emphasis on differential diagnosis. Am J Clin Pathol. 2002;118(Suppl):S100–15.
Okada F, Honda K, et al. Salivary duct carcinoma of the extra-glandular segment of Stensen's duct: radiological findings and pathological correlation (2008: 10b). Eur Radiol. 2009;19(1):254–7.
Rhys R. Ultrasound of the neck. In: Allan PL, Baxter GM, Weston MJ, editors. Clinical ultrasound, vol. 2. London: Churchill Livingstone Elsevier; 2011. p. 890–919.
Rosai J. Major and minor salivary glands. In: Rosai J, editor. Rosai and Ackerman's surgical pathology, vol. 1. Edinburgh: Mosby Elsevier; 2011. p. 817–56.
Shah AA, LeGallo RD, et al. EWSR1 genetic rearrangements in salivary gland tumors: a specific and very common feature of hyalinizing clear cell carcinoma. Am J Surg Pathol. 2013;37(4):571–8.
Shi L, Wang YX, et al. CT and ultrasound features of basal cell adenoma of the parotid gland: a report of 22 cases with pathologic correlation. AJNR Am J Neuroradiol. 2012;33(3):434–8.
Skalova A, Vanecek T, et al. Mammary analogue secretory carcinoma of salivary glands, containing the ETV6-NTRK3 fusion

gene: a hitherto undescribed salivary gland tumor entity. Am J Surg Pathol. 2010;34(5):599–608.
Stanley MW. Selected problems in fine needle aspiration of head and neck masses. Mod Pathol. 2002;15(3):342–50.
Stanley MW, Bardales RH, et al. Sialolithiasis. Differential diagnostic problems in fine-needle aspiration cytology. Am J Clin Pathol. 1996a;106(2):229–33.
Stanley MW, Bardales RH, et al. Primary and metastatic high-grade carcinomas of the salivary glands: a cytologic-histologic correlation study of twenty cases. Diagn Cytopathol. 1995;13(1):37–43.
Stanley MW, Horwitz CA, et al. Basal cell carcinoma metastatic to the salivary glands: differential diagnosis in fine-needle aspiration cytology. Diagn Cytopathol. 1997;16(3):247–52.
Stanley MW, Horwitz CA, et al. Basal-cell adenoma of the salivary gland: a benign adenoma that cytologically mimics adenoid cystic carcinoma. Diagn Cytopathol. 1988;4(4):342–6.
Stanley MW, Horwitz CA, et al. Basal cell (monomorphic) and minimally pleomorphic adenomas of the salivary glands. Distinction from the solid (anaplastic) type of adenoid cystic carcinoma in fine-needle aspiration. Am J Clin Pathol. 1996b;106(1):35–41.
Tsuneki M, Maruyama S, et al. Podoplanin is a novel myoepithelial cell marker in pleomorphic adenoma and other salivary gland tumors with myoepithelial differentiation. Virchows Arch. 2013;462(3):297–305.
Wenig BM. Major and minor salivary glands. In: Atlas of head and neck pathology. Philadelphia: Saunders Elsevier; 2008. p. 536–702.
Yuan WH, Hsu HC, et al. Gray-scale and color Doppler ultrasonographic features of pleomorphic adenoma and Warthin's tumor in major salivary glands. Clin Imaging. 2009;33(5):348–53.
Zhang C, Cohen JM, et al. Fine-needle aspiration of secondary neoplasms involving the salivary glands. A report of 36 cases. Am J Clin Pathol. 2000;113(1):21–8.

Chapter 6
The Head and Neck: Miscellaneous Lesions

Ricardo H. Bardales

The Neck by Regions

We will topographically address lesions found in these regions when they are evaluated by US and USG-FNA. The regions included are submental and sublingual (Figs. 6.1 and 6.2), anterior infrahyoid, submandibular (Fig. 6.3), lateral (Figs. 6.4, 6.5, and 6.6), supraclavicular (Fig. 6.7), posterior (Fig. 6.8), and parotid. The pathology of the thyroid, parotid, and submandibular glands and lymph nodes is addressed in other sections of this book and is not included here. However, some of the minor salivary gland lesions are included.

Cystic lesions of the head and neck are commonly approached by FNA. When cyst fluid is obtained, it should be processed by centrifugation and smears made from the pellet or processed by liquid-based techniques. The most important is the US evaluation of the lesion after fluid drainage, looking for a residual solid component, which must be sampled by USG-FNA.

R.H. Bardales, MD, MIAC, ECNU
Department of Pathology and Cytopathology,
Outpatient Pathology Associates,
7750 College Town Drive, 95826 Sacramento, CA, USA
e-mail: rhbardales@aol.com

R.H. Bardales (ed.), *The Invasive Cytopathologist*, Essentials in Cytopathology 16, DOI 10.1007/978-1-4939-0730-4_6,

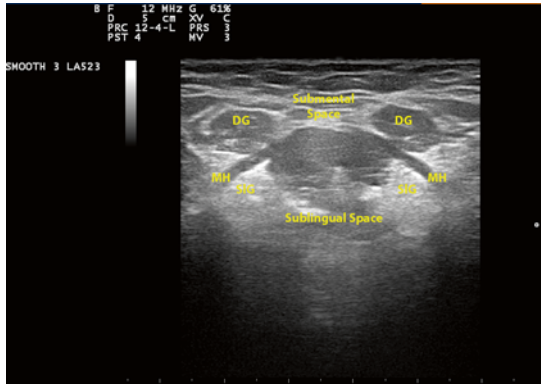

FIGURE 6.1 Submental and sublingual regions, axial view. The transducer is held in transverse position. *DG* digastric muscle, *MH* mylohyoid muscle, *SlG* sublingual gland

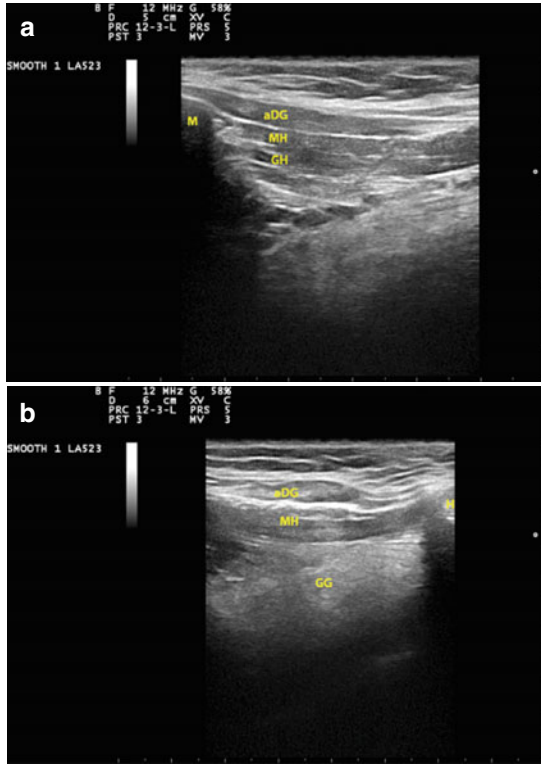

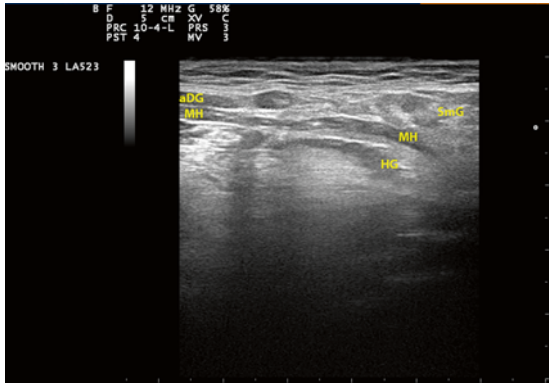

FIGURE 6.3 Left submandibular region. The transducer is held parallel to the mandible. *aDG* anterior belly of digastric muscle, *SmG* submandibular gland, *MH* mylohyoid muscle, *HG* hyoglossus muscle

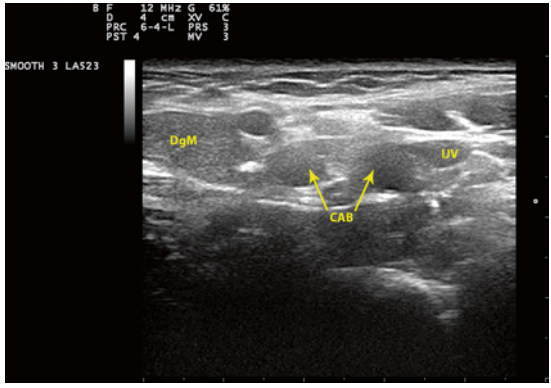

FIGURE 6.4 Left level II neck region. The transducer is held in transverse position at the level of common carotid artery bifurcation. *DgM* posterior belly of digastric muscle, *CAB* carotid artery bifurcation, *IJV* internal jugular vein

FIGURE 6.2 Submental region, sagittal view. The transducer is held parallel to the midline below the mandible (**a**) and superior to the hyoid bone (**b**). *M* mandible, *aDG* anterior belly of digastric muscle, *MH* mylohyoid muscle, *GH* geniohyoid muscle, *GG* genioglossus, *H* hyoid bone

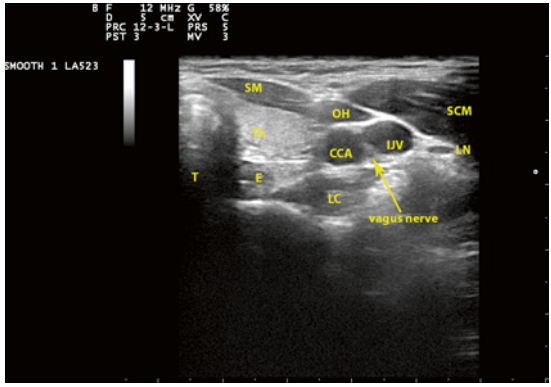

FIGURE 6.5 Left level III neck region. The transducer is held in transverse position in the mid-neck at the level of the omohyoid muscle, which is seen crossing from medial to lateral over the common carotid artery. *T* trachea, *SM* strap muscles (sternohyoid, sternothyroid), *Th* thyroid, *E* esophagus, *OH* omohyoid, *SCM* sternocleidomastoid muscle, *LC* longus colli, *CCA* common carotid artery, *IJV* internal jugular vein, *LN* lymph node

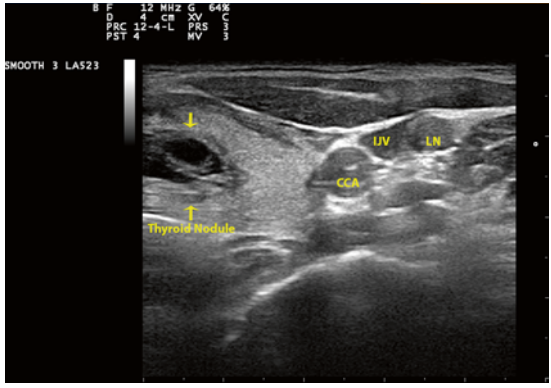

FIGURE 6.6 Left level IV neck region. The transducer is placed transverse in the upper portion of the supraclavicular fossa. *CCA* common carotid artery, *IJV* internal jugular vein, *LN* lymph node

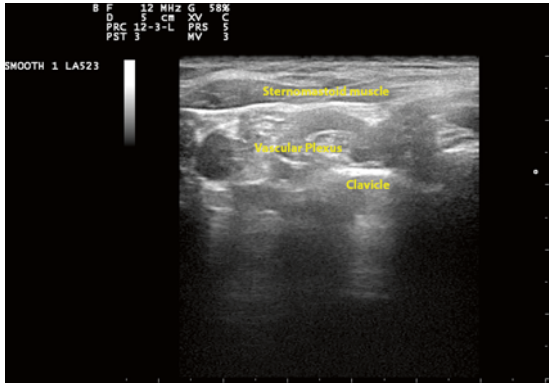

FIGURE 6.7 Left level V neck region. The transducer is placed parallel to the clavicle in the mid-posterior region

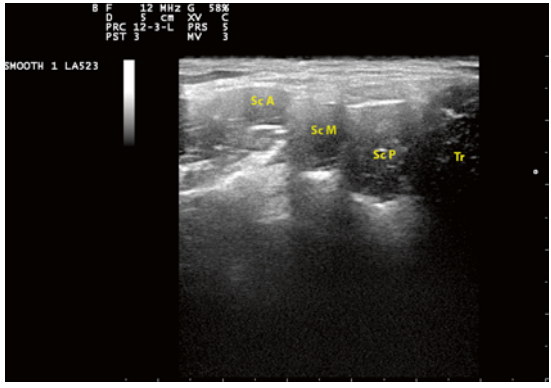

FIGURE 6.8 Left mid-level V neck region. The transducer is placed transverse in the mid-posterior neck region. *ScA* scalene muscle anterior, *ScM* scalene muscle medius, *ScM* scalene muscle posterior, *Tr* trapezius muscle

Submental/Sublingual Region

Cysts of various types, including the thyroglossal duct cyst, may be present in this region.

Ranula

Ranula is a mucus retention cyst of the sublingual gland and presents as a painless and cystic swelling in the floor of the mouth. The lining epithelium may be cuboidal, columnar, or squamous of non-keratinizing type. The so-called plunging ranula or pseudocyst lacks the lining epithelium. Aspirates show a granular precipitate, crystals, histiocytes, columnar cells, and occasionally metaplastic squamous cells. Differentiation of foamy histiocytes from mucin-producing malignant cells may be difficult, and separation from mucoepidermoid carcinoma may be impossible (Fig. 6.9). The reader is referred to the salivary gland section for further discussion. By US, the cyst is situated off line in the sublingual space, well defined, anechoic, and uniloculated and shows posterior acoustic enhancement. A large lesion is called "diving ranula."

Epidermoid Cysts

These lesions are located in the midline of the submental space; however, they are not attached to the hyoid bone and do not move with swallowing or tongue protrusion. By US, they are well defined with internal echoes which vary with the amount of keratin present.

Dermoid Cysts

Most lesions arise in the anterior portion of the floor of the mouth particularly in the sublingual space and become mani-

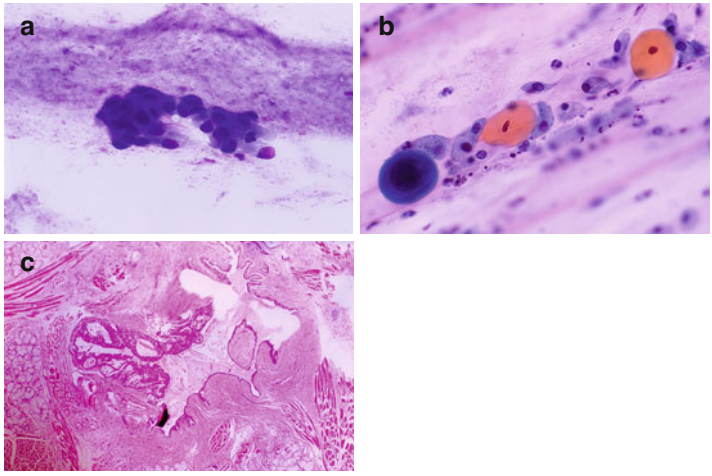

FIGURE 6.9 Mucocele. Cytologic features include scattered small aggregates of bland-appearing epithelial cells, squamous metaplastic cells, mucinophages, and mucus (**a**, **b**). The cytologic pattern is very similar, if not identical, to that of low-grade mucoepidermoid carcinoma, and surgical excision is necessary (**c**) (**a** Diff-Quik stain high magnification; **b** Papanicolaou stain, high magnification; **c** hematoxylin and eosin stain, low magnification)

fest during the second or third decades of life. They are not related to the hyoid bone and do not move with swallowing.

FNA findings. Smears show numerous anucleated squamous cells, keratinaceous debris, and acute inflammatory cells. Giant cells are found in a ruptured cyst. The differential diagnosis includes a well-differentiated squamous carcinoma, a consideration in older patients. Nucleated squamous cells with anaplastic nuclei are seen in squamous carcinoma.

US features. Dermoid cysts may be more heterogeneous than epidermoid and may have hyperechogenic streaks due to the presence of adipose tissue. Echogenic foci with posterior shadowing may be seen in the presence of bone or teeth.

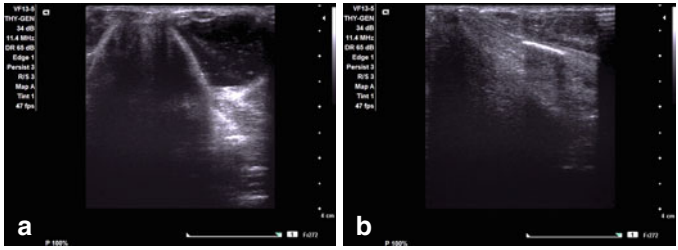

Figure 6.10 Thyroglossal duct cyst. Off-midline left unilocular well-defined cyst with posterior acoustic enhancement at the level of the hyoid bone and laryngeal cartilage (**a**). The cyst collapsed totally after drainage (**b**)

Thyroglossal Duct Cyst

Occasionally, a midline hyoid or suprahyoid thyroglossal duct cyst may develop and should be considered in the differential diagnosis of submental lesions (Fig. 6.10).

Undescended Thyroid

An undescended thyroid gland is often located in the base of the tongue; however, it may occur along the thyroglossal tract. It presents as an anterior midline neck mass, often mistaken as a thyroglossal duct cyst. Aspirates show benign follicular cells and colloid.

Tongue Tumors

The depth of tongue tumors may be assessed by US imaging of this area having the probe in a longitudinal position from the hyoid bone to the chin.

Anterior Infrahyoid and Suprasternal Region

The most common pathology of this area is the thyroglossal duct cyst and less frequently laryngocele and laryngeal tumors, chondroid tumors of the laryngeal cartilages (the

most common the cricoid), and a pharyngeal pouch. The thymus may be seen in the suprasternal area.

Thyroglossal Duct Cyst and Thyroglossal Duct Carcinoma

The thyroglossal duct involutes at the eighth gestational week; failure to involute results in the presence of a thyroglossal duct cyst or ectopic thyroid tissue. A thyroglossal duct cyst is the most common congenital mass and is often below the hyoid bone (65 %), at the level of the hyoid bone (20 %) and suprahyoid in 15 %. The cysts are often located in the midline, particularly when suprahyoid, and off the midline and surrounded by the strap muscles when infrahyoid. When located off midline, they are always located medial to the jugular vein. Most patients are under the age of 10 years, but the cysts may occur in adults as a slowly growing, painless mass that moves vertically with swallowing or tongue protrusion due to attachment to the hyoid bone.

Histopathology. The lining epithelium is columnar and may have a squamous component. The wall may contain thyroid tissue in various proportions. Both benign and malignant neoplasms can develop in a setting of a thyroglossal duct cyst. Neoplasms are of follicular derivation, i.e., follicular adenoma, follicular carcinoma, papillary thyroid carcinoma, and anaplastic carcinoma. Squamous cell carcinoma occurs rarely and in all likelihood arises from the squamous epithelium and not from the follicular epithelium. Papillary thyroid carcinoma is the most common. Medullary carcinoma does not occur for C cells have a different embryologic origin.

FNA findings. Smears are sparsely cellular and show scattered degenerated columnar, ciliated, or squamous cells, macrophages, few inflammatory cells, proteinaceous fluid, and granular debris. Squamous metaplastic cells may be seen in cases of infection or inflammation (Fig. 6.11a–c). In cases of papillary thyroid carcinoma, the smear findings are similar to those seen in the cystic variant of papillary thyroid carcinoma, including sheets of degenerated malignant cells, metaplastic cells, and psammoma bodies; the cytomorphology is identical to that described in the thyroid section (Fig. 6.11d–i).

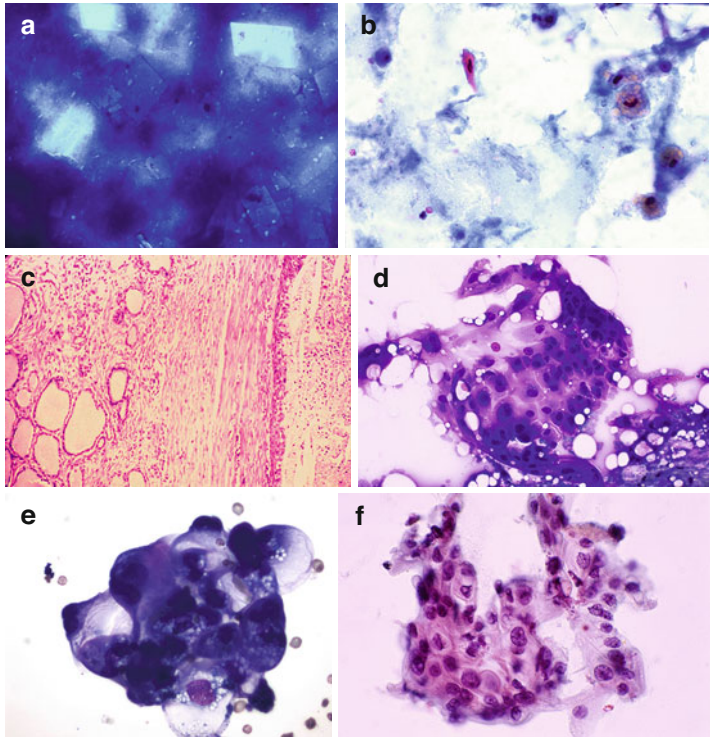

FIGURE 6.11 Thyroglossal duct cyst shows scattered macrophages, squamous cells, cholesterol crystals, and colloid (**a**, **b**). Tissue sections show the lining squamous epithelium and thyroid parenchyma toward the left side of the frame (**c**). Thyroglossal duct papillary carcinoma shows complex aggregates of large squamous metaplastic cells (**d**), "histiocytoid" cells (**e**), atypical cells (**f**), and psammoma bodies (**g**). Histology confirms the cytologic diagnosis (**h**). Cytologic findings of a different case of thyroglossal duct squamous carcinoma is shown in Fig. 6.11i (**a** Diff-Quik stain high magnification; **b** Papanicolaou stain, high magnification; **c** hematoxylin and eosin stain, low magnification; **d** Diff-Quik stain, high magnification; **e** MGG stain, high magnification; **f**, **g** Papanicolaou stain, high magnification; **h** hematoxylin and eosin, low magnification; **i** Papanicolaou stain, high magnification)

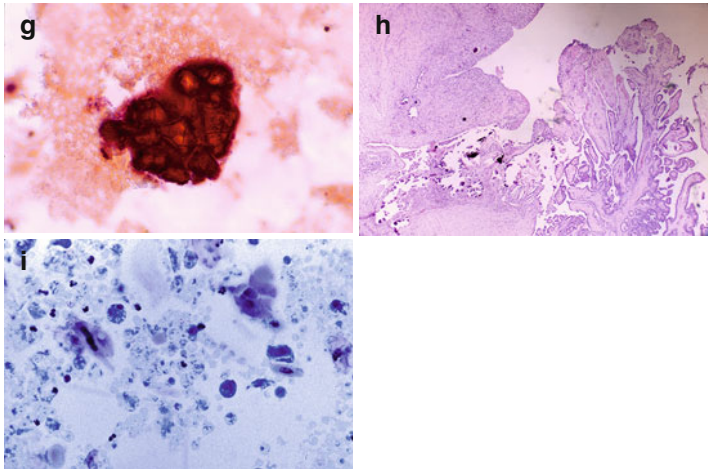

FIGURE 6.11 (continued)

US features. The US image shows a well-defined, smooth, unilocular, cystic mass with a thin wall. The relationship with the hyoid bone in the sagittal or longitudinal midline view helps in the US identification. The mass may be anechoic with posterior acoustic enhancement when purely cystic, hypoechoic when it contains debris, hypoechoic and heterogeneous when there is infection or hemorrhage, or "pseudo-solid" when there is dense proteinaceous content (Fig. 6.12a, b). The diagnosis of malignancy is suspected when there is a solid component within the cyst wall, i.e., nodules or excrescences by US imaging (Fig. 6.12c, d).

Thymus

The normal thymus gland may be seen in children and is located deep in the suprasternal notch. By US, the thymus is hypoechoic with well-defined and smooth borders. The gland may have a sparkly appearance due to the presence of comet-tail-like artifacts. A thymic cyst may be identified in the sternal notch.

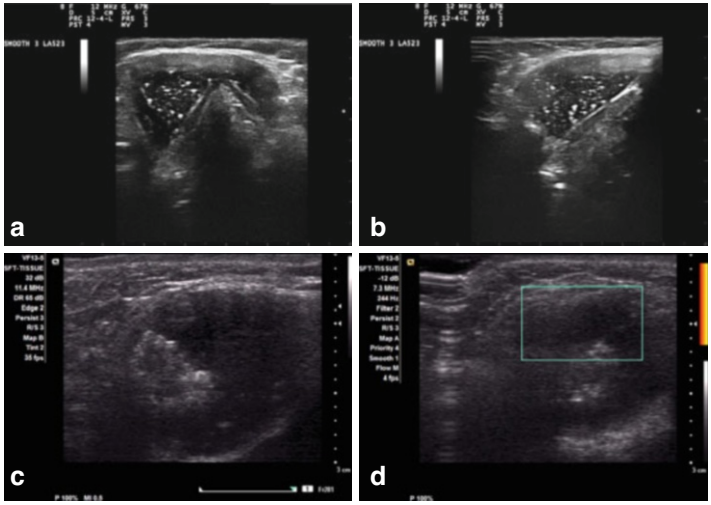

FIGURE 6.12 Ultrasound findings in thyroglossal duct cyst (**a**, **b**) and thyroglossal duct papillary carcinoma (**c**, **d**). Prominent "comet tails" are seen in the thyroglossal cyst and micro reflectors in the solid component of the papillary carcinoma. Vascularity by Doppler exam is not prominent in the carcinoma (**d**)

Submandibular Region

Lipoma

The US image of a lipoma is characteristic and shows a hypoechoic mass with fine, bright, echogenic striations producing a "feathery" appearance, characteristic if not pathognomonic of lipoma. The striations remain parallel to the probe regardless of the direction of the scan.

Parotid Region

Pilomatrixoma

This lesion is seen predominantly in children and affects mainly the preauricular region and proximal upper extremities. It is a slow-growing tumor that arises from the hair

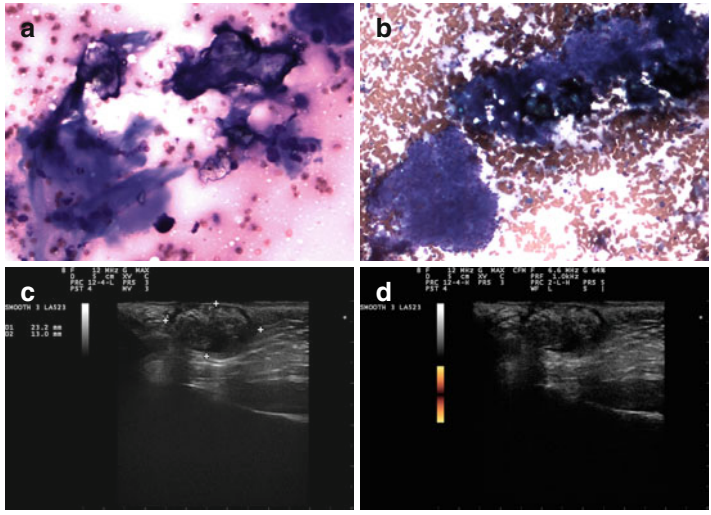

FIGURE 6.13 Parotid region pilomatrixoma. Smears show anucleated squamous cells and calcific material (**a**) as well as aggregates of basaloid cells (**b**). Ultrasound shows a superficial dermis-based skin lesion with internal hyperechoic foci suggestive of microcalcifications; minimal or no vascularity is seen by Doppler examination (**c**, **d**). (**a**, **b** MGG stain, medium magnification)

follicles and presents as a hard subcutaneous nodule. The US image shows a well-defined, irregular, hypoechoic nodule with inner echogenic foci and a peripheral hypoechoic rim. The mass may be completely echogenic, with strong posterior acoustic shadowing suggestive of calcification (Fig. 6.13).

Branchial Cleft Cyst

Branchial cleft cyst as a result of the first branchial cleft anomaly is located in the pre-, post-, or infra-auricular region and may be mistaken as a parotid gland tumor. This lesion is rare and histologically may or may not have adnexal elements in addition to the keratinizing squamous epithelium. However, in contrast to the findings in branchial cleft cysts derived from the second branchial left anomaly, the lymphoid component is not prominent unless the cyst becomes infected.

Other lesions that occur predominantly in the masticator space/masseter regions include dental abscesses, vascular malformations, lipomas, ectopic salivary gland, and muscle hypertrophy as a result of bruxism.

Lateral Region

Carotid Body Paraganglioma / Tumor

Parasympathetic paragangliomas can occur in various locations in the head and neck: glomus jugulare in the skull base, glomus vagale below the skull base, glomus tympanicum in the middle ear, and carotid body tumor in the carotid bifurcation. Carotid body tumor is a benign neuroendocrine tumor that arises from the carotid body paraganglia. Cells contain cytoplasmic neurosecretory granules by electron microscopy.

Clinical findings. The carotid body tumor usually affects adults and presents as a painless and progressively growing lateral neck pulsatile mass deep to the anterior border of the sternocleidomastoid muscle below the angle of the mandible. It can be reliably visualized by US imaging. About 10 % are multiple and may be familial and 10 % are malignant.

Histopathology. There is a cell nest or organoid growth pattern surrounded by fibrovascular stroma. Chief cells are round or oval, with abundant eosinophilic cytoplasm, granular uniform chromatin, and slight anisonucleosis. The sustentacular cells are spindle and basophilic, are located surrounding the nests of chief cells, and are difficult to identify on tissue sections. Cellular pleomorphism may be present; necrosis and mitosis are rare and do not indicate malignancy. Metastasis is the only true criterion for a malignant paraganglioma.

Immunoprofile. Chief cells are neuron-specific enolase, chromogranin, and synaptophysin positive. Sustentacular cells are S-100 protein positive.

FNA findings. Most aspirates are bloody and show tumor cell aggregates and single cells of variable nuclear size. Microfollicular architecture may be present. The nuclear to cytoplasmic ratio, chromatin clumping, and nucleolar prominence

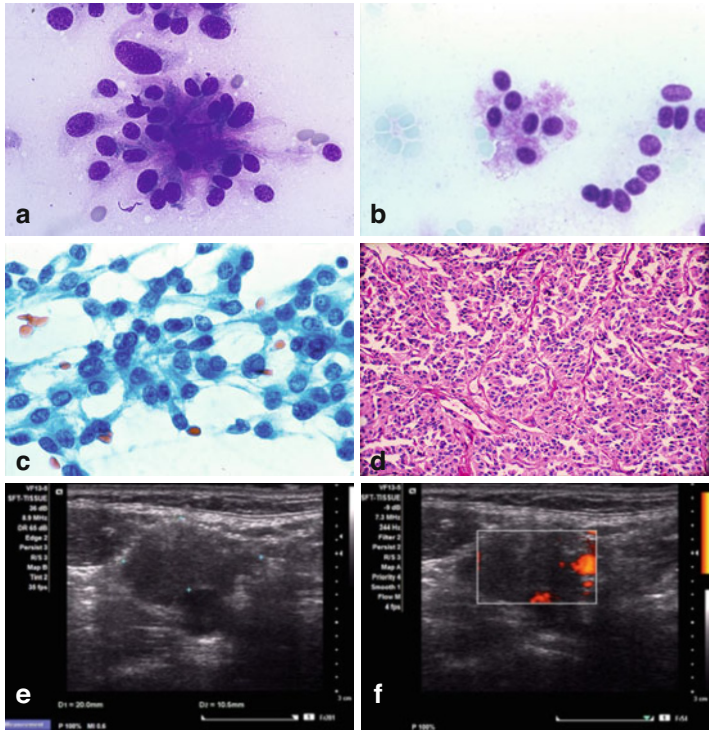

FIGURE 6.14 Carotid body tumor. Smears are cellular and show moderate to marked cell pleomorphism, microfollicular architecture (**a**), red cytoplasmic granules (**b**), nuclear inclusions (**c**), and "salt and pepper" chromatin with inconspicuous nucleoli. An organoid/trabecular pattern is evident in the resected tumor (**d**). Ultrasound shows an ill-defined hypoechoic mass with subtle merging of the normal vessels and the tumor mass (**e**, **f**) (**a**, **b** Diff-Quik stain, high magnification; **c** Papanicolaou stain, high magnification; **d** hematoxylin and eosin stain, low magnification)

are variable. Most nuclei are round or oval and eccentric and may show intranuclear inclusions. The cytoplasm is cyanophilic with Papanicolaou stain and finely granular with Romanowsky stains. Cells may show interlacing cytoplasmic processes. Cellular pleomorphism may be present, but necrosis or mitosis is absent (Fig. 6.14a–d).

The differential diagnosis includes neuroendocrine carcinomas, metastatic follicular and medullary carcinomas of the thyroid, and metastatic renal cell carcinoma. Careful clinical examination, identification of cell clusters and single cells with cytoplasmic granules, and variation in size and shape are helpful. Special stains and electron microscopy are also contributory.

US features. By US imaging, the tumor is well defined, heterogeneous, and hypoechoic. It has multiple anechoic foci that light up on Doppler examination and correspond to blood vessels. Doppler examination shows a chaotic pattern usually coming from the external carotid artery (Fig. 6.14e, f).

Peripheral Nerve Sheath Tumors

Schwannomas or neurilemomas and neurofibromas are included in this group. In general, these tumors are rare, schwannomas being the most common in the head and neck. Local resection is curative, and local recurrences are infrequent.

Schwannoma is a benign tumor, usually encapsulated, that originates in the Schwann cells. Patients commonly have a nonpainful, slowly growing mass that can be displaced horizontally and not vertically, as in carotid body tumors. Schwannomas most commonly affect the lateral aspect of the neck, often of adult patients, and there is no gender preference.

Histopathology. The tumor shows alternating Antoni A (cellular) and Antoni B (loose) areas. The cells have spindle and hyperchromatic nuclei and are embedded in a fibrillary stroma with scattered lymphoid cells. Whorling and palisading of nuclei may be seen. Rare mitosis and necrosis may be present and are not indicative of malignancy. Histologic variants include melanotic, plexiform, epithelioid, glandular, and neuroblastoma-like.

FNA findings. Smears show scant to moderate cellularity with uniform spindle cells held within glassy, dense, collagenous tissue fragments. The cells show slender and twisted nuclei and indistinct cytoplasmic borders and may show elongated fibrillary processes. The amount of matrix predominates

over the cellular elements in most cases, and the tissue fragments are sharply defined. The cell clusters may show more compact (Antoni A) and loose hypocellular (Antoni B) areas. Verocay bodies are uncommon, but diagnostic; there is a zone of palisading nuclei separated by a zone of fibrillary substance. High cellularity, sparse mitoses, and pleomorphism are not indicative of malignancy; pleomorphism is a feature present in ancient schwannomas. Moderate numbers of free-lying twisted nuclei with pointy ends are present in the background. Scattered lymphoid cells may be seen admixed in the tissue fragments. Cystic degeneration, necrosis, hemorrhage, and calcification are considered retrogressive changes (Fig. 6.15a–d).

The differential diagnosis includes neurofibromas of the head and neck that may have similar FNA cytomorphology. Diagnostic keys include the cutaneous–subcutaneous location, non-twisted spindle cell shape, cellular arrangement, and stromal features that distinguish them from schwannomas.

US features. Characteristically, the tumors are oval with well-defined edges, homogeneous, and markedly hypoechoic with a "pseudocystic" appearance showing posterior enhancement. They can be confused clinically with lymph nodes; however, they lack fatty hilum and, when scanned longitudinally, they have tapered ends that merge with the echogenic fibrillary nerve. These lesions tend to be hypervascular, although less so than carotid body tumors. When occurring in the parotid area, schwannoma is difficult to distinguish from pleomorphic adenoma (Fig. 6.15e, f).

Branchial Cleft Cyst

Branchial cleft cyst is the most common congenital anomaly of the second branchial cleft and can occur anywhere along a tract that passes inferiorly from the junction of the middle and lower thirds of the sternocleidomastoid muscle (anterior border) to the tonsillar fossa, passing between the internal and external carotid arteries. The position in the neck is identical to that of the jugulodigastric lymph node (neck level II).

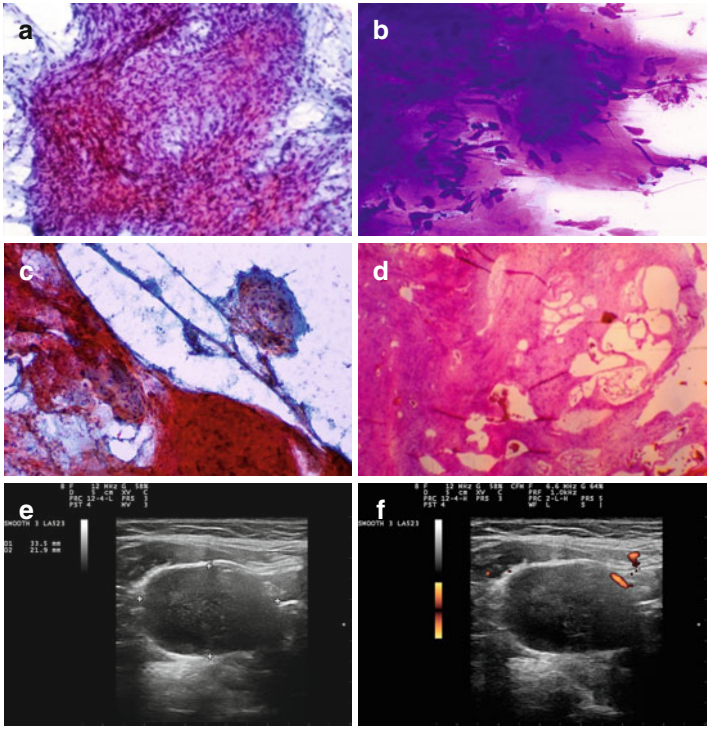

FIGURE 6.15 Schwannoma. Smear shows cellular fragments of spindle cells (**a**) supported by dense fibrillary stroma (**b**). Cellular and less cellular aggregates correspond to Antoni A and B areas, respectively (**a**). Cystic degeneration is present in (**c**) and correlates with findings in the excised tumor (**d**). Ultrasound shows a hypoechoic slightly heterogeneous and slightly elongated mass with posterior acoustic enhancement and minimal if any vascular flow by Doppler exam (**e**, **f**) (**a**, **c** Papanicolaou stain, medium magnification; **b** Diff-Quik stain, medium magnification; **d** hematoxylin and eosin stain, low magnification)

The most common location is at the level of the angle of the mandible, posterior to the submandibular gland, anterior to the sternocleidomastoid muscle, and superficial to the great vessels. Patients are usually younger than 40 years and

have a fluctuant, painless mass. The mass is of variable size and may be tender, larger, and firmer at the time of an upper airway infection.

Histopathology. The cyst lining is of the keratinized squamous type in 90 % of cases, being columnar or mixed in the remaining 10 %. The cyst wall contains nodular lymphoid tissue, often with germinal centers. The cyst fluid contains squamous cells, lymphocytes, and cholesterol crystals.

FNA findings. The FNA yields a turbid yellow fluid. Smears show numerous often anucleated squamous cells and variable numbers of columnar, mucinous, and lymphoid cells in a background of debris and cholesterol crystals (Fig. 6.16a). Inflamed cysts may show epithelial atypia, but frank anaplasia is absent (Fig. 6.16b, c). Acellular fluid is occasionally encountered. The differential diagnosis includes other congenital cysts, cystic squamous cell carcinoma (with nuclear anaplasia), and salivary gland cysts (which may contain crystalloids). Of note, a jugulodigastric lymph node with cystic necrosis associated with metastasis from squamous cell or thyroid carcinoma should be kept in mind particularly in patients older than 40 years, before the diagnosis of a branchial cleft cyst is made (Fig. 6.16d).

US features. The image shows a well-defined mass with a thin, uniform wall, regular borders, anechoic or hypoechoic with internal debris, and posterior acoustic enhancement. Occasionally, homogeneous internal echoes may be present mimicking a solid mass ("pseudosolid") (Fig. 6.16e–i).

Cervical Thymic Cyst

Remnants of thymic tissue, either solid or cystic, may occur in the neck along the course of the carotid sheath from the angle of the mandible to the sternal notch. They are more common in men and occur in the first decade of life and less commonly up to the third decade. Patients have a slow-growing painless mass that increases in size with the Valsalva maneuver.

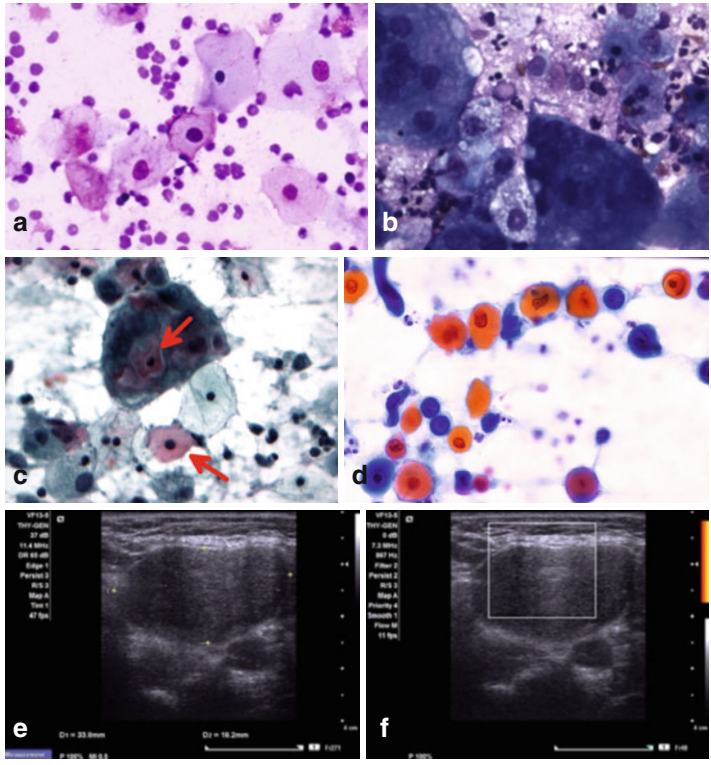

FIGURE 6.16 Branchial cleft cyst. Rare squamous cells and proteinaceous fluid are present when the cyst is not inflamed (**a**). Reactive cytologic changes including foreign body giant cell reaction are seen in the presence of rupture and inflammation (**b**, **c** *arrows* point squamous cells), but frank anaplasia is absent. Keratinized and non-keratinized anaplastic cells are seen in cystic metastasis from squamous cell carcinoma (**d**). Ultrasound imaging shows a well-circumscribed oval-shaped mass with posterior acoustic enhancement, thin wall, and no blood flow by Doppler exam (**e**, **f**). Inflamed cysts may have a heterogeneous echotexture and increased blood flow by Doppler exam (**g**, **h**). Cystic degeneration in squamous carcinoma may show a thick-walled cyst (**i**) and USG-FNA from the wall yields viable malignant cells (**d**) (**a**, **c**, **d** Papanicolaou stain, high magnification; **b** MGG stain, high magnification)

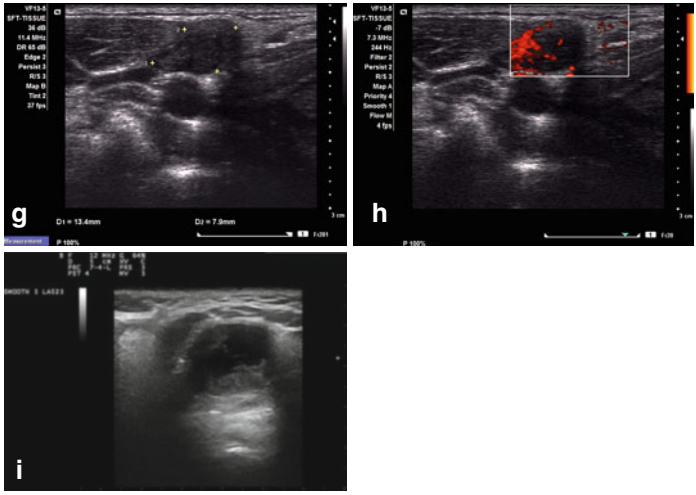

FIGURE 6.16 (continued)

Histopathology. Cysts are unilocular or multilocular; contain clear fluid; are lined with cuboidal, columnar, or squamous epithelium; and contain thymic tissue. Because of the common embryologic origin, parathyroid tissue may be present in the wall.

FNA findings. Smears show epithelial elements as described, lymphocytes, and proteinaceous fluid. The distinction from branchial cleft cyst is based on clinical and histologic grounds.

US features. The findings are not specific and include a well-defined, smooth, anechoic cystic mass with a thin wall and posterior acoustic enhancement.

Dermoid Cyst

This lesion occurs mainly in the first decade of life and has no gender preference. Patients often have a subcutaneous lesion in the orbit, nasal and oral cavities, and less commonly in the anterior, lateral, or upper neck.

Histopathology. The cyst wall is lined with keratinized squamous epithelium and contains cutaneous adnexal structures.

The cyst cavity contains keratin and sebaceous material. When there is rupture into the surrounding soft tissue, a foreign body tissue reaction occurs. The differential diagnosis with epidermal inclusion cysts rests on histologic evaluation and the demonstration of cutaneous adnexal elements.

FNA findings. The material obtained in both dermoid and epidermal cysts is "cheesy" with a peculiar odor. Smears show numerous anucleated squamous cells. The presence of acute inflammatory cells and foreign body-type multinucleated giant cells indicates cyst rupture, and the cells may show reactive changes that may suggest squamous cell carcinoma; attention to nuclear characteristics is essential (Fig. 6.17a, b).

US features. There is a well-defined, smooth, hypoechoic, "pseudosolid" mass with a thin wall and posterior acoustic enhancement. The borders are irregular in the presence of cyst rupture (Fig. 6.17c, d).

Cystic Hygroma

Cystic hygroma, presumably an anomaly of the jugular lymphatic sac, commonly occurs in the head and neck regions, predominantly in the lateral neck (posterior and anterior triangles) of children under the age of 2 years; it rarely occurs in adults. The mass is slowly growing and may be of considerable size, occupying the entire side of the neck, and may extend into the thorax.

Histopathology. The endothelium-lined cysts contain lymphoid cells and proteinaceous fluid, and the FNA cytology recapitulates these findings.

US features. US imaging shows a well-circumscribed, uniform, solitary or multicystic, anechoic mass with a thin wall and posterior acoustic enhancement.

Teratoma

Most patients are newborns and infants with a large mass and signs and symptoms of compression of the upper airways.

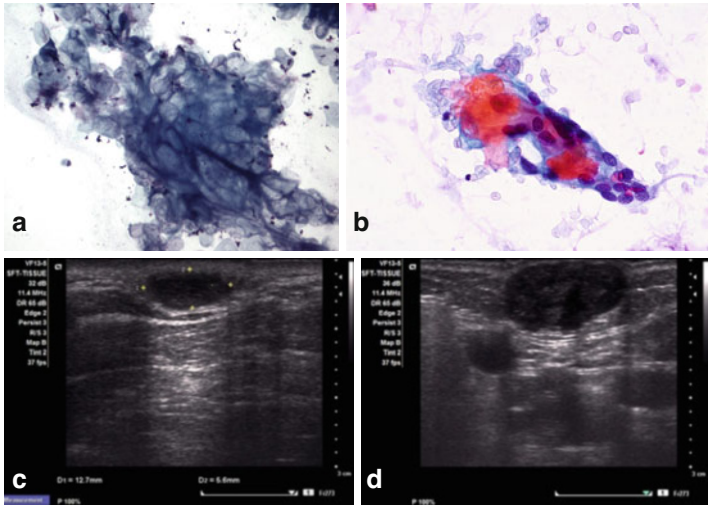

FIGURE 6.17 Epidermal inclusion cyst. Single and clustered anucleated squamous cells are present in unruptured epidermal inclusion cysts (**a**). Reactive squamous changes, multinucleated foreign body-type giant cells, and inflammation are present in ruptured cysts (**b**). Ultrasound in unruptured cysts shows thin and uniform capsule (**c**). In the presence of rupture, the cyst wall is ill-defined, thick, and fuzzy (**d**). Note the posterior acoustic enhancement in both examples and heterogeneous echotexture, more prominent in (d) (**a** MGG stain, high magnification; **b** Papanicolaou stain, high magnification)

Histologically, there are elements derived from the epithelial, neuroectodermal, and mesenchymal layers. Complete surgical excision is the treatment of choice and is curative.

Supraclavicular Region

Lymphadenopathy is the most common mass in the supraclavicular region. Among the rare non-nodal lesions, benign adipose tissue prominence or lipomas predominate. Occasionally, a prominent vertebral transverse process may be present as a pseudomass in this area.

Posterior Region

Non-nodal pathology is rare in this region, and among these peripheral nerve sheath tumors, cystic hygroma (in children) and lipomas predominate.

Lipoma

Lipomas are the most common tumors in adults and may occur in any part of the head and neck area, most commonly in the posterior triangle. They are usually solitary, but may be multiple.

Histopathology. Conventional lipomas are composed of mature adipose tissue. Types of lipomas include spindle, pleomorphic, myxoid, angiolipoma, myolipoma, fibrolipoma, myelolipoma, and intramuscular; however, with the exception of pleomorphic lipoma that often occurs in the posterior neck, they usually do not involve the neck.

FNA findings. Smears show fragments of mature adipose tissue with vacuolated cells and peripheral regular oval and uniform nuclei. Atypical lipoblasts and a conspicuous vascular pattern are absent (Fig. 6.18a).

The differential diagnosis includes well-differentiated sclerosing liposarcoma and pleomorphic lipoma, which shows pleomorphic, bizarre, multinucleated giant cells (Fig. 6.18b). Liposarcomas are deeply seated, usually intramuscular or retroperitoneal masses; lipomas are superficial. Smears of well-differentiated liposarcoma contain small fragments of fatty tissue similar to those of lipomas; however, numerous capillaries, occasional nuclear atypia, and lipoblasts are present.

US features. There is a homogeneous, oval, well-circumscribed, isoechoic mass when compared with the subcutaneous tissue. The lipoma has fine linear striations ("feathering") (Fig. 6.18c, d).

The Skin and Scalp

FNA is rarely used for the diagnosis of skin tumors, mainly because of their size and accessibility to surgical biopsies. However, aspirates can be used successfully in the diagnosis of

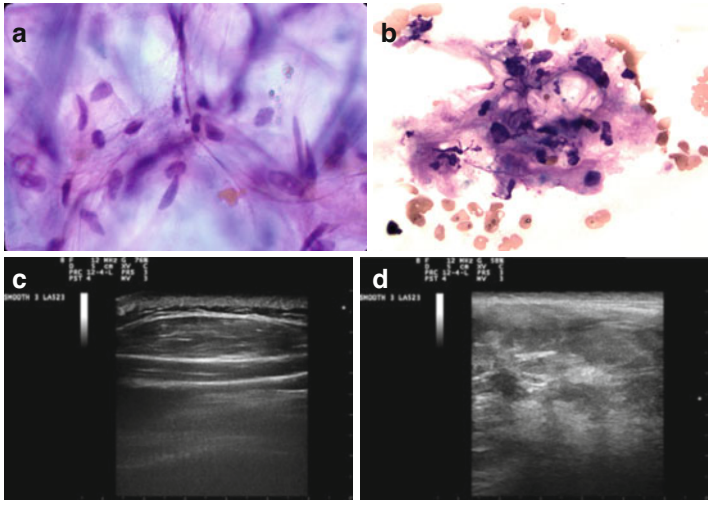

FIGURE 6.18 Lipoma. Adipose tissue without atypia or pleomorphism is present (**a**). Rare complex aggregates of slightly pleomorphic cells were obtained from a 12 cm lipomatous mass in the back of a patient's neck (**b**). Ultrasound of lipomas shows a characteristic "feathering" (**c**). The ultrasound from the 12 cm posterior neck mass shows a heterogeneous mass with areas of hypo- and hyperechogenicity and lack of "feathering" (**d**) (**a** Papanicolaou stain, high magnification; **b** MGG stain, high magnification)

suspected metastatic disease, in the evaluation of recurrent skin neoplasms, or in the diagnosis of tumors of unclear nature.

Pilomatrixoma

This benign adnexal (hair matrix) skin tumor is a hard subcutaneous tissue nodule often seen in the face, neck, and upper extremities, most commonly seen in the first two decades of life.

FNA findings. Smears show scattered single and dense groups of overlapping, non-molding, degenerating basaloid cells admixed with a pink background substance (Diff-Quik stain). The cells are usually stripped of cytoplasm and exhibit round to oval nuclei, regular nuclear contours, evenly distributed granular chromatin, and small, prominent nucleoli. Foreign body giant cells, ghost cells with keratinization,

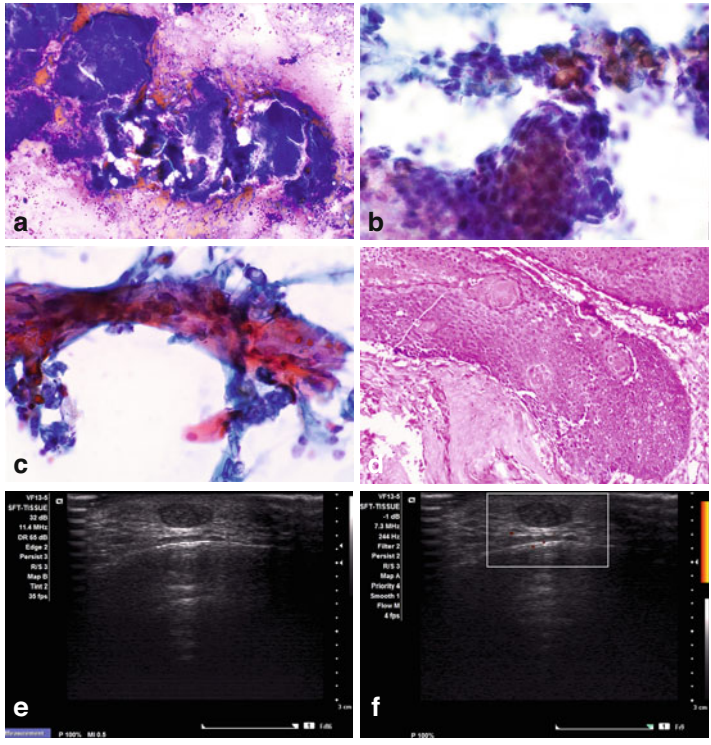

FIGURE 6.19 Pilomatrixoma. Smear shows complex 3-dimensional aggregates of basaloid cells (**a**), tight squamous pearls, anucleated squamous cells, and calcific fragments admixed with the basaloid cells (**b**), and foreign body-type giant cell reaction to keratin (**c**). Histologic section confirms the cytologic findings (**d**). A hypoechoic oval mass with well-circumscribed edges, homogeneous echotexture, uniform halo/capsule, posterior acoustic enhancement, and lack of vascularity by Doppler exam (**e**, **f**) is seen in the subcutaneous tissue area (**a** Diff-Quik stain, low magnification; **b**, **c** Papanicolaou stain, medium magnification; **d** hematoxylin and eosin stain, medium magnification)

elongated reactive fibroblasts, and calcium debris may be present (Fig. 6.19a–d).

The differential diagnosis includes carcinomas with basaloid cells (skin, salivary glands) and small blue cell tumors.

Diagnostic key features include ghost squamous cells, multinucleated cells, and clinical history including physical examination.

US features. As mentioned in the section on parotid region masses, an ill-defined, irregular, hypoechoic subcutaneous nodule that may have calcifications is identified (Fig. 6.19e, f).

Cylindroma

Because of its multinodular and diffuse distribution, this tumor of skin appendage origin is called a "turban tumor of the scalp."

FNA findings. Features are identical to those of basal cell carcinoma, except for an occasional layer of hyaline material surrounding the periphery of some cell clusters.

Basal Cell Carcinoma

Aspirates from basal cell carcinomas are usually performed to verification of recurrence of an excised primary tumor.

FNA findings. Smears show variable cellularity, complex aggregates, and single basaloid cells with hyperchromatic nuclei, mitosis, and necrosis (Fig. 6.20).

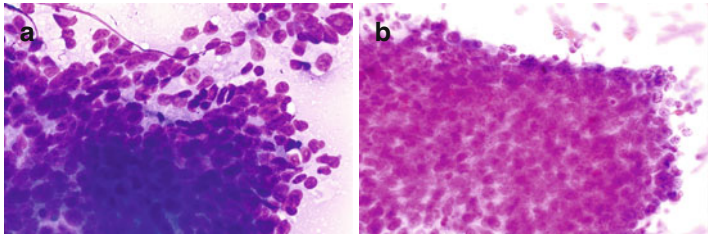

FIGURE 6.20 Basal cell carcinoma. Recurrence in the site of prior surgery (**a** Diff-Quik stain; **b** Papanicolaou stain medium magnifications)

Cutaneous Squamous Cell Carcinoma

The smears are cellular, showing keratinizing cells with mild to moderate nuclear atypia. The differential diagnosis includes ruptured epidermal inclusion cysts, trichilemmal cysts, and branchial cleft cysts. Diagnostic key is nuclear characteristics.

Merkel Cell Tumor

These uncommon malignant neoplasms occur in the dermis of elderly patients and behave aggressively, with frequent metastases to regional lymph nodes. Cytology and differential diagnosis are discussed in the section on metastatic tumors to lymph nodes (Fig. 6.21).

Sebaceous Carcinoma

Aspirates from this neoplasm show two cell types and a necrotic background. Larger cells show vacuolated cytoplasm, vesicular nuclei, and prominent nucleoli. Smaller cells show basaloid to intermediate cell characteristics. When the former predominate, they must be differentiated from other clear cell neoplasms; the latter can be confused with basal cell carcinoma and basaloid squamous cell carcinoma.

Kaposi's Sarcoma

It may be present in the oral cavity and lymph nodes in patients with AIDS.

FNA findings. There are cohesive clusters and single plump spindle cells in a bloody background. The cytoplasmic borders are ill-defined, and many of the individual cells are stripped of cytoplasm. Slit-like spaces may be found in the cell clusters (Fig. 6.22).

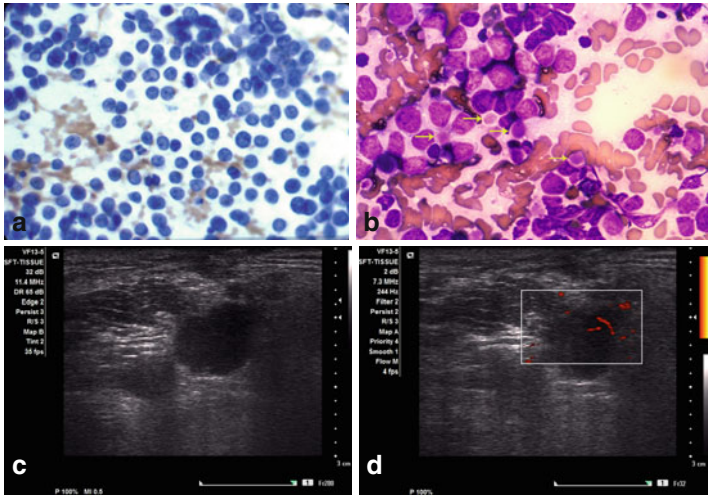

FIGURE 6.21 Merkel cell carcinoma, soft tissue of neck metastasis. The smear shows a small-/ intermediate-sized blue cell tumor (**a**). Romanowsky stain shows a paranuclear condensation of intermediate filaments (keratin) (**b** *arrows*). Ultrasound shows nonspecific findings and includes hypoechogenicity, irregular and fuzzy margins, and peripheral blood flow by Doppler examination (**c**, **d**) (**a** Papanicolaou stain, high magnification)

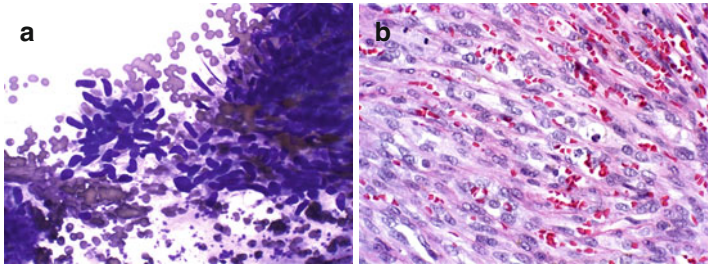

FIGURE 6.22 Kaposi's sarcoma. Spindle cell pattern and red blood cells (**a**). This cytologic pattern needs clinical correlation to support the diagnosis. Tissue section shows poorly formed slit-like pattern filled with red blood cells (**b**) (**a** Diff-Quik stain, high magnification; **b** hematoxylin and eosin stain, medium magnification)

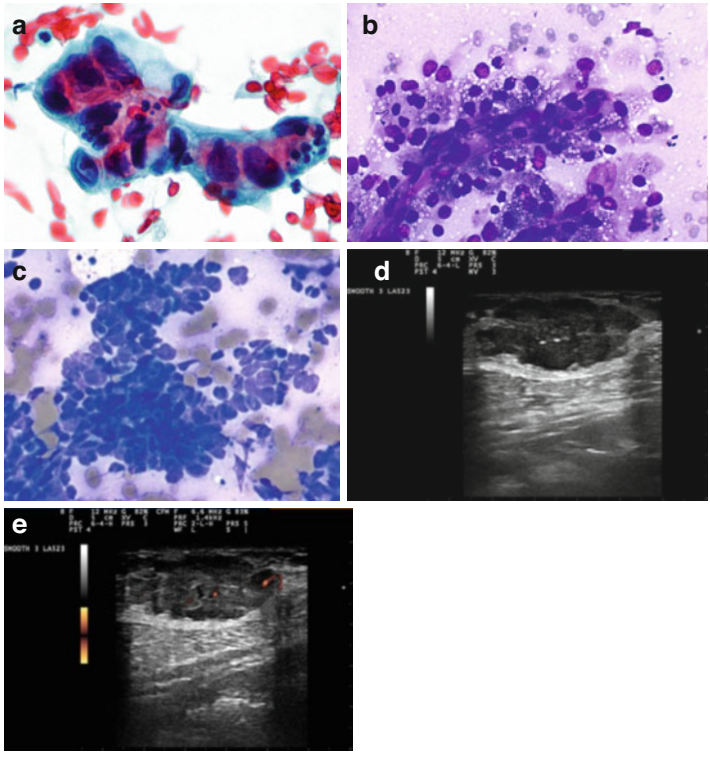

Figure 6.23 Metastatic carcinomas. Breast ductal carcinoma (**a**), renal cell clear cell carcinoma (**b**), and small cell carcinoma of the lung (**c**) to subcutaneous tissue of the clavicular area (**a**) and scalp (**b**, **c**). Subcutaneous tissue mass with lobulated and fuzzy edges and minimal vascular flow by Doppler exam (**d**, **e**) (**a** Papanicolaou stain, high magnification; **b**, **c** Diff-Quik stain, medium magnification)

The differential diagnosis includes other reactive and neoplastic spindle cell processes. The diagnostic key is the clinical history.

Metastatic Carcinomas

The majority of carcinomas metastasize late in the course of the disease process (Fig. 6.23a). However, scalp metastasis from renal cell carcinoma (Fig. 6.23b) or small cell carcinoma of the lung

(Fig. 6.23c) may be the first evidence of malignancy. Diagnostic keys include a high grade of suspicion, clinical history, and careful evaluation of aspirate smears. US findings are not specific and usually show a hypoechoic mass with heterogeneous echotexture and irregular indistinct margins (Fig. 6.23d, e).

Uncommon Masses of the Head and Neck

Myositis Ossificans

The progressive form of myositis ossificans affects the muscles of the face and neck and progresses to the thoracic musculature. The sporadic form is usually posttraumatic and affects the sternocleidomastoid or masseter muscles.

Aspirates are composed of osteoblasts, osteoclasts, and fibroblasts with reactive-appearing large nuclei. Osteoid is absent. Lack of nuclear anaplasia or atypical mitoses distinguishes this process from sarcomas. The presence of osteoid favors the diagnosis of osteosarcoma.

Proliferative Myositis

This rapidly growing lesion usually affects the sternocleidomastoid muscle. A checkerboard appearance felt on physical examination reflects the admixture of affected and nonaffected muscle tissue.

Aspirates consist of fragments of skeletal muscle fibers, degenerated multinucleated muscle cells, large polygonal cells with prominent nucleoli, and reactive fibroblasts. The differentiation from sarcoma is based on the lack of nuclear anaplasia.

Nodular Fasciitis

This lesion is most commonly seen in the upper extremities, trunk, and neck of young adults. It is a reactive, rapidly growing mass (less than a month), in direct association with the fascia and extending into the subcutaneous tissue and muscle.

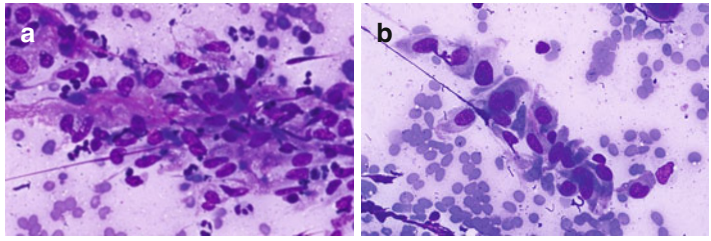

FIGURE 6.24 Nodular fasciitis. Spindle plump fibroblastic cells (**a**) and myofibroblasts (**b**) are present along with myxoid stroma and inflammatory cells. The lesion resolves spontaneously in less than 3 months (**a**, **b** Diff-Quik stain, high magnification)

The clinical evolution of the lesion should be carefully monitored because it will regress in a period of 8–10 weeks.

FNA findings. Spindle and plump *fibroblastic cells* are present singly and in small interwoven clusters in a loose myxoid stroma and admixed with various numbers of chronic inflammatory cells. Large *myofibroblasts* ranging from elongated to polygonal shape with stellate appearance and dense cytoplasm, eccentric nuclei, and prominent nucleoli are also seen. Capillaries and typical mitotic figures are frequently encountered (Fig. 6.24).

The differential diagnosis includes low-grade sarcomas with myxoid component. Diagnostic keys are lack of anaplasia, reactive nuclei, adequate sampling, and clinical picture.

Dermatofibrosarcoma Protuberans (DFSP)

DFSP is a spectrum of spindle cell tumors that typically involve both the dermis and subcutis of the trunk, proximal extremities, and occasionally the scalp. It is a firm, nodular (protuberant) cutaneous mass growing over a period of months to years.

FNA findings. Aspirates are of variable cellularity and are frequently bloody. Useful cytologic features are the presence of storiform stromal fragments, entrapped adipose tissue, and

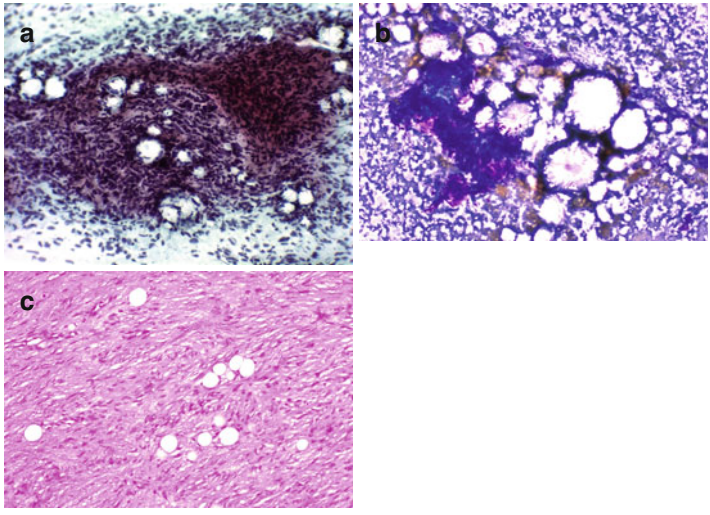

FIGURE 6.25 Dermatofibrosarcoma protuberans. Cellular smear showing fascicles of bland-appearing spindle cells admixed with adipose tissue elements (**a**, **b**). Histopathology recapitulates the FNA pattern (**c**) (**a** Papanicolaou stain, medium magnification; **b** Diff-Quik stain, medium magnification; **c** hematoxylin and eosin, low magnification)

the recognition of fibrohistiocytic spindle cells. The fat entrapped within the storiform fragments reflects the infiltrative growth pattern of DFSP. The stromal fragments (best seen with Romanowsky stains) are of variable cellularity, showing a finely fibrillar and metachromatic matrix. The spindle cells have abundant cytoplasm, ill-defined cytoplasmic borders, and bland nuclear features. Occasional mitotic figures and pleomorphic spindle cells may be found, but the absence of inflammatory cells is prominent (Fig. 6.25).

The differential diagnosis includes both benign and low-grade malignant spindle cell lesions. Nodular fasciitis shows more angular fibroblasts with prominent nucleoli admixed with inflammatory cells. Fibrous histiocytoma shows multinucleate giant cells with hemosiderin deposition, and inflammatory cells. Kaposi's sarcoma contains delicate spindle cells and

abundant blood. Spindle cell melanoma displays more pleomorphic nuclei. Clinicopathologic correlation is necessary, and occasionally a specific diagnosis may not be possible.

US features. Tumors are oval, entirely hypoechoic with posterior acoustic enhancement or with mixed echogenicity and hyperechoic streaks. They have well-defined and focally lobulated margins and a thin hypoechoic rim that may be disrupted by tumor protrusions.

Chordoma

This neoplasm arises from remnants of the notochord and may be found in the spheno-occipital region. It has an infiltrative growth pattern causing neuro-ophthalmologic and otologic symptoms.

FNA findings. Aspirates show abundant mucoid–myxoid substance of magenta color (with Romanowsky stains). Two cell types can be identified. The larger cells have multivacuolated and bubbly cytoplasm with round, bland nuclei; the smaller exhibit oval nuclei and are usually present in lesser numbers. The larger cells, arranged in nests and clusters, correspond to the physaliphorous cells seen in tissue sections. Binucleation and multinucleation are occasionally observed.

The differential diagnosis includes chondrosarcomas and metastatic mucin-producing adenocarcinomas. Large multivacuolated cells are rarely present in chondrosarcomas and adenocarcinomas. Clinical correlation is necessary.

Chondrosarcoma

This rare neoplasm affects the jaw, nasal septum, larynx, and trachea.

FNA findings. Aspirates show extracellular matrix and cells in various proportions. The extracellular matrix stains magenta with Romanowsky stains. Cellularity depends on the grade of the sarcoma. The neoplastic chondrocytes are single, can be located in lacunae, and range from oval to round. The

cells have a well-demarcated, vacuolated cytoplasm encasing bubble-like peripheral vacuoles. No mitotic figures are seen, except in de-differentiated chondrosarcoma. A fibroblast-like cell component may be present. Intermediate- to high-grade chondrosarcomas have characteristic cytologic features, but the low-grade ones require tissue confirmation. Clinical and radiographic correlation is necessary.

Osteogenic Sarcoma

Head and neck osteosarcomas are rare and comprise 6 % of all osteogenic sarcomas. Sites of involvement include the mandible, maxilla, paranasal sinuses, and skull. Depending on which component predominates, osteosarcomas are divided into osteoblastic, chondroblastic, and fibroblastic types.

FNA findings. The stromal cells are spindled to polygonal with hyperchromatic nuclei, with or without nucleoli, and exhibit variable anaplasia. Necrosis and mitoses are commonly seen. Fragments of pink osteoid and chondroid and multinucleated osteoclast-type tumor giant cells are frequently found (Fig. 6.26).

Differential diagnosis. When the osteoclast-type tumor giant cells predominate, giant cell tumors, giant cell reparative granulomas, and brown tumors of hyperparathyroidism are differential diagnostic considerations. Anaplastic stromal cells are a key diagnostic feature for osteosarcoma. The recognition of the osteoid matrix distinguishes osteosarcomas from other sarcomas. Radiographic correlation is crucial.

Synovial Sarcoma

Synovial sarcoma frequently occurs in the lower extremities, but occasionally occurs in the neck and nasopharynx. The biphasic pattern with fibrous and epithelioid components is usually seen in typical lesions. Metastases are mainly to the lungs and lymph nodes and may be biphasic or monophasic.

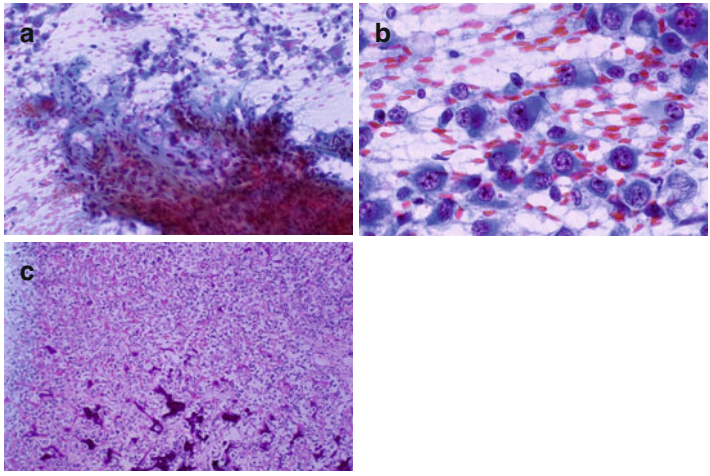

FIGURE 6.26 Osteosarcoma of the maxillary bone. Smears are cellular (**a**) and show spindle and pleomorphic epithelioid-appearing cells with anaplasia (**b**). The osteoid is evident in the tissue section (**c**) (**a**, **b** Papanicolaou stain, medium and high magnification; **c** hematoxylin and eosin stain, low magnification)

FNA findings. Aspirates are highly cellular, showing tightly packed monomorphic bipolar spindle cells with oval nuclei and faintly staining cytoplasm. A background of numerous free-lying monotonous oval or spindle small nuclei with a bland chromatin pattern and small nucleoli is usually present. The epithelioid cells are larger and cuboidal, columnar, or polygonal with round vesicular nuclei and rounded and distinct cell borders, and they occur in clusters of different sizes. Mast cells and calcific deposits are often seen. Only the fibrous or epithelioid component is present in aspirates of monophasic synovial sarcoma. The presence of calcific deposits and mast cell suggests the diagnosis (Fig. 6.27a–c).

Differential diagnosis. Large clusters of epithelioid cells may suggest the diagnosis of adenocarcinoma; however, the presence of a spindle cell component will be very unusual in such cases.

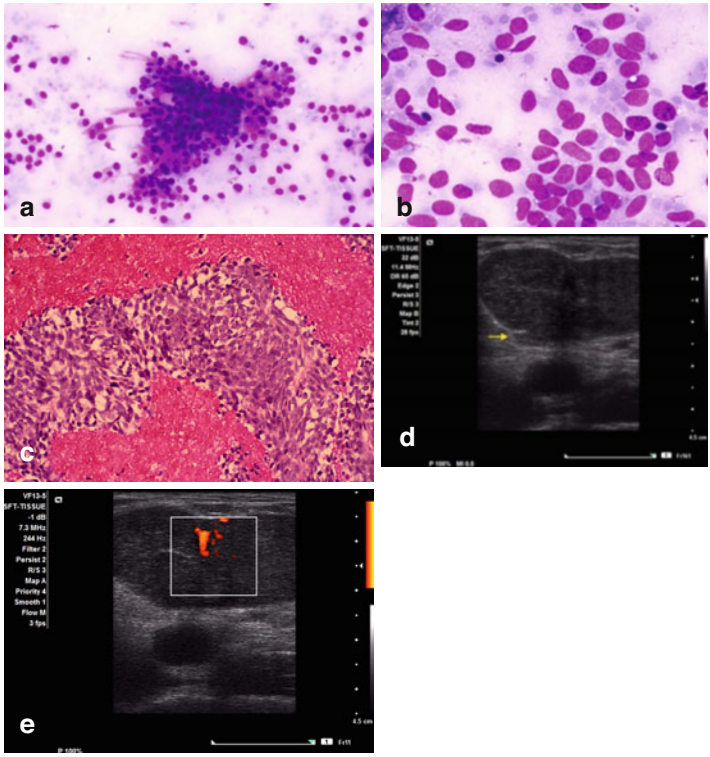

FIGURE 6.27 Synovial sarcoma. Both epithelioid (**a**) and spindle (**b**) cell components are seen. The cell block preparation shows the spindle cell component (**c**). Ultrasound shows a large hypoechoic mass with homogeneous echotexture, well-defined and smooth borders, and an area of stromal invasion (**d** *arrow*). Vascular flow is moderate by power Doppler (**e**) (**a** Diff-Quik stain, medium magnification; **b** Diff-Quik stain, high magnification; **c** hematoxylin and eosin, low magnification)

US features. Tumors show homogeneous, hypoechoic, solid, nodular, oval, and well-defined borders. Synovial sarcoma from the abdominal wall may show a "honeycomb" pattern of echotexture (Fig. 6.27d, e).

Suggested Reading

Ahuja A, Evans R. Lumps and bumps in the head and neck. In: Practical head and neck ultrasound. London: Greenwich Medical Media; 2000. p. 87–104.

Barnes L, Tse LLY, et al. Carotid body paraganglioma. In: Barnes L, Eveson JW, Reichart P, Sidransky D, editors. Pathology and genetics of head and neck tumors. Lyon: IARC Press; 2005. p. 364–5.

El-Naggar AK. Celular and molecular pathology of head and neck tumors. In: Bernier J, editor. Head and neck cancer: multimodality management. New York: Springer; 2011. p. 57–79.

Fletcher CD. Distinctive soft tissue tumors of the head and neck. Mod Pathol. 2002;15(3):324–30.

Hamilton BE, Nesbit GM, et al. Characteristic imaging findings in lymphoceles of the head and neck. AJR Am J Roentgenol. 2011; 197(6):1431–5.

Klijanienko J, Caillaud JM, et al. Cytohistologic correlations of 24 malignant peripheral nerve sheath tumor (MPNST) in 17 patients: the Institut Curie experience. Diagn Cytopathol. 2002;27(2):103–8.

Layfield LJ. Cytopathology of bone and soft tissue tumors. New York: Oxford University Press; 2002.

Lee YYP, Wong KT, et al. Ultrasound investigations in head and neck cancer patients. In: Bernier J, editor. Head and neck cancer: multimodality management. New York: Springer; 2011. p. 221–33.

Leyfield L. Cysts and neoplasms of the neck. In: Cytopathology of the head and neck. Chicago: ASCP Press; 1997. p. 141–58.

Rhys R. Ultrasound of the neck. In: Allan PL, Baxter GM, Weston MJ, editors. Clinical ultrasound, vol. 2. London: Churchill Livingstone Elsevier; 2011. p. 890–919.

Shin YR, Kim JY, et al. Sonographic findings of dermatofibrosarcoma protuberans with pathologic correlation. J Ultrasound Med. 2008;27(2):269–74.

Stanley MW, Skoog L, et al. Nodular fasciitis: spontaneous resolution following diagnosis by fine-needle aspiration. Diagn Cytopathol. 1993;9(3):322–4.

Yuan WH, Hsu HC, et al. Differences in sonographic features of ruptured and unruptured epidermal cysts. J Ultrasound Med. 2012; 31(2):265–72.

Chapter 7
The Lymph Nodes

Ricardo H. Bardales

Clinical Considerations

Lymph nodes are "absent" by palpation in newborns. They are more numerous in children than in adults and are soft and oval. Anterior cervical, axillary, and inguinal lymph nodes may be found in healthy children and measure <1 cm. The only palpable lymph nodes in adults may be found in the inguinal region and measure <1.5 cm.

Localized or regional lymphadenopathy is defined as lymph node enlargement in contiguous anatomic regions. *Generalized lymphadenopathy* is defined as the involvement of more than two noncontiguous lymph node regions.

Lymphadenopathy may be the result of a local or systemic etiologic process, i.e., metastases, lymphoma, infection, or inflammation. The clinical differential diagnosis is based on the physical examination, location of the lymph node, and particularly the age of the patient. Although these factors are important, they should not overinfluence the interpretation. The history of immunosuppression, particularly in HIV-positive individuals, contributes to the frequency of certain

R.H. Bardales, MD, MIAC, ECNU
Department of Pathology and Cytopathology,
Outpatient Pathology Associates,
7750 College Town Drive, Sacramento, CA 95826, USA
e-mail: rhbardales@aol.com

R.H. Bardales (ed.), *The Invasive Cytopathologist*, Essentials in Cytopathology 16, DOI 10.1007/978-1-4939-0730-4_7,

lymph node-based reactive, malignant, or infectious processes. A nonneoplastic pathologic process is the most common cause of regional or generalized lymphadenopathy in children and adults.

In the pediatric age group, the most common causes of regional lymphadenopathy are viral, bacterial, and mycobacterial processes, depending on the geographic environment; the most frequent malignancies presenting as a cervical lymphadenopathy are small blue cell tumors including, but not limited to, lymphomas and leukemias, followed by solid tumors such as neuroblastoma, rhabdomyosarcoma, and Wilms' tumor. In the adolescent group, Hodgkin's and non-Hodgkin's lymphomas, nasopharyngeal carcinoma, and metastatic germ cell tumors are the predominant malignancies present in a neck lymph node. Metastatic carcinoma, predominantly of the squamous type, from lung and head and neck organs becomes the most common diagnostic consideration in or above the fourth decade of life.

In general, a round, firm, well-defined lymph node present for >8 weeks or a lymph node that is fixed to surrounding tissues including the skin, deep anatomic planes, or other lymph nodes should be considered for FNA regardless of clinical findings. Likewise, a regional or generalized lymphadenopathy associated with constitutional symptoms should be considered for FNA.

Lymph Node Anatomy and Histology

The normal lymph node has a bean shape, measures <1 cm, has a cortex and medulla, and is surrounded by a capsule. The afferent lymphatic vessels penetrate the convex surface of the lymph node, and the efferent vessel exits at the level of the hilum, which is indented, contains the vein and artery, and is contiguous with the medulla.

The cortex contains the lymphoid follicles, which have germinal centers. The medulla contains the sinuses, stroma, and vessels. The sinuses converge in the hilum. The afferent

lymphatic vessels drain into the subcapsular sinus, a remarkably important structure because it is the first site of entry for any benign or metastatic process. Reactive lymphoid hyperplasia produces diffuse cortical widening; if the process continues, there is formation of germinal centers in the hilar area, causing widening of the hilum. Metastatic processes produce irregular cortical widening.

US features. The US findings reflect the histology. The cortex is densely cellular with little stroma and appears hypoechoic and essentially avascular on Doppler examination. In contrast, the medulla has more stroma, converging sinuses, and vessels and appears hyperechoic and vascular. Also, since the antigenic stimulus triggers lymph node enlargement, vascular increment, and follicular response, the cortex becomes variably vascular (Fig. 7.1a, b).

The Neck Levels, US Examination, and Lymphatic Drainage

There are more than 300 lymph nodes in the head and neck region and range from 3 mm to 3.0 cm in size. The neck has been divided in topographic compartments or levels to facilitate the localization of a particular lymph node. They were first described to map metastases from head and neck squamous cell carcinomas to cervical lymph nodes. The six levels of the neck are: (I) submental and submandibular, (II) upper lateral, (III) mid-lateral, (IV) lower lateral, (V) posterior, and (VI) antero-lateral (Fig. 7.1c). The suprasternal/superior mediastinum is considered level VII.

Level I

Submental (Ia) and submandibular (Ib) area lymph nodes. Level I lymph nodes are important for non-thyroid head and neck carcinomas, particularly those located in the oral cavity.

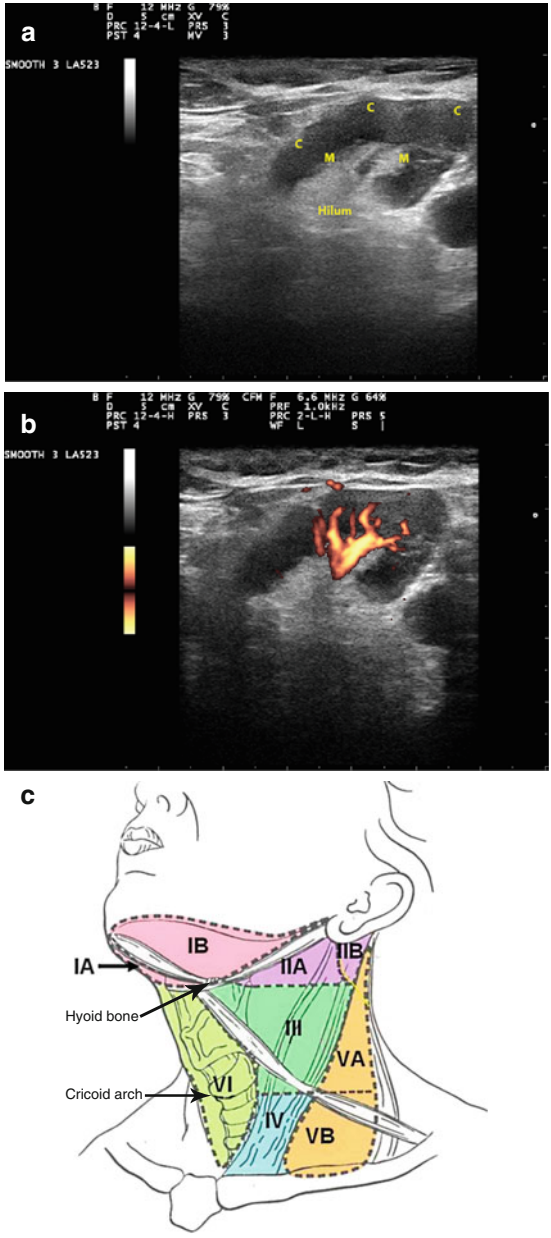

Figure 7.1 Ultrasound anatomy of a reactive lymph node showing cortex (*C*), medulla (*M*), and hilum (*H*) with a prominent vascular pole by Doppler examination (**a**, **b**). Anatomic levels of the neck (**c**)

US examination. For *submental nodes*, elevate the chin, place the probe transverse to the chin, and scan from the chin down to the hyoid bone. The nodes are superficial in the midline between the anterior bellies of both digastric muscles; they drain the anterior tongue, floor of the mouth, lips, chin, and cheeks (Fig. 7.2). For *submandibular nodes*, turn the head to the opposite side, place the probe transverse to the neck parallel to the mandible, and scan

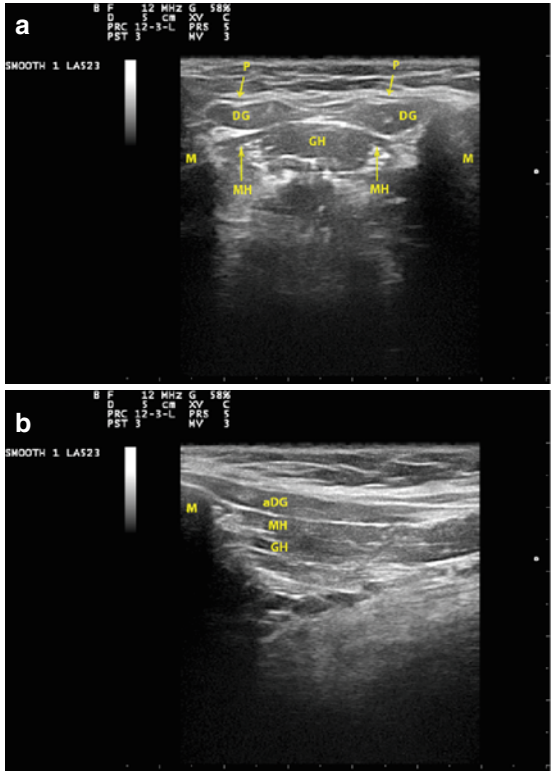

FIGURE 7.2 Submental (level 1a) region. The normal anatomy is shown in (**a**) (transverse view) and (**b**) (longitudinal view along the midline). A small reactive lymph node between the digastric muscles is seen in (**c**) (transverse view) and (**d**) (longitudinal view). Abbreviations: *P* platysma, *aDG* digastric muscle, anterior belly, *M* mandible, *GH* geniohyoid muscle, *MH* mylohyoid muscle, *LN* lymph node

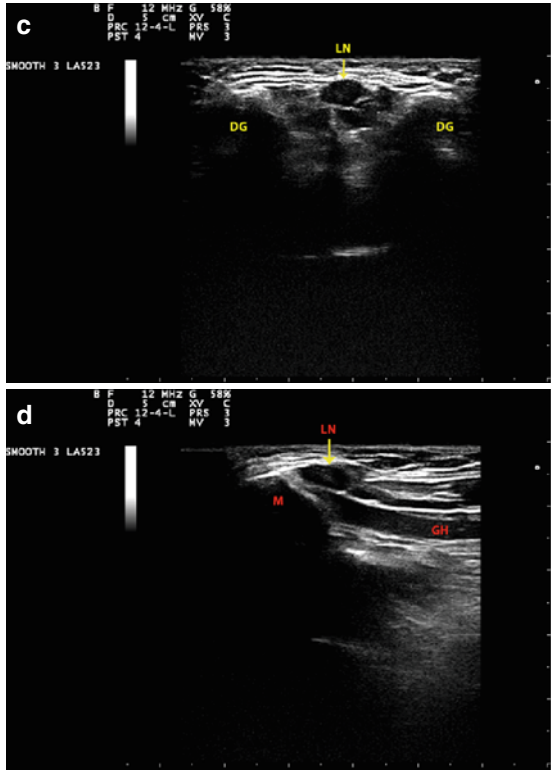

FIGURE 7.2 (continued)

from the chin back to the angle of the mandible and identify the submandibular gland. The nodes are grouped superior and anterior to the gland and lateral to the anterior belly of the digastric muscle; they drain the anterior face, anterior oral cavity, and floor of the mouth (Fig. 7.3). Of note, there are no lymph nodes within the submandibular gland.

Levels II, III, and IV

These levels correspond to lymph nodes deep to the cervical/internal jugular chain that follows the course of the internal jugular vein extending from the angle of the mandible to the

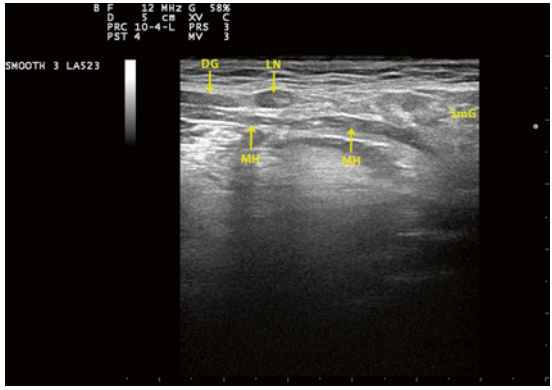

FIGURE 7.3 Left submandibular region (level 1b). The transducer is placed parallel to the mandible. There is a small reactive lymph node posterior to the anterior belly of the digastric muscle. Abbreviations: *LN* lymph node, *DG* digastric muscle, anterior belly, *MH* mylohyoid muscle, *SmG* submaxillary gland

midclavicular region and are the main lymphatic drainage for lesions located in the head and neck, draining the submental, submandibular, parotid, and retropharyngeal nodes. The jugulodigastric node is the most superior and prominent node in the chain, lies behind the submandibular gland, and is virtually visible by US examination in all individuals, measuring up to 4 cm in length in healthy young teenagers.

US examination. Identify the jugulodigastric node with the transducer transversally placed below the angle of the mandible and smoothly sweep down the chain keeping the internal jugular vein in the center of the field while evaluating all levels. In the mid-cervical region, the omohyoid muscle that divides levels III and IV lies deep to the sternocleidomastoid muscle and crosses the vessels mimicking a lymph node; the issue is solved by placement of the transducer in a longitudinal position.

Level II. Lymph nodes located from the skull base to the level of the hyoid bone (Fig. 7.4).

Level III. Lymph nodes located between the levels of the hyoid bone and the cricoid cartilage (Fig. 7.5).

Level IV. Lymph nodes located below the levels of the cricoid cartilage and the clavicle (Fig. 7.6).

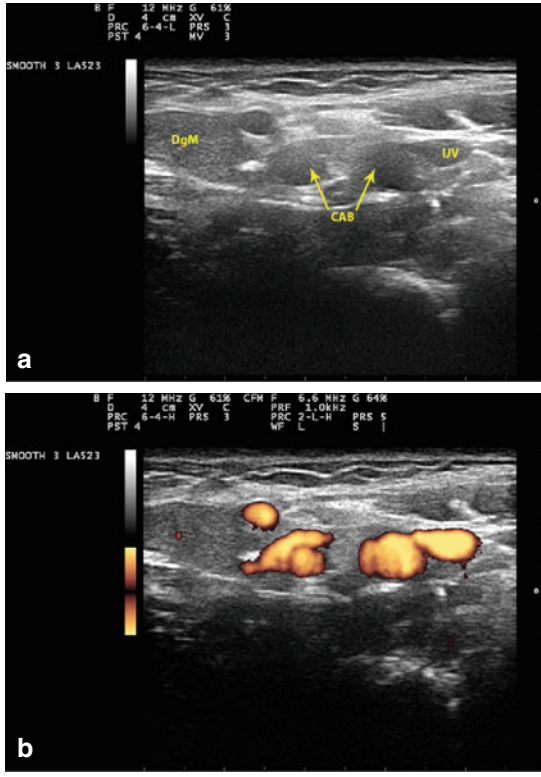

FIGURE 7.4 Left neck level II. The transducer is placed slightly superior to the carotid bulb and both carotid branches are visualized in (**a**). The corresponding findings by Doppler examination are seen in (**b**). Abbreviations: *DgM* digastric muscle, posterior belly, *CAB* carotid artery bifurcation, *IJV* internal jugular vein

Level V

This level corresponds to lymph nodes located in the supraclavicular fossa/transverse cervical chain posterior to the sternocleidomastoid muscle and superior to the subclavian vein and in the posterior triangle. The boundaries of the triangle are the sternocleidomastoid muscle anteriorly, the clavicle inferiorly, and the trapezius muscle posteriorly (Fig. 7.7). The lymph nodes are located *superficially* within this triangle filled with

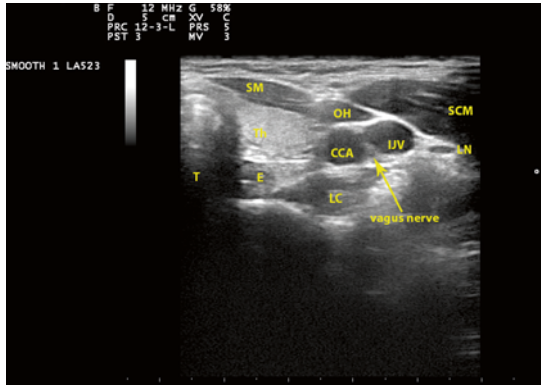

FIGURE 7.5 Left neck level III. Normal US anatomy showing the trachea (*T*), esophagus (*E*), left thyroid lobe (*Th*), strap muscles (*SM*), omohyoid muscle (*OH*), common carotid artery (*CCA*), internal jugular vein (*IJV*), sternocleidomastoid muscle (*SCM*), and longus colli (*LC*). A small lymph node with hilum (*LN*) and the vagus nerve are also seen

adipose tissue. Enlargement of the left supraclavicular lymph node (Virchow's node) often indicates a primary malignancy located below the diaphragm. The posterior triangle lymph nodes drain the skin of the occipital and mastoid regions, posterior scalp, lateral neck, and the postnasal space.

US examination. Scan transversally along the superior border of the midclavicle to the lateral end of the clavicle to evaluate the supraclavicular fossa. The posterior triangle is scanned with the transducer transverse to the mastoid process, moving inferiorly along the posterior border of the sternocleidomastoid muscle toward the acromioclavicular joint and the anterior border of the trapezius.

Level VI

These lymph nodes are located in the anterior central neck compartment. The prelaryngeal and pretracheal lymph nodes are superficial and the paratracheal are lateral to the trachea, medial to the carotid artery, and deeper in the tracheoesophageal groove. The prelaryngeal and pretracheal nodes drain the

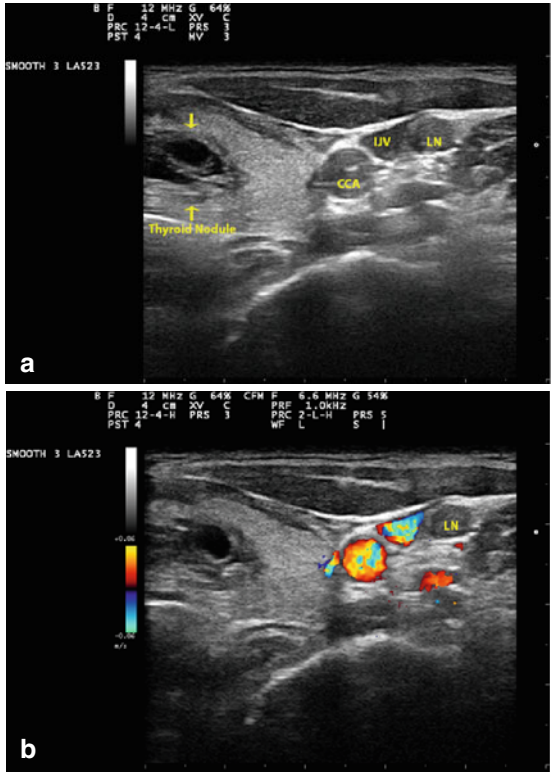

FIGURE 7.6 Left neck level IV. US images show a predominantly cystic complex left thyroid nodule, the common carotid artery (*CCA*), internal jugular vein (*IJV*), and a round-shaped lymph node (*LN*) posterior to the IJV (**a**). Corresponding findings by Doppler exam (**b**). US-guided FNA of both the thyroid nodule and lymph node showed papillary thyroid carcinoma

skin and muscles of the anterior neck and the thyroid gland. The prelaryngeal lymph node drains the subglottic area of the larynx. The paratracheal lymph nodes are difficult to visualize by US because they lie posterior to the thyroid gland; they drain the larynx, the pyriform fossae, the thyroid gland, and the esophagus.

US examination. Scan moving the probe in the transverse plane with the probe in a longitudinal position from the level of the hyoid bone down to the sternal notch.

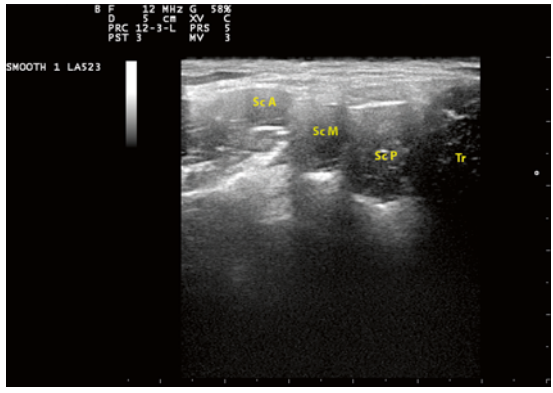

FIGURE 7.7 Left neck level V, supraclavicular area. Normal anatomy is seen in this image and include the trapezius muscle (*Tr*), and anterior, medial, and posterior scalene muscles (*ScA*, *ScM*, *ScP*)

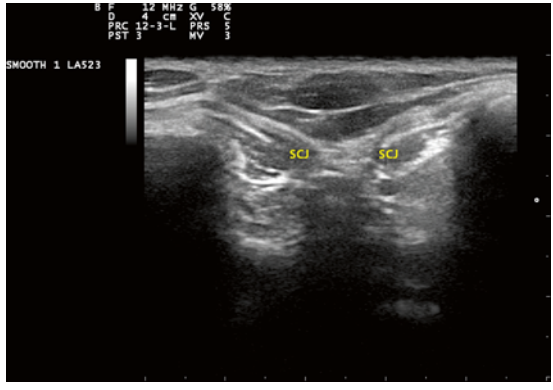

FIGURE 7.8 Neck level VII. The transducer is placed above the sternal notch and is used for evaluation of suprasternal/superior mediastinum lymph nodes. *SCJ* sternoclavicular joint

Level VII

These lymph nodes are located in the suprasternal/superior mediastinum. Best evaluated using a small-footprint curvilinear probe placed above the sternal notch (Fig. 7.8).

The *parotid-area lymph nodes* have no numbered level. They drain the skin of the lateral forehead, temple, external auditory meatus, posterior cheek, gums, and buccal mucosa. Likewise, the *buccal region lymph nodes* are not numbered, lie anterior to masseter muscle adjacent to the facial artery in the buccal fat space, and drain the facial skin from the upper eyelid to the upper lid.

The retroauricular and occipital lymph nodes drain corresponding areas of the scalp and should be examined in cases of scalp malignancy.

US can typically identify between 6 and 20 neck lymph nodes. Most enlarged lymph nodes are reactive secondary to inflammatory or infectious processes located in the head and neck area. Lateral compartment lymph nodes are easier to detect and amenable to USG-FNA. Central-compartment lymph nodes are more difficult to detect by US and sample using US guidance.

US Features in Lymph Node Evaluation

The US features to be evaluated in a lymph node include, size, shape, border, confluence, echogenicity, hilum, calcification, necrosis, parenchymal reticulation, intranodal vascular pattern, and surrounding edema. Because no abnormality of these features by itself is diagnostic of malignancy, a combination of the ultrasound findings helps in predicting malignancy. The lymph node number in a given lymph node chain is a consideration for abnormality when >3 US-abnormal lymph nodes are present.

1. Size. Lymph node size is an important consideration; however, the most important factor is the variation in the lymph node size over a period of time. Size may be of limited value in differentiating benign from malignant nodes. Nodal size is important for TNM cancer staging: N1 <3 cm, N2 3–6 cm, and N3 >6 cm. The lymph node size

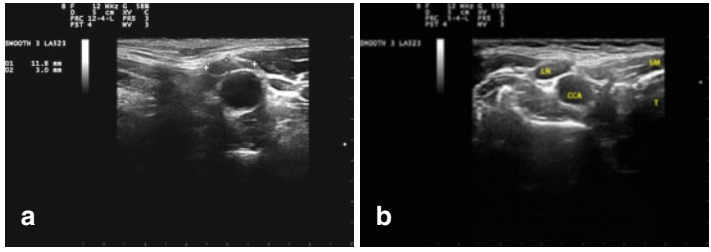

FIGURE 7.9 Lymph node size. Small oval level III left (**a**) and right (**b**) neck lymph nodes. Metastatic papillary thyroid carcinoma (calipers, **a**) and reactive follicular hyperplasia (**b**) were the US- guided FNA diagnoses. Abbreviations: *LN* lymph node, *CCA* common carotid artery, *SM* strap muscles, *T* trachea

should be measured transversally and not longitudinally (Fig. 7.9).

2. Shape. A normal node has a flat bean shape. An irregular or round shape is seen in metastasis instead of the oval shape often seen in benign and reactive lymph nodes. An irregular lymph node cortex is suggestive of a subcapsular metastatic deposit. It has been found that 85 % of benign lymph nodes have a ratio of antero posterior (AP) axis/transverse (T) axis <0.5, and 85 % of malignant nodes have an AP/T axis ratio >0.5 in the transverse view. Of note, level Ia and Ib benign lymph nodes are often round (Fig. 7.10).
3. Border. The border of a normal lymph node is smooth and slightly indistinct from the surrounding tissue. A sharp lymph node border is seen in metastasis and lymphoma instead of an ill-defined border seen in a reactive lymph node. Extracapsular nodal involvement of malignancy and response to radiotherapy also cause ill-defined borders. Ill-defined and spiculated/irregular margins in a metastatic node indicate extranodal metastatic spread (Fig. 7.11).

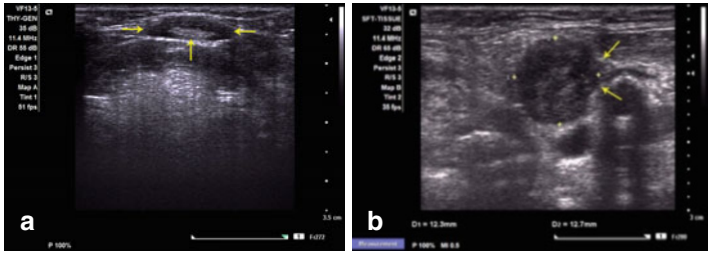

FIGURE 7.10 Lymph node shape. Oval (antero posterior/transverse <0.5) level 1a lymph node (*horizontal arrows*) with regular borders and prominent hilum (*vertical arrow*) (**a** US-guided FNA diagnosis was reactive follicular hyperplasia). Left neck lymph node with heterogeneous echotexture, irregular borders (*arrows*), and taller than wide (antero posterior/transverse >0.5) in the transverse view (**b** US-guided FNA diagnosis was poorly differentiated metastatic squamous cell carcinoma)

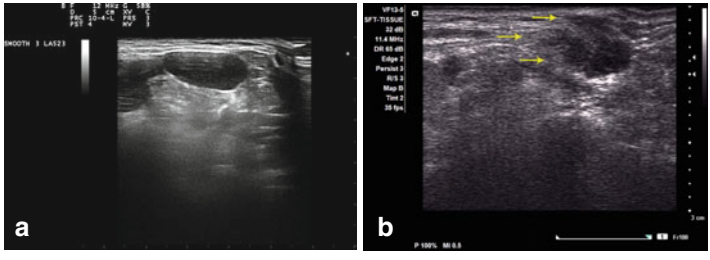

FIGURE 7.11 Lymph node borders. Neck lymph node with oval, homogeneous, and slightly lobulated well-defined sharp borders (**a** Hodgkin lymphoma was the US-guided FNA diagnosis). Neck level 1 lymph node with spiculated borders (*arrows*) and heterogeneous echotexture (**b** metastatic breast carcinoma was the US-guided FNA diagnosis)

4. Confluence. Matted lymph nodes can be seen in tuberculosis, postradiation, chemotherapy, metastasis, and lymphoma as a result of perinodal inflammation and fibrosis (Fig. 7.12).

FIGURE 7.12 Lymph node confluence. Matted hypoechoic homogeneous lymph nodes. Non-Hodgkin lymphoma was the US-guided FNA diagnosis

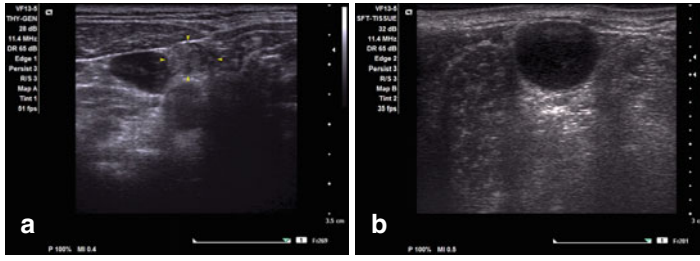

FIGURE 7.13 Lymph node echogenicity. Hyperechic lymph node in a patient with metastatic Hurthle cell carcinoma of the thyroid gland (**a** *arrow heads*). Lymph node with marked hypoechogenicity ("pseudocystic" pattern) and posterior acoustic enhancement in a patient with non-Hodgkin lymphoma (**b**)

5. Echogenicity. Hypoechogenicity is seen in metastatic malignancies; however, metastatic papillary thyroid carcinoma may be hyperechoic when compared with adjacent muscle. A "pseudocystic" pattern (marked hypoechogenicity with posterior acoustic enhancement) is seen in lymphoma when evaluated at conventional US resolution (Fig. 7.13).

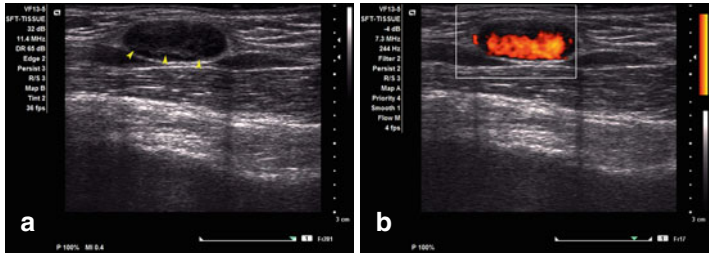

FIGURE 7.14 Benign lymph node with a prominent hilum (**a** *arrow heads*) highlighted by Doppler examination (**b**)

6. Hilum. A vascular hilum is usually seen in 90 % of lymph nodes >5 mm. An enlarged lymph node with a prominent echogenic vascular hilum is probably benign. Metastatic lymph nodes usually lack a hilum; however, a hilum can be seen in metastasis, particularly in early metastatic nodal involvement. Thus, hilum absence in an enlarged lymph node is highly suspicious for malignancy. Of note, tuberculous lymph nodes usually lack a hilum (Fig. 7.14).
7. Calcification. Metastasis from papillary thyroid carcinoma, medullary carcinoma, or lymph nodes in patients with a history of radiotherapy or chemotherapy may show foci of macrocalcification. Macrocalcifications are also seen in tuberculous lymphadenitis (Fig. 7.15).
8. Necrosis. Cystic necrosis can be seen in metastases, i.e., squamous cell carcinoma, papillary thyroid carcinoma, and benign processes such as tuberculosis (Fig. 7.16). A cystic nodal metastasis >3 cm in squamous cell carcinoma appears anechoic and, if it involves the jugulo digastric lymph node, should be differentiated from a branchial cleft cyst, particularly in patients older than 30 years. Coagulative necrosis may appear hyperechoic and may be confused with hilum when located close to the nodal capsule; however, it is not continuous with the perinodal fat as the hilum is.
9. Intranodal reticulation. A micronodular reticulated pattern is seen in lymphoma when evaluated with high-resolution US. Under conventional resolution, lymph nodes have a "pseudocystic" appearance with marked hypoechogenicity and posterior acoustic enhancement.

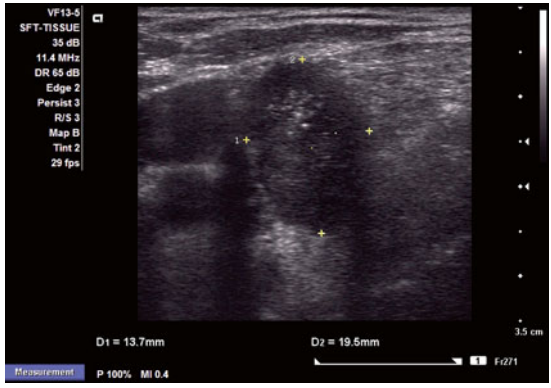

FIGURE 7.15 Metastatic thyroid carcinoma to a level V lymph node. Note microcalcifications in the upper part of the node

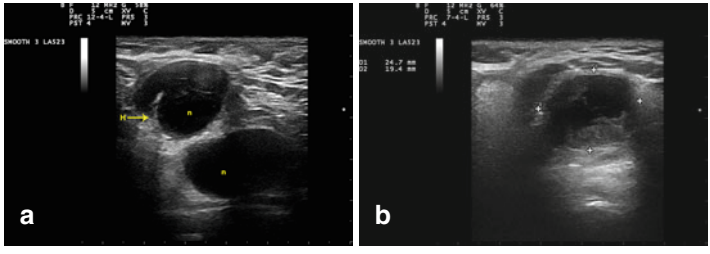

FIGURE 7.16 Necrosis. Tuberculous lymphadenitis with focal necrosis (*n*) and preserved hilum (**a** *arrow*). Level V cervical lymph node with metastatic squamous cell carcinoma with central necrosis (**b**)

10. Nodal vascular pattern. Normal or reactive lymph nodes usually have no vascularity when they measure <5 mm. Metastatic lymph nodes may have hilar and peripheral (mixed) or peripheral subcapsular flow and perfusion defects (Fig. 7.17a). Peripheral subcapsular flow is also seen in tuberculosis, which disrupts the nodal vascular architecture in a manner similar to malignancy. An exaggerated normal vascular appearance with a branching hilar vascular pattern is often seen in lymphoma (Fig. 7.17b).

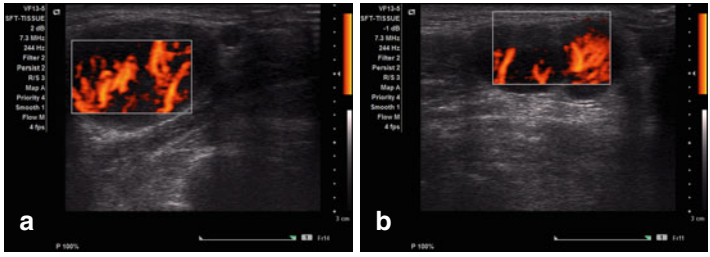

FIGURE 7.17 Vascular pattern. Metastatic poorly differentiated carcinoma showing a chaotic vascular flow pattern (**a**). Non-Hodgkin lymphoma showing an exaggerated branching hilar vascular pattern (**b**)

Thus, the US characteristics and topographic distribution of the lymph nodes, and the clinical scenario including physical examination, are paramount for the cytopathologist to provide a useful microscopic interpretation, which in some instances does not need to be specific but only descriptive. The lack of specific findings is also useful in some cases.

Fine-Needle Aspiration of Lymph Nodes

The clinical history and the characteristics of a lymph node are factors important for deciding on the need for additional diagnostic modalities, i.e., imaging studies and FNA. FNA is the modality of choice for evaluating an abnormal lymph node and, in many instances, avoiding an unnecessary open biopsy. The use of US as an aid in locating and performing FNA of superficial and deep-seated lymph nodes offers significant benefits, i.e., sampling of solid areas in cystic necrosis and reducing nondiagnostic samples, procurement of sample for cultures, and obtain material for flow cytometry in lymphomas. USG-FNA has a sensitivity of 97 % and a specificity of 93 %.

A thorough cytologic evaluation answers questions which the cytopathologist should keep in mind when evaluating lymph node FNAs. The questions include the following: (1)

Is it really a lymph node? (2) Adequate? (3) Is it benign or malignant? (4) If benign, is it infectious? Can we identify the infectious agent? (5) If malignant, lymphoma? Metastasis? (6) If lymphoma, non-Hodgkin? Hodgkin?, (7) If non-Hodgkin, B- or T-cell type? Grade? (8) If Hodgkin, subtype? (9) If metastasis, type? Source? Most answers can be based on morphologic evaluation, and others need the support of ancillary tests, i.e., cultures, special stains, flow cytometry, cytogenetics, molecular studies, etc., for reaching a definitive diagnosis.

The use of Romanowsky-type stains (Diff-Quik, Wright, May–Grunwald–Giemsa) performed on air-dried smears is fundamental for FNA cytologic interpretation, because they provide excellent evaluation of cell size, cytoplasmic detail, and background elements. Papanicolaou and hematoxylin and eosin stains performed on alcohol-fixed smears provide excellent visualization of nuclear morphology in both single cells and cell aggregates. Thus, both air-dried and alcohol-fixed stains are complementary. We caution against the use of liquid-based preparations for lymph node FNA because cells appear smaller, cell aggregates are fragmented, lymphocytes may become artificially aggregated, and background elements are difficult to evaluate.

Cell Patterns in Fine-Needle Aspiration of Lymph Nodes

To facilitate the cytologic interpretation, the FNA of lymph nodes can algorithmically be classified in the following smear cell patterns:

1. Polymorphous. Nonspecific reactive lymphoid hyperplasia, early HIV lymphadenitis, primary and secondary syphilis lymphadenitis, toxoplasma and leishmania lymphadenitis, rheumatoid arthritis, Castleman lymphadenopathy plasma cell variant, Kimura lymphadenopathy, early dermatopathic lymphadenopathy, Sézary syndrome, early cat scratch lymphadenitis, follicular lymphoma grade 2, diffuse follicular center cell lymphoma, and nodal marginal B-cell lymphoma

2. Monotonous small size. Quiescent benign lymph node, Castleman disease hyaline vascular variant, B-cell chronic lymphocytic leukemia/small lymphocytic lymphoma, T-cell chronic lymphocytic leukemia, lymphoplasmacytic lymphoma, T-cell/histiocyte-rich diffuse large B-cell lymphoma, and Hodgkin lymphoma lymphocyte-predominant type
3. Monotonous intermediate size. Follicular lymphoma grade 1, diffuse follicle center cell lymphoma grade 1, mantle cell lymphoma, nodal marginal zone lymphoma, Burkitt lymphoma, precursors of B- and T-cell lymphomas, adult T-cell leukemia/lymphoma, peripheral T-cell lymphoma, Sézary syndrome, and metastatic small cell malignancies
4. Monotonous large size. Diffuse large B-cell lymphoma and its variants, follicular lymphoma grade 3, Richter's transformation of small lymphocytic lymphoma, blastoid variant of mantle cell lymphoma, peripheral T-cell lymphoma, NK-/T-cell lymphoma, granulocytic sarcoma, nodal Langerhans cell histiocytosis, dendritic cell neoplasms, metastatic carcinoma, metastatic melanoma, metastatic sarcoma, and metastatic seminoma
5. Pleomorphic. Hodgkin lymphoma, anaplastic large cell lymphoma, Hodgkin-type Richter's transformation of small lymphocytic lymphoma/chronic lymphocytic leukemia, diffuse large B-cell lymphoma variants, thymoma, metastatic melanoma, and metastatic mesenchymal malignancies

Tables 7.1 and 7.2

Select Examples of Lymphadenopathy

Reactive Lymphoid Hyperplasia

Reactive lymphoid hyperplasia is the prototype of a cytologic polymorphous lymphoid cell pattern commonly associated with benign, reactive and reversible, lymphadenopathy. The etiology remains unknown in most cases. Bacteria, viruses,

Table 7.1 Lymphadenitis/lymphadenopathy – clues for the cytologic diagnosis

Viral	
Infectious mononucleosis	Immunoblasts with marked atypia
Herpes simplex	Cowdry A inclusions, ground-glass nuclei, multinucleation
Cytomegalovirus	Large cells with large eosinophilic nuclear inclusion
Varicella-Zoster	Rare small intranuclear inclusions
Measles	Polykariocytes (not specific)
Human immunodeficiency virus	Polymorphous lymphoid cell pattern. Plasma cells in late stages
Bacterial	
Cat scratch	Granulomas, necrosis, acute inflammation
Lymphogranuloma venereum	Granulomas, necrosis, acute inflammation
Syphilis	Small granulomas and plasma cells
Tuberculosis	Granulomas and caseation necrosis
Mycobacterium avium-intracellulare complex	Histiocytes and background smear with numerous bacilli (Pseudo-Gaucher cells and negative images)
Leprosy, tuberculoid	Small non-caseating granulomas
Fungal	
Cryptococcus	Yeast with mucoid thick capsule. Mucous background. Narrow-based buds
Pneumocystis	Foamy exudates

(continued)

Table 7.1 (continued)

Histoplasma	Intracytoplasmic yeasts. Granular calcific background
Coccidioides	Large spherules with yeast forms
Protozoal	
Toxoplasma	Crescent-shaped organisms (2–6 μm)
Leishmania	Amastigotes 1–3 μm with histiocytes (Donovan bodies) and multinucleated giant cells
Filaria	Fragments of dead calcified organisms
Non-infectious	
Kimura disease	Polymorphous lymphoid cell pattern with polykariocytes (not specific)
Kikuchi disease	Necrosis
Dorfman-Rosai disease	Histiocytes with cytophagocytosis (emperilopolesis, erythrocytes, plasma cells)
Sarcoidosis	Cell damage, non-necrotizing granulomas. Schaumann and cytoplasmic asteroid bodies
Systemic lupus erythemathosus	Necrosis. Hematoxylin bodies
Rheumatoid arthritis	Polymorphous lymphoid cell pattern and plasma cells
Castleman disease, plasma cell variant	Plasma cells
Dermatopathic	Lipid or pigment (melanin)-laden histiocytes
Amyloid	Amorphous "waxy" material, lymphocytes, multinucleated giant cells
Silicone	Histiocytes with clear cytoplasmic vacuoles, multinucleated giant cells
Lipid	Histiocytes with small cytoplasmic vacuoles, multinucleated giant cells (lipogranulomas)

Modified from Pambuccian and Bardales (2011), with permission

Table 7.2 The various cytologic patterns as clues for the diagnosis

Necrosis	Granulomas with necrosis
Infectious mononucleosis (focal)	Cat-scratch disease
Herpes simplex (focal)	Mycobacterial infection
Kikuchi disease (marked)	Fungal infection
Systemic lupus erythematosus (marked)	Kikuchi disease
Pneumocystis (marked)	Lymphogranuloma venereum
Infarcted lymph node (marked)	Leishmania
Neutrophils	**Granulomas without necrosis**
Bacterial infection (marked)	Toxoplasma
Anaplastic large cell lymphoma (scattered)	Sarcoidosis (rare with necrosis)
Anaplastic carcinoma (scattered)	Syphilis
	Whipple disease
	Tuberculoid leprosy
	Filaria
	Tumor-associated lymphadenitis

Modified from Pambuccian and Bardales (2011), with permission

chemicals, and iatrogenic drugs are identified in a minority of cases. The lymph nodes are small, oval, soft, and single or regional, often cervical in children and inguinal in all age groups.

The cytologic pattern reflects the expansion of a particular lymph node area (follicular, paracortical, medullary, sinusoidal), which depends on the antigenic stimulus. *Follicular hyperplasia* represents a B-cell response and includes the presence of small round lymphocytes, centroblasts, centrocytes, immunoblasts, plasmacytoid lymphocytes, plasma cells,

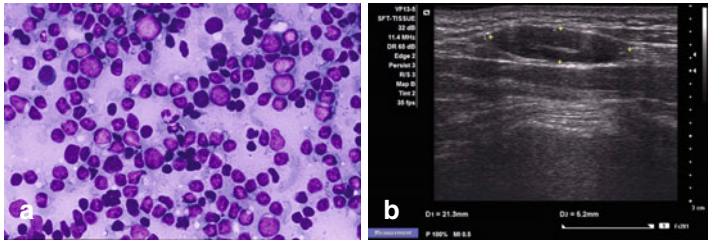

FIGURE 7.18 Reactive lymph node. The smear shows a characteristic polymorphous population of lymphoid cells (**a**). The US evaluation shows an oval (AP/T < 0.5 in the transverse view), hypoechoic, homogeneous, and well-defined lymph node with regular borders and presence of hilum (**b**). *AP* antero posterior axis, *T* transverse axis)

and histiocytes/tingible-body macrophages in various numbers. *Paracortical hyperplasia* with predominance of immunoblasts represents a T-cell response. An inflammatory pattern is frequently associated with bacteria and fungi. An immune pattern is usually the result of drugs and viruses, and it often elicits a paracortical hyperplasia. Occasionally, the differential diagnosis includes follicular lymphoma grades 2 and 3, and the use of ancillary tests on FNA material is needed.

The smears are cellular and show a polymorphous population of lymphoid cells and lymphohistiocytic aggregates, which are fragments of germinal centers containing centrocytes, centroblasts, dendritic cells, small lymphocytes, and tingible-body macrophages. After a single triggering factor, the smears show a polymorphous pattern lasting 3–4 weeks; progressively, the smear shows a predominance of small round lymphocytes and centrocytes for 3–4 weeks. The background shows histiocytes, scattered plasmacytoid cells, plasma cells, and lymphoglandular bodies (Fig. 7.18).

The immunophenotype shows positive pan-B-cell markers CD19, CD20, CD22, and CD79a with a K/L ratio of 3–5/1 and no light-chain restriction.

Of note, this pattern is seen as a smear background in Hodgkin lymphoma and along with histiocytes in cases of draining lymph nodes in metastatic disease, regardless of the presence or absence of actual metastatic deposits.

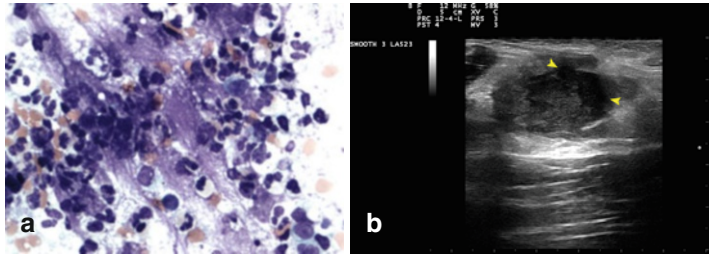

FIGURE 7.19 Bacterial lymphadenitis. Smear shows a purulent smear pattern (**a**). The US exam shows a lymph node with ill-defined margins, heterogeneous echotexture, and a cystic component (**b** *arrow heads*)

Bacterial Lymphadenitis

This process is seen in the head and neck of children draining, an area of bacterial infection. Patients have fever, the lymph node is enlarged and tender, and the overlying skin is usually hyperemic.

The smear pattern shows numerous intact and degenerated neutrophils; degenerated lymphoid cells and macrophages may also be present. This pattern may be seen in systemic lupus erythematosus and rarely in Hodgkin lymphoma. Bacterial organisms may be seen best with Romanowsky-stained smears inside phagocytes and extracellularly (Fig. 7.19).

Granulomatous Lymphadenitis

Etiologic agents for this smear pattern include infections, foreign body reactions, and sarcoidosis.

Mycobacterium tuberculosis is prevalent in HIV-infected individuals and in foreign-born young immigrants to the US. The most common form of extrapulmonary tuberculosis is lymphadenitis that commonly affects cervical (frequently posterior triangle) chains. The lymph nodes may be matted and markedly necrotic and fluctuant. The *M. tuberculosis*

activates CD4+ T cells and produces tissue necrosis, and the macrophages transform into uni- or multinucleated epithelioid macrophages. Thus, the smears of tuberculous lymphadenitis show epithelioid granulomas, caseation necrosis, lymphocytes, and occasional Langhans-type giant cells. The nuclei of such cells are arranged peripherally in a horseshoe shape rimming in the cytoplasm. The bacilli can be detected by special acid-fast staining and are detected predominantly in the background smear. The bacilli are bright red, slender, and beaded by the Ziehl–Neelsen acid-fast stain; however, only 20 % of culture-positive cases have a positive stain. Culture in Lowenstein–Jensen medium can take up to 6 weeks for a definitive diagnosis, thus delaying treatment. Polymerase chain reaction in fluids, smears, and tissue samples, including paraffin-embedded tissue, can detect the organism in less than 6 h.

Atypical mycobacteria are a cause of chronic granulomatous lymphadenitis in children. In adults, the infection occurs in the presence of immunosuppression. The organisms are widely spread in nature and include *M. marinum*, *M. fortuitum*, *M. scrofulaceum*, and *M. kansasii*. Commonly affected sites include cervical lymph nodes and may be associated with erythema of the overlying skin and with abscess formation. *Mycobacterium avium intracellulare* (MAI), found in the soil and in tap water, is highly pathogenetic in patients with AIDS and may produce regional or generalized lymphadenitis and systemic disease. The smears show necrosis, poorly formed granulomas, and numerous large histiocytes with foamy cytoplasm (pseudo-Gaucher cells) filled with bacilli. Occasionally, the histiocytes develop a spindle cell phenotype (MAI spindle cell pseudotumor). The characteristic negative images within the cytoplasm of macrophages and in the background are best seen in Romanowsky-stained smears. The definite diagnosis is made by cultures and polymerase chain reaction in smears and formalin-fixed, paraffin-embedded tissue (Fig. 7.20).

The differential diagnosis of granulomatous lymphadenitis includes tuberculosis, histoplasma, Kikuchi and cat scratch

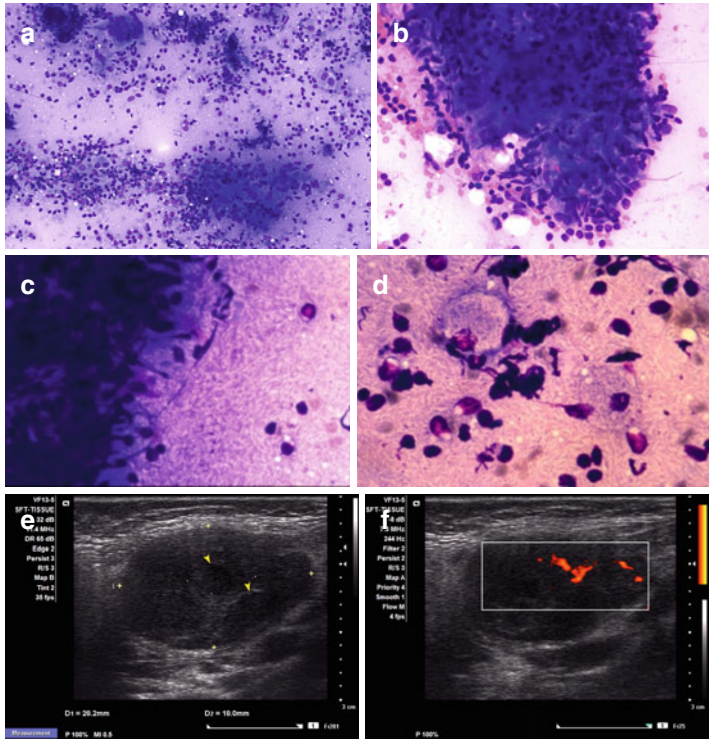

FIGURE 7.20 Tuberculous lymphadenitis. Smears show necrosis, damaged inflammatory cells, histiocytes, multinucleated giant cells, and granulomas (**a**, **b** *Mycobacterium tuberculosis*). Atypical mycobacteria with numerous thick and long organisms that appear as "negative images" both in the background of the smear (**c**) and within histiocytes ("pseudo-Gaucher" cells) (**d** *Mycobacterium avium intracellulare*). The US exam shows a large lymph node with hypoechogenicity, smooth distinct margins, foci of cystic degeneration (**e** *arrow heads*), and mild central and peripheral vascularity on Doppler examination (**f**) (**a**, **d** DiffQuik stain, medium and high magnification)

lymphadenitis, and sarcoidosis. Non-necrotizing granulomas are often seen in sarcoidosis, which shows tightly packed granulomas and damaged lymphoid cells; cultures are

negative. Fungal infections may involve the lymph nodes, particularly when immunocompetency is affected. The prevalence of these infections is influenced by the incidence of mycoses, i.e., histoplasmosis and coccidioidomycosis, in certain geographic areas. The identification of the organism in cytologic material permits the application of early antifungal therapy before culture and serologic results are available.

Cat Scratch Disease

Cat scratch disease is a common cause of chronic lymphadenitis in children and adolescents. In the United States, 55 % of cases occur in patients age 18 years or younger, commonly in the months of September to January. The pathogenic organism is *Bartonella henselae*, a Gram-negative bacillus transmitted by fleas to kittens and then transmitted to humans by a cat bite or lick.

The patients have enlarged, nodular, and matted regional lymphadenopathy that is fixed to surrounding tissues and commonly occurs in the upper extremities and face. The lymphadenopathy develops 1–3 weeks after the primary skin lesion and is usually accompanied by systemic symptoms. In immunocompetent individuals, the disease is self-limited and resolves in 6–12 weeks in the absence of treatment. Suppuration occurs in 10 % of cases. A systemic life-threatening disease may occur in immunosuppressed patients.

The smears show a reactive lymphoid hyperplasia pattern with monocytoid cells and scattered tingible-body macrophages in the early stages of the disease. A suppurative granulomatous pattern with necrosis, neutrophils, epithelioid histiocytes, granulomas, and rare multinucleated Langhans-type giant cells is seen in more established processes (Fig. 7.21).

Microbiologic detection is difficult, and the diagnosis is supported by clinical history, serology, and histopathology. The organisms can be visualized by the Warthin–Starry silver stain, immunoperoxidase stain with anti-*B. henselae*

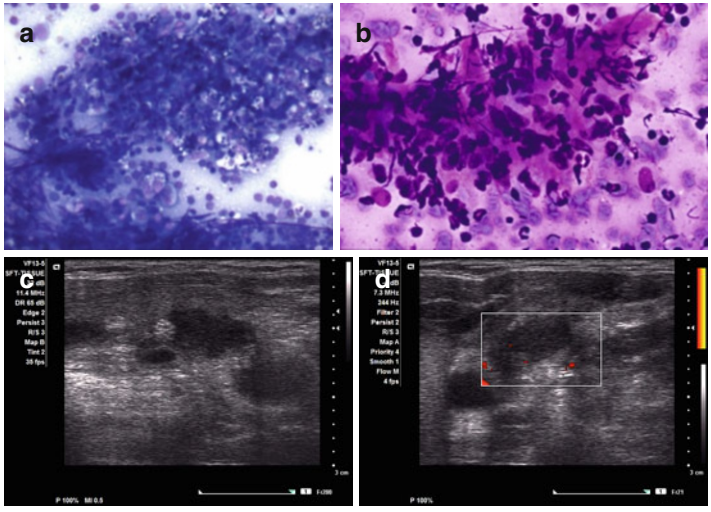

FIGURE 7.21 Cat scratch disease. Smears show a purulent pattern with necrosis, acute inflammation damaged lymphocytes, and granulomas (**a**, **b**). The US exam shows irregularly-shaped, coalescent lymph nodes with necrosis and no vascularity on Doppler examination (**c**, **d**) (**a**, **b** DiffQuik stain, high magnification)

antibodies in tissue sections, PCR, indirect immunofluorescence, and enzyme immunoassay. The diagnostic sensitivity of all tests is low. The silver stain is the most sensitive, but is the least specific. Lymphogranuloma venereum is cytologically identical, and immunofluorescence and serology are necessary for the diagnosis. The differential cytologic diagnosis also includes bacterial suppurative lymphadenitis, tularemia, and other granulomatous processes, including tuberculosis; special stains and cultures are needed to rule out these processes.

Infectious Mononucleosis

Infectious mononucleosis is an acute self-limited disease caused by the Epstein–Barr virus (EBV) that affects predominantly adolescents and young adults, who have fever,

pharyngitis, and cervical or generalized lymphadenopathy. The lymph nodes are enlarged and soft, but not matted. The viral spread is via direct contact with oral secretions. The EBV infects both epithelial cells and B cells in the oropharynx; B cells can be infected via the CD3d complement receptor (CD21) causing an antibody response with cell proliferation during the first week of the disease. Lymphocytosis with atypical lymphocytes is commonly seen in the peripheral blood. The disease resolves in 3–4 weeks in most patients. A life-threatening disease is seen in immunosuppressed individuals.

The cytology preparations show numerous large reactive immunoblasts, large and small lymphocytes, histiocytes, tingible-body macrophages, and rare plasma cells. Numerous mitoses and apoptotic nuclei are also present. The immunoblasts are large and show a basophilic cytoplasm, a large nucleus, and a single central round or polyhedral nucleolus. Necrosis may be present (Fig. 7.22).

No light-chain restriction is identified, and the immunostains for B and T cells demonstrate a reactive pattern. EBV can be demonstrated by immunohistochemistry, in situ hybridization, and other types of molecular analysis in tissue sections. The differential diagnosis includes large cell lymphoma, anaplastic large cell lymphoma, nodular lymphocyte predominance Hodgkin lymphoma, and classical Hodgkin lymphoma.

Human Immunodeficiency Virus

The human immunodeficiency virus 1 (HIV-1) is a lentivirus, a subfamily of retroviruses that infects CD4+ lymphocytes, macrophages, and dendritic cells; the first disseminates the virus, and the last two are the reservoirs. In the late stage, the CD4 lymphocytes and the dendritic cells are destroyed, the viremia resurges, and opportunistic infections and tumors develop in the immunosuppressed host.

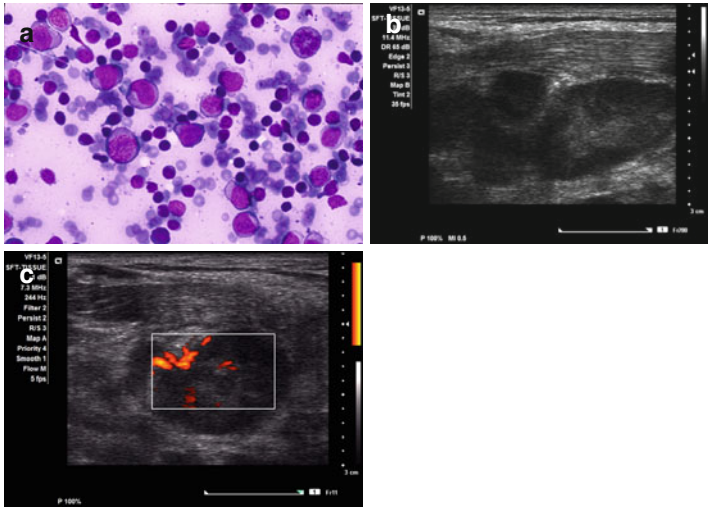

FIGURE 7.22 Infectious mononucleosis. Smears show numerous reactive immunoblasts with bluish cytoplasm, large nuclei, prominent nucleoli, and scattered mitoses (**a**). The US exam shows large odd-shaped hypoechoic lymph nodes with predominant medullary and polar vascularity (**b**, **c**) (**a** DiffQuik stain, high magnification)

In the acute and chronic phase of HIV infection, there is generalized lymphadenopathy that harbors processes that may be reactive, infectious (mycobacterial and fungal), or neoplastic (lymphoma, Kaposi's sarcoma). In the acute phase, the smear shows a florid reactive lymphoid hyperplasia, scattered large monocytoid cells with clear cytoplasm and round nuclei, neutrophils, multinucleated cells (polykaryocytes of Warthin–Finkeldey), and tingible-body macrophages. The smears are less cellular, and the present plasma cells are notorious in the subacute phase of HIV lymphadenitis. Hypocellular smears with a paucity of lymphocytes and predominance of plasma cells are characteristic of the chronic burned-out phase of HIV infection.

The main role of FNA in HIV patients is to rule out opportunistic infections and neoplasms such as lymphoma or Kaposi's sarcoma.

Ultrasound Features of Reactive and Infectious Lymph Nodes

Reactive lymph nodes usually have the following characteristics: hypoechoic, slightly ill-defined margins, hilum present, hilar vascular pattern except lymph nodes <5 mm, lack of peripheral blood flow by Doppler examination, and flat or oval shape (AP/T axis <0.5) except lymph nodes involving level I, which may be round. Lymph nodes involved by granulomatous infectious processes including cat scratch disease and tuberculosis may have pronounced cystic necrosis and lymph node confluence in addition to the mentioned findings (Figs. 7.18b, 7.19b, 7.20e, f, 7.21c, d, and 7.22b, c).

Non-Hodgkin Lymphoma (NHL)

The use of FNA cytology for diagnosing NHLs is well established. In fact, most malignant lymphomas can be diagnosed and treated on the basis of cytomorphology and special studies done on FNA material. Judicious use of ancillary tests is paramount, and flow cytometry is most important in the detection of cell surface markers to establish light-chain monoclonality and characterize the clonal proliferation. Normal mature B cells express CD19, CD20, and CD22 and are good markers in B-cell lymphomas. Plasma cells lack such markers; instead, they express CD38 and CD138. CD10 is expressed by both early B- and T-cell progenitor cells and follicular lymphoma. The T-cell markers CD5 and CD43 may normally be expressed in a small percentage of B cells; CD5 is aberrantly coexpressed in some small cell types of B-cell lymphomas. T-cell clonality is difficult to establish by flow cytometry.

Table 7.3 CD5 and CD10 expression in most common nodal NHLs

CD5-positive, CD10-negative
Chronic lymphocytic leukemia/small lymphocytic lymphoma (CLL/SLL)
Mantle-cell lymphoma (MCL)[a]
Diffuse large B-cell lymphoma, including Richter transformation of CLL
Lymphoplasmacytic leukemia
CD5-negative, CD10-positive
Follicular lymphoma (FL)[a]
Diffuse large B-cell lymphoma (DLBCL)[a]
Burkitt lymphoma (BL)[b]
CD5-negative, CD10- negative
Marginal zone lymphoma (MZL)[c]
Lymphoplasmacytic lymphoma

Modified from Pambuccian and Bardales (2011), with permission
[a]FL, DLBCL, and MCL can be CD5+/CD10+ or CD5–/CD10–
[b]BL can be CD5+/CD10+
[c]MZL can be CD5+

The various types of NHLs are defined by their morphology, immunophenotype, cytogenetics, and clinical features (Table 7.3).

Combining cytomorphology and immunophenotype, the diagnosis of NHL can be reached successfully in FNA material. In the following paragraphs, we will briefly review the characteristics of the common NHLs found in clinical practice.

Large Cell Lymphoma

This is one of the most common neoplasms diagnosed by FNA and affects mainly adults in the seventh decade of life.

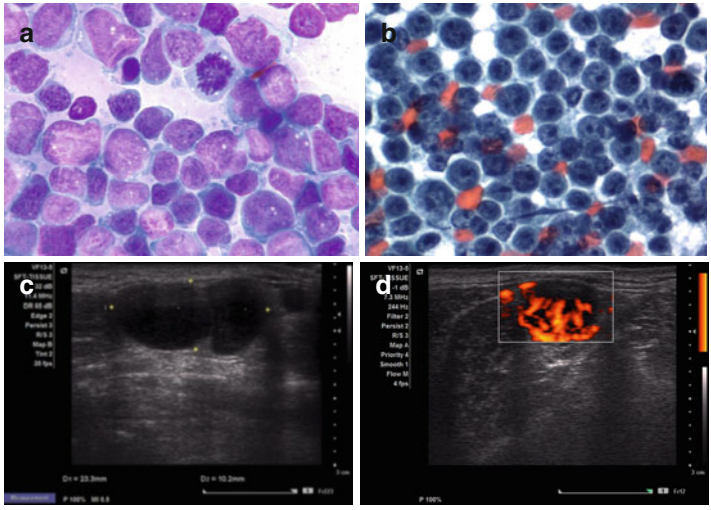

FIGURE 7.23 Diffuse large B-cell lymphoma. Large monomorphous cells with dark blue cytoplasm, some plasmacytoid features, irregular nuclear contours, mitoses, and apoptotic bodies (**a**). Large cells with round nuclei, basophilic cytoplasm, and prominent nucleoli are characteristic of immunoblastic lymphoma (**b**). The US exam shows dysmorphic coalescent lymph nodes with well-defined, margins, marked hypoechogenicity, and intense chaotic hilar blood flow by Doppler examination (**c**, **d**) (**a** From Pambuccian and Bardales (2011). Reprinted with permission)

Young adults and children may be affected occasionally. The primary presentation is usually nodal, but extranodal spread or presentation may be seen. B cell is the most common phenotype and is usually diffuse on tissue examination.

The cytology shows monomorphous large lymphoid cells; however, the particular cytomorphology is variable, i.e., centroblasts, centroblasts and immunoblasts, and less frequently true immunoblasts may be seen (Fig. 7.23a–d). Variable anaplasia including large cells with irregular multilobed nuclei can also be seen. The rare anaplastic B-cell lymphoma shows less pleomorphism than does the T-cell counterpart. The T-cell-rich B-cell lymphoma shows rare large pleomorphic

tumor cells and a background of numerous small lymphocytes and mimics Hodgkin lymphoma, carcinoma, or melanoma.

Cells show light-chain monoclonality and positive B-cell markers CD19, CD20, and CD79a. CD10 is positive in centroblastic lymphoma and CD30 in the anaplastic variants. Large-cell lymphoma has a high proliferation index and frequently expresses bcl-2 and bcl-6. One third of cases show t(14;18).

Follicular (Small Cleaved and Mixed Small Cleaved and Large-Cell) Lymphoma

Follicular lymphomas arise in the lymph node follicular centers and affect mainly middle-aged patients who usually have generalized lymphadenopathy. The lymph nodes in small cleaved follicular lymphoma have a nodular or diffuse histologic pattern that gives the lymphoma a low or intermediate grade, respectively, with prognostic implications. The mixed type is an intermediate-grade lymphoma. Follicular lymphomas need tissue confirmation for precise classification. The clinical course depends on the stage and grade, and cure is rare. Large-cell malignant transformation occurs in 30 % of patients, who have a poor prognosis.

The cytology of the small cell type shows a monotonous population of small lymphocytes (centrocytes) with irregular nuclear contours, i.e., indentations, notches, and clefts, which are best seen in Papanicolaou-stained smears; nucleoli are rarely identified. The mixed cell type shows a polymorphous population of centrocytes and medium-sized atypical lymphocytes with a round nucleus and peripheral nucleoli (centroblasts), usually with predominance of the former; this pattern must be differentiated from that of reactive follicular hyperplasia. Cell aggregates may suggest a nodular pattern when smears are evaluated at low magnification. Small T lymphocytes are also present in the background (Fig. 7.24).

Cells show light-chain monoclonality and CD19, CD20, CD79a, and CD10 positivity. CD5 and CD43 are negative.

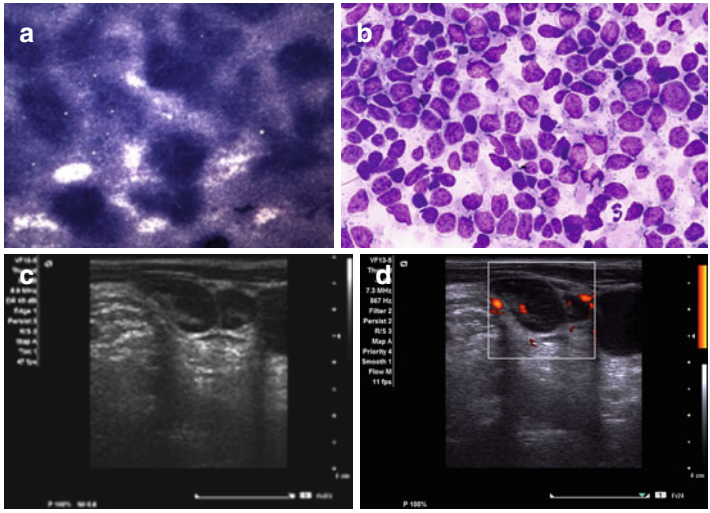

FIGURE 7.24 Follicular lymphoma. Smear shows a follicular pattern at screening magnification (**a**). Cells are monomorphous of small to intermediate size and have irregular nuclear contours (**b**). The US exam, in this particular case shows coalescent lymph nodes with presence of hilum, thick and irregular cortex, well-defined margins, hypoechogenicity, and hilar vascular blood flow by Doppler examination (**c**, **d**) (**a**, **b** MGG stain, low and high magnification) (**b** From Pambuccian and Bardales (2011). Reprinted with permission)

Cells express bcl-2 in most cases. In 95 % of cases, t(14;18) is seen.

Small Lymphocytic Lymphoma

This mainly B-cell neoplasm is the nodal counterpart of chronic lymphocytic leukemia, affects middle-aged and older populations, involves multiple lymph nodes, and is a low-grade malignancy. The clinical course is indolent; however, in rare instances, it may undergo a high-grade large B-cell transformation (Richter's lymphoma).

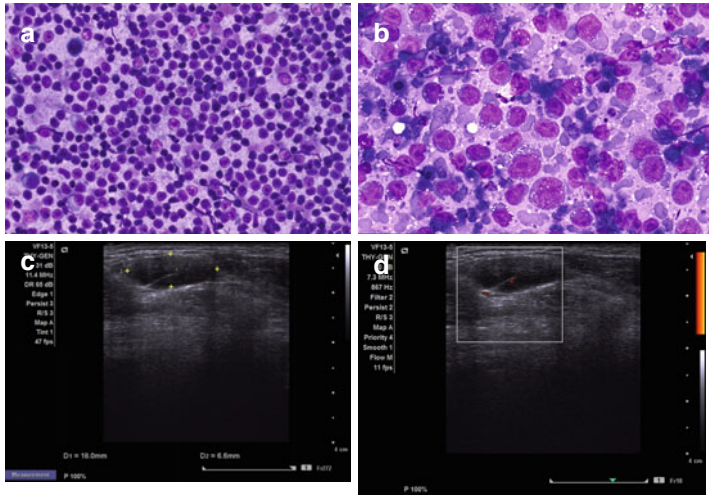

FIGURE 7.25 Small cell lymphocytic lymphoma. The smear shows a monotonous population of small round lymphoid cells (**a**). The precise diagnosis is made based on flow cytometric analysis. Large cell lymphoma transformation may occur (Richter lymphoma) and the vacuolated cytoplasm is often the result of prior chemotherapy (**b**). The US evaluation showed slightly enlarged cervical lymph nodes with linear hilum (**c**) and minimal blood flow by Doppler exam (**d**) (**a**, **b** DiffQuik, high magnification) (**a** From Pambuccian and Bardales (2011). Reprinted with permission)

The cytology shows a monotonous pattern of small lymphocytes with a round nucleus, coarse chromatin, and inconspicuous nucleoli. Scattered large cells (paraimmunoblasts and prolymphocytes) can be found. Distinction from other lymphomas of the small cell type is based on flow cytometry and not on pure cytomorphology (Fig. 7.25) (Table 7.4).

Cells show CD19, CD20, CD23, and CD79a positivity. CD5 positivity is characteristic, and cells are negative for CD10 (positive in follicular lymphoma) and FMC7 (positive in mantle cell lymphoma). Deletion (13q14) is present in 50 % of the patients and is associated with a favorable prognosis. Trisomy 12, t(11;14), and t(14;19) have been described.

Table 7.4 Immunophenotypic profile of small- and intermediate-sized-cell lymphmas

	B-CLL/ SLL	MCL	Nodal MZL	FL-1	LPL
Surface κ/λ	+ dim	+ strong	+ strong	+ strong	+ strong
CD5	+	+	+ dim 10 %	–	–
CD10	–	–	–	+	–
CD20	+ dim	+	+	+	+
CD23	+ 90 %	+ dim 10 %	+ 10 %	–	+ dim/–
FMC7	–	+	+	+	+ (40% cases)
BCL-1	–	+	–	–	–
BCL-2	+	+	+ most cases	+	+
BCL-6	–	–	–	+	–
Cyclin D1	–	+	–	–	–

Abbreviations: *B-CLL/SLL* B-chronic lymphocytic leukemia/small lymphocytic lymphoma, *MCL* mantle cell lymphoma, *MZL* marginal zone lymphoma, *FL-1* follicular lymphoma, grade 1, *LPL* lymphoplasmacytic lymphoma

Mantle Cell Lymphoma

Mantle cell lymphoma occurs in middle-aged to older individuals, with male predominance. Most patients have generalized lymphadenopathy, hepatosplenomegaly, and GI and bone marrow and peripheral blood involvement. Most patients cannot be cured.

Cytologic preparations show monotonous lymphoid cells of intermediate size with irregular nuclear contours resembling centrocytes with dispersed chromatin and inconspicuous nucleoli; the larger cells may have single small, distinct nucleoli. Rare plasmacytoid lymphocytes may be seen.

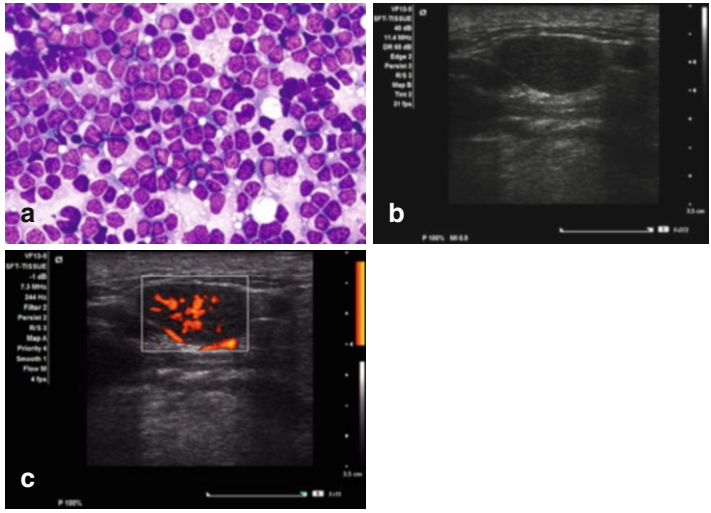

FIGURE 7.26 Mantle cell lymphoma. The smear shows a monotonous population of small slightly irregular lymphoid cells (**a**). The diagnosis needs flow cytometry evaluation in material obtained by FNA. The US exam shows a lymph node with well-defined margins, hypoechogenicity, homogeneous echotexture, and prominent vascular pattern by Doppler exam (**b**, **c**) (**a** DiffQuik stain, high magnification) (**a** From Pambuccian and Bardales (2011). Reprinted with permission)

Scattered epithelioid histiocytes and plasma cells are commonly present (Fig. 7.26).

Cell show CD5+, FMC7+, CD43+, BCL2+, BCL6–, and CD10– (Table 7.4). All cases express bcl-2 and cyclin D1. Neoplastic cells showing t(11;14)(q13;q32) with *CCND1* translocation are seen in almost all cases.

Marginal Zone Lymphoma

Monocytoid B-cell lymphoma and mucosa-associated lymphoid tissue (MALT) lymphoma have been grouped as nodal and extranodal types of marginal zone lymphoma, respectively,

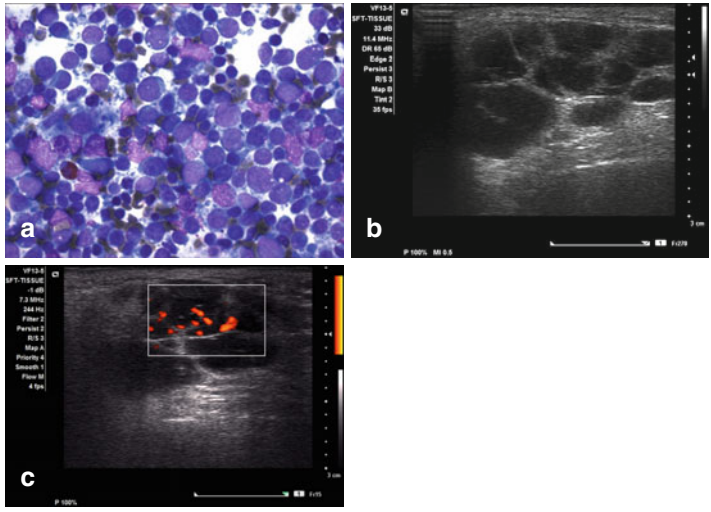

FIGURE 7.27 Marginal zone lymphoma. A monotonous population of intermediate size centrocyte-like lymphoid cells with slightly irregular nuclei is seen (**a**). The precise diagnosis is made by flow cytometry on FNA material. Ultrasound shows coalescent lymph nodes with hypoechogenicity, well-defined margins, and chaotic vascular flow by Doppler exam (**b**, **c**) (**a** DiffQuik stain, high magnification) (**a** From Pambuccian and Bardales (2011). Reprinted with permission)

and have identical histology and cytology. The nodal type that comprises <2 % of all non-Hodgkin lymphomas is a primary lymph node B-cell neoplasm without splenic or extranodal involvement and affects mostly adults and older individuals who have asymptomatic regional, often cervical or generalized lymphadenopathy. It is clinically indolent, and most patients survive longer than 5 years. Some patients may have serologic evidence of hepatitis C infection or autoimmune disorders.

The cytology shows monocytoid cells or medium-sized cells with irregular contours (centrocyte-like cells), or cells resembling small-/intermediate-sized round lymphocytes, or a combination of the three in various proportions. Plasma cell differentiation may be prominent in some cases, and scattered eosinophils may be present (Fig. 7.27).

As seen in Table 7.4, CD5, CD10, BCL6, and cyclin D1 are negative and bcl-2 is positive. CD23 may be faintly positive. Trisomy 3 (60 %) or t(11;18) may be seen.

Small Non-cleaved Cell (Burkitt) Lymphoma (BL)

Three variants, endemic, sporadic, and immunodeficiency associated, have been described and differ clinically, morphologically, and biologically. Endemic BL occurs in equatorial Africa in areas of endemic malaria and affects predominantly children. Sporadic BL is seen throughout the world, represents <2 % of all non-Hodgkin lymphomas in the United States, and affects predominantly children and young adults. Immunodeficiency-associated BL is often associated with HIV infection. Patients have bulky disease and signs and symptoms of a few weeks' duration due to the short doubling time of the tumor. Endemic and sporadic BL may be cured with intensive chemotherapy regimens.

The cytology shows tumor cells of medium size with round nuclei and evenly distributed chromatin with multiple nucleoli. The cytoplasm is moderate in amount, deeply basophilic, and usually contains a number of clear-lipid-containing vacuoles. Numerous mitoses are present as well as numerous macrophages with ingested apoptotic tumor cells. The spectrum of BL is wide, and some cases may show tumor cells with plasmacytoid features or nuclear pleomorphism with prominent nucleoli (Fig. 7.28).

Tumor cells are monoclonal and CD10, CD19, and CD20 positive. bcl-2 is negative and bcl-6 is positive. The Epstein–Barr virus (EBV) genome is present in the neoplastic cells in all cases of endemic BL and in approximately 30 % of sporadic and immunodeficiency-associated BL. Most cases have an (8;14) translocation.

Precursor B- and T-Cell Lymphomas

The term lymphoblastic lymphoma (LBL) is used when the process is confined to a mass lesion with minimal or no

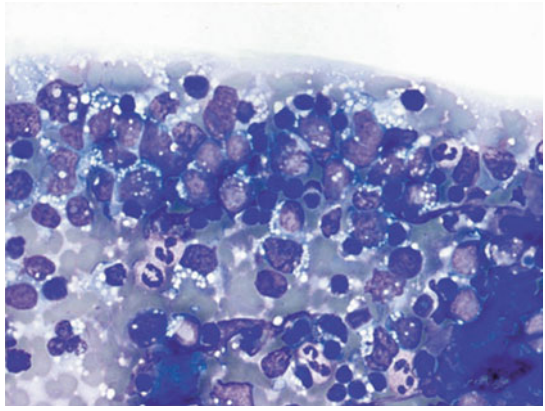

FIGURE 7.28 Burkitt's lymphoma. The smear shows a population of intermediate-size cells with multiple nucleoli and distinct minute cytoplasmic vacuoles (DiffQuik stain, high magnification) (From Pambuccian and Bardales (2011). Reprinted with permission)

peripheral blood and bone marrow involvement. Whereas the B-cell lineage predominates in lymphoblastic leukemia, only 10 % of LBLs have a B-cell phenotype. In general, LBLs are seen often in children and adolescents. The most frequent sites of involvement in B-LBL are the skin, soft tissue, bone, and lymph nodes. Mediastinal (thymic) involvement is often present in T-LBL and infrequent in B-LBL. Any extranodal site may be involved in T-LBL. Lymphadenopathy, hepatomegaly, and splenomegaly are frequent in B- and T-LBL.

The cytology shows cells of small or intermediate size. The small cells are uniform and have scant cytoplasm; round nuclei with occasional clefting and indentations; homogeneous, fine, and delicate chromatin; and multiple variably prominent nucleoli. When intermediate-sized cells predominate, the pattern shows more anisocytosis; moderate cytoplasm; fine and delicate chromatin; often irregular, clefted, and indented nuclear contours; and two to three small nucleoli. Mitotic figures are often numerous (Fig. 7.29).

Tumor cells are positive for the enzyme terminal deoxynucleotidyl transferase (TdT) in most cases of B- and T-LBL.

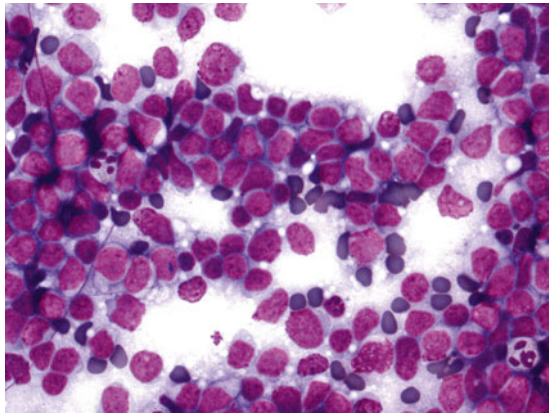

FIGURE 7.29 Lymphoblastic lymphoma. A monotonous population of intermediate-size lymphoid cells some with slight nuclear irregularities is seen (MGG stain, high magnification)

The lymphoblasts in B-LBL are almost always positive for the B-cell markers CD19, CD22, cytoplasmic CD79a, and PAX5. The lymphoblasts in T-LBL are positive for the T-cell markers CD7, CD99, CD34, and CD1a. Almost all cases of B-LBL have cytogenetic abnormalities. T-LBL almost always has T-cell receptor gene rearrangements, commonly of α and δ loci.

Adult T-Cell Leukemia/Lymphoma

The disease is caused by the human T-cell leukemia virus type I (HTLV-I) and is endemic in southwestern Japan, the Caribbean basin, and Central Africa. Most patients have generalized disease with lymph node and peripheral blood involvement. Generalized lymphadenopathy, skin rash, leukocytosis, eosinophilia, and hypercalcemia are common in acute ATLL. Generalized lymphadenopathy without peripheral blood involvement is seen in the lymphomatous variant of ATLL.

The cytology shows neoplastic lymphocytes of intermediate to large size with marked nuclear irregularities, coarse

chromatin, and distinct nucleoli. Giant cells with convoluted nuclei may be present.

The tumor cells express T-cell-associated antigens (CD2, CD3, and CD5) and lack CD7. The large cells may be CD30+, but are negative for ALK. The tumor cells frequently express CCR4 and FOXP3. Neoplastic cells have a clonal rearrangement of T-cell-receptor genes and monoclonal integration of HTLV-I.

Peripheral T-Cell Lymphoma

Peripheral T-cell lymphoma (PTCL) is rare and is especially common in African-American males in the sixth decade of life or older. Patients commonly have lymphadenopathy, extranodal (skin, GI tract, liver, spleen, bone marrow) involvement, and systemic symptoms. Pruritus, eosinophilia, and hemophagocytic syndrome may be present, but leukemia is uncommon.

The cytology shows small, intermediate, and large cells in various combinations resulting in a polymorphous pattern or may be monotonous when one cell pattern predominates. The small cell pattern is the least common. Cells exhibit clear cytoplasm, irregular nuclei, prominent nucleoli, and numerous mitoses. Clear cells and Reed–Sternberg-like cells may be seen. In addition, small lymphocytes, histiocytes, eosinophils, and plasma cells are present. Tight sarcoid-like granulomas can be seen.

The neoplastic cells express pan-T-cell and T-cell-associated antigens including CD2, CD3, CD5, CD7, CD43, and CD45RO. Most are CD4+ and express TCR αβ. Ki67 is usually high. T-cell-receptor genes are clonally rearranged in most cases.

Sézary Syndrome

Sézary syndrome is rare and occurs in adults, usually older than 60 years, and has a male predominance. It is an aggressive disease with an overall survival of 20 % at 5 years. Patients have erythroderma and generalized lymphadenopathy.

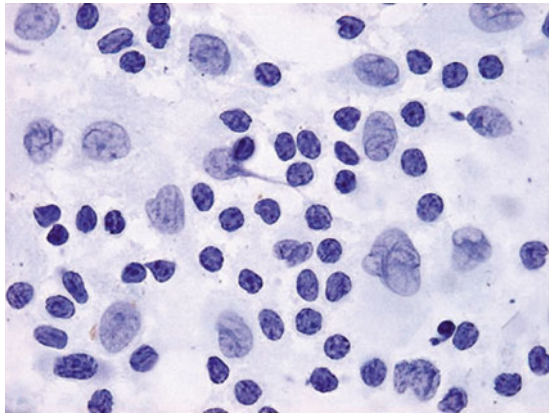

FIGURE 7.30 Sezary syndrome. Monotonous population of intermediate-size lymphocytes with prominent nuclear irregularities in a background of dermatopathic lymphadenopathy is seen (Papanicolaou stain, high magnification) (Courtesy Dr. Javier Saenz de Santamaria, Badajoz, Spain. From Pambuccian and Bardales (2011). Reprinted with permission)

Palmar and plantar hyperkeratosis and onychodystrophy may be present.

The neoplastic T cells are of small to intermediate size, have irregular "cerebriform" nuclei (Sézary cells), and are found in the skin, lymph nodes, and peripheral blood. The cells have moderate amounts of cytoplasm, and the nucleus may have a monocytoid appearance with one to three nucleoli. The smear background may show melanin-laden histiocytes as a manifestation of dermatopathic lymphadenopathy (Fig. 7.30).

Tumor cells are CD2+, CD3+, TCRβ+, CD5+, and often CD4+. They express cutaneous lymphocyte antigen (CLA) and the skin-homing receptor CCR4 and have a T-cell-receptor gene rearrangement.

Anaplastic Large Cell Lymphoma

Anaplastic large cell lymphoma (ALCL) is a mature T-cell lymphoma that accounts for approximately 20 % of all T-cell

lymphomas and occurs in young adults, but may occur in children. According to the presence or absence of ALK protein expression, it can be divided into the morphologically indistinguishable but clinically distinct ALK+ ALCL (50–80 % of cases) and ALK–ALCL. ALK+ ALCL involves both lymph nodes and extranodal sites (skin, musculoskeletal system, lungs, liver) of young, predominantly male patients, whereas ALK-ALCL tends to affect elderly patients. The response to treatment and the prognosis of patients with ALK+ ALCL are better than that for ALK– ALCL and other peripheral T-cell lymphomas.

ALCL has a number of morphologic variants or patterns, the *common* (or *classic*) (75 %), the *lymphohistiocytic* (10 %), and the *small cell* (5–10 %). The small cell variant is composed of neoplastic cells that are neither large nor anaplastic and may enter the differential diagnosis of small blue cell tumors and of lymphomas composed of intermediate-sized neoplastic cells.

Common to all morphologic variants of ALCL is the presence of "hallmark" cells, large or very large cells, with horseshoe-shaped or kidney-shaped nuclei, abundant clear or basophilic cytoplasm, and prominent perinuclear clear hofs, corresponding to the Golgi regions. Nucleoli are round or angular and prominent. The cytoplasm may show peripheral blebs and small vacuoles. A continuum of sizes of the abnormal cells can usually be seen. Other characteristic neoplastic cells include "half-doughnut cells," "doughnut cells," multinucleated giant "wreath cells," "embryo cells," "tennis racket" or "hand mirror" cells, and cells with polylobed nuclei and Reed–Sternberg-like cells. Frequent mitoses and apoptotic cells are present. Erythrophagocytosis or cell cannibalism, reactive lymphocytes, neutrophils, histiocytes, or eosinophils can occasionally be seen (Fig. 7.31).

Immunohistochemistry is useful in the differentiation of ALCL from Hodgkin lymphoma and metastatic malignancies (Table 7.5). The large, pleomorphic neoplastic cells of ALCL are positive for CD30 in a membranous and Golgi pattern. The vast majority of cases express one or more T-cell markers

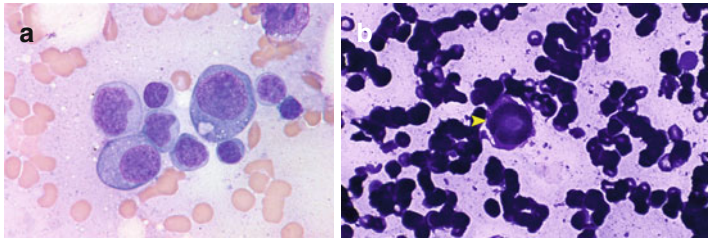

FIGURE 7.31 Anaplastic large cell lymphoma. Large pleomorphic cell population is characteristic of this lymphoma (**a**). "Doughnut" cells also are some of the pleomorphic cells seen (**b** *arrow head*) (DiffQuik stain, high magnification) (**a** From Pambuccian and Bardales (2011). Reprinted with permission)

(CD2, CD4, CD5), but CD3 is frequently lost. The neoplastic cells are consistently CD45 and EMA positive. The t(2;5) or t(1;2) translocation is present in 90 % of systemic cases.

Hodgkin Lymphoma (HL)

Hodgkin lymphoma accounts for 30 % of lymphomas, principally affects adolescents and young adults, and initially involves cervical and mediastinal lymph nodes. Lymph nodes are enlarged and usually non-tender, and patients are usually asymptomatic at diagnosis. The HL tends to spread to contiguous lymph node regions. Constitutional symptoms including fever, night sweats, and weight loss usually occur with widespread disease.

The REAL/WHO classification of HL includes:

1. Nodular lymphocyte-predominant HL (NLPHL) – 5 % of all HL cases
2. Classical Hodgkin lymphoma (cHL) – 95 % of all HL cases
   (a) Nodular sclerosis cHL – 65 to 70 % of all HL cases
   (b) Mixed-cellularity cHL – 20 % of all HL cases
   (c) Lymphocyte-rich cHL – 5 % of all HL cases
   (d) Lymphocyte-depleted cHL – 1 % of all HL cases

Table 7.5 Immunohistochemistry in Hodgkin lymphoma and its mimics

	CD15	CD30	CD45	CD3, CD5, CD7	CD20	PAX5	EMA
cLH	+	+	–	–	–80 %	+	–
NLPHL	–	–	+	–	+	+	+/–
TC/HRLBCL	–	–	+	–	+	+	–/+
ALCL	–	+	+	+/–	–	–	+
pTCL	–	–	+	+/–	–	–	–
PMBL	–	+ weak	+	–	+	+	–

Modified from Pambuccian and Bardales (2011), with permission
Abbreviations: *cLH* classical Hodgkin lymphoma, *NLPHL* nodular lymphocyte-predominant Hodgkin lymphoma, *TC/HRLBCL* T-cell/histiocyte-rich large B-cell lymphoma, *ALCL* anaplastic large-cell lymphoma, *pTCL* peripheral T-cell lymphoma, *PMBL* primary mediastinal B-cell lymphoma

The neoplastic cells in HL are B cells that have lost most of their B-cell markers. The L&H cells of NLPHL are also named LP or popcorn cells; the mononuclear Hodgkin and multinucleated Reed–Sternberg cells of cHL are collectively called HRS cells. By polymerase chain reaction, it has been demonstrated that HRS cells have immunoglobulin gene rearrangements with somatic mutations that indicate their clonal origin in the germinal center. Likewise, the LP cells of NLPHL have cell rearrangements and mutations similar to those of HRS. However, the B-cell differentiation program is downregulated in HRS cells and fully active in LP cells. Thus, neoplastic cells have lost most B-cell markers in cHL and are preserved in NLPHL. The neoplastic cells of cHL are variably positive for EBV; however, no EBV positivity is found in NLPHL.

Treatment with radiation and chemotherapy results in a >85 % cure rate.

FNA findings. Smears show a background of reactive polymorphous lymphoid cells with predominance of small mature lymphocytes. The cellularity tends to be relatively low, and neoplastic cells are found scattered in the background. The cellularity is the lowest due to fibrosis in nodular sclerosis HL, the most common form of HL. The background also shows variable numbers of eosinophils, plasma cells, and even epithelioid cells to the point that such a finding in a lymph node aspirate should trigger the diligent search for neoplastic cells of HL. A granulomatous response is also seen in HL. These findings may also be present in lymphadenopathies secondary to allergic reactions and parasitic infestations. Occasionally, the background shows numerous neutrophils and simulates bacterial lymphadenitis. Of note, the syncytial variant of nodular sclerosis HL, particularly when present in the mediastinal lymph nodes, must be distinguished from metastatic carcinoma and primary mediastinal large B-cell lymphoma. Large cell T- and B-cell lymphomas, metastatic malignancies, especially melanoma and carcinoma or viral-driven lymphadenitis, should be included in the differential diagnosis.

The FNA diagnosis requires finding the neoplastic cells. Classic Reed–Sternberg cells usually have a moderate amount of pale cytoplasm with two or more eccentrically placed large, complex, or lobulated nuclei exhibiting irregular borders, coarse chromatin, and prominent irregular inclusion-like nucleoli. The mononuclear variants of neoplastic cells show similar nuclear features. Immunoblasts, commonly mistaken for the mononuclear variant, are smaller and show basophilic cytoplasm, a round nucleus, and a prominent but smooth round nucleolus (Fig. 7.32).

Immunoprofile. Table 7.5 summarizes the markers that are useful in the differential diagnosis of HL.

Ultrasound Features of Lymph Nodes Involved by Lymphomas

Lymphomas commonly involve the levels I and V of the neck. Lymph nodes are usually round or oval, very hypoechoic reticulated/micronodular, and rarely necrotic and have sharp margins, and the hilum may be absent or present, usually with an exaggerated vascular pattern (Figs. 7.23c, d, 7.24c, d, 7.25b, c, 7.26b, c, 7.27b, c, and 7.32d, e).

Metastases

Lymph nodes are the most common sites of metastasis, and metastatic malignancies outnumber primary lymphoid malignancies in most lymph node locations. The topography of lymph node chains and their territories of lymphatic drainage are helpful clues for determining the primary site of malignancy and are covered early in this chapter. When possible, the original tumor should be reviewed for comparison of the cytomorphology. In the absence of a known primary malignancy, a metastatic deposit can be correctly classified only by the cytomorphology in many cases. However, poorly differentiated or undifferentiated malignancies, particularly of the

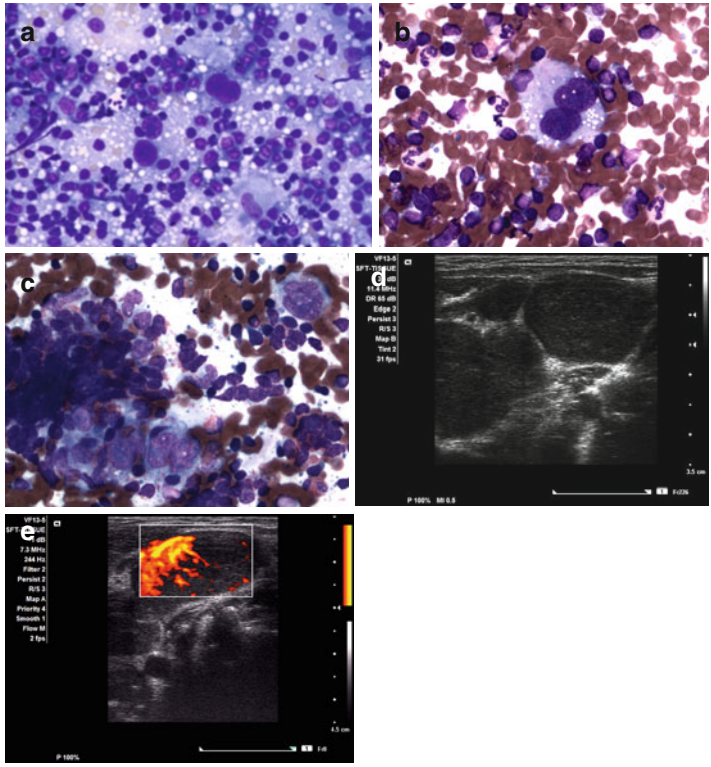

FIGURE 7.32 Hodgkin lymphoma. The smear shows a polymorphous population of lymphoid cells, rare eosinophils, and plasma cells. Present in this background are Reed-Sternberg cells, mononuclear variants, and multinucleated cells (**a**–**c**). Large, matted, and hypoechoic lymph nodes with well-defined margins are seen (**d**). The vascular pattern is exaggerated and chaotic (**e**) (**a**–**c** DiffQuik stain, high magnification)

small cell type (blue cell tumors), may be difficult to distinguish from each other and from lymphomas. Because distinction is important for management purposes, the use of immunostains is helpful in the diagnosis of carcinoma, lymphoma, melanoma, or other malignancies and can be done preferably in cell block preparations (Table 7.6). It must be

Table 7.6 Panel of immunostains helpful in classifying lymph node metastasis

Marker	Malignancy
CD45RB (leukocyte common antigen)	Hematolymphoid
Cytokeratin cocktail (AE1/AE3 and 8/18)	Epithelial
EMA (epithelial membrane antigen)	Epithelial
S100 protein	Melanocytic
Vimentin	Mesenchymal and others
Specific markers	Organ-specific malignancy
Thyroglobulin	Thyroid
Calcitonin	Thyroid (medullary carcinoma)
HepPar1	Liver
Renal cell carcinoma antigen	Kidney
Uroplakin	Urothelium
TTF1 (thyroid transcription factor 1)	Thyroid, lung
CDX2	GI tract, neoplasms with intestinal differentiation
Cytokeratins 7 and 20	Lung, GI tract, Urothelium

noted that no antibody is organ specific and cross-reactivity with other tissues is being reported increasingly. Material from needle rinses may also be used for measurement of thyroglobulin and thyroglobulin antibody levels when differentiated thyroid carcinoma is suspected. Likewise, calcitonin levels in needle rinses are helpful when metastasis from medullary thyroid carcinoma is suspected.

Table 7.7 Lymph node metastasis by cell patterns

Monotonous intermediate cell	Neuroendocrine tumors: carcinoid, atypical carcinoid, small-cell carcinoma, Merkel cell carcinoma
	Basal cell carcinoma
	Melanoma
	Small blue cell tumors: metastatic neuroblastoma, Ewing sarcoma/peripheral neuroectodermal tumor, rhabdomyosarcoma
	Nasopharyngeal carcinoma
Monotonous large cell	Carcinoma
	Melanoma
	Sarcoma
	Seminoma
Pleomorphic cell	Carcinoma
	Melanoma
	Sarcoma

The Table 7.7 summarizes metastatic malignancies by patterns, monotonous and pleomorphic, as an attempt to ease and narrow the differential diagnosis in lymph node aspirates.

Common Metastatic Malignancies in Adults

Metastatic Squamous Cell Carcinoma

This is the most common metastatic malignancy to the head and neck and frequently follows or presents with a primary tumor in the head and neck.

FNA findings. Well-differentiated squamous cell carcinoma shows high cellularity, with keratinized cells exhibiting

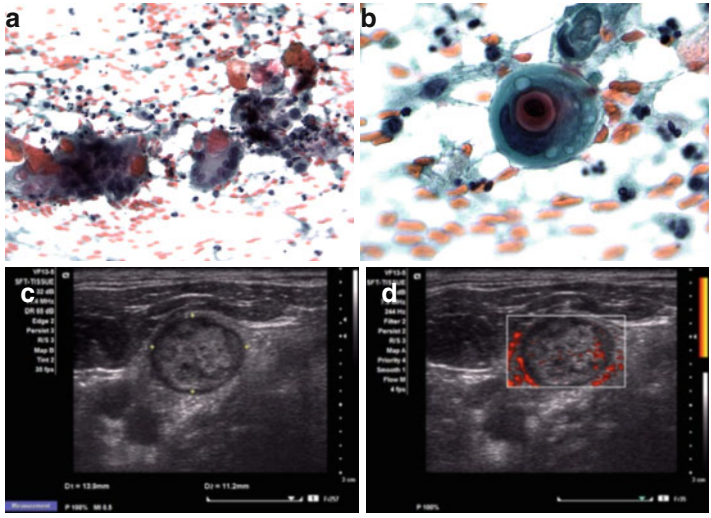

FIGURE 7.33 Metastatic squamous carcinoma, well-differentiated. The smears show keratinization with anucleated squamous cells, foreign body type reaction with giant cells "engulfing" keratin flakes (**a**), and keratinized malignant cells showing cytophagocytosis with clearly malignant nuclear features (**b**). The US exam shows slightly hyperechoic lymph node with round shape, slightly lobulated borders, and heterogeneous echotexture (**c**). Minimal peripheral and central vascularity is seen by Doppler examination (**d**) (**a**, **b** MGG stain, high magnification)

pyknotic, minimally irregular, and slightly enlarged nuclei, with no mitotic activity (Fig. 7.33). The diagnosis is usually straightforward in these cases. Cystic squamous cell carcinoma shows scant cellularity, anucleated squamous cells, and scattered intermediate squamous cells with hyperchromatic and minimally irregular nuclei in a necrotic and variably inflamed background (Fig. 7.34). Necrosis and granulomatous foreign body-type reaction to the keratin may be seen.

The differential diagnosis includes cystic squamous cell carcinomas versus benign inflamed branchial cleft cysts and abscess. Malignant cells with anaplastic nuclei are important for diagnosis. Poorly differentiated squamous carcinomas may be difficult to differentiate from other high-grade neo-

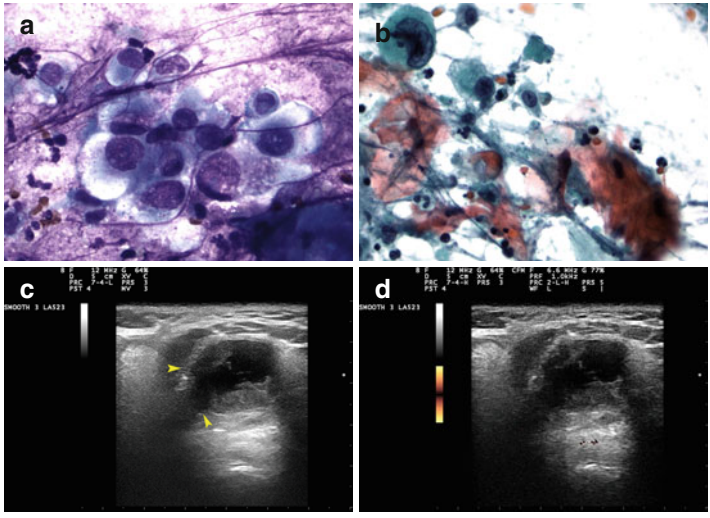

FIGURE 7.34 Metastatic squamous carcinoma with cystic degeneration. The smears clearly malignant squamous cells with focal keratinization and a background of tissue damage (**a**, **b**). The US images show an irregular lymph node with cystic necrosis, ill-defined margins with focal extracapsular invasion (*arrowheads*), and no vascularity by Doppler exam (**c**, **d**) (**a** MGG stain high magnification; **b** Papanicolaou stain, high magnification)

plasms. Cell block material is useful to perform special stains such as p16, which is a subrogate for HPV-driven squamous carcinomas of the head and neck (Fig. 7.35).

Metastatic Nasopharyngeal Carcinoma

This is particularly prevalent among the Asian ethnic group, is associated with Epstein–Barr virus infection, and has a bimodal age presentation with one peak between 15 and 25 years and the other between 60 and 70 years. Involvement of level II and III neck lymph nodes are frequent and is the first evidence of the tumor in 90 % of cases. Histologic types include keratinizing, nonkeratinizing, and undifferentiated.

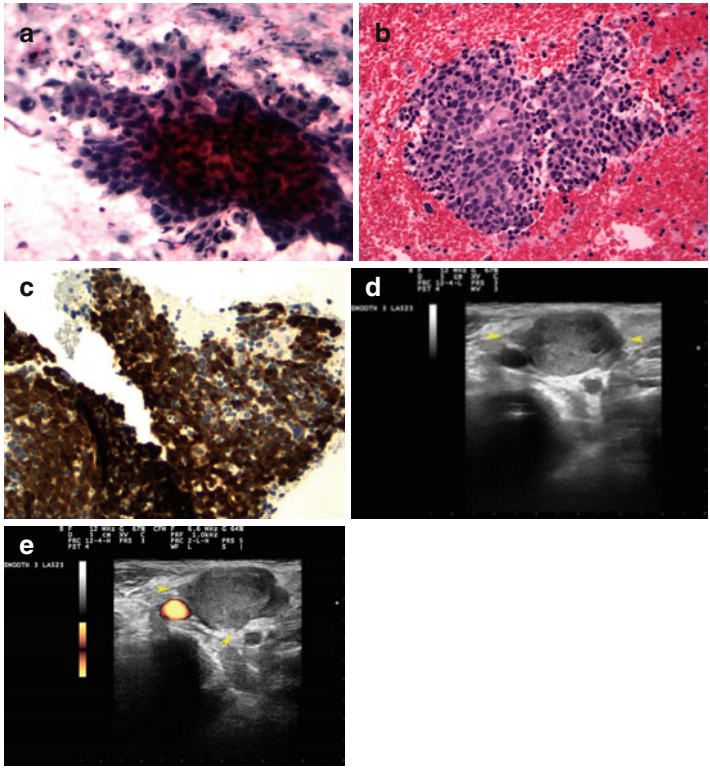

FIGURE 7.35 Metastatic squamous carcinoma, poorly differentiated. The smear shows complex aggregates with spiculated ends and no evidence of keratinization (**a**). The cell block shows scattered aggregates of malignant squamous cells (**b**). Immunostain or p16 is positive (**c**). The US exam shows a hypoechoic lymph node with fuzzy margins, extracapsular invasion (*arrowheads*), and no vascularization by Doppler exam (**d**, **e**) (**a** MGG stain high magnification; **b** H-E stain, medium magnification; **c** immunostain for p16, medium magnification)

FNA findings. The smears are cellular. The nonkeratinizing type shows numerous tridimensional aggregates and single round or elongated cells with scant cytoplasm, large nuclei, and prominent nucleoli. The undifferentiated type shows single and aggregated basaloid cells and small lymphocytes

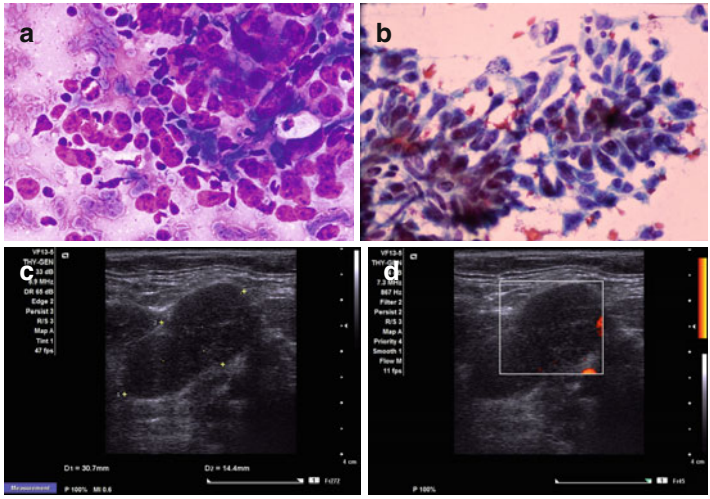

FIGURE 7.36 Metastatic nasopharyngeal carcinoma. Non-keratinizing poorly-differentiated carcinoma with spindle cell features admixed with lymphocytes (**a**, **b**). US features are not specific and include hypoechoic coalescent lymph nodes with sharp and irregular margins, and minimal vascularity by Doppler exam (**c**, **d**) (**a** DiffQuik stain high magnification; **b** Papanicolaou stain high magnification)

within the cell aggregates and in the background. Mitosis and necrosis are common (Fig. 7.36). Tumors with similar histomorphology can arise in the palatine and lingual tonsils, thymus, and larynx.

The differential diagnosis includes large cell lymphoma, carcinomas, and germ cell tumors. Immunocytochemistry for keratin, leukocyte common antigen, alpha-fetoprotein, and β-chorionic gonadotropin is helpful. The neoplastic cells are positive for EBV-associated markers such as EBV-latent membrane protein type 1 and in situ hybridization for EBV small-encoded RNA (EBER).

Metastatic Papillary Thyroid Carcinoma

US is useful in the preoperative evaluation and postsurgical follow-up of patients with well-differentiated thyroid

carcinoma, in particular for evaluation of lymphadenopathy in the central and lateral neck compartments. Also, in cases of elevated serum thyroglobulin in post-thyroidectomy patients with thyroid carcinoma, US is used for evaluation of neck lymph nodes and thyroid bed nodules followed by USG-FNA, looking for thyroid carcinoma. Needle rinses looking for thyroglobulin and thyroglobulin antibody levels complement the cytologic evaluation in these cases. Secondary cystic changes are common in both primary and metastatic papillary carcinomas.

FNA findings. Solid lymph node metastases from papillary carcinoma show diagnostic features sufficient for a diagnosis. Aspirates from cystic metastasis show small sheets of monolayered epithelium in a hemorrhagic cystic background; cytoplasmic septate vacuoles and macrophages are often seen, and other cytologic characteristics may be inconspicuous (Fig. 7.37).

The differential diagnosis includes medullary carcinoma that may exhibit a pseudo-papillary pattern, as well as intranuclear inclusions and nuclear grooves which may be erroneously interpreted as features of papillary carcinoma. Furthermore, amyloid may be mistaken for colloid. Measurements of thyroglobulin and thyroglobulin antibody levels and calcitonin levels in needle rinses are helpful.

Metastatic Breast Carcinoma

The single most important predictor of clinical outcome is the sentinel lymph node, which is the ipsilateral axillary lymph node closest to the breast cancer tumor and likely to be the first to harbor a metastatic deposit. Touch preparation cytology evaluation of a sentinel lymph node is the preferred technique. Alternatively, sampling by means of FNA can be done pre- or intraoperatively at the time of lumpectomy. If the sentinel lymph node is positive, the patient undergoes axillary lymph node dissection. Skip metastasis involving axillary lymph nodes other than the sentinel lymph node occurs in 5 % of cases (Fig. 7.38).

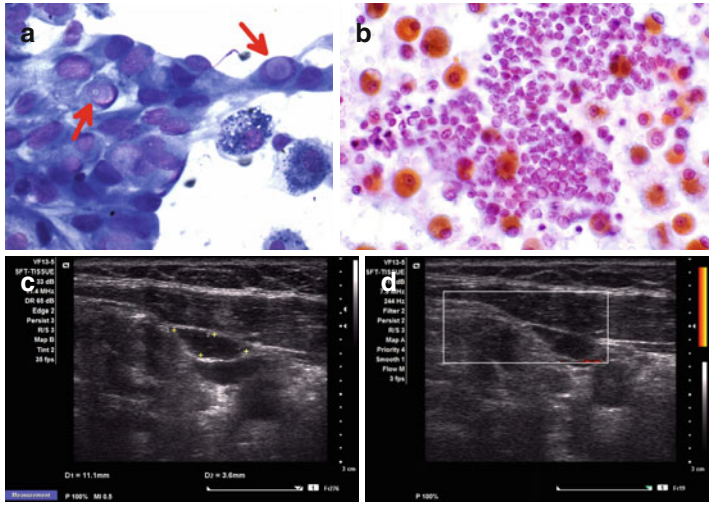

FIGURE 7.37 Metastatic papillary thyroid carcinoma with cystic degeneration. Metaplastic cells with intranuclear cytoplasmic invaginations (*arrows*), numerous macrophages, and rare sheets of cells with pale chromatin, nuclear grooves, and intranuclear cytoplasmic invaginations (**a**, **b**). US exam shows an oddly-shaped angulated lymph node with marked hypoechogenicity and no vascularity by Doppler exam (**c**, **d**) (**a** MGG stain, high magnification; **b** Papanicolaou stain, high magnification)

Metastatic Melanoma

If the thickness of a cutaneous melanoma exceeds 0.76 mm, the risk of lymph node metastasis increases in parallel to the tumor thickness. The regional (sentinel) lymph nodes are involved before the melanoma spreads more distally. However, approximately 4 % of melanomas show axillary, cervical, and inguinal lymph node metastases in the absence of a known primary site (spontaneous regression).

FNA findings. The diagnosis is facilitated by the clinical history and the demonstration of melanin pigment in tumor cells or histiocytes (melanophages), but melanin may be entirely absent, and a history of melanoma may not be

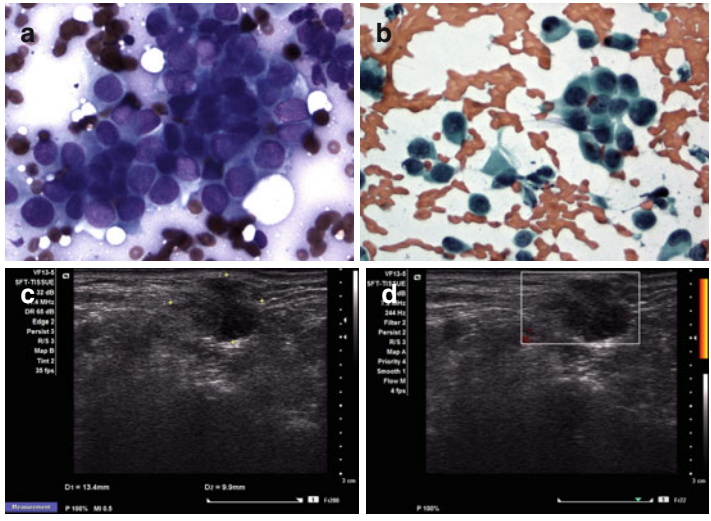

FIGURE 7.38 Metastatic breast carcinoma. Neck level I LN. Aggregates of malignant cells with thin cytoplasm, ill-defined cytoplasmic borders, round nucleus and prominent nucleoli are seen (**a**, **b**). Comparison with the cytomorphology of the primary tumor is necessary for an accurate diagnosis. The US exam shows a lymph node with ill-defined and spiculated borders, and poor vascularization by Doppler exam (**c**, **d**) (**a** MGG stain high magnification; **b** Papanicolaou stain, high magnification)

available. Aspirates are usually cellular, containing round or oval, spindle-shaped, and pleomorphic cells in various proportions. This pleomorphic pattern is characteristic of metastatic melanoma; however, anaplastic nuclei, prominent nucleoli, intranuclear cytoplasmic invaginations, and melanin pigment may not be present in all cell types (Fig. 7.39). Melanoma may mimic the cytomorphology of any neoplasm, including large cell lymphoma, although metastatic melanoma cells are usually larger and more pleomorphic. The rare amelanotic melanoma with lymphocyte-like or plasmacytoid-like cytomorphology may also resemble lymphoma or plasmacytoma; however, the smear background lacks lymphoglandular

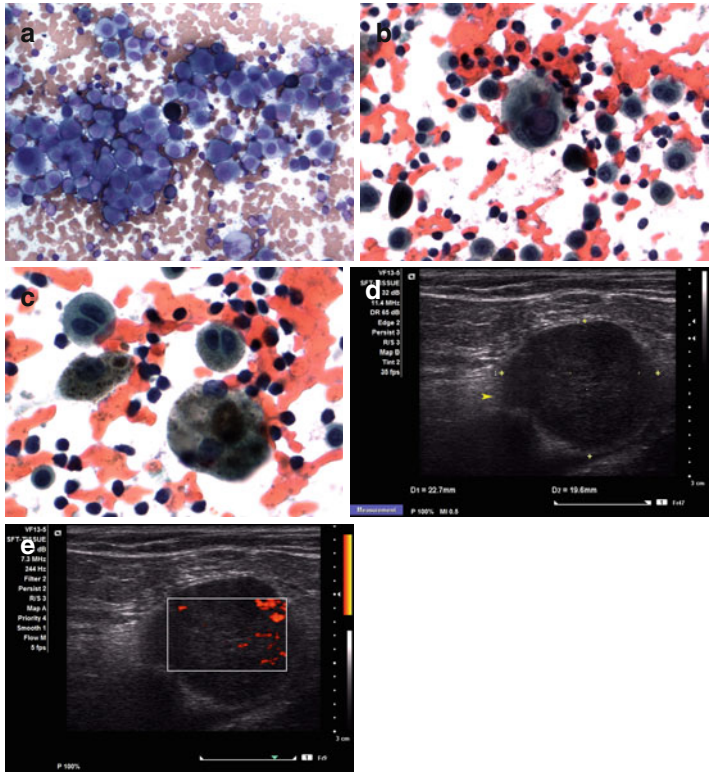

FIGURE 7.39 Metastatic pigmented melanoma. Markedly pleomorphic cells with cytoplasmic brown melanin pigment, prominent nucleoli, and rare large cells with intranuclear cytoplasmic invaginations (**a**–**c**). US evaluation shows large round lymph nodes, focal fuzzy margins, extracapsular invasion (*arrowhead*), and moderate but abnormal vascularity (**d**, **e**) (**a** MGG stain, high magnification; **b**, **c** Papanicolaou stain, high magnification)

bodies. The spindle cell type must be distinguished from spindle cell neoplasms (Fig. 7.40). In equivocal cases, stains for S-100 protein, melan-A, and HMB-45 are helpful. Of note, the S-100 protein stain is also positive in the interdigitating reticulum cells of the lymph node.

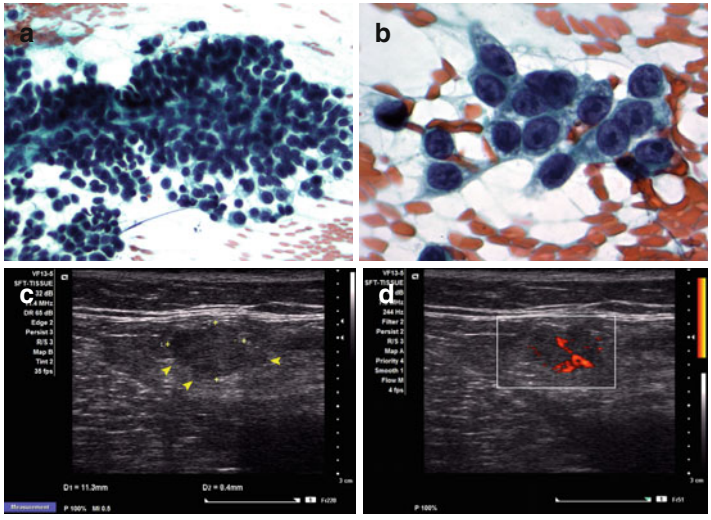

FIGURE 7.40 Metastatic amelanotic melanoma, spindle cell type. Elongated cells with pleomorphic nuclei, prominent nucleoli, and lack of melanin pigment (**a**, **b**). US show slightly hypoechoic lymph nodes with ill-defined margins, areas of extranodal invasion (*arrowheads*), and abnormal vascularity on Doppler examination (**c**, **d**) (**a**, **b** Papanicolaou stain, moderate and high magnification)

Metastatic Merkel Cell Carcinoma

Merkel cell carcinoma is a rare primary neuroendocrine tumor of the skin which occurs particularly in the head and upper extremities of elderly individuals. This tumor is aggressive and may produce multiple distant metastases, including the lymph nodes.

FNA findings. Aspirates are cellular, composed of intermediate-sized cells with a variable degree of cohesiveness. Cells have uniform round or oval nuclei with fine chromatin and small nucleoli. The cytoplasm is scant and fragile. Cell molding is not a feature. Scattered mitoses and apoptotic nuclei are present, and the background lacks lymphoglandular bodies. The most characteristic feature is the presence of

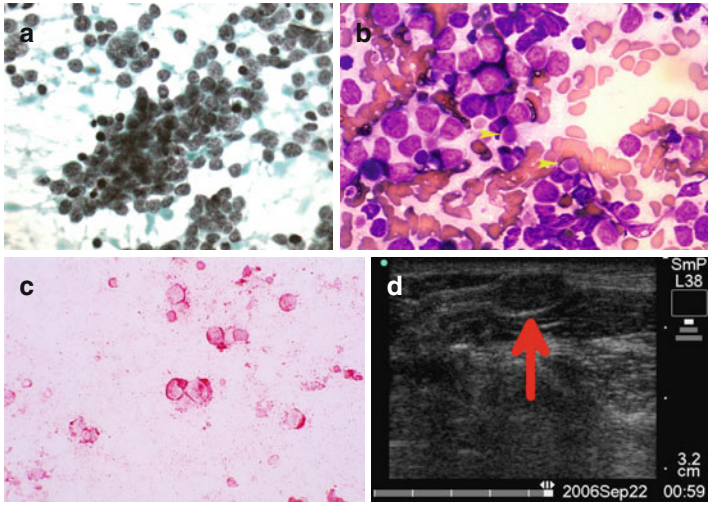

FIGURE 7.41 Metastatic Merkel cell carcinoma. Complex aggregates of intermediate size cells with scan cytoplasm, granular coarse chromatin, and paranuclear dense cytoplasmic round aggregates of intermediate filaments or "buttons" (**a**, **b** *arrowheads*) highlighted by the keratin immunocytochemical stain (**c**). The US features are not specific and include oval shape hypoechoic lymph node with well-defined margins (**d** *arrow*) (**a** Papanicolaou stain high magnification; **b** DiffQuik stain high magnification; **c** immunocytochemical stain for keratin, high magnification)

an inconspicuous small spherical perinuclear cytoplasmic aggregate ("button") of intermediate filaments (keratin). The cells show a positive immunostain for low-molecular-weight keratin, neurofilaments, and NSE. The keratin stain highlights the cytoplasmic condensation (Fig. 7.41).

The differential diagnosis includes small cell carcinoma of salivary gland or lung origin, lymphoma, and solid adenoid cystic carcinoma. The presence of "buttons" and small perinuclear clear zones is important for diagnosing Merkel cell carcinoma. In some cases, the use of special stains is necessary. The demonstration of the Merkel cell polyomavirus is diagnostic.

Metastatic Mesenchymal Malignancies

Lymph node metastases from sarcomas are unusual; however, when they occur, they may mimic carcinomas or lymphomas of Hodgkin or non-Hodgkin type, including anaplastic large cell lymphoma (ALCL) due to the presence of pleomorphic single cells or loose clusters in a lymphoid background. Of the metastatic mesenchymal neoplasms, the most likely to be confused with such entities are metastatic high-grade undifferentiated sarcomas (malignant fibrous histiocytomas), metastatic rhabdomyosarcomas, and metastatic neuroblastomas. Metastatic neuroblastoma may show a spectrum of neuroblastic to ganglion cell differentiation, with large, frequently multinucleated ganglion-like cells which may mimic Hodgkin/Reed–Sternberg cells or ALCL cells. The identification of neutrophil-like material in the background is diagnostically useful. The correct diagnosis is made by clinical correlation and immunostains (desmin and myogenin in rhabdomyosarcoma and NSE in neuroblastoma).

The Virchow's Lymph Node

The supraclavicular lymph nodes are the most likely site to harbor cancer. Left supraclavicular lymphadenopathy is usually an ominous sign of disseminated disease from a primary site below the diaphragm, including but not restricted to the stomach, prostate, ovary, colon, biliary tract, pancreas, and uterus (Fig. 7.42). It may be the first evidence of disease in patients with prostatic adenocarcinoma.

Ultrasound Features of Lymph Nodes Involved by Metastases

Lymph nodes affected by metastases are usually in the territory of lymphatic drainage of the primary tumor, unless in a widely metastatic process. In squamous cell carcinoma, the metastatic lymph node may be as small as 0.5 cm. Lymph nodes often have the following characteristics: round (AP/T

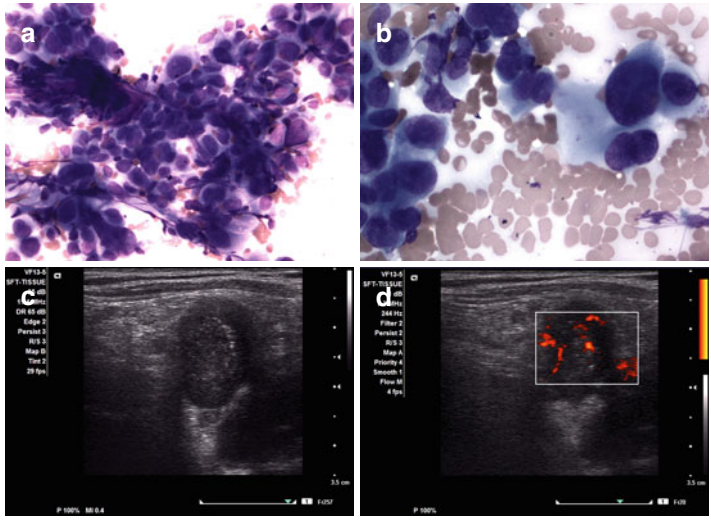

FIGURE 7.42 Virchow's node. Metastatic anaplastic-type carcinoma showing marked cell pleomorphism (**a**, **b**). The US evaluation shows a taller than wide hypoechoic lymph node with microcalcifications, fuzzy margins (**c**), and abnormal vascularity by Doppler examination (**d**) (**a**, **b** MGG stain, high magnification)

axis >0.5 in the transverse view), usually hypoechoic, absent hilum, eccentric cortical hypertrophy, partial or total cystic necrosis, sharp margins, and abnormal peripheral vascularization. The lymph node may be hyperechoic with microcalcifications in metastatic papillary medullary, and anaplastic thyroid carcinoma and ovarian serous papillary carcinoma. The lymph node margins are ill defined and spiculated when there is lymph node extracapsular spread.

Suggested Reading

Cook JR. Nodal and leukemic small B-cell neoplasms. Mod Pathol. 2013;26 Suppl 1:S15–28.

Ioachim HL, Medeiros LJ. Ioachim's lymph node pathology. Philadelphia: Lippincott Wlliams and Wilkins; 2009.

Pambuccian SE, Bardales RH. Lymph node cytopathology. Philadelphia: Springer; 2011.

Rhys R. Cervical lymph nodes. In: Allan PL, Baxter GM, Weston MJ, editors. Clinical ultrasound, vol. 2. London: Churchill Livingstone Elsevier; 2011. p. 920–37.

Said JW. Aggressive B-cell lymphomas: how many categories do we need? Mod Pathol. 2013;26 Suppl 1:S42–56.

Skoog L, Tani E. FNA cytology in the diagnosis of lymphoma. Basel: Karger; 2009.

Swerdlow SH, Campo E, et al. WHO classification of tumors of haematopoietic and lymphoid tissues. Lyon: IARC WHO; 2008.

Twist CJ, Link MP. Assessment of lymphadenopathy in children. Pediatr Clin North Am. 2002;49(5):1009–25.

Weiss LM, O'Malley D. Benign lymphadenopathies. Mod Pathol. 2013;26 Suppl 1:S88–96.

Chapter 8
The Breast

Ricardo H. Bardales and Eugenio Leonardo

Background and General Concepts

Breast imaging has become the main tool in breast cancer screening and diagnosis and has a major impact on breast cancer staging. Interventional radiologists and cytopathologists may obtain adequate tissue samples for pathologic evaluation of palpable and non-palpable but ultrasound (US)-visible lesions. However, the cytopathologist is more skilled in obtaining FNA cytology samples under US guidance (USG-FNA), a minimally invasive and cost-effective technique that avoids a more costly core biopsy for a potentially benign condition. Microcalcifications without a palpable or US-visible lesion are sampled under stereotactic guidance.

It is our experience that FNA sampling by capillarity without aspiration (Zajdela technique) with the use of a 25-gauge

R.H. Bardales, MD, MIAC, ECNU (✉)
Department of Pathology and Cytopathology,
Outpatient Pathology Associates,
7750 College Town Drive, Sacramento,
CA 95826, USA
e-mail: rhbardales@aol.com

E. Leonardo, MD, PhD
Pathology Department,
University Hospital of Trieste,
Strada di Fiume 447, Trieste 34100, Italy
e-mail: eugenio.leonardo@tiscali.it

R.H. Bardales (ed.), *The Invasive Cytopathologist*, Essentials in Cytopathology 16, DOI 10.1007/978-1-4939-0730-4_8,

needle may yield less cellular samples, but provides sufficient material for diagnosis of most breast lesions. It has been suggested that adding aspiration lowers the yield of nondiagnostic specimens when benign breast lesions are studied. This is in part due to the fibrofatty tissue composition of the normal breast tissue that yields sparsely cellular samples. For smaller or non-palpable lesions, USG-FNA samples are adequate and diagnostic.

In experienced hands, FNA of breast lesions can be highly accurate, with sensitivity between 80 and 100 % and specificity of 99 % when radiologic evaluation is provided and clinical evaluation and FNA are performed by the cytopathologist who also interprets the FNA. The so-called triple test (clinical, radiology, and FNA) results must be congruent for guiding an appropriate therapeutic management. If the cytopathologist did not perform the FNA, he or she must know the clinicoradiologic findings before the FNA interpretation is given. If one of the three is discrepant, an open biopsy or a frozen section may be required prior to definitive surgery.

Immediate interpretation for evaluation of sample adequacy and often providing a preliminary diagnosis are important and will prompt the operator to obtain material to perform additional studies, i.e., receptor studies, cultures, and flow cytometry. As mentioned in the technical section of this book, in our practice the cytopathologist triages the material on site and, if necessary, obtains core biopsies (CBxs) under ultrasound (US) guidance. Alternatively, a cell block may be obtained for performing hormone receptor immunohistochemistry or other ancillary tests, including molecular studies.

A specimen is considered adequate when at least six clusters or sheets of at least 15 epithelial cells each are present. Specimen adequacy is influenced by the clinical impression of the operator and by radiologic findings. An adipose tissue mammary prominence or lipoma does not have epithelial elements and should not be considered a nondiagnostic specimen.

FNA cytology cannot distinguish between in situ and invasive carcinoma and cannot further define all “atypias.” For most benign conditions, cytology cannot give a specific diagnosis. However, when FNA diagnoses of “malignancy,”

"atypia," or "no malignancy" are reached, CBxs, open biopsy, or lumpectomy will follow in the first two instances and a conservative approach in the last.

CBx and FNA are complementary tests for evaluating palpable and non-palpable US-visible breast masses and can modify decisions before surgery, may affect surgical outcome, or may avoid unnecessary surgery in benign conditions.

Complications of breast FNA are rare. Local pain and hematoma are the most common, and the latter can be minimized by applying firm pressure to the area of the FNA. Pneumothorax is a very rare complication. Needle track seeding of malignancy has been reported with large core needle biopsies, but is exceedingly rare with FNA. Histologic changes and epithelial displacement have been reported post FNA. The latter may be seen in breast carcinoma in situ and simulates invasive malignancy.

The FNA Report

The FNA diagnostic categories should include the following: "nondiagnostic," "negative for malignancy," "atypia," "suspicious for malignancy," and "positive for malignancy." The type of malignancy must be stated when a suspicious or malignant diagnosis is given. The report also includes a brief clinical history and physical examination, microscopic description, and a note or assessment that correlates all findings. The note section is also used to address physician notification in case of a malignant diagnosis or other clinically relevant discussions. Although optional, our report includes photomicrographs and ultrasound images of the mass.

The Normal Breast

The normal female breast is a modified sweat gland showing ducts, ductules, and acini surrounded by stromal elements, mainly adipose tissue (Fig. 8.1). Aspiration cytology smears of a nonlactating breast show fibroadipose tissue stroma and

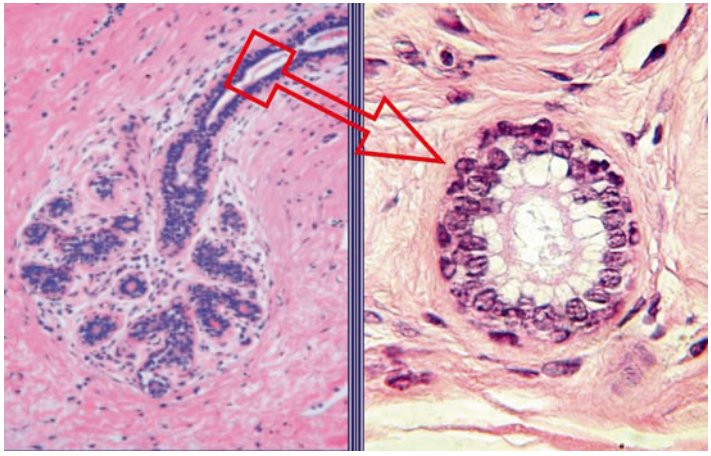

FIGURE 8.1 Normal breast histology. Tubulo-lobular unit and cross section of the duct showing epithelial and myoepithelial cell layers (H&E stain, medium and high magnification)

few ductal and acinar elements. The ductal epithelial cells are arranged cohesively in monolayers with honeycomb architecture and have a cuboidal or columnar shape with oval nuclei, finely dispersed chromatin, and inconspicuous nucleoli (Fig. 8.2). The myoepithelial cells have indiscernible cytoplasm and appear as small dark, oval nuclei both admixed with the ductal cells (but in a different plane of focus) and in the smear background. Acinar cells are arranged in small aggregates and show a cuboidal shape and slightly granular cytoplasm; they are rarely seen in aspirates from normal breast (Fig. 8.3).

Immunohistochemistry

The wall of the terminal ducts and acini consists of secreting cells, cylindrical or cubic, resting on a *basal lamina* that can be highlighted by the use of antibodies for vimentin, type IV collagen, and laminin. *Acinar cells* are usually positive for low-molecular-weight cytokeratins (CK7, CK8, CK18, and CK19).

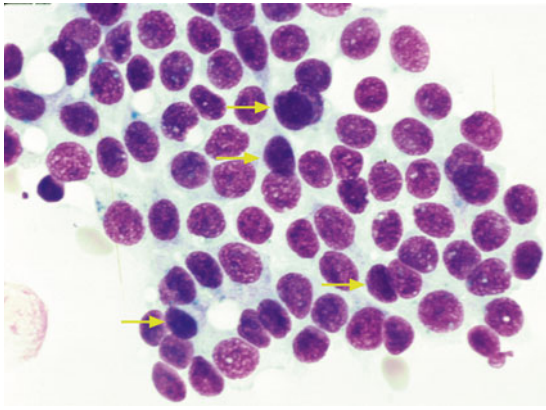

FIGURE 8.2 Cytology benign ductal cells. Sheet of benign ductal epithelial cells and myoepithelial cell nuclei seen as small overlapping darker nuclei (*arrows*) (Diff-Quik stain, high magnification)

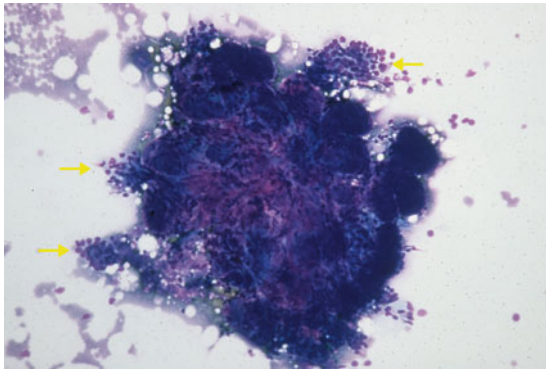

FIGURE 8.3 Cytology benign breast lobule. Tightly packed lobular cells arranged as small nodular aggregates surrounded by stromal elements. Note a small sheet of terminal ductal epithelial cells in the periphery of the lobule (*arrows*) (Diff-Quik stain, medium magnification)

Myoepithelial cells in the interlobular and terminal ducts intensely express CK5, CK14, and CK17, and myoepithelial cells in the alveoli also show positivity for vimentin, α-SMA,

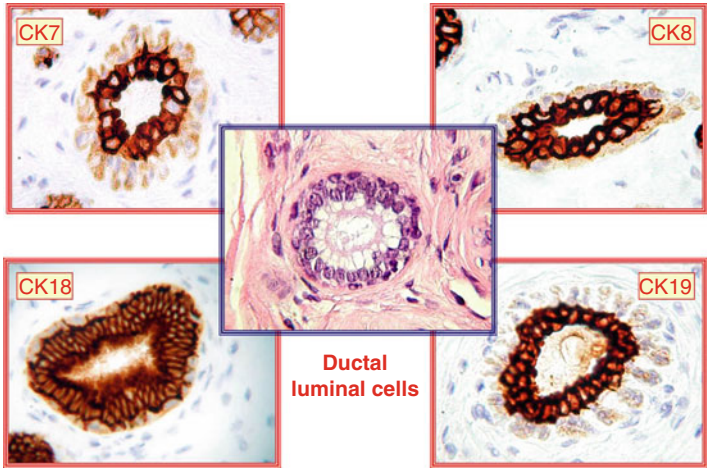

FIGURE 8.4 Immunohistochemistry of normal ductal luminal cells (immunoperoxidase stain, high magnification)

smooth muscle myosin heavy chain, and bone calponin. Myoepithelial cells are also positive for p63, maspin, and CD10. The terminal ducts have a mosaic of reactivity for cytokeratins, being positive for low-molecular-weight cytokeratins (except CK20) or CK5, CK14, and CK17. Some ductal cells are also positive with maspin and CD10. Cells positive for steroid receptors (ER and PR) are confined to the ducts and lobules. The lobule positive cells occupy a luminal position, or they are arranged in an intermediate zone between epithelial luminal cells and basal elements. In interlobular ducts, the positive cells are distributed predominantly in the basal level (Fig. 8.4, 8.5, and 8.6).

Ultrasound of the Normal Breast

Breast US is not a screening test; however, it can be used as an adjunct to mammography in palpable or not palpable breast masses. Breast US can also be used as an adjunct to

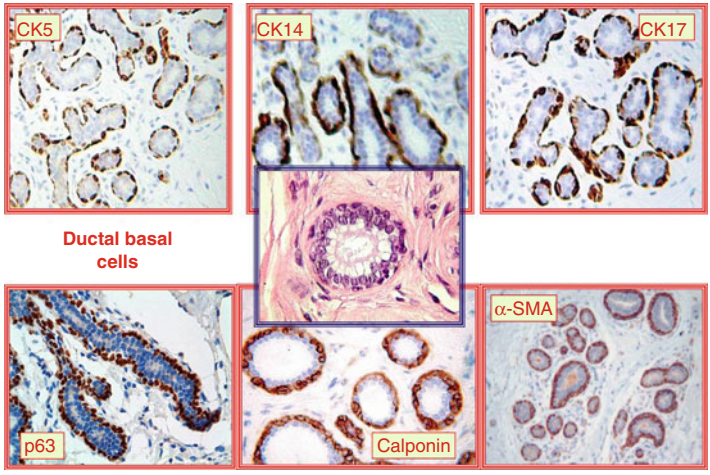

FIGURE 8.5 Immunohistochemistry of normal ductal basal cells (immunoperoxidase stain, high magnification)

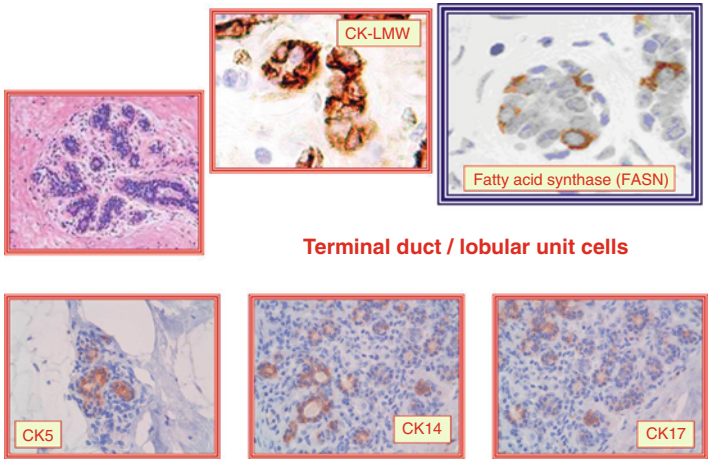

FIGURE 8.6 Immunohistochemistry of the normal tubulo-lobular unit (immunoperoxidase stain, high magnification)

mammogram in patients with dense breasts or breast cancer risk factors. In patients under the age of 35 years, US is the main tool for evaluating breast lesions. Of note, approximately 15 % of US-visible lesions are not detected on mammography, particularly in young women with dense breasts or women with lobular carcinoma; on the contrary, US detects only few additional cancers in women with large breasts, increasing the screening cost and slightly lowering the specificity. In women with a history of familial breast cancer, the preferred screening modality is MRI with a 91 % detection rate in contrast to mammography (33 %) and US (40 %).

Fat in the breast is hypoechoic compared to glandular tissue, which is relatively hyperechoic. Thus, normal glandular breast tissue is isoechoic or slightly hyperechoic. A dense fibroglandular tissue often shows round, oval, or elongated areas of hypoechogenicity in a more echogenic background. Breast tissues that can be distinguished by US include skin, fat, fibrous tissue stroma, Cooper's ligaments, fibroglandular tissue, and mammary ducts. The skin is 1–2 mm thick and has a hypoechoic band surrounded by a superficial and deep dermal echogenic lines. Bundles of fatty tissue are seen demarcated by echogenic lines coursing through tissue (Cooper's ligaments) (Fig. 8.7). The nipple can simulate a hypoechoic subareaolar mass by US (Fig. 8.8); angling the transducer around the nipple helps to distinguish this artifactual shadowing also called hypoechoic nipple shadow. Ribs appear as oval hypoechoic masses and pleura as an echogenic line immediately below the rib. Pectoral muscle appears hypoechoic with parallel echogenic striations.

Ultrasound of Breast Masses

US features are not entirely specific or sensitive for predicting benign or malignant breast lesions. US features of benign conditions such as inflammation, fat necrosis, or radial scar can mimic a malignant lesion.

Benign solid lesions show hypoechogenicity compared with fat and have an oval shape, well-circumscribed lobulated margins (macrolobulation), homogeneous internal echo pattern,

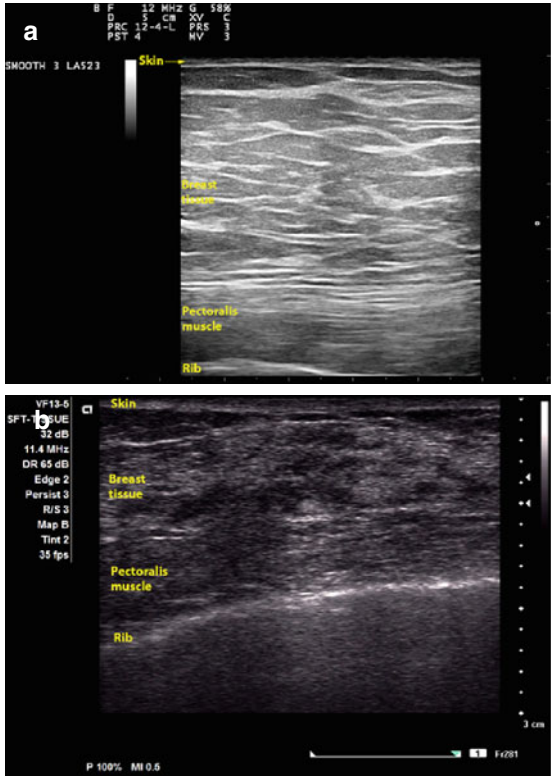

FIGURE 8.7 Ultrasound features of normal breast in a young woman (**a**) and in a 65-year-old woman (**b**)

posterior acoustic enhancement, parallel orientation (long axis of lesion parallels skin), compressibility, gentle bi- or trilobulation, and a thin echogenic pseudocapsule. For example, fibroadenomas are usually oval, well-circumscribed, smooth, and hypoechoic. These tumors have pushing borders and are oriented in a horizontal fashion and not vertically. They show posterior acoustic enhancement (Fig. 8.9). Intramammary lymph nodes are found more frequently in the upper outer quadrant of the breast, but they may be found in any quadrant.

However, not all well-circumscribed lesions are benign. Most circumscribed malignancies represent specific breast

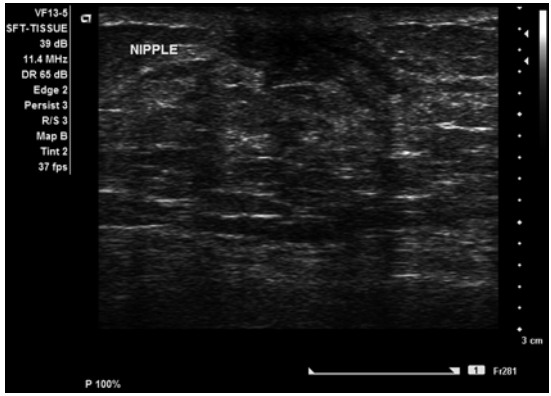

FIGURE 8.8 Nipple. The nipple appears hypoechoic with irregular and poorly defined borders. These features may be confused with those of malignancy

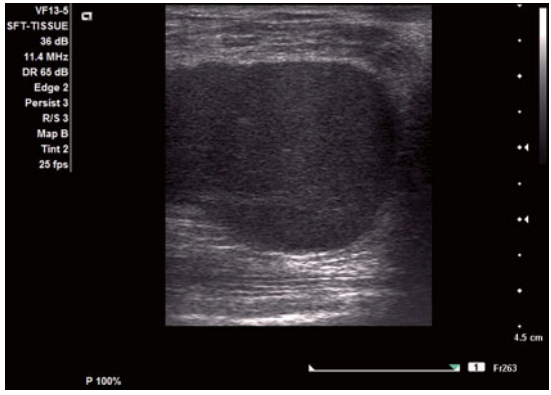

FIGURE 8.9 Fibroadenoma. The mass is oval, hypoechoic, and wider than tall and shows circumscribed distinct margin, pushing borders, slight lobulation in the left upper portion, and posterior acoustic enhancement

tumor types such as medullary carcinoma, colloid carcinoma, cystic papillary carcinoma, and high-grade infiltrating ductal carcinoma (Fig. 8.10). Some fast-growing malignant tumors are circumscribed by US due to a lack of tumor-induced desmoplastic stromal reaction. For the same reason, these

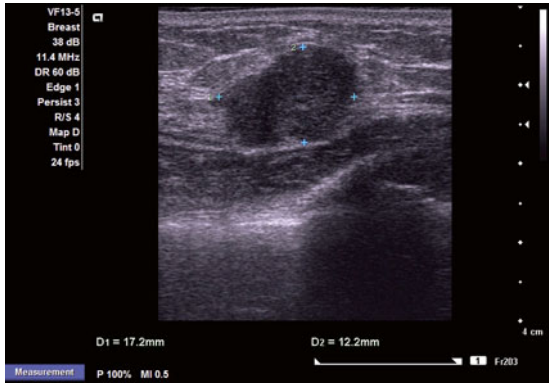

FIGURE 8.10 Medullary carcinoma. The mass is oval, hypoechoic, wider than tall and has a circumscribed slightly fuzzy margin, slight lobulation, slight spiculation at 5 o'clock, and disruption of surrounding breast parenchyma

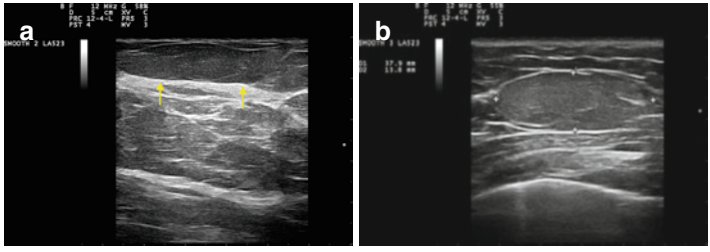

FIGURE 8.11 Breast adipose tissue prominence (**a**) and lipoma (**b**). The mass (*arrows*) is oval, slightly hypoechoic or hyperechoic, homogeneous, and has a circumscribed margin, with no lobulations, spiculations, or disruption of breast architecture. Lipoma has tapered ends and better defined margins.

tumors often show posterior acoustic enhancement that may be augmented by the presence of a host inflammatory response, as seen in medullary carcinoma.

Hyperechoic lesions are usually benign and include prominent and dense fibroglandular tissue and lipomas (Fig. 8.11). Lesions that are anechoic are usually cystic and have posterior acoustic enhancement (Fig. 8.12). If a breast cyst has an echogenic vascular focus on Doppler examination, it is

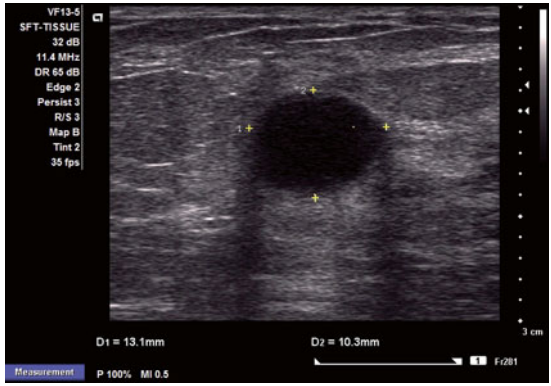

FIGURE 8.12 Simple cyst. The mass is round and anechoic and has well-circumscribed distinct margin, with posterior acoustic enhancement, edge shadows (representing a thick cyst wall), and no lobulations or spiculations

probably a papillary neoplasm, and USG-FNA (preferably using the Zajdela technique) must be directed to the solid component after cyst drainage. When the mass is heterogeneous, the sound waves do not pass through, and an acoustic shadowing posterior to the mass is seen (Fig. 8.13).

Malignant breast lesions are typically hypoechoic and are easily identified in normal or dense breast tissue. These lesions appear white on screening mammogram. US findings suspicious for malignancy include the following: marked hypoechogenicity, spiculation, taller than wide or round, irregular angular ill-defined margins, posterior acoustic shadowing, microlobulated borders, intraductal extension, solid echotexture, inhomogeneous internal echotexture, ill-defined echogenic halo, no compressibility, and calcifications (Fig. 8.14). Some infiltrating breast cancers elicit a desmoplastic stromal reaction surrounding the malignant glandular component, which appears as slightly hyperechoic irregular rims (Fig. 8.15). Posterior acoustic enhancement may be seen in rapidly growing tumors such as poorly differentiated carcinomas and in colloid and intracystic papillary carcinoma (Fig. 8.16).

Spiculated lesions usually correlate with a slow tumor growth and the presence of tumor-induced desmoplastic stromal response formation as seen in low- and intermediate-grade

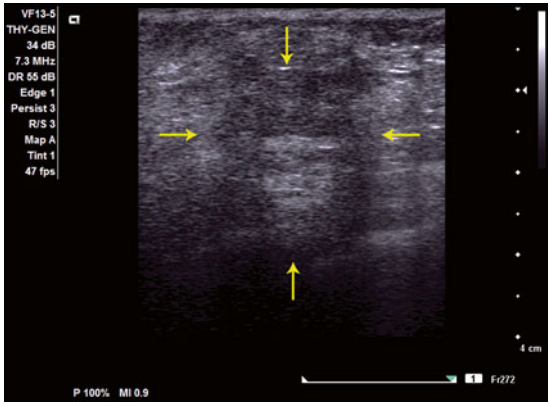

FIGURE 8.13 Fat necrosis. The mass has an irregular shape, complex echotexture, poorly circumscribed and indistinct margins and is taller than wide with disruption of breast architecture. The lesion mimics a malignant mass. The *top arrow* shows a hyperechoic linear area of dense fibrous tissue (also present in the center right and center low surrounded by a hyperechogenic area)

FIGURE 8.14 Malignant lesion. The mass is wider than tall and has an irregular shape, slight complex echotexture, poorly circumscribed and indistinct margins in the lower left part of the mass, and microlobulation. The mass seems to invade the superficial breast tissue causing slight retraction of the skin with disruption of the deep subcutaneous tissue hyperechoic plate (*arrow*), superior and left from the area of spiculation

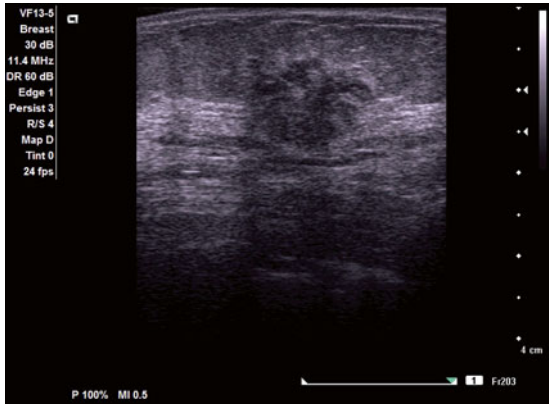

FIGURE 8.15 Malignant lesion. Hyperechoic stromal reaction is seen in the right upper portion of the mass. The mass is slightly round with complex echotexture and ill-defined margins

FIGURE 8.16 Malignant lesion. The mass is irregular, hypoechoic, with slight heterogeneous echotexture, ondulations or macrolobulations, one spiculated border at 1 o'clock, and irregular posterior acoustic enhancement. Cooper's ligaments are disrupted

ductal carcinoma, invasive tubular carcinoma, and lobular carcinoma. Also, these tumors show posterior acoustic shadowing by US (Fig. 8.17).

It must be remembered that not all smooth and well-circumscribed tumors are benign and spiculated ones malignant. The US error rate is 1–2 %.

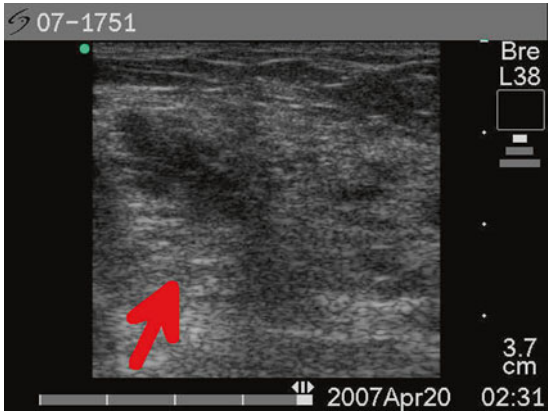

FIGURE 8.17 Malignant lesion. The mass (*arrow* at 7 o'clock) is large, irregular, and wider than tall, poorly circumscribed, heterogeneous, complex and ill-defined. Diagnosis was infiltrating lobular carcinoma. Breast architecture is disrupted

Useful US information essential for the cytopathologist to know in regard to a lesion include the following: (1) borders well circumscribed or irregular; (2) echotexture solid, cystic, or solid and cystic; (3) size; (4) physical changes over time; and (5) disappeared or collapsed after fluid drainage. Also important are the clinical findings, the patient's age, evidence of stability over a period of time, and mammographic findings, when evaluating the likelihood chance of malignancy of a solid mass.

American College of Radiology Ultrasound: Summarized Bi-Rads[a] terminology and categories

Mass:

Shape: oval (may have slight undulations, macrolobulations), round, irregular

Orientation: long axis parallel to skin (wider than tall) or not parallel ("taller than wide")

Margin: circumscribed, not circumscribed (indistinct, angular, microlobulated, or spiculated)

Boundary: abrupt interface, echogenic halo

American College of Radiology Ultrasound: Summarized Bi-Rads[a] terminology and categories

Echo pattern: (relative to fat) anechoic, hypoechoic, isoechoic, hyperechoic, complex

Posterior acoustic features: enhancement, shadowing, combined, none

Surrounding tissue changes: ducts, Cooper's ligament, edema, architectural distortion, skin thickening/retraction/irregularity

Calcifications:

Macrocalcifications (≥0.5 mm in size)

Microcalcifications out of the mass (<0.5 mm in size)

Microcalcifications in the mass

Special cases:

Clustered microcysts, complicated cysts, mass in or on skin, foreign body, lymph nodes (intramammary, axillary)

Vascularity:

Not present, present in lesion, present adjacent to lesion, diffuse in surrounding tissue

Assessment categories:

Category 0: incomplete, need additional imaging evaluation

Category 1: negative findings

Category 2: benign findings

Category 3: probably benign

Category 4: suspicious abnormality (consider biopsy)

Category 5: highly suggestive of malignancy

Category 6: known malignancy (biopsy proven)

[a]BI-RADS, Breast Imaging Reporting and Data System

Breast Masses

Palpable and US visible breast masses can be neoplastic or nonneoplastic and can be sampled and interpreted by FNA under palpation or US guidance. Nonneoplastic masses include mastitis, breast abscesses, fibrocystic change, fat necrosis, cysts, lactation changes/adenoma, etc. An abridged classification of tumors of the breast is listed in Table 8.1. Ductal carcinoma in situ (DCIS) may be palpable, and precursor and intraductal proliferative lesions may be visible by US and also be targets for USG-FNA.

Nonneoplastic Breast Masses

Cysts

The most common lesions of the female breast are solitary or multiple cysts, particularly in the premenopausal age. The FNA is a diagnostic and therapeutic procedure and yields clear, opaque, or turbid fluid that may be clear, yellow, or red (bloody). Turbid and bloody fluids should be examined cytologically because they may harbor a papillary neoplasm, including intracystic papillary carcinoma. It is also important to reexamine the area manually and/or by US after cyst drainage to search for a solid-phase component, which must be sampled by FNA, preferably under US guidance. The smears show macrophages in various numbers and epithelial cells, often of apocrine appearance (Fig. 8.18a, b).

US features. Cysts have well-circumscribed margins; are anechoic, rounded, or oval; and show thin edge shadows and a characteristic posterior acoustic enhancement due to the presence of fluid (Fig. 8.18c). Posterior acoustic enhancement is not always seen in small cysts or in those located deep close to the chest wall. In some cysts, dot-like moving internal

Table 8.1 Abridged WHO classification of tumors of the breast

Epithelial tumors		
	Invasive breast carcinoma	Carcinoma of no special type
		Lobular carcinoma
		Tubular carcinoma
		Cribriform carcinoma
		Mucinous carcinoma
		Carcinoma with medullary features
		Metaplastic carcinoma
		Micropapillary carcinoma
		Rare types: neuroendocrine, secretory, acinic cell, mucoepidermoid, oncocytic, etc.
	Epithelial–myoepithelial tumors	Pleomorphic adenoma
		Adenomyoepithelioma
		Adenoid cystic carcinoma
	Precursor lesions	Ductal carcinoma in situ
		Lobular neoplasia
	Intraductal proliferative lesions	Ductal hyperplasia
		Columnar lesions
		Atypical ductal hyperplasia
	Papillary lesions	Intraductal papilloma
		Intraductal papillary carcinoma
		Solid papillary carcinoma
	Benign epithelial proliferations	Adenosis, radial scar
		Adenomas
Mesenchymal tumors		Benign and malignant

Table 8.1 (continued)

Fibroepithelial tumors	Fibroadenoma
	Phyllodes tumor
Tumors of the nipple	Adenoma
	Paget disease of the nipple[a]
Malignant lymphoma	B- and T-cell types
Metastatic tumors	
Tumors of the male breast	Gynecomastia
	Carcinoma

[a]Scraping of the lesion can provide cytologic material for diagnosis

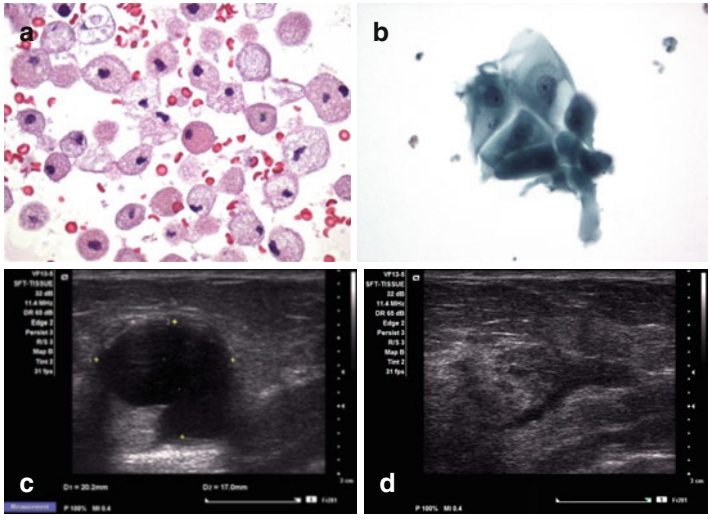

Figure 8.18 Simple cyst. Macrophages (**a**) and metaplastic cells (**b**). The cyst is anechoic with no mural nodules (**c**) and collapsed after fluid drainage (**d**) (**a**, **b**, Papanicolaou stain, medium and high magnification)

echogenic signals ("gurgling cyst") are seen upon cyst compression with the US transducer, confirming a fluid internal matrix. Occasionally, small echogenic septations may be seen, particularly when apocrine metaplasia is present. Again, a mural solid component present after fluid drainage must be sampled by USG-FNA (Fig. 8.18d).

Mastitis

Bacterial, mycobacterial, fungal, parasitic, and viral, among others, are rare causes of mastitis. Less than 3 % of lactating women develop acute suppurative mastitis, and staphylococci and streptococci are the most common agents. Localized acute mastitis may result in abscess formation. Inflammatory mastopathy may be associated with duct/cyst rupture and diabetes mellitus. Granulomatous mastitis may be due to sarcoidosis, infections, reaction to tumor, fat necrosis, foreign body reaction (suture, ruptured squamous cyst, silicone implant leakage), and idiopathic granulomatous mastitis. These entities can clinically and radiologically mimic carcinoma. USG-FNA can be used as diagnostic and therapeutic tools, i.e., for abscess drainage associated with antibiotic therapy.

FNA findings. The inflammatory cells vary in type and number according to the type of mastitis; however, the epithelial cell morphology has variable reactive changes ranging from minimal to severe and can be confused with malignancy. The epithelial cells are arranged in cohesive sheets and have variable reactive inflammatory changes and reparative features (Fig. 8.19). Polarity is maintained, and myoepithelial cells are present in the background. A purulent smear pattern including neutrophils, macrophages, and debris is found in *acute mastitis*. In *chronic mastitis*, smears are less cellular due to underlying fibrosis and show plasma cells and lymphocytes. Multinucleated giant cells and macrophages may be present. Plasma cell mastitis is a common chronic inflammatory condition and is most probably caused by duct rupture. In granulomatous mastitis, smears show granulomas, a foreign body-type giant cell reaction, aggregates of epithelioid

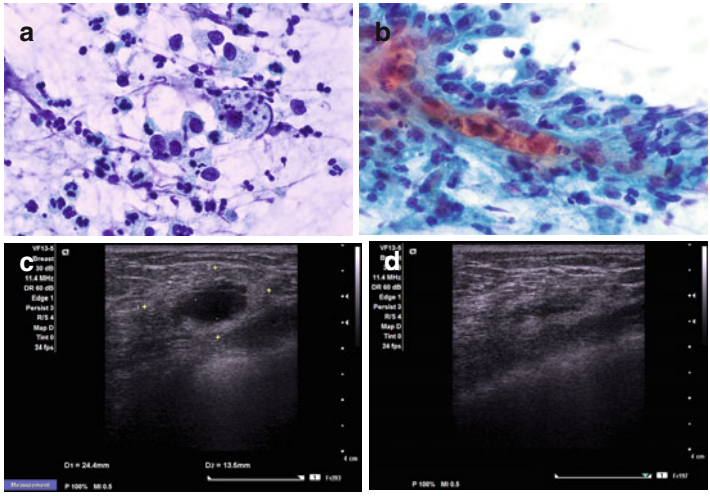

FIGURE 8.19 Acute and chronic mastitis. Acute inflammatory exudate, variable numbers of macrophages (**a**), and granulation tissue fragments (**b**) are seen. This particular US image shows an abscess with thick echogenic wall and anechoic center (**c**) that collapsed partially after drainage (**d**) (**a**, Diff-Quik stain high magnification; **b**, Papanicolaou stain high magnification)

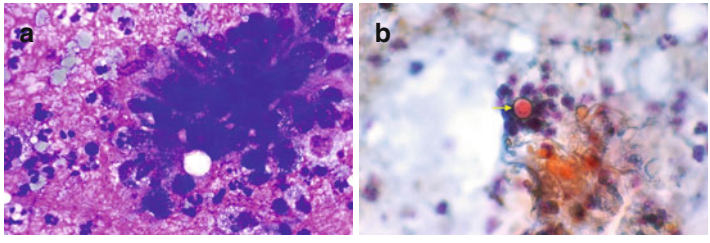

FIGURE 8.20 Granulomatous mastitis. Blastomycosis. Necrosis, granulomas, markedly reactive stromal and epithelial elements (**a**), and fungal organisms (**b**, *arrow*) are seen (**a**, Diff-Quik stain high magnification; **b**, Papanicolaou stain high magnification)

histiocytes, lymphocytes, and plasma cells, and variable necrosis (Figs. 8.20 and 8.21). Special stains for mycobacteria

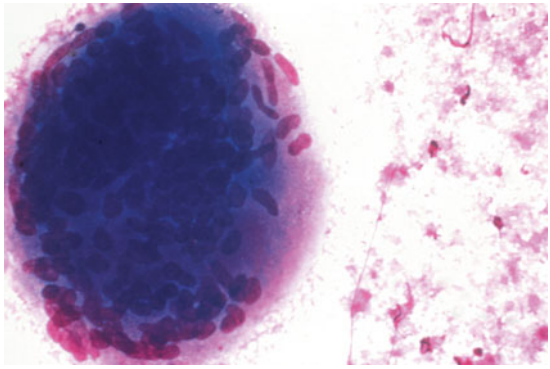

FIGURE 8.21 Granulomatous mastitis. Tuberculosis. Multinucleated histiocytes and a background of necrosis (Diff-Quik stain, high magnification)

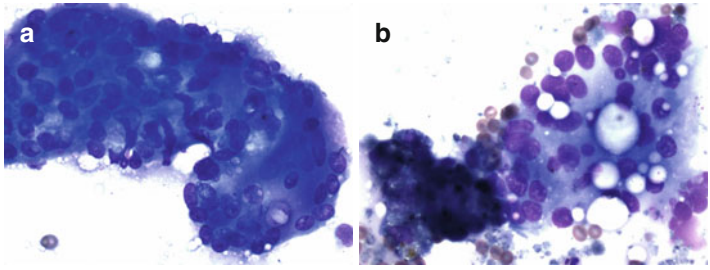

FIGURE 8.22 Silicone mastitis. Granulomas (**a**) and multinucleated giant cells containing round empty vacuoles (**b**) (MGG stain, high magnification)

and fungus performed in smears or cell blocks are useful for rapid diagnosis and for initiation of therapy. Cultures are confirmatory and used to modify therapy according to sensitivity to specific drugs. *Silicone granulomas* can be suspected when histiocytes contain empty, round vacuoles and amorphous nonstaining material in Romanowsky stains; the clinical history is important (Fig. 8.22).

US features. Mastitis shows diffusely increased echogenic tissue with loss of normal tissue planes including Cooper's

ligaments, reflecting the presence of tissue edema; increased vascularity may be seen on Doppler examination. Areas of increased echogenicity may be associated with areas of decreased echogenicity, resulting in a not well-circumscribed mass. An abscess is hypoechoic, well defined, and may be uni- or multiloculated, showing interconnecting complex cystic masses that may extend to the skin. The abscess content has an echogenic signal that results in movement of particles when there is compression of the mass with the US transducer. The overlying skin and the surrounding soft tissue are thickened and show edema (Fig. 8.19c, d). A "snow-storm" appearance is characteristic of silicone granuloma; the same appearance can be seen in axillary lymph nodes in cases of extracapsular rupture of the implant and migration of the silicone to the lymph nodes.

Subareolar Abscess

This process usually occurs in nonlactating premenopausal women who have recurrent abscess formation in the subareolar area and draining of a periareolar fistula. Squamous metaplasia of the distal lactiferous ducts with obstruction is considered to be the etiologic factor. The abscess is usually sterile, but a superimposed bacterial infection may occur.

FNA findings. Smears show a mixed acute and chronic inflammatory background, multinucleated giant cells of foreign body type, and squamous cells (anucleated, parakeratotic). Variable numbers of foamy macrophages, cholesterol crystals, and reactive ductal epithelial cells and granulation tissue may be present (Fig. 8.23). Sebaceous cysts also show numerous anucleated squamous cells and may show multinucleated giant cells if there is cyst rupture; cholesterol crystals may be seen (Fig. 8.24a). The distinction between these two entities needs US correlation.

US features. Subareolar abscess by US shows a complex hypoechoic to nearly anechoic oval or lenticular mass with irregular margins, heterogeneous echotexture with minute particles, and mixed solid and cystic areas with posterior acoustic enhancement. Hypoechoic tubular areas associated

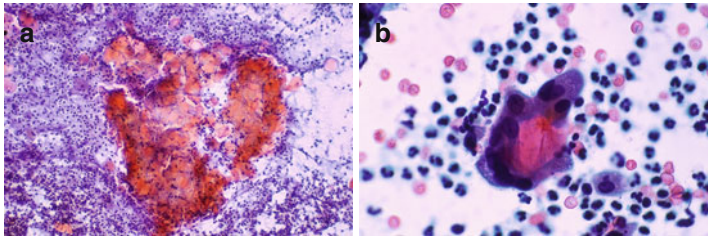

FIGURE 8.23 Subareolar abscess. Cluster of anucleated squamous cells are surrounded by acute inflammatory cells (**a**). Multinucleated giant cell phagocytizing anucleated squamous cells and a background of acute inflammation present (**b**) (Papanicolaou stain, medium (**a**) and high magnification (**b**)

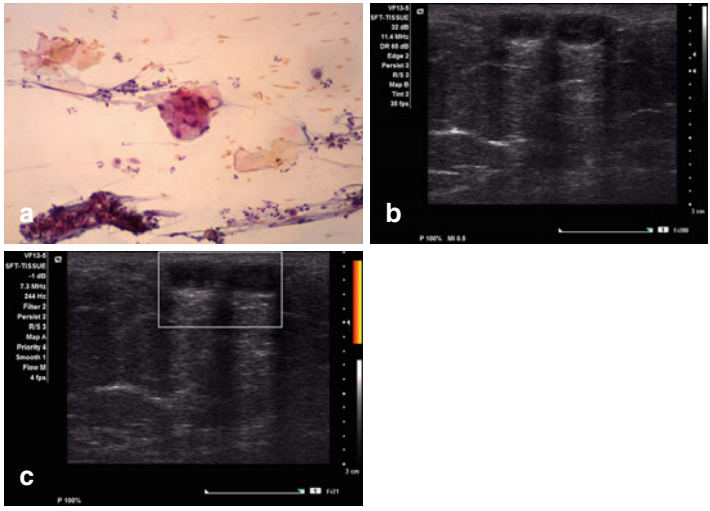

FIGURE 8.24 Epidermal inclusion cyst. These lesions developed in the inframammary fold. Anucleated squamous cells, acute inflammation, macrophages, and multinucleated giant cells phagocytizing squamous cells are present (**a**). Ultrasound image shows two skin-based hypoechoic oval lesions with uniform well-defined margins, edge shadows, and posterior acoustic enhancement (**b**). No vascular flow is noted by Doppler exam (**c**) (**a**, Papanicolaou stain intermediate magnification)

with the skin and subcutaneous tissue, skin thickening, and dilated subdermal lymphatics may be seen. A sebaceous cyst is superficial and arises from the skin. Early in sebaceous cyst development, a hypoechoic mass is seen causing skin thickening; the echogenic deep dermal layer may disrupt as the cyst enlarges. Sebaceous cysts may be completely anechoic, hypoechoic, or echogenic with posterior acoustic enhancement or a complex cystic mass and may be irregular with indistinct margins (Fig. 8.24b, c).

Fibroadipose Tissue Prominence/Lipoma

True lipomas are rare. These lesions are palpable and often not visible by mammography or US. They are soft to slightly firm and often poorly circumscribed. Occasionally, lipomas may become more evident if there is weight loss.

FNA findings. Aspiration smears from lipomas show benign adipose tissue fragments of variable sizes. Benign ductal epithelial cell sheets and myoepithelial cell nuclei may be seen in addition to adipose tissue in cases of adipose tissue prominence. Cytologic findings need clinical and US correlation; the accuracy of such a diagnosis is the highest when the cytopathologist performs FNA under US guidance and interprets the cytology findings.

US features. The US features of lipoma are characteristic and include a well-defined oval, compressible, isoechoic, or slightly hyperechoic homogeneous mass with a thin echogenic capsule (Fig. 8.11). Fatty tissue prominence shows bundles of hypoechoic tissue surrounded and delineated by echogenic lines (Cooper's ligaments) (Fig. 8.25).

Fat Necrosis

This trauma-related inflammatory lesion resembles malignancy clinically, radiologically, and cytologically. The problem is compounded because the patient often does not recall having trauma. The mass is commonly firm, irregular, and fixed to deep planes and may not always be tender.

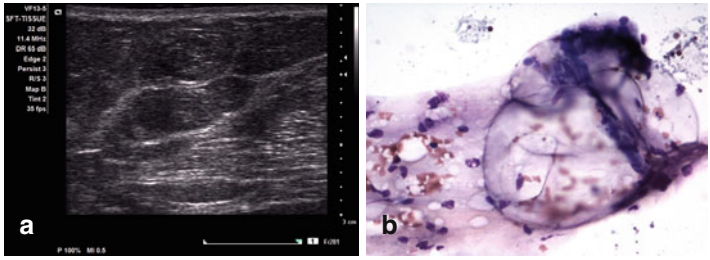

FIGURE 8.25 Adipose tissue breast prominence. Patient usually has an ill-defined and slightly firm palpable breast lesion, which is not distinctly visible by US as in this case; instead, lobules of adipose tissue are seen (**a**). The FNA smears show small fragments of fibro-fatty tissue (**b**). (**b**, MGG stain, intermediate magnification)

FNA findings. Necrotic and degenerating adipocytes, lipid-laden macrophages, and mixed inflammatory cells are present along with scattered multinucleated foreign body-type giant cells. Myospherulosis, which is the result of aggregated red blood cells altered by the contact with lipid resembling a "bag of marbles," possibly represents a sequel of fat necrosis (Fig. 8.26a–c).

US features. The lesion may be irregular and hypoechoic with variable posterior acoustic enhancement. The lesions may have ill-defined borders and be slightly hyperechoic or mixed complex solid/cystic when there is cystic degeneration. Old lesions may have dystrophic calcification and, in some cases, have a calcific rim (Fig. 8.26d, e). Old lesions may also be complex solid and cystic or cystic and nearly anechoic, with or without posterior acoustic enhancement on US.

Fibroepithelial Tumors

Fibroadenoma

This benign biphasic stromal and epithelial neoplasm arises in the terminal duct lobular unit and affects women particularly between the ages of 20 and 35 years. It is usually a

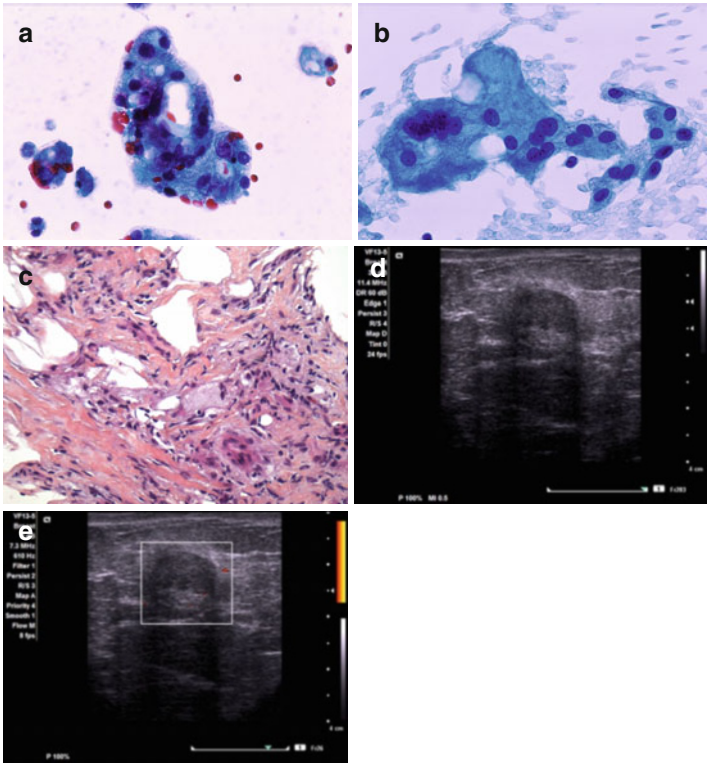

FIGURE 8.26 Fat necrosis. Damaged adipocytes are arranged predominantly in cohesive aggregates with rare single cells showing finely vacuolated cytoplasm, low nuclear to cytoplasm ratio, and bland nuclear features. Variable anisocytosis and anisonucleosis may be present (**a**, **b**). Core biopsy performed confirms the diagnosis (**c**). Ultrasound shows an ill-defined, round, taller than wide mass with heterogeneous echotexture and minimal vascularity by Doppler exam (**d**, **e**) (**a**, **b** Diff-Quik stain, high magnification; **c**, H&E stain intermediate magnification)

mobile, firm, solitary, slow-growing, well-circumscribed tumor and usually measures <3 cm. However, it may be larger, multiple, and bilateral. Juvenile fibroadenomas are larger than 5 cm. A complete surgical excision is curative.

Histopathology. The stromal component may surround the ducts (pericanalicular) or may separate the ducts, forming clefts (intracanalicular) (Fig. 8.27a). Hypercellular stroma, calcification, myxoid change or hyalinization, scattered giant cells, and rare mitoses may be present and have no clinical significance (Fig. 8.28a). Complex fibroadenomas show calcifications and superimposed fibrocystic changes including cysts >3 mm, sclerosing adenosis, ductal epithelial hyperplasia of usual type, and apocrine and squamous metaplasia. Juvenile fibroadenomas show hypercellular stroma, a stromal pericanalicular pattern, and ductal epithelial hyperplasia. Atypical ductal or atypical lobular hyperplasia, lobular carcinoma in situ, and ductal carcinoma in situ may develop within the fibroadenoma.

Molecular profile. Both epithelial and stromal components are polyclonal. No alterations in DNA copy have been shown by comparative genomic hybridization. Rare cases of numerical chromosomal abnormalities have been reported. There is no detectable stromal expression of nuclear α-catenin or E-cadherin.

FNA findings. Smears are usually hypercellular with epithelial cells arranged in sheets, fingerlike branching and staghorn-like structures, numerous myoepithelial cell nuclei in the background and adherent to the epithelial elements,

---

Figure 8.27 Fibroadenoma. Low-power tissue sections show the typical features of a pericanalicular fibroadenoma (**a**). Cytologic features include branching and "staghorn-like structures, cohesive cell sheets, numerous myoepithelial cells both in the background and within the epithelial cells, and stromal fragments (**b**–**e**). Ultrasound shows a homogeneous, isoechoic, or hypoechoic wider than tall mass with ondulations or macrolobulations. A thin echogenic pseudocapsule and a homogeneous echotexture may be seen. Posterior acoustic enhancement is variably present. Vascular flow by Doppler exam is also variably present (**f**–**j**) (**a**, H&E stain low magnification; **b**, **d** Diff-Quik stain low and high magnification; **c**, **e** Papanicolaou stain low and intermediate magnification)

and fragments of fibrous and fibromyxoid stroma; apocrine and foam cells may be present. This smear pattern overlaps that of fibrocystic change; however, the clinical findings including US are different (Figs. 8.27b–e and 8.28b).

US features. A well-defined oval mass with gently lobulated margins is seen. The mass is homogeneous, isoechoic,

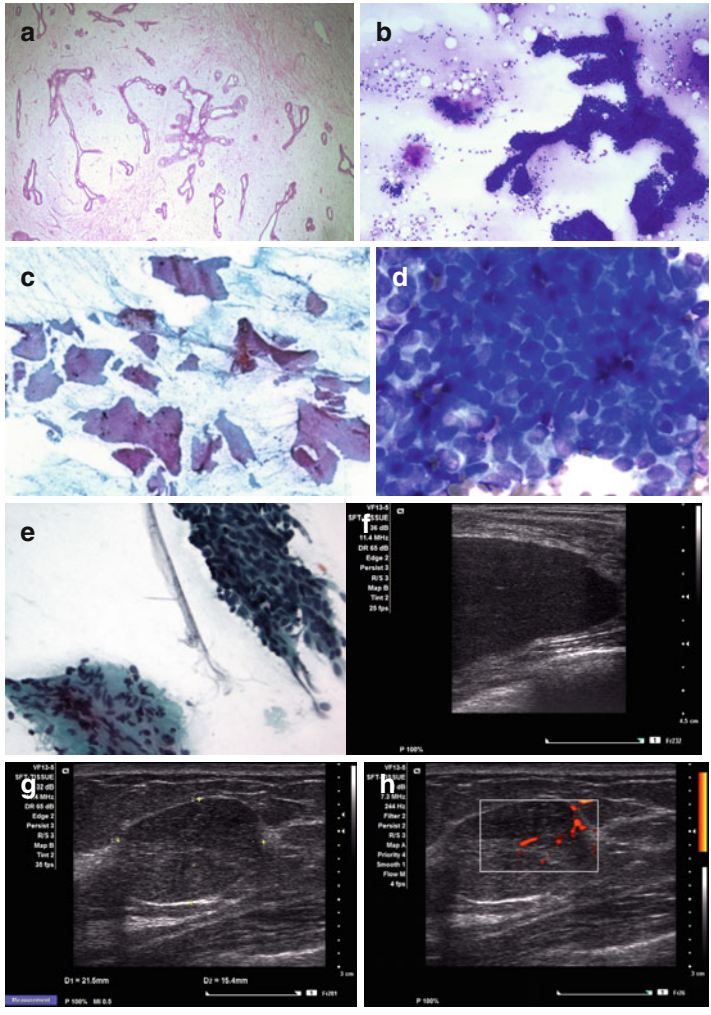

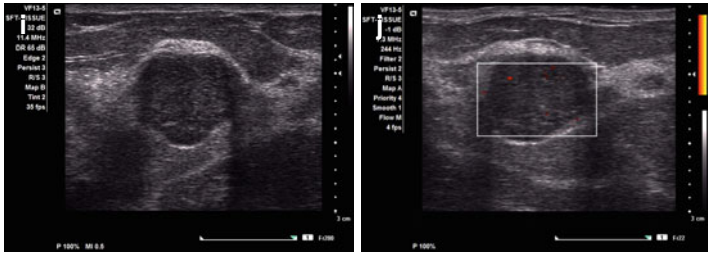

FIGURE 8.27 (continued)

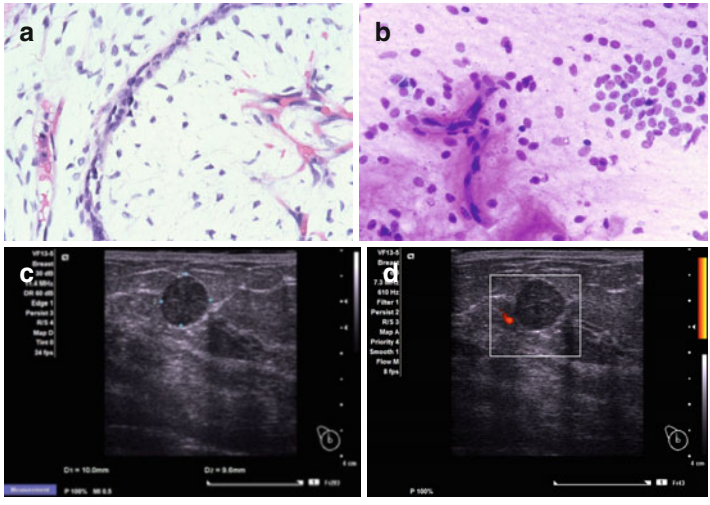

FIGURE 8.28 Myxoid fibroadenoma. The myxoid stroma is prominent in both the histology and cytology (**a**, **b**). Ultrasound shows a round hypoechoic mass with circumscribed distinct margins, homogeneous echotexture, posterior acoustic enhancement, and little or no vascular flow by Doppler exam (**c**, **d**) (**a**, H&E stain, low magnification; **b**, Diff-Quik stain high magnification)

or hypoechoic to the adjacent fat. A thin echogenic pseudocapsule, characteristic of a benign lesion, and a "pseudocystic pattern" due to the homogeneous echotexture may be seen. Posterior acoustic enhancement is variably present; slight posterior acoustic shadowing may be present in long-lasting lesions due to sclerosis. The echotexture may be

slightly heterogeneous with small cystic lesions. Calcifications may be seen in complex and long-lasting fibroadenomas; coarse benign "pop-corn" calcifications are typical of calcified fibroadenomas and show posterior acoustic shadowing. Cysts >3 mm and calcifications are seen in complex fibroadenomas. Juvenile fibroadenomas are well circumscribed and hypoechoic and may have heterogeneous echotexture and posterior acoustic enhancement (Figs. 8.27f–j and 8.28c, d).

Phyllodes Tumors

This biphasic stromal and epithelial tumor accounts for less than 0.3 % of all breast tumors and 2.5 % of all fibroepithelial tumors. These tumors occur in middle-aged women, although they may occur at a younger age in Asian women. Patients have a bulging, well-circumscribed, unilateral painless breast mass, not attached to the skin. Most phyllodes tumors behave in a benign fashion; recurrence occurs within 3 years, particularly in the case of borderline and malignant tumors. Most deaths occur within 5–8 years post diagnosis, and lung and skeletal metastases are most common. Mediastinal involvement secondary to chest wall invasion has been reported.

Histopathology. These tumors have hypercellular stroma and an intracanalicular stromal growth pattern with leaflike projections into elongated and variably dilated lumina. Archlike clefts are lined with epithelial and myoepithelial cell layers and surround stromal mounds. Marked usual ductal epithelial hyperplasia is common. Tumor size, mitotic activity, cytologic atypia, stromal overgrowth, and the status of borders/margins are histologic parameters useful for assessment of the biologic behavior of these tumors. Based on these parameters, phyllodes tumors are classified as benign, borderline, and malignant. Benign phyllodes tumors have pushing borders, accentuated subepithelial stromal cellularity, and <5 mitoses per 10 high-power fields (Fig. 8.29a). Malignant phyllodes tumors have infiltrating borders, marked stromal cellularity, inconspicuous epithelial component, cellular stromal pleomorphism, and >10 mitoses per 10 high-power fields. In summary, the stromal component is the basis for the diagnosis and grading of phyllodes tumor.

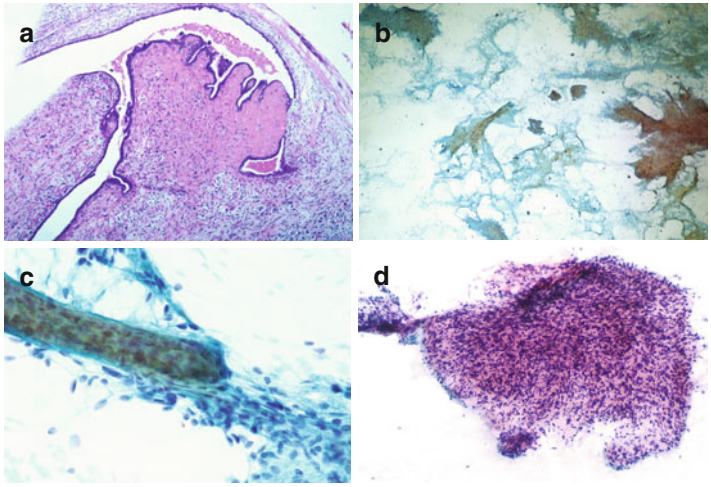

FIGURE 8.29 Phyllodes tumor. Tissue section shows hypercellular stroma and archlike clefts lined with epithelial and myoepithelial cell layers that surround stromal mounds (**a**). The FNA smear pattern is similar to that of fibroadenoma, except for the marked cellular stroma (**b**–**d**). Diagnosis of benign, borderline, or malignant phyllodes requires examination of the excised tumor (**a**, H&E low magnification; **b**–**d** Papanicolaou stain low and intermediate magnification)

Immunoprofile. No specific marker distinguishes phyllodes tumors from fibroadenomas or accurately diagnoses benign, borderline, or malignant phyllodes tumors. However, the proliferation index Ki-67 expression correlates with tumor grade. Likewise, p53 (tumor suppressor for cell cycle control) nuclear stain and CD10 expression may correlate with tumor grade, but do not differentiate between fibroadenoma and benign phyllodes since the stain is negative in both.

Molecular profile. There is evidence of epithelial influence over stromal growth via the Wnt signaling pathway, upregulation of transcriptionally active β-catenin, and downstream effectors such as cyclin D1. α- and β-catenins in stromal cells may be important in early stages of phyllodes tumors development, and E-cadherin may be required for malignant

transformation. β-catenin binds to the cytoplasmic domain of E-cadherin and to α-catenin in cell–cell adhesion. Stromal β-catenin correlates with α-catenin expression and is significantly higher in borderline than in benign phyllodes tumors, but lower in malignant tumors. Thus, malignant phyllodes tumors show loss of β-catenin and, in addition, show *MYC* amplification and aberrant expression of *TP53*. The stroma also influences the epithelium via IGF (insulin-like growth factor) signaling pathway and IGFR1 and IGFR2 (insulin-like growth factor polypeptide hormones 1 and 2) that are overexpressed in the stroma of fibroepithelial tumors. The expression of α-catenin by stromal cells is associated with tumor recurrence.

FNA findings. Smears show both epithelial and stromal elements. The distinction from fibroadenomas is based mainly on the cellularity of the stromal fragments. In addition, and in contrast to fibroadenomas, stromal cells have larger nuclei, irregular nuclear contours, and occasional nucleoli (Fig. 8.29b–d). Malignant phyllodes tumors show large atypical stromal cells and mitoses. Marked ductal epithelial hyperplasia with varying degrees of atypia is common and may lead to an erroneous diagnosis of mammary carcinoma.

US features. The US features of phyllodes tumors can be indistinguishable from those of fibroadenomas. The tumor is hypoechoic, well circumscribed with smooth distinct borders and typical internal hyperechoic bands and shadows, and with variable posterior acoustic enhancement and shadowing. Calcifications may be present. Occasionally, a complex cystic mass may be seen and can suggest the diagnosis of a malignant phyllodes tumor.

Myoepithelial and Epithelial–Myoepithelial Lesions

Myoepithelial lesions encompass myoepithelial hyperplasia, collagenous spherulosis, and myoepithelial carcinoma.

Epithelial–myoepithelial lesions encompass pleomorphic adenoma, adenomyoepithelioma, adenomyoepithelioma with carcinoma, and adenoid cystic carcinoma. Adenoid cystic carcinoma is covered later in this chapter.

Antibodies selected to high-molecular-weight keratins (CK 5, CK 5/CK6, CK 14, CK 17), p63, actin, calponin, smooth muscle heavy-chain myosin, S-100 protein, and H-caldesmon (variable) will react with myoepithelial cells in most lesions.

Adenomyoepithelioma and Adenomyoepithelioma with Carcinoma

These are rare tumors that affect adult women and that may also be seen in men. Patients may have tenderness or nipple discharge.

Histopathology. Adenomyoepithelioma shows a proliferation of myoepithelial cell layers around epithelium-lined spaces. The histologic pattern may be lobulated, papillary, tubular, or mixed. Myoepithelial cells may be spindle, epithelioid, or glycogen-rich with clear cytoplasm. Either the epithelial or the myoepithelial cells or both may undergo malignant change. The malignant epithelial component may give rise to invasive carcinoma of no special type, to undifferentiated carcinoma, or to metaplastic carcinoma. The tumor has a low malignant potential, and there may be local recurrence particularly after incomplete excision.

Immunoprofile. Immunostains for estrogen receptor (ER) and progesterone receptor (PR) are negative or focally weakly positive. HER2 is negative.

Molecular profile. Allelic imbalance, microsatellite instability, and reciprocal translocations between chromosomes 8 and 16 have been described in adenomyoepithelioma.

FNA findings. Smears are variably cellular and show cohesive aggregates of epithelial and myoepithelial cells supported by variable amounts of fibrillary magenta stroma admixed with delicate branching capillaries. Myoepithelial cells have clear cell, spindle, or plasmacytoid characteristics

or appear naked and bipolar and dissociated in the smear background. The epithelial cells are small and may be arranged in small sheets or tubules. Metachromatic stroma may also be seen in the background and may be fibrillary or clumpy, resembling collagenous spherulosis.

US Features. The tumors are round or lobulated and are circumscribed with well-defined margins.

Epithelial Tumors

Benign Epithelial Proliferations

Adenosis, Sclerosing Adenosis, and Adenosis Tumor

Adenosis is a benign proliferation of glandular elements involving terminal ducts and lobular units. Sclerosing adenosis is a benign and microscopic lesion. Adenosis tumor is the palpable (average size 2.5 cm) counterpart of sclerosing adenosis, occurs commonly in the fourth decade of life, and is rare. Adenosis tumor can be mistaken for carcinoma on clinical and histologic evaluation.

Immunoprofile. In sclerosing adenosis, the presence of myoepithelial cells, masked by architectural distortion, can be detected by immunoreactions with CK5, CK14, CK17, α-SMA, p63, and calponin. Adenosis shows a normal epithelial monolayer immersed in a fibrous stroma, sometimes surrounded by a hyaline basal membrane without myoepithelial cells. Immunostaining for collagen IV, laminin, and vimentin shows the presence of a basement membrane, which is not always obvious on conventional H&E stain. In this lesion, unlike sclerosing adenosis, the myoepithelial markers are negative, whereas the S-100 protein is positive.

FNA findings. The smear pattern is similar to that of proliferative fibrocystic change, including sheets of ductal epithelial cells, numerous myoepithelial cell nuclei, and stromal fragments. The specific diagnosis of adenosis tumor is not possible on FNA; however, the diagnosis of benign proliferative fibrocystic change can be made.

US features. Adenosis tumor may be seen as a hypoechoic mass with posterior acoustic shadowing. Angular margins and tubular-like extensions may be present.

Radial Scar and Complex Sclerosing Lesion

Radial scar is a small stellate lesion, whereas a complex sclerosing lesion is larger and more complex and may occasionally be palpable. These lesions are usually found incidentally on imaging studies and they may be mistaken for carcinoma on clinical, imaging, and histologic grounds, in particular for tubular carcinoma.

Histopathology. Both lesions show a lobular architecture, epithelial proliferation, and prominent sclerosis and elastosis. They have a central zone of fibroelastosis with radiating ducts and lobules showing ductal dilatation, various patterns of epithelial hyperplasia, apocrine metaplasia, sclerosing adenosis, and micropapillomas. The compressed tubules, particularly in the sclerotic areas, are distorted and angular and have a myoepithelial cell layer that may be inconspicuous on routine histologic evaluation. Radial scar may exhibit atypical ductal hyperplasia, DCIS, or lobular neoplasia.

Immunoprofile. The myoepithelial cell layer is detected with immunostains (p63, calponin, smooth muscle actin, smooth muscle myosin heavy chain); however, caution is suggested in the interpretation particularly in small biopsies since results may vary.

FNA findings. Cytologically, smears show variable cellularities, usually small to moderate; as in fibrocystic change, sheets of ductal epithelial cells, myoepithelial cell nuclei, apocrine metaplasia, and macrophages with cyst debris may be variably present.

US features. Ultrasound, in a few patients, may show a hypoechoic lesion with irregular stellate borders and a central hyperechoic area corresponding to the fibroelastotic central area, similar to low-grade carcinomas; however, an echogenic halo, distal attenuation, a taller than wide shape, and distortion are more common in cancer, whereas small cysts and an echogenic component are more frequent in radial scar.

Tubular Adenoma

This is a well-circumscribed (not truly encapsulated), painless nodule that occurs mainly in young women.

Histopathology. The tumor is composed of a proliferation of tubular structures lined by epithelial and myoepithelial cells separated by scant stroma.

FNA findings. Cytologically, the presence of smaller tubules and myoepithelial cells distinguishes tubular adenoma from tubular carcinoma; otherwise, smears resemble fibroadenoma without stroma.

US features. US shows a well-circumscribed hypoechoic oval mass with homogeneous echotexture, smooth borders, and posterior acoustic enhancement or shadowing; margins may be variable.

Apocrine Adenoma

This lesion is rare and occurs in both males and females. Patients have a painless nodule usually measuring <2 cm. Histologically, there is a nodular collection of glands lined with apocrine epithelium with no cytologic atypia. The lesion is benign and is cured by local excision.

Pregnancy-Related Lesions

These changes are the result of a hormonal effect on de novo (lactating adenoma, Fig. 8.30a) or preexistent (fibroadenoma, fibrocystic change) palpable or non-palpable breast lesions. Most are benign, and they often regress within 6 months' postpartum. Pregnant or lactating women may develop a galactocele, which is a milk-filled cystic lesion and may be seen up to several years post-lactation.

FNA findings. The smears are cellular and show numerous complex cellular aggregates, loose clusters, and numerous dissociated cells with clear or vacuolated cytoplasm. Acinar cells have round nuclei, prominent nucleoli, abundant vacuolated cytoplasm, and frayed edges. The background shows bubbly and finely vacuolated granular lipid-rich cytoplasmic contents and variable numbers of stripped epithelial cell nuclei

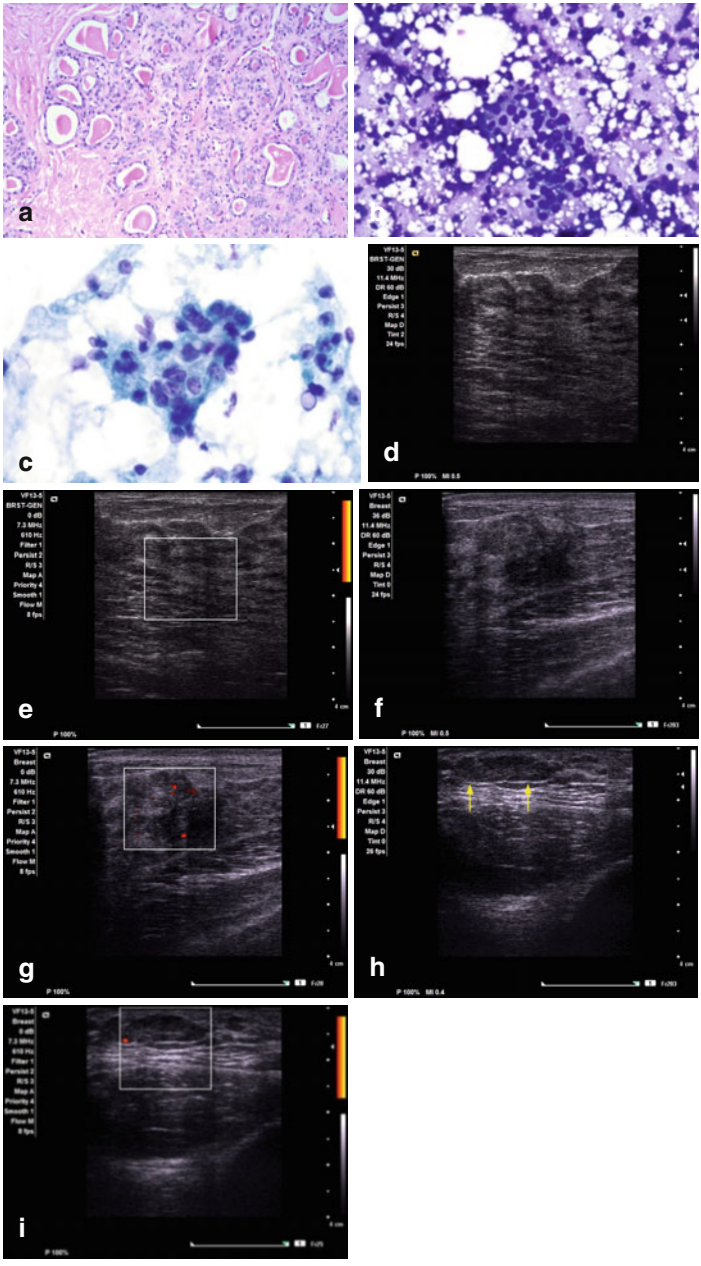
a
c
d
e
f
g
h
i

FIGURE 8.30 Pregnancy-related lesions. A medium-power view of a lactating adenoma is seen in (**a**). Smears show a background of fine lipid vacuoles, scattered single and aggregates cells with cytoplasm, prominent nucleoli, and complex architecture (**b**–**c**). Awareness and clinical history is necessary to avoid an erroneous diagnosis of atypia or malignancy. Normal lactating breast with accentuated parenchyma and no increased vascularity is seen in (**d**, **e**). Ultrasound features from palpable masses range from ill-defined vascularized complex masses to well-defined hypoechoic masses in cases of fibroadenoma (*arrows* point the mass) with lactational changes (**f**–**i**) (**a**, H&E stain low magnification; **b**, Diff-Quik stain high magnification; **c**, Papanicolaou stain high magnification)

with prominent nucleoli. Except in fibroadenomas with lactational change, myoepithelial cell nuclei are lacking (Fig. 8.30b, c). The differential diagnosis includes breast adenocarcinoma, which can be minimized or avoided with clinical correlation and the fact that breast malignancy in pregnancy usually shows greater cellular and architectural atypia, cell dissociation, and hyperchromasia than lactational changes. An aspirate of milk confirms the diagnosis of galactocele (Fig. 8.31).

US features. Normal lactating breast shows a subtle diffusely increased tissue echogenicity with loss of normal tissue planes including Cooper's ligaments, reflecting the presence of lactational changes (Fig. 8.30d). Features of *lactating adenoma* are similar to those of fibroadenoma, including a macrolobulated, oval, hypoechoic well-circumscribed mass with posterior acoustic enhancement; however, irregular margins, heterogeneous echotexture, small cystic spaces, and posterior acoustic shadowing may be present (Fig. 8.30e–i). Multiple internal linear or curvilinear echogenic bands are commonly present. *Galactocele* has features of a cyst or may have echogenic material within the fluid, probably representing an admixture of fatty globules and water, resulting in a US pattern similar to that of fibroadenoma. Compression of the mass with the US probe identifies the movement of particles in galactocele, confirming the diagnosis. Occasionally, galactocele may appear complex and have horizontal band-like hypoechogenic areas (fluid–fluid level) with slight posterior acoustic shadowing.

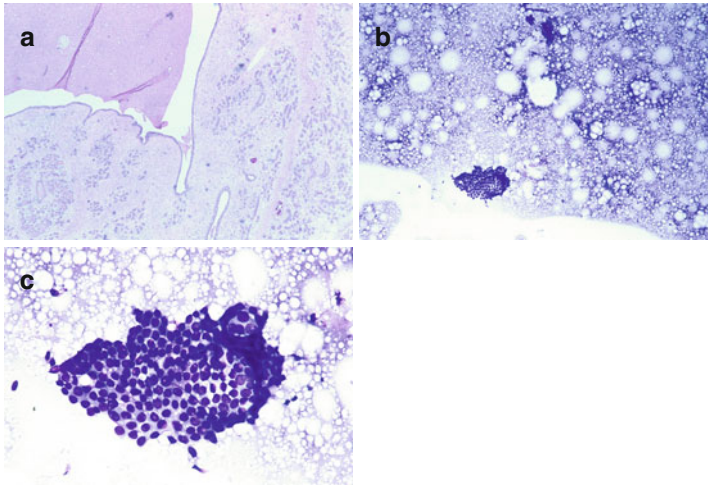

FIGURE 8.31 Galactocele. Tissue section shows a cystically dilated duct with intraluminal fluid consistent with milk (**a**). Smears show rare cyst lining epithelial cells surrounded by fluid with lipid vacuoles consistent with milk (**b**, **c**) (**a**, H&E stain low magnification; **b**, **c**, Papanicolaou stain low and high magnification)

Nipple Adenoma

This benign epithelial proliferation affects the collecting ducts of women at any age, with an average of 47 years, who complain of nipple discharge, nipple erosion, or a nodule. The lesion may recur if it is excised incompletely.

FNA findings. The smear pattern is similar to that of fibrocystic change, with marked ductal epithelial hyperplasia including numerous sheets of benign ductal epithelial cells and myoepithelial cell nuclei.

US features. The mass is oval, circumscribed, and hypoechoic and may have associated calcifications; however, US findings may suggest carcinoma in the presence of sclerosis.

Adenomas of Skin Adnexal Origin and Other Adenomas

Because these tumors originate in the skin, they can be suspected based on clinical and US evaluation. Ductal adenoma,

syringomatous adenoma, and pleomorphic adenoma (chondroid syringoma) are some of these tumors. Syringomatous adenoma affects the dermis of the nipple or the areolar region. Pleomorphic adenoma usually affects the periareolar area.

FNA findings. The specific diagnosis cannot always be made by FNA cytology; however, the tumors can be recognized as benign.

US features. US may show a stellate subareolar mass that may suggest malignancy. When the nodule is round, it may suggest adenoma; its association with the skin may suggest an adnexal origin.

Fibrocystic Change

This lesion represents the most common palpable lesion in women above the age of 30 years and is considered to represent an exaggerated hormonally mediated breast tissue response.

Histopathology. Histologically, there are duct dilatation, cysts, apocrine metaplasia, fibrosis, chronic inflammation, and varying degrees of ductal epithelial hyperplasia, which should be evaluated carefully (Fig. 8.32a).

FNA findings. Smears show sparse epithelial representation due to the presence of fibrosis. Ductal epithelial cells are arranged in flat, cohesive honeycomb sheets with round or oval nuclei and fine granular chromatin with small inconspicuous nucleoli. Stripped myoepithelial cell nuclei are present adherent to the epithelial cell sheets and in the smear background. Apocrine metaplastic cells are polygonal with ample granular cytoplasm and conspicuous nucleoli. Foam cells are often present in the background. Higher numbers of ductal epithelial cells with slight anisocytosis and anisonucleosis without atypia are seen in proliferative fibrocystic change, always accompanied by bipolar myoepithelial cell nuclei (Fig. 8.32b–d). However, no distinct cytomorphologic features can distinguish between nonproliferative and proliferative fibrocystic change without atypia.

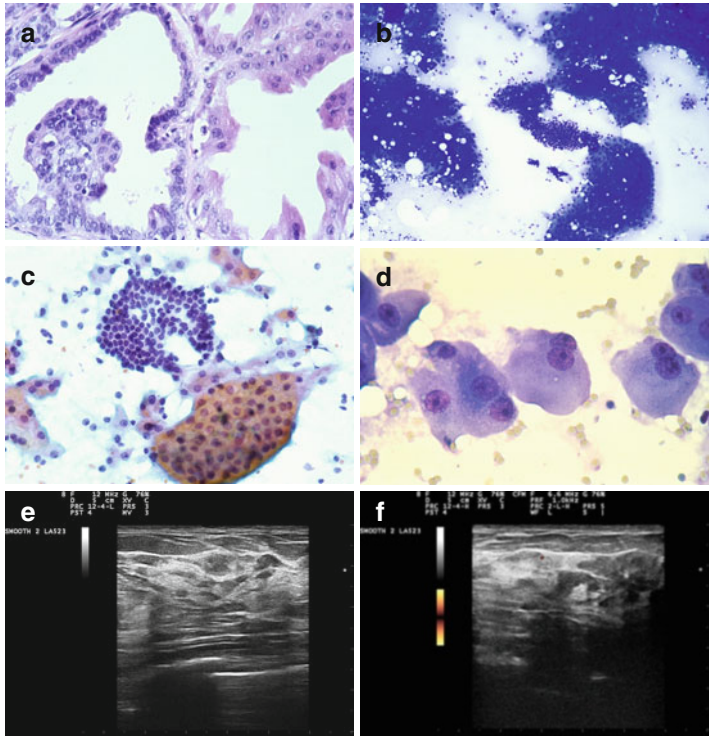

FIGURE 8.32 Fibrocystic change. Histology showing cystic dilatation, ductal epithelial hyperplasia, apocrine metaplasia, and lack of epithelial atypia (**a**). The FNA smear shows high cellularity (**b**) composed of sheets of ductal epithelial cells without atypia (**b**), apocrine metaplasia (**a**–**c**), stripped myoepithelial cell nuclei (**c**), and cystic background (**c**). Apocrine metaplastic cells with slight nuclear atypia may be seen (**d**). Ultrasound shows dense slightly hyperechoic tissue bands surrounding hypoechoic nodular areas (**e**) and minimal vascular flow by Doppler exam (**f**) (**a**, H&E stain, medium magnification; **b**, **d** Diff-Quik stain low and high magnification; **c**, Papanicolaou stain intermediate magnification)

US features. These lesions show slight hyperechogenicity due to fibrosis and small (<5 mm) hypoechoic or anechoic nodules (Fig. 8.32e, f).

Molecular Pathology Aspects of Epithelial Precancerous Breast Lesions

Despite the insight of molecular biology and genetics in breast tumor progression, our understanding still remains incomplete. The traditional model of linear progression from normal epithelium to hyperplasia to atypical hyperplasia to carcinoma secondary to cumulative genetic abnormalities seems to be too simple. The following concepts summarize some of the most relevant advances of molecular biology and genetics in the study of precancerous breast epithelial lesions:

1. Usual ductal hyperplasia (UDH) shares few genetic abnormalities with atypical ductal hyperplasia (ADH), ductal carcinoma in situ (DCIS), or invasive breast carcinoma.
2. ADH share many similarities with DCIS.
3. ADH and DCIS (all grades) appear to be clonal proliferations.
4. Low-grade DCIS and high-grade DCIS give place to different forms of invasive breast carcinoma that seem to be genetically different from one another, but similar along the low-grade or high-grade lines of development.
5. Lobular in situ and invasive carcinoma share genetic and molecular similarities with DCIS and invasive duct breast carcinoma.
6. Tumor microenvironment (myoepithelial cells and epithelial–stromal interactions) may be critical in the progression of these lesions to invasive breast carcinoma.

Intraductal Proliferative Lesions

These lesions originate in the terminal duct lobular unit and are confined to the mammary ductal–lobular system. They are associated with a variably increased risk for the development of breast carcinoma. They can be classified as columnar cell lesions (CCLs), usual ductal epithelial hyperplasia (UDH), and atypical ductal hyperplasia (ADH).

Columnar Cell Lesions (CCLs)

CCLs are not palpable and are often identified on screening mammography. Occasionally, the lesion is palpable, being part of nonproliferative or proliferative fibrocystic change.

Histopathology. The standardized histologic term of CCLs describes lesions showing dilated acini lined by columnar cells that frequently have apical cytoplasmic snouts. They are classified into 4 categories: columnar cell change (one or two cell layers thick) with or without atypia and columnar cell hyperplasia (cell stratification or tufting) with or without atypia. The lesions with atypia are categorized as "flat epithelial atypia" (well-developed arcades, bridges, or micropapillary structures are absent). The atypia is of low grade and monomorphic, and, for practical purposes, "flat" proliferations with high-grade nuclei should be regarded as DCIS. There is a strong association of these lesions with the coexistence of lobular carcinoma in situ (LCIS), atypical lobular hyperplasia (ALH), ADH, low-grade DCIS, and low-grade invasive carcinoma.

Immunoprofile. Flat epithelial atypia shows positive ER and negative HER2.

Molecular profile. Loss of 16q is the most frequent change found in flat epithelial atypia. Thus, these lesions are considered more likely to be precursors to ADH and low-grade DCIS.

FNA findings. CCLs are commonly identified in aspiration smears as small cohesive crowded aggregates of bland ductal cells with peripheral columnar cells, which may show apical snouts. Varying degrees of atypia may be seen. When there is coexistent fibrocystic change, the background may show sheets of ductal epithelial cells, myoepithelial cell nuclei, macrophages, and proteinaceous fluid.

Usual Ductal Hyperplasia (UDH)

The risk of UDH for the subsequent development of breast cancer is 1.5 times that of the reference population. Recent molecular data suggest that "flat epithelial atypia" is a more

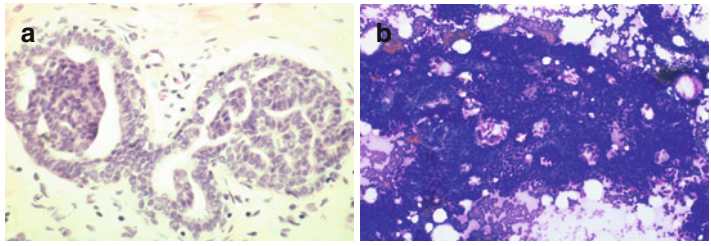

FIGURE 8.33 Ductal epithelial hyperplasia without atypia. Histologic section shows two ducts with hyperplasia of epithelial cells and streaming and fenestration of variable shape (**a**). The smears are cellular and show sheets of ductal epithelial cells with myoepithelial cell nuclei and fenestrations of variable shape (**b**) (**a**, H&E stain low magnification; **b**, Diff-Quik stain low magnification)

likely precursor to ADH and DCIS than is UDH. DCIS is recognized as a true precursor to invasive breast cancer. UDH is most common in the late premenopausal years. When it is associated with fibrosis, lesions may be palpable. Otherwise, they are usually found incidentally to other lesions.

Histopathology. Characteristically, there is a cohesive intraductal proliferation of benign epithelial cells with prominent cellular streaming, and there are peripherally distributed fenestrations of variable sizes (Fig. 8.33a).

Immunoprofile. Proliferating cells show immunohistochemical positivity for CK5, CK8, CK14, CK17, CK18, CK19, and S-100 protein. Myoepithelial markers are usually absent or only occasionally present. Positivity for ER is heterogeneous and variable; DCIS shows diffuse and strong ER positivity.

Molecular profile. No consistent genetic alterations have been found in UDH. The molecular and genetic alterations seen in ADH and DCIS are not found in UDH. The vast majority of these lesions are not thought to progress to invasive mammary carcinoma.

FNA findings. The cellularity is moderate to high, with fragments of ductal epithelial cells with numerous myoepithelial cells both adherent to the cell aggregates and in the smear background. Cells are mildly enlarged and crowded (Fig. 8.33b). Elements of fibrocystic change may be present in UDH.

Atypical Ductal Hyperplasia

The risk for subsequent development of breast cancer is 3–5 times that of the reference population.

Histopathology. This process involves the terminal duct lobular units with a proliferation of evenly placed monomorphic epithelial cells that lack the streaming, swirling, and overlapping of UDH. Cytomorphology is similar to that of low-grade DCIS; however, ADH is smaller (<2 mm or <2 ducts) and does not involve the full cross- section of the duct.

Immunoprofile. Cells are typically negative for high-molecular-weight keratins (CK 5/CK6, in contrast to UDH) and diffusely positive for ER. The proliferating cells express CK8, CK18, CK19, and sometimes CK7. The myoepithelial cells that line the tubulo-lobular terminal units express CK5, CK14, and CK17 simultaneously with myoepithelial cell markers.

Molecular profile. Common molecular and genetic alterations seen in ADH, low-grade DCIS, and invasive carcinomas include loss of heterozygosity in chromosome segments 16q, 17p, and 11q13, with losses at 16q being frequent.

FNA findings. The smears show high epithelial cellularity with cytologic and architectural atypia, with cellular and nuclear enlargement, loss of polarity, considerable cellular and nuclear overlapping, monomorphic atypical cells, nuclear hyperchomasia, prominent nucleoli, and variable numbers of myoepithelial cells (Fig. 8.34). However, myoepithelial cells may be absent, and variable numbers of single atypical epithelial cells may be seen in the background. A cribriform architecture and complex epithelial cell aggregates may be present. Thus, FNA cytology cannot reliably distinguish ADH from the non-comedo type of DCIS. Nevertheless, FNA

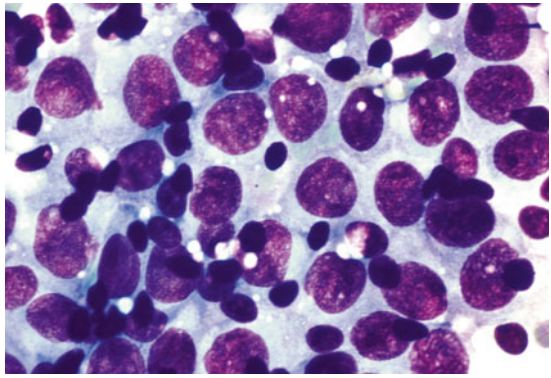

FIGURE 8.34 Ductal epithelial hyperplasia with atypia. Observe atypical epithelial cells and myoepithelial cell nuclei (Diff-Quik stain, high magnification)

cytology is useful in identifying these overlapping entities and prompts an excisional biopsy.

US features. The lesion is not US visible unless it is associated with other lesions such as papilloma, in which case it may be visible.

Papillary Lesions

Intraductal Papilloma

Intraductal papillomas often occur in women in the seventh and eighth decades of life. Solitary or central papilloma originates from the large ducts and usually develops in the areolar area. Multiple or peripheral papillomas develop from the terminal duct lobular units. They manifest as a bloody nipple discharge. A palpable lesion may be present particularly in central papillomas.

Histopathology. Papillomas show arborescent structures lined with myoepithelial and ductal epithelial cell layers which are supported by a fibrovascular stroma (Fig. 8.35a). The layer of myoepithelial cells may be inconspicuous, and immunostains may be needed to demonstrate its presence.

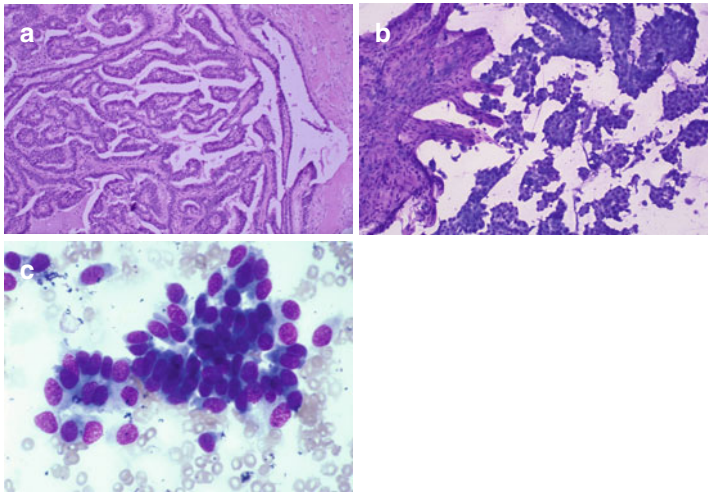

FIGURE 8.35 Intraductal papilloma. Histology shows arborescent papillary structures supported by fine fibrovascular cores and lined by columnar epithelial cells and inconspicuous myoepithelial cell layer (**a**). Papilloma may show focal sclerosis of the supporting stroma as seen in this FNA smear; sheets of lining cells are also present as well as columnar cells (**b**, **c**). The distinction from intracystic papillary carcinoma cannot be made with certainty on pure cytology grounds and excision of the lesion is needed (**a**, H&E stain low magnification; **b**, **c**, Diff-Quik stain low and high magnification)

The epithelial layer shows columnar or cuboidal cells and may show varying degrees of ductal epithelial hyperplasia as well as various types of metaplasia. Stromal fibrosis is commonly seen and may be prominent and extensive (sclerosing papillomas). ADH or DCIS may be seen particularly in peripheral papillomas. The risk of subsequent carcinoma increases to 7-fold or more in the presence of ADH or DCIS.

Immunoprofile. Tumors show positive stains for myoepithelial cells (smooth muscle myosin, calponin, p63), positive high-molecular-weight keratins (CK 5/CK6 and CK14), and patchy positivity for ER and PR.

Molecular profile. Benign papillomas are monoclonal proliferations. Activating point mutations of *PIK3CA*, *AKT1*, and *RAS* family genes are found in higher frequency than in papillary carcinomas.

FNA findings. The lesion and dilated duct may be visible by US and sampled by USG-FNA. Smears show a bloody background and papillary aggregates of cuboidal and columnar cells. Variable cellular aggregates supported by a fibrovascular stroma are seen (Fig. 8.35b, c). Larger lesions may show necrosis. The distinction from intracystic papillary carcinoma is not possible by FNA, and surgical excision is necessary.

US features. Lesions have smooth borders. They may show a dilated duct with a well-defined mural solid mass or a lobulated homogeneous solid and cystic lesion with a smooth wall. Adjacent ducts are often dilated. However, sonographic features of benign papillomas overlap with those of papillary carcinomas.

Intracystic (Encapsulated) Papillary Carcinoma

This tumor occurs in older women (average, 65 years old) who show a circumscribed round mass with or without nipple discharge. If the lesion is central, there may be nipple retraction and a palpable subareolar lobulated mass. Intracystic papillary carcinomas are noninvasive and have a good prognosis. A wide local resection is usually curative; however, associated DCIS in the surrounding tissue confers a higher risk for local recurrence.

Histopathology. Central papillary carcinomas are usually solitary, whereas peripheral lesions are commonly multiple. A thick fibrous capsule is present surrounding an arborescent proliferation of delicate fibrovascular stalks decorated by monomorphic cuboidal or columnar cells with low or intermediate nuclear grade and loss of the myoepithelial cell layer.

Immunoprofile. Tumors show negative myoepithelial cell markers (p63, calponin), negative high-molecular-weight

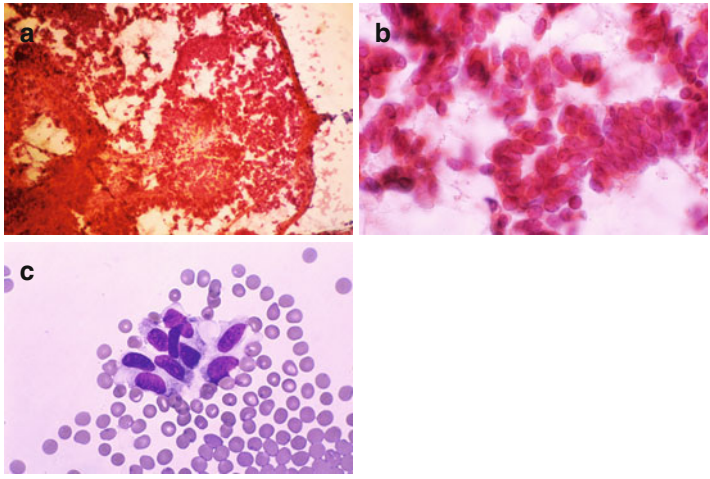

FIGURE 8.36 Intracystic papillary carcinoma. Cytologic features overlap with those of papilloma (**a**–**c**). The lesion should be excised and examined histologically (**a**, **b**, Papanicolaou stain low and high magnification; **c**, Diff-Quik stain high magnification)

keratins (CK5/CK6, CK14), and diffuse and strongly positive ER and PR stains.

Molecular profile. Patterns of gene copy-number aberrations and prevalence of *PIK3CA* mutations are similar to those of breast carcinoma of no special type.

FNA findings. The diagnosis of encapsulated papillary carcinoma cannot be made with certainty by FNA. Smears have variable cellularities, although moderate cellularity is more common, and show three-dimensional papillary structures with fibrovascular cores in a bloody background with scattered hemosiderin-laden macrophages. The decorating epithelial cells are often palisading the edges of aggregates and are bland appearing and of columnar shape (Fig. 8.36). Myoepithelial cells are not present; however, larger and more elongated stripped nuclei of malignant cells are identified and may be confused with myoepithelial cells. The differential diagnosis includes fibroadenoma (lacks fibrovascular cores and has myoepithelial cells) and papilloma (cannot be diagnosed by

FNA cytology). Thus, surgical excision is advised whenever a papillary neoplasm is diagnosed by FNA cytology.

US features. Sonographic features of benign papillomas overlap with those of papillary carcinomas and are more difficult to differentiate on US than are other breast neoplasms. Malignant papillary lesions frequently show a round or oval shape and have a circumscribed lobulated margin; these are findings suggestive of benign lesions in other breast neoplasms. A complex mass with irregular shape, a noncircumscribed margin, and a complex echo pattern is not uncommonly seen in papillary carcinomas, but their presence is not statistically significant. Irregular posterior acoustic enhancement may be present.

Solid Papillary Carcinoma

As the name implies, the solid component predominates, and no fluid collection is associated. This tumor is rare and peripherally located and occurs in postmenopausal women with a mean age in the seventh decade of life. The patients may have a palpable mass, and nipple discharge is seen in 25 % of patients.

Histopathology. The tumor shows multiple circumscribed cellular and expansile nests or nodules having thin and delicate fibrovascular cores. Of note, the tumor lacks an obvious papillary or cribriform architecture; however, the presence of thin fibrovascular cores is important for the diagnosis. Occasionally, the neoplastic growth shows a geographic or jigsaw pattern of epithelial islands. Cells are small and monomorphic, with polygonal or, less commonly, elongated shape, finely granular cytoplasm, and hyperchromatic nuclei. Mitoses are present, although rare. Neuroendocrine features are not uncommon.

Immunoprofile. Tumors are ER and PR positive and HER2 negative. Low-molecular-weight keratins 8 and 18 are positive. High-molecular-weight keratins 5/6 are negative. Partial or sometimes complete loss of myoepithelial cells may be seen at the periphery of the nests. Neuroendocrine markers (chromogranin A, synaptophysin, and CD56) are positive in 50 % of cases.

Molecular profile. Gene expression confirms the *luminal* phenotype (Table 8.2).

FNA findings. Smears are cellular and show compact fibrovascular structures decorated with columnar or elongated/spindle cells. Variable amounts of intracellular or extracellular mucin may be seen as well as neuroendocrine features.

US features. Solid papillary carcinomas may be associated with mucin production, which is not found in benign papillomas; this might be why posterior acoustic enhancement may be a characteristic finding of papillary carcinomas when present. Noninvasive papillary carcinomas more frequently show a circumscribed margin than do invasive papillary carcinomas. Differences in the shape, orientation, echo pattern, lesion boundary, posterior acoustic features, calcification, and duct dilatation are not statistically significant. High-resolution US may show the papillary features. Microcalcifications may be seen.

Molecular Pathology and Gene Expression Profile of Breast Carcinoma

Breast cancer is a heterogeneous disease with variable histopathologies, metastatic potential, and a variable prognosis. The histopathologic classification alone has limited value, whereas new markers seem to be of greater clinical relevance with higher prognostic value and better predictive therapeutic response. Thus, pathologic examination and immunohistochemical results for ER, PR, and HER2 overexpression are standard practice to guide the therapeutic modality. Breast cancer is also remarkably heterogeneous at the genomic level, and there is a correlation between the patterns of gene aberrations, histologic grade, and ER expression in breast carcinoma, including DCIS.

Grade 1 invasive carcinomas of no special type are usually diploid or near diploid and harbor recurrent deletions of 16q (>85 %), gains of 1q (60 %), and gains of 16p (40 %). Grade 3 invasive carcinomas are heterogeneous and often show aneuploidy, and deletions of 16q (found in<30 %) are almost

TABLE 8.2 Immunohistochemical classification of breast cancer

IHC classification	Risk		Therapy response			
	Recurrence	**Metastasis**	**Adjuvant**	**Hormonal**	**Biological**	**Traditional**
Luminal A	Low	Low	No	Yes	No	No
Luminal B	Intermediate	Intermediate	Yes	Yes	Yes	Yes
Luminal C	High	High	Yes	Yes	Yes HER2+	Yes
Basal TN	High	High	Yes	No	No	Yes
Basal no TN	Intermediate	Intermediate	Yes	Yes ER+	Yes HER2+	Yes
HER2 positive	High	High	Yes	No	Yes	Yes
Normal-like	Low	Low	No	Yes	No	No

Abbreviations: *IHC* immunohistochemical, *TN* triple negative

restricted to ER-negative tumors. Approximately 50 % of grade 3 ER-positive cancers harbor the genetic pattern found in grade 1 tumors (deletion of 16q and gain of 1q), suggesting that progression from low- to high-grade and invasive carcinoma only applies to the ER-positive tumors. Molecular evidence suggests that grade 2 tumors are the end stage of grade 1 tumors. Of note, lobular neoplasia and invasive lobular carcinoma harbor similar findings (deletion of 16q, gains of 1q and 16p).

Genetically distinct subgroups of invasive breast carcinoma have been described based on gene expression profiling. These subtypes appear to be clinically important and reflect the phenotype of the underlying cell of origin, and they are luminal (A, B, or C hybrid), HER2 positive, basal-like ("triple negative" and "no triple negative"), and normal breast-like. The methodology for defining these subtypes may not be fully accessible by all laboratories; thus, comparable immunohistochemistry panels have been described as being equivalent to luminal A, luminal B, HER2-positive, basal-like, and normal breast-like genomic groups (Table 8.2).

Luminal Subtype

Luminal-subtype carcinoma expresses a cancer gene profile similar to that of breast duct epithelial cells. All luminal carcinomas show the expression of genes related to hormonal receptors. *Luminal A subtype* tumors comprise 55 % of cancers and are commonly of histologic grade 1 and ER positive HER2 negative. CK7, CK8, CK18, and CK19 are positive and CK5, CK14, and CK17 are negative (Fig. 8.37). These cancers have a good prognosis and respond to antiestrogen therapy. Most cases are ductal mucinous, tubular, cribriform, and papillary, as well as classic and pleomorphic lobular carcinoma. *Luminal B subtype* tumors comprise 15 % of carcinomas and are of histologic grade 2 or 3 (ductal and lobular), positive for CK7, CK8, CK18, and CK19, whereas there is no immunoreactivity to CK5, CK14, and CK17. Furthermore, the immunostainins for ER, PR, and HER2 are always positive (Fig. 8.38). The proliferation index is higher and prognosis is poorer than that for luminal A carcinoma. *Luminal C or hybrid* tumors are rare and show immunopositive staining

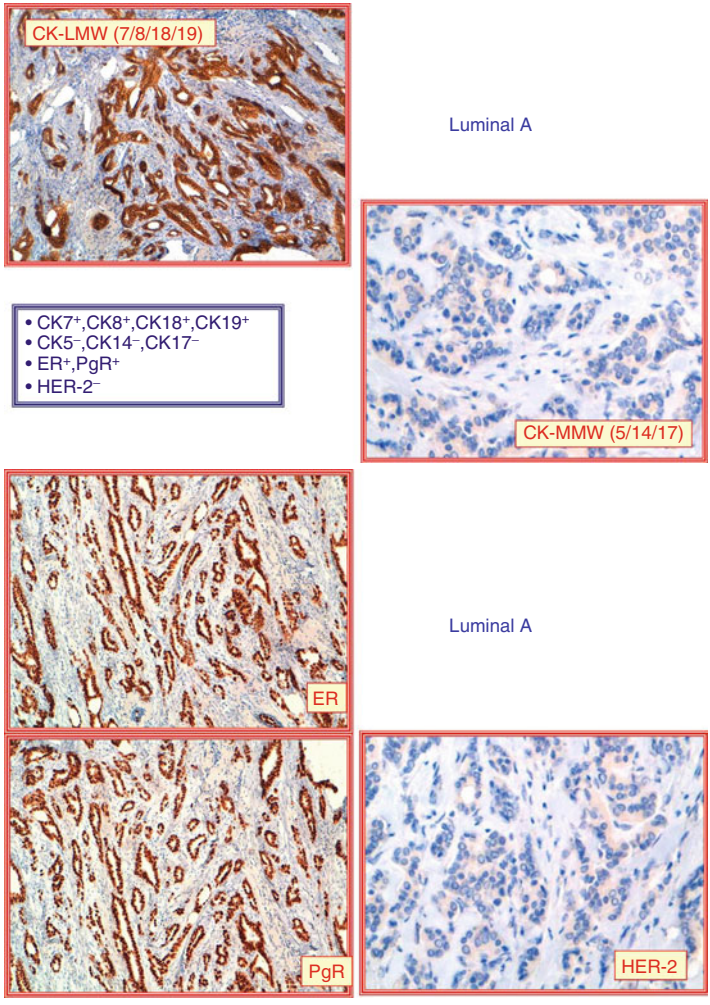

FIGURE 8.37 Breast carcinoma, luminal A subtype. Immunohistochemistry

for CK7, CK8, CK18, and CK19 and absence of CK5, CK14, and CK17. One of the hormone receptors (ER or PR) and the HER2 protein can be absent (Fig. 8.39). This immunophenotype is expressed in about 10 % of breast carcinomas

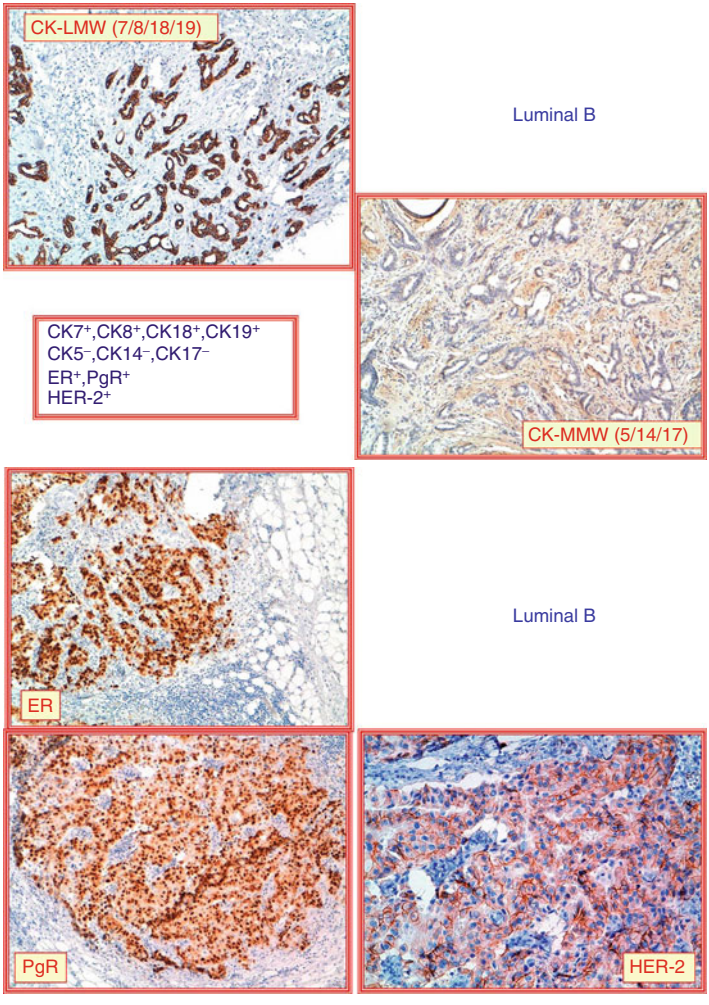

FIGURE 8.38 Breast carcinoma, luminal B subtype. Immunohistochemistry

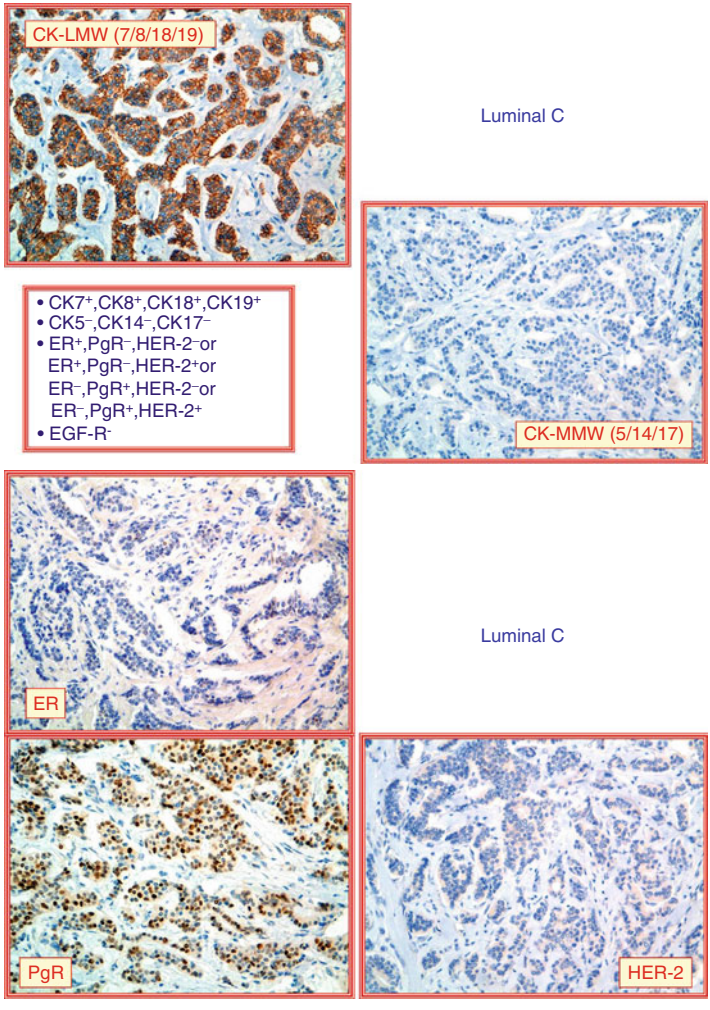

FIGURE 8.39 Breast carcinoma, luminal C subtype. Immunohistochemistry

with morphologic aspects of moderately differentiated ductal carcinoma of no special type or lobular carcinomas, including the pleomorphic variant. Likely luminal B and C cancers are part of the spectrum of ER-positive cancers and have a more aggressive phenotype and worse prognosis than the luminal A subtype. Thus, the ER, PR, HER2, and Ki-67 proliferation index are important for identifying this subtype. The response to antiestrogen therapy may be partial.

The ER-negative cluster encompasses HER-positive, basal-like, and normal breast-like cancers.

HER2-Positive Subtype

This carcinoma comprises approximately 4–5 % of cases of breast carcinoma. These tumors show amplification of the *HER2* gene that is localized on chromosome 17 and are ER negative; the ER-positive tumors belong to the luminal B subtype. Low-molecular-weight keratins (CK7, CK8, CK18, and CK19) are positive and EGFR is variable (Fig. 8.40). This subtype is often of histologic grade 3, may show apocrine differentiation, may have lymphoid infiltrates, and can potentially be aggressive, with increased risk for local recurrence or metastatic disease. HER2 overexpression/amplification predicts a favorable response of these tumors to treatment with the monoclonal antibody trastuzumab (Herceptin) or other HER2 antagonists as well as to anthracycline-based chemotherapy.

Basal-Like Subtype

These tumors comprise approximately 15 % of cases of breast cancer and have a broad immunohistochemical profile. Some authors include the so-called "triple-negative" tumors in this subtype (Fig. 8.41); others include tumors showing at least one positive basal cytokeratin antibody (CK 5/CK6, CK 14, CK 17), irrespective of the ER or HER2 positivity; and others define this subtype as being ER-, HER1-/EGFR-, HER2-, and CK5-/CK6-positive tumors (Fig. 8.42). Approximately 20 % are ER, PR, or HER2 positive. The positivity with "basal markers" (CK5/CK6, CK 14, CK17, EGFR, P-cadherin, p63,

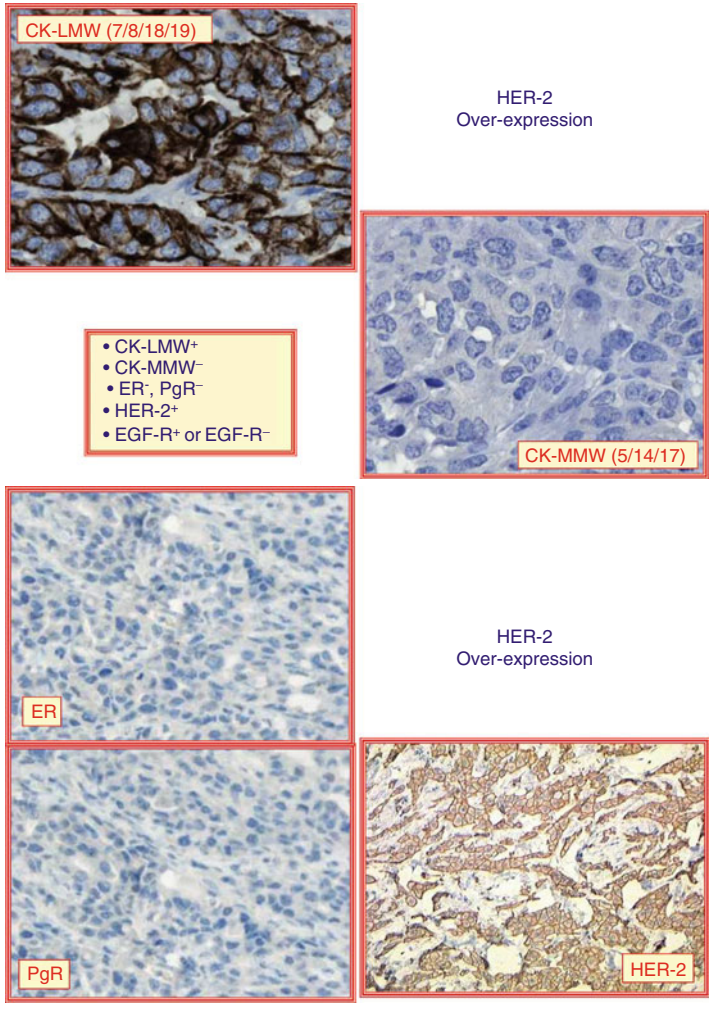

FIGURE 8.40 Breast carcinoma, HER2-positive subtype. Immunohistochemistry

laminin, and c-Kit) is variable as well as with caveolins 1 and 2, nestin, and CD44. "Luminal cytokeratins" (CK 8/CK18 and 19) and myoepithelial cell markers (p63, SMA, smooth muscle myosin heavy chain) may be positive. These tumors are

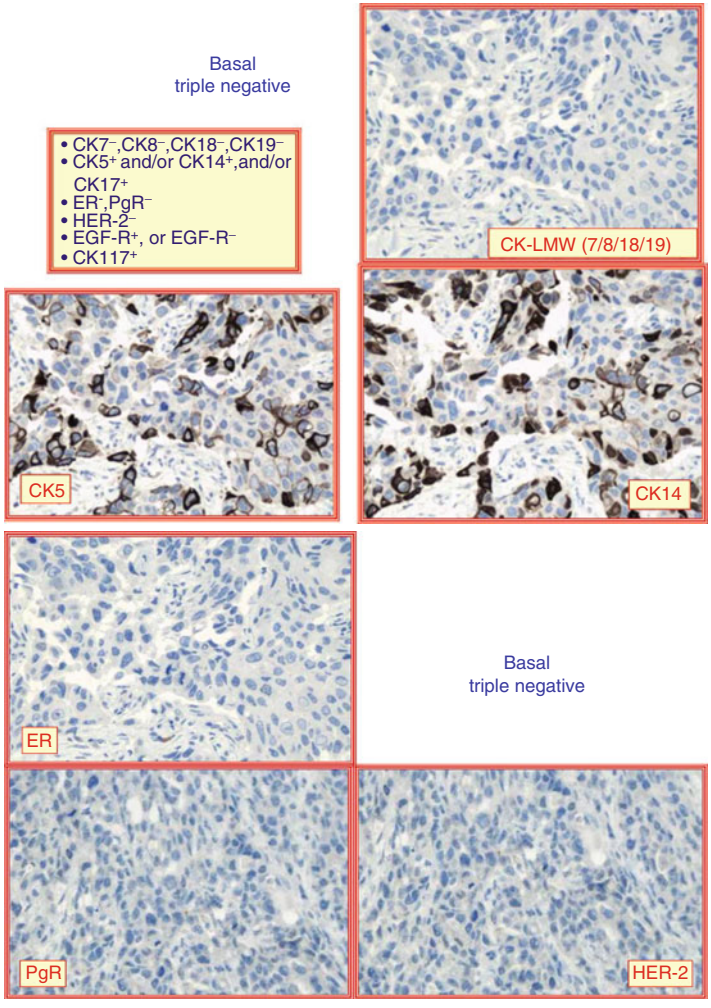

Figure 8.41 Breast carcinoma, basal triple negative subtype. Immunohistochemistry

common in younger Hispanic women, frequently carry the germline *BRCA1* gene mutation, are grade 3 with a ductal/no specific type morphology, and do not respond to HER2-targeted or antiestrogen therapy. Most BRCA1 cancers lack

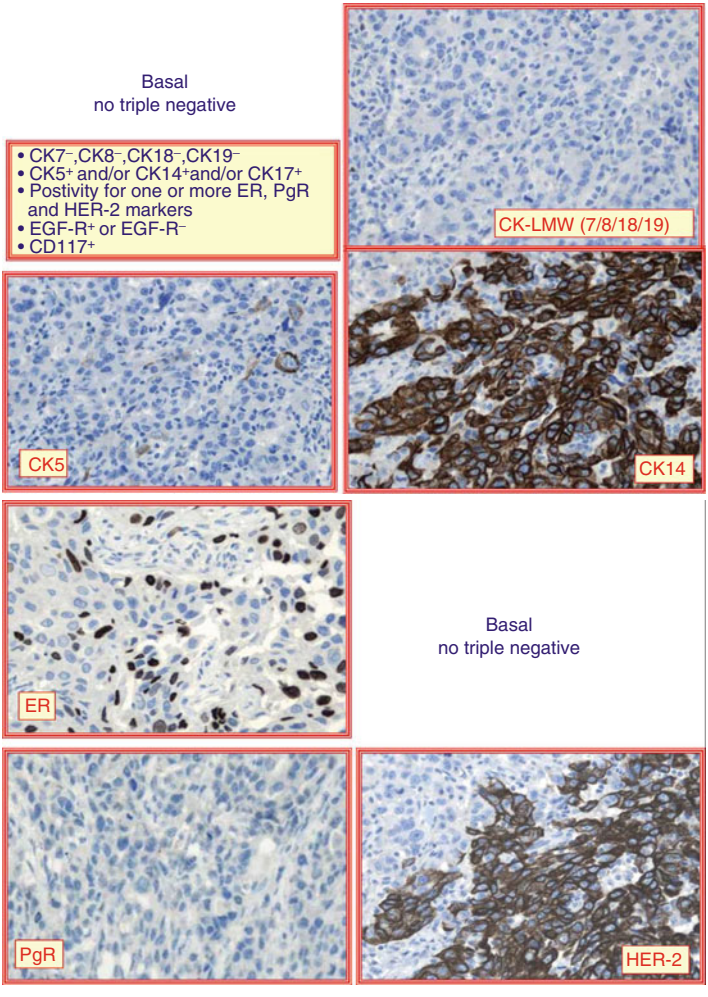

FIGURE 8.42 Breast carcinoma, basal no triple negative subtype. Immunohistochemistry

ER, PR, and HER2 expression and express basal markers (CK5/CK6, CK14, CK17, EGFR, and P-cadherin) in 80 % of cases. Carcinoma with medullary features, metaplastic carcinoma, secretory carcinoma, and adenoid cystic carcinoma

tend to have a basal-like phenotype. The Ki-67 proliferation index is high, and some of these tumors have an aggressive clinical course and a poor prognosis. These tumors often have benign-appearing US features, i.e., well-defined borders, an oval shape, and no or very little posterior acoustic shadowing. BRCA2 cancers comprise often invasive lobular, pleomorphic lobular, tubular, and cribriform carcinoma types. Germline mutations of *BRCA1* and *BRCA2* genes are seen in 5 % of breast carcinomas. If the tumor is ER negative and "basal" markers positive, BRCA1 should be sequenced.

Normal Breast-Like Subtype

This carcinoma was not considered as a distinct subtype, because of the strong expression of non-epithelial genes, mainly of adipose tissue, together with genes of basal and luminal ductal epithelium present in the normal breast and fibroadenomas. Therefore, these carcinomas were initially considered as unclassifiable luminal types. The use of immunohistochemical staining with molecular gene expression "surrogate" markers has shown that this group exhibits an immunophenotype similar to that of tubulo-lobular terminal units of normal breast with variable immunostainings for cytokeratins, ER and/or PR, and negativity for HER2. A characteristic is the expression of adipose tissue antigen, i.e., adipose acid synthetase (NSAIDs, fat acid synthase) (Fig. 8.43). At the moment, there are not many publications about the correlation of the immunophenotype of this group of carcinomas and the histopathology. However, preliminary studies suggest that this group comprises about 5–6 % of breast cancer cases and that the usual histomorphology is that of invasive lobular carcinoma.

Precursor Lesions

Ductal Carcinoma in Situ

Ductal carcinoma in situ (DCIS) represents 20–25 % of newly diagnosed breast cancers in the United States. DCIS

is uncommon before the age of 40 years and the incidence rises progressively to a peak at ages of 65–69 years. Age, race, family history and genetics, nulliparity, late age at first birth, late menopause, breast density, body mass index, and use of

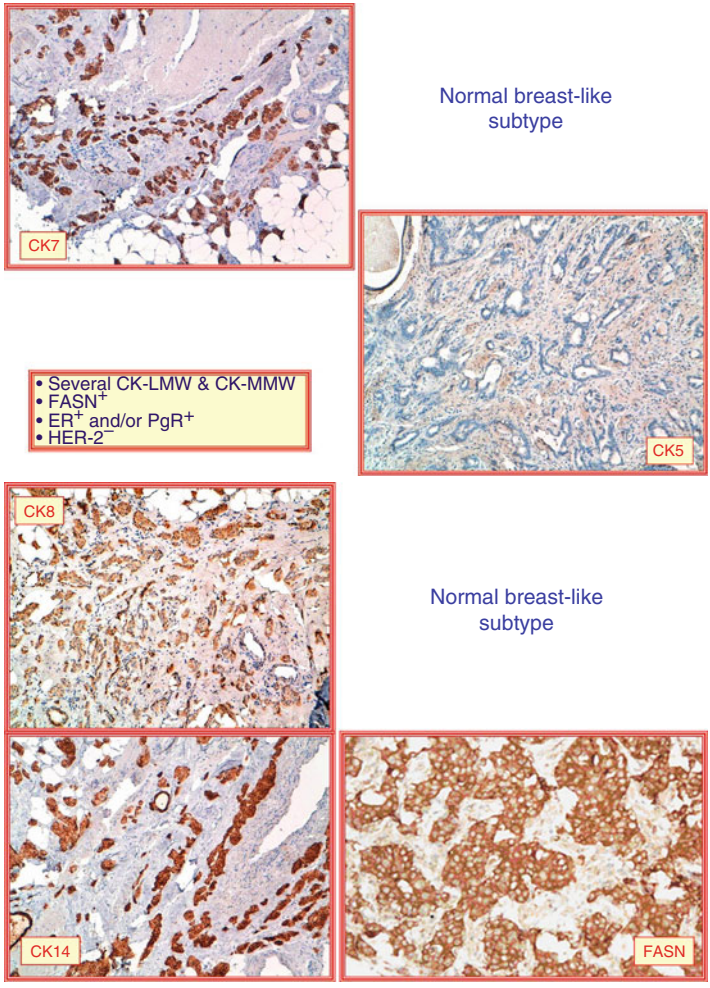

FIGURE 8.43 Breast carcinoma, normal breast-like subtype. Immunohistochemistry

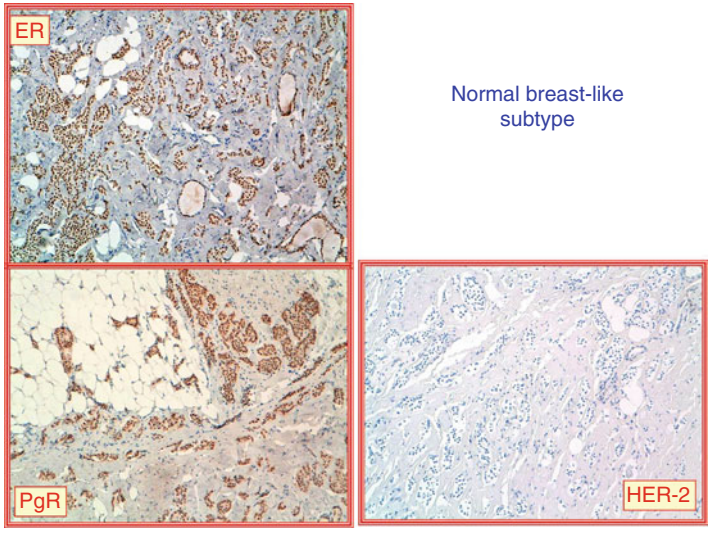

FIGURE 8.43 (continued)

hormone replacement therapy have been associated with an increased risk for DCIS. This lesion is often unilateral, although 22 % develop DCIS or invasive carcinoma in the contralateral breast. The risk of DCIS for subsequent development of breast cancer is 8–10 times that of the reference population. DCIS is a precursor to invasive breast carcinoma. Usually, 80–90 % of DCIS are detected mammographically by a finding of calcifications; however, occasionally coalescent areas of high-grade DCIS may form a firm palpable mass. Prognostic factors for local recurrence or progression to invasive carcinoma include tumor size, nuclear grade, comedo necrosis, and resection margins status.

Histopathology. The neoplastic proliferation develops in the terminal duct lobular unit and progresses distally in the main duct and peripherally toward the adjacent branches of a given duct system segment. The rare lesions that develop in larger ducts and lactiferous ducts close to the nipple progress toward the nipple, resulting in Paget disease and nipple discharge. Current trend suggests that grading of DCIS

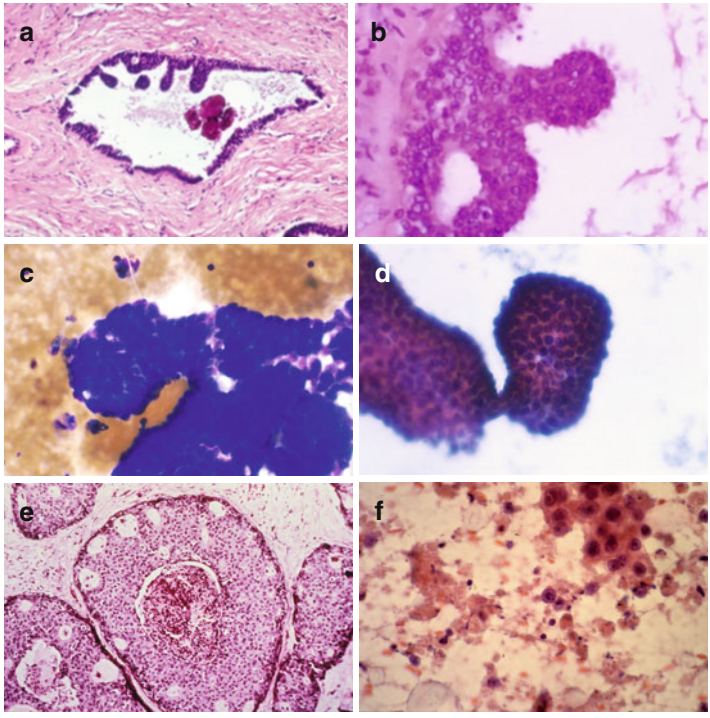

FIGURE 8.44 Ductal carcinoma in situ. Histology of non-comedo-type DCIS shows bland-appearing neoplastic ductal cells arranged as micropapillary projections and rigid arches; rare microcalcifications are also seen (**a**, **b**). FNA smears show complex aggregates of bland-appearing cells with slight anisonucleosis and anisocytosis (**c**, **d**). Histology of comedo-type ductal carcinoma in situ showing central necrosis surrounded by high-grade tumor cells confined to the duct (**e**). Cytology smear shows high-grade tumor cells with prominent nucleoli and necrotic background (**f**) (**a**, **b**, **e** H&E stain low and high magnifications; **c**, Diff-Quik stain high magnification; **d**, **f** Papanicolaou stain high magnification)

should be based primarily on nuclear features rather than on the architectural (solid, comedo, cribriform, micropapillary, or papillary) pattern (Fig. 8.44a, b, e). Thus, DCIS is divided into low, intermediate, and high grade, although nuclear

heterogeneity may occur in the same lesion. Cell polarity, small to intermediate nuclear size, inconspicuous nucleoli, and rare mitoses are features of low-grade to intermediate-grade DCIS; lack of cell polarity, nuclear pleomorphism, mitoses, and prominent nucleoli are seen in high-grade DCIS. Apocrine, clear, and neuroendocrine types of DCIS may be seen occasionally, the latter often associated with papillary areas. Intracystic (encapsulated) papillary carcinoma is a variant of papillary carcinoma that occurs in older women and is considered as an in situ tumor by some.

Immunoprofile. For both ER and PR immunostain positivity in tissue sections is required ≥1 % of cells showing nuclear staining. High-grade DCIS expresses ER less frequently than does low-grade DCIS. HER2 overexpression is more common in high-grade DCIS (50–60 % of cases) than in invasive breast carcinoma (20 % of cases). Likewise, the rate of luminal B phenotype is significantly higher in DCIS than in invasive carcinomas. Some high-grade DCIS express a "basal-like" (Table 8.2) immunophenotype (CK5 + and CK14 +) in varying degrees likely representing the precursor of basal-like invasive carcinoma. High-grade DCIS frequently has a luminal B, HER2, or "basal-like" including "triple-negative" immunophenotype (Table 8.2). No markers can distinguish between low-grade DCIS and ADH.

Molecular profile. Recent molecular and genetic results suggest that low-grade and high-grade DCIS are distinct disorders. Low-grade DCIS is usually positive for ER, PR, E-cadherin, Bcl-2, and cyclin D1 and negative for HER2. They are also diploid/near diploid, with deletion of 16q (>70 %), gain of 1q (>70 %), and lack of expression of "basal-like" markers (luminal A > B). High-grade DCIS is more heterogeneous and often shows amplifications at 17q12 and 11q13 and is frequently aneuploid. This immunoprofile and genetic features, with the exception of E-cadherin that is negative, are similar to those seen in ADH and ALH/LCIS. Again, low-grade and high-grade DCIS are direct precursor lesions of invasive breast carcinoma and appear to have distinct and separate pathways of preinvasive epithelial neoplasia.

FNA findings. The comedo type of DCIS yields cellular smears with loose aggregates and single large malignant cells with coarse chromatin, large nucleoli, mitoses, and a necrotic background. In contrast, the non-comedo type of DCIS shows medium-sized bland-appearing uniform cells. Complex flat cell aggregates and well-defined punched-out lumens with or without metachromatic stroma are seen in cribriform DCIS. Numerous small papillary fragments composed of small cells and having a slender base and bulbous ends with smooth contours are seen in the micropapillary DCIS. No myoepithelial cell nuclei are present (Fig. 8.44c, d, f). Histologic confirmation is needed for distinguishing DCIS from invasive ductal carcinoma.

US features. DCIS can rarely be a mass with circumscribed, indistinct, or spiculated borders; the mass may be taller than wide and hypoechoic. However, most lesions are often microscopic and, US examination may be normal or calcifications may be seen in dilated ducts. DCIS of low grade may be visible and lack calcification or obvious US features of malignancy, as seen in invasive cancers. We should remember that DCIS may be associated with benign or proliferative lesions, and the US may be non-revealing or show the underlying benign condition, i.e., a radial scar.

Lobular Neoplasia (LN)

The term LN encompasses atypical lobular hyperplasia (ALH) and lobular carcinoma in situ (LCIS), lesions that develop in the terminal duct lobular unit and do not involve the terminal ducts (Fig. 8.45). The distinction between ALH and LCIS is based on the extent of lobular units involved. The average age for diagnosis is 49 years, and there are no specific or grossly recognizable clinical features. The LN is usually a microscopic incidental finding in breast tissue removed for other reasons. The lesion is often bilateral and multicentric and carries an increased risk for developing invasive lobular carcinoma (4–5 times for ALH and 8–10 times for LCIS).

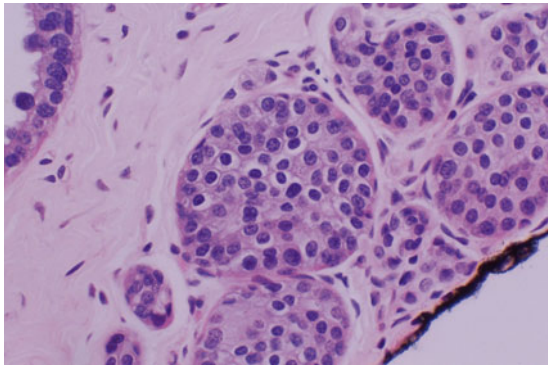

FIGURE 8.45 Lobular carcinoma in situ. The lobules are distended and filled with uniform and bland-appearing cuboidal cells with eccentrically placed nuclei (H&E stain, intermediate magnification)

Histopathology. There is distention of lobules by a proliferation of round cells with eccentric nuclei. Cells often have an intracytoplasmic mucin vacuole conferring a targetoid appearance. Cells are uniform, are of variable sizes, and lack pleomorphism. Necrosis, mitoses, cell pleomorphism, nucleoli, and large cell size are seen in pleomorphic LCIS, which may rarely show apocrine features.

Immunoprofile. Most cases of LN are positive for ER and PR and negative for both HER2 and for the cell adhesion molecule E-cadherin. Pleomorphic LCIS is also negative for E-cadherin and likely negative for ER and positive for HER2 and has a high proliferation index. The immunoprofile and genetic features are similar to those seen in ADH and low-grade DCIS, with the exception of E-cadherin, which is positive. Immunohistochemical stains are also positive for CK7, CK8, CK18, CK19, CK14, and/or CK17.

Molecular profile. ALH and LCIS are usually diploid/near diploid, show deletion of 16q (>70 %) and gain of 1q (>70 %), and lack of expression of "basal-like" markers (luminal A > B). Loss of heterozygosity at loci frequently seen in invasive lobular carcinoma, i.e., 11q13, 16q, 17p, and 17q, has been reported in LN. Pleomorphic LCIS has greater genomic

instability and reflects the more aggressive features of this tumor compared with LN.

FNA findings. Smears have low to moderate cellularity and show single monomorphous isolated cells with plasmacytoid features, round eccentric nuclei, powdery chromatin, and inconspicuous nucleoli. Except for the smear cellularity in adequate samples, the cytologic findings of LCIS and invasive lobular carcinoma overlap. Pleomorphic LCIS shows cellular pleomorphism, necrosis, mitosis, and large cells similar to the smear pattern of comedo-type DCIS.

US features. ALH and LCIS have no distinct radiologic features. However, when LN involves sclerosing adenosis or fibroadenoma, a mass lesion may be visible on US evaluation; otherwise, US evaluation is normal.

Invasive Breast Cancer

Breast carcinomas with a favorable prognosis include papillary carcinoma, tubular carcinoma, cribriform carcinoma, colloid carcinoma, adenoid cystic carcinoma, medullary carcinoma, and secretory carcinoma. Unfavorable breast carcinomas include metaplastic carcinoma, pleomorphic lobular carcinoma, inflammatory carcinoma, and sarcomas. Therefore, it is important to subclassify the type of mammary carcinoma on FNA samples.

Ductal Carcinoma of No Special Type

This is a large and heterogeneous group of breast cancers that do not have sufficient histologic characteristics to be specifically classified, i.e., lobular carcinoma, medullary carcinoma, and tubular carcinoma. This group comprises 50–75 % of breast cancers and is rare before the age of 40 years. Grossly, the tumors have a stellate or nodular appearance, and the size ranges between <1 cm and >10 cm.

Histopathology. The tissue diagnosis is based on exclusion of known types of breast carcinoma. Thus, the histologic pattern is highly variable including, solid, syncytial, glandular,

tubular, or trabecular, with variable amounts of desmoplastic stroma. The cellular appearance is also variable, and the nuclei range from uniform to highly pleomorphic with multiple and prominent nucleoli. Mitoses are also variable. Mixed, pleomorphic, osteoclast-like, choriocarcinomatous, and melanotic are morphologic variants encountered. Papillary, neuroendocrine, and signet ring cell differentiation may be present (Fig. 8.46a–c).

Immunoprofile. Between 70 and 80 % are ER + (Fig. 8.46d).

Molecular profile. Cases of familial breast cancers associated with mutations in the *BRCA1* and *BRCA2* genes are commonly breast carcinomas of no special type.

FNA findings. Smears are highly cellular with numerous cell groups and single cells. Cell groups are arranged in crowded groups, gland-like, and in syncytial patterns with loss of polarity and nuclear molding. Cells are large with a high nuclear to cytoplasmic ratio, irregular and thickened nuclear contours, coarsely granular chromatin, and nucleoli of variable sizes. The cytoplasm may be finely to coarsely vacuolated. Tumor necrosis may be present, and no myoepithelial cells are seen in the background. Occasionally, and particularly in elderly women, cells may be uniform

FIGURE 8.46 Ductal carcinoma of no special type. Histologic appearance of carcinomas of low- (**a**), intermediate- (**b**), and high- (**c**) histologic grade, all surrounded by desmoplastic stroma. Most carcinomas are ER positive (**d**). Papillary differentiation may be present and these cases should not be considered as papillary carcinoma (**e**). Cytologic features include cell dissociation, variable cellular pleomorphism, anisonucleosis, and variably prominent nucleoli (**f**, **g**, low grade; **h**, intermediate grade; **i**, **j**, high grade). Papillary fronds with wide fibrovascular stromal core may be seen in cases of papillary differentiation (**k**). Corresponding ultrasound features are shown in figures **l**, **m** (low grade), **n** (intermediate grade), and **o**, **p** (high grade) (**a**–**c**, **e** H&E stain low to intermediate magnification; **d**, positive immunoperoxidase stain for estrogen receptor; **f**, **h**–**k** Diff-Quik stain high magnification; **g**, Papanicolaou stain high magnification)

and plasmacytoid, resembling those of lobular carcinoma. Poorly differentiated mammary carcinomas show bizarre and multinucleated tumor cells (Fig. 8.46e–k).

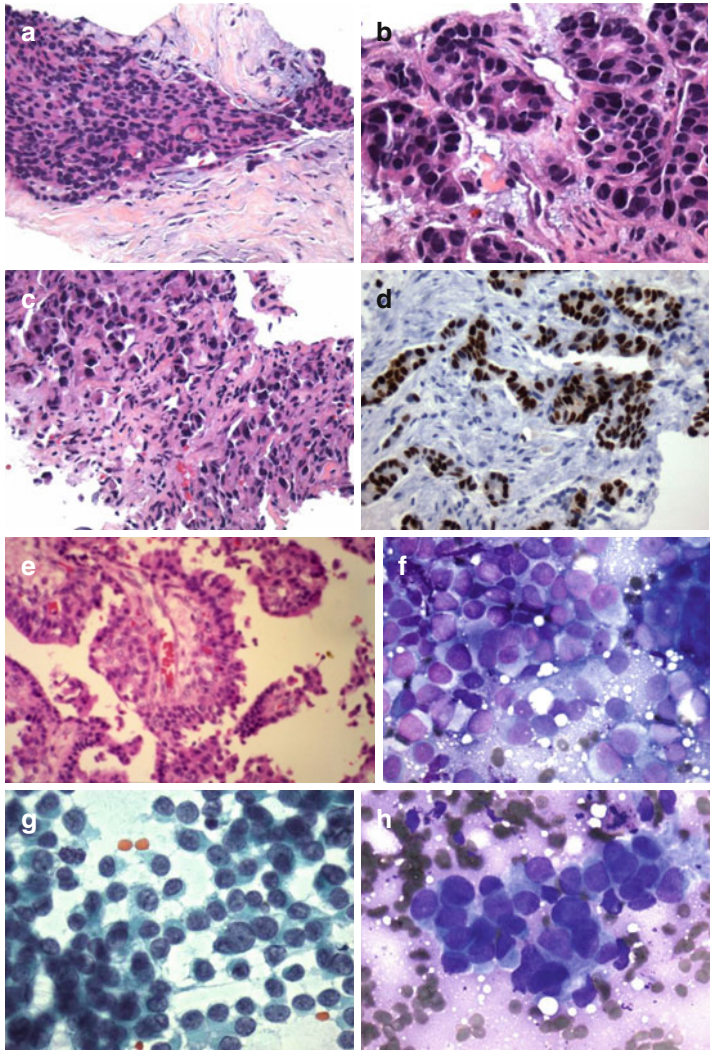

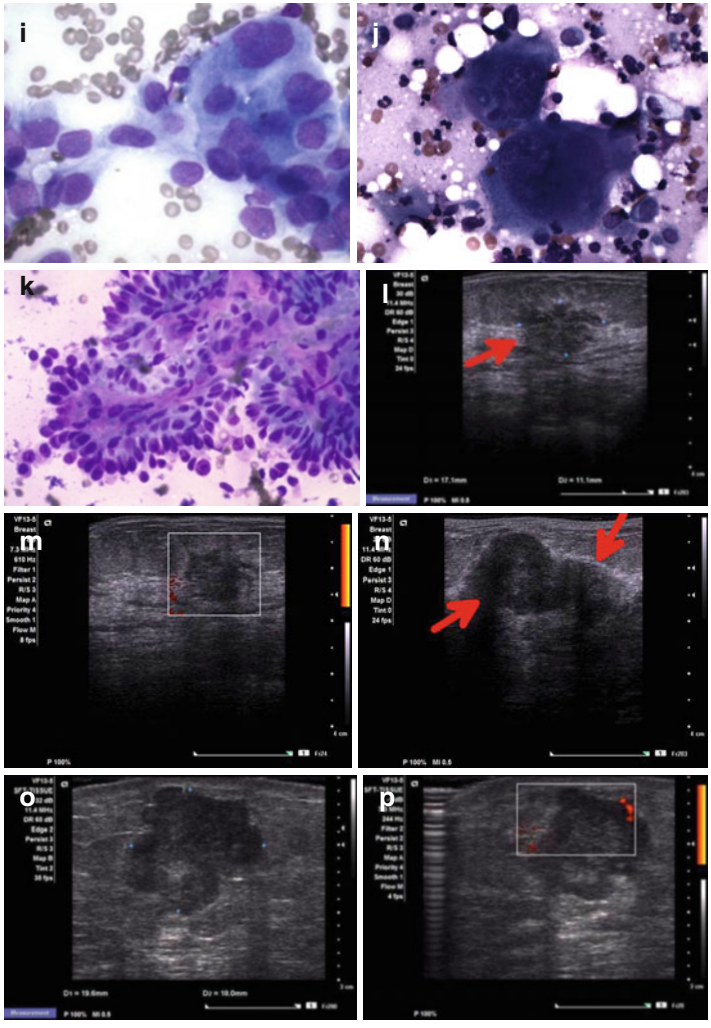

FIGURE 8.46 (continued)

US features. The mass is irregular, vertically oriented, and hypoechoic with indistinct spiculated and angular margins, microlobulation, and posterior acoustic shadowing as in low-grade invasive carcinomas. The mass can be round, oval,

lobular, or irregular with marked hypoechogenicity and variable posterior acoustic enhancement, as in high-grade carcinomas. When skin is secondarily involved, there is disruption of the linear echogenicity of the deep dermal layer. Rarely, advanced breast carcinoma extends to the nipple to cause ulceration; when this occurs, a hypoechoic mass is seen in the subareolar area, with angular and spiculated borders and posterior acoustic shadowing (Fig. 8.46l–p).

Lobular Carcinoma

Lobular carcinoma is often bilateral and multicentric and accounts for approximately 5–15 % of all invasive breast carcinomas. Women have an ill-defined palpable mass, and the mean age at diagnosis is 60 years. The prognosis in the first 10 years is similar to or better than that of invasive carcinoma of no special type; however, the incidence of distant metastases, recurrence, and mortality is higher in invasive lobular carcinoma than in "no specific type." Common sites of metastases include bone, the GI tract, uterus, meninges, ovaries, and serosal surfaces, in contrast to the lung, the most common site for invasive carcinoma of no specific type. Pleomorphic lobular carcinoma is a more aggressive tumor than the classic invasive lobular carcinoma; the prognosis is worse than that of low-grade ductal carcinoma and similar to that of high-grade ductal carcinoma.

Histopathology. The classic lobular carcinoma shows infiltrating small tumor cells that lack cell cohesion and appear individually scattered and characteristically arranged in a single-line pattern and arranged concentrically around ducts in a targetoid pattern. Cells have smooth or slightly irregular round or ovoid nuclei. There is an intense desmoplastic fibrous response that is in great part responsible for the sparse cellularity seen in FNA samples. Histologic variants include classic, solid, alveolar, pleomorphic, tubulo-lobular, and mixed. Focal apocrine or prominent signet ring cell differentiation may be present (Fig. 8.47a–c).

Immunoprofile. The expression of ER is high, although variable, depending on the variant. The classic and alveolar variants are almost invariably ER+; in contrast, 10 % of the

pleomorphic variant, which has an aggressive phenotype, is ER+. PR+ is seen in 60–70 % of classic and pleomorphic variants. HER2 amplification and overexpression are rare

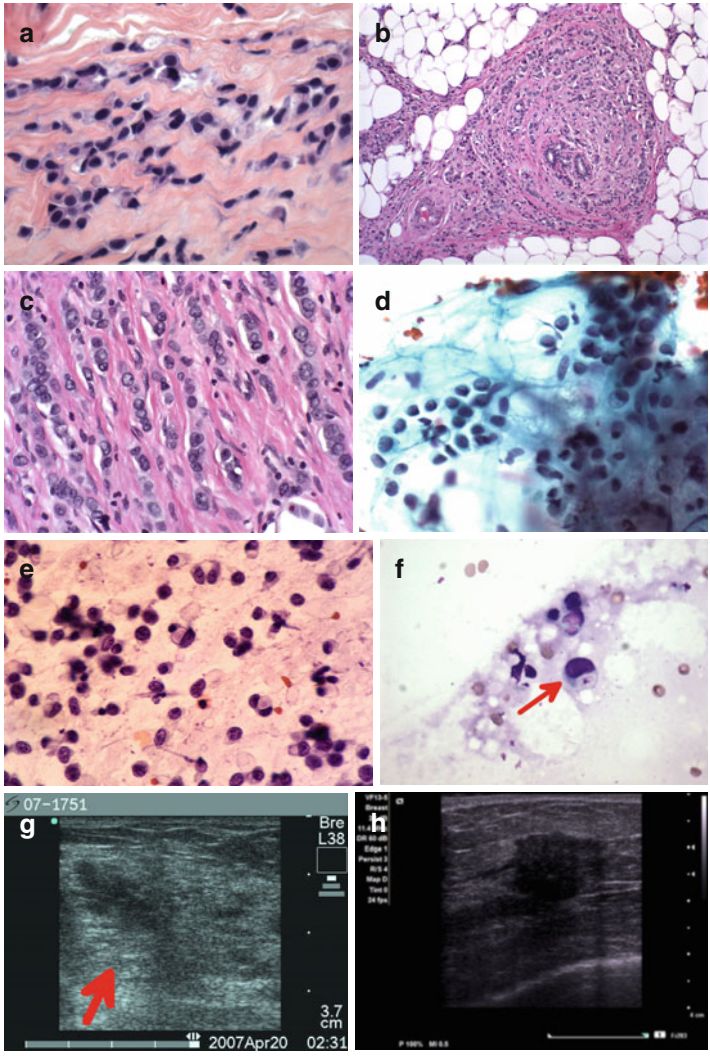

in infiltrating lobular carcinoma, although present in some pleomorphic variant cases. The proliferative index is low. Expression of p53 and basal markers (CK14, CK5/CK6) is rare. There is intense cytoplasmic immunostaining for catenin p120 in cases of lobular carcinoma, whereas ductal carcinoma and normal ducts show a linear membranous pattern. The immunostaining for p120, therefore, appears useful for confirmation of cases of dubious negativity for E-cadherin and particularly in cases of mixed ductal/lobular carcinoma. Pleomorphic variant with apocrine differentiation shows gross cystic disease fluid protein-15 (GCDFP-15) positivity in 40 % of cases. Furthermore, the pleomorphic variant may be a peculiar type of breast cancer with mixed ductal and lobular clinical, pathological, and immuno- and molecular profiles including features of lobular (morphology, negative E-cadherin, and lack of basal keratins) and ductal (aggressive clinical behavior and a subgroup with aggressive immunophenotype of triple negative and positive HER2) carcinomas.

Molecular profile. Loss of expression of the membranous adhesion molecule E-cadherin, the result of a somatic mutation of the E-cadherin gene *CDH1* located on chromosome

FIGURE 8.47 Lobular carcinoma. Tissue sections of the classic lobular carcinoma show linear arrangement of cancer cells surrounded by desmoplastic stroma (**a**). Periductal circumferential arrangement (**b**) and linear distribution (**c**) are also evident in this example of lobular carcinoma of pleomorphic type. Cell dissociation, medium-sized cells with minimal anisonucleosis and anisocytosis, and cytoplasmic "target-like" mucin accumulation (**f** *arrow*) are present in classic lobular carcinoma (**d**–**f**). The ultrasound characteristics are not specific and range from ill-defined to well-circumscribed, irregular, and spiculated hypoechoic masses of variable size (**g**, *arrow* points a large mass) as seen in these three examples (**g**–**k**). Variable posterior acoustic shadowing may be present. Vascular flow by Doppler exam is also variable (**a**–**c**, H&E stain high and low magnification; **d**, **e**, Papanicolaou stain high magnification; **f**, Diff-Quik stain high magnification)

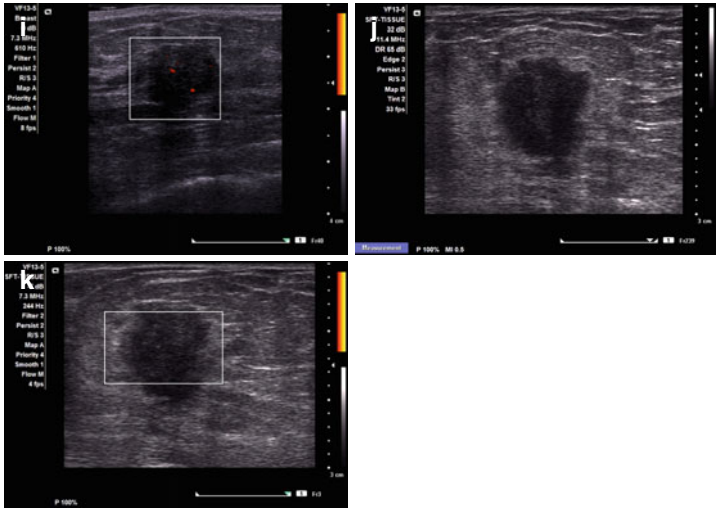

FIGURE 8.47 (continued)

16 (16p22.1), is the most consistent alteration in infiltrating lobular carcinoma and helps in the distinction from low-grade invasive ductal carcinoma of no special type. The most common chromosomal abnormalities are loss of 16q and gain of material on 1q. Pleomorphic lobular carcinoma shows similar alterations, but, in addition, has 8q24, 17q12, and 20q13 amplifications, which are characteristic of high-grade invasive ductal carcinoma of no special type. In addition, 50 % are found to be near diploid.

By gene expression profiling, infiltrating lobular carcinomas are most frequently classified as *luminal A* molecular tumors, but they can also be classified as luminal B, HER2 positive, normal-like, or basal-like.

Studies suggest that 95 % of infiltrating lobular carcinomas, in particular the classic variant, do not show *topoisomerase* IIα gene amplification either in the primary or matched metastasis predicting lack of response with traditional anthracycline-based chemotherapy.

FNA findings. Smears show scant to moderate cellularity, small aggregates, cords, and single cells. Cells are uniform and monomorphic with a high nuclear to cytoplasmic ratio, scant indistinct cytoplasm, and uniform and mildly hyperchromatic nuclei with slightly irregular contours. The cytoplasm shows mucin vacuoles and an occasional cytoplasmic lumen, often with a central mucoid inclusion. Signet ring-type cells may be present. The background shows naked tumor cell nuclei and lacks myoepithelial cell nuclei (Fig. 8.47d–f).

US features. The sensitivity of US in detecting lobular carcinoma is at the level of 90 %. The tumor has an irregular shape, ill-defined, or spiculated margins, hyper- or isoechogenicity compared to fat, and shows posterior acoustic shadowing and architectural distortion. The tumors may not be taller than wide, as in invasive ductal carcinomas. Precise measurement of the tumor size may be difficult to determine by US due to the ill-defined borders (Fig. 8.47g–k).

Tubular Carcinoma

Tubular carcinoma comprises 2 % of invasive breast cancers, usually measures < 1.5 cm, and has a favorable prognosis even in the presence of axillary lymph node metastasis.

Histopathology. The infiltrating tumor has haphazardly arranged, angulated comma-shaped and tubular structures lined by a single layer of cells and surrounded by a prominent desmoplastic fibrous stroma. The cellular elements are small and monotonous, showing bland-appearing uniform nuclei and inconspicuous nucleoli. Focal apocrine differentiation may be present (Fig. 8.48a, b).

Immunoprofile. Tubular carcinoma is almost always ER + and PR + and is typically negative for HER2, EGFR, P-cadherin, p53, and high-molecular-weight keratins (CK 5/CK6, CK14).

Molecular profile. The most frequent chromosomal alterations include loss of 16q, gain of 1q material, gain of 16p, and loss of 8p, 3p, and 11q.

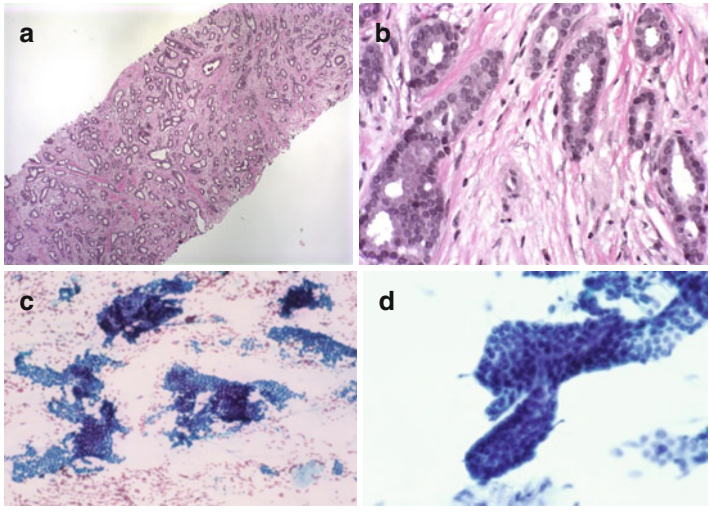

FIGURE 8.48 Tubular carcinoma. Core biopsy showing the characteristic features of tubular carcinoma including angulated and comma-shaped tubules lined with cuboidal bland-appearing cells, surrounded by a desmoplastic stroma (**a**, **b**). Smears show striking resemblance with features of fibroadenoma when examined a low magnification; however, in contrast with fibroadenoma, myoepithelial cells are absent in tubular carcinoma when the smear is evaluated at high magnification (**c**, **d**) (**a**, **b**, H&E stain low and intermediate magnification; **c**, **d**, Papanicolaou stain low and high magnification)

By gene expression profiling, infiltrating tubular carcinomas belong to the *luminal A* molecular class of breast cancer.

FNA findings. Variably cellular smears show small uniform cells arranged in sheets, small aggregates, and tubular structures (Fig. 8.48c, d). Myoepithelial cells may be present due to the small tumor size and sampling of the surrounding benign breast tissue.

US features. A small vertically oriented hypoechogenic mass with irregular spiculated and angular borders and marked posterior acoustic shadowing is usually seen. These tumors usually have an ill-defined echogenic halo and show no vascularity on Doppler examination.

Cribriform Carcinoma

This invasive carcinoma accounts for <1 % of breast carcinomas, occurs in patients at a mean age of 55 years, has an excellent prognosis, and often has a component of tubular carcinoma. The mean tumor size is 3 cm.

Histopathology. A cribriform pattern composed of arches of cells of small to moderate size, and mild to moderate pleomorphism is embedded in a fibroblastic stroma. Invasive cribriform carcinomas with tubular carcinoma comprising less than 50 % are still considered to be of the cribriform type. Osteoclast-like giant cells are occasionally present.

Immunoprofile. This tumor is almost always ER+and is PR+in 65 % of cases. It lacks HER2 overexpression. Myoepithelial markers (calponin, smooth muscle myosin heavy chain) are negative. p63 and CD117 are negative and allow the distinction from adenoid cystic carcinoma that shows positive immunoreactions.

Molecular profile. The molecular profile is similar to that of invasive tubular carcinoma.

By gene expression profiling, infiltrating cribriform carcinomas belong to the *luminal A* molecular class of breast cancer.

FNA findings. Smears show cohesive sheets and three-dimensional cribriform clusters of bland-looking and mitotically inactive ductal cells. Associated scattered multinucleated, osteoclast-like giant cells, some containing hemosiderin granules, have been described. Myoepithelial cells and naked nuclei are not identified.

US features. This tumor appears as an ill-defined inhomogeneous mass with lobulated margins and an ill-defined echogenic halo. Usually there is minimal or no posterior acoustic shadowing.

Mucinous (Colloid) Carcinoma

Colloid carcinoma usually occurs in elderly women, comprises <5 % of breast carcinomas, and has a good prognosis.

Histopathology. The mass has pushing margins and shows nests of cells of variable sizes and shapes floating in mucin lakes. Cytologic atypia is usually mild. Hypercellular mucinous

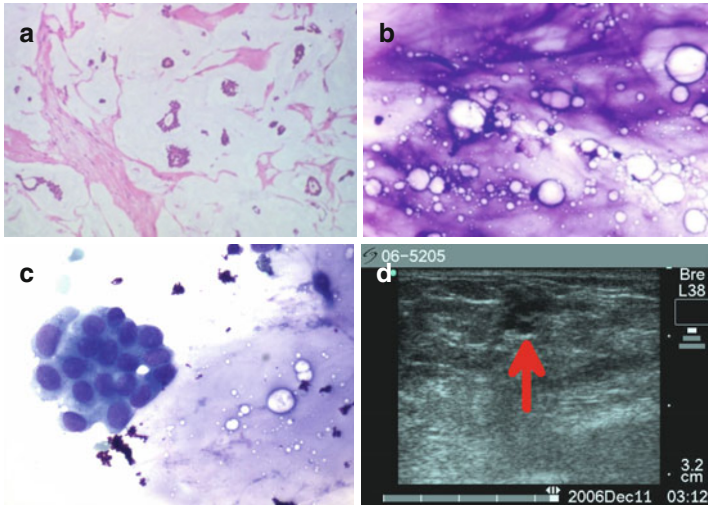

FIGURE 8.49 Colloid (mucinous) carcinoma. Tissue sections show scattered islands of bland-appearing neoplastic cells embedded in an abundant mucinous background (**a**). Cytologic features include small aggregates of bland-appearing monomorphic neoplastic cells and abundant mucus (**b**, **c**). The ultrasound features are not specific and include lobulated borders and hypoechogenicity (*arrow*) with variable presence of posterior acoustic enhancement (**d**) (**a**, H&E stain low magnification; **b**, **c**, Diff-Quik and MGG stain high magnification)

carcinoma may have neuroendocrine differentiation and show neuroendocrine marker positivity. Pure and mixed variants have been described, being the most common component found in invasive carcinoma of no special type. A pure tumor must be composed of >90 % mucinous carcinoma (Fig. 8.49a).

Immunoprofile. The tumor is ER + and PR +. HER2 is not overexpressed.

Molecular profile. Hypercellular mucinous tumors show a pattern of gene expression similar to that of neuroendocrine carcinomas.

Mucinous tumors are of *luminal A* molecular profile.

FNA findings. The mass is soft instead of gritty upon insertion of the needle. Aspirates yield mucous material and

variable cellularities. Characteristically, the cellular elements are monomorphic and arranged in small ball-like tridimensional aggregates surrounded by mucinous material that appears magenta with Romanowsky stains and fibrillary with Papanicolaou stain. The cells are small, with a bland-appearing chromatin pattern and a small nucleolus (Fig. 8.49b, c). High-grade tumor cell elements and stromal fragments are not uncommon in cases of ductal carcinoma with a mucinous component. Thus, the definitive cytologic diagnosis of mucinous carcinoma should be avoided; instead, the diagnosis of mammary carcinoma with a mucinous component should be rendered. The differential diagnosis includes mainly fibroadenoma with myxoid component and mucocele-like tumors of the breast; myoepithelial cells are seen in the former and benign ductal cells without atypia in the latter.

US features. The tumor is hypo- to nearly isoechoic and inhomogeneous with circumscribed lobulated edges, instead of the stellate or irregular appearance. There is variable posterior acoustic enhancement, likely related to the mucin present in these tumors (Fig. 8.49d).

Carcinoma with Medullary Features

This tumor usually occurs in women in the fifth and sixth decades of life. Typical medullary carcinoma, atypical medullary carcinoma, and a subset of invasive carcinomas of no special type are included under this category. Therefore, the diagnosis of medullary carcinoma requires careful gross and microscopic evaluation of the resected specimen. Classic medullary carcinoma comprises <1 % of invasive breast carcinomas. Traditionally, the medullary type is associated with a good prognosis; however, due to the low reproducibility of the diagnosis, these tumors are treated with aggressive therapy as for "basal-like triple-negative" carcinomas.

Histopathology. These tumors exhibit all or some of the following: circumscribed or pushing borders, a syncytial histologic pattern in >75 % of the tumor mass, lack of gland formation, a prominent diffuse lymphoplasmacytic infiltrate, and high-nuclear grade tumor cells with abundant cytoplasm,

pleomorphic nuclei, and prominent nucleoli. Mitoses, necrosis, and tumor giant cells may be present. Focal apocrine differentiation may be present. Because histologic evaluation may be subjective and not fully reproducible, use of the term carcinoma with medullary features is suggested instead of subclassifying this tumor (Fig. 8.50a).

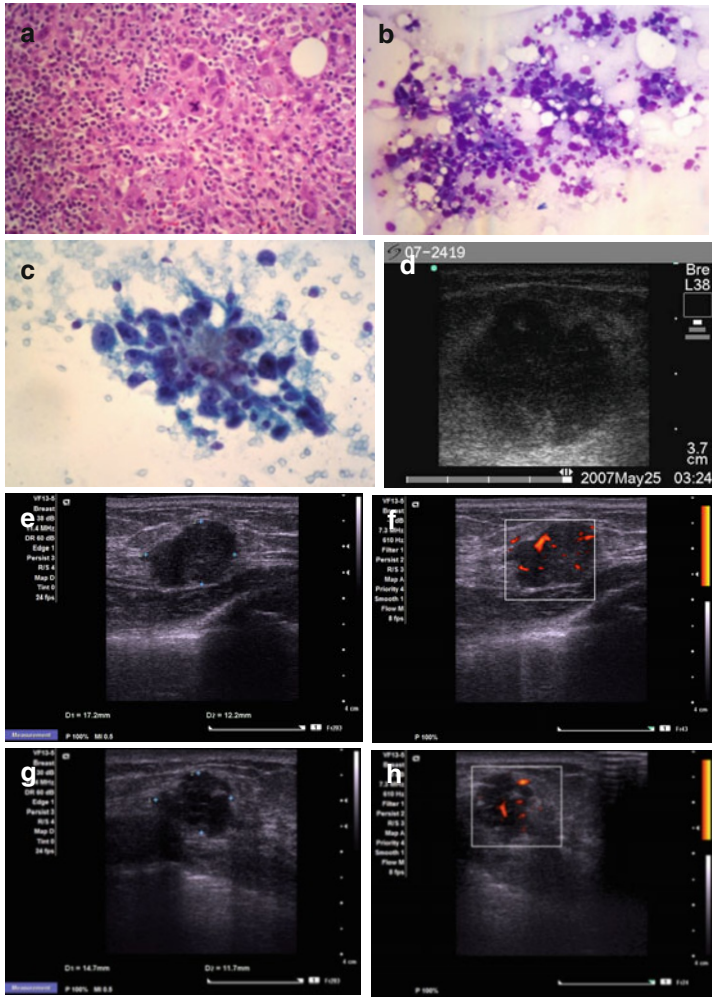

Immunoprofile. These tumors are often ER, PR, and HER2 negative ("triple negative") and variably express high-molecular-weight keratins (CK 5/CK6 and CK14), EGFR, P-cadherin, p53, and caveolin-1.

Molecular profile. Many of these tumors are recognized as "basal-like," and 13 % of patients with these tumors have *BRCA1*germline mutations.

FNA findings. Carcinoma with medullary features should be suspected when the tumor is well circumscribed and the smear shows high-grade tumor cells with lymphocytes and plasma cells. Smears show syncytial sheets of poorly differentiated epithelial cells with high nuclear grade, admixed with a lymphoplasmacytic infiltrate and occasional necrosis. Cells have a considerable size and nuclear enlargement with multiple irregular macronucleoli. Individual high-grade tumor cells and naked malignant nuclei are also present in the background (Fig. 8.50b, c).

US features. These tumors may appear as a well- or ill-defined homogeneously hypoechoic round mass with lobulated margins and a variable posterior acoustic effect. Fast-growing tumors may have a "pseudocystic" pattern with posterior acoustic enhancement (Fig. 8.50d–h).

Adenoid Cystic Carcinoma

Adenoid cystic carcinoma of the breast comprises <0.1 % of breast carcinomas and is associated with a good prognosis.

FIGURE 8.50 Carcinoma with medullary features. Histology shows high-grade tumor cells arranged in a syncytial pattern surrounded by a lymphoplasmacytic infiltrate. Atypical mitoses may be seen (**a**). High-grade pleomorphic tumor cells admixed with lymphocytes and plasma cells are noted in the smears (**b**, **c**). Ultrasound images show an irregular, hypoechoic mass with lobulated borders (**d**–**f**); spiculated borders in addition to the lobulated margins may be seen focally (**g**–**h**). The vascular flow by Doppler exam is variable. (**a**, H&E stain, intermediate magnification; **b**, Diff-Quik stain intermediate magnification; **c**, Papanicolaou stain high magnification)

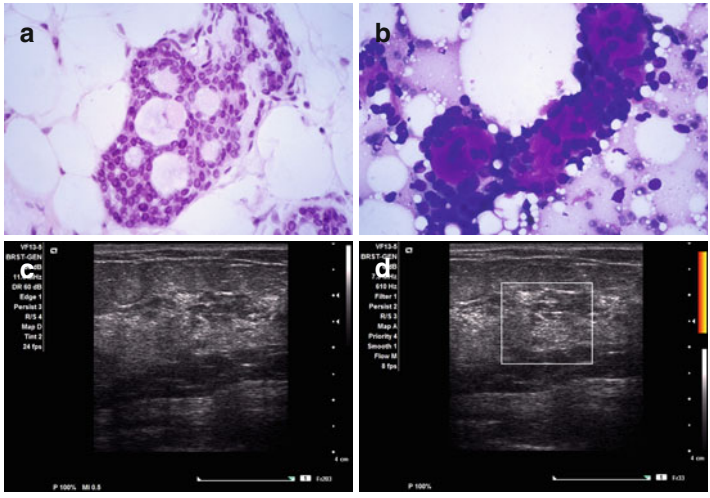

FIGURE 8.51 Adenoid cystic carcinoma. Histologic findings are similar to those of adenoid cystic carcinoma of salivary gland and show pseudolumens filled with basement membrane material (**a**). Cytologic findings include bland-appearing neoplastic cells surrounding globules of dense metachromatic stroma; the cell stroma interface is sharp and well defined (**b**). By ultrasound, this mass is heterogeneous, poorly circumscribed, and focally hyperechoic and shows no vascular flow by Doppler exam (**c**, **d**) (**a**, H&E stain intermediate magnification; **b**, Diff-Quik stain high magnification)

The mean age at diagnosis is 64 years. The carcinoma develops in the subareolar region in 50 % of cases. The tumor is generally cured by simple mastectomy, and the 10-year survival rate is >90 %.

Histopathology. The tumor is usually well circumscribed and is histologically similar to the counterpart in the salivary gland, showing pseudoluminal spaces containing spherules of basement membrane material and glandular lumens. The tumor may show a solid variant composed of basaloid cells (Fig. 8.51a).

Immunoprofile. The pseudoluminal spaces are decorated by small basal–myoepithelial cells that are positive for p63, calponin, smooth muscle actin, and high-molecular-weight

keratins (CK 5/CK6, CK 14) and negative for CD10. The glandular lumens, which may be inconspicuous, are decorated by epithelial cells that are positive for CD117 (membrane staining), CK 7, and CK 8/CK18. This tumor is generally ER, PR, and HER2 negative. EGFR overexpression is found in 65 % of cases.

Molecular profile. Adenoid cystic carcinoma harbors a recurrent chromosomal translocation t(6;9) leading to the formation of a chimeric fusion gene, *MYB–NFIB*. Many of these tumors are recognized as "basal-like" subtype.

FNA findings. The smear pattern is identical to that seen in the counterpart tumor located in the salivary gland. Smears show basaloid cells arranged in nests intimately associated with metachromatic matrix forming three-dimensional spheres. Usually, the metachromatic matrix has a sharp border, and there is a distinct separation between the matrix and surrounding cellular elements. The differential diagnosis includes collagenous spherulosis; however, collagenous spherulosis is a microscopic finding and adenoid cystic carcinoma is a neoplasm. Furthermore, adenoid cystic carcinoma lacks the fibrillary texture of collagenous spherulosis. The differential diagnosis also includes pleomorphic adenoma, and the differential diagnosis criteria are those listed in the chapter on salivary gland tumors (Fig. 8.51b).

US features. The mass may be oval and complex with well-circumscribed margins and posterior acoustic enhancement (Fig. 8.51c, d).

Metaplastic Carcinoma

This rare mammary carcinoma accounts for <2 % of breast malignancies. The tumors are usually large (mean size 4 cm), with borders that may be well circumscribed or indistinct and irregular, and histologically heterogeneous, characterized by the presence of ductal carcinoma with areas of squamous or mesenchymal (spindle, chondroid, osseous, or rhabdomyoid) elements. When there is a predominance of pseudosarcomatous metaplasia, the prognosis is poor, and the survival rate is 25 % at 5 years. Distant metastasis (lung and brain) can be

found in the absence of lymph node metastasis, similar to other triple-negative breast cancers.

Histopathology. This malignancy includes tumors with malignant squamous differentiation, spindle cell morphology, and heterologous mesenchymal elements (osseous, chondroid, rhabdomyoid), either alone or combined with another metaplastic component, and/or ductal carcinoma of no special type. It may have prominent mesenchymal differentiation. The histologic diagnosis should be descriptive, i.e., low-grade adenosquamous carcinoma, fibromatosis-like metaplastic carcinoma, squamous cell carcinoma, spindle cell carcinoma, metaplastic carcinoma with mesenchymal differentiation, mixed metaplastic carcinoma (Fig. 8.52a, b).

Immunoprofile. These tumors are usually negative for ER, PR, and HER2 and express high-molecular-weight keratins (CK 5/CK6, CK14) and EGFR. Low-molecular-weight keratins are commonly negative. P63 positivity, seen in >90 % of metaplastic breast carcinomas, is a useful marker for differentiating it from other spindle and mesenchymal neoplasms, including sarcomas.

Molecular profile. These tumors are triple-negative basal-like tumors and have multiple and complex chromosomal abnormalities. Mutations of the tumor suppressor gene *TP53* are found in most tumors, and loss of *p16* and *PTEN* is seen in other subgroups.

These tumors are classified as "basal-like" subtype. Some tumors are currently being classified into a recently described claudin-low tumor molecular subtype (tumors with epithelial to mesenchymal transition features).

FNA findings. Cytologic findings reflect the tumor composition such as ductal carcinoma and areas of spindle, squamous, chondroid, and osseous metaplasia in a background of necrosis. Smears may be hypercellular with cells showing marked pleomorphism, bi- or multinucleated bland-appearing or pleomorphic giant cells, and fibroblast-like spindle cells that may be tightly packed or loosely aggregated. Metaplastic carcinoma with chondrosarcomatous differentiation shows large high-grade tumor cells surrounded by a chondromyxoid

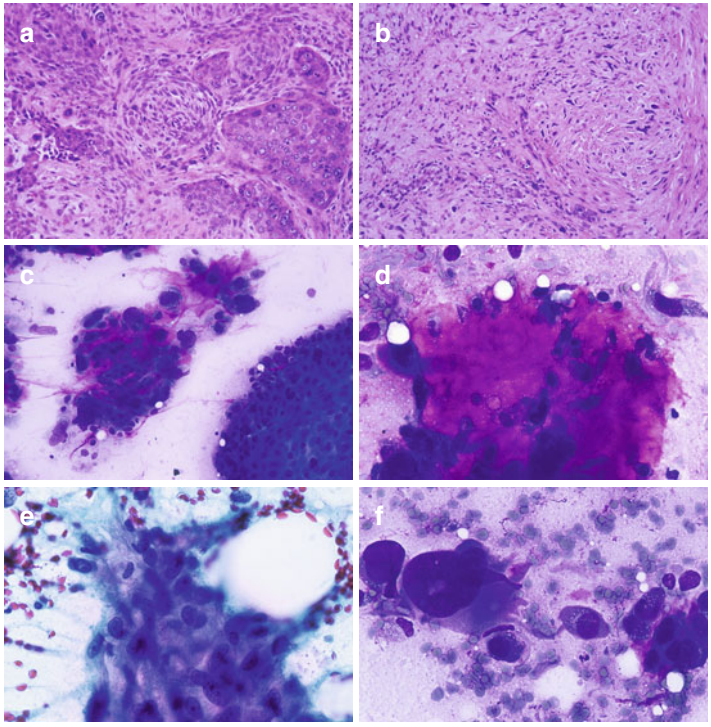

FIGURE 8.52 Metaplastic carcinoma with mesenchymal differentiation. Rapidly growing tumor in a 27-year-old woman. Sections show chondromyxoid and squamous differentiation (**a**, **b**). Cellular pleomorphism, squamous and chondroid metaplasia, and fibrillary magenta stroma are prominent findings in the FNA smears (**c**–**f**) (**a**, **b**, H&E stain intermediate magnification; **c**–**f**, Diff-Quik stain intermediate and high magnification)

stroma. Squamous carcinoma usually shows pleomorphic keratinizing, nonkeratinizing, and spindle squamous cells forming sheets, cords, or nests or is single in a necrotic cystic background (Fig. 8.52c–f). The differential diagnosis of sarcomas includes reactive processes such as nodular fasciitis, fibromatosis, myofibroblastoma, and adenomyoepithelioma.

US features. These tumors tend to have oval-shaped and well-defined borders. Cystic changes are common, and coarse calcification is seen when there is osteochondroid differentiation. Posterior acoustic shadowing is rarely present.

Papillary Carcinoma

This tumor is rare and is defined as being >90 % papillary in the invasive component. Thus, by definition, invasive carcinoma of no specific type with papillary differentiation, solid papillary carcinoma, and encapsulated papillary carcinoma should not be classified as invasive papillary carcinoma. The differential diagnosis includes metastasis from ovary or lung. The prognosis appears to be mandated by the grade and stage of the tumor. Myoepithelial cell markers are absent. There are no available data on the molecular profile of this tumor.

Micropapillary Carcinoma

This is a rare tumor that accounts for <2 % of breast cancers and is composed of small mini-papillary or morular-like cell aggregates surrounded by a clear space. The cells are columnar or cuboidal and show eosinophilic cytoplasm, variable nuclear pleomorphism, and a reverse polarity with cytoplasmic snouts facing the clear space and not the luminal surface. Focal apocrine differentiation may be present. Angiolymphatic invasion is more frequent in this tumor than in invasive ductal carcinoma of no special type.

Immunoprofile. Most carcinomas are ER and PR positive with variable HER2 overexpression. EMA positivity restricted to the basal portion of the neoplastic cells distinguishes this tumor from ductal carcinoma of no specific type that shows an apical homogeneous cytoplasmic immunostain.

Molecular profile. These tumors are classified as *luminal A or B subtype*. Recurrent gains of chromosome arms 8q, 17q, and 20q and deletions of chromosome arms 6q and 13q are seen. Deep sequencing techniques have shown microRNA patterns different from that of invasive ductal carcinoma of no special type.

FNA findings. Smears show increased cellularity, cell clusters with angular and papillary configuration without a

fibrovascular core, tumor clusters showing an "inside–out" pattern, irregular crowded nuclei, and the presence of single discohesive cells. Few malignant-appearing multinucleated giant cells, cells with apocrine features, little mucin, psammoma bodies, and tumor diathesis may be seen. No mitoses are present. The diagnosis is suspected in the presence of morule formation, isolated malignant cells, and branching epithelial structures.

US features. The tumor is hypoechoic, but occasionally isoechoic; it is irregular, or microlobulated, with hypoechoic internal areas, and with or without posterior acoustic enhancement.

Inflammatory Carcinoma

This is a rare and aggressive breast carcinoma. The skin has the appearance of an "orange peel" and is engorged, red, and tender with or without an underlying distinct breast mass (Fig. 8.53a). Inflammatory carcinoma is a descriptive clinical term that has a distinctive underlying pathologic finding, the presence of tumor emboli plugging the lymphatic vascular channels of the breast dermis with no inflammation (Fig. 8.53b). Aspiration cytology may not be revealing, and in such cases, sampling of the commonly found ipsilateral axillary metastasis fulfills diagnostic and staging purposes.

Immunoprofile. This carcinoma is ER and PR positive in 50 % of cases and HER2 positive in 40 %. Characteristically, E-cadherin is overexpressed and there is high expression of p53 and MUC1.

Molecular profile. There is no characteristic genetic alteration for inflammatory carcinoma. Molecular subtyping often classifies this cancer in the HER2 or basal subtypes. Activation of the anaplastic lymphoma kinase (ALK) pathway has recently been suggested to occur, and if this is confirmed, these patients may benefit from targeted therapy.

FNA findings. The cytomorphology is similar to that of poorly differentiated infiltrating breast carcinoma. Smears are sparsely cellular due to lymphatic permeation and stromal edema. High-grade cells are arranged in small aggregates

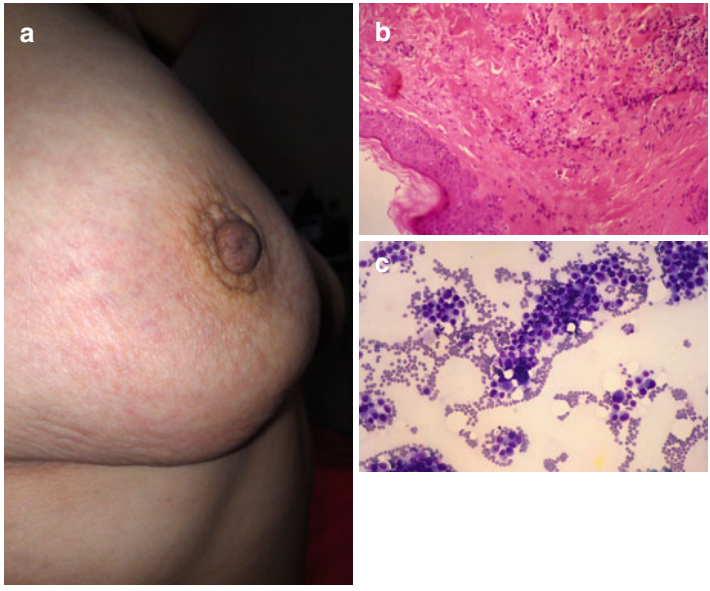

Figure 8.53 Inflammatory carcinoma. Hyperemia and orange peel-appearing skin are characteristic on breast exam (**a**); this picture corresponds to a patient with micropapillary breast carcinoma. Dermal lymphatics with tumor emboli and no inflammatory reaction are present (**b**) in tissue sections. Scattered groups of malignant cells are seen in the FNA smears (**c**) (**b**, H&E stain, intermediate magnification; **c**, MGG stain intermediate magnification)

and show a vacuolated cytoplasm, large pleomorphic nuclei, coarse chromatin, and prominent nucleoli (Fig. 8.53c).

US features. The skin thickening seen by US is the combination of dilated subdermal lymphatics and edema. There is tissue hyperechogenicity and disruption of normal tissue planes. A hypoechoic, irregular, ill-defined mass with posterior acoustic shadowing may be identified. Axillary lymph nodes with suspicious US features are commonly seen.

Paget Disease of the Nipple

This eczema-like change in the nipple and areola is commonly associated with underlying in situ or invasive mammary carcinoma. Paget disease of the nipple without underlying

carcinoma is rare. It affects both sexes and can be bilateral. Patients may have erythema or eczema of the nipple, ulceration, inversion, and nipple discharge. The prognosis depends on the presence or absence of underlying DCIS or invasive carcinoma. However, rarely advanced breast cancer extends out to involve the surface of the nipple and produce ulceration.

Histopathology. The presence of large cells having ample clear cytoplasm and large nuclei with prominent nucleoli is characteristic within the epidermis. Cells are placed singly or in small clusters in the dermoepidermal junction and lower layers of the epidermis (Fig. 8.54a).

Immunoprofile. Paget cells are positive for CK 7 and CAM5.2. ER and PR are positive in 40 % of cases, and HER2 is positive in 90 %, similar to the underlying carcinoma. Negative immunoreaction with S-100 protein, HMB-45 and melan-A excludes melanoma; pancytokeratin and high-molecular-weight cytokeratin are positive in Bowen's disease.

Molecular profile. Paget cells have no distinct or specific gene mutation profile, and they are genetically similar to the underlying breast carcinoma.

Cytologic findings. The diagnosis can be made by scraping of the lesion or by FNA if there is an underlying mass. Smears usually show high-grade malignant cells (Fig. 8.54b).

US features. The nipple is thickened, and an underlying calcification/mass lesion may be seen.

Rare Types of Breast Carcinoma

Included but not restricted to secretory, mucoepidermoid, neuroendocrine, acinic cell, and oncocytic carcinomas.

Secretory Carcinoma

This low-grade invasive carcinoma is very rare; occurs in young patients of both sexes, with a median age of 25 years; and has a favorable prognosis. The tumors are well circumscribed and mobile, occurring close to the areola.

Histopathology. Tumors have pushing borders and have microcystic, solid and tubular patterns, usually in combination (Fig. 8.55a).

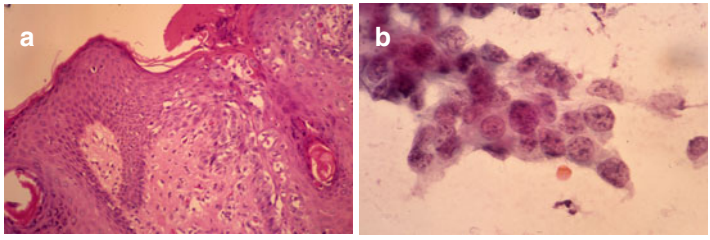

FIGURE 8.54 Paget's disease. Large malignant cells with vacuolated cytoplasm are present in the dermoepidermal interface (**a**). Smears show high-grade malignant cells (**b**) (**a**, H&E stain intermediate magnification; **b**, Papanicolaou stain high magnification)

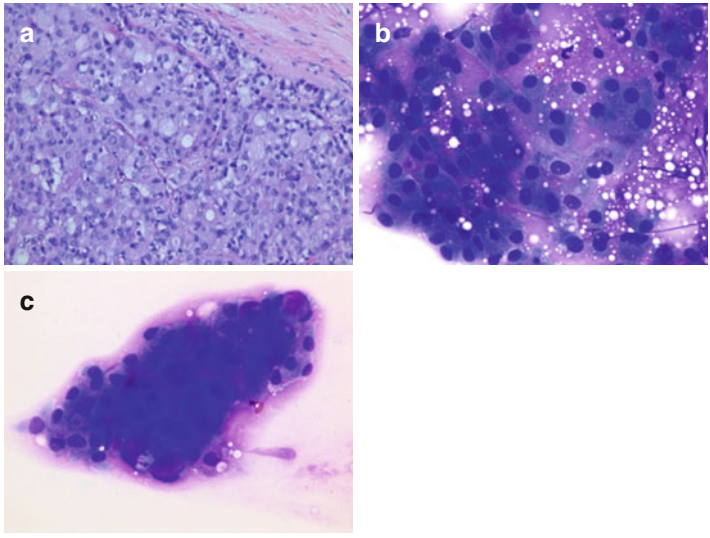

FIGURE 8.55 Secretory carcinoma. Histopathology shows pushing borders and microcystic architecture (**a**). The smears show cohesive sheets and aggregates of large cells with ample slightly vacuolated dense cytoplasm, bland-appearing round nuclei, ill-defined cytoplasmic borders, and clean background (**b**, **c**). Other areas show a proteinaceous mucoid background (**a**, H&E stain; **b**, **c**, Diff-Quik stain high magnification) (Courtesy Dr. Margarita Elices Apellaniz. Madrid, Spain)

Immunoprofile. The tumors are S-100 protein and lactalbumin positive and ER, PR, HER2, and p63 negative. The basal-like marker (CK5/CK6 or EGFR) is expressed in 90 % of cases.

Molecular profile. Secretory carcinoma harbors a recurrent chromosomal translocation t(12;15)(q13;q25) leading to the formation of the chimeric fusion gene *ETV6-NTRK3*, which is considered specific for secretory carcinoma. These tumors are classified as "basal-like" subtype.

FNA findings. Smears are cellular and show grape-like clusters and single large cells with granular to vacuolated cytoplasm, uniform round nuclei, minimal nuclear atypia, and prominent nucleoli in a mucinous background. Cells may have a plasmacytoid appearance and may be binucleate. Diagnosis of this carcinoma on FNA is difficult and important because the cytologic findings can be confused with those of the lactating breast. The differential diagnosis includes lipid-secreting carcinoma, glycogen-rich clear cell carcinoma, and cystic hypersecretory carcinoma (Fig. 8.55b, c).

US features. Ultrasonography and breast computed tomography show a subareolar oval-shaped tumor exhibiting homogeneous echogenicity with clear margins.

Mucoepidermoid Carcinoma

This very rare breast tumor is similar histologically to the salivary gland counterpart, is well circumscribed, and can reach a large size. The tumor shows basaloid, intermediate, squamous, and mucinous cells. Most tumors are of low grade, with predominance of the mucinous cells. High-grade mucoepidermoid are usually solid with predominance of intermediate and squamous cells.

Carcinomas with Neuroendocrine Differentiation

Pure neuroendocrine tumors are rare, comprising <1 % of breast carcinomas, and include large cell and small cell neuroendocrine carcinomas. Neuroendocrine differentiation of breast carcinomas of no special type, mucinous carcinomas,

and solid papillary carcinomas are more frequent. Clinical neuroendocrine syndromes related to hormone production are rarely present.

Histopathology. These tumors show features similar to those seen in the lung or GI tract.

Immunoprofile. Well-differentiated tumors are positive for ER and PR; poorly differentiated small cell neuroendocrine carcinoma shows ER and PR positivity in 50 % of cases.

Molecular profile. These tumors have a *luminal A* molecular profile.

FNA findings. Cytomorphologic features are similar to those of neuroendocrine carcinomas of other sites, i.e., lung and GI tract.

Acinic Cell Carcinoma

This tumor is similar to the parotid gland counterpart, and it may be well to poorly differentiated to undifferentiated. It appears to have good prognosis, although axillary lymph node metastasis may occur.

Immunoprofile. There is cytoplasmic reactivity with alpha-1-anti-chymotrypsin, amylase, lysozyme, EMA, and S-100 protein. This tumor is negative for ER, PR, and HER2.

FNA findings. Cells have abundant granular cytoplasm, a round nucleus, and prominent nucleoli. The cytoplasm contains zymogen granules or may be clear ("hypernephroid").

Oncocytic Carcinoma

The tumor occurs in both sexes and predominantly in the seventh decade of life.

Histopathology. Oncocytic carcinoma is defined as breast carcinoma with >70 % oncocytic differentiation. Oncocytes have ample eosinophilic cytoplasm with numerous mitochondria. It is predominantly solid with variable nuclear pleomorphism and prominent nucleoli. Oncocytic carcinoma is indistinguishable from apocrine carcinoma on H&E stain.

Immunoprofile. The tumor is ER, PR, and HER2 positive in 80, 60, and 25 % of cases, respectively. GCDFP-15 (gross

cystic disease fluid protein-15) is negative and antimitochondrial antibody stain is strong and diffuse.

Molecular profile. The tumor often displays chromosomal gains of 11q and 19p13 similar to renal and thyroid oncocytic tumors.

Apocrine Carcinoma

Data suggest that many subtypes of breast cancer show apocrine differentiation in various proportions and that "apocrine carcinomas" do not represent a distinct entity.

Histopathology. This is a rare breast tumor that is indistinguishable from oncocytic carcinoma on usual histologic grounds. The eosinophilic cytoplasm has predominance of electron-dense cytoplasmic granules. Some cells may have empty vesicles and correspond to the foam cells seen histologically in the clear cell variant.

Immunoprofile. The tumor is CK 7 negative, ER and PR negative, and androgen receptor positive; HER2 is overexpressed in 45 % of cases. GCDFP-15 is diffusely positive, and the antimitochondrial antibody stain is weak and focal.

FNA findings. Smears show fragments with a syncytial arrangement and single cells showing abundant granular eosinophilic cytoplasm, large nuclei, and prominent nucleoli. In contrast to apocrine metaplasia, the carcinoma shows cell dissociation, a syncytial arrangement, cellular atypia, and pleomorphic, irregular, and hyperchromatic nuclei (Fig. 8.56).

Lipid-Rich Carcinoma

The tumor occurs in women from the fourth to ninth decade of life. Half of the patients have axillary nodal metastases at diagnosis, and 38 % die within the first year after diagnosis. The tumor is defined as breast carcinoma with >90 % of cells containing cytoplasmic neutral lipids. Most cases show histologic grade 3 and are ER and PR negative. There are no data on the genetic features of these tumors. Neoplastic cells show large, vacuolated, foamy lipid-laden cytoplasm.

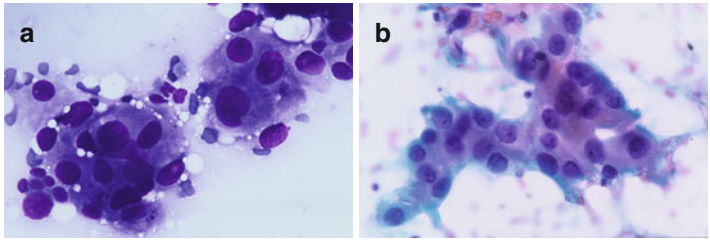

FIGURE 8.56 Breast carcinoma with apocrine differentiation. Large cells with abundant granular cytoplasm, large nuclei, and prominent nucleoli are identified forming a syncytial pattern (**a**, Diff-Quik stain high magnification; **b**, Papanicolaou stain high magnification)

Glycogen-Rich Clear Cell Carcinoma

This tumor is more aggressive than carcinoma of no specific type. The median age at diagnosis is 57 years. This is defined as breast carcinoma with >90 % cells having glycogen-containing clear cytoplasm. The cells are polygonal with granular clear cytoplasm, hyperchromatic nuclei, and prominent nucleoli. ER is positive in 50 % of cases. HER2 and PR are negative in most cases. The differential diagnosis includes other clear cell primary or metastatic breast tumors, i.e., lipid-rich carcinoma, myoepithelioma, and metastatic renal cell carcinoma.

Squamous Cell Carcinoma

The diagnosis is made histologically. This carcinoma may occur as part of metaplastic carcinoma or as a pure tumor. The WHO includes this tumor under the category of metaplastic carcinoma.

Mesenchymal Tumors

Benign and malignant mesenchymal tumors such as nodular fasciitis, hemangiomas, desmoid-type fibromatosis, inflammatory myofibroblastic tumor, leiomyoma, rhabdomyosarcoma, osteosarcoma, and leiomyosarcoma occur in the breast.

True sarcomas, i.e., osteogenic sarcoma, rhabdomyosarcoma, liposarcoma, and angiosarcoma, are rarer than metaplastic carcinoma, with malignant fibrous histiocytoma being the most common.

FNA findings of benign and malignant mesenchymal tumors are similar to those described in other chapters of this book. We describe granular cell tumor and angiosarcoma next.

Granular Cell Tumor

This almost always benign tumor of neural (Schwann cell) origin can be seen in the breast as a painless mass that measures up to 3 cm. It is multiple in 20 % of cases. These tumors can appear malignant clinically and radiologically. Tumors are firm and may cause skin and nipple retraction or involve pectoralis fascia.

Histopathology. The tumor shows infiltrative sheets, cords, or clusters of polygonal cells with indistinct cell borders; abundant granular cytoplasm (rich in lysosomes); a round, uniform nucleus; and conspicuous nucleoli (Fig. 8.57a).

Immunoprofile. The tumor is positive for S-100 protein and CD68 (lysosomal). Staining for keratins, myoglobin, GFAP, and lysozyme is negative. A tumor with a high level of Ki67 should be considered malignant, even if the tumor has few pathological features of malignancy.

FNA findings. Aspirates show numerous single and grouped cells with eosinophilic granular cytoplasm and oval to round nuclei with variable atypia. The cytoplasm is fragile, and its rupture results in a granular background and numerous free-lying nuclei (Fig. 8.57b, c). Atypia and necrosis may indicate a malignant granular cell tumor. The differential diagnosis includes alveolar soft-part sarcoma and rhabdomyosarcoma that show nuclear atypia; rhabdomyoma, a glycogen-rich benign tumor of striated muscle that has cells with granular cytoplasm and elongated cells showing squared well-defined borders; and cytoplasmic cross-striations standing out in a clean background. Rhabdomyomas are PAS positive, but S-100 protein negative.

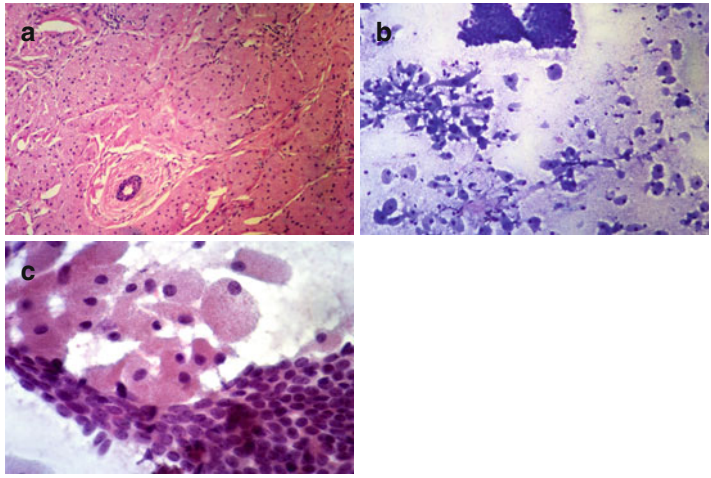

FIGURE 8.57 Granular cell tumor. Cords of large cells with abundant granular cytoplasm and round nuclei surround a benign breast duct (**a**). The smears show numerous cells with polyhedral appearance, abundant granular cytoplasm, and a granular background (**b**). The eosinophilic cytoplasm is best seen in the Papanicolaou-stained smear (**c**) (**a**, H&E stain intermediate magnification; **b**, Diff-Quik stain intermediate magnification; **c**, Papanicolaou stain high magnification)

US features. US shows an oval hypoechoic spiculated nodule with combined posterior acoustic enhancement and shadowing. The tumor may not be well circumscribed.

Angiosarcoma

This tumor can arise de novo in the breast or secondarily in the skin, breast, or chest wall in patients with a history of breast carcinoma treated with radiotherapy (the latent period is 7–10 years or more). Angiosarcoma associated with lymphedema in patients treated with mastectomy and axillary lymph node dissection has been described. Primary angiosarcoma is the second most common sarcoma after malignant phyllodes tumor. Patients may have a painless mass or a diffuse breast enlargement with a bluish-red discoloration

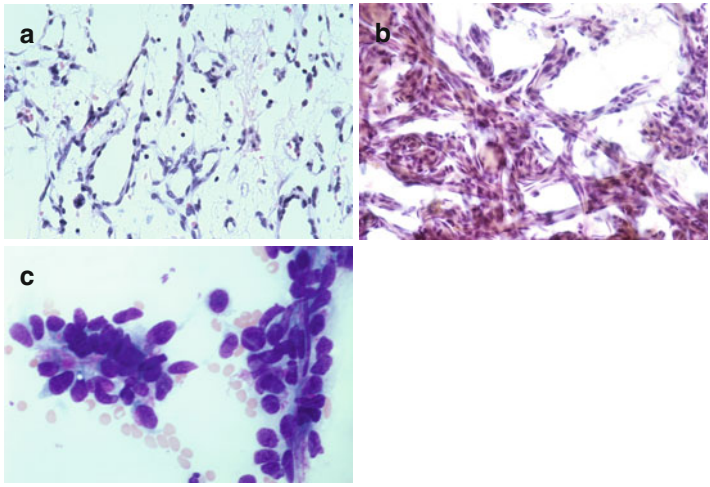

FIGURE 8.58 Angiosarcoma. Histologic section shows anastomosing vascular channels lined with endothelial cells (**a**). Similar anastomosing vessels are seen in the cytology smears (**b**). Rare aggregates of cuboidal cells forming microacini are also seen along with linear vessels (**c**) (**a**, H&E stain low magnification; **b**, Papanicolaou stain low magnification; **c**, Diff-Quik stain high magnification)

when the skin is involved. Violaceous or erythematous skin nodules or variably sized plaques may be seen. The prognosis is dismal, and recurrence, metastases, and survival are independent of tumor grade.

Histopathology. Well-differentiated angiosarcomas show anastomosing vascular channels with dilated or angulated lumina lined with endothelial cells that have large hyperchromatic nuclei (Fig. 8.58a). Poorly differentiated angiosarcomas show vascular channels admixed with solid cellular areas exhibiting spindle or epithelioid cells, blood lakes, necrosis, and mitoses.

Immunoprofile. CD31, CD34, and nuclear Fli-1 positivity support the diagnosis of angiosarcoma, particularly in poorly differentiated tumors. Of importance, keratin may be focally positive.

Molecular profile. Activating mutations of the receptor tyrosine kinase gene *KDR* have been described in some angiosarcomas. A high level of *MYC* amplification may be seen in angiosarcomas secondary to radiotherapy.

FNA findings. The cellularity may be sparse. Epithelioid and/or spindle cells with hyperchromatic nuclei and prominent nucleoli are seen. Smears show a background of blood, necrosis, and hemosiderin-laden macrophages (Fig. 8.58b, c).

US features. US shows a hyperechoic or a mixed hyper- and hypoechoic mass with indistinct, angular, or spiculated margins; the echotexture may be homogeneous or heterogeneous. Sometimes the mass may be lobular with circumscribed margins ("cloud-like") and coarse calcifications. When the skin is involved, there is a round, oval, or irregular hypoechoic mass associated with the dermis with skin thickening. The hypoechoic dermal nodules usually disrupt the dermal plate and extend to the underlying breast tissue.

Lymphoid Malignancies

Lymphomas in the breast are rare and may be primary or secondary to a systemic lymphoma. Most patients are postmenopausal women, although lymphoma can occur in young women or in men. A painless mass or a multinodular breast is usually identified. The most common type of lymphoma in the breast is diffuse large B-cell lymphoma followed by extranodal marginal zone lymphoma of the MALT type and follicular lymphoma. Burkitt lymphoma, lymphoblastic lymphoma, and T-cell lymphomas including anaplastic large cell lymphoma (ALCL) have been described.

Histopathology. Histologic findings are identical to those of lymphomas in other sites.

Immunoprofile. Diffuse large B-cell lymphoma has a mature B-cell phenotype expressing CD20, CD79a, and PAX5.

Burkitt lymphoma has a mature B-cell phenotype expressing CD20, CD79a, and PAX5. Staining for CD10 and BCL6 is

positive and is negative for BCL2 and terminal deoxynucleotidyl transferase. EBV sequences are detected by EBV-encoded RNA (EBER) in situ hybridization.

T-cell lymphoma cells express the T-cell-associated markers CD2 and CD3. ALCL is positive for CD30 and EMA and negative for CD15 and CD20.

MALT lymphomas express CD20, CD79a, PAX5, and BCL2 and are negative for CD5, CD10, CD23, BCL6, and cyclin D1.

Follicular lymphomas express pan-B-cell markers CD20 and CD79a as well as CD10, BCL6, and BCL2.

Molecular profile. Burkitt lymphoma has translocations involving the MYC gene and one of the immunoglobulin genes, most often *IGH@*, and less often *IGK@* or *IGL@*.

Most ALCLs show a clonal rearrangement of the T-cell receptor gene.

MALT lymphomas of the breast show a clonal rearrangement of the immunoglobulin genes. Cytogenetic abnormalities characteristic of other MALT lymphomas, e.g., t(11;18)(q21;q21), have not been reported.

The characteristic t(14;18)(q32;q21) seen in follicular lymphomas has not been systematically evaluated in primary follicular lymphomas of the breast.

FNA findings. Cytologic findings are similar to those of lymphomas in lymph nodes or other sites.

US features. Breast involvement shows a well-defined to irregular hypoechoic mass or masses, skin thickening, and dilated subdermal lymphatics. Lymph nodes are markedly hypoechoic with thickening of the hypoechoic cortex, a bulging contour, and attenuation of the central fatty hilum.

Tumors of the Male Breast

Gynecomastia

Gynecomastia is a hormonally dependent, often unilateral lesion that occurs in adolescents and older male patients.

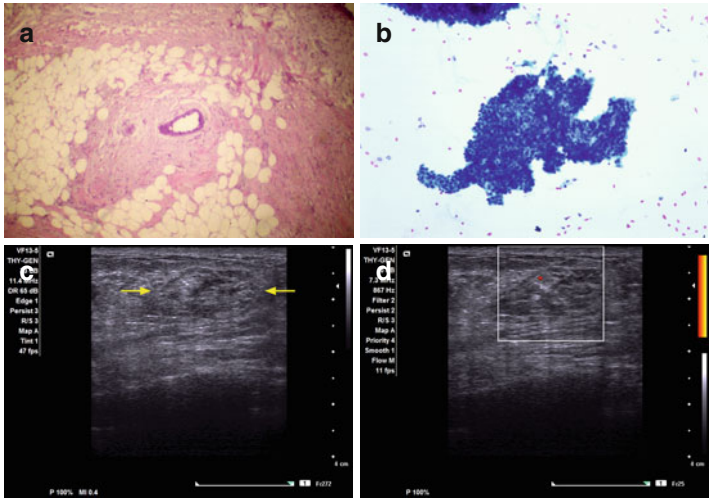

Figure 8.59 Gynecomastia. There is proliferation of mesenchymal stroma and ductal epithelium (**a**). Smears show sheets of benign ductal epithelial cells with myoepithelial cell nuclei similar to those seen in fibrocystic change (**b**). The US images in this case show slight breast tissue prominence (**c** *arrows*) with minimal vascularity by Doppler exam (**c**, **d**) (**a**, H&E stain low magnification; **b**, Diff-Quik stain high magnification)

It may be idiopathic or drug related, i.e., related to digitalis, reserpine. Patients have a palpable tender subareolar and ill-defined mass.

Histopathology. There is proliferation of the ductal and mesenchymal elements. Branching ducts with variable degrees of cellular hyperplasia are seen. Squamous and apocrine metaplasia may occasionally be present, and atypical ductal hyperplasia is rarely seen (Fig. 8.59a).

Molecular profile. Except in gynecomastia associated with Klinefelter syndrome, there is no underlying genetic abnormality.

FNA findings. Cellularity is variable and is higher in early lesions and sparse in long-standing lesions. The smear pattern is similar to that of fibrocystic change, including benign ductal epithelial cells and myoepithelial cell nuclei. Cellular smears

resemble those of fibroadenoma (Fig. 8.59b). Slight cellular and nuclear atypia with nucleoli may be seen.

US features. The area of palpable abnormalities shows normal tissue on US (Fig. 8.59c, d).

Carcinoma

Male breast DCIS and invasive carcinoma are rare and affect slightly older men than women. Conditions that may increase the risk of breast cancer in men include obesity, cryptorchidism, liver cirrhosis, diabetes, and hyperthyroidism. Occupational exposure to petrol and airline fuel has been suggested to increase the risk of breast cancer. Approximately 15 % of males with breast cancer have a family history of breast or ovarian carcinoma. Patients have a palpable painless mass, usually in the subareolar area, and often have nipple retraction, fixation, ulceration, and discharge. Axillary lymphadenopathy may be present in 50 % of cases. The overall survival is poor compared with women who have breast cancer.

Histopathology. The histopathology is similar to that of female breast carcinoma. It seems that papillary carcinoma and Paget disease are more prevalent in men than in women. Invasive carcinoma of no special type is the most common, and lobular carcinoma is very rare.

Immunoprofile. Positivity for ER and PR is present in >80 % of cases and HER2 overexpression is rare. PR negativity and p53 accumulation seem to correlate with high-grade phenotype, aggressive clinical course, and decreased 5-year survival rate. High-grade tumors with high mitotic activity also have been correlated with HER2 overexpression, low bcl-2 expression, high Ki67, and high p21 expression.

Molecular profile. Luminal A (ER + and/or PR+ and *HER2*- or Ki67 low) is the most common subtype (75 % of cases), followed by luminal B (ER + and/or PR+ and *HER2*+ or Ki67 high) subtype (21 %). Basal-like (ER−, PR−, *HER2*−, CK5/6+ and/or CK14+ and/or EGFR+) and unclassified (triple negative for all markers) subtypes are very rare. No *HER2*-driven (ER−, PR−, *HER2*+) subtype cases have been

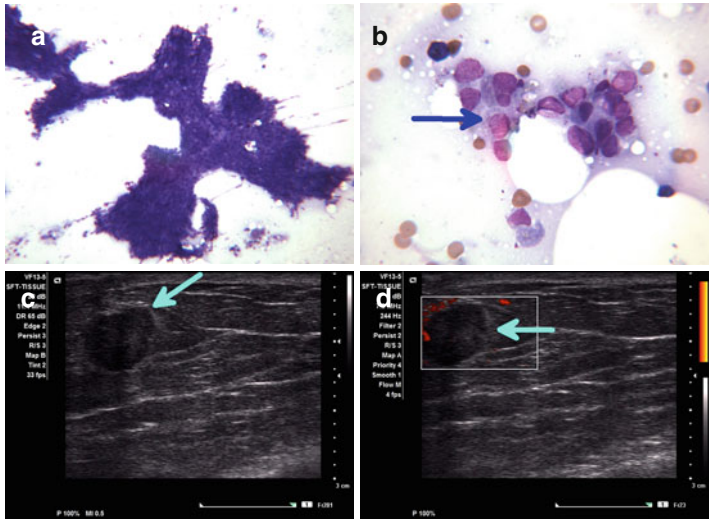

FIGURE 8.60 Male breast carcinoma. Cytologic features (**a**, **b** *arrow* points tumor cells) and US characteristics (**c**, **d** *arrows* point breast mass) are similar to those seen in female breast carcinoma (**a**, **b**, MGG stain intermediate high magnification)

reported in a study of 134 male breast cancers. Male carriers of *BRCA2* gene mutations have a 7 % risk of developing breast cancer at the age of 70 years. The association of male breast cancer and *BRCA1* germline mutation is weaker than that for *BRCA2*. The distribution of molecular subtypes is different from that of female breast cancer and suggests differences in carcinogenesis.

FNA findings. Smear patterns are similar to those described for female breast cancer (Fig. 8.60a, b).

US features. US features are similar to those of female breast carcinoma (Fig. 8.60c, d).

Metastasis in the Breast

Metastases to the breast are rare, but occasionally they may be the first manifestation of the malignancy. Primary mammary carcinoma is mimicked in these cases. The most common

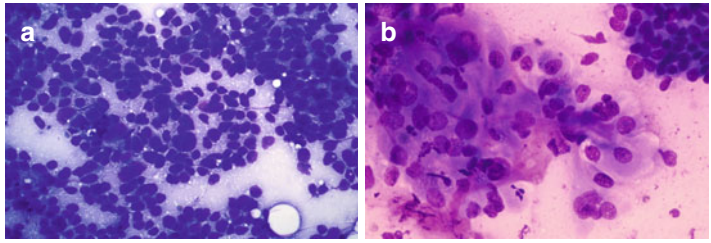

FIGURE 8.61 Unusual cases of metastatic malignancy to the breast include small cell carcinoma (**a**) in a 40-year-old woman with primary lung small cell carcinoma. In males, metastatic prostatic carcinoma may be seen (**b**) (**a**, **b**, MGG stain high magnification)

primary sites of origin include melanoma, lymphoma, as well as lung, ovary, and soft tissue sarcomas. Prostate carcinoma is the most common source in men (Fig. 8.61). Melanoma and carcinoma of the ovary or kidney may be the source of metastasis years after the primary diagnosis. In children, rhabdomyosarcoma and lymphoma are the most common primary sites. The patients usually have a single palpable, painless, round mass; multiple masses are rare. Mass calcifications and spiculated borders are less common than in primary breast carcinomas. In questionable cases, comparison with the original tumor histopathology (known in 80 % of cases) is important for a definitive diagnosis, along with immunohistochemistry. Clinical history and imaging studies are also crucial for diagnosis.

Immunoprofile. ER-, PR-, and HER2-negative tumors in the absence of an in situ component should alert the pathologist to strongly consider a metastatic deposit. However, triple-negative breast cancer shows the same immunophenotype; ER and PR positivity is seen in metastasis from gynecologic primaries; GCDFP-15 has been reported in 5 % of lung carcinomas and TTF-1 in 2.5 % of breast carcinomas. Of note, GCDFP-15 and mammaglobin A are the most specific breast markers, but they have low sensitivity.

US features. There is usually a single round, hypoechoic mass, sometimes showing a heterogeneous echotexture and well or poorly defined borders with no posterior acoustic shadowing.

Axillary Lymph Node Evaluation in Breast Cancer

The status of the axillary lymph nodes is the most important prognostic factor in the evaluation of a patient with breast cancer. Evaluation of the sentinel lymph node is important for prediction of the status of the axillary lymph nodes. Thus, lymph node US characteristics and pathologic study are essential before a management decision is made. USG-FNA is simple, inexpensive, minimally invasive, and accurate for evaluating axillary nodes, including sentinel lymph nodes, and can be made under US guidance (Fig. 8.62a, b).

Axillary lymph node dissection is associated with significant morbidity; thus, accurate lymph node evaluation to detect macrometastasis (>2 mm) or micrometastasis (≤2 mm), both intraoperatively and on permanent sections, is paramount in patient management. Pancytokeratin immunostains are commonly used to highlight the metastatic deposits. It is clear that US exam and USG-FNA are simple and cost-effective methods to detect axillary metastasis and proceed to axillary lymph node dissection and avoid sentinel lymph node biopsy. Obviously, this is useful in sizable metastatic involvement and may not be useful to accurately detect small foci including micrometastasis. This practice needs further evaluation in view of undergoing treatment trials in patients with sentinel lymph node micrometastasis that may not require axillary lymph node dissection.

US features. A normal US appearance of an axillary lymph node includes size <2 cm, cortical thickness <2 mm, regular uniform borders, oval shape, presence of hilum, and hilar vascularity. Abnormal nodes may show >2 mm uniform concentric cortical thickening, eccentric cortical thickening, a bulging contour, round shape (taller than wide), loss of fatty hilum, an irregular cortical shape, and irregular vascular flow (central and peripheral/cortical) (Fig. 8.62c). None of these features is specific for a benign or malignant process.

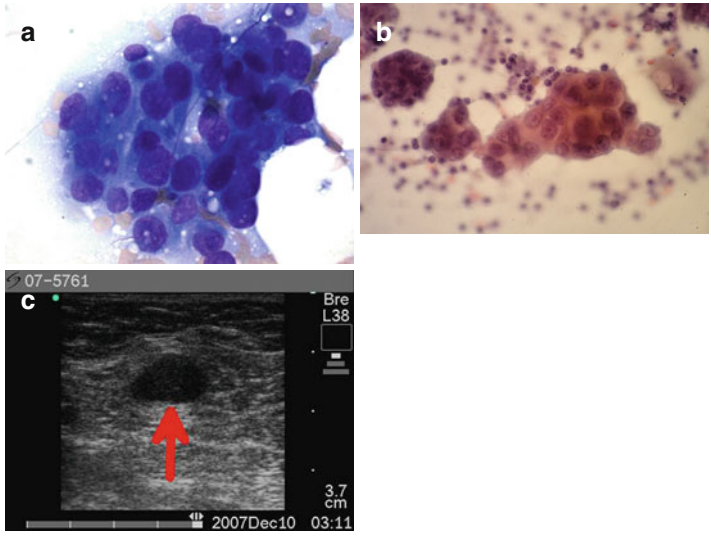

FIGURE 8.62 Axillary lymph node metastasis. Axillary lymph node metastasis is not uncommon in patients with "inflammatory" carcinoma; while FNA of the primary breast mass may not be fully diagnostic due to the marked desmoplasia often present in these cases, FNA sampling of ipsilateral axillary lymph nodes yields diagnostic material as seen in this case. Aggregates of high-grade tumor cells are present (**a**, **b**) surrounded by small lymphocytes (**b**). US image of the lymph node shows intense hypoechogenicity, irregular shape, well-defined borders, and lack of vascular hilum (**c** *arrow*) (**a**, Diff-Quik stain high magnification; **b**, Papanicolaou stain high magnification)

Suggested Reading

Ali SZ, Parwani AV. Breast cytopathology. New York: Springer; 2007.

Bardales RH, Stanley MW. Benign spindle and inflammatory lesions of the breast: diagnosis by fine-needle aspiration. Diagn Cytopathol. 1995;12(2):126–30.

Bardales RH, Suhrland MJ, et al. Papillary neoplasms of the breast: fine-needle aspiration findings in cystic and solid cases. Diagn Cytopathol. 1994;10(4):336–41.

Bleiweiss I, Jaffer S, et al. Breast core biopsy: a pathologic-radiologic approach. Philadelphia: Saunders Elsevier; 2008.

Brunello E, Brunelli M, et al. Classical lobular breast carcinoma consistently lacks topoisomerase-IIalpha gene amplification: implications for the tailored use of anthracycline-based chemotherapies. Histopathology. 2012;60(3):482–8.

Cardenosa G. Breast ultrasound. Breast imaging companion. Philadelphia: Wolters Kluwer/Lippincott Williams & Wilkins; 2008. p. 146–79.

Chang MC, Crystal P, et al. The evolving role of axillary lymph node fine-needle aspiration in the management of carcinoma of the breast. Cancer Cytopathol. 2011;119(5):328–34.

Farmer C, Stanley MW, et al. Mycoses of the breast: diagnosis by fine-needle aspiration. Diagn Cytopathol. 1995;12(1):51–5.

Geisinger KR, Stanley MW, et al. Breast. Modern cytopathology. Philadelphia: Churchill Livingstone; 2004. p. 873–929.

James JJ, Evans AJ. Breast. In: Allan PL, Baxter GM, Weston MJ, editors. Clinical Ultrasound, vol. 2. London: Churchill Livingstone Elsevier; 2011. p. 987–1004.

Kornegoor R, Verschuur-Maes AH, et al. Immunophenotyping of male breast cancer. Histopathology. 2012a;61(6):1145–55.

Kornegoor R, Verschuur-Maes AH, et al. Molecular subtyping of male breast cancer by immunohistochemistry. Mod Pathol. 2012b; 25(3):398–404.

Lakhani SR, Ellis IO, et al. WHO classification of tumours of the breast. Lyon: IARC Press; 2012.

Leonardo E. Mammella. Morfologia Molecolare: Principi Generali e Diagnostica Sistematica. Padova: Libreria Universitaria; 2012. p. 739–62.

Li D, Xiao X, et al. Secretory breast carcinoma: a clinicopathological and immunophenotypic study of 15 cases with a review of the literature. Mod Pathol. 2012;25(4):567–75.

Lopez-Garcia MA, Geyer FC, et al. Breast cancer precursors revisited: molecular features and progression pathways. Histopathology. 2010;57(2):171–92.

Mentzel T, Schildhaus HU, et al. Postradiation cutaneous angiosarcoma after treatment of breast carcinoma is characterized by MYC amplification in contrast to atypical vascular lesions after radiotherapy and control cases: clinicopathological, immunohistochemical and molecular analysis of 66 cases. Mod Pathol. 2012; 25(1):75–85.

Monhollen L, Morrison C, et al. Pleomorphic lobular carcinoma: a distinctive clinical and molecular breast cancer type. Histopathology. 2012;61(3):365–77.

O'Malley FP, Pinder SE, et al. Breast pathology. Philadelphia: Elsevier Saunders; 2011.

Perou CM, Sorlie T, et al. Molecular portraits of human breast tumours. Nature. 2000;406(6797):747–52.

Rakha EA, Ellis IO. Modern classification of breast cancer: should we stick with morphology or convert to molecular profile characteristics. Adv Anat Pathol. 2011;18(4):255–67.

Rinaldi P, Ierardi C, et al. Cystic breast lesions: sonographic findings and clinical management. J Ultrasound Med. 2010;29(11): 1617–26.

Rosa M, Masood S. Cytomorphology of male breast lesions: diagnostic pitfalls and clinical implications. Diagn Cytopathol. 2012;40(2): 179–84.

Ross DS, Wen YH, et al. Ductal carcinoma in situ: morphology-based knowledge and molecular advances. Adv Anat Pathol. 2013; 20(4):205–16.

Sauer T. Fine-needle aspiration cytology of extra mammary metastatic lesions in the breast: a retrospective study of 36 cases diagnosed during 18 years. Cytojournal. 2010;7:10.

Schnitt SJ. Molecular biology of breast tumor progression: a view from the other side. Int J Surg Pathol. 2010;18(3 Suppl): 170S–3.

Stanley MW, Henry-Stanley MJ, et al. Atypia in breast fine-needle aspiration smears correlates poorly with the presence of a prognostically significant proliferative lesion of ductal epithelium. Hum Pathol. 1993a;24(6):630–5.

Stanley MW, Tani EM, et al. Primary spindle-cell sarcomas of the breast: diagnosis by fine-needle aspiration. Diagn Cytopathol. 1988;4(3):244–9.

Stanley MW, Tani EM, et al. Adenoid cystic carcinoma of the breast: diagnosis by fine-needle aspiration. Diagn Cytopathol. 1993b; 9(2):184–7.

Stanley MW, Tani EM, et al. Cystosarcoma phyllodes of the breast: a cytologic and clinicopathologic study of 23 cases. Diagn Cytopathol. 1989a;5(1):29–34.

Stanley MW, Tani EM, et al. Metaplastic carcinoma of the breast: fine-needle aspiration cytology of seven cases. Diagn Cytopathol. 1989b;5(1):22–8.

Stanley MW, Tani EM, et al. Mucinous breast carcinoma and mixed mucinous-infiltrating ductal carcinoma: a comparative cytologic study. Diagn Cytopathol. 1989c;5(2):134–8.

Stanley MW, Tani EM, et al. Fine-needle aspiration of fibroadenomas of the breast with atypia: a spectrum including cases that cytologically mimic carcinoma. Diagn Cytopathol. 1990;6(6): 375–82.

Tsang JY, Mendoza P, et al. Involvement of alpha- and beta-catenins and E-cadherin in the development of mammary phyllodes tumours. Histopathology. 2012;61(4):667–74.

Index

R.H. Bardales (ed.), *The Invasive Cytopathologist*, Essentials in Cytopathology 16, DOI 10.1007/978-1-4939-0730-4,